Regulatory and self-protection implications of gliotoxin bisthiomethylation in *Aspergillus fumigatus*

Stephen Dolan BSc

Maynooth University
National University of Ireland Maynooth

Thesis submitted to Maynooth University for the degree of Doctor of Philosophy

October 2015

Supervisor:

Prof. Sean Doyle,

Biotechnology Laboratory,

Department of Biology,

Maynooth University,

Maynooth,

Co. Kildare, Ireland

Head of Department:

Prof. Paul Moynagh

Regulatory and self-protection implications of gliotoxin bisthiomethylation in *Aspergillus fumigatus*

Stephen Dolan BSc

Maynooth University
National University of Ireland Maynooth

Thesis submitted to Maynooth University for the degree of Doctor of Philosophy

October 2015

Supervisor:

Prof. Sean Doyle,

Biotechnology Laboratory,

Department of Biology,

Maynooth University,

Maynooth,

Co. Kildare, Ireland

Head of Department:

Prof. Paul Moynagh

Table of Contents

Declaration of Authorship

This thesis has not previously been submitted, in whole or in part, to this, or any other University, for any other degree. This thesis is the sole work of the author with the exception of the solving of the GtmA crystal structure, which was carried with the assistance of Tobias Bock at the Helmholtz Centre for Infection Research, Braunschweig, Germany.

_____

Stephen Dolan BSc.

Acknowledgements

I wish to extend my sincere gratitude to my supervisor, Professor Sean Doyle, to whom I am indebted for all of the guidance and support throughout my studies. My thanks are also extended to Dr Gary Jones, my co-supervisor, whose advice and ideas were greatly appreciated. I would also like to thank Dr Rebecca Owens and Dr Grainne O'Keeffe for the invaluable training at the start of this process. Thanks to Caroline Batchelor for the superior Mass Spec assistance, Dr David Fitzpatrick for the bioinformatic analysis and to Ica Dix for the help with confocal microscopy. Dr Özgür Bayram and Dr Özlem Bayram were of the utmost help, especially when it came to protein localisation studies.

I wish to thank the Irish Research Council and the Department of Biology, Maynooth University for funding this PhD. Also, I am grateful for the support that I had from numerous societies in the pursuit of various courses and lab visits during my PhD; FEBS, FEMS, SGM, ISCA and the Biochemical Society. Special thanks go to Prof. Gustavo Goldman and Dr Wulf Blankenfeldt for generously hosting me in their labs. The structural work of this project would not have been possible without Tobias Bock and Vanessa Hering at the HZI in Braunschweig. My appreciation to Dr John Flood for all of the help with administration.

Thanks to the Biotechnology and Yeast Genetics Labs for making this whole experience a very enjoyable one. Nicola, who was always guaranteed to have at least 6 spare bottles of sterile PBS. Lara, who always knew when you took her PBS. Kevin, for all those times I beat him at table tennis and Eoin, for that one incredible time I beat him at table tennis: definitely a 2015 highlight! Elizabeth for being the best prank victim there ever was, Daragh for the many stories about his car and Linan for his help, unusual food and discussions. I would also like to thank Niamh, Rose, Cindy and Stephen H.

A special thanks to my good friend Brian who was always up for a chat, a crash course in driving or a game of pitch and putt on the weekends.

I would like to thank my family. To my parents, Emer and Tom, for all of their help and support throughout my time in Maynooth. Darina, for some fancy dinners during my brief stint at home when writing up. Aisling, for all the extended coffee chats over the last few months and for the Mrs Doyle-like “put your money away” arguments that ensued every time.

Bríd for all her help, support and encouragement during just about everything I put my mind to over the last 7 years. And for understanding that when I said I’d be home in an hour, it was a very crude estimate.

Publications

Manzanares L., Sarikaya-Bayram, Ö. **Dolan S.K**, Bayram, Ö., Jones G.W. and Doyle S. (2015) Quantitative proteomics reveals the mechanism and consequence of gliotoxin-mediated dysregulation of the methionine cycle in *Aspergillus niger.* J. Proteomics. In Revision.

Owens, R. A., O'Keeffe, G., Smith, E. B., **Dolan, S. K.**, Hammel, S., Sheridan, K. J., Fitzpatrick, D. A., Keane, T. M., Jones, G. W., and Doyle, S. (2015). Interplay between Gliotoxin Resistance, Secretion, and the Methyl/Methionine Cycle in Aspergillus fumigatus. *Eukaryot. Cell* 14, 941–57. doi:10.1128/EC.00055-15.

Dolan, S. K., O'Keeffe, G., Jones, G. W., and Doyle, S. (2015). Resistance is not futile: gliotoxin biosynthesis, functionality and utility. *Trends Microbiol.*, 1–10. doi:10.1016/j.tim.2015.02.005.

Winkelströter, L. K., **Dolan, S. K.**, Fernanda Dos Reis, T., Bom, V. L. P., Alves de Castro, P., Hagiwara, D., Alowni, R., Jones, G. W., Doyle, S., Brown, N. A., et al. (2015). Systematic Global Analysis of Genes Encoding Protein Phosphatases in Aspergillus fumigatus. *G3 (Bethesda).* 5, 1525–39. doi:10.1534/g3.115.016766.

Sheridan, K. J., **Dolan, S. K.**, and Doyle, S. (2015). Endogenous cross-talk of fungal metabolites. *Front. Microbiol.* 5, 10.3389. doi:10.3389/fmicb.2014.00732.

Dolan, S. K., Owens, R. a, O'Keeffe, G., Hammel, S., Fitzpatrick, D. a, Jones, G. W., and Doyle, S. (2014). Regulation of Nonribosomal Peptide Synthesis: bis-Thiomethylation Attenuates Gliotoxin Biosynthesis in Aspergillus fumigatus. *Chem. Biol.* 21, 999–1012. doi:10.1016/j.chembiol.2014.07.006.

Johnson, G., Ferrini, A., **Dolan, S. K.**, Nolan, T., Agrawal, S., Doyle, S., and Bustin, S. a (2014). Biomarkers for invasive aspergillosis: the challenges continue. *Biomark. Med.* 8, 429–51. doi:10.2217/bmm.13.129.

Gallagher, L., Owens, R. A., **Dolan, S. K.**, O'Keeffe, G., Schrettl, M., Kavanagh, K., Jones, G. W., Doyle, S. (2012). The Aspergillus fumigatus protein GliK protects against oxidative stress and is essential for gliotoxin biosynthesis. *Eukaryot. Cell* 11, 1226–38. doi:10.1128/EC.00113-12.

Oral Presentations

Combining reverse genetics and X-ray crystallography to elucidate the structure and function of a gliotoxin bis-thiomethyltransferase in *Aspergillus fumigatus*, Biology Research Day, Maynooth University, June 2015. Awarded runner-up best presentation.

Regulation of Nonribosomal Peptide Synthesis: bis-Thiomethylation Attenuates Gliotoxin Biosynthesis in *Aspergillus fumigatus*. NCIB Proteomics Conference, Dublin City University, September 2014.

Discovering New Biochemistry in *Aspergillus fumigatus*. Irish Fungal Society Annual Meeting. NUI Galway. June 2014. Awarded best presentation.

Bis-thiomethylation of gliotoxin in *Aspergillus fumigatus*: Exploring the implications for gliotoxin biosynthesis and self-protection. 3rd Biology Research Day, Maynooth University, September 2014. Awarded best presentation.

Poster Presentations

Thiol directed natural product methyltransferases: new tools for synthetic biology, Synthetic Biology UK, London, September 2015.

Bis-Thiomethylation of Gliotoxin: Insights into the enzymatic structure and global effects of a post-biosynthetic regulatory system in *A. fumigatus*, Irish Fungal Society Annual Meeting, Trinity College Dublin, June, 2015. Awarded best poster prize.

Bis-Thiomethylation of Gliotoxin: Exploring the effects and enzymatic mechanism of a post-biosynthetic regulatory system in *A. fumigatus*. FEBS Advanced Lecture Course Human Fungal Pathogens, La Colle sur Loup, France, May 2015.

Regulating Nonribosomal Peptide Synthesis: Post-biosynthetic bis-Thiomethylation of Gliotoxin Attenuates Gliotoxin Biosynthesis in *Aspergillus fumigatus*. Asperfest, 28th Fungal Genetics Conference, California, March 2015. Awarded best poster prize.

Exploring the Enzymatic Mechanism and Biological Function of Gliotoxin S-methylation in *Aspergillus fumigatus.* BioCrys course on Macromolecular Crystallography, Oeiras, Portugal, September 2014.

Exploring the Enzymatic Mechanism and Biological Function of Gliotoxin S-methylation in *Aspergillus fumigatus*. The Eleventh International Aspergillus Meeting. Hotel Silken-Al Andalus, Seville, Spain. March 2014. Awarded best poster prize.

S-Methylation of Gliotoxin: Uncovering the Biosynthetic Pathway Responsible for a Novel Self-Protection Mechanism. Irish Fungal Society Annual Meeting, Maynooth University, June 2013.

Microbiology Meets Chemical Biology: The *Aspergillus fumigatus* Protein GliK is Involved in Gliotoxin Biosynthesis and Self-Protection. FEBS Advanced Lecture Course Human Fungal Pathogens, La Colle sur Loup, France, May 2013.

Abbreviations

AMM	*Aspergillus* minimal media
ATCC	American Type Cell Culture
ATP	Adenosine triphosphate
bp	Base pairs
BSA	Bovine serum albumin
bZIP	Basic leucine zipper
CADRE	Central *Aspergillus* Data Respository
cDNA	Complementary deoxyribonucleic acid
CIAP	Calf intestine alkaline phosphatase
CoA	Coenzyme A
DIG	Digoxigenin
DMSO	Dimethyl sulfoxide
DNA	Deoxyribonucleic acid
EDTA	Ethylenediaminetetraacetic acid
gDNA	genomic deoxyribonucleic acid
GOI	Gene of interest
GST	Glutathione *s*-transferase
GSH	Glutathione
H_2O_2	Hydrogen peroxide
IA	Invasive Aspergillosis
Kb	Kilobase
RNA	Ribonucleic acid
ROS	Reactive oxygen species
RP-HPLC	Reverse-phase High performance liquid chromatography
RPM	Revolutions per minute

RT-PCR	Reverse-transcriptase polymerase chain reaction
SAM	s-adenosyl methionine
SDS	Sodium dodecyl sulphate
SDS-PAGE	Sodium dodecyl sulphate polyacrylamide gel electrophoresis
TAE	Tris:acetate:EDTA
TCA	Trichloroacetic acid
TFA	Trifluroacetic acid
tRNA	transfer RNA
UPR	Unfolded protein response
UV	Ultraviolet
v/v	volume per volume
w/v	weight per volume
X-gal	1,5-bromo-4-chloro-3-indoyl-β-DNA-galactosidase
mAU	milli Absorbance Unit

Summary

Gliotoxin is an epipolythiodioxopiperazine (ETP) produced by the opportunistic fungal pathogen *Aspergillus fumigatus*. It contains an intact disulphide bridge, which mediates its toxic effects via redox cycling. Like many other ETPs, a bisthiomethylated form is also produced. In the case of gliotoxin, bis(methyl)gliotoxin is formed for unknown reasons by a cryptic enzyme. The work presented uncovered the S-adenosylmethionine dependent gliotoxin bis-thiomethyltransferase (GtmA), which converts dithiol gliotoxin to bis(methyl)gliotoxin. Disruption of this non-*gli* cluster encoded methyltransferase completely abrogated organismal ability to biosynthesize and secrete bis(methyl)gliotoxin, while gliotoxin production and secretion were increased (p=0.0056). Label-free quantitative (LFQ) proteomics of *A. fumigatus* wild-type, *ΔgtmA*, and *gtmAC* strains cultured in Czapek-Dox media revealed an elevated abundance of *gli* cluster encoded enzymes in the *ΔgtmA* mutant strain. Phylogenetic analysis of this enzyme revealed that there are 124 GtmA homologs within the Ascomycota phylum. Furthermore, through the characterisation of changes in SAM homoeostasis within *A. fumigatus*, this work also illuminates a direct link between gliotoxin biosynthesis and primary metabolic processes. Recombinant GtmA was shown to bismethylate dithiol GT using S-adenosyl methionine (SAM) as a methyl donor. Additionally, the crystal structure of GtmA was solved by multiple-wavelength anomalous diffraction to 2.3 Å resolution. This information was used to identify GtmA structural homologs, to uncover residues in involved in GtmA substrate binding and to facilitate targeted engineering of this enzyme. We now propose that the purpose of GtmA mediated bis(methyl)gliotoxin formation primarily serves to attenuate gliotoxin biosynthesis. This appears to be the first example of postbiosynthetic regulation of nonribosomal peptide synthesis in any organism.

Chapter 1

Introduction

1.1 General Characteristics of *Aspergillus fumigatus*

Aspergillus fumigatus is an opportunistic human pathogen found in the Ascomycota Phylum (Dagenais and Keller, 2009). It is one of the most ubiquitous of the airborne saprophytic fungi and plays an important role in recycling environmental carbon and nitrogen (Latgé, 1999). *A. fumigatus* has achieved worldwide distribution due to the production of small buoyant spores called conidia which have an average size of 2-3.5 µm. Due to their remarkable hydrophobicity these conidia are capable of dispersing in the air and persisting in the atmosphere (O'Gorman, 2011). They also have the ability to survive prolonged periods of freezing or dehydration (Kwon-Chung and Sugui, 2013). In addition to airborne dispersal, conidia which are imbedded in soil may be effectively transported to favourable growth conditions by swarming soil bacteria such as *Paenibacillus vortex* (Ingham et al., 2011). As a major component of the biomass in a self-heating compost pile *A. fumigatus* grows optimally at 37°C and a pH 3.7 to 7.6, but it can be isolated when temperatures range between 12° and 65°C and the pH ranges between 2.1–8.8 (Kwon-Chung and Sugui, 2013). In contrast, most other fungi are mesophilic, displaying temperature optima in the range of 25–35°C (Bhabhra and Askew, 2005).

A. fumigatus reproduction is predominantly asexual and is mediated by the abundant production of haploid conidia (Rokas, 2013). The asexual life cycle of *A. fumigatus* is initiated by germination of these conidia into mycelia composed of hyphal cells. After a period of vegetative growth, conidiophores develop from these hyphae which are dandelion head-like structures bearing long chains of conidia (Ward et al., 2005). *A. fumigatus* also possesses a fully functional sexual reproductive cycle. It was shown to produce mature cleistothecia (sexual bodies containing the sexual spores called ascospores) in cultures grown on oatmeal agar plates at 30°C in the dark after a 6 month incubation period (O'Gorman et al., 2009).

1.2 Pathogenesis of *Aspergillus fumigatus*

Among the human pathogenic species of *Aspergillus*, *A. fumigatus* is the primary causative agent of human infections. It is followed by *A. flavus*, *A. terreus*, *A. niger*, and *A. nidulans* (Dagenais and Keller, 2009). *A. fumigatus* attacks immunocompromised patients: particularly those who are suffering from prolonged neutropenia or severe haematological malignancies, transplant recipients and, also, individuals with genetic immunodeficiencies such as chronic granulomatous disease (CGD) are particularly sensitive (Edmond et al., 1999; Bodey et al., 1992; Pfaffenbach et al., 1994). The susceptible patient population is expanding due to the increased use of transplantation for end organ disease, the development of immunosuppressive and myeloablative therapies for autoimmune and neoplastic disease and the human immunodeficiency virus/AIDS pandemic (Hohl and Feldmesser, 2007). The primary route of human infection is via the inhalation of airborne conidia which is followed by conidial deposition in the bronchioles or alveolar spaces (Pandey et al., 2013). *Aspergillus* primarily affects the lungs and causes the following four main syndromes: allergic bronchopulmonary aspergillosis (ABPA), chronic necrotizing *Aspergillus* pneumonia, aspergilloma and invasive aspergillosis (IA) (Pathak et al., 2011).

` IA is the most common invasive mould disease worldwide and this devastating illness has been associated with high rates of mortality (Dagenais and Keller, 2009). IA is usually seen in the lungs as invasive pulmonary aspergillosis (IPA) which is defined as an invasion of the pulmonary parenchyma by the growing hyphae of *Aspergillus*. This is further refined as angioinvasive IPA if there is evidence of vascular invasion by the hyphae (Hope et al., 2005). In 10%–25% of cases dissemination is reported to occur from pulmonary sites to other tissues. These include the central nervous system (CNS), sinuses, bone, heart, kidney, eye, blood and skin (Johnson et al., 2014). Mortality rates range from 40% to 90% in high-risk populations and are dependent on factors such as the host's

immune status, the site of infection and the treatment regimen applied (Lin et al., 2001). A recent study suggested that respiratory failure is the most frequent cause of IA related death and that 83.9% of IA-related deaths occurred within 21 days following diagnosis (Garcia-Vidal et al., 2015)

The inhalation of *A. fumigatus* conidia rarely has an adverse effect on immunocompetent individuals as innate immune mechanisms such as mucociliary clearance and alveolar macrophages efficiently remove the conidia. Conidia that evade macrophage killing and germinate become the target of infiltrating neutrophils which are able to destroy hyphae. Conversely, in the case of immunosuppressed patients, inhaled conidia adhere to airway epithelial cells or pulmonary macrophages, are internalized and undergo germination (Latgé, 1999). As shown in Figure 1.1, hyphal growth occurs by apical extension with the angiogenic properties giving the fungus access to the vascular compartment. Dissemination occurs via the bloodstream, colonizing other organs (Dagenais and Keller, 2009). The fungus appears to sense the bloodstream and adapts to it within hours. It shuts down all unnecessary pathways in order to obscure itself for as long as is viable in the blood and then escapes as quickly as possible (Irmer et al., 2015). This results in the dissemination and invasion of deep tissues whereby *A. fumigatus* can cause severe, and usually fatal, invasive infections.

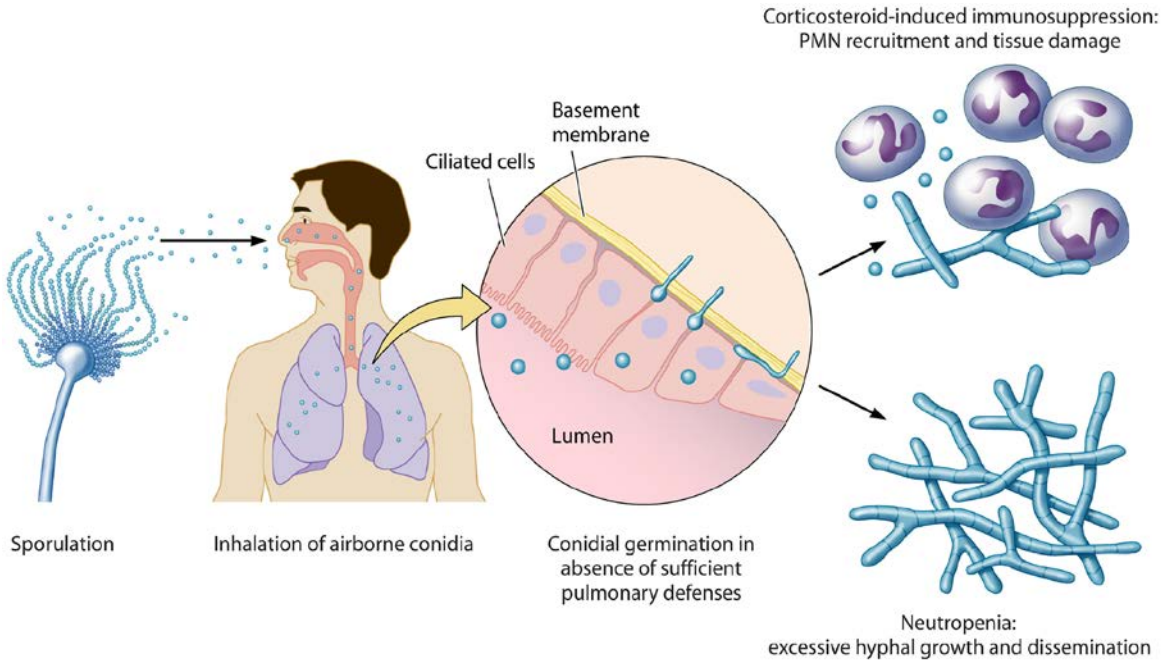

Figure 1.1. Infectious life cycle of *A. fumigatus*. *Aspergillus* is ubiquitous in the environment and asexual reproduction leads to the production of airborne conidia. Inhalation by specific immunosuppressed patient groups results in conidium establishment in the lung which is followed by germination and either PMN-mediated fungal control with significant inflammation (corticosteroid therapy) or uncontrolled hyphal growth with a lack of PMN infiltrates and, in severe cases, dissemination (neutropenia) (Dagenais and Keller, 2009).

1.3 Virulence factors of *Aspergillus fumigatus*

Virulence factors are defined as any factor that causes damage to the infected host (Rhodes, 1988). As illustrated in Figure 1.2, the genes and molecules related to *A. fumigatus* virulence can be classified according to the process they are involved in, e.g., thermotolerance; cell wall composition and maintenance; resistance to the immune response; toxins; nutrient uptake during invasive growth and response to stress conditions (Abad et al., 2010).

Reflecting elevated temperatures present in composting substrates, *A. fumigatus* is well adapted to temperature stress and displays an exquisite thermotolerance of up to 70 °C (Bhabhra and Askew, 2005). This metabolic adaptation means that *A. fumigatus* is capable of growing at 37°C, the actual body temperature of humans, which represents an essential characteristic for pathogenicity (Amich and Krappmann, 2012). Several lines of evidence suggest that high temperature is a significant stress for the process of ribosome biogenesis. Consequently, deletion of the *A. fumigatus* gene encoding nucleolar protein CgrA was shown to impair thermotolerant growth and reduce the virulence of this organism (Bhabhra et al., 2004). Additionally, trehalose synthesis was shown to play an important role in mediating thermotolerance in *A. fumigatus* (Al-Bader et al., 2010).

The cell wall (CW) is the main line of defense of the fungus against a hostile environment. It provides both structural integrity and physical protection to the cell. The fungal cell wall is also responsible for the interaction with the host and its components are often the targets of the host immune system during fungal infections (Abad et al., 2010). In *A. fumigatus*, the cell wall is mainly composed of the polysaccharides β-glucan, chitin, galactomannan, α-glucan and a variety of proteins (Gastebois et al., 2009). Several of these cell wall components and associated pathways have been targeted by gene deletion studies. Of the current *A. fumigatus* mutant strains which have a defect in the CW, more than 20

were affected in virulence (Valiante et al., 2015). Surprisingly, many mutant strains with defects in CW biosynthesis enzymes were still virulent in the applied infection models. As an example, both of the α-1,3-glucan synthase mutant strains (Δ*ags1,* and Δ*ags2*) were still pathogenic despite their α-1,3-glucan content being reduced by 50% when compared to the wild-type strain (Beauvais et al., 2005). However, the deletion of the genes encoding for a β-1,3-glucanosyltransferase (*gel2*) and a α-1,2-mannosyltransferase (*mnt1*) resulted in a decrease of virulence (Mouyna et al., 2005; Wagener et al., 2008).

Mammalian organisms present a broad variety of microenvironments in which *A. fumigatus* must survive in order to cause disease and these environmental conditions are subject to rapid change depending on the current stage of infection (Abad et al., 2010). Among micronutrients of the environment iron is an essential nutrient for *Aspergillus* sp. and a key component of several enzymes that participate in a variety of cellular processes (Haas et al., 2008). The iron sequestration is an important factor in host defence against invading fungi since it prevents *in vivo* fungal development. Low-molecular mass iron-specific chelators called siderophores are employed by the fungus to regulate iron load which is of great importance in fungal virulence (Schrettl et al., 2007; Sales-Campos et al., 2013). Additionally, the concentration of free zinc in living tissues is much lower than that required for optimal fungal growth *in vitro* because most of it is tightly bound to proteins (Outten and O'Halloran, 2001). To efficiently obtain zinc from a living host, *A. fumigatus* uses the zinc transporters ZrfA, ZrfB, and ZrfC. The ZrfA transcriptional regulator induces the expression of all these transporters and is essential for virulence (Moreno et al., 2007; Vicentefranqueira et al., 2015).

The environmental conditions found by pathogenic fungi in the colonization and infection of the host are different to those found in their normal environmental niche. *A. fumigatus* must be able to adapt to stress in the microenvironment during host invasion and

systemic spread. Several regulatory mechanisms have been studied in *A. fumigatus*. These include mitogen-activated protein kinase (MAPK) pathways and signal transduction pathways which are activated by G-proteins, Ras proteins, histidine kinases, calcium signaling and others (Abad et al., 2010). The high-osmolarity glycerol (HOG) mitogen-activated protein kinase (MAPK) signaling pathway is a key element in regulating morphology, growth and adaptation to stress and virulence in *A. fumigatus* (Ma and Li, 2012).

A. fumigatus has a combination of characteristics that helps the fungus to evade or interfere with the immune response (Heinekamp et al., 2015). Genes and molecules involved in the resistance to the host immune response could be considered defensive virulence factors (Abad et al., 2010). Dihydroxynaphtalene (DHN)-melanin pigmentation on *A. fumigatus* conidial surface has been shown to affect virulence by limiting C3 complement deposition and neutrophil activation (Langfelder et al., 1998). Also, the rodlet layer, composed by the hydrophobic RodA protein and the pigment DHN-melanin on the surface of resting *A. fumigatus* conidia, renders the conidia largely inert towards recognition by the immune system (Aimanianda et al., 2009). This surface protein was also shown to enhance fungal survival in the cornea during fungal keratitis (de Jesus Carrion et al., 2012).

Mycotoxins are a group of chemically diverse, low molecular mass compounds which are produced by fungi as secondary metabolites. They are formed in the hyphae during growth and may be actively expelled into the environment or released after the death of the hyphae (Richard, 2007). Toxins are apparently produced by the fungus as competitive weapons which are used against predators and competitors in its ecological niche. However, they could also contribute to *A. fumigatus* pathogenesis by modulating the disease progress (Scharf et al., 2014b). Fungal toxins have also been shown to act as interspecies signals,

affecting filamentous fungal development via oxidative stress regulation (Zheng et al., 2014).

A fumigatus produces a wealth of potent mycotoxins including gliotoxin, festuclavine, fumigaclavines A–C, helvolic acid and pseurotin A (Frisvad and Larsen, 2015). Gliotoxin will be discussed in detail in Section 1.4. The ergot alkaloids are a complex family of indole derivatives with diverse biological activities (Wallwey et al., 2010). Due to their ability to act as partial agonists or antagonists at different adrenaline, noradrenaline, dopamine, and serotonin receptors they affect nervous, circulatory, reproductive, and immune systems. This results in a large variety of symptoms including changes in blood pressure, lowered immune response, hallucinations and gangrene of the limbs (Mulinti et al., 2014). The ergot alkaloids festuclavine and fumigaclavines A–C are present in, or on, conidia of *A. fumigatus* (Mulinti et al., 2014). Two other toxins which are produced by *A. fumigatus* are helvolic acid and fumagillin. Helvolic acid is part of a small family of steroidal antibiotics known as fusidanes (Mitsuguchi et al., 2009). At high concentrations it can affect the oxidative burst of macrophages, the metabolism of low density lipoproteins and, *in vivo*, it induces ciliostasis and rupture of epithelial cells (Mitchell et al., 1997). Fumagillin is a monoterpenoid antibiotic which inhibits angiogenesis and, *in vitro*, directly inhibits endothelial cell proliferation and cilial movement in respiratory epithelium (Lin et al., 2013; Amitani et al., 1995).

.

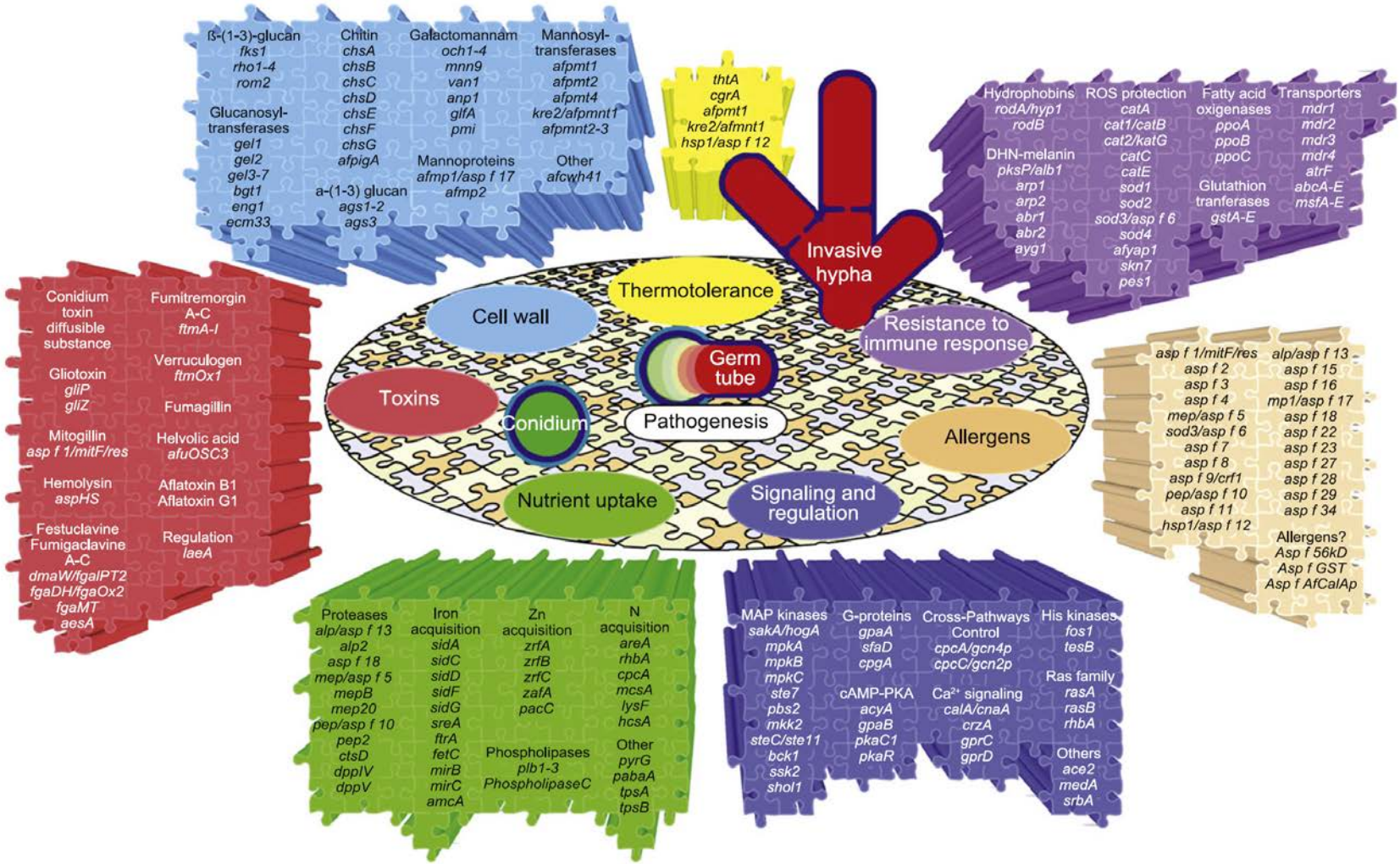

Figure 1.2. Summary of genes and molecules associated with the virulence of *Aspergillus fumigatus* (Abad et al., 2010).

1.4 Gliotoxin

Gliotoxin is a non-ribosomally synthesised, redox-active metabolite which is secreted by several fungal species (Figure 1.3). It was the first antibiotic to be utilised in the control of plant diseases and was purified prior to the discovery of penicillin (Anitha and Murugesan, 2005). This metabolite also significantly contributes to the virulence of the human fungal pathogen *A. fumigatus* (Dagenais and Keller, 2009). Gliotoxin is an epipolythiodioxopiperazine (ETP) class fungal toxin equipped with a transannular disulphide bridge which mediates its toxic effects via redox cycling as shown in Figure 1.4 (Kwon-Chung and Sugui, 2008).

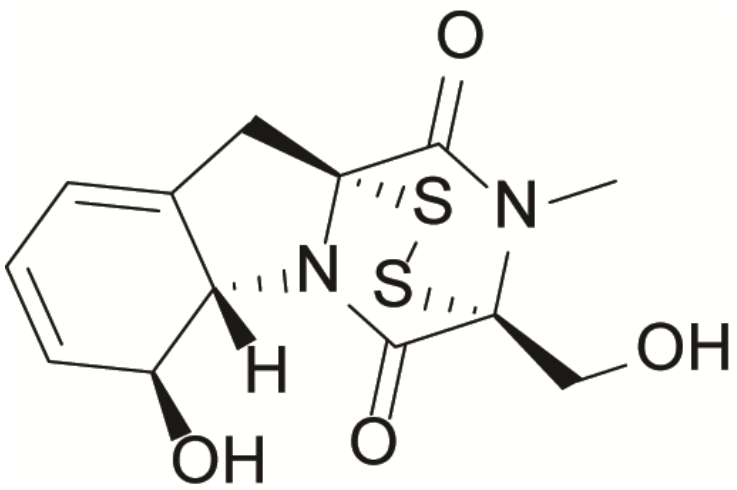

Gliotoxin

Figure 1.3. The structure of gliotoxin ($C_{13}H_{14}N_2O_4S_2$).

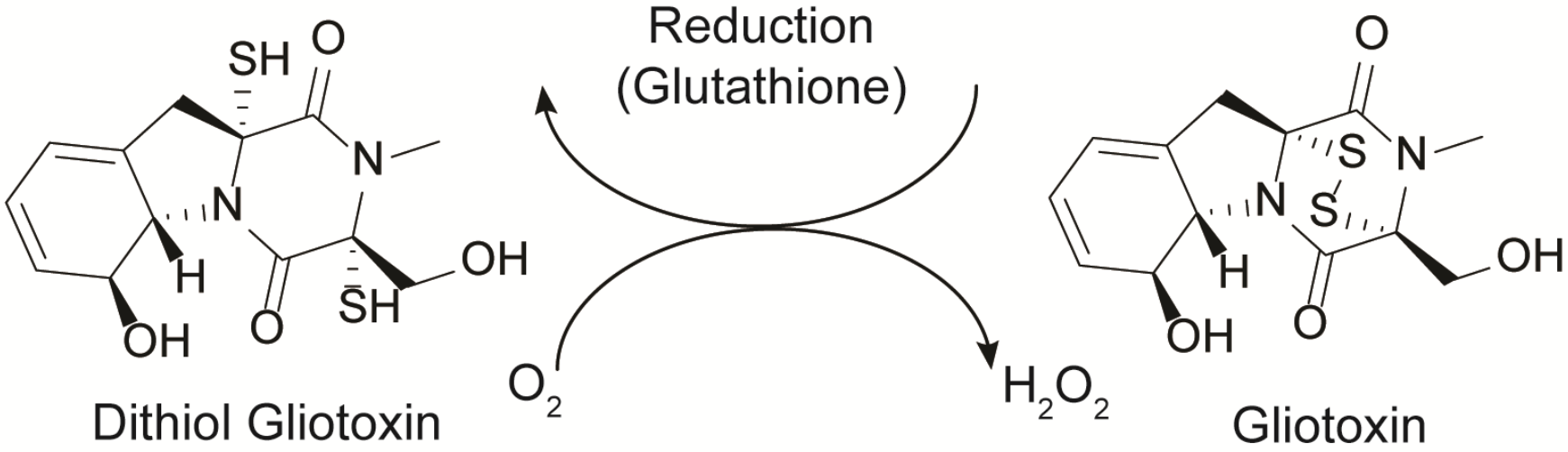

Figure 1.4. Interconversion of gliotoxin between the reduced (dithiol) and oxidized (disulfide) forms.

1.4.1 Gliotoxin Biosynthesis

The *in silico* identification of the *gli* cluster in *A. fumigatus* (Figure 1.5) (Gardiner and Howlett, 2005; Schrettl et al., 2010) paved the way for multiple functional genomic studies which have revealed that the *gli* cluster, comprising 13 genes, encodes the key enzymes responsible for gliotoxin biosynthesis. The $Zn(II)_2$-Cys(6) binuclear cluster domain transcription factor *gliZ* was confirmed as the regulator of the *gli* cluster (Bok et al., 2006) as deletion of this gene abrogated the expression of key biosynthetic genes and concomitant gliotoxin biosynthesis. Interestingly, upon *gliZ* reconstitution in *A. fumigatus* Δ*gliZ*, the biosynthesis of unrelated natural products was induced. The non-ribosomal peptide synthetase, GliP, catalyzes the formation of cyclo-phenylalanyl-serine, the first biosynthetic intermediate in the gliotoxin biosynthetic pathway (Balibar and Walsh, 2006) and multiple groups undertook *gliP* deletion, which results in complete loss of gliotoxin biosynthesis (Cramer et al., 2006; Kupfahl et al., 2006; Spikes and Xu, 2008; Sugui et al., 2007) (Figure 1.6). Interestingly, Cramer *et al*. observed that exogenous gliotoxin induced *gli* cluster gene expression in *A. fumigatus*, which was somewhat attenuated in *A. fumigatus* Δ*gliP* (Cramer et al., 2006). Although not unheard of, it is certainly unusual for a fungal natural product to induce its own biosynthesis and the biological significance of this phenomenon is only beginning to emerge. Cyclo-phenylalanyl-serine is subsequently converted to a highly reactive acyl imine intermediate prior to *bis*-glutathionylation. GliC has been shown to catalyze hydroxylation of the α-carbon of L-Phe in cyclo-phenylalanyl-serine prior to *bis*-glutathionylation (Chang et al., 2013). The demonstration that *gliG* encodes a glutathione *S*-transferase (GST) which conjugates two glutathione (GSH) molecules to a biosynthetic intermediate to form a *bis*-glutathionylated biosynthetic intermediate (Figure 1.6), and which is therefore responsible for the sulfurization of gliotoxin, was an important finding as it was one of the first demonstrations that GSTs played a biosynthetic, as opposed to

detoxification, role in fungi (Davis et al., 2011; Scharf et al., 2011). The *bis*-glutathionylated intermediate is subsequently processed by GliK, a γ-glutamyl cyclotransferase, to remove both γ-glutamyl moieties (Gallagher et al., 2012; Scharf et al., 2013). Subsequent processing via GliI (Scharf et al., 2012) yields a biosynthetic intermediate, which is *N*-methylated via the *N*-methyltransferase GliN, prior to the gliotoxin oxidoreductase GliT-mediated disulfide bridge closure (Figure 1.6) (Scharf et al., 2013, 2014a). Gliotoxin secretion from *A. fumigatus* ensues and is now known to be facilitated in part, or completely, by the MFS transporter GliA (Wang et al., 2014; Owens et al., 2015).

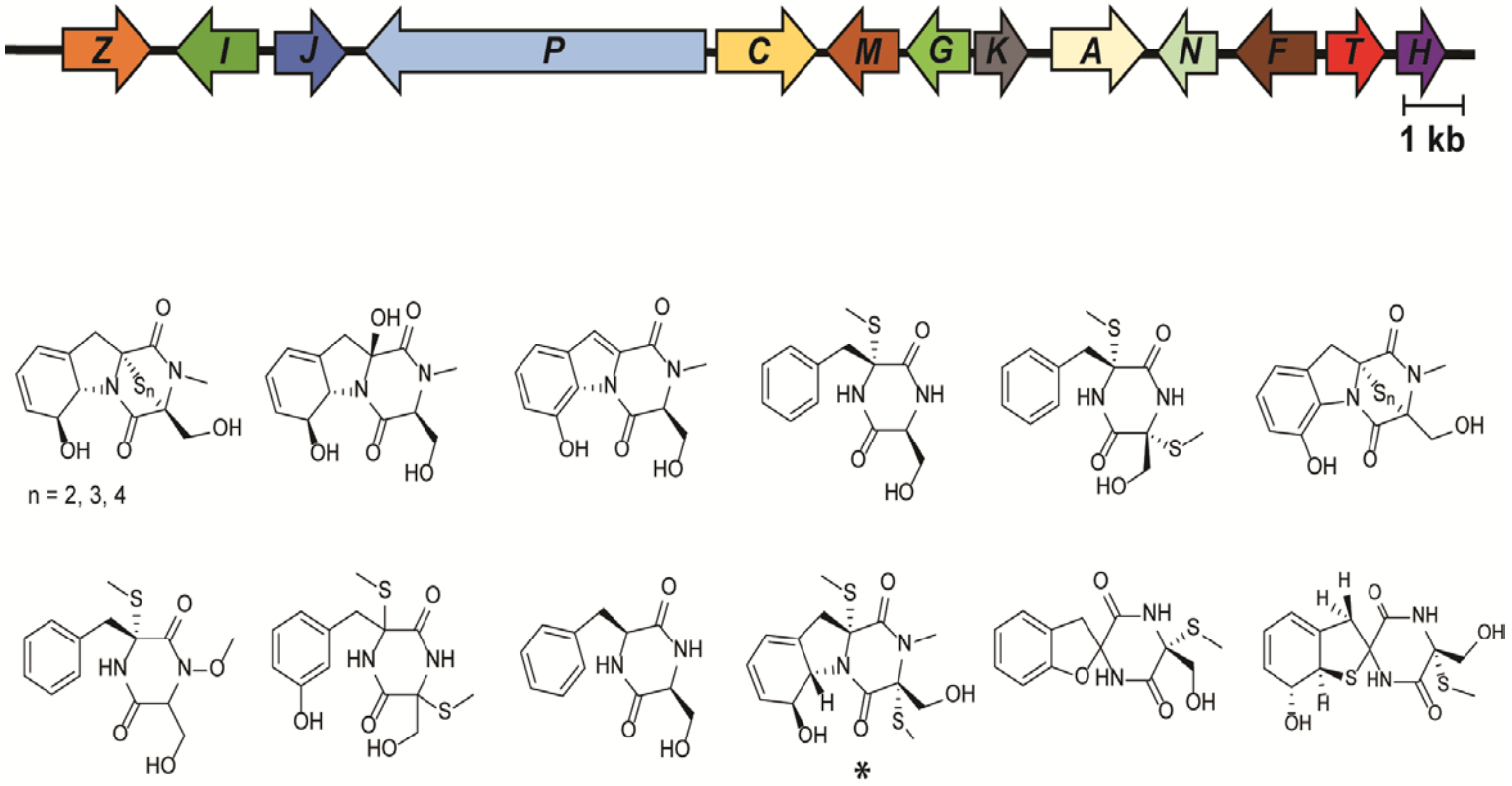

Figure 1.5. In *A. fumigatus*, the *gli* cluster which encodes gliotoxin biosynthesis and consists of 13 genes (in colour and labelled with their last letter) is located on chromosome 6 (Gardiner and Howlett, 2005; Schrettl et al., 2010). Multiple metabolites are produced via the activity of the gliotoxin biosynthetic pathway (shown at the bottom of the figure). These include BmGT (indicated by an asterisk) (Forseth et al., 2011).

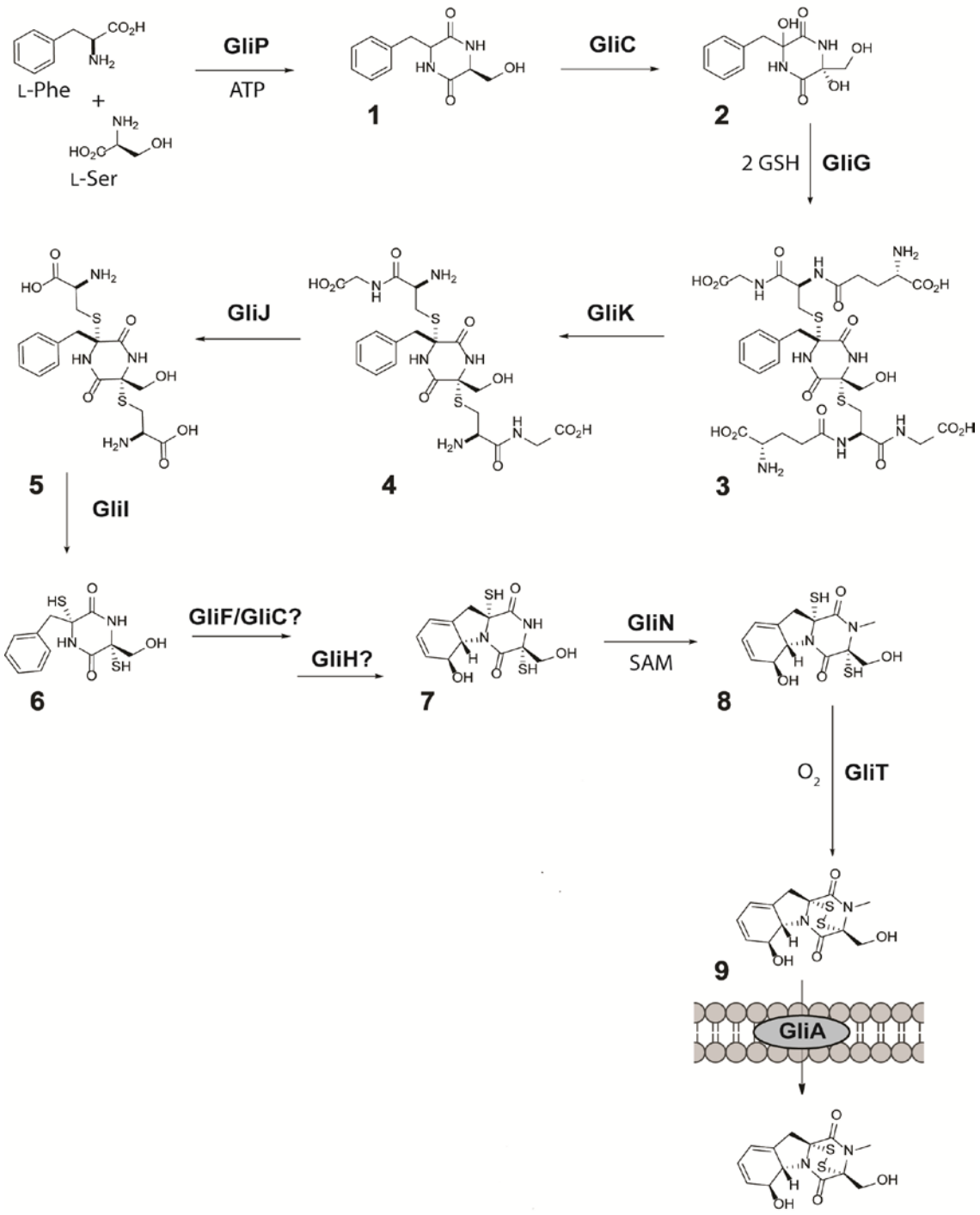

Figure 1.6. Gliotoxin biosynthesis and secretion. The GliP enzyme catalyzes the formation of the diketopiperazine (DKP) cyclo(l-Phe-l- Ser) (1) from phenylalanine and serine. GliC, a cytochrome P450 monooxygenase is responsible for the twofold hydroxylation of the DKP (2). This step a prerequisite for subsequent sulfuration of 2 by the dedicated glutathione S-transferase GliG, resulting in the cis-bis(glutathione) DKP 3. The γ-glutamate cyclotransferase GliK is responsible for processing 3 to an intermediate

Cys-Gly adduct 4 and pyroglutamate. Subsequently, GliJ, a di-peptidase, removes the two glycine fragments to generate the unstable bis(cysteinyl) DKP 5. GliI, a pyridoxal phosphate dependent C-S lyase, led to conversion of 5 into epidithiol 6. GliN was shown to be an N-methyltransferase responsible for the conversion of 7 to 8. GliT was found to be capable of forming the disulfide bridge in gliotoxin (9) from dithiol gliotoxin (8), which is subsequently secreted by GliA. The precise order of some reaction steps and *gliM*/*H* involvement have yet to be fully elucidated (Dolan et al., 2015).

1.4.2 Regulation of Gliotoxin Biosynthesis

Interestingly, apart from *gliZ*, many other transcription factors and regulatory genes influence gliotoxin biosynthesis (Table 1.1). The C_2H_2 transcription factor *gipA* regulates *gliA* interdependently with *gliZ* (Schoberle et al., 2014). Additionally, it is well-established that *laeA*, a global regulator of secondary metabolism, which interacts with the Velvet proteins VeA and VelB in the nucleus (Perrin et al., 2007; Bayram et al., 2008; Bok and Keller, 2004; Bok et al., 2005), augments gliotoxin biosynthesis because either *laeA* or *veA* deletion results in impaired gliotoxin production in *A. fumigatus* (Dhingra et al., 2012; Bok and Keller, 2004). Other transcription factors found to regulate the *gli* cluster include *mtfA* (a C_2H_2 transcription factor (Smith and Calvo, 2014)), *rsmA* (a bZIP transcription factor (Sekonyela et al., 2013)), and *stuA* (an APSES family transcription factor (Gravelat et al., 2008; Twumasi-Boateng et al., 2009)) (Table 1.1). The developmental regulators *flbB* and *flbE* positively influence gliotoxin biosynthesis as deletion mutants exhibit reduced or abolished gliotoxin production (Kim and Shin, 2013; Xiao et al., 2010; Kwon et al., 2010). The MAP kinase, *mpkA*, and the class 2 histone deacetylase, *hdaA*, also positively regulate gliotoxin biosynthesis while the histone methyltransferase, *cclA*, negatively regulates gliotoxin production as increased gliotoxin levels were evident in Δ*cclA*, consequent to increased *gliZ* expression (Palmer et al., 2013) (Table 1.1). As such, it is now apparent that regulation of gliotoxin biosynthesis is a hierarchical, multi-factorial process which is affected by many regulatory elements, and which is highly integrated into *A. fumigatus* metabolism.

Table 1.1. Transcriptional regulators which impact upon *gli* cluster gene expression and gliotoxin biosynthesis

Transcriptional Regulator	**Effect on Gliotoxin Biosynthesis**	**Other Phenotypes**	**Reference**
GliZ (Zn_2Cys_6 binuclear transcription factor)	Essential for gliotoxin biosynthesis. Deletion results in loss of expression of some of the other *gli* cluster genes (e.g. *gliI*).	*gliZ* regulates the production of other secondary metabolites (SM) e.g. OE*gliZ* produced helvolic acid at 37 °C unlike wild-type. Δ*gliZ* virulence in a mouse model is not significantly different to wild-type although slightly decreased. Involved in apoptotic but not necrotic cell death	(Bok et al., 2006)
GipA (C_2H_2 transcription factor)	Regulates gliotoxin biosynthesis genes; deletion of *gipA* results in decreased expression of *gliA*, *gliZ*, *gliP*, and *gliT*, while conversely, overexpression of *gipA* led to increased expression of said genes. Reduced gliotoxin production in Δ*gipA*. The *gli* genes (except *gliM*) contain potential GipA binding sites. GipA cannot induce *gliA* or *gliP* independent of *gliZ*, while *gliZ* induction of *gliA* is GipA dependent.	GipA potentially induces other SM clusters as at least one gene from 18 SM clusters was increased in expression in an OE*gipA* strain.	(Schoberle et al., 2014)
LaeA (transcriptional regulator)	Positively regulates gliotoxin biosynthesis as impaired gliotoxin production in Δ*laeA*.	Global regulator of SM production in *A. fumigatus* as in Δ*laeA* reduced expression of 13/22 SM clusters was observed. Δ*laeA* had reduced virulence in a mouse model of IA. Δ*laeA* conidia had increased susceptibility to macrophage phagocytosis, while hyphae displayed decreased ability to kill neutrophils. Δ*laeA* demonstrated impaired conidia and conidiophore production in liquid shake culture. Δ*laeA* conidia were defective in rodlet production.	(Bok and Keller, 2004; Bok et al., 2005)

VeA (regulatory gene)	Positively regulates gliotoxin biosynthesis as there is reduced gliotoxin production in Δ*veA*. *gliZ* and *gliP* expression is decreased in Δ*veA*.	VeA predominantly positively regulates other SM clusters; fumagillin, fumitremorgin G, fumigaclavine C and glionitrin A production is reduced in Δ*veA*. VeA regulates development; Δ*veA* demonstrates reduced conidiation but increased pigmentation of conidia, reduced protease activity, and increased expression of *brlA* (a developmental activator) during development compared to wild-type. VeA is dispensable for virulence in a neutropenic mouse infection model. VeA is highly conserved; *veA* from *A. nidulans* complements deletion in *A. fumigatus*.	(Dhingra et al., 2012, 2013; Park et al., 2012)
FlbA (regulator of G-protein signalling protein)	Does not affect gliotoxin biosynthesis, however, expression of *gliT* and secretion of GliT is increased in Δ*flbA*. Consequently, Δ*flbA* displays enhanced tolerance to exogenous gliotoxin.	*laeA* expression is reduced in Δ*flbA* suggesting that other SM clusters may be effected by FlbA. FlbA is necessary for normal cell death progression and autolysis in submerged cultures. Deletion of *flbA* results in increased SOD and catalase activity and demonstrated enhanced resistance to menadione and paraquat. FlbA downregulates hyphal differentiation by inactivating GpaA and thus induces asexual development.	(Shin et al., 2013; Mah and Yu, 2006)
MpkA (Map Kinase)	Regulates gliotoxin production which is reduced in Δ*mpkA* compared to wild-type. Expression of *gliN* and *gliT* is decreased in Δ*mpkA*.	MpkA is activated by iron starvation and acts in response by reshuffling the amino acid pool (increased ornithine levels) leading to increased siderophore biosynthesis. Δ*mpkA* exhibits increased sensitivity to menadione and diamide but decreased sensitivity to H_2O_2. Involved in cell wall integrity signalling.	(Valiante et al., 2008; Jain et al., 2011)

MtfA (C_2H_2 transcription factor)	Gliotoxin levels were increased in a OE*mtfA* strain, but were not changed in Δ*mtfA*. Expression of *gliZ* and *gliP* was increased in OE*mtfA*.	Involved in growth and development; reduced growth and conidiation was observed in Δ*mtfA* and OE*mtfA*. Positive regulator of protease production Δ*mtfA* exhibited attenuated virulence in *Galleria mellonella*.	(Smith and Calvo, 2014)
RsmA (restorer of secondary metabolism A – bZIP transcription factor)	The production of twelve *gli* cluster metabolites were increased 2-100 fold in the OE*rsmA* strain compared to wild-type.	Involved in growth and oxidative stress resistance; OE*rsmA* exhibits a growth defect at low growth temperature (25°C). OE*rsmA* mutants show increased resistance to menadione.	(Sekonyela et al., 2013)
CclA (Histone methyltransferase)	Increased gliotoxin production in *ΔcclA* mediated by a substantial increase in *gliZ* transcription.	Increased production of other unidentified secondary metabolites. Severe growth defects and sensitivity to 6-Azauracil (6AU); an inhibitor of guanine nucleotide synthesis and an indicator of transcriptional defects.	(Palmer et al., 2013)
FlbB (Developmental Regulator containing a basic leucine zipper domain (bZIP)	Drastically reduced gliotoxin production (approx. 85 %) in the *ΔflbB* mutant compared to wild-type.	Delayed/Reduced sporulation; precocious cell death; lack of conidiophore development in submerged culture, reduced (approx. 90%) fumagillin production.	(Xiao et al., 2010; Kim et al., 2013)
FlbE (Developmental Regulator Interacts with FlbB)	Gliotoxin production was abolished in the *ΔflbE* deletion strain.	Controls asexual development: Deletion results in reduced conidiation, delayed expression of *brlA* and *vosA*. Necessary for salt-induced development in liquid submerged culture.	(Kwon et al., 2010; Kim et al., 2013)

HdaA (Class 2 histone deacetylase)	Deletion of the *hdaA* gene decreased gliotoxin production and over-expression of *hdaA* increased gliotoxin production.	*ΔhdaA* demonstrated a reduction in both germination rate and vegetative growth; altered colony morphology and increased expression of several NRPS genes.	(Lee et al., 2009)
StuA (APSES family transcription factor)	*gliP* expression, and likely gliotoxin production, is dependent on StuA *in vivo*.	*ΔstuA* had severely impaired conidiation; six secondary metabolite clusters were found to be regulated by StuAp.	(Gravelat et al., 2008; Twumasi-Boateng et al., 2009)

1.4.3 Gliotoxin Toxicity

Gliotoxin and related epipolythiodioxopiperazines (ETPs) directly inactivate multiple enzymes and proteins in animal cells, including nuclear factor-kappaB (NF-kB), NADPH oxidase and glutaredoxin by conjugation to thiol groups (Pahl et al., 1996; Tsunawaki et al., 2004; Srinivasan et al., 2006). It has been conclusively demonstrated that gliotoxin is taken up by animal cells in a GSH-dependent manner whereby this normally protective molecular species facilitates the concentration of gliotoxin within animal cells (Bernardo et al., 2003). Specifically upon uptake, intracellular gliotoxin is reduced to the dithiol form (Figure 1.4), resulting in GSH depletion and concomitant formation of GSSG. Apoptosis ensues and is followed by the oxidation of dithiol gliotoxin to re-form gliotoxin (Bernardo et al., 2003). Gliotoxin then effluxes from the cell in a pseudocatalytic manner and may be taken up by adjacent cells to continue its cytocidal effects. In addition to having an essential role in gliotoxin biosynthesis as a sulfur donor (Davis et al., 2011; Scharf et al., 2011), GSH has also been shown to have an important role in mediating gliotoxin-induced cytotoxicity in animal cells and fungi. It is worth noting that the diminution of intracellular GSH levels using L-buthionine-sulfoxamine (BSO), a specific inhibitor of GSH synthesis, significantly attenuated the cytotoxic effect of gliotoxin towards human neuroblastoma SH-SY5Y cells, possibly due to a deficit in GSH-mediated cleavage of the disulfide bridge of gliotoxin to produce reactive dithiol gliotoxin (Axelsson et al., 2006). This study highlighted the seemingly contradictory effects of antioxidants in enhancing cellular sensitivity to disulfide compounds.

Peroxiredoxins (Prxs) constitute a ubiquitous family of antioxidant enzymes that catalyze the reduction of peroxides. This is achieved with 2 electrons derived from NADPH via an electron-conveying system comprising thioredoxin and thioredoxin reductase. Nanomolar levels of gliotoxin can protect against oxidative damage by converting H_2O_2 to water in HeLa cells, where it functions to accept electrons from

NADPH in the thioredoxin redox system (Choi et al., 2007). Gliotoxin could, in turn, attenuate H_2O_2-induced angiogenesis in a dose-dependent manner, thereby acting as an anti-angiogenic agent. The anti-angiogenic effect of *A. fumigatus* was completely attenuated by deletion of *laeA*, the global regulator of secondary metabolism (Ben-Ami et al., 2009). These studies also revealed that gliotoxin was responsible for approximately 50% of this anti-angiogenic activity since culture extracts from *A. fumigatus* Δ*gliP*, deficient in gliotoxin biosynthesis only, did not abolish angiogenesis. In murine melanoma cells, Prx II silencing enhanced lung metastasis *in vivo*. Gliotoxin, due to its ability to exert a Prx-like activity, inhibited the proliferation and migration as well as lung metastasis of Prx II-deficient melanoma cells. This *in vivo* study implicated the Prx II mimetic ability of gliotoxin as a promising therapeutic drug for preventing melanoma metastasis (Lee et al., 2013a).

Further studies have dissected the molecular basis and investigated applications of ETP-mediated anti-angiogenesis. Tumor cells must adapt to a hypoxic environment in order to survive and grow. This is mediated by hypoxia-inducible factor (HIF-1), whereby the O_2-regulated HIF-1α subunit of the HIF-1 transcription factor is required for the activation of multiple genes involved in tumor progression and angiogenesis (Reece et al., 2014). Under hypoxic conditions, HIF-1α undergoes nuclear translocation where it interacts with HIF-1β and binds to target DNA sequences. Upon recruitment of additional proteins (e.g., p300), gene expression is activated to mount an adaptive response to hypoxia (Palazon et al., 2014). It has been speculated that disruption of this hypoxic response could form an effective anti-cancer strategy. Interestingly, gliotoxin and the ETPs chaetocin and chetomin can inhibit the HIF-1α–p300 interaction by ejecting an essential Zn^{2+} co-factor from p300 via the formation of a $Zn^{2+}(ETP)_2$ moiety (Cook et al., 2009). Moreover, exposure to gliotoxin resulted in anti-proliferative effects on cultured tumor cells, which was reversible by Zn^{2+} supplementation. Furthermore, Zn^{2+} can protect

HepG2 cells against toxicity of the ETP sporidesmin from *Pithomyces chartarum* which causes facial eczema in sheep (Duncan et al., 2005). Indeed, Zn^{2+} supplementation of ruminant diets is an effective prophylactic treatment for this disease (Munday et al., 2001) and it is tempting to speculate that this could be effected via disruption of the HIF-1α–p300 adaptive response. More recently it has been shown that gliotoxin, chaetocin, and chetomin could significantly decrease tumor growth in a prostate cancer xenograft model system (Reece et al., 2014). Although, gliotoxin exposure did not impact on the expression of HIF-1α regulated genes, these authors speculated that the anti-tumor activity of gliotoxin could be mediated via farnesyltransferase inhibition, as inhibition of this enzyme can attenuate angiogenesis by interfering with endothelial cell migration (Peng et al., 2012).

As described in Figure 1.7, gliotoxin induces apoptotic cell death by activating the pore-forming proapoptotic Bcl-2 family member Bak to elicit ROS generation, the mitochondrial release of apoptogenic factors, and caspase-3 activation. As such, not only has this work elucidated the mechanism of gliotoxin-induced apoptosis, but it also has uncovered the molecular mechanisms of Bcl-2 family initiation (Geissler et al., 2013; Häcker, 2013). It is possible that induction of gliotoxin-dependent apoptosis could impact on the severity and course of *Aspergillus* infection by destroying lung epithelium or by killing alveolar macrophages (Pardo et al., 2006). NF-κB is a ubiquitously expressed proinflammatory transcription factor composed of different combinations of members of the Rel family of proteins. As shown in Figure 1.7 gliotoxin has been well-characterised as an inhibitor of NF-κB activation (Pahl et al., 1996) which has then led to a plethora of studies which utilize gliotoxin as a specific NF-κB inhibitor (Fitzpatrick et al., 2002; Herfarth et al., 2000; Ward et al., 1999). Gliotoxin has also been utilized to demonstrate that NF-κB inhibition reverses tumor necrosis factor-α (TNF-α)-induced eosinophil

survival, highlighting the major role of NF-κB in TNF-α induced inhibition of eosinophil apoptosis (Kankaanranta et al., 2014).

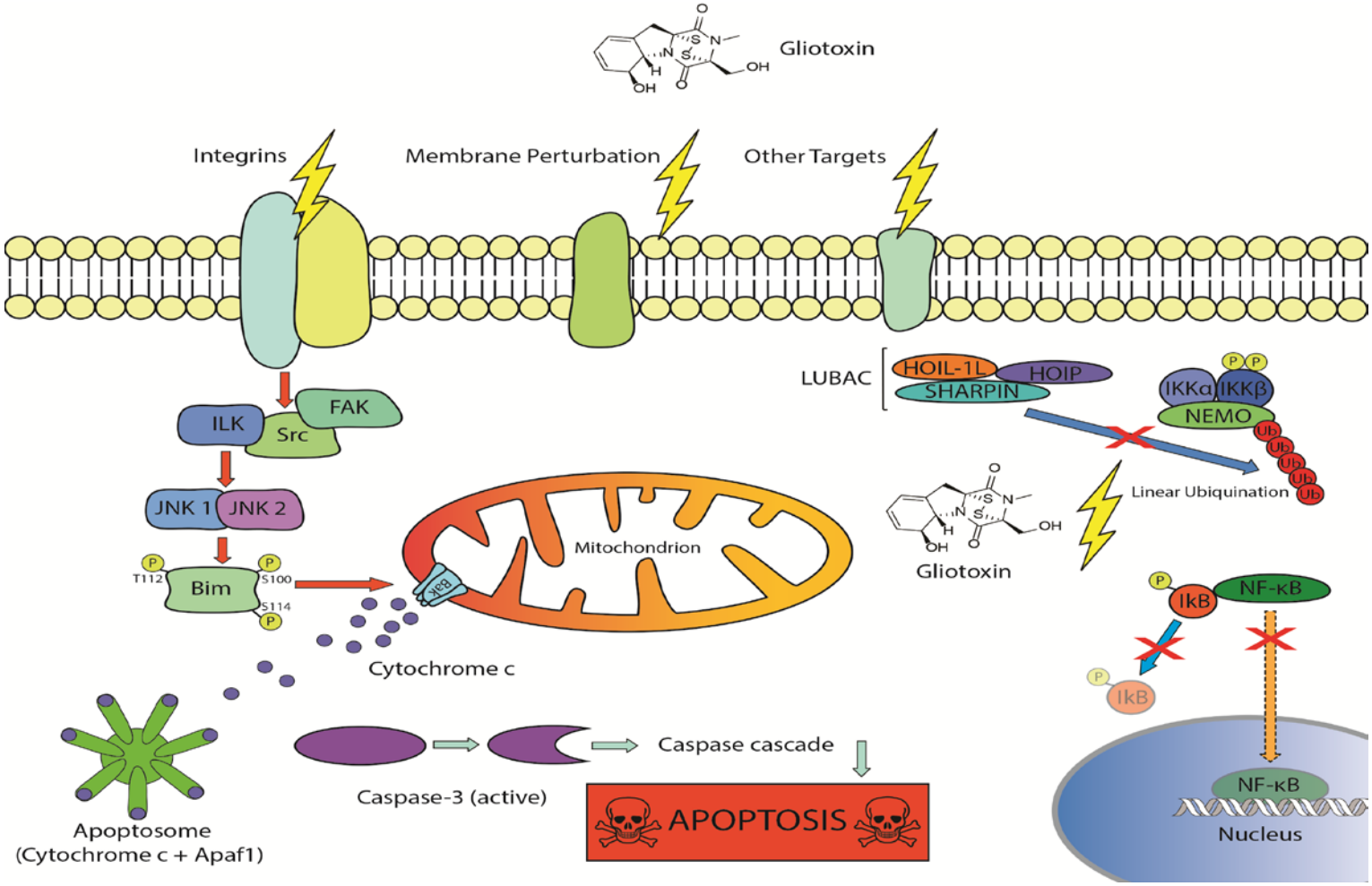

Figure 1.7. Gliotoxin induction of apoptosis in mammalian cells through various specific cellular targets. Upstream of the pore-forming proapoptotic Bcl-2 family member Bak, gliotoxin-mediated apoptosis requires the c-Jun N-terminal kinase 1 and 2 (JNK1/2)-mediated phosphorylation of the BH3-

only protein BimEL at three sites (S100, T112, and S114). This triple phosphorylation increases the stability of BimEL, increases its binding affinity for Bcl-2-like survival factors and activates Bak more effectively. Notably, triple-mutated Bim is unable to transduce the gliotoxin-JNK-initiated apoptotic stimulus to Bak. Compared to wild-type, mice lacking Bak were significantly less susceptible to *A. fumigatus* infection which demonstrates the *in vivo* relevance of this gliotoxin-induced apoptotic pathway (Geissler et al., 2013; Pardo et al., 2006; Häcker, 2013). In resting cells, NF-kB is localized to the cytoplasm because of binding to inhibitory protein IkB. Upon activation, NF-κB inducing kinase (NIK) is activated, which in turn activates a complex of specific IkB kinases (IKKs) resulting in IkB phosphorylation. Phosphorylation of IkB leads to a rapid ubiquitination which makes it a substrate for the proteasome. The active NF-κB complex then translocates to the nucleus and initiates the expression of target genes. Gliotoxin inhibits NF-κB activation by preventing IκB degradation (Pahl et al., 1996). Gliotoxin also suppresses NF-κB activation by inhibiting the linear ubiquitin (Ub) chain assembly complex (LUBAC). This is the first selective small-molecule inhibitor of this complex to be identified (Sakamoto et al., 2014). Abbreviations: ILK, Integrin-linked kinase; Src, Sarcoma family nonreceptor protein tyrosine kinase; FLK, Focal adhesion kinase; Apaf1, Apoptotic protease activating factor 1; NEMO, NF-κB essential modulator; HOIL-1L, Haem-oxidized IRP2 ubiquitin ligase-1; HOIP, HOIL-1L Interacting Protein; SHARPIN, SHANK-associated RH domain interacting protein (Dolan et al., 2015).

1.5 Epipolythiodioxopiperazine (ETP) type toxins

Nearly twenty distinct families of ETP fungal metabolites have been reported since the seminal discovery of gliotoxin in 1936 (Welch and Williams, 2014). This unique class of natural products is characterized by a sulfur-bridged dioxopiperazine, a feature generally requisite for the potent biological activity prevalent among the class (Patron et al., 2007). All natural epidithiodioxopiperazines which have been discovered are derived from at least one aromatic amino acid. Representative ETPs are shown in Figure 1.8. Besides gliotoxin, the gene clusters responsible for the biosynthesis of the ETPs sirodesmin and acetylaranotin have been identified in the organisms *L. maculans* and *A. terreus*, respectively (Gardiner et al., 2004; Guo et al., 2013). ETP clusters have been inherited relatively intact and are believed to have a single origin (Patron *et al.*, 2007). As shown in Figure 1.9, the distribution of ETP clusters in ascomycetes is discontinuous. Also, the relationship of cluster subclades does not always reflect the relationship of organisms. In the case of some closely related species, one taxon had a cluster whilst the other taxon did not. Although several *Aspergilli* species have ETP-like clusters, *A. nidulans* does not (Patron et al., 2007).

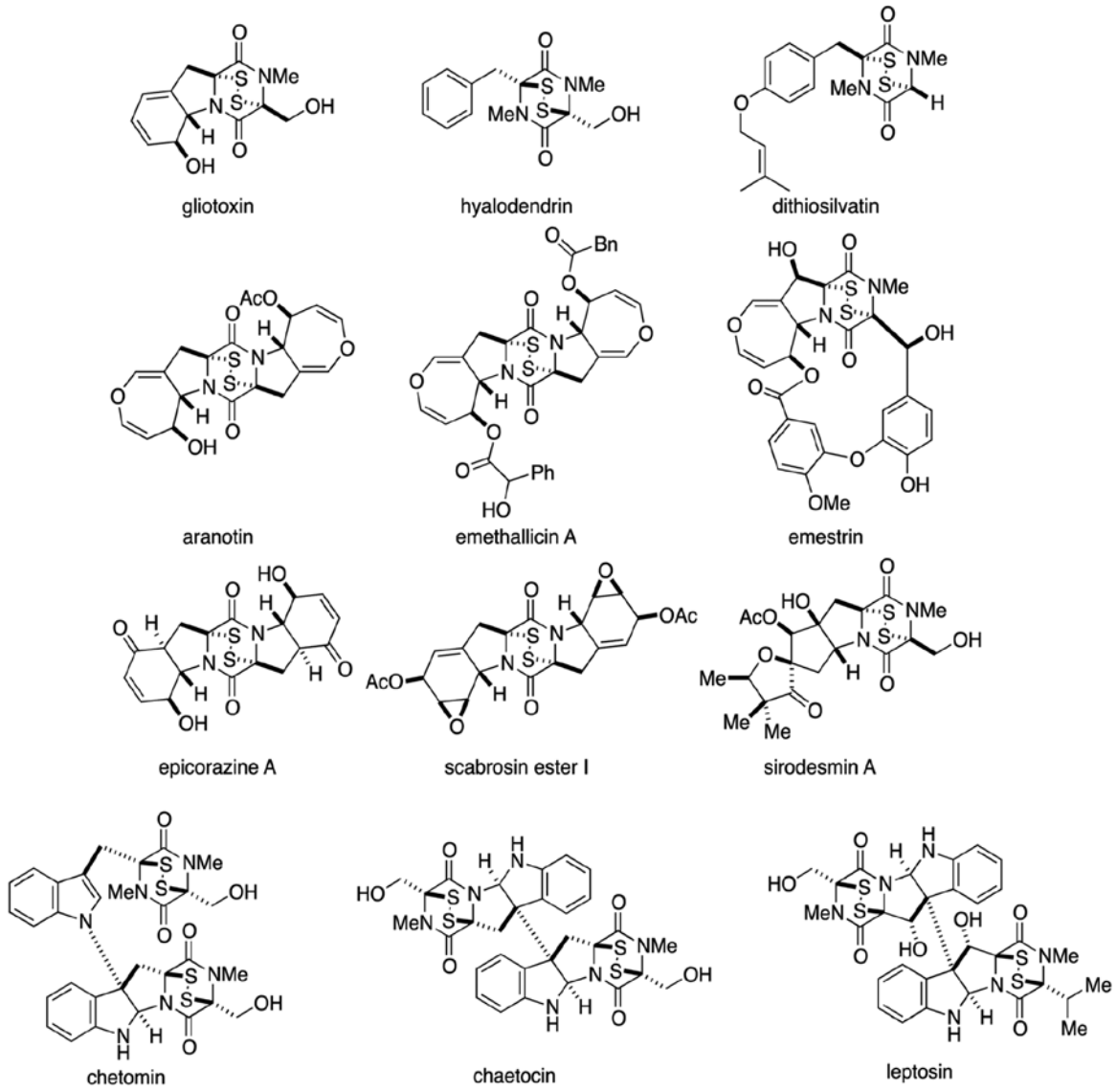

Figure 1.8. Representative epidithiodioxopiperazines derived from tyrosine, tryptophan and/or phenylalanine (Welch and Williams, 2014).

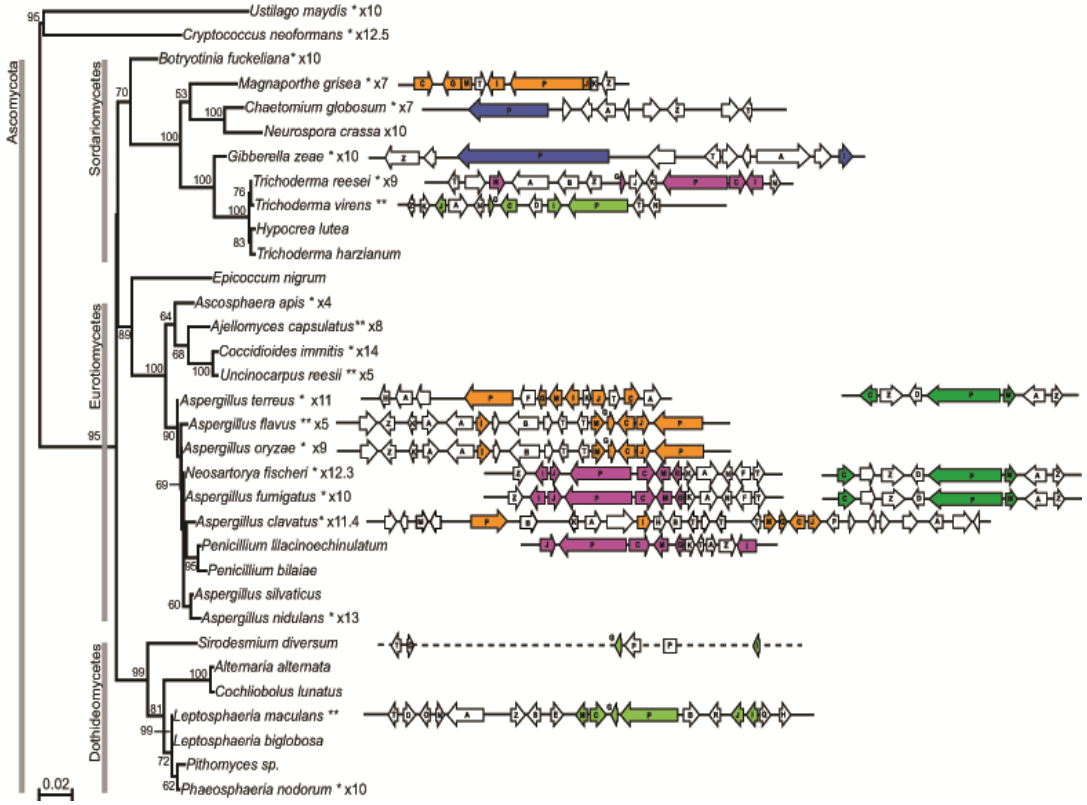

Figure 1.9. Phylogenetic relationships between ascomycetes derived from 18S ribosomal DNA sequences showing the presence and subclade type of ETP-like gene clusters. Cluster genes are coloured according to position within the phylogeny. xN indicates present coverage of the genome sequence. Consistent cluster relationships across the six proteins are indicated by orange (subclade I), pink (subclade II) and light and dark green (subclades IIIA and IIIB, respectively). Proteins encoded in clusters outside of the main cluster clade are on blue branches (Patron et al., 2007).

1.5.1 Bis(methyl)gliotoxin and Thiomethylated ETPs

Several mono- and bismethylthio derivatives of gliotoxin have also been discovered in various fungi. Bis(methyl)gliotoxin is the most well characterised of these gliotoxin derivatives (Forseth et al., 2011). First identified in *Gliocladium deliquescens,* bis(methyl)gliotoxin appears to be formed by the irreversible disulfide bridge reduction and *S*-methylation of exogenous gliotoxin; this is demonstrated by feeding [^{14}C]-gliotoxin to *G. deliquescens* (Kirby et al., 1980). The enzyme which catalyses this biotransformation and the purpose of the functionality have remained elusive. Bis(methyl)gliotoxin has also been detected in *A. fumigatus* (Amitani et al., 1995), *Colletotrichum gloeosporioides* (Guimarães et al., 2010), *Penicillium* sp. BCC16054 (Intaraudom et al., 2013), FO2047 (Van der Pyl et al., 1992), JMF034 (Sun et al., 2011), *Pseudallescheria* sp. MFB165 (Li et al., 2006) and several other fungi.

Methylthio-derivatives of ETP-type fungal toxins (i.e., hyalodendrin (Boente and Kirby, 1991), sporidesmin (Taylor, 1963), rostratin (Tan et al., 2004), haematocin (Suzuki et al., 2000), leporizine (Reategui et al., 2013), epicoccin (Guo et al., 2009), glionitrin (Park et al., 2011), etc.) have been identified in the majority of ETP-producing fungi (Figure 1.10). *S*-methylation of dithiol metabolites also extends to bacteria as *Streptomyces clavuligerus* has been shown to produce a bisthiomethylated derivative of the dithiolpyrrolone antibiotic, holomycin (Li et al., 2012).

Although initially regarded as inactive versions of toxic ETPs, there has been a renewed interest in the biological properties of ETP bisthiomethyl derivatives. Five of seven bisthiomethyl ETP derivatives tested for the ability to eliminate trypanosomes (trypanocidal potential) displayed positive responses and bis(methyl)gliotoxin showed moderate trypanocidal activity (IC_{50} = 40.2 ±5.2 μM), while appearing to be non-toxic towards T-cell leukemia cells (Watts et al., 2010). Bis(methyl)gliotoxin has also been

shown to display anti-angiogenic activity (Lee et al., 2001), antibacterial activity against both methicillin-resistant and multidrug-resistant *Staphylococcus aureus* (Li et al., 2006). It has also demonstrated the ability to specifically inhibit platelet activating factor (PAF) induced platelet aggregation (Okamoto et al., 1986). Compellingly, glionitrin B (the non-toxic *bis*-thiomethyl derivative of the ETP, glionitrin A) caused the suppression of DU145 (human prostate cancer cell line) invasion whereas the disulfide-containing glionitrin A and gliotoxin exhibited significant cytotoxicity therefore eliminating their use in a clinical setting. This highlights the potential of these derivatives as antimetastatic agents (Park et al., 2011).

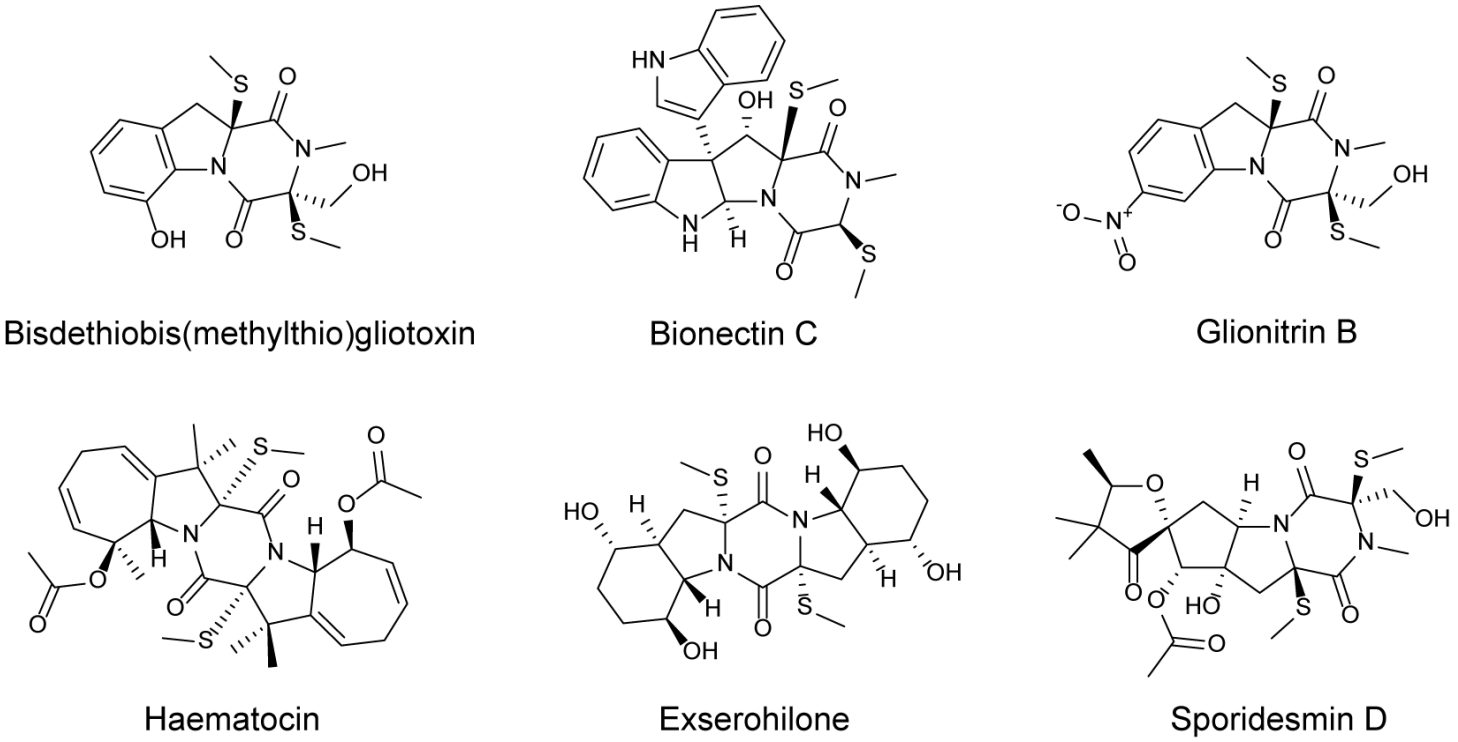

Figure 1.10 Selected *bis*-thiomethyl metabolites (ETPs) biosynthesized by fungi. No data are available on the enzyme(s) required for, or mechanism of, *bis*-thiomethylated ETP formation.

1.6 Self-protection against ETPs

Resistance genes are required to allow a toxin producer to grow in the presence of its own metabolic weaponry and ETPs are no exception to this rule (Carberry et al., 2012). Indeed one of the genes in the gliotoxin biosynthetic gene cluster in *A. fumigatus*, *gliT*, is required for self-protection against the toxin. Deletion of this gene renders *A. fumigatus* sensitive to exogenous gliotoxin. In addition, heterologous expression of *gliT* in *Saccharomyces cerevisiae* and *A. nidulans* facilitated resistance to gliotoxin (Schrettl et al., 2010). This sensitivity is thought to occur through the accumulation of dithiol gliotoxin, the immediate biosynthetic precursor to gliotoxin in the fungal cytosol (Scharf et al., 2010). In bacteria, thiomethylation has been posited as an additional or backup strategy, to disulfide bridge closure, for self-protection during holomycin biosynthesis, and it has been proposed that *S*-methylation of biosynthetic intermediates, or possibly shunt metabolites, protects cellular components against these reactive species (Guo et al., 2013; Li et al., 2012).

O'Keeffe *et al*. (2014) have demonstrated that an intact gliotoxin self-protection mechanism (Schrettl *et al*., 2010; Scharf *et al*., 2010), which is mediated by GliT, is essential to regulate the biosynthesis of apparently unrelated metabolites such as pseurotin A, fumagillin and fumitremorgins. Specifically, using RNA-seq these authors have demonstrated that gene cluster expression encoding the biosynthesis of helvolic acid, pseurotin A, fumagillin and fumitremorgins is significantly attenuated in *A. fumigatus* Δ*gliT* upon gliotoxin exposure. Unexpectedly, alterations in the expression of genes involved in siderophore-mediated iron transport and siderophore biosynthesis was also observed, which was suggestive of a deficiency in iron-sensing. This leads to the question of how exactly the modification of a single fungal secondary metabolite pathway leads to downstream effects on apparently unrelated secondary metabolite clusters.

1.7 Interactions between Primary and Secondary Metabolism

Non-ribosomal peptide synthesis (NRPS) in fungi is mediated by a combination of large multi-functional enzymes known as non-ribosomal peptide (NRP) synthetases: these include adenylation, thiolation, condensation and, sometimes, tailoring domains. NRP synthetases require post-translational modification via 4'-phosphopantetheinylation, mediated by 4'-phosphopanteheinyl transferase (4'-PPTase), to yield the active holo-NRP synthetase. This modification, which requires Coenzyme A (CoA) as the 4'-phosphopantetheine source, requires that each Thiolation domain within an NRP synthetase is modified at a specific serine residue (Stack et al., 2007). In addition, so-called decorating enzymes or domains are responsible for the modification of non-ribosomal peptide biosynthetic intermediates, which may be either tethered to, or released from, the NRP synthetase during the modification process. Likewise, polyketides are biosynthesized from acyl CoA precursors (e.g., malonyl CoA) by multi-modular enzymes consisting of essential ketosynthase, acyl carrier protein and acyltransferase, amongst other, domains (Weissman, 2015). As shown for *Streptomyces* spp. intracellular ATP levels may also affect non-ribosomal peptide production in fungi (Li et al., 2008). Unlike polyketide synthases (PKS), NRPS require ATP for their catalysed reactions.

Both proteogenic and non-proteogenic amino acids (e.g., ornithine) may be essential precursor substrates for non-ribosomal peptide formation and during NRPS they are generally conjugated together via peptide bond formation. Moreover, substrate amino acids can be modified either prior to, or during, NRPS (Chocklett and Sobrado, 2010; Thykaer and Nielsen, 2003). Furthermore, many other cellular components which are more commonly associated with primary metabolism are required for NRPS and PKS. These include, amongst others, *S*-adenosylmethionine (SAM), isoprenyl and mevalonyl moieties, NADPH, glutathione (GSH), malonyl CoA and acetyl CoA (Davis et al., 2011; Scharf et al., 2011; Haas, 2012; Yasmin et al., 2012). This suggests a significant interplay

between what is currently considered to be primary and secondary metabolism. As a result of this, essential re-consideration must be given to the integration of these two historically-defined discrete systems.

In fungi, the biosynthesis of a specific non-ribosomal peptide is generally encoded by genes located within a gene cluster (Figure 1.5). These are often located in the sub-telomeric regions of chromosomes (McDonagh et al., 2008). The activity of these secondary metabolite (SM) gene clusters is controlled by local chromatin structure – this is effected via histone post-translational modification (e.g., methylation or acetylation). The influence of histone modifying enzymes on SM production was first reported for sterigmatocystin (ST) production and gene regulation in *A. nidulans*. The authors uncovered that the histone deacetylase mutant Δ*hdaA* bypassed the requirement for the general SM activator LaeA, resulting in overproduction of the subtelomeric metabolites ST and penicillin (Shwab et al., 2007). In the endophytic filamentous fungus *Epichloë festucae*, the gene clusters responsible for the production of bioprotective lolitrems and ergot alkaloids were shown to be derepressed following deletion of the genes encoding either the H3K9- (ClrD) or H3K27- (EzhB) histone methyltransferases. A further enhancement of cluster expression was evident when both of these methyltransferases were deleted (Chujo and Scott, 2014). Indeed, the production of many SM in *Aspergillus spp*. is controlled by a methyltransferase, *laeA*, and orthologs of this gene are found in numerous fungi (Bok and Keller, 2004). It is interesting to note that LaeA has been shown to counteract the establishment of heterochromatic marks thus activating SM production. Deletion of *laeA* in *A. nidulans* resulted in highly elevated H3K9 methylation levels suggesting that LaeA counteracts H3K9 trimethylation and, therefore heterochromatin formation at the ST locus (Reyes-Dominguez et al., 2010). The Velvet complex, which is comprised of the light-dependent regulators VeA and VelB, also regulates SM production and serves to coordinate SM production and fungal development. It is now clear that the

VelB–VeA–LaeA complex coordinates fungal sexual development and secondary metabolism (Bayram et al., 2008).

As such, it appears that a truly phenomenal degree of cross-talk exists between so-called primary and secondary metabolism, with the involvement of genetic regulation, which facilitates non-ribosomal peptide and polyketide and, indeed, other SM, production. Primary metabolism is required to provide the essential biosynthetic precursors for NRPS, many non-ribosomal peptides share substrate amino acids and additional co-substrates. Evidence is also emerging that NRPS pathways interact such that alterations in the biosynthesis of specific non-ribosomal peptides may impact on the production of apparently unrelated metabolites (O'Keeffe et al., 2014; Wiemann et al., 2014).

1.7.1 Primary metabolite involvement in SM biosynthesis

It is essential to consider the sources of primary metabolites used during fungal NRPS and PKS in order to begin to see why there may be interactions between apparently independent biosynthetic pathways.

SAM is the major source of methyl groups for cellular reactions involving methylation, and is directly synthesized via the action of SAM synthetase (Sauter *et al*., 2013). In fungi, the methionine cycle enables SAM biosynthesis; L-homocysteine is converted to L-methionine via methionine synthase and, in turn, SAM is formed via SAM synthetase which requires ATP (Sieńko *et al*., 2009). Cellular methylation reactions (e.g., NRPS and PKS) then consume SAM to produce *S*-adenosylhomocysteine (SAH). This is then converted to L-homocysteine, thereby completing the methionine cycle (Liao *et al*., 2012). In *A. nidulans*, a SAM synthetase, SasA, has been demonstrated to affect SAM availability which is important for the production of sterigmatocystin, and may also play a role in coordinating fungal secondary metabolism and development (Gerke *et al*., 2012). SAM availability is essential for the biosynthesis of a range of polyketides and non-

ribosomal peptides including gliotoxin, where it acts as a methyl source for the *N*-methyltransferase GliN (Scharf *et al*., 2014). SAM is also the provider of methyl groups for the biosynthesis of many other non-ribosomal peptides and polyketides such as butyrolactone III (Guo *et al*., 2013a). Forseth *et al*. (2011) identified a plethora of methylated biosynthetic intermediates/shunt metabolites associated with gliotoxin biosynthesis which allowed the authors to speculate about the complex reactions required within this metabolic pathway.

The biosynthesis of gliotoxin, acetylaranotin and related ETP compounds requires biosynthetic intermediate sulfurization and it has been established that GSH is this sulfur source (Davis *et al*., 2011; Scharf *et al*., 2011; Guo *et al*., 2013b). Furthermore, Atanasova *et al*. (2013) have noted an elevated expression of genes predicted to be involved in GSH formation, possibly as a precursor to enable the biosynthesis of gliotoxin in *Trichoderma virens*. In any case, during gliotoxin biosynthesis a gene cluster-encoded glutathione *S*-transferase (GST) mediates GSH conjugation to a highly reactive acyl imine intermediate which results in a *bis*-glutathionylated product. This is subsequently processed by a suite of enzymes, initially by a γ-glutamyl cyclotransferase (GliK in the case of gliotoxin biosynthesis) to the final product (Davis *et al*., 2011; Gallagher *et al*., 2012; Scharf *et al*., 2011, 2013).

1.7.2 Enzyme and cluster cross-talk in Fungal Secondary Metabolism

In addition to the clear interactions between primary and secondary metabolism described above, there are also several examples of cross-talk amongst gene clusters which are responsible for the synthesis of fungal SMs. Over-expression of the silent *inp* putative secondary metabolism cross-pathway regulator gene (*scpR*) in *A. nidulans* resulted in the overproduction of both the *inp* gene cluster (encoding the interacting NRPSs *inpA* and *inpB*) and also production of the polyketide, asperfuranone. As no link had previously been described between these unrelated metabolites, this work highlighted some

additional complexity in the regulatory cross-talk within fungal secondary metabolism (Bergmann et al., 2010). Furthermore, recent findings are changing previously held views of distinct SM clusters encoding for single classes, or closely related groups of secondary metabolites. A FAD-dependent monooxygenase (FqzB) which is encoded by the fumiquinazoline biosynthetic pathway in *A. fumigatus* was also shown to catalyse spiro-carbon formation in the indole alkaloid spirotryprostatin A via an epoxidation route. The authors speculated that the interactions between unrelated fungal SM-encoding cluster genes may be a strategy employed by natural product producers to generate structural diversity (Tsunematsu et al., 2013).

The *A. fumigatus* genes *psoF* (putative dual function methyltransferase and monooxygenase) or *psoG* (hypothetical protein) were predicted to be required for fumagillin biosynthesis due to their proximity to the characterised fumagillin encoding genes *fmaA* and *fmaB*. Surprisingly, deletion of *psoF* and *psoG* resulted in the abolition of pseurotin A biosynthesis. The Δ*psoF* strain accumulated a demethyl-deepoxy-synerazol (*m/z* 384.1447) compound instead of pseurotin A which agrees with the putative role of this enzyme (Wiemann et al., 2013). PsoF was recently characterised by Tsunematsu *et al.* (2014). One of the most dramatic examples of cross-talk between fungal metabolites at the genetic level has been elucidated by Wiemann *et al*. (2013) in *A. fumigatus*. Here, the gene clusters encoding fumagillin and the non-ribosomal peptide/polyketide hybrid, pseurotin A, are physically intertwined and co-regulated by LaeA via the $Zn(II)_2Cys_6$ Transcription Factor, FapR. In addition, fumitremorgin is also encoded by this supercluster. However, the genes encoding the biosynthesis of fumitremorgin are distinct from the intertwined region. It is worth noting that although this supercluster is not present in completely intact form in related fungal species, there is a sufficient co-localization of orthologs to allow Wiemann *et al*. to speculate that co-production of the aforementioned metabolites confers survival advantages on producing

species. It is tempting to speculate that the products of this supercluster act synergistically or in a complementary manner, almost like subunits of a heteromeric enzyme, to effect survival of *A. fumigatus*, and related species in defined ecological niches.

The efflux of secondary metabolites is another aspect of secondary metabolism where evidence exists of the occurrence of cross-metabolite interactions. The rice pathogen *Magnaporthe grisea* produces the PKS-NRPS fusion natural product ACE1 from a 15-gene cluster. Although this cluster encodes a transporter for the MFS superfamily (MFS1), it has been shown that *MFS1* is not involved in the efflux of ACE1 as this gene has a deletion of a single base pair which results in an early stop codon. Therefore, it has been suggested that ACE1 must rely on another transporter which is encoded outside of the ACE1 gene cluster (Coleman and Mylonakis, 2009). Moreover, deletion of the sirodesmin ABC transporter gene *sirA* from *Leptosphaeria maculans* actually resulted in an increase (39%) of sirodesmin production and secretion when compared to the wild-type strain. The production of deacetyl sirodesmin in the Δ*sirA* mutant also increased 27% when compared to the wild-type. This seemingly contradictory result may be explained by the presence of alternate efflux mechanisms for these metabolites or by a degree of redundancy across SM transporters. These alternate efflux mechanisms may be more effective than SirA, resulting in differential sirodesmin cluster feedback regulation which leads to the overexpression of this NRPS cluster (Gardiner et al., 2005). In contrast, deletion of *gliA* from the gliotoxin gene cluster significantly decreased gliotoxin efflux, indicating that some ETP-producing fungi may not have compensatory mechanisms to mediate natural product efflux (Wang et al., 2014; Owens et al., 2015). Evidence also exists to suggest that the MFS transporter DotC encoded within the dothistromin gene cluster of *Dothistroma septosporum* is not the only mechanism of toxin efflux in this organism (Bradshaw et al., 2009).

Recent data have also described what may be cross-talk of natural products from different organisms. Culturing *A. fumigatus* MBC-F1-10 in the presence of *Streptomyces bullii* leads to the production of a diversity of *A. fumigatus* metabolites; these include ergosterol and the seven diketopiperazine (DKP) class of alkaloids. Production of the antibiotic-antitumor metabolite glionitrin was induced in *A. fumigatus* following co-culture with a *Sphingomonas* isolate KMK-001 derived from mine-drainage system (Rateb et al., 2013). Moreover, physical interaction between the *Streptomyces rapamycinicus* and *A. fumigatus* resulted in the activation of a silent PKS gene cluster encoding fumicycline A (König *et al*., 2013). Bacterial metabolites have also been demonstrated to act as precursors of fungal metabolites, whereby phenazine metabolites from *Pseudomonas aeruginosa* were converted by *A. fumigatus* into new molecular species with enhanced toxicity and additional properties (Moree *et al*., 2012). It is likely that further examples of inter-kingdom interactions, which describe cross-talk leading to metabolite production, will be described as the focus on the impacts of co-culturing of microorganisms receives increasing attention.

In summary, it is clear that significant cross-talk exists between (i) primary and secondary metabolism, (ii) different fungal metabolites, (iii) the enzymes involved in synthesizing different metabolites and (iv) various metabolite-encoding gene clusters. Indeed cross-talk even exists between kingdoms.

1.8 Natural Product Methyltransferases (NPMTs)

Methylation is a ubiquitous biotransformation in nature which is used throughout all branches of metabolism and is often key to metabolic homeostasis. These transformations modulate diverse biological processes such as cell signaling and the biosynthesis of complex and specialized metabolites (Liscombe et al., 2012). These reactions are most often catalysed by methyltransferases that rely on the co-substrate S-adenosyl-L-methionine (SAM). S-Adenosyl-methionine (SAM)-dependent methyltransferases

(MTases) catalyse the transfer of methyl groups from SAM to a large variety of acceptor substrates ranging from small metabolites to bio-macromolecules and generate S-adenosyl-homocysteine (SAH) as the by-product (Figure 1.11).

Natural product methyltransferases (NPMTs) participate in the biosynthesis and modification of bioactive molecules derived from several branches of primary and secondary metabolism; these include membrane components, cofactors, prosthetic groups, pigments and signaling and defense compounds. Surprisingly, all currently known NPMT structures belong to either of two (Class I and Class III) currently recognized protein fold superfamilies of SAM-binding proteins. However, the vast majority belong to the Class I or Rossmann-like fold family (Liscombe et al., 2012).

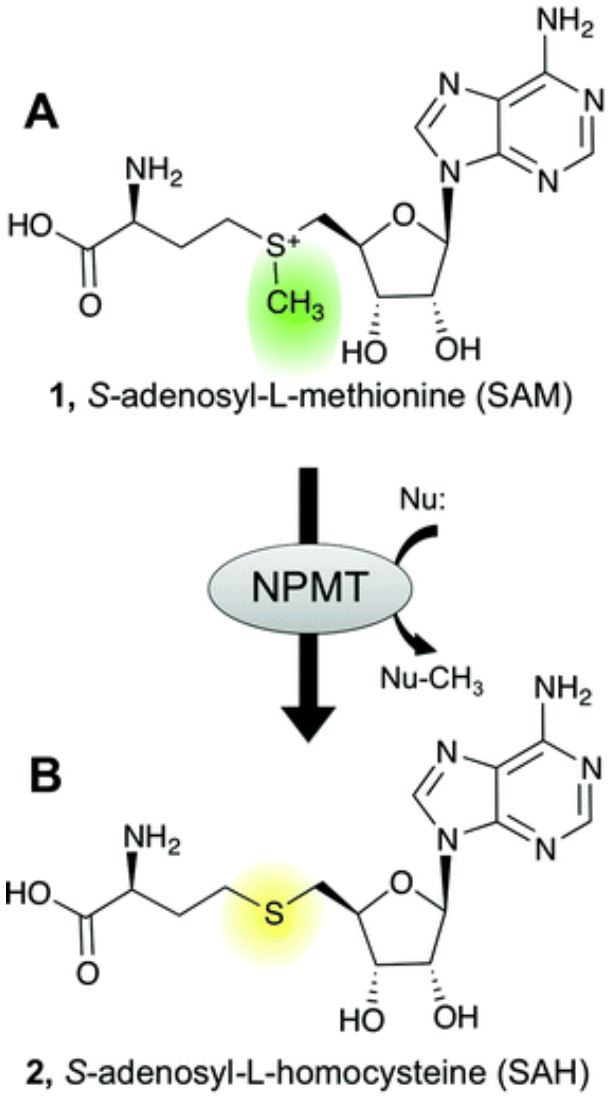

Figure 1.11. NPMTs use S-Adenosyl-L-methionine (SAM) co-substrate as a reactive electron deficient methyl group (green) donor for transfer to a electron-rich methyl acceptor (Nu:). In addition to the methylated product, S-adenosyl-L-homocysteine (SAH) forms and is a potent inhibitor of SAM-dependent MTs (Liscombe et al., 2012).

1.8.1 MTase Classification and Motifs.

All MTases (EC 2.1.1.-) are classified according to the substrate atom that accepts the methyl group - usually O (54% of EC subclass), N (23%), or C (18%). The S-directed MTs (3% of EC subclass) and NPMTs which accommodate other acceptors such as halides (2%) are rare but notable (Liscombe et al., 2012). The enzymatic methylation of arsenic compounds is well established in certain bacteria, fungi and animals. The structure of CmArsM, an As(III) S-adenosylmethionine methyltransferase from the thermophilic eukaryotic alga *Cyanidioschyzon merolae* has provided insight into this transformation (Ajees et al., 2012). Some NPMTs have multiple acceptor atoms: AtHTMT, a promiscuous halide methyltransferase from *Arabidopsis thaliana* was shown to have a preference for thiocyanate despite being responsible for halomethane production (Schmidberger et al., 2010).

Few S-directed NPMTs have been identified and characterized to date. Human thiopurine S-MTs (TPMT) participate in the detoxification of xenobiotics. A NPMT isolated from *Brassica oleracea* L (cTMT1) was shown to methylate thiocyanate. As thiocyanate is an extremely reactive product of glucosinolate degradation, cTMT1 is most likely responsible for enzymatic detoxification within this pathway (Attieh et al., 2000). PpSABATH1, a TMT from the moss *Physcomitrella patens* showed a high level of activity towards thiobenzoic acid. Interestingly, the expression of *PpSABATH1* was induced by the treatment of *P. patens* with thiobenzoic acid. Additionally, the constitutive expression of *PpSABATH1* in tobacco plants resulted in an enhanced tolerance to thiobenzoic acid. These results suggest that PpSABATH1 may have a role in the detoxification of xenobiotic thiols (Zhao et al., 2012). The Madagascar periwinkle (*Catharanthus roseus*) *O*-methyltransferase CrSMT1, the true biological function of which remains unknown, has been shown to methylate a wide range of aliphatic and aryl alcohols and thiols (Coiner et al., 2006). Remarkably, *S*-methyltransferases have only

been definitively classified in relation to detoxification mechanisms and primary metabolism, although the activity have long been implicated in numerous secondary metabolite pathways (Boente and Kirby, 1991; Kirby et al., 1980; Taylor, 1963). The *Streptomyces lasaliensis* SAM dependent methyltransferase Ecm18 was shown to catalyze the conversion of a disulfide bond in the precursor antibiotic triostatin A to the thioacetal bridge of the nonribosomal dipsipeptide echinomycin (Hotta et al., 2014). This appears to be the only published example of a thiol-directed methyltransferase involved in secondary metabolism.

The NPMTs vary in length, typically spanning 200–500 amino acid residues corresponding to monomeric molecular masses of ca. 25–55 kDa. Almost all of the NPMTs which have been isolated to date possess an α/β structure: alternating α-helices and β-strands along the length of the polypeptide chain. A series of conserved motifs h which are shared among SAM-dependent MTs have been identified. Motifs I–VI reside in regions associated with SAM co-substrate binding and they are generally arranged in sequential order across the core MT domain. These motifs, which are shown in Figure 1.12 and 1.13, are widely conserved across NPMTs and are considered to be defining features of SAM-dependent MTs (Liscombe et al., 2012).

Motif I is present in the majority of MTs. This motif spans the loop preceding the first β-strand (β1) of the core Rossmann fold leading into the following α-helix (αA). It includes a nine-residue amino acid block with the consensus sequence (V/I/L)(L/V)(D/E)(V/I)- G(G/C)G(T/P)G. This nine-residue structure incorporates the glycine-rich ‘‘GxGxG’’ signature sequence, the hallmark of a nucleotide binding site (Loenen, 2006). Although none of the three glycines of the GxGxG motif are universally conserved, substitutions typically encompass small sidechains. Motif II spans β2 and the adjoining turn. Only two residues, DA, are common to both consensus sequences with the aspartate residue reflecting the conservation of an acidic residue near the C-terminus

of β2. Motif III spans β3 and is followed by Motif IV spanning β4 and the adjoining loops. Both motifs include a partially-conserved acidic residue at the C-terminus. Motif V, occurring in the helix (αC) following Motif IV, sometimes harbours hydrophobic residues which sandwich the adenine moiety of SAM. A well-conserved glycine residue is characteristic of Motif VI, which corresponds to β5 and the loop between αC and β5 (Liscombe et al., 2012).

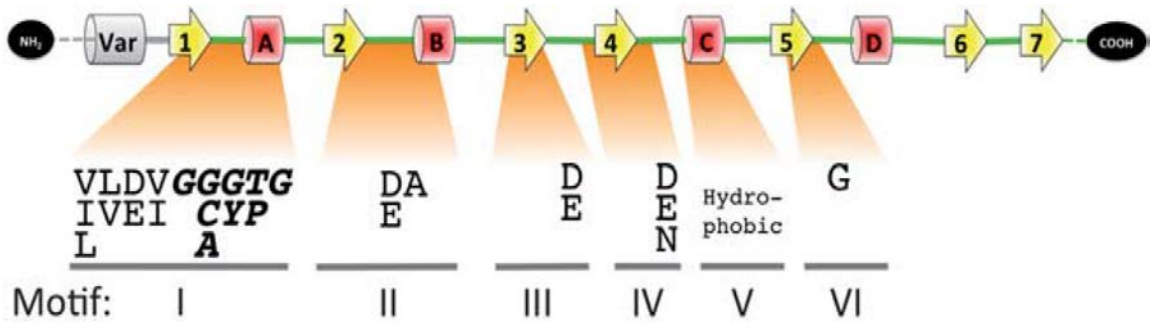

Figure 1.12. A schematic diagram of the primary and secondary structure of a typical NPMT, emphasizing conserved motifs used to identify a putative MT. N- and C- termini are shown in black circles. α-Helices are shown in red, β-strands in yellow and adjoining loops are green. Conserved residues are stacked for each motif (I–VI), and the highly-conserved ‘‘GxGxG’’ motif is in bold fonts (Liscombe et al., 2012).

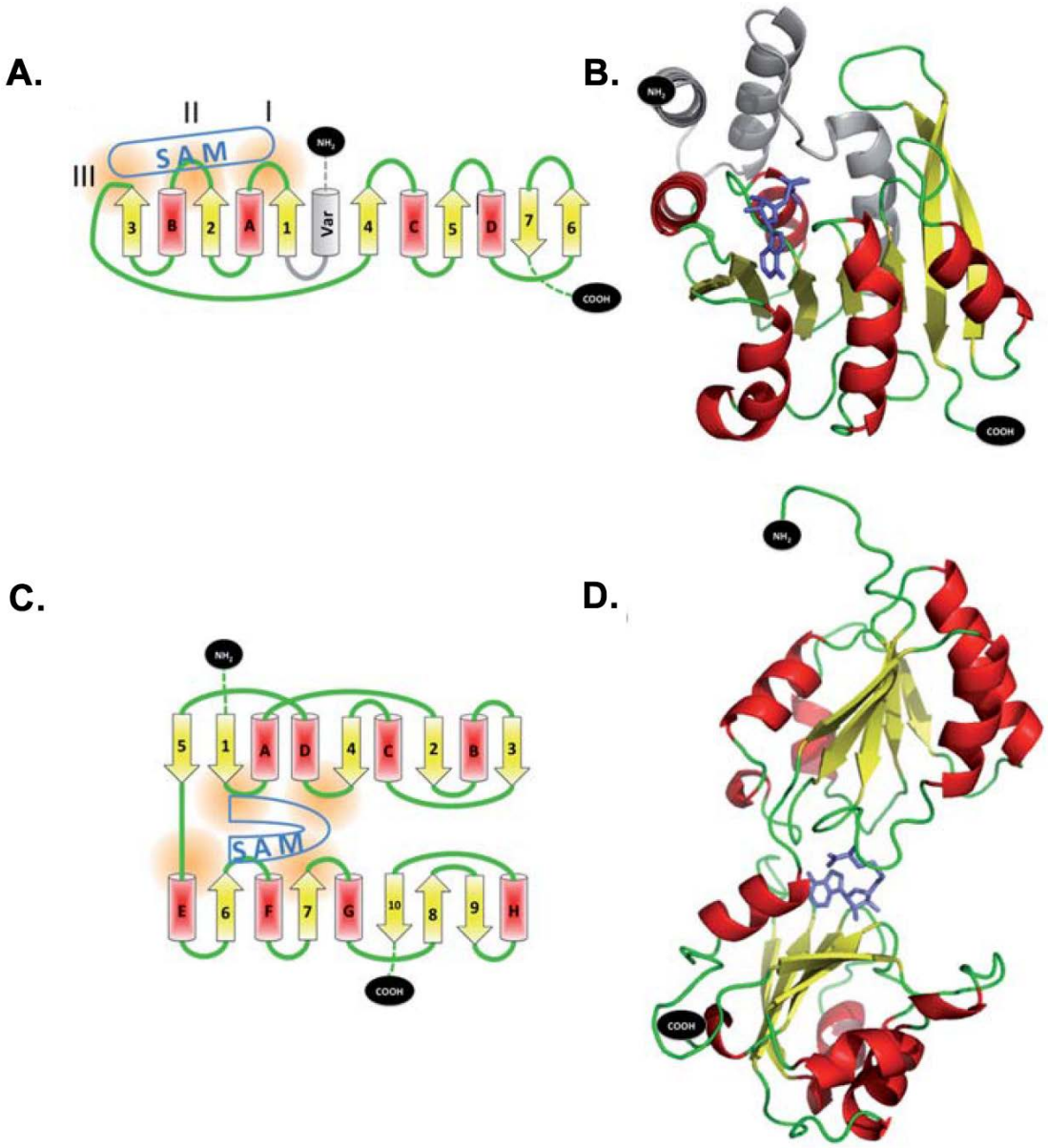

Figure 1.13. Topologies and folds of NPMTs. **(A)** Typical topology of a Class I, Rossmann-like NPMT. **(B)** Tertiary structure of catechol-O-methyltransferase (COMT) with bound SAH, representative of the Class I fold. **(C)** Topology and **(D)** Tertiary structure of cobalt-precorrin-4 C(11)-methyltransferase (CbiF) with bound SAH illustrate the typical Class III NPMTs. The diverse N-terminal region of Class I NPMTs is shown in grey. The SAM/SAH binding site is highlighted in orange, bound SAH ligands are shown in light blue, and conserved motifs are indicated with Roman numerals (I, II, III). α-Helices are shown in red, β-strands in yellow, and adjoining loops are green (Liscombe et al., 2012).

1.8.2 Biotechnological Applications of NPMTs

NPMTs have significant potential for application in biotechnology and, also, in emerging areas of chemical biology and synthetic biology such as metabolic engineering. The structural and functional diversity of this family of enzymes means that they can be applied for the biocatalytic methylation of a diverse range of synthetic and natural compounds which are necessary for the production of pharmaceuticals, agrochemicals and fine chemicals through to bulk chemicals such as biofuels (Struck et al., 2012). Following cofactor supply modifications, a key *O*-methyltransferase in vanillin biosynthesis was overexpressed in yeast resulting in a 30% increase in the production of this flavouring agent (Brochado and Patil, 2013).

MTases are amongst the enzymes most commonly found in the biosynthetic pathways of all major classes of natural products; these include the polyketides, nonribosomal peptides, terpenoids, alkaloids and flavonoids. The presence or absence of specific methyl groups within natural product scaffolds can dramatically affect their properties (Scharf et al., 2014a). Consequently, considerable effort has been focused on characterising MTases from natural product biosynthetic pathways. This has led to the development of biosynthetic and metabolic engineering methods which alter the methylation patterns of natural products, with the aim of improving their properties for therapeutic and other applications (McCarthy and McCarthy, 2007).

Traditionally, methylation reactions are carried out with methyl iodide. However, the harsh reaction conditions together with the environmental and safety considerations associated with the use of methyl iodide are far from ideal (Struck et al., 2012). In addition, such chemical methylation reactions often lack selectivity and this in turn leads to the use of complex and expensive synthetic strategies. The major advantage of chemoenzymatic synthesis lies in the ability of enzymes to perform regio- and stereoselective transformations on complex molecules. Advances in chemoenzymatic

methods and microbial engineering will offer avenues to new synthetic designs and ultimately expand our access to bio-based materials and therapeutics (Lipson et al., 2013).

1.9 Current Detection and Treatment of Invasive Aspergillosis

In addition to the biotechnological applications of secondary metabolite pathway enzymes, the products of these pathways may have significant potential for the specific diagnosis of fungal infection. Invasive aspergillosis (IA) is the most common of invasive mould diseases and is a major source of mortality in immunocompromised individuals. Incidence of IA has increased markedly over recent years (Perfect, 2013). Despite the fact that early initiation of antifungal therapy is key to a favourable outcome, early diagnosis of this condition poses many challenges. Unlike many infections, blood culture is almost always negative for *A. fumigatus* (Duthie and Denning, 1995). Bronchoalveolar lavage sampling of the lower respiratory tract secretions for *A. fumigatus* is also a low sensitivity technique. These caveats of diagnosis have led to the adoption of an empirical system in many treatment centres whereby even in the absence of fungal pathogen identification early antifungal treatment is commenced. This pre-emptive implementation is known to result in the administration of antifungal therapies to patients without invasive fungal disease (Valerio et al., 2014). As a result of this, several attempts have been made to develop sensitive nonculture-based diagnostic mechanisms to rapidly detect the onset of infection and permit the rational administration of antifungal drugs. The success of this strategy is dependent on the development of reliable biomarker assays or imaging techniques.

In recent years attention has focused on the detection of signature molecules of fungal infection. These include the targeting of fungal antigens such as galactomannan or 1, 3-β-D-glucan by ELISA or lateral flow devices (LFDs), detection of siderophores and the amplification of fungal nucleic acids from tissue and body fluids as well as application of mass spectrometry (Johnson et al., 2014).

Galactomannan (GM) is a carbohydrate molecule which is composed of a backbone of mannose residues with side chains of β 1–5 linked galactofuranosyl residues. It is a major cell wall component in *Aspergillus* species. Detection of this molecule is carried out using a monoclonal antibody (EB-AB) which was raised in rats (Stynen et al., 1992). Pure GM is readily released from *Aspergillus sp.* during *in vitro* growth as a molecule of about 20 kDa in size. GM release *in vivo* is thought to occur following cell lysis as nutrients are limited and growth is restricted by the host response. It has been suggested that GM is not released into circulation during infection until the fungus invades the endothelial compartment. This also means that serum GM levels may act as a marker for this stage of host colonisation (Hope et al., 2007).

A double-sandwich ELISA, the Platelia™ Aspergillus enzyme immunoassay (Bio-Rad, France), has been developed. This uses the EBA2 monoclonal antibody both as detector and acceptor for GM. The test has been commercially available in Europe since the mid-1990s and was approved by the US Food and Drug Administration in 2003 (Maertens et al., 2007). It can detect as little as 0.5 μg/ml of GM and a positive result can be obtained in 65% of patients approximately 5–8 days before clinical signs of IA develop (Wheat, 2003).

Nevertheless, there are some doubts about the clinical utility of recording a serum-positive GM result in the nonculture-based diagnosis of IA. Although early reports indicate both high sensitivity and specificity, more recent studies have found a lower sensitivity, ranging from 40 to 50%, particularly in the setting of antifungal agents (Patterson, 2011). Other studies challenge the specificity of the GM ELISA and suggest that it may actually more suitable for the detection of non-*fumigatus* species (Hachem et al., 2009). It detects a soluble antigen produced during infection with *Geotrichum capitatum*, with no evidence of aspergillosis, cross-reacts with other opportunistic fungi in some other fungal infections (such as histoplasmosis) and may react with antigens from

Cryptococcus neoformans in patients with cryptococcosis (Giacchino et al., 2006; Min et al., 2012). Furthermore, false-positive *Aspergillus* GM tests have been reported in patients taking certain antibiotics (e.g. piperacillin–tazobactam and amoxicillin–clavulanate) (Boonsarngsuk et al., 2010). Antibodies to GM can also develop and this has been suggested as a cause of false negative serum GM results in patients with IA (Herbrecht et al., 2002)

1,3-β-D-glucan (BDG) is a carbohydrate moiety in the cell walls of most fungal species, with the exception of Zygomyces and *Cryptococcus* spp. (Marty and Koo, 2009). Similar to GM, BDG is excreted into the culture fluid of *A. fumigatus* (Odabasi et al., 2006). The measurement of BDG using the Fungitell assay (Associates of Cape Cod, Inc.) is based on the *Limulus* test that has traditionally be used for the detection of bacterial endotoxin (Miyazaki et al., 1995). BDG activates factor G, a serine protease zymogen of the *Limulus* amebocyte lysate, which is extracted from amebocytes of the horseshoe crab species. This in turn activates a coagulation cascade. The activity of this reaction can be measured with use of the colorimetric or turbidimetric methods (Pickering et al., 2005). A positive BDG result in serum, along with the presence of appropriate host factors, clinical features and other mycological evidence, allows possible IFI to be upgraded to probable IFI in the revised criteria of both the European Organization for Research and Treatment of Cancer/Invasive Fungal Infections Cooperative Group and the National Institute of Allergy and Infectious Diseases Mycoses Study Group (EORTC/MSG) (De Pauw et al., 2008). The major limitations of BG testing are the false-positive results which can occur with interfering substances. Gauze dressings, dialysis, and some bacteria have been shown to result in highly elevated BDG values (Onishi et al., 2012; Kanamori et al., 2009). Despite these major limitations, combining GM and BG assays may strengthen IA diagnosis (Sulahian et al., 2014).

Aspergillus spp. produces a range of extracellular enzymes as well as primary and secondary metabolites which may serve as specific biomarkers of infection. Although ELISA methodology has traditionally dominated for the detection of biomarkers, the flexibility of MS to analyze all kinds of molecules under optimal conditions makes it likely that it can soon be used for the detection of *Aspergillus*-specific metabolites and nucleic acids. A recent study highlights the potential of thermal desorption-gas chromatography/mass spectrometry to diagnose IA based on the detection of exogenous fungal metabolites in breath (Koo et al., 2014).

Siderophore detection is emerging as a potential strategy for IA diagnosis. Iron, an indispensable cofactor for many cellular processes including electron transport, amino acid metabolism and biosynthesis of DNA, is a key nutrient for most organisms, including *Aspergillus* (Schrettl and Haas, 2011). However, since iron excess can catalyze the formation of reactive oxygen species, *Aspergillus* has evolved complex mechanisms to balance its acquisition, storage and consumption. Under iron-limited conditions one strategy involves the biosynthesis of siderophores, which are low molecular mass iron chelators that acquire iron from the environment (Haas et al., 2008). Fusarinine C (FsC) and triacetylfusarinine C (TAFC), the major siderophores produced by *A. fumigatus* to mobilize extracellular iron are produced within hours of spore germination and, along with the intracellular siderophore ferricrocin, are essential for its virulence (Schrettl et al., 2007). In a rat infection model, radiolabelled TAFC shows highly selective accumulation in infected lung tissue and good correlation with severity of disease, strongly suggesting that it is a promising agent for *A. fumigatus* infection imaging (Petrik et al., 2010).

The detection of nonribosomal cyclic peptides and depsipeptides by MS may serve as highly specific fungal markers (Jegorov and Hajduch, 2006). Gliotoxin is produced by most *A. fumigatus* strains and is present both in plasma and serum. The inactive gliotoxin derivative bis(methylthio)gliotoxin has been shown to be recoverable

from blood (Domingo et al., 2012). A recent report describes the MS detection of a gliotoxin precursor cyclo (L-Phe-L-Ser) in the lungs of mice colonised by *A. fumigatus*. This metabolite may serve as an alternative marker for the diagnosis of invasive aspergillosis (Sekonyela et al., 2013). Immunodetection of human IgG directed against the *Aspergillus* gliotoxin oxidoreductase may have potential as a diagnostic biomarker of IA in nonimmunocompromised individuals (Shi et al., 2012).

Overall, this section summarises the important role of fungal secondary metabolites during infection, the complex biosynthetic routes by which these molecules are produced, and finally the commercial and diagnostic potential of both the enzymes involved in these pathways and the metabolites themselves.

1.10 Thesis rationale and objectives

As such, the overall work objectives presented in this thesis are as follows:

(i) The identification and targeted deletion of the thiol methyltransferase responsible for gliotoxin bismethylation in *A. fumigatus* ATCC26933.

(ii) Phenotypic and metabolomic characterisation of the *A. fumigatus* gene deletion mutant in response to various stresses and the abolition of any identified phenotype through restoration of gene functionality via complementation.

(iii) Biochemical and structural characterisation of this methyltransferase.

(iv) Development of antibodies reactive to bis(methyl)gliotoxin in order to develop a competitive ELISA for the detection of this metabolite.

Chapter 2

Materials and Methods

2.1 Materials

All chemicals were purchased from Sigma-Aldrich Chemical Co. Ltd. (U.K.), unless otherwise stated.

2.1.1 *Aspergillus* Media and Agar

2.1.1.1 Sabouraud Agar

Sabouraud agar (65 g) (Oxoid, Cambridge, UK) was added to 1 L dH_2O and dissolved. The solution was autoclaved, and allowed to cool to ~50 °C. Agar (25 ml) was subsequently poured into 90 mm petri dishes, under sterile conditions. The plates were allowed to set and stored at 4 °C.

2.1.1.2 Malt Extract Agar

Malt extract agar (50 g) (Difco, Maryland, USA) was added to 1 L dH_2O and dissolved. The solution was autoclaved, and allowed to cool to ~50 °C. Agar (25 ml) was then poured into 90 mm petri dishes, under sterile conditions. The plates were allowed to set and stored at 4 °C.

2.1.1.3 Czapeks Dox Broth

Difco™ Czapeks Dox powder (35 g) (BD Biosciences) was dissolved in 1 L of dH_2O and autoclaved at 121 °C for 15 min.

2.1.1.4 Czapeks Dox Agar

Agar (18 g) (Scharlau Chemie S.A., Barcelona, Spain) was added to 1L of Czapeks Dox broth. The solution was autoclaved at 121 °C for 15 min and allowed to cool to ~50 °C before being poured into 90 mm petri dishes under sterile conditions. The plates were allowed to set and were stored at 4 °C.

2.1.1.5 Yeast Glucose Broth

Yeast extract (5 g) (Oxoid Ltd., Basinstoke, Hampshire, England) and glucose (20 g) were added to 800 ml dH_2O and dissolved. The solution was brought to 1 L with dH_2O, autoclaved at 121 °C for 15 min and stored at 4 ºC.

2.1.1.6 *Aspergillus* Minimal Media

2.1.1.6.1 50 X Salt Solution

KCl (26 g), $MgSO_4.7H_2O$ (26 g), and KH_2PO_4 (76 g) was dissolved in 1 L dH_2O and autoclaved at 105 °C for 30 min. The solution was stored at 4 °C.

2.1.1.6.2 100 X Ammonium Tartrate

Ammonium Tartrate (92 g) was dissolved in 1 L dH_2O. The solution was 105 °C for 30 min and stored at room temperature.

2.1.1.6.3 Trace Elements

$Na_2B_4O_7.7H_2O$ (40 mg), $CuSO_4.5H_2O$ (400 mg), $FeSO_4.7H_2O$ (800 mg), $Na_2MoO.2H_2O$ (800 mg), and $ZnSO_4.7H_2O$ (8 g) were dissolved in 800 ml dH_2O allowing each to dissolve completely before addition of the next component. A few drops of conc. HCl was added to maintain the solution. The solution was then brought up to 1 L with dH_2O and filter sterilised.

2.1.1.7 *Aspergillus* Minimal Media (AMM) Liquid

2.1.1.7.1 AMM with Ammonium Tartrate

Salt solution (50 X; 20 ml), Ammonium tartrate (100 X, 10 ml) and glucose (10 g) were added to 800 ml dH_2O. Trace elements containing iron (1 ml) (Section 2.1.1.6.3) were added and the pH of the solution was adjusted to pH 6.8. The solution was brought to 1 L with dH_2O, mixed and autoclaved at 105 °C for 30 min. The solution was stored at room temperature.

2.1.1.8 *Aspergillus* Minimal Media Agar

2.1.1.8.1 AMM Agar with Ammonium Tartrate

Agar (18 g) was added to 1 L of AMM liquid medium with ammonium tartrate (Section 2.1.1.6.2). The solution was autoclaved at 105 °C for 30 min and allowed to cool to about 50 °C and the agar mixture (25 ml) was poured into 90 mm petri dishes under sterile conditions and stored at 4 °C.

2.1.1.9 Regeneration Agar

2.1.1.9.1 1.8 % (w/v) Regeneration Agar

Aspergillus salt solution (50 X; 20 ml), ammonium tartrate (100 X; 10 ml), and trace elements (1 ml) (Section 2.1.1.6.3) were added to 800 ml dH_2O and dissolved. The solution was adjusted to pH 6.8. Sucrose (342 g) was added and the solution was made up to 1 L dH_2O. Agar (18 g) was added to the solution. The solution was autoclaved at 105 °C for 30 min and kept at 65 °C until required.

2.1.1.9.2 0.7% (w/v) Regeneration Agar

Aspergillus salt solution (50 X; 20 ml), ammonium tartrate (100 X; 10 ml), and trace elements (1 ml) (Section 2.1.1.6.3) were added to 800 ml dH_2O and dissolved. The pH of the solution was adjusted to pH 6.8. Sucrose (342 g) was added and the solution was made up to 1 L dH_2O. Agar (7 g) was added to the solution. The solution was autoclaved at 105 °C for 30 min and kept at 65 °C until required.

2.1.2 *E. coli* Media and Agar

2.1.2.1 Luria-Bertani Broth

LB Broth (25 g) (Difco, Maryland, USA) was dissolved in 1 L dH_2O and dissolved. The solution was autoclaved at 121 °C for 15 min and stored at 4 °C.

2.1.2.2 Luria-Bertani Agar

LB Agar (40 g) (Difco, Maryland, USA) was dissolved in 1 L dH_2O. The solution was autoclaved at 121 °C for 15 min, and allowed to cool to ~50 °C. Agar (25 ml) was then poured into 90 mm petri dishes, under sterile conditions and allowed to set. They were stored at 4 °C.

2.1.2.3 Terrific Broth

Terrific Broth (47.6 g) (Fluka) and 8 ml glycerol was dissolved in 1 L dH_2O. The solution was autoclaved at 121 °C for 15 min and stored at 4 °C.

2.1.2.4 M9 Minimal Media Components

2.1.2.4.1 5x M9 Salts

64 g $Na_2HPO_4.7H_2O$, 15 g KH_2PO_4, 2.5 g NaCl and 5 g NH_4Cl were dissolved in 800 ml dH_2O. The pH was adjusted to 7.2 and the volume was adjusted to 1 L with dH_2O. The solution was autoclaved at 121 °C for 15 min.

2.1.2.4.2 20% Glucose

10 g glucose was dissolved in 40 ml dH_2O. This was then brought to 50 ml with dH_2O and filter sterilised with a 0.22 μm syringe filter. The solution was stored at room temperature.

2.1.2.4.3 1M $MgSO_4$

4.8 g $MgSO_4$ (1M) was dissolved in 40 ml dH_2O. The solution was filter sterilised using a 0.22 μm syringe filter and stored at room temperature.

2.1.2.4.4 1M $CaCl_2$

4.4 g MgSO4 (1M) was dissolved in 40 ml dH_2O. The solution was filter sterilised using a 0.22 μm syringe filter and stored at room temperature.

2.1.2.4.5 1000x Trace Metals Solution

0.60 g $CaCl_2.H_2O$, 0.60 g $FeSO_4.7H_2O$, 0.12 g $MnCl_2.4H_2O$, 0.08 g $CoCl_2.6H_2O$, 0.07 g $ZnSO_4.7H_2O$, 0.03 g $CuCl_2.2H_2O$, 2 mg Boric acid, 25 mg $(NH_4)6Mo_7O_{24}.4H_2O$ and 0.50 g EDTA was added to 100 ml of dH_2O in a 500 ml Erlenmeyer flask in the stated order. Each compound was fully dissolved by stirring before adding the next. The solution was filter sterilised and stored in the dark at room temperature.

2.1.2.4.6 Amino Acid Mix

100 mg Lysine, 100 mg Phenylalanine, 100 mg Threonine, 50 mg Isoleucine, 50 mg Leucine and 50 mg Valine were added to a 2 ml eppendorf immediately before use.

2.1.2.5 M9 Minimal Media

780 ml deionized water (ddH_2O) was autoclaved in a 3-liter flask. To this solution 200 ml 5x M9 Salts, 20 ml 20% Glucose, 2 ml 1M $MgSO_4$, 100 µl 1M $CaCl_2$ and 200 µl 1000x Trace Metals (Section 2.1.2.4.5) were added.

2.1.3 Solutions for pH Adjustment

2.1.3.1 5 M Hydrochloric Acid (HCl)

Deionised water (40 ml) and hydrochloric acid (43.64 ml) were added slowly to a graduated cylinder (glass). The final volume was adjusted to 100 ml. The solution was stored at room temperature.

2.1.3.2 5 M Sodium Hydroxide (NaOH)

NaOH pellets (20 g) were added to ddH_2O (80 ml) and dissolved using a magnetic stirrer. The final volume was adjusted to 100 ml. The solution was stored at room temperature.

2.1.4 Phosphate Buffer Saline

One PBS tablet (Oxoid, Cambridge, UK) was added to 200 ml of dH_2O, and dissolved by stirring. The solution was autoclaved and stored at room temperature.

2.1.5 Phosphate Buffer Saline-Tween 20 (PBST)

Tween-20 (0.5 ml) was added to 1 L PBS (Section 2.1.4). The solution was stored at room temperature.

2.1.6 Antibiotics and Supplements

All antibiotics and supplements were prepared as stock solutions in water or methanol and filter sterilised. All were stored at – 20 °C. Further information is provided in Table 2.1.

2.1.7 80 % (v/v) Glycerol

Glycerol (80 ml) was added to 20 ml ddH_2O. The solution was autoclaved at 121 °C for 15 min and stored at 4 °C.

2.1.8 Molecular Biology Reagents

2.1.8.1 Agarose Gel Electrophoresis Reagents

2.1.8.1.1 0.5 M Ethylenediaminetetraacetic acid (EDTA)

Ethylenediaminetetraacetic acid disodium salt dihydrate (186.12 g) was dissolved in 800 ml dH_2O. The pH was adjusted to pH 8.0 using 5 M NaOH (Section 2.1.3.2) and the final volume was brought up to 1 L.

2.1.8.1.2 50 X Tris-Acetate Buffer (TAE)

Trizma base (242 g) was added to 57.1 ml glacial acetic acid and 100 ml of 0.5 M EDTA, pH 8.0 (Section 2.1.8.1.1). The volume was adjusted to 1 L with dH_2O. The solution was stored at room temperature.

2.1.8.1.3 1 X Tris-Acetate Buffer (TAE)

50 X TAE (20 ml) (Section 2.1.8.1.2) was added to dH2O (980 ml). The solution was stored at room temperature.

2.1.8.1.4 Ethidium Bromide

Ethidium bromide (Sigma-Aldrich) was supplied at 1 mg/ml of which 4 µl was used per 100 ml agarose gel.

2.1.8.1.5 6 X DNA Loading Dye

Loading dye (Promega, Southampton, UK) was used at the concentration supplied.

2.1.8.1.6 1 % (w/v) Agarose Gel

Agarose powder (1 g) was dissolved into 100 ml 1 X TAE (Section 2.1.8.1.3). This mixture was heated in a microwave oven until the agarose had dissolved and the mixture was molten. Ethidium Bromide solution (Section 2.1.8.1.4) was added. The gel was left to set for at least 30 minutes.

2.1.8.1.7 Roche molecular weight marker VII

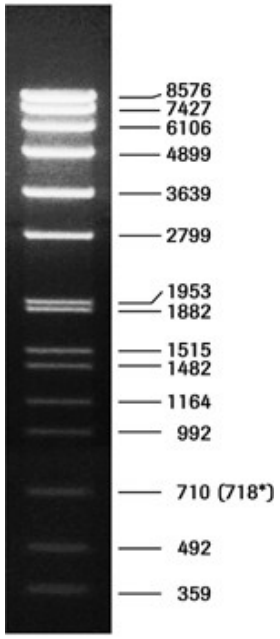

Figure 2.1. Image of the Roche molecular weight marker VII.

2.1.8.1.8 New England BioLabs (NEB) 1 kb DNA Ladder

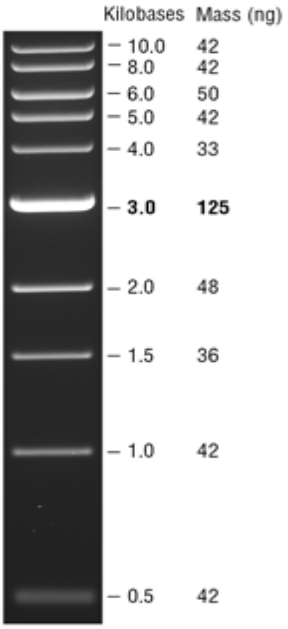

Figure 2.2. Image of the NEB 1 kb DNA Ladder

Table 2.1. Additives and antibiotics used during this study.

Condition Tested	Reagent Used	Stock Concentration	Tested Concentration
Sensitivity to Oxidative Stress	H_2O_2	1 M (prepared in H_2O)	0.25 - 2 mM
Gliotoxin Sensitivity	Gliotoxin	1 mg/ml (prepared in methanol)	2.5 -20 µg/ml
Pyrithiamine Resistance	Pyrithiamine Hydrochloride	0.1 mg/ml (prepared in H_2O)	0.1 µg/ml
Phleomycin Resistance	Phleomycin	25 mg/ml (prepared in H_2O)	40 µg/ml
Hygromycin Resistance	Hygromycin B	100 mg/ml (prepared in H_2O)	100 µg/ml
Ampicillin Resistance	Ampicillin	100 mg/ml (prepared in H_2O)	0.1 µg/ml

2.1.9 *Aspergillus* Transformation Reagents

2.1.9.1 0.7 M Potassium Chloride

KCl (26.1 g) was dissolved in 500 ml dH2O. The solution was autoclaved and stored at room temperature.

2.1.9.2 25 mM Potassium Phosphate Monobasic

KH_2PO_4 (1.7 g) was dissolved in 500 ml dH_2O.

2.1.9.3 25 mM Potassium Phosphate Dibasic

K_2HPO_4 (0.87 g) was dissolved in 200 ml dH_2O.

2.1.9.4 Lysis Buffer

KCl (26.1 g) was dissolved in 25 mM KH_2PO_4 (350 ml) (Section 2.1.9.2). The pH was adjusted to pH 5.8 with 25 mM K_2HPO_4 (Section 2.1.9.3). The solution was brought to 500 ml with dH_2O.

2.1.9.5 Lytic Enzymes solution for protoplast generation

Lytic enzymes from *Trichoderma harzianum* (Sigma Aldrich) (0.45 g) were added to 15 ml lysis buffer (Section 2.1.9.4) and filter sterilised with a 0.45 µm filter.

2.1.9.6 Buffer L6

Sorbitol (1 M), Tris-HCl (10 mM), and $CaCl_2$ anhydrous (10 mM) was prepared by dissolving sorbitol (72.88 g), Tris-HCl (0.484 g), and $CaCl_2$ (0.444 g) in dH_2O. The pH was adjusted to pH 7.5 before the final volume was adjusted to 400 ml with dH_2O. The solution was autoclaved and stored at room temperature.

2.1.9.7 Buffer L7

PEG 6000 (60 g) was dissolved in dH_2O (40 ml). Tris-HCl (0.157 g) and $CaCl_2$ anhydrous (0.444 g) was added and the solution was heated gently whilst covered with tin foil until completely dissolved. After dissolution the solution was placed on a cool plate. To

adjust the pH, concentrated HCl was added dropwise. This was done over a time period of 1 – 2 h until the pH was 7.5. The solution was autoclaved and stored at room temperature.

2.1.10 Southern Blot Reagents

2.1.10.1 Southern Transfer Buffer

Sodium hydroxide (0.6 M; 16 g) and Sodium chloride (0.4 M; 35.07 g) were dissolved in 800 ml dH_2O. The volume was adjusted to 1 L with dH_2O.

2.1.10.2 20 X SSC

Sodium chloride (175.3 g) and sodium citrate (88.2 g) were added to dH_2O (800 ml). The pH was adjusted to pH 7 and the volume brought up to 1 L dH_2O. The solution was autoclaved and stored at room temperature.

2.1.10.3 2 X SSC

SSC (100 ml, 20 X) (Section 2.1.10.2) was added to 900 ml dH_2O and stored at room temperature.

2.1.10.4 10 % SDS (w/v)

SDS (10 g) was dissolved into 1 L dH_2O. The solution was stored at room temperature.

2.1.10.5 0.1 % (w/v) SDS / 1 X SSC

20 X SSC (50 ml) (Section 2.1.10.2) and 10 ml of SDS 10 % (w/v) (Section 2.1.10.4) were dissolved in 1 L dH_2O. The solution was stored at room temperature.

2.1.10.6 Digoxigenin (DIG) Detection Buffers

2.1.10.6.1 10 % (w/v) Lauroylsarcosine

Lauroylsarcosine (1 g) was dissolved in 10 ml dH_2O.

2.1.10.6.2 Membrane Pre-hybridisation Buffer

SDS (35 g), formamide (250 ml), 100 ml 10 % Blocking reagent (Roche Applied

Science, Mannheim, Germany), 5 ml 10 % (w/v) laurylosarcosine were dissolved in 500 ml dH_2O. The solution was prepared under sterile conditions and stirred well before storage at 4 °C. Before use the solution was pre-heated at 65 ^oC for 15 min.

2.1.10.6.3 DIG Buffer 1 (1 X)

Maleic Acid (2.32 g) (0.1 M) and NaCl (1.75 g) (0.15 M) were added to 180 ml dH_2O. The pH was adjusted to pH 7.5 before the final volume was adjusted to 200 ml with dH_2O. The solution was filter sterilised and stored at room temperature for up to one month.

2.1.10.6.4 Antibody Blocking Reagent

Blocking reagent (0.4 g) (Roche Applied Science, Mannheim, Germany) was dissolved in 40 ml of DIG Buffer 1 (Section 2.1.10.6.3) at 50 °C. The solution was prepared fresh on the day.

2.1.10.6.5 DIG Buffer 3

Tris-HCl (1.575 g) (0.1 M), NaCl (0.584 g) (0.1 M) and $MgCl_2.6H_20$ (1.02 g) (50 mM) were dissolved in dH_2O (80 ml). The pH was adjusted to pH 9.5 and the final volume brought up to 100 ml. The solution was filtered sterilised and then stored at room temperature for up to one month.

2.1.10.6.6 DIG Wash Buffer

Tween 20 (0.15 g) was dissolved in DIG Buffer 1 (50 ml) (Section 2.1.10.6.3). The solution was mixed and filter sterilised before being stored at room temperature.

2.1.10.6.7 Anti-Digoxigenin-Alkaline Phosphatase (AP),Fab fragment conjugate

Anti-Digoxigenin- AP, Fab fragments (Roche, Mannheim, Germany) (1 µl) was added to 10 ml antibody blocking reagent (Section 2.1.10.6.4).

2.1.10.6.8 Chemiluminescent substrate phosphatase detection (CSPD) Substrate

CSPD (50 µl) (Roche, Mannheim, Germany) was added to DIG Buffer 3 (4.95 ml) (Section 2.1.10.6.5).

2.1.10.6.9 DIG-labelled deoxynucleotide Triphosphates (dNTPs)

Pre-mixed DIG-labelled dNTPs were purchased from Roche and used according to the manufacturers guidelines for the generation of DIG-labelled probes for Southern detection probes.

2.1.10.6.10 Developer Solution

Developer (Kodak) was diluted 1/4 in dH_2O and stored in a tinfoil covered Duran in a dark room.

2.1.10.6.11 Fixer Solution

The fixer solution (Kodak) was diluted 1/5 in dH_2O and stored in a tinfoil covered Duran in a dark room.

2.1.11 *E. coli* Lysis Buffer

50 mM Tris-HCl, 100 mM NaCl, 1 mM EDTA, 10 % Glycerol, pH 8.0. Autoclave and store at 4 °C. Immediately before use add 0.4 % Sodium Deoxycholate (Make 5% stock in ddH_2O), 1 mM PMSF (250 mM Stock in ethanol), 1 µg/ml Pepstatin A (1 mg/ml stock in ethanol), 1 µg/ml Leupeptin (1 mg/ml stock in ethanol), 300 µg/ml Lysozyme (10 mg/ml stock solution in 10 mM Tris-HCl, pH 8.0).

2.1.12 SAM and SAH Extraction Buffer

4 ml 5 M HCl (Section 2.1.3.1) was added to 196 ml ddH_2O resulting in a 0.1 M HCl solution. This was stored at room temperature.

2.1.13 Reverse-Phase High Performance Liquid Chromatography (RP-HPLC) Solvents

2.1.13.1.1 Solvent A: 0.1 % (v/v) Trifluoroacetic acid (TFA) in HPLC grade water

TFA (1 ml) was added to HPLC Grade Water (1 L) in a darkened Duran.

2.1.13.1.2 Solvent B: 0.1 % (v/v) TFA in HPLC grade Acetonitrile

TFA (1 ml) was added to HPLC Grade Acetonitrile (1 L) in a darkened Duran.

2.1.14 AKTA FPLC Buffers and Reagents

2.1.14.1 Gel Filtration Calibrant Mixture

Thyroglobulin (25 mg/ml) (200 µl), Aldolase (25 mg/ml) (160 µl) and RNAse A (25 mg/ml) (160 µl) were brought to 1 ml with PBS (Section 2.1.4). The solution was stored at 4 °C. All calibrants used were included in the HMW gel filtration calibration kit (GE Healthcare).

2.1.14.2 Glutathione Affinity Chromatography Buffers

The Equilibration/Wash Buffer: 50 mM Tris-HCl (7.88 g), 100 mM NaCl (5.84 g) and 10 % Glycerol (100 ml) was added to 800 ml dH2O. The pH of the solution was adjusted to pH 8.0 and volume was brought to 1 L with dH2O. The solution was autoclaved and store at 4 °C. The Sample Elution Buffer was prepared as described above and brought to 10 mM reduced glutathione which was added immediately before use.

2.1.14.3 Q-Sepharose Ion Exchange Chromatography (IEX) Buffers

The IEX Equilibration Buffer; 20 mM Tris-HCl (3.14 g) and 20 mM NaCl (1.17 g) were added to 800 ml dH_2O. The pH of the solution was adjusted to pH 8.5. The volume was brought to 1 L with dH_2O. The solution was autoclaved and store at 4 °C. The IEX Sample Elution Buffer was prepared as described above with 1 M NaCl (58.44 g) instead of 20 mM NaCl.

2.1.14.4 GtmA Gel Filtration Buffer

50 mM Tris-HCl (7.88 g) and 50 mM NaCl (2.92 g) were added to 800 ml ddH_2O. The pH of the solution was adjusted to pH 7.4. The volume was brought to 1 L with ddH_2O. The solution was autoclaved and store at 4 °C. The buffer was degassed using vacuum filtration before use.

2.1.15 SDS-PAGE and Western Blotting Reagents

2.1.15.1 10 % (w/v) Sodium Dodecyl Sulfate (SDS)

SDS (10 g) was added to 80 ml of dH_2O and dissolved. The solution was adjusted to 100 ml with dH_2O and stored at room temperature.

2.1.15.2 1.5 M Tris-HCl pH 8.3

Trizma-hydrochloride (23.64 g) was dissolved in 60 ml dH_2O. The pH was adjusted to 8.3 using 5 M NaOH (Section 2.1.3.2). The volume was adjusted to 100 ml with dH_2O and stored at 4 °C.

2.1.15.3 0.5 M Tris-HCl pH 6.8

Trizma-hydrochloride (7.88 g) was dissolved in 60 ml dH_2O. The pH was adjusted to 6.8 using 5 M NaOH (Section 2.1.3.2). The volume was adjusted to 100 ml with dH_2O and stored at 4 °C.

2.1.15.4 10% (w/v) Ammonium Persulfate (APS)

Ammonium persulfate (0.1 g) was added to 1 ml dH_2O. The solution was stored at 4 °C and used within 8 h.

2.1.15.5 5 X Solubilisation Buffer

Trizma-hydrochloride (23.64 g) was dissolved in 60 ml dH_2O. The pH was adjusted to 8.3 using 5 M NaOH (Section 2.1.3.2). The volume was adjusted to 100 ml with dH_2O and stored at 4 °C.

2.1.15.6 5 X SDS Electrode running buffer

Trizma base (30 g), glycine (144 g) and SDS (10 g) were added to 1600 ml dH_2O, and dissolved using a magnetic stirrer. The pH was adjusted to between 8.6 and 8.8. The final volume was adjusted to 2 L. The solution was stored at room temperature.

2.1.15.7 1 X SDS Electrode running buffer

5 X SDS Electrode running buffer (200 ml) (Section 2.1.15.6) was added to 800 ml dH_2O.

2.1.15.8 Coomassie® Blue Stain Solution

dH_2O (600 ml), glacial acetic acid (100 ml) and methanol (300 ml) were added to a glass bottle containing 1 g Coomassie® Brilliant Blue R. The solution was stored at room temperature.

2.1.15.9 Destain Solution

Glacial acetic acid (100 ml) was added to dH_2O (600 ml) and methanol (300 ml). The solution was stored at room temperature.

2.1.15.10 Towbin Electrotransfer Buffer for Semi-Dry Transfer

Trizma base (6.06 g) and glycine (28.8 g) were added to dH_2O (600 ml) and methanol (200 ml). The final volume was adjusted to 1 L with dH_2O. The solution was stored at room temperature.

2.1.15.11 Blocking Solution

Marvel® powdered milk (5 g) was added to 100 ml PBST (Section 2.1.5) 100 ml PBST (Section 2.1.5)

2.1.15.12 Antibody Buffer

Marvel® (powdered milk) (1 g) was added to 100 ml PBST (Section 2.1.5)

2.1.15.13 DAB Substrate Buffer

Trizma-HCl (15.76 g) was added to 700 ml dH_2O and the pH was adjusted to 7.6 with 5 M NaOH (Section 2.1.3.2). The final volume was adjusted to 1 L.

2.1.16 Mass Spectrometry Reagents

2.1.16.1 *A. fumigatus* Whole Protein Lysate Extraction Buffer

100 mM Tris-HCl (15.7 g), 50 mM NaCl (2.92 g), 20 mM EDTA (5.85 g), 10% (v/v) Glycerol (100 ml) was added to 800 ml dH_2O. The pH was adjusted to 8.0 and the solution was brought to 1 L with dH_2O. Autoclave and store at 4 °C. Immediately before use 1 mM PMSF (Section 2.1.16.2), 1 µg/ml Pepstatin A (Section 2.1.16.3) and 1 mM DTT (final concentrations) were added to the buffer.

2.1.16.2 100 mM Phenylmethylsulfonyl fluoride (PMSF)

PMSF (17.4 mg) was dissolved in 1 ml methanol. The solution was stored at room temperature.

2.1.16.3 Pepstatin A (1 mg/ml)

Pepstatin A (10 mg) was brought to 10 ml with ethanol. The solution was split into 1 ml aliquots and stored at -20 °C.

2.1.16.4 100 % (w/v) TCA

Trichloroacetic acid (100 g) was added to 45.4 ml dH_2O and dissolved. The solution was stored in the dark at 4 °C.

2.1.16.5 50 mM Ammonium bicarbonate (NH_4HCO_3)

100 mM ammonium bicarbonate (Section 2.1.16.5) (5 ml) was added to 5 ml of ddH_2O. The solution was prepared fresh on day of use.

2.1.16.6 0.5 M Dithiotreitol (DTT)

DTT (77 mg) was dissolved in 100 mM ammonium bicarbonate (Section 2.1.16.5) (1 ml). The solution was prepared fresh on day of use.

2.1.16.7 0.55 M Iodoacetamide

Iodoacetamide (50.8 mg) was dissolved in 100 mM ammonium bicarbonate (Section 2.1.16.5) (.5 ml). The solution was prepared fresh on day of use.

2.1.16.8 Protein Resuspension Buffer

1.21 g Tris-HCl (100 mM) was dissolved in 50 ml ddH_2O. 36 g Urea (6 M) and 15.2 g Thiourea (2 M) were then dissolved. The pH was adjusted to 8.0 and the volume was brought to 100 ml with ddH_2O. The solution was filtered with a 0.22 µm filter and stored at room temperature.

2.1.16.9 Trypsin

Immediately before use a vial containing 20 µg Sequencing Grade Modified Trypsin (Promega) was resuspended in 20 µl Trypsin Resuspension Buffer (1 mg/ml). The vial was kept on ice until use. Remaining trypsin was snap frozen and stored at – 20 °C.

2.1.16.10 Trypsin Diluent

100 mM ammonium bicarbonate (Section 2.1.16.5) (1 ml) and acetonitrile (1 ml) were brought to 10 ml with distilled water. The solution was prepared fresh on day of use.

2.1.16.11 0.1 % (v/v) Formic Acid

Formic Acid (1 ml) was added to LC-MS grade water (1 L).

2.1.16.12 ProteaseMAX Surfactant Trypsin Enhancer

Immediately before use a vial containing 1 mg ProteaseMAX was resuspended in 50 mM ammonium bicarbonate (Section 2.1.16.5). The vial was kept on ice until use. Remaining ProteaseMAX was snap frozen and stored at – 20 °C.

2.1.17 Enzyme Linked Immunoassay (ELISA) Reagents

2.1.17.1 Carbonate Buffer (5 X)

200 ml of 250 mM Na_2CO_3 (5.3 g in ddH_2O) was added to 400 ml of 250 mM $NaHCO_3$ (8.4 g/ 400 ml ddH_2O) pH 9.6.

2.1.17.2 ELISA Wash Buffer

Biotrin Wash Buffer was used for all ELISA wash steps

2.1.17.3 ELISA Sera and Calibrator Diluent

1 % (w/v) BSA (1 g) was added to 100 ml PBST (Section 2.1.5). The solution was stirred gently and sorted at 4 °C.

2.1.17.4 3,3′,5,5′-Tetramethylbenzidine (TMB) Liquid Substrate

TMB Substrate was purchased from MOSS Inc.

2.1.17.5 ELISA Blocking Solution

1% BSA (w/v) (1 g) and 10% sucrose (10 g) was added to 100 ml PBST. The solution was stirred gently and sorted at 4 °C.

2.1.17.6 ELISA Stop Solution

13.5 ml of an 18.4 M H_2SO_4 stock solution (Sigma Aldrich) was added to 486.5 ml ddH_2O to prepare a 0.5 M H_2SO_4 solution.

2.2 Methods

2.2.1 Microbiological Methods – Strain Storage and Growth

Fungal and bacterial strains used in this study are listed in Table 2.2 and Table 2.3.

Table 2.2. *A. fumigatus* strains used in the study.

Strain	Reference
*A. fumigatus*ATCC26933	http://www.atcc.org/
A. fumigatus Δ*gliT*^{26933}	Schrettl et al., 2010
A. fumigatus Δ*gliK*^{26933}	Gallagher et al., 2012
A. fumigatus Δ*gliA*^{26933}	Owens et al., 2015
A. fumigatus Δ*gtmA*^{26933}	This work
A. fumigatus Δ*gtmA*::*gtmA* (*gtmA*^{c})	This work
A. fumigatus Δ*gliT*::Δ*gtmA*^{26933}	This work
A. fumigatus Δ*gliA*:: Δ*gtmA*^{26933}	This work

Table 2.3. Bacterial strains used, including antibiotics and supplements used.

Species	Strain	Antibiotics/Supplements
E. coli	TOP10	Ampicillin (100 μg/ml)
E. coli	DH5α^{TM}	Ampicillin (100 μg/ml)
E. coli	*pSK275*	Pyrithiamine (100 ng/ml)
E. coli	*pAN7-1*	Hygromycin (100 μg/ml)
E. coli	*pUCGH*	Hygromycin (100 μg/ml)
E. coli	*H2A::mRFP*	Phleomycin (40 μg/ml)
E. coli	*pEX-N-GST*	Ampicillin (100 μg/ml)
E.coli	*Pet19m*	Ampicillin (100 μg/ml)

2.2.1.1 *A. fumigatus* Growth, Maintenance and Storage

A. fumigatus strains were maintained on MEA (Section 2.1.1.2). A single inoculation loop of spores from a stock spore solution was streaked onto a plate and incubated at 37 ^{o}C in a static incubator for 5 days. Conidia were harvested from the plate by adding sterile PBST (10 ml) (Section 2.1.5) to the conidia and rubbing the surface with a sterile inoculation loop to dislodge the spores. The spore solution was centrifuged at 2000 x g for 5 min. The supernatant was removed and the spore pellet was resuspended in sterile PBS (5 ml) (Section 2.1.4). This was repeated. The spores were counted using a haemocytometer to determine the spore density (spores/ml). The spore solution was stored at 4 ^{o}C until required.

2.2.1.2 *E. coli* Growth, Maintenance and Storage

E. coli strains were grown on Luria-Bertani agar (Section 2.1.2.2) overnight at 37 ^{o}C or in Luria-Bertani broth (Section 2.1.2.1) at 37 ^{o}C overnight, shaking at 200 rpm. Where appropriate, media was supplemented with suitable antibiotics.

2.2.2 Molecular Biological Methods

2.2.2.1 Isolation of Genomic DNA from *A. fumigatus*

A. fumigatus conidia were harvested described in Section 2.2.1. An aliquot of the resulting conidial suspension (100 µl) was used to inoculate 50 ml cultures of Sabouraud Dextrose broth. The cultures were incubated at 37 ^{o}C for 24 h with constant agitation. The cultures were then filtered through autoclaved miracloth and the mycelia was collected, flash frozen in liquid nitrogen and ground to a fine powder using a pestle and mortar. The DNA extractions were carried out using the ZR Fungal/Bacterial DNA kit supplied by Zymo Research (California, U.S.A). All buffers and reagents were supplied with the kit. For each sample, mycelia (100 mg) was added to 750 µl DNA

buffer in the ZR Bead Bashing tube. DNA extraction was carried out according to the product protocol.

2.2.2.2 Polymerase Chain Reaction (PCR)

Polymerase chain Reaction (PCR) was used to amplify fragments of DNA for cloning, transformation constructs, DIG-labelled probes and colony PCR. Reactions were carried out using Accu*Taq* LA polymerase (Sigma-Aldrich). Annealing temperatures were estimated as *ca.* 4 ^{o}C below the melting temperature (T_m) of the primers used. Extension times used were *ca.* 1 min/kb of DNA to be synthesised. Reactions were carried out using the G-Storm PCR (Roche) System. Primers used in this study are listed in Table 2.4.

The general reaction constitutes for Accu*Taq* LA polymerase used was as follows:

10X reaction buffer	2 µl
dNTP mix (10 µm)	2 µl
Primer 1 (100 pmol/µl)	1 µl
Primer 2 (100 pmol/µl)	1 µl
DMSO	0.8 µl
DNA template	10 – 100 ng
Accu*Taq*	0.2 µl
Sterile water	to a total of 20 µl

The following reaction cycle was used unless otherwise stated:

95 °C (denaturing)	5 min	
95 °C (denaturing)	1 min	
55 °C (annealing)	1 min 30 sec	x 30-35 cycles
68 °C (extending)	1 min	
68 °C (extending)	10 min	

Table 2.4. Oligonucleotide primers used in the study. Restriction sites are underlined.

Primer Name	**Sequence (5' to 3')**
calm-qPCR-F	CCGAGTACAAGGAAGCTTTCTC
calm-qPCR-R	GAATCATCTCGTCAACTTCGTCGTCAGT
gtmA-qPCR-F	CGTCTGGAAAGATCTGGAAG
gtmA-qPCR-R	CGTCTGGAAAGATCTGGAAG
PTRoptrA1	GAGGACCTGGACAAGTACCAT
PTRoptrA2	CATCGTGACCAGTGGTAC
HYoptrA1	GCTCCATACAAGCCAACCAC
YGoptrA2	GTCCTGCGGGTAAATAGCTG
Δ*gtmA*-P1	ACCCTCATAGCTGCGACTTC
Δ*gtmA*-P2	GCACCGGTGGTCAACAAAGCTCTTGGTC
Δ*gtmA*-P3	GCGGTACCAAGACACCTATGGGGCGAAT
Δ*gtmA*-P4	GCAAAGCACTGAACAGCAAC
Δ*gtmA*-P5	CGGTTTGCGACTAAGCAGTT
Δ*gtmA*-P6	ACAGTGACAGTCCCGACGTT
Δ*gtmAHYG*-P2	GACTCGAGGGTCAACAAAGCTCTTGGTC
Δ*gtmAHYG*-P3	GACCTGCAGGAAGACACCTATGGGGCGAAT
*gtmA_eGFP*_F	TAGGTACCCGGTTTGCGACTAAGCAGT
*gtmA_eGFP*_R	TACCCGGGTCTGGGCTTGAGGCCGGTT
rGtmA-*HindIII*	GCAAGCTTATGTCCAAGTCAGACTACATCCA
rGtmA-*XhoI*	ATCTCGAGCTAGGGCTTGAGGCCG
GtmA_W157V_F	GGAATCCAGTTGAAGTTCTGCACTGTTGAGCTTGCAAGTATAC
GtmA_W157V_R	GTATACTTGCAAGCTCAACAGTGCAGAACTTCAACTGGATTCC
GtmA_W162V_F	GCGGCTTTCATAATTGGAATCACGTTGAAGTTCTGCCATGTTG

GtmA_W162V_R	CAACATGGCAGAACTTCAACGTGATTCCAATTATGAAAGCCGC
GtmA_N159V_F	CATAATTGGAATCCAGTTGAAGACCTGCCATGTTGAGCTTGCAAG
GtmA_N159V_R	CTTGCAAGCTCAACATGGCAGGTCTTCAACTGGATTCCAATTATG
GtmA_F185G_F	CGGCGTTGTGAAGAGCGATGCCCTCTTTCTGTGTTGGAAAC
GtmA_F159G_R	GTTTCCAACACAGAAAGAGGGCATCGCTCTTCACAACGCCG
GtmA_F127V_F	AAGCTCTGGAAGCCACCAGCGACAAAAACGTGCGTATAATG
GtmA_F127V_R	CATTATACGCACGTTTTTGTCGCTGGTGGCTTCCAGAGCTT

2.2.2.3 DNA Gel Electrophoresis

2.2.2.4 Preparation of Agarose Gel

Agarose gel electrophoresis was used to visualise restriction digest reactions, to separate DNA for Southern analysis, to separate differently sized DNA fragments prior to purification and for estimation of DNA yield. Agarose gels were cast and run using Bio-Rad electrophoresis equipment. Agarose gels of between 0.7 – 2 % (w/v) in 1X TAE buffer (Section 2.1.8.1.3) were used, although for the majority of applications a 1 % (w/v) agarose content was suitable. Powdered agarose was added to the appropriate volume of 1X TAE buffer in a 200 ml flask with loose stopper. This was then gently heated in a microwave, with frequent mixing, until the agarose had dissolved. While allowing the gel to cool, a mould was prepared by inserting the casting unit in a casting holder and sealed. A gel comb was inserted. After allowing the gel to cool to 40 – 50 ^{o}C, ethidium bromide (Section 2.1.8.1.4). The molten gel was then poured into casting unit, and allowed to set on a level surface. Once set, the gel comb was removed gently, and the gel casting unit containing the set gel was placed into the gel tank, with the wells nearer the negative (black) electrode. 1 X TAE buffer (Section 2.1.8.1.3) was then poured into the gel tank to fully submerge the gel.

2.2.2.5 Loading and Running Samples

DNA samples were prepared for loading by adding 5 volumes of DNA sample to 1 volume of 6 X loading dye (Section 2.1.8.1.5). DNA fragment size was estimated by running molecular weight markers alongside the unknown samples. Two different molecular weight markers were used throughout this study; marker VII (Roche) and 50 bp ladder (Roche). Gels were electrophoresed at 60 – 120 volts for 30 – 90 min.

2.2.2.6 DNA Gel Extraction

DNA gel extraction was carried out using the QIA quick gel extraction kit (Qiagen, UK). All reagents and columns were supplied with the kit and the procedure was carried out according to the manufacturer's instructions. DNA was eluted in 30 µl of sterile molecular grade water.

2.2.2.7 Restriction Enzyme Digest

Restriction enzymes, 10 X reaction buffers, and bovine serum albumin (BSA) were obtained from Promega. Reactions were carried out according to the manufacturer's instructions as follows:

DNA	1- 5 µg
Enzyme	1 µl
10 X Buffer	2.5/5 µl
10 X BSA	2.5/5 µl
Sterile water	to a total of 25/50 µl

2.2.2.8 Ligation of DNA Fragments

Ligation of DNA fragments was required for the generation of gene disruption constructs. DNA was digested (Section 2.2.2.7) to produce compatible fragments. These fragments were then separated by DNA gel electrophoresis (Section 2.2.2.3). Ligation of DNA fragments was carried out using the Ligafast Rapid DNA Ligation System (Promega)

which employs T4 DNA ligase. Ligations were carried out as per manufacturer's instructions. Restriction digests either produce a DNA fragment with an overhang of single-stranded DNA at either end of the double-stranded section, called a cohesive end or where no overhangs exist, called a blunt end. For cohesive ended ligation, the preferred molecular ration of insert to backbone is 3:1. This was estimated based off the size of the DNA fragment using the following formula. Ligations were carried out using 50 – 200 ng of vector DNA. T4 DNA ligase (1 µl), and 2X Rapid ligation buffer. For ligations where inserts were ligated to vectors, a control ligation was also carried out where the insert DNA was omitted from the reaction. For the generation of complementation constructs a ratio of insert to backbone of 3 : 1 was used. This was estimated based on the above formula.

2.2.2.9 Transformation of DNA into Competent DH5α Cells

LB agar plates (Section 2.1.2.2) containing Ampicillin (Section 2.1.6) were pre-heated to 37 ^{o}C for at least 1 h. For DH5α transformation, competent cells (50 µl) were removed from -70 ^{o}C freezer and were defrosted on ice for 2 min. DNA (1-10 ng) was added to the DH5α cells. The mixture was incubated on ice for 5 min. The mixture was spread onto the agar plates as quickly as possible and the plates were incubated at 37 °C overnight.

2.2.2.10 TOPO TA Cloning

One step cloning of PCR products were carried out using the TOPO TA Cloning kit from Invitrogen, according to the manufacturer's instructions. The principle behind one step Cloning is based on the non-template dependent activity of Taq polymerase that results in the addition of a single deoxyadenosine (A) to the 3' ends of the PCR products. The linearised cloning vector has single 3' deoxythymidine (T) residues therefore facilitating PCR inserts to ligate efficiently with the vector. The TOPO TA Cloning kit contains TOP 10 One Shot competent *E. coli* cells, Super Optimal Catabolite repression (SOC) media,

TOPO vector and salt solution. Prior to cloning, TOP10 cells were thawed on ice and LB agar plates (Section 2.1.2.2) containing 100 µg/ml Ampicillin (Section 2.1.6) pre-warmed in a 37 °C incubator. Genomic DNA PCR product (4 µl), Salt solution (1 µl) and TOPO vector (1 µl) were added to a sterile 0.5 ml tube and left at room temperature for 30 min. A 2 µl aliquot of this reaction mixture was added to a vial of TOP10 *E. coli* cells and placed on ice for 30 min. Cells were heat shocked at 42 °C for 30 s in a water bath and pre-warmed SOC media (200 µl) was added to the vial. The cell suspension was transferred to a 15 ml tube and incubated at 37 ºC for 1 h with constant agitation (200 rpm). During this incubation period, 32 µl of 5-bromo-4-chloro-3-indolyl-beta-D-galactopyranoside (X-gal) (Promega) (Southampton, UK) (40 mg/ml) was spread over the pre-warmed agar plates using a sterile glass spreader and the plates were returned to the incubator. This reagent facilitates blue/white colony screening which greatly aids in the identification of desired clones. A 50 µl aliquot of the cell suspension was spread on the selection plates using a sterile disposable spreader and the plates were incubated overnight at 37 °C. White colonies were selected and sub-cultured on to LB agar plates (Section 2.1.2.2) with Ampicillin (100 µg/ml) (Section 2.1.6). Restriction digest (Section 2.2.2.7) was carried out to verify the presence and orientation of the desired insert in the vector of the sample clones.

2.2.2.11 Small Scale Plasmid Purification

Plasmid purification was carried out according to the Qiagen Plasmid purification manual using the QIA prep Mini-prep kit. All buffers and columns were supplied with the kit and details of buffer constituents are outlined in the Qiagen Plasmid Purification Handbook. An isolated colony was picked aseptically and used to inoculate LB broth (Section 2.1.2.1) (10 ml) containing 100 µg/ml Ampicillin (Section 2.1.6). Cultures was grown overnight at 37 °C and the cells harvested by centrifugation at 13,000 x g for 10 min at 4 °C. Procedures were then carried out according to the manufacturer's guidelines. Purified

plasmids were subsequently analysed by restriction digestion followed by DNA gel electrophoresis (Section 2.2.2.3).

2.2.3 Generation of *A. fumigatus ΔgtmA* Mutant Strains

2.2.3.1 Generation of Constructs for *A. fumigatus gtmA* Gene Deletion

The bipartite gene disruption strategy was employed for the generation of *A. fumigatus* mutant strains in this study (Nielsen et al., 2006). Briefly, this strategy involved the generation of two constructs which each contain a partial fragment to the pyrithiamine (PT) resistance gene (*ptrA*) from *A. oryzae* (Kubodera et al., 2000) which is ligated to respective 5' and 3' flanking regions of A. fumigatus *gtmA*. This facilitates overlapping of the two constructs and reconstitution of the deletion cassette *in vivo*. The *ptrA* gene was excised from a plasmid vector pSK275 (a kind gift from Prof. Sven Krappmann, Göttingen, Germany), using two restriction enzymes. Both the 5' and 3' flanking regions of *A. fumigatus gtmA* were amplified from *A. fumigatus* genomic DNA by PCR (Section 2.2.2.2), where restriction sites were incorporated to the PCR products. This facilitates cloning of the PCR products to *ptrA*. About 1.0 – 1.2 kb of the flanking region were amplified. The resulting PCR products were digested with the same restriction enzymes as *ptrA* to make the ends compatible for ligation (Section 2.2.2.8). The ligation products were used as template for a subsequent second round of PCR, where nested primers amplified the majority of the flanking region and only a partial section of *ptrA*. Schematic representation of the bipartite gene deletion strategy is illustrated in (Chapter 3, Figure 3.1). All primers used in this study are listed in Table 2.4. Both first and second round PCR were performed with AccuTaq (Section 2.2.2.2). PCR products were extracted from 1 % (w/v) agarose gels and purified using a Qiagen gel extraction kit (Section 2.2.2.6). Successful transformation of *A. fumigatus* protoplasts generated potential *A. fumigatus* transformants which had the ability to grow on pyrithiamine (PT) selection plates. This ability only occurred with the successful integration of a fully reconstituted *ptrA*. These

transformants were then screened by Southern blot analysis where a single homologous integration of *ptrA* in place of *A. fumigatus gtmA* was desired.

2.2.3.2 Constructs for Complementation Transformations

To restore *A. fumigatus gtmA* back into the genome of *A. fumigatus* Δ*gtmA*, a construct containing a new selectable marker gene and the full *gtmA* sequence with the respective 5'and 3' flanking regions was generated. The primers used for the complemented construct are listed in Table 2.4. The *gtmA* coding sequence was PCR amplified from wild-type genomic DNA with Δ*gtmA*-P5 and Δ*gtmA*-P6. The PCR products were cloned into the TOPO vector. For the selection marker, the hygromycin resistance plasmid, pAN7-1 was used where the hygromycin resistance gene (*hph*) was excised using *BamH*I and *Mfe*I. This was then cloned into the topo*gtmA* plasmid via the single *EcoRII* site in this plasmid. A diagnostic restriction digest was performed using *NcoI* to confirm the correct orientation of *hph*. This vector, topo*gtmA*hph, was then linearised using a restriction enzyme that had a unique site in the sequence. In this case, *NotI* was chosen. The linearised plasmid was then transformed into protoplasts of *A. fumigatus* Δ*gtmA*. The selection marker used to complement *ΔgtmA* was *hph*. Hygromycin is also lethal to *A. fumigatus*, however with the insertion of *hph*, growth in the presence of hygromycin is possible. In this study it was possible to generate a complementation construct that contained both *gtmA* and *hph*, allowing for the targeted insertion of *hph* with *gtmA*.

2.2.3.3 *A. fumigatus* Protoplast Preparation

A. fumigatus conidia were harvested from 5 day old plates grown on AMM agar (Section 2.2.1.1). A 500 ml conical flask containing AMM medium (100 ml) (Section 2.1.1.6) was inoculated with *A. fumigatus* conidia. The culture was incubated overnight at 37 °C, whilst shaking at 200 rpm. The mycelia were harvested by filtering through sterile

miracloth and washed with sterile dH_2O. Excess water was removed by gentle blotting. Mycelia (1.5 g) was weighed out in duplicate, and each was added to 15 ml Lysis buffer (Section 2.1.9.4) containing lytic enzymes (Section 2.1.9.5). The tubes were inverted vigorously to ensure that all mycelial clumps were removed. The tubes were then incubated laying down flat at 30 °C while shaking at 100 rpm for 3 h. The samples were placed on ice for 5 min to inhibit the lytic enzymes therefore terminating the lysis. The mycelial solution was centrifuged at 132 x g for 18 min with the brake off. The supernatant was filtered through sterile filter paper and brought up to 40 ml with 0.7 M KCl (Section 2.1.9.1). The solution was centrifuged at 1769 x g for 12 min with the brake off. The supernatant was poured off and discarded. The pellet was resuspended in 10 ml 0.7 M KCl (Section 2.1.9.1). The solution was centrifuged at 1769 x g for 12 min with the brake off. The supernatant was poured off and discarded. The tubes were then left upside down on sterile tissue for 1 min. The pellet was resuspended in 70 µl of Buffer L6 (Section 2.1.9.6) by gentle pipetting and swirling the resuspended pellet. The samples were centrifuged at 58 x g for 1 min with the brake off to gather the entire protoplast suspension in the bottom of the tube. Duplicate protoplast solutions were pooled at this point. Finally, the protoplasts were viewed on a haemocytometer to ensure adequate yield and viability was assessed prior to the transformation. The protoplasts were stored on ice for up to 1 h before use in transformation experiments.

2.2.3.4 *A. fumigatus* Protoplast Transformation

For each transformation event approximately 5 µg of 5' and 3' constructs were mixed together in a 50 ml sterile tube and the final volume was brought up to 50 µl with Buffer L6 (Section 2.1.9.6). *A. fumigatus* protoplasts (150 µl), of at least 1 x 10^7 / ml were added to the constructs. Buffer L7 (50 µl) (Section 2.1.9.7) was added to the protoplast / DNA mixture. This was mixed by gentle swirling and placed on ice for 20 min. Once on ice. Buffer L7 (1 ml) (Section 2.1.9.7) was added to the mixture and left at room temperature

for 5 min, to allow for recovery of protoplasts. Buffer L6 (5 ml) (Section 2.1.9.6) was added, and the mixture was left on ice until required for plating. This incubation time on ice did not exceed 30 min. Control plates were set up simultaneously where Buffer L6 (185 µl) was added to *A. fumigatus* protoplasts (15 µl). The tube was swirled gently before the addition of Buffer L7 (50 µl).

2.2.3.5 Plating of Transformation Protoplasts

Regeneration agar (1.8% (w/v), 25 ml) (Section 2.1.1.9.1) containing pyrithiamine (0.1 µg/ml) or hygromycin (100 µg/ml) (Section 2.1.6) was poured into 90 mm petri dishes on the transformation day. These plates were stored at room temperature until required for use. For each transformation, six plates containing the selective reagent were prepared and two plates without this reagent were prepared. The two plates without the selective reagent were used for the protoplast viability check. For the negative control, protoplasts (1.25 ml) were added to a sterile tube, which was brought to 6 ml with the 0.7 % (w/v) regeneration agar (Section 2.1.1.9.2). This was then poured onto one of the transformation plates that contained the selective agent. For the protoplast viability control plate dilutions of the protoplasts were plated for a viable titration. To do this two protoplast dilutions were prepared in fresh 50 ml tubes. One of these contained 1.25 ml of the *A. fumigatus* protoplast suspension and the other contained 1.25 µl of the *A. fumigatus* protoplast suspension. Independently, the protoplast dilutions were brought to 6 ml with the 0.7 % (w/v) regeneration agar (Section 2.1.1.9.2). These were then separately poured onto transformation plates that contained no selective agent. Finally, transformed *A. fumigatus* protoplasts were topped up to 30 ml with the 0.7 % (w/v) regeneration agar. This was mixed by inversion once and then 5 ml was poured onto each of the five transformation plates that contained the selective agent. All the plates were left upright at room temperature overnight (as long as the room temperature did not drop below 20 °C).

2.2.3.6 Overlaying of Transformation Plates

0.7 % (w/v) regeneration agar (50 ml) (Section 2.1.1.9.2) containing pyrithiamine (0.1 µg/ml) or hygromycin (40 µg/ml) (Section 2.1.6) was mixed and 6 ml was poured over the 5 transformation plates, and the negative control plate. For the positive control plates, 6 ml of 0.7 % (w/v) regeneration agar (Section 2.1.1.9.2) without pyrithiamine or hygromycin was added to each of the plates. Once the agar had set, all the plates were incubated upside down in a 37 ^{o}C static incubator for approximately 5 – 7 days or until colonies were observed through the top of the overlay layer. The appearance of colonies on the protoplast viability plates after 2 – 3 days confirmed viable protoplasts had been generated.

2.2.3.7 Isolation of *A. fumigatus* Transformants after Transformation

Potential transformants exhibited the ability to grow on the transformation plates, which contained the selective agent. Spores from the transformants were picked aseptically from the transformation plates and point inoculated onto fresh selective plates (Section 2.1.1.1) which contained the selective agent (Section 2.1.6). The plates were then incubated at 37 °C in a static incubator until colonies were observed. The individual potential transformant colonies were aseptically excised from the plates by plugging with the base of a blue pipette tip. The plug was transferred to an Eppendorf tube containing PBST (750 µl) (Section 2.1.5). The tubes were then vortexed vigorously to release the conidia from the agar and into the solution. The conidial suspensions were stored at 4 ^{o}C until required. Putative transformant conidial suspensions (500 µl) were inoculated into Sabouraud Dextrose Broth (20 ml) in a 50 ml conical flask. The cultures were incubated overnight at 37 ^{o}C, whilst shaking at 200 rpm. The cultures were then harvested and DNA extraction (Section 2.2.2.1) was performed for Southern blot analysis (Section 2.2.4).

2.2.3.8 Single Spore Isolation of Transformant Colonies

Following a first round of Southern blot analysis, transformants which showed the correct signal on the Southern blot were selected for single spore isolation. This was to ensure that a transformant contained a homogenous single nucleus and that it was not a heterokaryon. Potential transformants were diluted by serial dilutions ranging from 10^{-2} to 10^{-6} in filter sterilised PBST (Section 2.1.5). One-hundred µl of the dilutions were spread onto AMM plates (Section 2.1.1.6) containing pyrithiamine (0.1 µg/ml) or hygromycin (100 µg/ml) (Section 2.1.6) and incubated at 37 °C in a static incubator until conidiation of colonies were observed. The individual colonies were numbered and isolated in PBST (Section 2.1.5) as described in Section 2.2.3.7 and were then subjected to a second round of Southern blot analysis (Section 2.2.4).

2.2.3.9 Synthesis of DIG-labelled Probes

The probes used in the Southern analysis (Table 2.2) were generated by PCR (Section 2.2.2.2) with the incorporation of DIG-labelled dNTP's. PCR products were resolved on a 1 % agarose gel and excised as previously described (Section 2.2.2.3). DNA was denatured by heating at 95 °C for 10 min on a heating block. The DNA was centrifuged for 1 min under a quick spin before it was placed on ice. The DNA (400 ng) was added to membrane pre-hybridisation buffer (10 ml) (Section 2.1.10.6.2) which had been pre-heated to 65 °C for at least 30 min. The probe was stored at – 20 °C and always heated at 65 °C for at least 30 min before use in Southern blot analysis.

2.2.4 Southern Blot Analysis

2.2.4.1 Southern Blot Analysis – DNA Transfer

Southern blot analysis was performed to determine whether the gene of interest has been deleted of replaced. Genomic DNA was isolated from the potential transformants (Section 2.2.2.1) and a restriction digest was performed using a suitable enzyme (Section 2.2.2.7).

The choice of enzyme depended on the sequence of the *A. fumigatus* wild-type and transformed strain. The enzyme of choice would cut upstream to the 5' or 3' flanking region and once within the gene of interest for the wild-type loci and it would also cut once within the replacement gene for the mutant loci. This digestion would generate one signal on the blot of different sizes in the wild-type and mutant strain. The digested DNA was resolved on 0.7 % (w/v) agarose gels (Section 2.2.2.3). After the digested DNA had resolved sufficiently. The gel was placed on a UV cross- linking machine (Strategene, La Jolla, CA) and pulsed at 800 KJ to nick the DNA which aids transfer to the nylon membrane. Following the DNA nicking the Southern tower was set up (Figure 2.3). A Bio-Rad electrophoresis tank was used for this procedure where the two reservoirs on each side of the tank were filled with Southern transfer buffer (Section 2.1.10.1). Two large sheets of Whatman filter paper were draped from reservoir to reservoir across the tank and left until they were soaked in the transfer buffer. On top of these, the DNA gel was placed with the loaded side face down. A piece of nylon membrane (H+ Bond Nylon Membrane, GE Electric) cut to the exact size of the gel was placed on top of the gel. Once contact was made with the gel, the membrane was not moved. Three pieces of filter paper cut to gel size were placed on top, followed by three stacks of pocket-sized tissue. A glass plate was placed on top of the stack and a duran bottle containing approximately 400 ml of water was used to balance the tower. The Southern blot was left overnight at room temperature (as long as room temperature was consistent and did not drop below 20 °C).

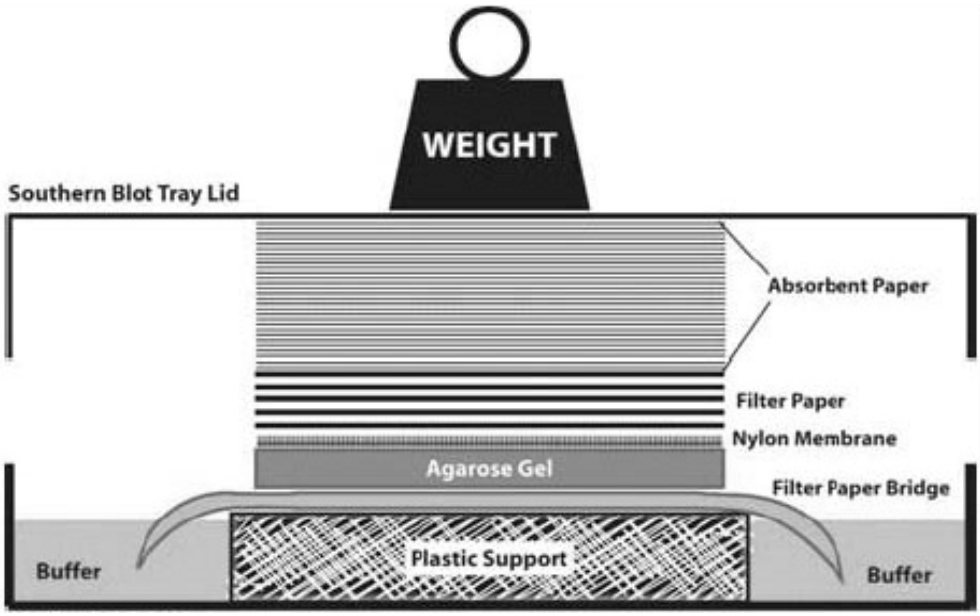

Figure 2.3. Schematic illustration of a Southern transfer tower.

2.2.4.2 Disassembly of the Southern Tower

The Southern Blot tower (Section 2.2.4.1) was taken apart and the membrane and gel were removed together and placed on a clean glass plate. The position of the wells was marked onto the corresponding place on the membrane, and the gel was peeled away from the membrane. The membrane was then washed in SSC buffer (2 X, 40 ml) (Section 2.1.10.3), and rocked gently for 10 min. The membrane was removed and placed on clean tissue paper to remove excess buffer. The membrane was then placed in a UV crosslinker (Strategene, La Jolla, CA) and crosslinked at 1200 μJ for 20 – 50 sec in order to fix the DNA onto the membrane.

2.2.4.3 Pre-hybridisation of the Nylon Membrane

After UV crosslinking the membrane was placed in a Hybaid tube (which had been heated to 42 °C) with the DNA side facing inwards. Pre-hybridisation buffer (20 ml) (Section 2.1.12.7.2), which had been heated to 65 °C was poured into the tube. The tubes were incubated at 42 °C in a Hybaid oven whilst rotating for 4 – 5 h to block the membrane.

2.2.4.4 Addition of DIG-labelled Probe to Southern Blots

After pre-hybridisation of Southern blots (Section 2.2.4.3), the pre- hybridisation buffer was removed. The DIG-labelled probe which had been heated to 65 °C was then poured into the tube. The tubes were then incubated overnight at 42 °C whilst rotating in a Hybaid oven to allow the probe to hybridise to regions of homology on the membrane. After probing the probe was removed from the tube and stored at – 20 °C.

2.2.4.5 DIG Detection

The membrane was removed from the Hybaid tube and washed with 0.1 % (w/v) SDS / 1 X SSC solution (Section 2.1.10.5) for 5 min. The Buffer was discarded and replaced again and the wash was repeated for another 5 min. The blot was placed in a clean Hybaid tube (which had been heated to 65 °C) and half filled with 0.1 % (w/v) SDS / 1 X SSC solution (Section 2.1.10.5). The membrane was rotated in the Hybaid oven for 15 min at 65 °C. The solution was discarded and replaced and the membrane was rotated for 15 min at 65 °C. Between each wash step the tubes were allowed to drip dry on clean tissue paper. The solution was poured off from the tube and DIG Wash Buffer (10 ml) (Section 2.1.10.6.6) was poured in with the membrane. The membrane was rotated for 5 min in the Hybaid oven at 25 °C. The buffer was poured off from the tube and the blots were blocked with Antibody Blocking buffer (Section 2.1.10.6.4) whilst rotating for 30 min at 25 °C. The Buffer was poured off from the tube and the Anti-Digoxigenin-Fab AP conjugate (10 ml) (Section 2.1.10.6.7) was added. The membrane was rotated for 30 min at 25 °C. The solution was poured off from the tube and DIG Wash Buffer (10 ml) (Section 2.1.10.6.6) was added to the tube. The membrane was rotated for 15 min at 25 °C. The wash step was repeated. The buffer was poured off from the tube and DIG Buffer 3 (10 ml) (Section 2.1.10.6.5) was added and the membrane was rotated at 25 °C for 5 min. The buffer was poured off from the tube and CSPD Substrate (5 ml) (Section

2.1.10.6.8) was added. The membrane was rotated at 25 °C for 5 min. The CSPD Substrate was collected from the tube covered in tinfoil and kept at 4 °C to be reused within one week. The membrane was removed from the Hybaid tube and placed on a clean tissue briefly. The membrane was carefully wrapped in a single layer of cling film and incubated at 37 °C for 15 min. This incubation step was performed to enhance the signal on the Southern blot.

2.2.4.6 Developing the Southern Blot membrane

The cling film wrapped membrane was taped into a photo developer case and an in the dark an X-ray film was placed over the membrane. Exposure time usually ranged between 1 – 3 h initially and an overnight exposure was usually performed also. After this, the X-ray film was removed from the case in complete darkness and placed into developer solution (Section 2.1.10.6.10) for a couple of seconds or until signals began to appear. The film was rinsed with water and then placed into Fixer Solution (Section 2.1.10.6.11). The film was then thoroughly rinsed with water and left to dry.

2.2.5 RNA Analysis

2.2.5.1 RNA Isolation

A. fumigatus liquid cultures which were incubated at the required temperature and time were filtered through autoclaved miracloth and the mycelia collected. Mycelia were then flash frozen in liquid Nitrogen and ground to a fine powder in a mortar by pestle. The RNA was isolated using the RNeasy plant mini kit supplied by Qiagen, according to the manufacturer's instructions. All buffers and columns were supplied with the kit, details of which are outlined in the kit handbook. β-mercaptoethanol (10 µl) was added to Buffer RLC (1 ml) before RNA extraction. For each sample, mycelia (100 mg) was placed in sterile microcentrifuge tubes. The procedure was then carried out as per manufacturer's guidelines. RNase-free water (50 µl) was added to the columns and the RNA was eluted

by centrifuging the column at 10,000 x g for 1 min. To increase RNA concentration, the eluent was passed through the RNeasy spin column for a second time and centrifuged at 10,000 x g for 1 min. The RNA samples were stored at – 20 °C up to 6 months and at – 70 °C long term.

2.2.5.2 DNase Treatment of RNA

A DNase kit (Sigma) was used to DNase treat RNA samples. RNA samples (Section 2.2.5.1) (500 ng) were adjusted to a final volume of 8 µl in Molecular Grade H_2O. 10 X Reaction Buffer (1 µl) and DNase (1 µl) were added to the RNA samples and the mixture was left to incubate at room temperature for 15 min. Stop Solution (1 µl) was added to the reaction and they were then incubated at 70 °C for 10 min. The samples were chilled on ice and stored at – 70 °C if not for immediate use.

2.2.5.3 cDNA Synthesis

cDNA synthesis was performed using the qScript™ cDNA SuperMix (Quanta BioSciences) using the supplied reagents in the kit and following the manufacturer's instructions.

2.2.5.4 Semi-quantitative RT-PCR

PCR was carried out on the cDNA samples (Section 2.2.5.3) as described in Section 2.2.2.3 using the primers 5' *gtmA* RT-PCR and 3' *gtmA* RT-PCR (Table 2.4). The *A. fumigatus* calmodulin (*calm*) gene (*Afu4g10050*) was used as a housekeeping gene (Burns et al., 2005)The primers calmF and calmR (Table 2.4) span an intronic region in *calm*, resulting in an amplicon size of 617 bp from gDNA and an amplicon size of 314 bp from cDNA. This allows the detection of any contaminating gDNA in the cDNA samples. The RT-PCR amplicons were resolved on a 2 % (w/v) Agarose Gel (Section 2.1.8.1.6) and visualised using a Syngene G:Box.

2.2.6 *A. fumigatus* Plate Assays

A. fumigatus wild-type and mutant strains were grown on MEA agar for 5 days at 37 °C after which conidia were harvested (Section 2.2.1.1). Conidia was serially diluted to 10^{-2} and 10^{-4} in PBS. Aliquots (5 µl) of each dilution was spotted onto agar plates containing various additives (Section 2.1.6). Plates were incubated at 37 °C and growth was monitored at specific time intervals by measuring the diameter of radial growth (cm) of each colony. Two-way ANOVA analysis was performed to determine the statistical significance between strains on the various additives.

2.2.7 GtmA Recombinant Expression in *E. coli* using PEX-N-GST and Pet19m

The PCR product of the *gtmA* gene was integrated into the expression vectors PEX-N-GST (Figure 2.4) and Pet19m by linearising the vector within the multiple cloning site and ligation of the free ends of the linearised vector and the digested PCR product together. The orientation of the ligation was restricted to only the correct one by ensuring that that linearizing digestion was conducted with two incompatible enzymes. The PCR that created the *gtmA* product had add-on nucleotides that ensured that the ligation did not shift any of the subsequential amino acid expression.

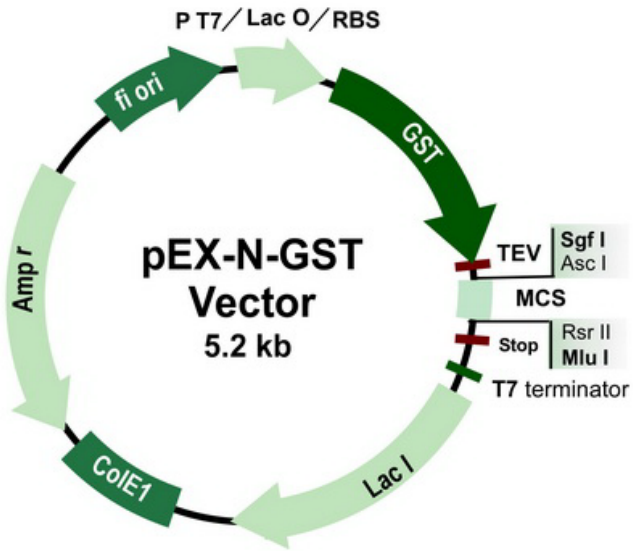

Figure 2.4. pEX-N-GST Vector for GST-GtmA Expression

2.2.7.1 Small scale induction of the recombinant pEX-N-GST-GtmA and Pet19m-GtmA

Once it was verified that the pEX-N-GST-GtmA vector had transformed correctly into *E. coli*, small-scale inductions were carried out to confirm GtmA production. A 10 ml LB broth (Section 2.1.2.1) culture was set up containing 100 µg/ml ampicillin (Section 2.1.6) which was then inoculated with the pEX-N-GST-GtmA plasmid and incubated overnight at 37 °C whilst shaking at 200 rpm. This culture was then used to inoculate a 50 ml LB broth culture (Section 2.1.2.1) containing 100 µg/ml ampicillin (Section 2.1.6). The culture was incubated at 37 °C whilst shaking at 200 rpm until an OD_{600} value of 0.5 – 0.7 was reached. Once the culture had reached the target growth level, a 1 ml aliquot was removed and kept as an un-induced aliquot used for reference. The expression was induced by adding IPTG (1 M stock) to a final concentration of 1 mM and the culture was incubated further, and at the time points, 1, 2 and 3 h, 1 ml aliquots were removed, and kept as post induced time-point samples. The remaining culture was centrifuged at 3200 x *g* at 4 ºC, for 20 min and the sample aliquots were centrifuged at 17900 x *g* for 1 min. The supernatants were discarded and the pellets were kept at -20 °C until required.

2.2.7.2 Site-Directed Mutagenesis

The previously described vector Pet19m_gtmA (Section 2.2.7) served as a template for *in vitro* site-directed mutagenesis using the QuikChange® XL Site-Directed Mutagenesis Kit (Stratagene) and oligonucleotides listed in Table 2.4. Mutagenesis was carried out as stated in the supplied protocol. Hereby, the plasmids Pet19m_GtmA_W157V, Pet19m_GtmA_W162V, Pet19m_GtmA_N159V, Pet19m_GtmA_F185G and Pet19m_GtmA_F127V were created. The resulting plasmids were propagated in *E. coli* DH5α cells. The DNA sequence was verified by sequencing and the vectors were

introduced into *E. coli* BL21(DE3) cells for protein overproduction as described in Section 2.2.7.1.

2.2.7.3 Protein extraction from pEX-N-GST-GtmA cultures

Lysis Buffer (9 ml) (Section 2.1.11) was added to every 2 g of pelleted cells. The samples were sonicated whilst sitting on ice. Lysozyme (80 µl) (Section 9.1.22.3) was added per 2 g of pellet, and the sample was incubated at 20 ^{o}C for 1 h constantly shaking. The samples were sonicated on ice. The samples were centrifuged at 12000 x g for 10 min at 4 ^{o}C. An aliquot (1 ml) was removed from the supernatant, and the rest of the supernatant was discarded. The pellets were resuspended in 1X Solubilisation buffer (Section 2.1.15.5) per original 1 g. The samples and aliquots were stored at -20 ^{o}C until required.

2.2.8 Analysis of GtmA-eGFP by Confocal Microscopy

The *gtmA*-eGFP strain transformed with H2A::mRFP (1x10^{4} conidia) was inoculated into 400 µl Czapeks dox media in a Lab-Tek Chambered Borosilicate Coverglass System. The chamber was incubated at 37°C for 21h and then gliotoxin (5 µg/ml final) was added to the chambers. An equivalent volume of MeOH was added to the control wells. As a second control a well containing Δ*gtmA* with gliotoxin was also prepared. Samples were viewed with an Olympus Flouview 1000 confocal microscope under the supervision of Dr. Ica Dix, Biology Dept., Maynooth University.

2.2.9 Sequence data and phylogenetic methods

The fungal protein dataset consisted of 103 genomes and 1001217 individual genes. Information on the sources of genome data are as in (Medina et al., 2011)). Using BlastP (Altschul et al., 1997), with an expectation (E) value of 10^{-5}, *A. fumigatus* GtmA (AFUA_2G11120) was searched against each individual fungal genome to locate all putative fungal homologs. Top significant hits were also searched back against the *A.*

fumigatus genome and reciprocal top hits to *A. fumigatus* GtmA were putatively labelled as orthologs. All GtmA homologs were aligned using MUSCLE (Edgar, 2004), with the default settings. Obvious alignment ambiguities were manually corrected. Phylogenetic relationships were inferred using maximum likelihood methods and the appropriate protein models of substitution were selected using the Bayesian information criterion implemented in ProtTest (Darriba et al., 2011). One hundred bootstrap replicates were then carried out with the appropriate protein model using the software program PHYML (Guindon and Gascuel, 2003) and summarized using the majority-rule consensus method.

2.2.10 Protein Characterisation Methods

2.2.10.1 Bradford Protein Assay

Bio-Rad protein assay dye was diluted 1/5 in sample buffer prior to use. The sample to be assayed was also diluted appropriately. 20 µl of the sample was added to 980 µl of the diluted Bio-Rad protein assay dye and mixed thoroughly. The final sample (1 ml) was transferred to a 1 ml plastic cuvette and incubated for 5 min at room temperature. The absorbance at 595nm was read relative to a blank and the protein concentration was determined based on values obtained from a standard curve. All samples were prepared and analysed in duplicate.

2.2.10.2 Sodium Dodecyl Sulphate Polyacrylamide Gel Electrophoresis (SDS-PAGE)

SDS-PAGE gels, both stacking and resolving, were prepared according to Table 2.5 and Table 2.6 respectively. The gels were cast using the Mini-Protean II gel casting apparatus (BioRad, CA, USA) according to the manufacturer's guidelines. Samples were prepared by adding one volume of 5X solubilisation buffer (Section 2.1.15.5) to every 4 volumes of sample in a 1.5 ml microfuge tube. The samples were boiled for 5 min and centrifuged briefly to collect the sample to the bottom of the tube. An appropriate volume of sample

was loaded onto the gel. A molecular mass marker was run alongside samples in order to estimate the relative size of observed proteins. The molecular mass marker used throughout this study ranged from 10-170 kDa (SM0671, Fermentas, Figure 2.5). The electrophoresis tank was filled with 1X SDS electrode running buffer (Section 2.1.15.7). Electrophoresis was carried out initially at 80 V for 30 min, followed by electrophoresis at 120 V until the dye front reached the bottom of the gel.

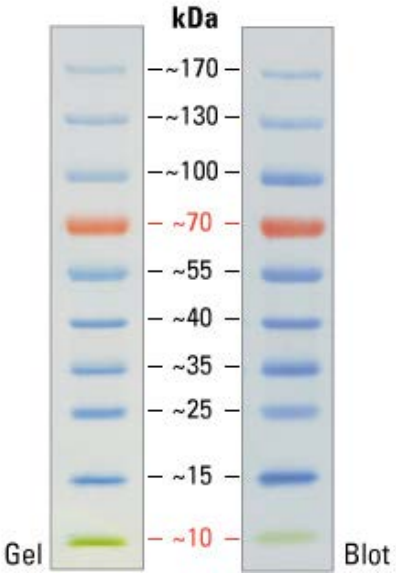

Figure 2.5. Protein ladder used in this thesis - Fermentas PageRuler™ Prestained Protein Ladder

Table 2.5. Reagents composition for SDS-PAGE Resolving Gels.

% Acrylamide	***10%***	***10%***	***12%***	***12%***	***15%***
Number of Minigels	5	8	5	8	5
1.5 M Tris-HCl pH 8.3	7.0 ml	10.5 ml	7.0 ml	10.5 ml	7.0 ml
10 % SDS	280 µl	420 µl	280 µl	420 µl	280 µl
30 % Acrylamide, 0.8 % Methylene bis Acrylamide	9.3 ml	13.9 ml	11.3 ml	16.9 ml	13.9 ml
Distilled water	12.3 ml	18.4 ml	9.3 ml	13.9 ml	6.3 ml
10 % Ammonium persulfate	100 µl	150 µl	100 µl	150 µl	100 µl

TEMED	23 µl	35 µl	23 µl	35 µl	23 µl

Table 2.6. Reagents composition for SDS-PAGE Stacking Gels.

Number of Minigels	2	5	8
0.5 M Tris-HCl pH 6.8	2.5 ml	4.0 ml	5.2 ml
10 % SDS	100 µl	160 µl	210 µl
30 % Acrylamide, 0.8 % Methylene bis Acrylamide	1.0 ml	1.5 ml	2.0 ml
Distilled water	6.4 ml	9.6 ml	12.8 ml
10 % Ammonium persulfate	100 µl	150 µl	200 µl
TEMED	10 µl	15 µl	20 µl

2.2.10.3 Semi-dry transfer of proteins to NCP

Nitrocellulose paper (NCP) and six sheets of filter paper were cut to the appropriate size of the gel and pre-soaked in Towbin Transfer Buffer (Section 2.1.15.10) for 15 min. The protein gels were removed carefully from the electrophoresis unit and assembled on the transfer unit in a NCP "sandwich" consisting of 3 sheets of saturated filter paper, soaked NCP, protein gel and an additional 3 sheets of saturated filter paper. Transfer was carried out at 18 V for 20 min using a semi-dry transfer unit. Ponceau S solution was applied to NCP to detect protein transfer with excess stain removed through washing with dH_2O.

2.2.10.4 Western Blot Analysis

Protein transferred to NCP using semi-dry transfer (Section 2.2.10.3) was used to carry out Western blot analysis. Blocking buffer (Section 2.1.15.11) was applied to the NCP and incubated for 1 h at room temperature with gentle rocking. The blocking buffer was poured off the blot and primary antibody, diluted in Antibody buffer (Section 2.1.15.12),

was added to the blot. This was incubated for 1 h at room temperature with gentle rocking. Three 10 min PBST (Section 2.1.5) washes were carried out on the blot. The secondary antibody was diluted in antibody buffer (Section 2.1.15.12) and incubated with the blot for 1 h at room temperature with gentle rocking. Three 10 min PBST washes were carried out and the blot was developed using 3, 3'-diaminobenzidine tetrachloride hydrate (DAB) (10 mg) was dissolved in DAB Substrate buffer (Section 2.1.15.13) (15 ml). Hydrogen peroxide (7 µl) was added to the substrate solution which was then applied to blots. Blots were allowed to develop for 10 min and dH_2O was applied to stop the reaction and reduce background staining.

2.2.10.5 Dialysis of protein samples

Dialysis tubing was pre-soaked in the appropriate buffer for 10 min. Protein sample was added to the dialysis tubing with an additional 50% free space included to allow for sample volume expansion. The sealed tubing, containing the sample, was dialysed against 50 volumes. Dialysis was carried out at 4 °C with stirring. A minimum of three buffer changes were carried out at 3 h intervals.

2.2.11 AKTA FPLC Methods

2.2.11.1 Glutathione Sepharose Affinity Chromatography

Glutathione Sepharose Affinity Chromatography was carried out using an ÄKTA purifier coupled with a XK 16/20 column (GE Healthcare, Germany) packed with 10 ml Glutathione Sepharose 4B (GE Healthcare, Germany). The column was first equilibrated with 2 column volumes (CV) of Equilibration/Wash Buffer (Section 2.1.14.2) at a flow rate of 4 ml/min. *E. coli* cell lysates containing GST-GtmA were passed through a 0.45 µm syringe filter to remove particulate matter then passed over the GSH-Sepharose column at 1 ml/min. As the GSH-GST interaction is flow-rate dependent, the flow-rate was not increased higher than 1 ml/min during binding to maximise the resin capacity.

After all the lysate was loaded the column was washed with 3 CV of Equilibration/Wash Buffer (Section 2.1.14.2) at 4 ml/min. The absorbance was monitored at 280 nm to ensure that it returned to the baseline after the wash step. The GST-GtmA was then eluted from the column using 3 CV of Sample Elution Buffer (Section 2.1.14.2) and the eluted GST-GtmA was collected in 1 ml fractions. Fractions containing protein were pooled and analysed using SDS-PAGE.

2.2.11.2 Anion Exchange Chromatography

Anion Exchange Chromatography was carried out using an ÄKTA purifier coupled with (i) a XK 16/20 column (GE Healthcare, Germany) packed with 10 ml Q-Sepharose High Performance (GE Healthcare, Germany). The column was first equilibrated with 2 column volumes (CV) of Equilibration/Wash Buffer (Section 2.1.14.2) at a flow rate of 2 ml/min. A solution containing TEV cleaved GST and GtmA was injected onto the Q-Sepharose column at 1 ml/min. After all the sample was loaded the column was washed with 2 CV of Equilibration/Wash Buffer (Section 2.1.14.2) at 2 ml/min. The absorbance was monitored at 280 nm to ensure that it returned to the baseline after the wash step. A linear gradient of 0-60 % Elution Buffer (Section 2.1.14.2) over 30 min was then used to elute the protein from the column. Due to their different isoelectric points, the GtmA and GST were eluted from the column as two separate peaks. The eluted GtmA was collected in .5 ml fractions. Fractions containing GtmA were pooled and analysed using SDS-PAGE.

2.2.11.3 Gel Filtration Chromatography

Gel filtration chromatography was carried out using an ÄKTA purifier coupled with a Superdex 200 10/300 GL column (GE Healthcare, Germany). Lines were purged prior to use and the column was equilibrated with GtmA Gel Filtration Buffer (Section 2.1.14.4). Samples were centrifuged at 10000 x *g* for 10 min to remove particulates prior to injection

onto column. A selection of molecular weight calibrants were applied to the column in order to prepare a standard curve based on molecular weight versus elution volume (Ve) (Section 2.1.14.1). The flow rate was set to 0.2 ml/min, with absorbance monitored at 215, 254 and 280 nm. Fractions were collected if required for further analysis.

2.2.12 Small Scale Organic Extraction of *A. fumigatus* Culture Supernatants

A. fumigatus culture supernatants (20 ml) were added to chloroform (20 ml) in 50 ml Falcon tubes. The mixtures were then placed on a rotating wheel for 1 h. The mixtures were removed and centrifuged for 10 min at 2000 x *g*. The top aqueous layers were removed and discarded and the bottom organic layers were stored at -20 ^{o}C until required.

2.2.13 Rotary evaporation of Organic Extraction Samples

Organic extracts (Section 2.2.12) were placed in an evaporation bulb and the bulb was evaporated under vacuum whilst sitting in a water bath set to 37 ^{o}C (Stuart RE300DB digital water bath). The chloroform evaporated leaving the dried organic extract in the bulb. The extracts were resuspended in HPLC grade methanol (200 – 500 µl) until all the dried material was fully resuspended. The resuspended extract was centrifuged at 13,000 x *g* for 5 min and then transferred to clean 1.5 ml eppendorf and stored at – 20 ^{o}C.

2.2.14 S-Adenosyl Methionine (SAM) Extraction and Quantification in *A. fumigatus*

Czapeks Dox media was inoculated with 10^6/ml conidia in triplicate, and incubated at 37 °C, shaking 200 rpm, for 21 h. Gliotoxin (5 µg/ml final) or methanol control was added and the cultures were incubated for a further 3 h before mycelia were harvested and snap frozen in liquid N_2. Mycelia was then ground to a fine powder using a pestle and mortar (Section 2.2.2.1). 100 mg of ground mycelia was weighed into an eppendorf and 250 µl of 0.1 M HCl (Section 2.1.12) was added to the sample. The sample was vortexed and incubated on ice for 60 min, with regular vortexing. The sample was then centrifuged at

13,000 x *g* for 10 min at 4 °C. The supernatant was transferred to a new eppendorf. Protein was removed from the supernatant by TCA precipitation (10% final TCA). Samples were diluted in 0.1 % (v/v) formic acid and analysed by LC-MS/MS using a porous graphitized carbon (PGC) Chip on an Agilent 6340 Ion-trap LC Mass Spectrometer (Agilent Technologies) using electrospray ionization. Quantification was enabled using commercially available SAM obtained from Sigma-Aldrich.

2.2.15 Metabolome Analysis using RP - HPLC

Organic extracts from supernatants (Section 2.2.13) were analysed by RP-HPLC with UV detection (Agilent 1200 system), using a C18 RP-HPLC column (Agilent Zorbax Eclipse XDB-C18 Semi-Preparative; 5 mm particle size; 4.6 x 250 mm) at a flow rate of 1 ml/min. A mobile phase of water (Section 2.1.13.1.1) and acetonitrile (Section 2.1.13.1.2) with TFA, was used under various gradient conditions. Injection volume was either 20 or 100 µl.

2.2.16 Mass Spectrometry Methods

2.2.16.1 In-gel Digestion of SDS-PAGE Samples

In-gel digestion of SDS-PAGE samples was carried out according to the protocol of (Shevchenko et al., 2006). Briefly, selected bands or spots from SDS-PAGE gels were excised and placed in individual 1.5 ml microfuge tubes. Gel pieces were destained by the addition of 100 µl of 100 mM ammonium bicarbonate (Section 2.1.16.5): acetonitrile (1:1 v/v). Samples were vortexed periodically for 30 min. Acetonitrile (500 µl) was added to samples, followed by vortexing until the gel pieces became white and shrunk. Acetonitrile was removed and replaced with 50 µl of trypsin, diluted to 13 ng/µl in trypsin buffer (Section 2.1.16.10). Samples were incubated at 4 °C for 2 h, with additional trypsin added to cover gel pieces if required. Samples were then incubated at 37 °C overnight. Gel pieces were subsequently placed in a sonication bath for 10 min followed by transfer

of the digest supernatant to fresh microfuge tubes. Samples were dried to completion using a speedy vac (DNA Speedy Vac Concentrator, Thermo Scientific) and resuspended in 0.1% formic acid (Section 2.1.3.8) (20 µl). The samples were filtered through 0.22 µm Cellulose Spin-filters (Costar) before transfer to polypropylene vials. Care was taken to ensure there was no air trapped in the vials.

2.2.16.2 LC-MS/MS Analysis of Peptide Mixtures

Peptide mixtures generated from in-gel digestion of protein spots or bands from SDS-PAGE (Section 2.2.16.1) were analysed using a 6340 Model Ion Trap LC-Mass Spectrometer (Agilent Technologies, Ireland) using electrospray ionisation. Samples (1 - 5 µl) were loaded onto a Zorbax 300 SB C-18 Nano-HPLC Chip (150 mm x 75 µm) with 0.1 % (v/v) formic acid at a flow rate of 4 µl/min. Peptides were eluted using the appropriate gradient with a post run of 5 min. The eluted peptides were ionised and analysed by the mass spectrometer. MSn analysis was carried out on the 3 most abundant peptide precursor ions at each time point, as selected automatically by the mass spectrometer. Singly charged ions were excluded from analysis by the mass spectrometer.

2.2.16.3 Database Search

MASCOT MS/MS Ion search, with interrogation of the NCBI (National Centre for Biotechnology Information, **http://www.ncbi.nlm.nih.gov**) database, was used for protein identification. Criterion for each search was set at (i) Taxonomy: Fungi, (ii) two missed cleavages by trypsin, (iii) fixed modification: carboxymethylation of cysteines, (iv) variable modification: oxidation of methionine, (i) mass tolerance of precursor ions ± 2Da and product ions ± 1Da.

2.2.16.4 LC-MS/MS Analysis of *A. fumigatus* Metabolites

Metabolites isolated by (i) organic extraction from culture supernatants of *A. fumigatus* (Section 2.2.12) or (ii) fractionation following RP-HPLC analysis were analysed by LC-

MS/MS. Samples were diluted in 0.1 % (v/v) formic acid (Section 2.1.16.11) prior to mass spectrometry and were loaded onto a Zorbax 300 SB C-18 Nano-HPLC Chip (150 mm x 75 µm) at a flow rate of 4 µl/min. Metabolites were eluted using the appropriate gradient with a post run of 5 min. MSn was carried out on the 3 most abundant precursor ions at each timepoint, with n ranging from 2 to 5, depending on the analysis. Singly charged ions were not excluded from analysis, with the precursor range adjusted to include ions with m/z between 15 and 2200.

2.2.16.5 Q-Exactive Mass Spectrometry

2.2.16.5.1 *A. fumigatus* Protein Extraction for Q-Exactive Mass Spectrometry

Harvested mycelia was snap frozen in liquid nitrogen and crushed into a fine powder using liquid nitrogen and a pestle. Mycelia powder (200 mg) was weighed into a 2 ml tube. Excess mycelial powder was collected and stored immediately at -70 °C. *A. fumigatus* Whole Protein Lysate Extraction Buffer (Section 2.1.16.1) (500 µl) was added to the mycelial powder. The suspension was sonicated using sonication probe MS72 at 10% power, cycle 6 for 10 sec. This was repeated two more times with the sample being cooled on ice between each sonication. The suspension was then sonicated using sonication probe MS73 at 10% power, cycle 6 for 10 sec. Lysates were incubated on ice for 1 h, followed by centrifugation at 12,000 x *g* for 10 min at 4 °C. The supernatants were transferred to new tubes and the centrifugation step was repeated to obtain clarified lysates. A Bradford assay was carried out to determine the protein concentration in each sample. Samples (1 mg) were brought to 15 % TCA by addition of the appropriate volume of cold 100 % TCA solution (Section 2.1.16.4), vortexed briefly, and incubated on ice for 30 min. Samples were centrifuged at 12,000 x *g*, 10 min, 4 °C and the supernatant was discarded. 500 µl of ice-cold acetone was added to the protein pellet, this was pipetted briefly and incubated at -20 °C for 2 h. Samples were centrifuged at 12,000 x *g*, 10 min, 4 °C and the supernatant was discarded. Pellets were washed twice with 500 µl of ice-

cold acetone. Acetone was removed after the final wash and the pellet was allowed to dry for no more than 5 min before resuspension with 80 µl of Protein Resuspension Buffer. A Bradford assay (Section 2.2.10.1) was carried out to determine the protein concentration in each sample.

2.2.16.5.2 Protein Digestion for Q-Exactive Mass Spectrometry

Samples (15 µl; 50 µg) in Protein Resuspension Buffer (Section 2.1.16.8) were brought to room temperature for 10 min to ensure urea was in solution. Ammonium bicarbonate (78.5 µl; 50 mM) was added to the samples. 1 µl DTT was added to the samples, followed by incubation at 56 °C for 20 min. Samples were allowed to cool to room temperature and 2.7 µl of IAA (Section 2.1.16.7) was added, followed by incubation at room temperature for 15 min in the dark. Following reduction and alkylation, 1 µl of ProteaseMAX stock and 1.8 µl of trypsin were added to each of the samples, followed by incubation at 37 °C overnight. The next day samples were spun briefly to collect any condensate and acidified by adding 1 µl of TFA, vortexed briefly, and incubated at room temperature for 5 min. Samples were centrifuged at 13,000 x *g* for 10 min at room temperature and the supernatant was aliquoted into 0.2 ml tubes and snap-frozen in liquid nitrogen. Samples were stored at -20 °C.

2.2.16.5.3 ZipTip® Pipette Tip Protocol

The sample was first resuspended with 20 µl Resuspension Buffer and sonicated for 2 minutes in a sonication bath to help resuspend the pellet. The sample was then centrifuged briefly. The ZipTip was then wet by aspirating and dispensing 10 µl wetting solution into the tip. This step was repeated 5 times. The ZipTip was then equilibrated by aspirating and dispensing 10 µl Equilibration Solution onto the tip. This was repeated 5 times. To bind the sample to the ZipTip, 10 µl of the resuspended sample was aspirated and dispensed. This step was repeated 10 times. The ZipTip was then washed by aspirating

and dispensing 10 µl of Washing Solution from the tip to a waste eppendorf. This step was repeated 5 times. To elute the peptide sample from the ZipTip 10 µl of Elution Solution was aspirated and dispensed from the tip into a new 1.5 ml eppendorf. This step was repeated 5 times. The eluted sample was then dried down with a SpeedVac and resuspended in 15 µl Q-Exactive Loading Buffer. The samples were stored at 4 °C until analysis.

Table 2.7. Solutions for ZipTip Protocol

Solution	Composition	Volume (µl) Acetonitrile	Volume (µl) ddH_2O	Volume (µl) TFA	Total Volume (µl)
Resuspension Buffer	0.5% TFA in ddH_2O	0	995	5	1000
Equilibration & Washing Solution	0.1% TFA in ddH2O	0	999	1	1000
Wetting Solution	0.1% TFA in 80% Acetonitrile	800	199	1	1000
Elution Solution	0.1% TFA in 60% Acetonitrile	600	399	1	1000

2.2.16.5.4 *A fumigatus* Q-Exactive Mass Spectrometry Method

All peptide mixtures were analysed via a Thermo Fisher Q-Exactive mass spectrometer coupled to a Dionex RSLCnano. LC gradients ran from 4-35 %B over 2 h, and data was collected using a Top15 method for MS/MS scans. Comparative proteome abundance and data analysis was performed using MaxQuant software (Version 1.3.0.5) (Cox and Mann, 2008), with Andromeda used for database searching and Perseus used to organise the data (Version 1.4.1.3). Carbamidomethylation of cysteines was set as a fixed modification, while oxidation of methionines and acetylation of N-termini were set as variable modifications. The maximum peptide/protein false discovery rates (FDR) were set to 1% based on comparison to a reverse database. The Label-Free Quantification (LFQ) algorithm was used to generate normalised spectral intensities and infer relative protein

abundance. Proteins that matched to a contaminants database or the reverse database were removed and proteins were only retained in final analysis if detected in at least three replicates from at least one sample. Quantitative analysis was performed using a t-test to compare pairs of samples, and proteins with significant change in abundance (*p* value <0.05; fold change ≥2) were included in the quantitative results. Qualitative analysis was also performed, to detect proteins that were found in at least 3 replicates of a particular condition, but undetectable in the other sample condition.

2.2.17 Gliotoxin Feeding Experiments Using *A. fumigatus*

A. fumigatus strains were cultured in Sabouraud dextrose broth (25 ml) at 37 ^{o}C, for 21 h. At 21 h the gliotoxin related metabolite was added to the cultures, and a 1 ml aliquot of the supernatant was removed. Cultures were incubated for a further 15, 60 and 180 min and an aliquot (1 ml) of the supernatant was removed at each time point. A control sample was treated the same except nothing was spiked into the culture. The 1 ml aliquots of supernatant from each time point were subjected to organic extraction (Section 2.2.12) at a 1:1 ratio of chloroform. The organic extracts were dried overnight in a fume hood until all chloroform had evaporated. The dried extract was resuspended in HPLC grade methanol (50 µl). Extracts (1 µl) were then analysed by LC-MS (Section 2.2.16.4) to determine whether the gliotoxin related metabolite had been taken up or converted by *A. fumigatus.*

2.2.18 Generation of mono(methylthio)gliotoxin (MmGT) using Methyl Iodide

5 mg gliotoxin (3 mg/ml in MeOH) was reduced to dithiol gliotoxin with 50 µl TCEP Bond-Breaker Solution. 5 µl Maleimide Conjugation Buffer (0.083 M sodium phosphate, 0.1M EDTA, 0.9 M NaCl, pH 7.2) was added to minimise sulfhydral oxidation to disulfides during the methylation reaction. The sample was evaporated in a Speedivac for 30 min at medium heat to 400 µl. 30 µl Iodomethane (0.5 M in MeOH) was then added

to the dithiol GT. The sample was then covered in aluminium foil to protect from the light an incubated at room temperature for 20 min with gentle shaking.

2.2.19 Mono(methylthio)gliotoxin Conjugate Generation

Lyophilised maleimide KLH (Pierce) or sulfo-SMCC BSA (Pierce) was resuspended at 1 mg/ml in degassed ddH_2O. 500 µl of the MmGT solution was immediately added dropwise to 5 mg of the maleimide KLH or sulfo-SMCC BSA. The reaction was left to incubate overnight at room temperature. The sample was then centrifuged at 13,000 x *g* for 2 min to remove precipitated immunogen. This precipitate was then combined with the final sample for immunisation. The MmGT-KLH sample was concentrated to 1 mg/ml using an Amicon Ultra Centrifugal Filter Unit (Merck Millipore).

2.2.20 Optimisation of MmGT-BSA Antigen ELISA Plate Coating Concentration and Sera Dilutions

Microtitre plates were coated with a titred range of MmGT-BSA concentrations, starting x gat 2 µg/ml, and double diluted down to 0.015 µg/ml. Control plates were also prepared coated with a titred range of SMCC-BSA. Plates were sealed and incubated overnight at 37 °C for 2 h. Plates were then washed using a plate washer (Programme: BTL4: 4 X 300 µl) with ELISA Wash Buffer (Section 2.1.17.2). The residual Wash Buffer was tapped out of the wells. 200 µl Blocking Solution (Section 2.1.17.5) was added to each well and the plates were incubated at 37 °C for 2 h. The blocking buffer was removed from the wells and plates were inverted and dried for 2 h at 37 °C. MmGT-KLH antisera (from mice A-C) was diluted in ELISA Sera and Calibrator Diluent (Section 2.1.17.3) at various dilutions. 100 µM BmGT was prepared in this buffer also. An antigen control was prepared by adding 1.2 % DMSO to ELISA Sera and Calibrator Diluent. 50 µl 100 µM MmGT or 1.2 % DMSO in diluent was added to the corresponding wells followed by 50 µl of the sera dilutions. The plates were incubated at 37 °C for 1 h. Plates were then

washed using the plate washer (BTL4) and 100 µl Anti-Mouse IgG-HRP diluted 1/2000 in antibody diluent was added to each well. Plates were incubated while sealed at 37° for 1 h. Plates were washed with using the plate washer (BTL4) and tapped on tissue to remove excess wash buffer. 100 µl TMB Substrate (pre-incubated at R.T for 30 min) was then added to each well. The plates were incubated at room temperature for 10 min. The reaction was terminated by the addition of 100 µl ELISA stop solution (Section 2.1.17.6). The absorbance was measured at wavelengths of 450 and 630 nm. The optimum coating concentration was determined for the MmGT-BSA antigen based on consistent absorbance values which fell within the dynamic range of the assay.

2.2.21 Statistical Analysis

All data was analysed using built-in GraphPad prism version 5.01 functions, as specified. The level of significance was set at $p < 0.05$ (*), $p < 0.001$ (**), and $p < 0.0001$ (***), unless otherwise stated. Post-hoc comparisons between groups were performed using the Bonferroni multiple comparisons test, unless otherwise stated.

2.2.22 Software Graphing

All graphs were compiled using Graphpad Prism version 5.01, unless otherwise stated.

Chapter 3

Genetic modification of Afu2g11120 (*gtmA*) in *A. fumigatus*

3.1 Introduction

ETP bis-thiomethylation is a widespread mechanism found in filamentous fungi which produce these disulfide containing metabolites. However, the enzyme which is responsible for this process has remained elusive (Boente and Kirby, 1991; Tan et al., 2004; Guo et al., 2009; Park et al., 2011). In addition, although O, C and N-directed methyltransferases are routinely identified and characterised within fungal secondary metabolite pathways, S-directed methyltransferases have been largely unexplored (Liscombe et al., 2012). *S*-methyltransferases have only been definitively classified in relation to detoxification mechanisms and primary metabolism, although this activity has long been implicated in numerous secondary metabolite pathways (Boente and Kirby, 1991; Kirby et al., 1980; Taylor, 1963). Recently, the *Streptomyces lasaliensis S*-adenosyl-L-methionine (SAM) dependent methyltransferase *Ecm18* has been shown to catalyze the conversion of a disulfide bond in the precursor antibiotic triostatin A to the thioacetal bridge of the nonribosomal dipsipeptide echinomycin (Hotta et al., 2014). This appears to be the only published example of thiol-directed methyltransferase involvement in secondary metabolism.

S-methylation of dithiol metabolites also extends to bacteria; *Streptomyces clavuligerus* has been shown to produce a *bis*-thiomethylated derivative of the dithiolpyrrolone antibiotic, holomycin (Li et al., 2012). This thiomethylation mechanism has been posited as an additional or backup strategy to disulfide bridge closure for self-protection during holomycin biosynthesis. It has been proposed that *S*-methylation of biosynthetic intermediates, or possibly shunt metabolites, protect cellular components against these reactive species (Guo et al., 2013; Li et al., 2012).

Prior to the work described in this chapter, an RNA-Seq analysis identified three methyltransferases which were highly increased in expression following gliotoxin

exposure (O'Keeffe et al., 2014). The identification of an uncharacterised methyltransferase encoding gene, Afu2g11120, which is highly upregulated upon gliotoxin exposure warranted further investigation. Afu2g11120 encodes an uncharacterised protein with predicted methyltransferase activity. The presence of the superfamily domain SSF53335 indicated that the protein is a predicted S-adenosyl-L-methionine-dependent methyltransferase. The *gli* gene cluster which contains all the genes required for gliotoxin biosynthesis is located on chromosome 6 and Afu2g11120 is located outside of this gliotoxin biosynthetic cluster (Gardiner and Howlett, 2005).

Gene deletion is a valuable reverse-genetic technique for the study of gene function and virulence in filamentous fungi such as *Aspergillus fumigatus* (Wiemann and Keller, 2013). The most commonly used method for gene deletion is the replacement of some, or all, of the open reading frame (ORF) of interest with a selection marker. *A. fumigatus* auxotrophic markers such as *pyrG* have been used for transformation. However, in some cases, these procedures can affect the growth rate of the organism even when the strains are complemented with the adequate gene (Díez et al., 1987). A reduction in growth rate can have a negative effect on secondary metabolite volumetric production due to the reduced biomass of the cultures. It is also possible that the use of auxotrophic markers could enhance secondary metabolite production through a reduction in protein or total RNA synthesis, in turn providing more NADPH and other precursors. Consequently, these precursors could feed into secondary metabolite pathways (Martin, 2015). Dominant selection through the use of drug resistance markers is more common and allows for the transformation of prototrophic strains. Two drug resistance markers are commonly used for selection of transformants: *hph* and *ptrA*. The *hph* cassette encodes hygromycin B phosphotransferase which confers resistance to hygromycin and the product of *ptrA* provides resistance to pyrithiamine (Cullen et al., 1987; Kubodera et al., 2002).

The use of a split-marker approach greatly improves the recovery of homologous integrants. In short, two hybrid DNA constructs are used for co-transformation. Each is comprised of a fusion product of one of the flanking sequences of the targeted gene with an incomplete portion of the drug resistance cassette. These drug resistance sequences overlap for approximately 600 bp. Neither marker fragment encodes sufficient sequences to reconstitute the functional resistance protein. Therefore, acquisition of drug resistance requires homologous recombination of the marker halves within their overlapping sequences (Figure 3.1). The highest probability for this event occurs when the fragment DNAs are in proximity to one another; for example, during integration at the target locus. This promotes a triple recombination event, replacing the target gene and reconstituting the functional drug resistance marker. Nonhomologous recombination events result in the integration of single non-functional cassettes into random locations within the genome and do not generate resistant transformants. To ensure that the phenotype of subsequent mutants is due to the deletion of the targeted gene, rather than a spontaneous secondary mutation, reintroduction of a wild-type allele of the gene using a second selection marker can be performed (Nielsen et al., 2006).

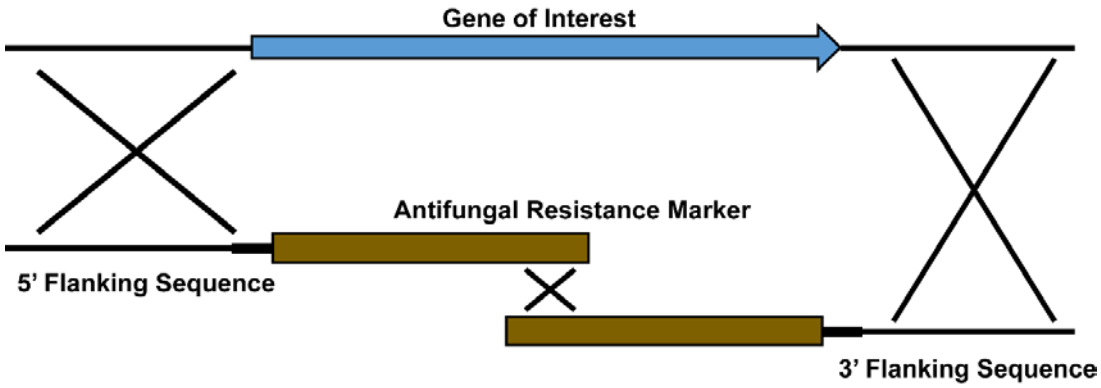

Figure 3.1. Illustration of the split-marker method for *A. fumigatus* gene deletion by targeted homologous recombination.

Reverse genetic analysis has been used to classify the role of several uncharacterised genes which are associated with secondary metabolism in *A. fumigatus* (Gallagher et al., 2012; Davis et al., 2011). This method has been applied in the work presented in this chapter to generate an Afu2g11120 mutant strain in order to study the impact of gene deletion on gliotoxin and/or bis(methyl)gliotoxin biosynthesis and resistance. As will be described in Chapter 4, functional characterisation of this gene resulted in its renaming as gliotoxin thiomethyltransferase A (*gtmA*). Consequently, this nomenclature will be used throughout this thesis for convenience and clarity.

The overall objectives presented in this chapter were to:

(i) Uncover the optimal growth conditions suitable for the examination of bis(methyl)gliotoxin biosynthesis in *A. fumigatus*.

(ii) Create and utilise replacement constructs for the targeted deletion, complementation and GFP labelling of *gtmA* in order to elucidate the function of this gene in *A. fumigatus* wild-type ATCC26933 and the gliotoxin sensitive mutants Δ*gliA* (Owens et al., 2015) and Δ*gliT* (Schrettl et al., 2010).

3.2 Results

3.2.1 RP-HPLC analysis confirms that bis(methyl)gliotoxin is produced at low levels by *A. fumigatus*

In order to determine the production levels of gliotoxin (GT) and bis(methyl)gliotoxin (BmGT), culture supernatants of *A. fumigatus* wild-type ATCC26933 were collected after growth in Czapeks Dox broth (CDB), *Aspergillus* minimal media (AMM) and yeast glucose (YG) broth in triplicate (72 h; 37 °C). The culture supernatants were then subjected to organic extraction followed by RP-HPLC analysis (Section 2.2.12).

Commercial standards of gliotoxin and bis(methyl)gliotoxin were analysed by RP-HPLC (Section 2.2.15). As shown in Figure 3.2, gliotoxin eluted with a retention time (RT) of 20.42 min and bis(methyl)gliotoxin eluted with a RT of 20.06 min. Comparison of the metabolite profiles from *A. fumigatus* in different growth conditions indicated that Czapeks Dox broth was the most suitable media for the production of gliotoxin and bis(methyl)gliotoxin (Figure 3.3). Bis(methyl)gliotoxin was shown to elute slightly earlier than gliotoxin by RP-HPLC. Additionally, the amount of bis(methyl)gliotoxin was shown to be substantially lower than the gliotoxin concentration in all of the media conditions tested.

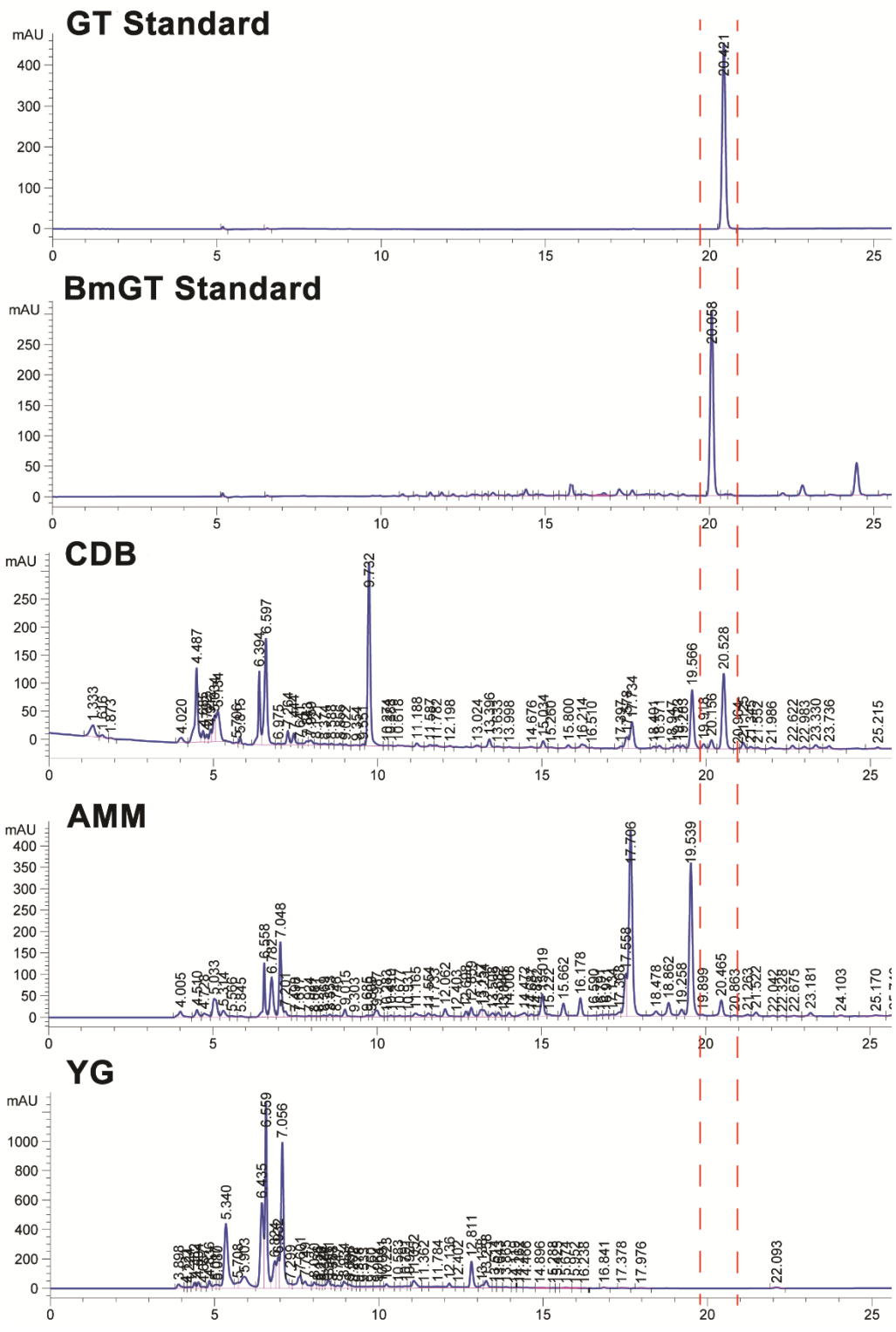

Figure 3.2. Representative RP-HPLC chromatograms highlighting gliotoxin and bis(methyl)gliotoxin production in various media conditions: Czapeks Dox broth (CDB), *Aspergillus* minimal media (AMM) and yeast glucose (YG). Absorbance was monitored at 254 nm.

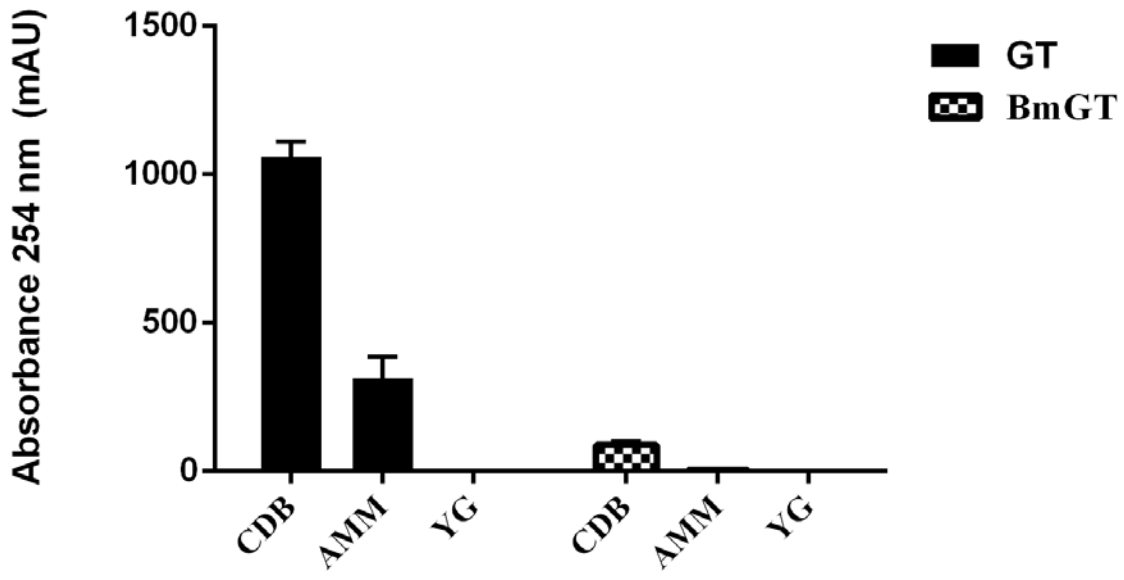

Figure 3.3. Relative amounts of gliotoxin and bis(methyl)gliotoxin in Czapeks Dox (CDB), *Aspergillus* Minimal Media (AMM) and Yeast Glucose (YG) liquid media. Cultures were incubated in triplicate at 37 °C, 200 rpm shaking for 72 h. Of the media conditions tested, CDB was shown to produce the highest amounts of gliotoxin and bis(methyl)gliotoxin after the 72 h incubation period.

3.2.2 Generation of replacement constructs for the transformation of *gtmA*

In order to determine the function of *gtmA,* a gene deletion strategy was employed (Figure 3.4). Protoplast transformations were performed using the background strain ATTC26933. This background has been previously used to characterise the roles of several genes within the gliotoxin biosynthetic cluster, such as *gliT* (Schrettl et al., 2010) and *gliK* (Gallagher et al., 2012). The *A. fumigatus* strain was co-transformed with two DNA constructs, each of which contained an incomplete fragment of the pyrithiamine (*ptrA*) resistance gene excised from the plasmid *pSK275*. These fragments were fused to 1.02 kb and 1.08 kb of *gtmA* flanking sequences. The fragments shared a 538-bp overlap within the *ptrA* cassette, serving as a potential recombination site during transformation. During transformation, homologous integration of each fragment into the genome flanking *gtmA* allows recombination of the *ptrA* fragments and generation of the intact resistance gene at the site of recombination.

Two rounds of PCR generated each fragment. Initially, each flanking region was amplified from ATCC26933 genomic DNA the primers *gtmA*-P1and *gtmA*-P2 for flanking region A (1.15 kb), and *gtmA*-P3 and *gtmA*-P4 for flanking region B (1.10 kb) (Figure 3.5). Following gel-purification, the fragments were digested with *Age*I and *Kpn*I, respectively. The *ptrA* selection marker was released from plasmid *pSK275* by digestion with *AgeI* and *KpnI* (Figure 3.6), and ligated with the two flanking regions, A and B, described above. Two overlapping fragments were amplified from the ligation product using primers *gtmA*-P5 and PTRoptrA2 for fragment C (2.4-kb); and primers *gtmA*-P6 and PTRoptrA1 for fragment D (2.2-kb) (Figure 3.7). Subsequently, ATCC26933 was transformed simultaneously with the overlapping fragments C and D. The PCR products were gel-purified to remove any non-specific products and then concentrated prior to protoplast transformation.

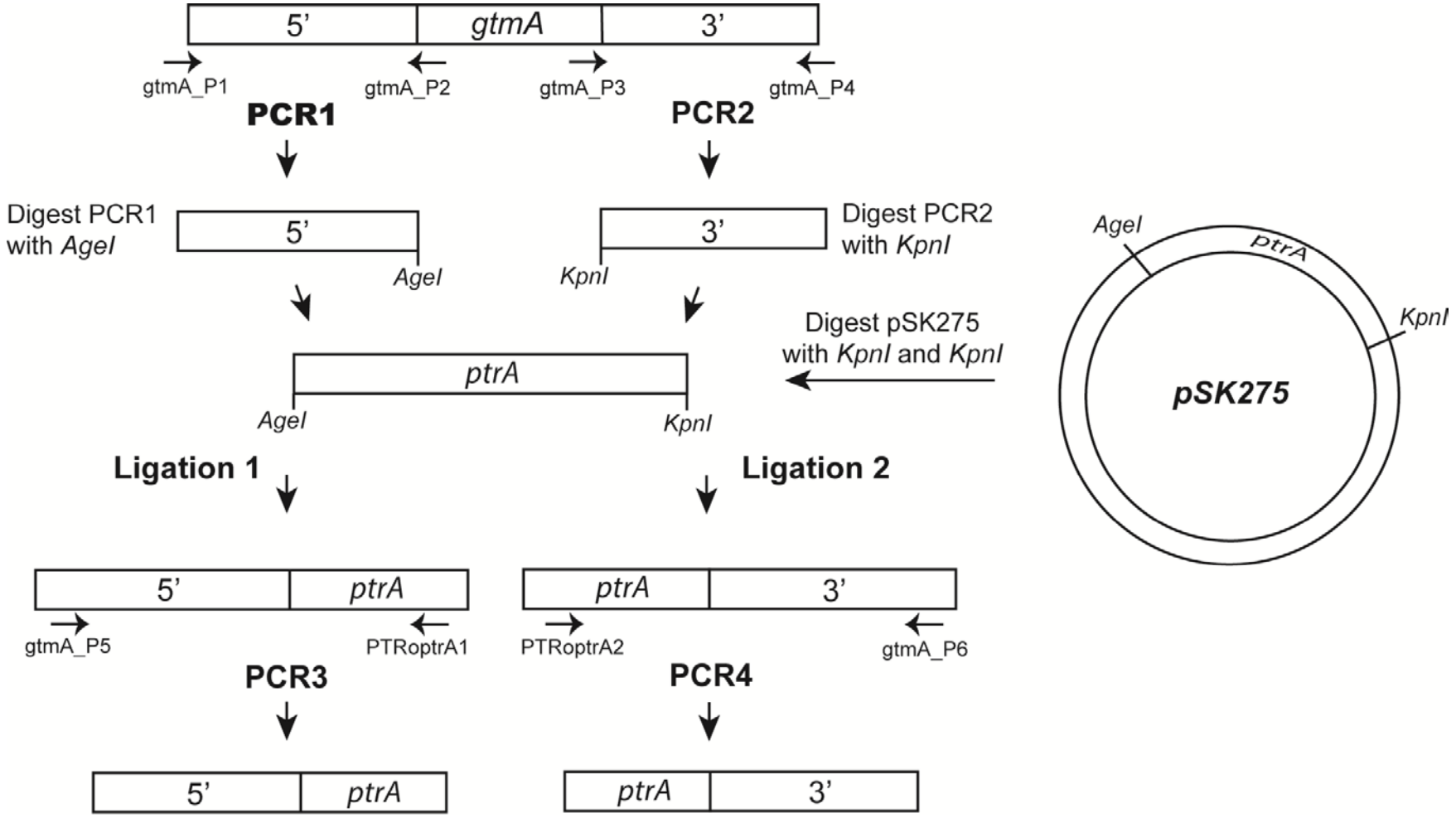

Figure 3.4. Schematic outlining the strategy used in the deletion of *gtmA* in *A. fumigatus* using the pyrithiamine resistance marker

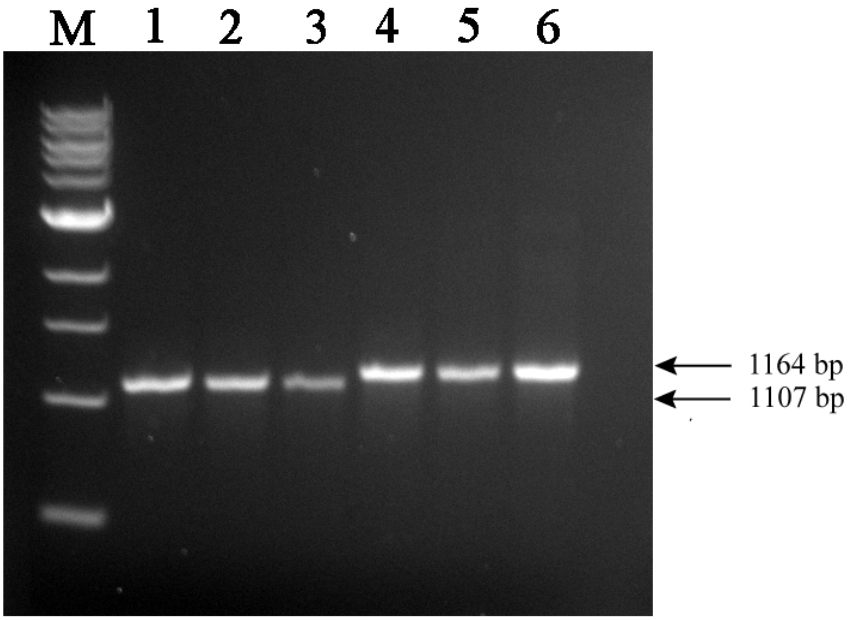

Figure 3.5. PCR products of the flanking regions of *gtmA*. Lane M: Molecular weight marker (NEB) (Section 2.1.8.1.8), Lane 1-3: PCR 1 (1164 bp) is the 5' flanking region of *gtmA*, Lane 4-6: PCR 2 (1107 bp) is the 3' flanking region of *gtmA*.

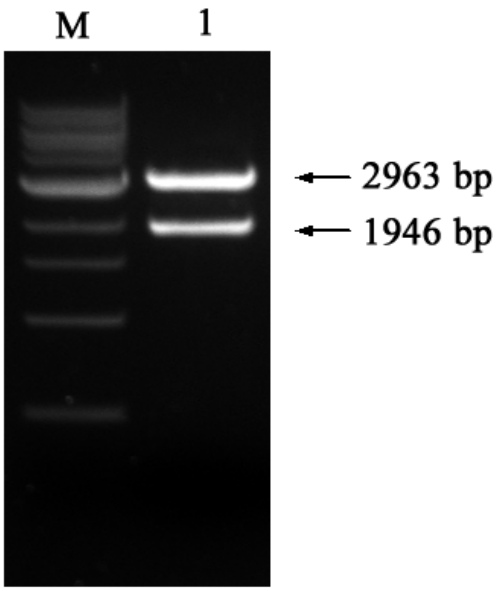

Figure 3.6. Lane M: Molecular weight marker (NEB) (Section 2.1.8.1.8), Lane 1: Restriction digestion of *pSK275* with the enzymes *AgeI* and *KpnI*. The *ptrA* selection marker was released (1946 bp) and ligated to the 5'and 3' flanking regions of *gtmA*.

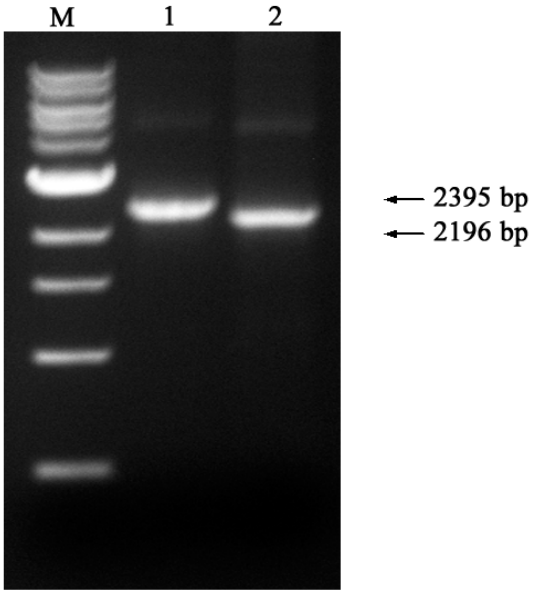

Figure 3.7. Final *gtmA-ptrA* gene deletion constructs. Lane M: Molecular weight marker (NEB) (Section 2.1.8.1.8), Lane 1: PCR 3 (2395 bp) is the 5' flanking region of *gtmA* fused to half of the *ptrA* selection marker, Lane 2: PCR 4 (2196 bp) is the 3' flanking region of *gtmA* fused to the second half of the *ptrA* selection marker.

3.2.3 Generation of DIG-labelled probe by PCR for Δ*gtmA* transformant identification

A single 5' upstream probe was prepared by PCR amplification for use in Southern blot analysis. As described in Section 2.1.10.6.9, the probe contained DIG-labelled nucleotides which facilitated detection using Southern blot analysis. A 5' probe was made using primers *gtmA*_P5 and *gtmA*_P2 which detected a region just upstream of *gtmA* (Figure 3.8).

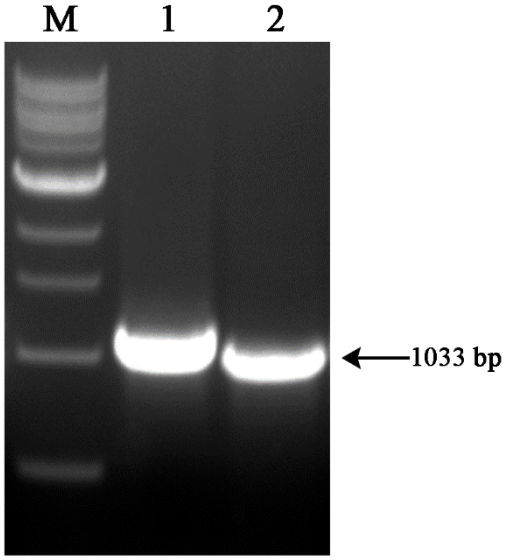

Figure 3.8. Generation of DIG-labelled nucleotide probe which facilitated Δ*gtmA* detection with Southern blot analysis. A 5' probe was made using primers *gtmA*_P5 and *gtmA*_P2 which detected a region just upstream of *gtmA*. Lane M: Molecular weight marker (NEB) (Section 2.1.8.1.8), Lane 1; DIG labelled nucleotide probe, Lane 2; positive control using standard dNTPs.

3.2.4 Protoplast transformation facilitated the deletion of *gtmA* from *A. fumigatus*^{ATCC26933}

The constructs from Section 3.2.2 were transformed into protoplasts of *A. fumigatus* ATCC26933. Approximately 3 µg of each 5' and 3' construct was used per transformation event. The transformation procedure was carried out as described in Section 2.2.3. The resultant transformants were selected on agar plates containing pyrithiamine (100 ng/ml). The colonies that grew on these plates were considered resistant and, therefore, predicted to have reconstituted *ptrA* incorporated into the genome.

For the transformation event, eight colonies were observed on pyrithiamine selection plates. Genomic DNA from these colonies was digested using an *Xho*I restriction enzyme. These were screened by Southern analysis using a 5' probe (Section 3.2.3). Figure 3.9 illustrates the Southern strategy which was employed in order to confirm Δ*gtmA* deletion. The mutant band (Δ*gtmA*; 3.99 kb) was present in colonies 7 and 8 (Figure 3.10). These two colonies were selected for single spore isolation. The single spore isolates of colonies 7 and 8 were digested with *Xho*I and a second round of Southern blot analysis using the 5' probe was performed. This confirmed the single integration of the Δ*gtmA* deletion cassette at the correct locus (Figure 3.11). To further confirm the absence of the wild-type locus from these transformants, PCR analysis (Section 2.2.2.2) was performed using primers *gtmA*_P5 and *gtmA*_P6 (Table 2.4). The predicted fragment size of 4.1 kb was observed for the mutants in comparison to 3 kb for the wild-type strain (Figure 3.12).

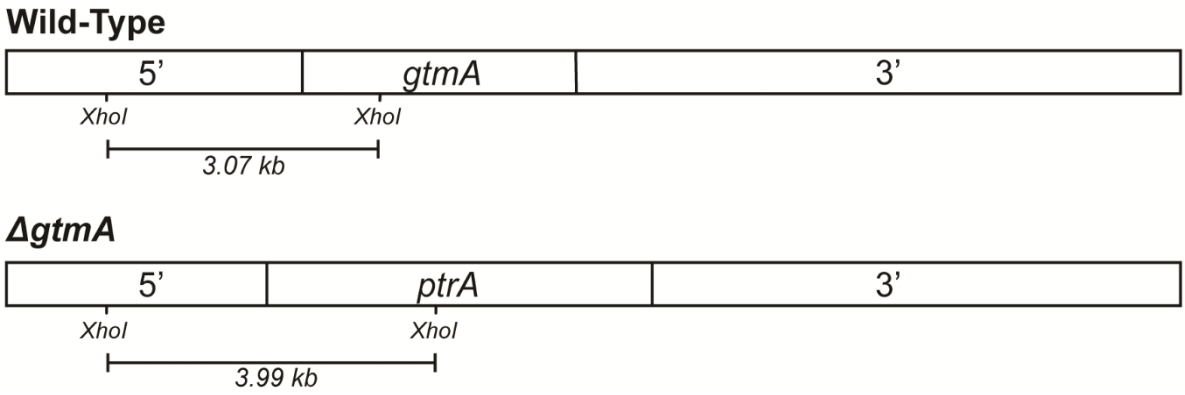

Figure 3.9. Schematic illustrating the Southern blot strategy employed to confirm the deletion of *gtmA*. The *XhoI* digested gDNA was screened using a 5' probe. A correct gene deletion event would result in a band of 3.99 kb. However, the wild-type *XhoI* digested gDNA would be 3.07 kb.

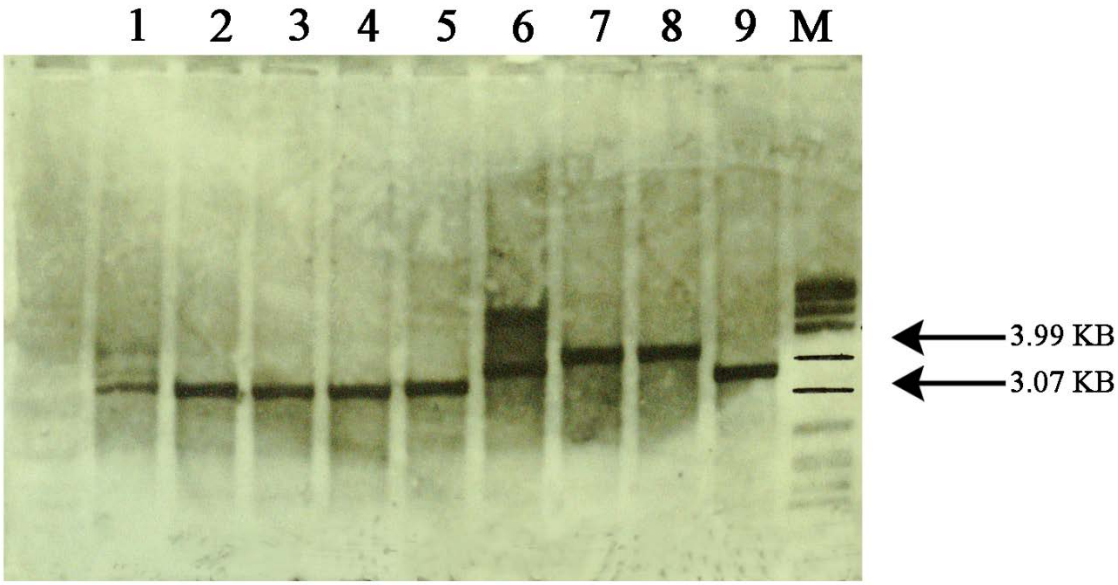

Figure 3.10. Southern analysis of potential Δ*gtmA* transformants. Here, the 5' DIG-labelled probe was used to detect the predicted presence of a 3.99 kb fragment in *XhoI* digested genomic DNA. Lane 1 - 8: genomic DNA from potential Δ*gtmA* transformants, Lane 9: WT positive control samples (3.07 kb). M; Molecular weight marker (Roche VII) (Section 2.1.8.1.7).

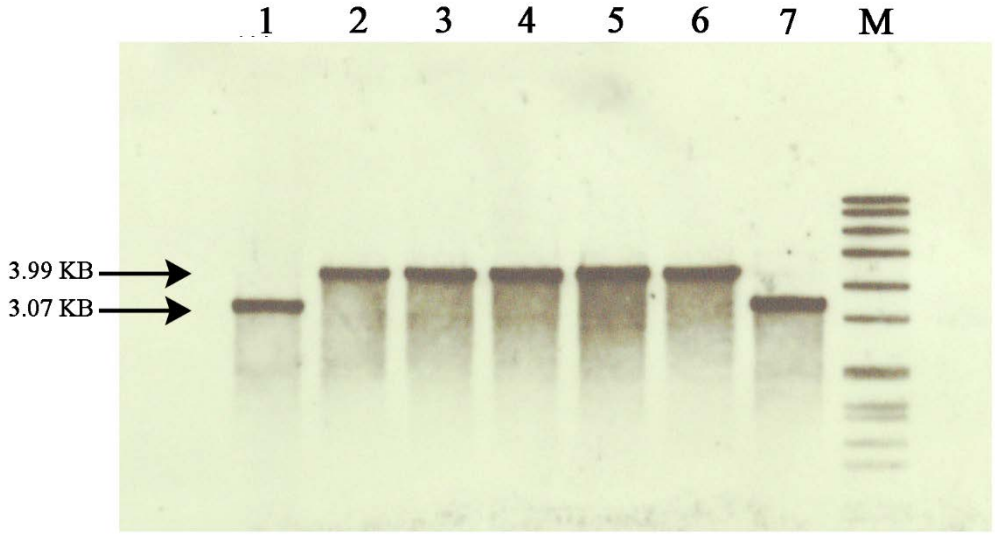

Figure 3.11. Second round Southern analysis of single spore isolates of Δ*gtmA* transformants. Here, the 5' DIG-labelled probe was used to detect the predicted presence of a 3.99 kb fragment in *XhoI* digested genomic DNA. Lane 2 - 6: Single spore isolates of potential mutant strain from colonies 7 and 8, Lane 1 and 7: Wild-type positive control samples (3.07 kb), M; Molecular weight marker (Roche VII) (Section 2.1.8.1.7).

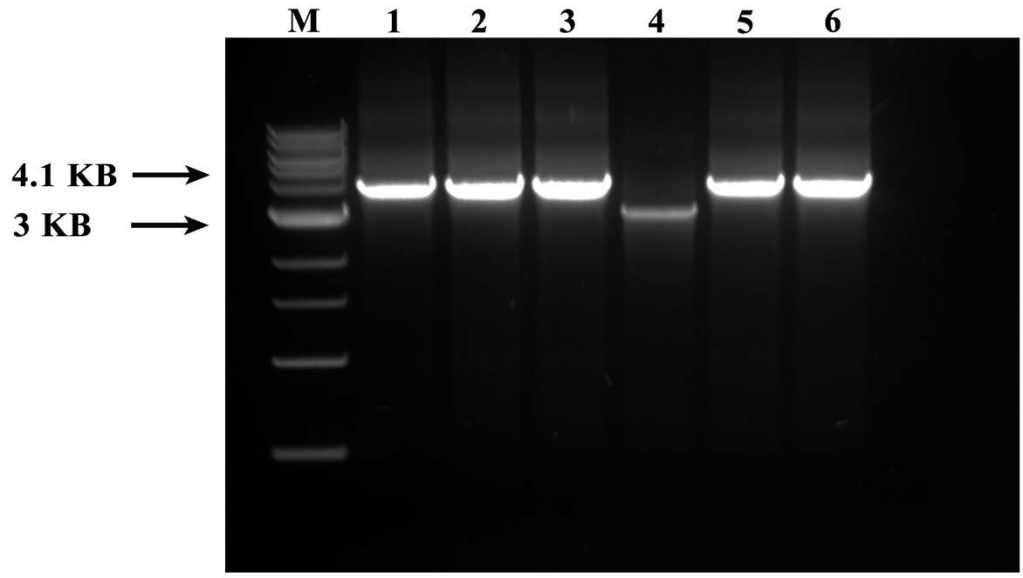

Figure 3.12. PCR analysis of genomic DNA extracted from wild-type and Δ*gtmA* transformants. M: Molecular weight marker (NEB) (Section 2.1.8.1.8), Lanes 1-3: Δ*gtmA* colony 7 single spore isolates, Lane 4: Wild-type, Lanes 5-6 Δ*gtmA* colony 8 single spore isolates

3.2.5 Complementation of *gtmA* into *ΔgtmA*

Once *gtmA* had been successfully deleted it was necessary to reintroduce the gene into the genome of *A. fumigatus ΔgtmA*::*ptrA*. This ensured that the phenotype which was observed could be solely attributed to the product of *gtmA*. The complementation method for *gtmA* reintroduction is described in Section 2.2.3.2.

3.2.6 Generation of a Complementation Construct

To complement Δ*gtmA*, a PCR fragment containing the *gtmA* locus, including promoter and terminator, was amplified using primers *gtmA*-P5 and *gtmA*-P6. This was then inserted into the pCR® 2.1-TOPO® TA vector (TOPO*gtmA*) (Figure 3.13). The *hph* resistance cassette was digested from the plasmid *pAN7-1* (Figure 3.14) and cloned into TOPO*gtmA* through the single *EcoRII* site in said plasmid, thus producing a TOPO*gtmAhph* vector (Figure 3.15).

The final vector, TOPO*gtmAhph,* was linearized with *NotI* and transformed into the Δ*gtmA* mutant strain. In order to confirm the correct cloning of *gtmA* and *hph*, a diagnostic digest was performed on potential plasmids. This established that the constructs were cloned correctly as *Nco*I yielded the predicted three fragments: 4262, 3214 and 1086 bp.

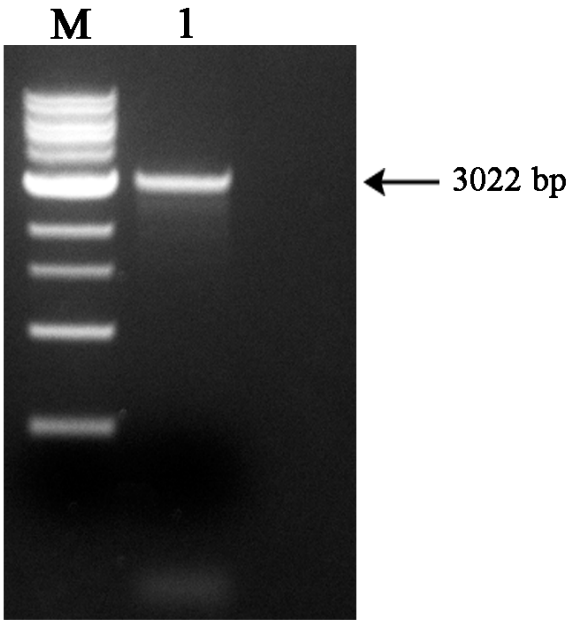

Figure 3.13. Amplification of *gtmA*, including 5' and 3' flanking regions, for TOPO cloning. Lane M: Molecular weight marker (NEB) (Section 2.1.8.1.8), Lane 1: *gtmA* amplified using primers *gtmA*-P5 and *gtmA*-P6 (3022 bp)

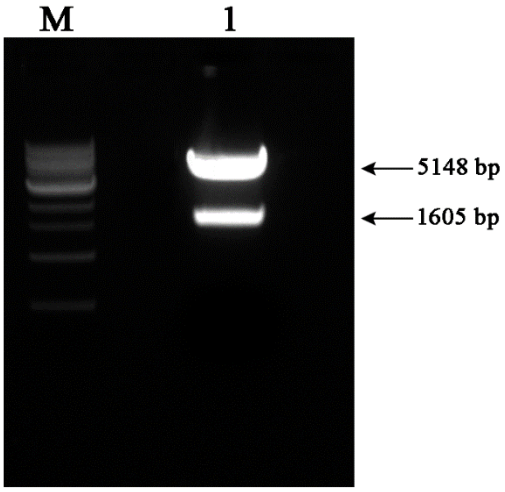

Figure 3.14. Restriction digestion of the *hph* resistance gene from the plasmid pAN7-1. M; Molecular weight marker (NEB) (Section 2.1.8.1.8), Lane 1: *pAN7-1* digestion with the restriction enzymes *BamHI* and *MfeI* resulted in the release of the *hph* hygromycin resistance gene (1605 bp).

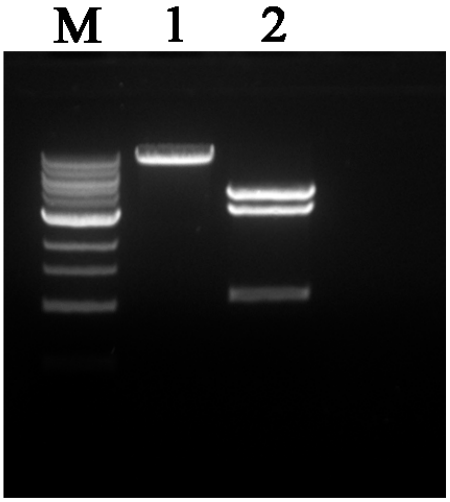

Figure 3.15. Linearization and diagnostic digestion of the TOPO*gtmAhph* plasmid. M: Molecular weight marker (NEB) (Section 2.1.8.1.8), Lane 1: Linearization of the TOPO*gtmA*hph plasmid using *NotI* (8562 bp). Digestion using *NcoI* yielded the predicted three fragments 4262, 3214 and 1086 bp. These fragments confirm that both of the plasmids were accurately cloned and suitable for complementation.

3.2.7 Southern blot Analysis of Transformants from *A. fumigatus gtmA*^{C} Complementation

Figure 3.16 illustrates the Southern strategy employed to confirm *gtmA*^{C} complementation. Genomic DNA from all potential transformants was digested with *Xho*I and probed with the 5' probe. Southern blot analysis (Section 2.2.4) identified two putative complemented transformants, termed 2 and 4 (Figure 3.17). Both the predicted fragment size of 3.99 kb and a single ectopic integration fragment of 7.5 kb were detected in these colonies when analysed by Southern blot.

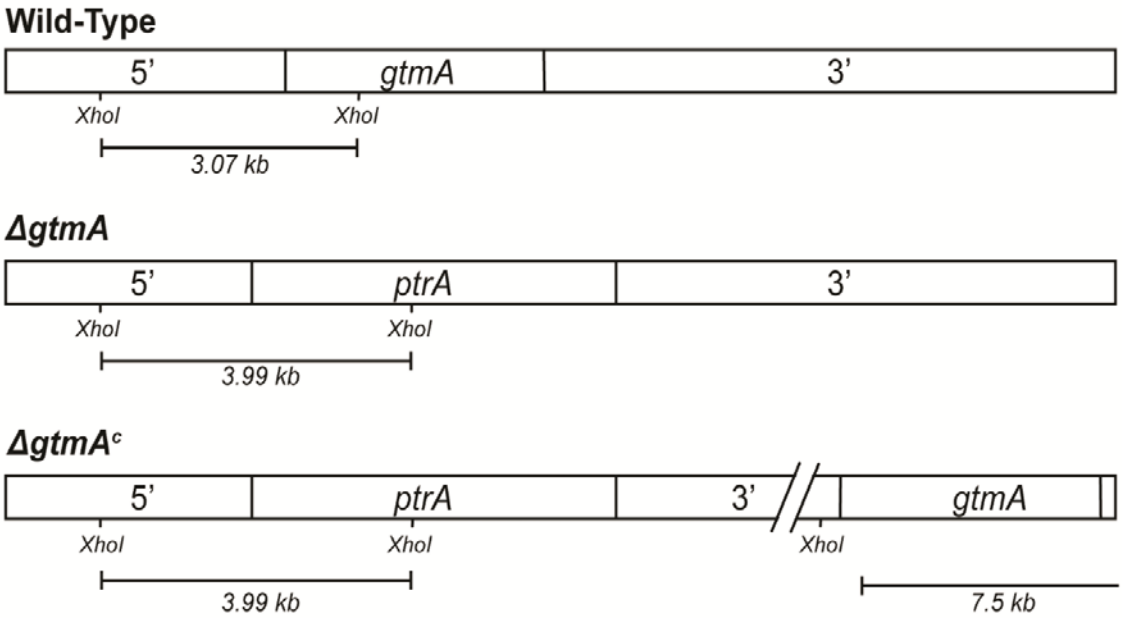

Figure 3.16. Schematic illustrating the Southern blot strategy employed for confirming the complementation of *gtmA*. The *Xho*I digested gDNA was screened using a 5' probe. A correct single ectopic complementation event would result in a band of 3.99 kb (Δ*gtmA*) and a second single integration (7.5 kb). The wild-type *Xho*I digested gDNA would be 3.07 kb.

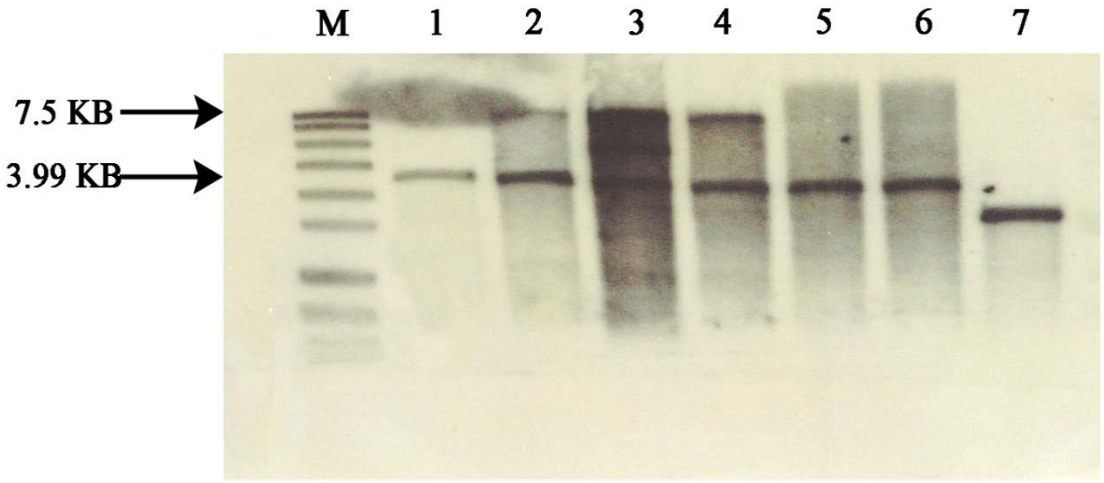

Figure 3.17. Southern blot of *gtmA*^{C} transformants. M: Molecular weight marker (Roche VII) (Section 2.1.8.1.7), Lanes 1-5: potential transformants, Lane 6: Δ*gtmA* (3.99 kb), Lane 7: Wild-type gDNA (3.07 kb)

3.2.8 RT-PCR Analysis of *gtmA* Expression following exposure to exogenous gliotoxin

The deletion of *A. fumigatus gtmA* from ATCC26933 and its subsequent complementation was confirmed by Southern analysis (Section 3.2.7). RT-PCR was employed to support that the deletion of *gtmA* resulted in the abolition of *gtmA* expression in Δ*gtmA* and that the restoration of *gtmA* expression was evident in $gtmA^c$. Both wild-type and mutant strains were cultured in Sabouraud Dextrose liquid broth and incubated at 37 °C for 21 h. This was followed by the addition of gliotoxin at a final concentration 5 µg/ml for 3 h. Gliotoxin was added to the cultures to induce the expression of *gtmA*. Total RNA was extracted and subjected to cDNA synthesis (Section 2.2.5.3). RT-PCR was carried out using the primers *gtmA*-qPCR-F and *gtmA*-qPCR-R (Table 2.4). Expression of *gtmA* was evident in *A. fumigatus* wild-type and the complemented strain $gtmA^c$ and absent from Δ*gtmA*. This confirmed that *gtmA* expression was restored in the complemented strain (Figure 3.18). The slightly higher *gtmA* expression in the complemented strain (Figure 3.18) may be due to the ectopic integration of the gene in its non-native location.

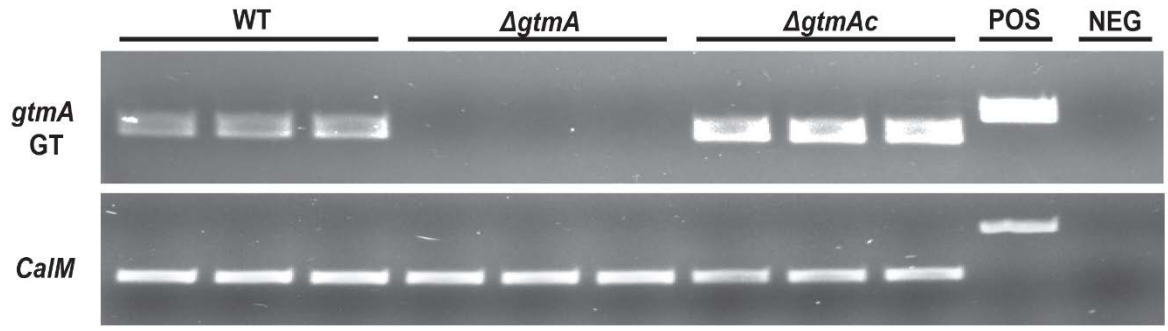

Figure 3.18. Confirmation of the absence of *gtmA* expression in *A. fumigatus* Δ*gtmA* and its restoration in *gtmA*^{c} by RT-PCR (n = 3 biological replicates per condition) following gliotoxin exposure (5 μg/ml for 3 h). Calm cDNA is used as cDNA control (Burns et al., 2005). POS represents amplification of genomic DNA. NEG: no cDNA or DNA present in amplification reactions.

3.2.9 Deletion of *gtmA* in the gliotoxin sensitive mutant backgrounds Δ*gliT* and Δ*gliA*

The *gtmA* gene was also deleted in the gliotoxin sensitive mutant backgrounds Δ*gliT* and Δ*gliA*. As these gene deletions were also carried out in the ATCC26933 background, the results could be compared to the Δ*gtmA* single mutant. However, Δ*gliT* and Δ*gliA* were prepared using the pyrithiamine resistance gene *ptrA*. As such, the hygromycin resistance gene (*hph*) from the plasmid *pAN7-1* had to be used for the Δ*gliT*::Δ*gtmA* and Δ*gliA*::Δ*gtmA* mutant selections. As shown in Figure 3.19, *A. fumigatus* Δ*gliT* and Δ*gliA* were co-transformed with two DNA constructs, each of which contained an incomplete fragment of *hph*. These fragments were fused to 1.1 kb and 1.1 kb of *gtmA* flanking sequences. These marker fragments shared a 572 bp overlap within the *hph* cassette which served as a potential recombination site during transformation. Throughout transformation, homologous integration of each fragment into the genome flanking *gtmA* allowed the recombination of the *hph* fragments and the generation of an intact resistance gene at the site of recombination.

Two rounds of PCR generated each fragment. Initially, each flanking region was amplified from ATCC26933 genomic DNA using the primers *gtmA*-P1and *gtmA_HYG*-P2 for flanking region A (1.15 kb) and *gtmA_HYG*-P3 and *gtmA*-P4 for flanking region B (1.10 kb). Following gel-purification the fragments were digested with *Xho*I and *Sbf*I, respectively. The *hph* selection marker was released from plasmid *pAN7-1* by digestion with *Xho*I and *Sbf*I and ligated with the two flanking regions, A and B. Two overlapping fragments were amplified from the ligation product using primers *gtmA*-P5 and PTRoptrA2 for fragment C (2.32 kb), and primers *gtmA*-P6 and PTRoptrA1 for fragment D (2.76 kb) (Figure 3.20). The PCR products were gel-purified to remove any non-specific products and then concentrated prior to protoplast transformation. Finally, Δ*gliT*

and Δ*gliA* were independently transformed in concert with the two overlapping fragments.

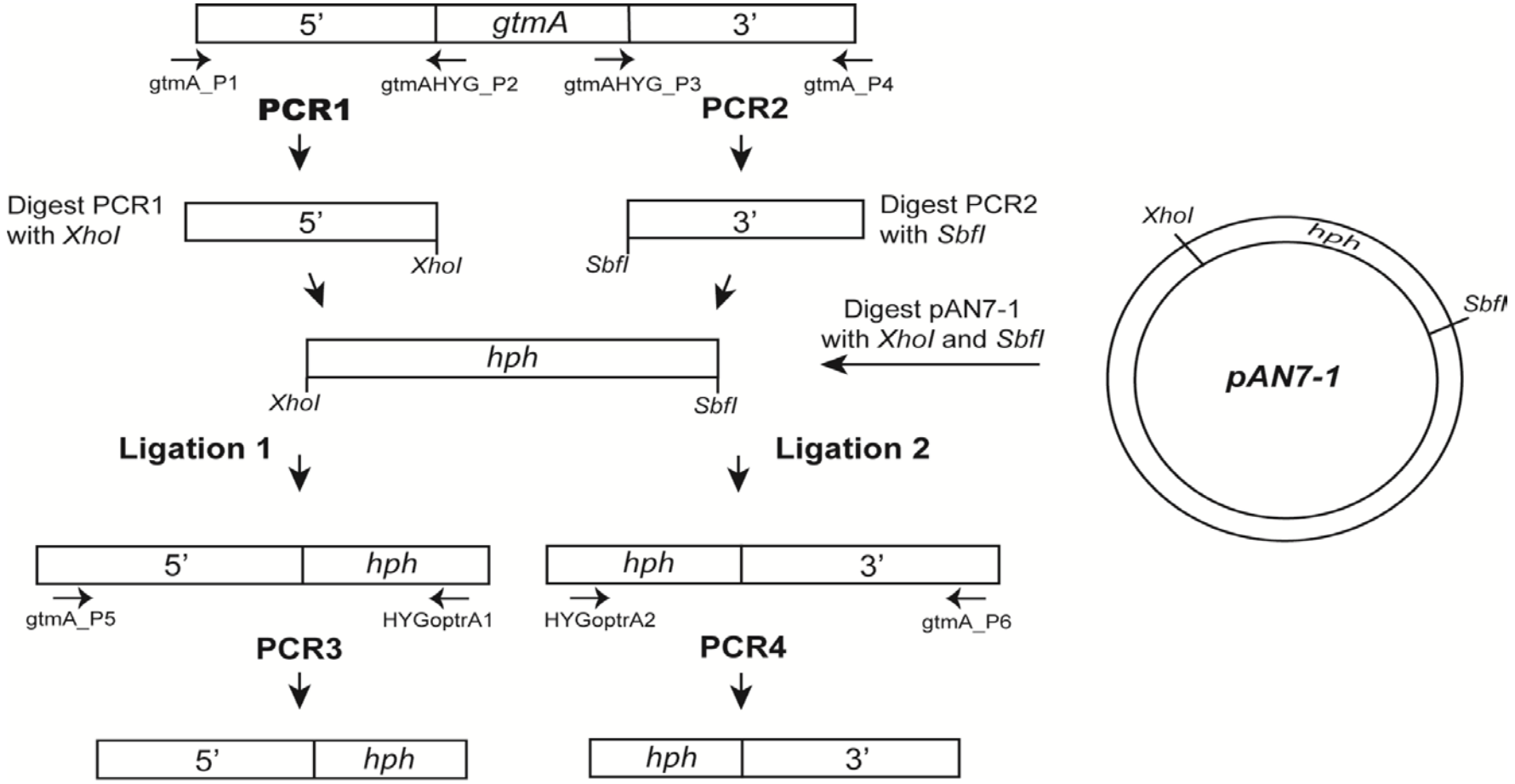

Figure 3.19. Schematic outlining the strategy used in the deletion of *gtmA* in *A. fumigatus* Δ*gliT* (Schrettl et al., 2010) and Δ*gliA* (Owens et al., 2015) using the hygromycin resistance marker.

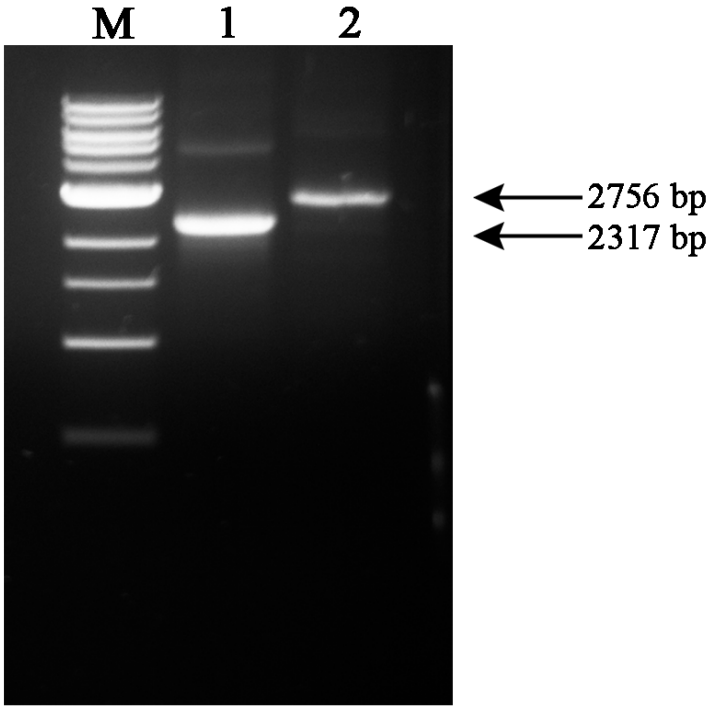

Figure 3.20. Final *gtmA-hph* gene deletion constructs. Lane M: Molecular weight marker (NEB) (Section 2.1.8.1.8), Lane 1: PCR 3 (2756 bp) is the 5' flanking region of *gtmA* fused to half of the *hph* selection marker, Lane 2: PCR 4 (2317 bp) is the 3' flanking region of *gtmA* fused to the second half of the *hph* selection marker.

3.2.10 Transformation and selection for deletion of *gtmA* from *A. fumigatus* ATCC26933 Δ*gliT* and Δ*gliA*

The transformation procedure was carried out as described in Section 2.2.3. Approximately 3 μg of both 5' and 3' construct were used per transformation event. The resultant transformants were selected on agar plates containing hygromycin (100 μg/ml). The colonies that grew on these were considered resistant and, therefore, predicted to have reconstituted *hph* incorporated into the genome.

For the transformation event, 12 Δ*gliT* background and 9 Δ*gliA* background colonies were observed on hygromycin selection plates. Genomic DNA from these transformants was-screened by Southern analysis using a 5' probe (Section 3.2.3). Figure 3.21 illustrates the Southern strategy employed to confirm Δ*gliT*::Δ*gtmA* and Δ*gliA*::Δ*gtmA* deletions. The mutant band (*ΔgtmA*; 1.83 kb) was present in two Δ*gliT*::Δ*gtmA* transformants and one Δ*gliA*::Δ*gtmA* transformant. These three colonies were selected for single spore isolation. Single spore isolates of Δ*gliT*::Δ*gtmA* (3) and Δ*gliA*::Δ*gtmA* (2) were digested with *Xho*I and a second round of Southern blot analysis using the 5' probe was performed. This confirmed the single integration of the *ΔgtmA* deletion cassette at the correct locus (Figure 3.22)

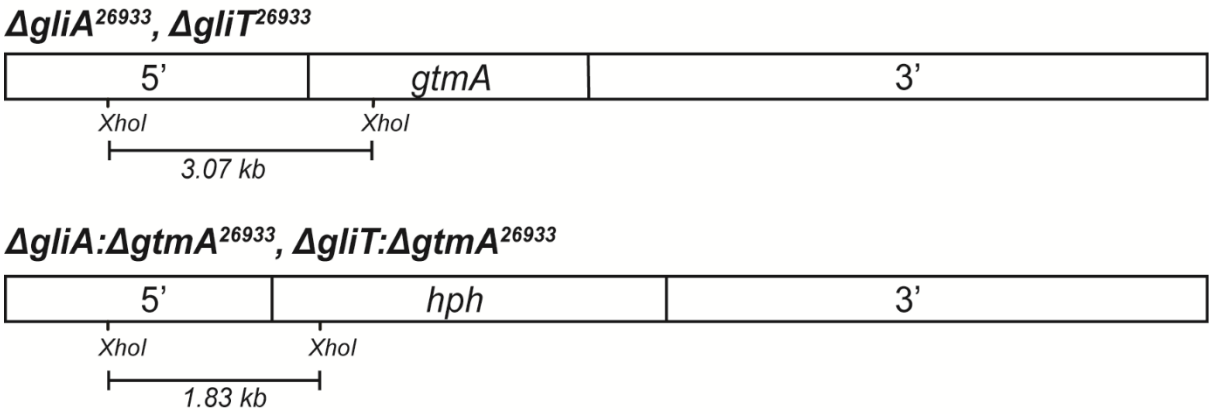

Figure 3.21. Schematic illustrating the Southern blot strategy employed for confirming the deletion of *gtmA* in Δ*gliT* and Δ*gliA*, respectively. The *XhoI* digested gDNA was screened using a 5' probe. A correct gene deletion event should result in a band of 1.83 kb. The wild-type *Xho*I digested gDNA would be 3.07 kb.

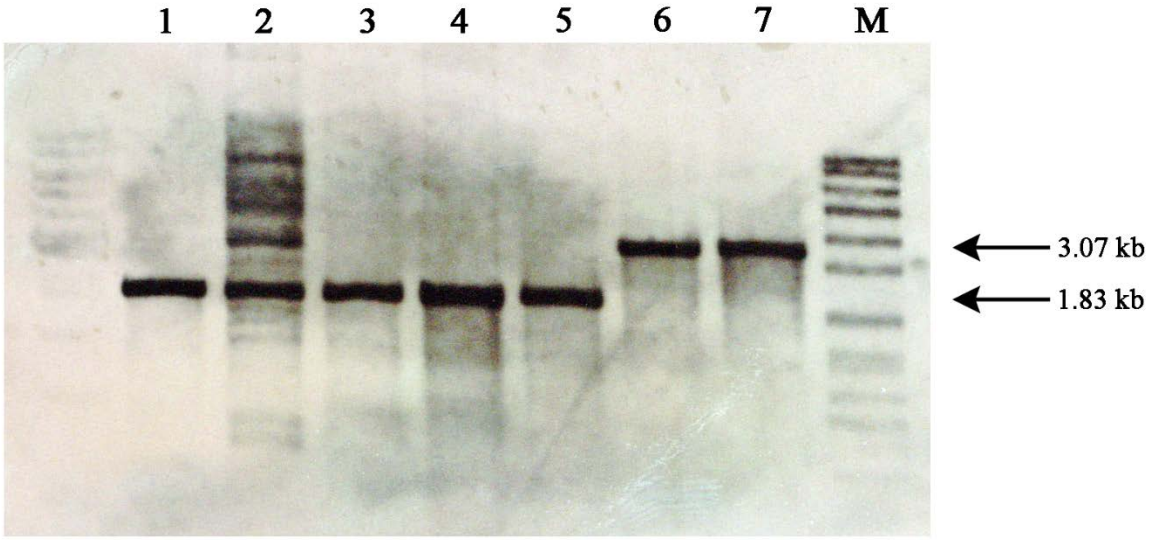

Figure 3.22. Identification of *A. fumigatus* Δ*gliT*::Δ*gtmA* and Δ*gliA*::Δ*gtmA* in second round Southern analysis of single spore isolates of Δ*gtmA-hph* transformants. Here, the 5' DIG-labelled probe was used to detect the predicted presence of a 1.83 kb fragment in *Xho*I digested genomic DNA. Lane 1 - 3: Single spore isolates of potential Δ*gliT*::Δ*gtmA* mutant strains, Lanes 4-5; Single spore isolates of potential Δ*gliA*::Δ*gtmA* mutant strains, Lane 6; Δ*gliT* positive control (3.07 kb), Lane 7; Δ*gliA* positive control (3.07 kb).

3.2.11 Generation of *gtmA-eGFP* Gene Fusion Construct

The *pUCGH* eGFP vector containing *hph* (Langfelder et al., 2001) under the control of a *Potef* constitutive promoter was digested with the enzymes *Kpn*I and *Xma*I. This released the *Potef* promoter from the vector and facilitated the cloning of *gtmA* under the control of its native promoter into the *pUCGH* vector. The *gtmA* gene with both 1 kb upstream and the stop codon removed was amplified from *A. fumigatus* 26933 DNA (2036 bp) using the primers *gtmA*_GFP_F and *gtmA*_GFP_R. This construct was then double digested with *Kpn*I and *Xma*I, gel purified and, finally, ligated to the digested *pUCGH* vector. An outline of the *pUCGHgtmA* vector is shown in Figure 3.23. The final vector (*pUCGHgtmA*) was linearized with *Kpn*I and transformed into *A. fumigatus* Δ*gtmA*. This strategy targeted the *gtmA-egfp-hph* construct to the original *gtmA* locus of the Δ*gtmA* mutant. 6 μg of the linearised construct was transformed into Δ*gtmA* protoplasts.

3.2.12 Southern blot Analysis of *A. fumigatus gtmA-eGFP* Transformants

Figure 3.24 illustrates the Southern strategy employed to confirm *gtmA-eGFP* insertion into Δ*gtmA*. Genomic DNA from all four potential transformants was digested with *XhoI* and probed with the 5' probe. Southern blot analysis (Section 2.2.4) identified a single transformant with *gtmA-GFP* insertion at the correct locus (Colony 4). This transformant had the predicted fragment size of 4.73 kb when analysed by Southern blot (Figure 3.25).

3.2.13 Transformation of *A. fumigatus* Δ*gtmA*::*gtmA-eGFP* with a Histone 2A monomeric red fluorescent protein fusion (H2A::mRFP) plasmid

In order to visualise the nuclei of Δ*gtmA:gtmA-eGFP* during confocal microscopy, a Histone 2A monomeric red fluorescent protein fusion (H2A::mRFP) plasmid (Sarikaya Bayram et al., 2010) was linearised using *EcoRI* (5 µg) and transformed into *ΔgtmA:gtmA-eGFP* protoplasts. The resultant transformants were selected for on agar plates containing phelomycin (100 µg/ml) at 30 °C and screened for mRFP expression by confocal microscopy.

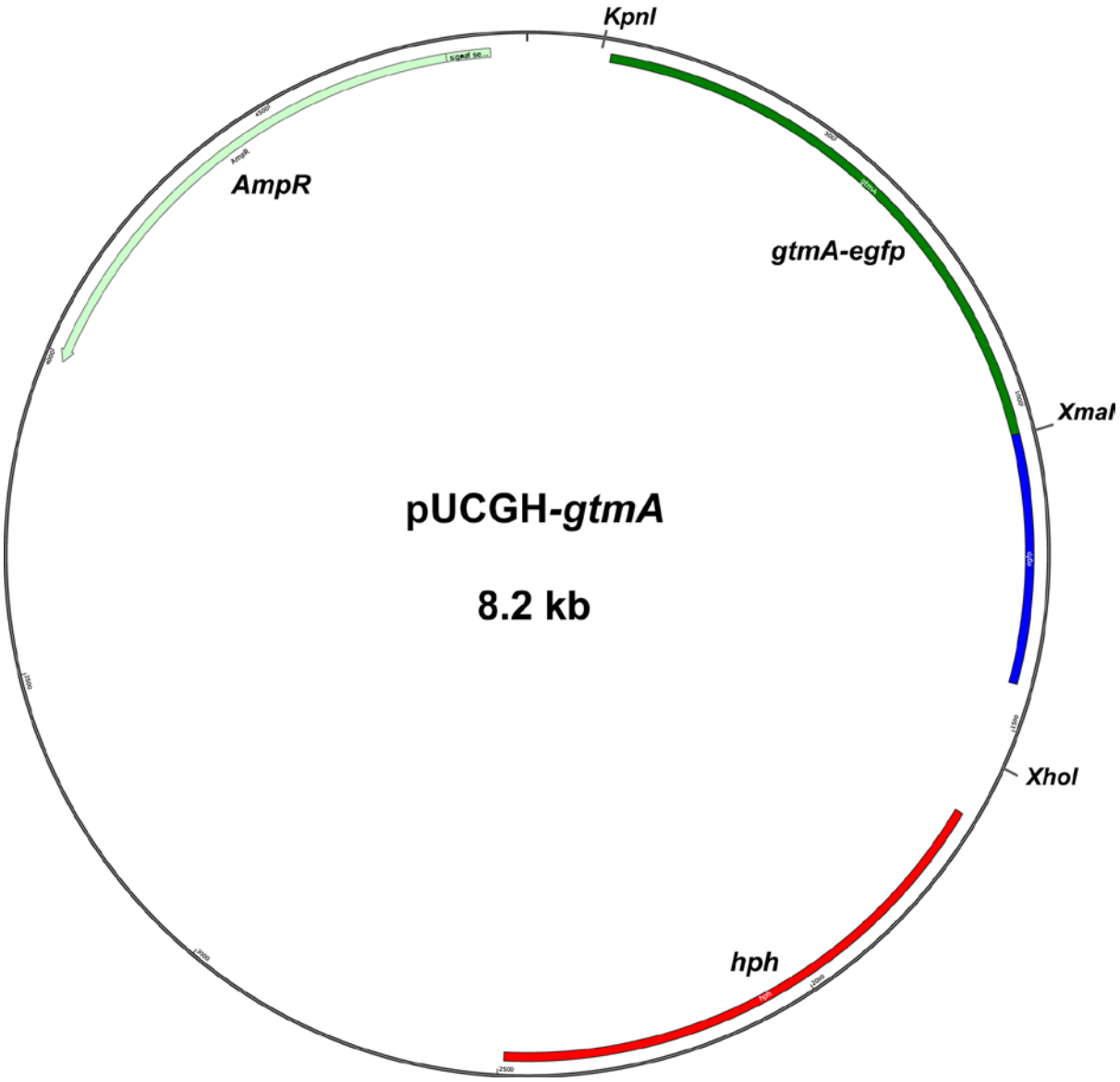

Figure 3.23. Plasmid map of *pUCGH-gtmA*. This vector contains the *hph* gene for hygromycin selection which is indicated by the red region. Restriction sites, *Kpn*I and *XmaI*, facilitated the cloning of *gtmA* with its promoter sequence (green) in frame with the *eGFP* gene (blue).

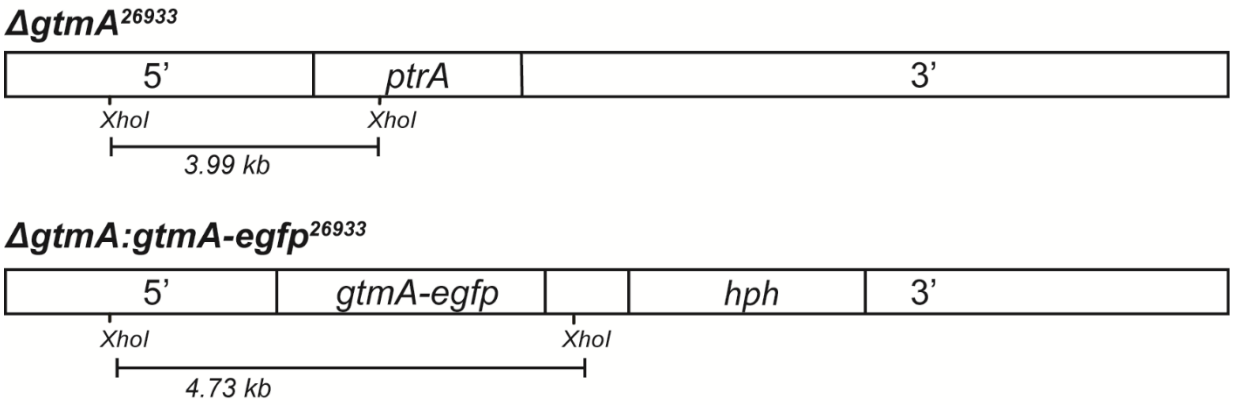

Figure 3.24. Schematic outlining the insertion of *gtmA-eGFP* into *A. fumigatus* Δ*gtmA*. A single homologous recombination between the 5' flanking region results in the insertion of the construct into the 5' flanking region of Δ*gtmA*, directly before the *ptrA* selection marker used to generate *A. fumigatus* Δ*gtmA: gtmA-eGFP* (4.73 kb).

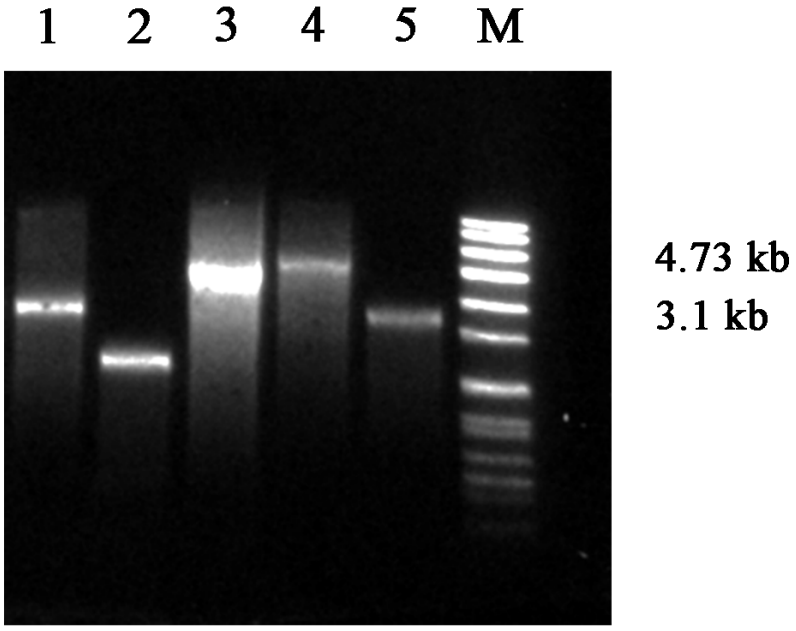

Figure 3.25. Identification of *A. fumigatus* Δ*gtmA: gtmA-eGFP* by Southern analysis. Second round Southern analysis of single spore isolates of Δ*gtmA*::*gtmA-eGFP* transformants. Here, the 5' DIG-labelled probe was used to detect the predicted presence of a 4.73 kb fragment in *XhoI* digested genomic DNA. Lane 1 - 4: Single spore isolates of potential Δ*gtmA*::*gtmA-eGFP* transformants, Lane 5; Wild-type positive control

3.3 Discussion

The work presented in this chapter describes the deletion of *gtmA* in *A. fumigatus* ATCC26933 wild-type, Δ*gliA* and Δ*gliT*. *A. fumigatus* Δ*gtmA* was complemented to restore *gtmA* function. Semi-quantitative RT-PCR confirmed expression of *A. fumigatus gtmA* in *A. fumigatus* ATCC26933 and $gtmA^{C}$; expression was absent in *A. fumigatus* Δ*gtmA* after gliotoxin exposure. The *gtmA* gene was also fused to eGFP and transformed into Δ*gtmA* under the control of the native promoter.

The split bipartite method (Nielsen et al., 2006) was employed in the deletion of *A. fumigatus gtmA*, a putative methyltransferase that has been previously shown to be highly expressed during gliotoxin exposure. Two constructs containing partial fragments of the pyrithiamine resistant gene, *ptrA* were generated according to this method. The constructs were transformed into protoplasts from *A. fumigatus* ATCC26933. A further two constructs were generated containing partial fragments of the hygromycin resistance gene, *hph*. These constructs were used to transform Δ*gliA* and Δ*gliT* mutant backgrounds to generate two double gene deletion mutants; *A. fumigatus* Δ*gliT*::Δ*gtmA* and Δ*gliA*::Δ*gtmA*, respectively.

A complementation construct was prepared containing *gtmA* and the selection marker *hph*. This was transformed into Δ*gtmA*. Five transformants were obtained and screened by Southern blot following restriction digest with *Xho*I. Two of the transformants displayed the fragment pattern 3.99 kb and 7.5 kb, indicating the generation of $gtmA^{C}$. The hygromycin resistance gene, *hph*, has been successfully used to complement other gene deletions in *A. fumigatus* where it has been co-transformed as a plasmid along with the complementation construct. The advantage of a single construct containing the gene to be complemented and the resistance marker is that it rules out the situation whereby the resistance marker randomly integrates into the genome.

Semi-quantitative Reverse Transcriptase PCR (RT-PCR) was undertaken to assess *A. fumigatus gtmA* expression in *gtmA*^{C} and its absence of expression in Δ*gtmA*. cDNA was prepared from RNA extracted from *A. fumigatus* ATCC26933, Δ*gtmA*, and *gtmA*^{C}. Expression of *A. fumigatus gtmA* was confirmed in ATCC26933 and *gtmA*^{C} whilst no expression was observed in Δ*gtmA*. This confirmed the successful deletion of *A. fumigatus gtmA* in ATCC26933 and complementation of Δ*gtmA*.

In addition, the Δ*gtmA* mutant was transformed with a construct containing *gtmA* under its native promoter fused to *eGFP*. As *gtmA* is known to be induced by gliotoxin exposure, the generation of this strain should facilitate localisation and expression studies to be carried out on this uncharacterised protein.

Chapter 4

Functional characterisation of *gtmA* – an uncharacterised methyltransferase encoded by *A. fumigatus*

4.1 Introduction

A. fumigatus gtmA has been identified as a putative methyltransferase of unknown function and specificity which is highly upregulated upon gliotoxin exposure (O'Keeffe et al., 2014). Chapter 3 detailed the deletion of *gtmA* from *A. fumigatus,* facilitating the comparative phenotypic analysis between wild-type and Δ*gtmA*. This data should aid in the identification of the specific role of *gtmA* in response to gliotoxin exposure. Characterisation of the *gtmA* null mutant will determine whether this enzyme plays a role in gliotoxin S-methylation or the biosynthesis of gliotoxin. In addition, the Δ*gtmA: gtmA-eGFP* strain will uncover the cellular localisation of this protein. This characterisation will involve subjecting the mutant and corresponding wild-type strain to the following:

The thiol-methyltransferase activity of *A. fumigatus* upon exposure to exogenous gliotoxin suggests a possible detoxification role of this enzyme in response to exogenous thiols (Li et al., 2012). Using a NMR-based comparative metabolomics method, 17 *gliZ*-dependent metabolites were shown to be produced by *A. fumigatus* and 7 of these metabolites were shown to contain thiomethyl groups (Forseth et al., 2011). It is possible that a single S-methyltransferase is responsible for the thiomethylation of these *gliZ* dependent metabolites. It is also conceivable that thiomethylation has a biosynthetic role in the stabilisation of the gliotoxin scaffold or shunt intermediates during gliotoxin biosynthesis.

The overall objectives of the work presented in this chapter were to:

(i) Determine if Afu2g11120*, gtmA*, has a role in bis(methyl)gliotoxin biosynthesis and/or gliotoxin biosynthesis, through comparative metabolite profile analysis of wild-type Δ*gtmA* and the complemented strain generated in Chapter 3.

(ii) Observe any phenotype associated with *A. fumigatus gtmA* in comparison to the corresponding wild-type under various conditions of oxidative stress or gliotoxin resistance through a series of phenotypic assays.

(iii) Perform quantitative proteomic analysis of the wild-type and Δ*gtmA* strain in response to either gliotoxin or bis(methyl)gliotoxin exposure.

(iv) Confocal microscopy to uncover the localisation of GtmA-eGFP upon gliotoxin exposure.

(v) Perform quantitative proteomic analysis of the wild-type, Δ*gtmA* and complemented strain under secondary metabolite producing conditions.

(vi) Perform a phylogenetic analysis on the GtmA protein across the fungal kingdom.

4.2 Results

4.2.1 Analysis of *A. fumigatus* wild-type, Δ*gtmA* and *gtmAc* metabolite profiles by LC-MS/MS

The alignment of total ion chromatographs (TIC) of wild-type, Δ*gtmA* and *gtmA*^{c} culture supernatant organic extracts was performed and revealed a single significant difference in the metabolite profiles. Reference standards of pure gliotoxin (GT) and bis(methyl)gliotoxin (BmGT) were also analysed alongside these samples. Wild-type and *gtmA*^{c} extracts produced spectra with a dominant peak at the retention time of 6.5 min. However, this was absent in Δ*gtmA*. This peak was attributable to the elution of bis(methyl)gliotoxin as confirmed by the presence of the precursor ion, (M + H)+ = 357.1, and characteristic product ions, (M + H)+ = 309, 243, 215 (Domingo et al., 2012). LC-MS/MS analysis also certified that gliotoxin was produced by wild-type, Δ*gtmA* and *gtmA*^{c}. Extracted ion chromatograms of bis(methyl)gliotoxin (m/z 357) and gliotoxin (m/z 327) for *A. fumigatus* wild-type, Δ*gtmA* and *gtmA*^{c} are shown in Figure 4.1. This confirmed that bis(methyl)gliotoxin production was abolished in *A. fumigatus* Δ*gtmA* and restored in the complemented strain (*gtmA*^{c}).

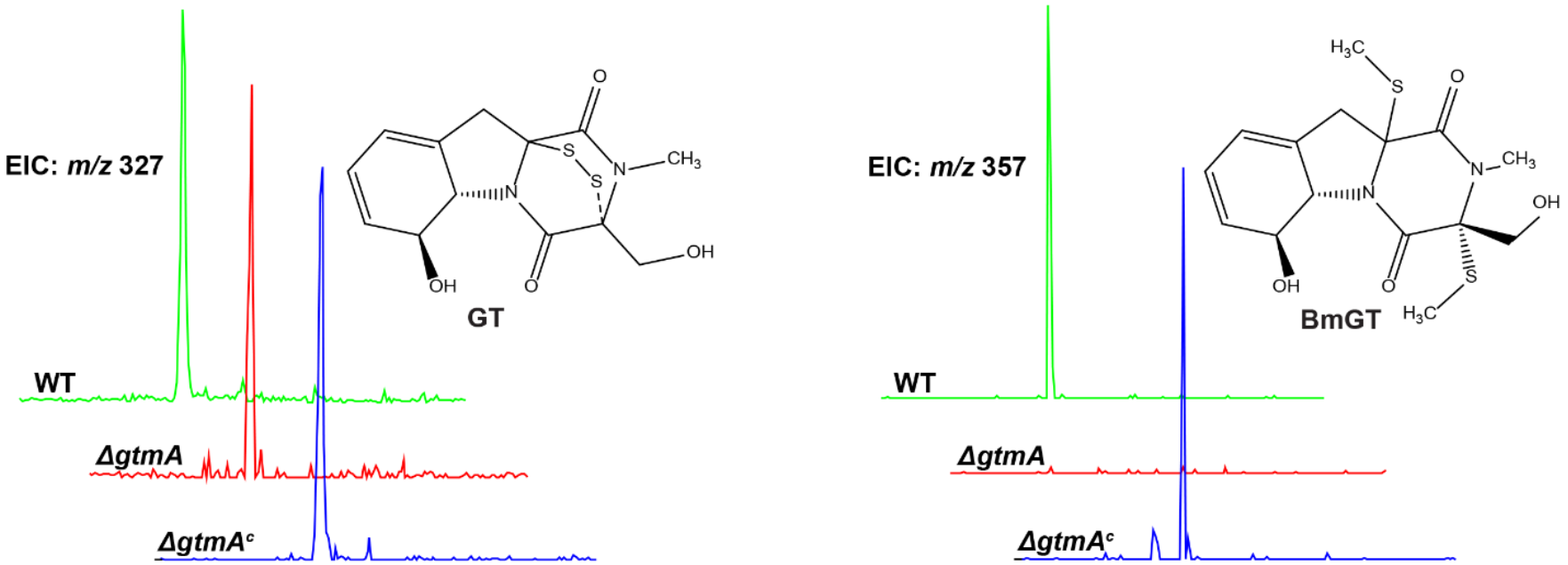

Figure 4.1. High sensitivity LC-MS analysis confirms complete abrogation and restoration of bis(methyl)gliotoxin biosynthesis in *A. fumigatus* Δ*gtmA* and *gtmA*^{c}, respectively. Gliotoxin (m/z 327) was detected in *A. fumigatus* wild-type, Δ*gtmA* and *gtmA*^{c}

4.2.2 Comparative metabolite profiling of *A. fumigatus* wild-type, Δ*gtmA* and *gtmA*^{c} by RP-HPLC

In order to elucidate the effect of *gtmA* absence on *A. fumigatus*, secondary metabolite production culture supernatants of *A. fumigatus* wild-type, Δ*gtmA* and *gtmA*^{c} were collected after growth (triplicate) in Czapeks Dox broth (CDB) at 200 rpm for 72 hr, 37 °C and, also, 7 d, 37 °C. The supernatants were then subjected to organic extraction prior to RP-HPLC analysis (Section 2.2.12). Reference standards of pure gliotoxin (GT) and bis(methyl)gliotoxin (BmGT) were also analysed alongside these samples by LC-MS and RP-HPLC (Section 2.2.16.4). Interestingly, as shown in Figures 4.2 and 4.3, a significant increase in gliotoxin production was evident in *A. fumigatus* Δ*gtmA* in comparison with the wild-type following culture in Czapeks-Dox media for both 72 h (p<0.0056) and 7 d (p<0.0001). No other metabolites were shown to be significantly altered by the absence of *gtmA*.

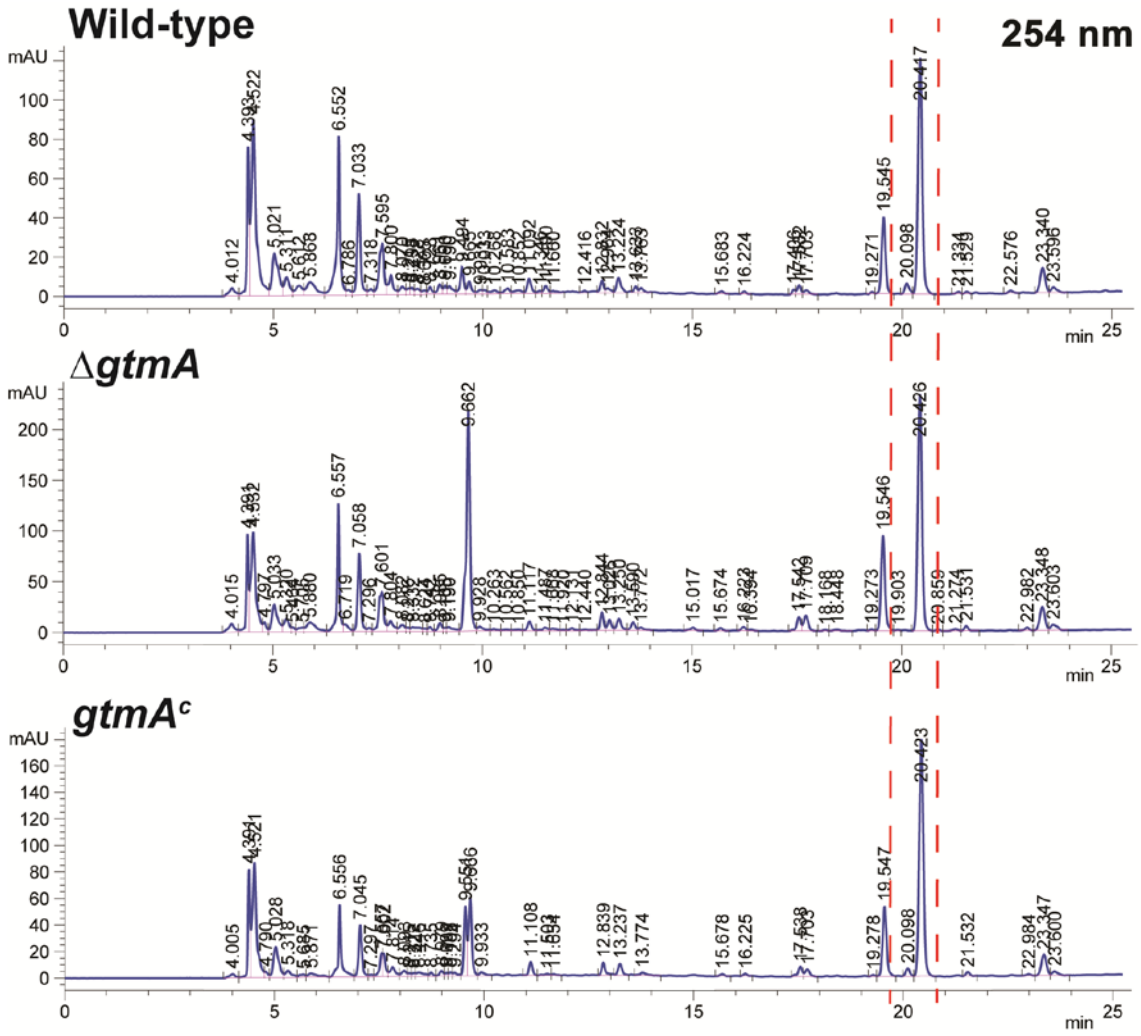

Figure 4.2. Comparative RP-HPLC analysis of *A. fumigatus* wild-type, Δ*gtmA* and *gtmA*^{c}. Gliotoxin and bis(methyl)gliotoxin were the only metabolites significantly altered across all three replicates (BmGT RT = 20.1, GT RT = 20.4). Absorbance was monitored at 254 nm.

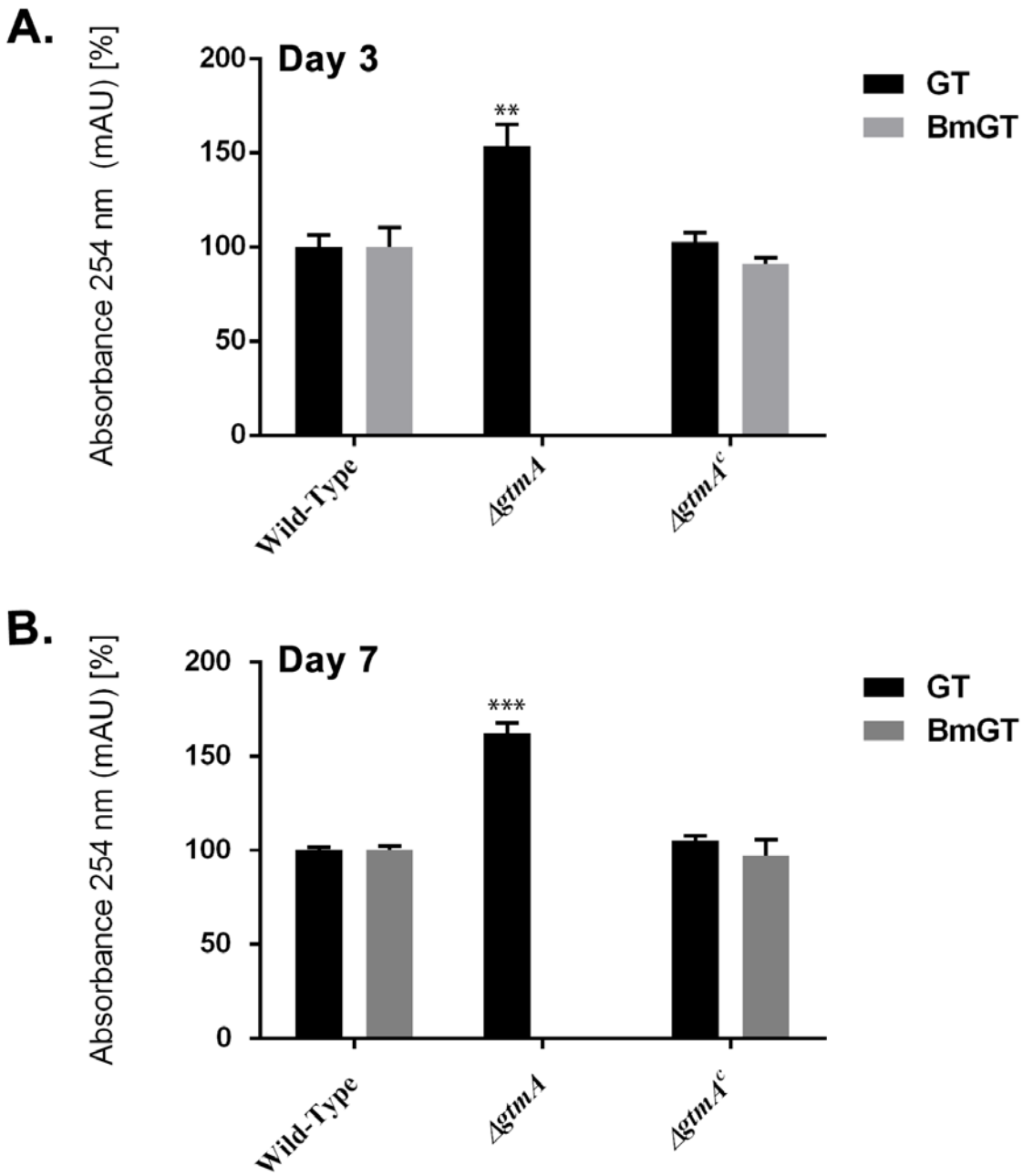

Figure 4.3. Deletion of *gtmA* significantly increases gliotoxin biosynthesis at day 3 (A) (p<0.0056) and day 7 (B) (p<0.0001) culture supernatants. *gtmA* complementation restores wild-type gliotoxin biosynthesis levels. The depicted values are from three independent samples. GT and BmGT levels in Δ*gtmA* and *gtmAC* are relative to the wild-type at day 3 and day 7. Error bars are SDs from the mean.

4.2.3 Phenotypic Analysis of *A. fumigatus* Δ*gtmA* in Response to Exogenous gliotoxin

In order to assess a possible role for *gtmA* in protection against gliotoxin-induced toxicity (Li et al., 2012), comparative phenotypic analysis of *A. fumigatus* Δ*gtmA* and wild-type was performed as described in Section 2.2.6. This analysis would determine any altered phenotype observed in the mutant strain thus identifying a role for *gtmA* expression in *A. fumigatus* following gliotoxin exposure.

In order to assess whether the loss of *gtmA* affected the growth rate of *A. fumigatus* Δ*gtmA*, the mutant was grown alongside the wild-type on Czapeks Dox agar alone - no difference in the growth rate between the two strains was observed. As shown in Figure 4.4, no significant difference in the growth rate of *A. fumigatus* Δ*gtmA* and the wild-type was observed for any of the concentrations of gliotoxin tested (0 – 10 µg/ml). However, growth of *A. fumigatus* Δ*gliT* (Schrettl et al., 2010) was completely inhibited upon exposure to 10 µg/ml gliotoxin.

4.2.4 Phenotypic Analysis of *A. fumigatus* Δ*gtmA* in Response to Hydrogen Peroxide

In the interest of assessing a possible role for *gtmA* in protection against hydrogen peroxide (H_2O_2) induced oxidative stress, comparative phenotypic analysis of *A. fumigatus* Δ*gtmA* and wild-type was performed as described in Section 2.2.6.

As shown in Figure 4.5, no significant difference in the growth rate of *A. fumigatus* Δ*gtmA* and wild-type was observed for any of the concentrations of H_2O_2 tested (0 – 2 mM). This result suggested that *gtmA* does not play a role in the protection against H_2O_2 induced oxidative stress.

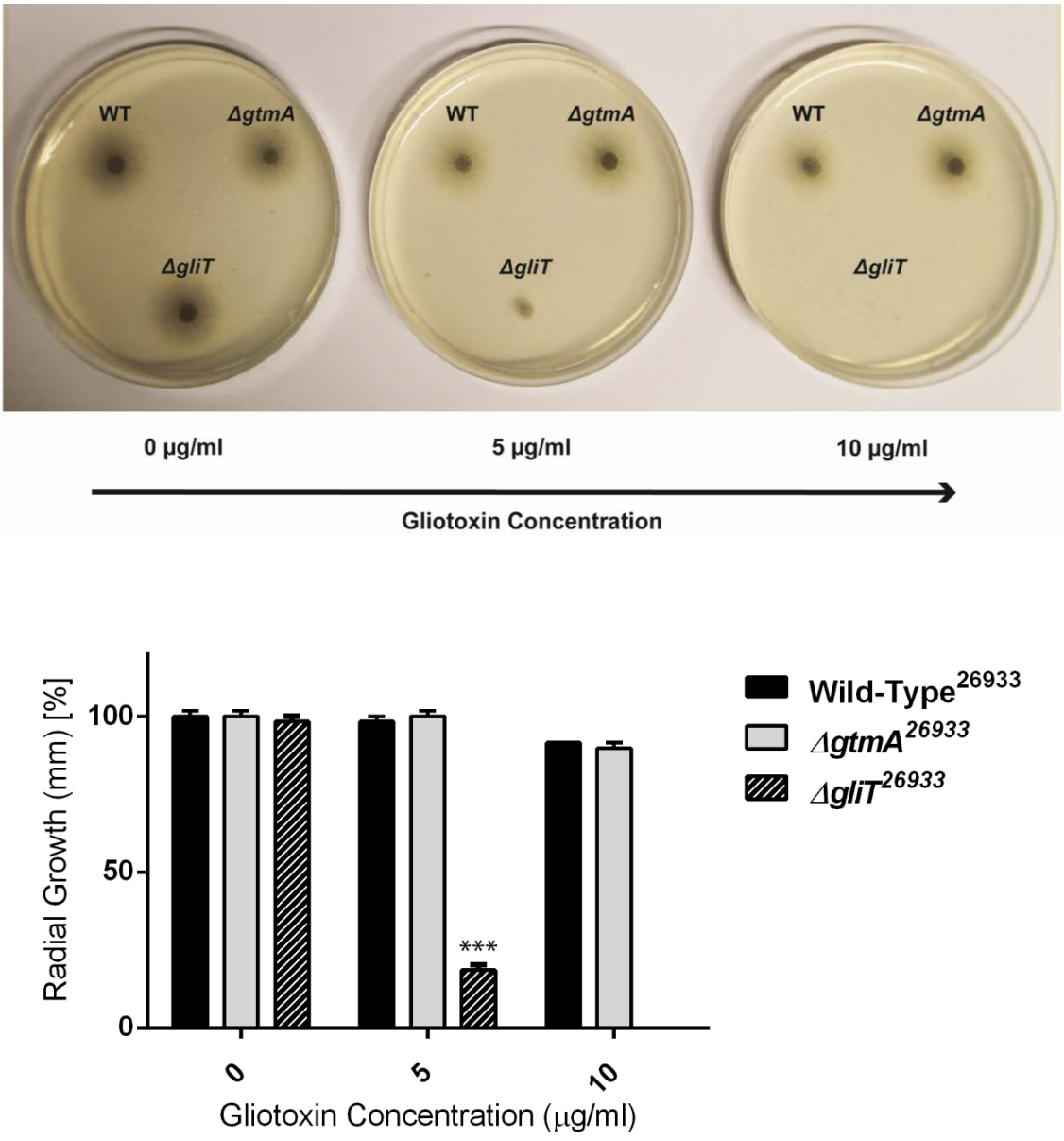

Figure 4.4. Exogenous gliotoxin (0 – 10 µg/ml) does not inhibit the growth of *A. fumigatus* Δ*gtmA* in comparison with the wild-type strain despite the growth of Δ*gliT* being completely inhibited at 10 µg/ml gliotoxin. Growth in Δ*gtmA* and Δ*gliT* are relative to the wild-type. The depicted values are from three independent samples. Error bars are SDs from the mean.

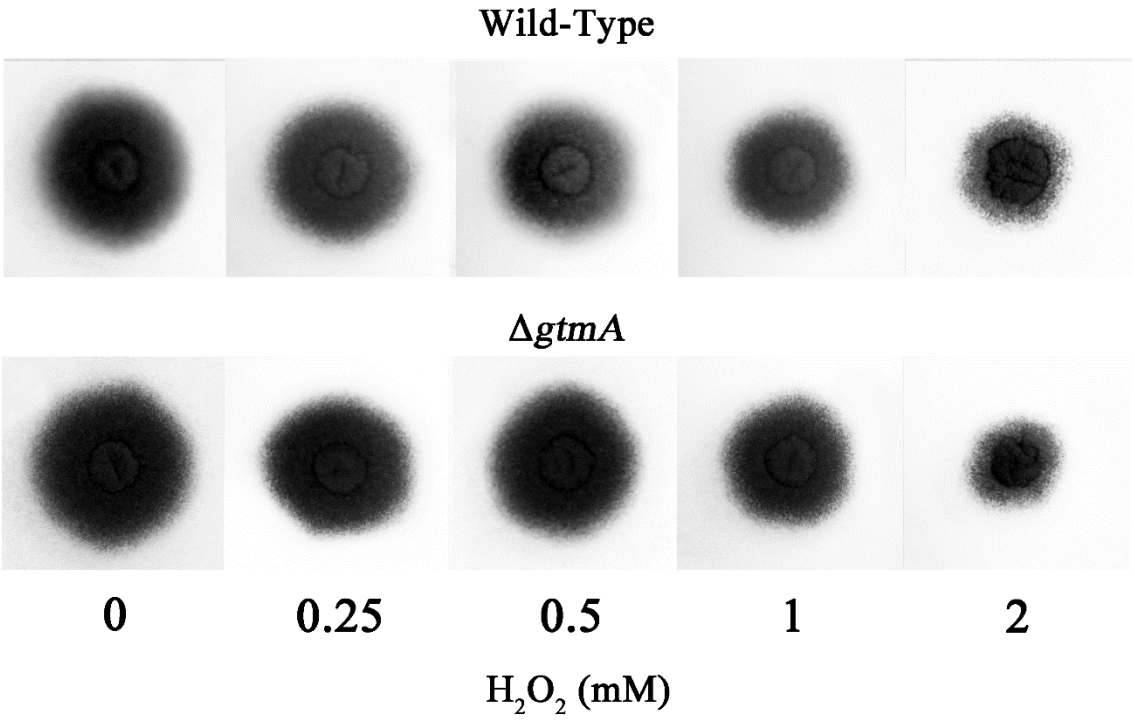

Figure 4.5. *A. fumigatus* wild-type and Δ*gtmA* respond identically to H_2O_2-induced oxidative stress (0 – 2 mM). No radial growth difference was noted at any of the concentrations tested.

4.2.5 *In Vivo* Gliotoxin Bisthiomethylation by *A. fumigatus*

Species which produce gliotoxin have been previously shown to take up this metabolite and convert it to its bisthiomethylated form (Kirby et al., 1980). *A. fumigatus* was treated with gliotoxin for 3 h (5 µg/ml final) as described in Section 2.2.17. Time point samples were taken every 30 min. The samples were organically extracted, as outlined in Section 2.2.12, and analysed by LC-MS. Figure 4.6 shows that the production of bis(methyl)gliotoxin (m/z 357) from spiked gliotoxin is evident in *A. fumigatus* ATCC26933. No bis(methyl)gliotoxin was detectable in the samples prior to gliotoxin treatment. Exogenously added gliotoxin (5 µg/ml) was taken up by *A. fumigatus* ATCC26933 and was converted to bis(methyl)gliotoxin over the course of 3 h. This was subsequently secreted into the culture medium over 3 h. Exogenously-added gliotoxin (5 µg/ml final) was taken up, but not converted, to bis(methyl)gliotoxin in *A. fumigatus* Δ*gtmA* whilst *gtmA* complementation restored the ability to biosynthesize bis(methyl)gliotoxin from exogenous gliotoxin. This result indicated that *gtmA* is directly, and likely solely responsible for the conversion of exogenously added gliotoxin to bis(methyl)gliotoxin.

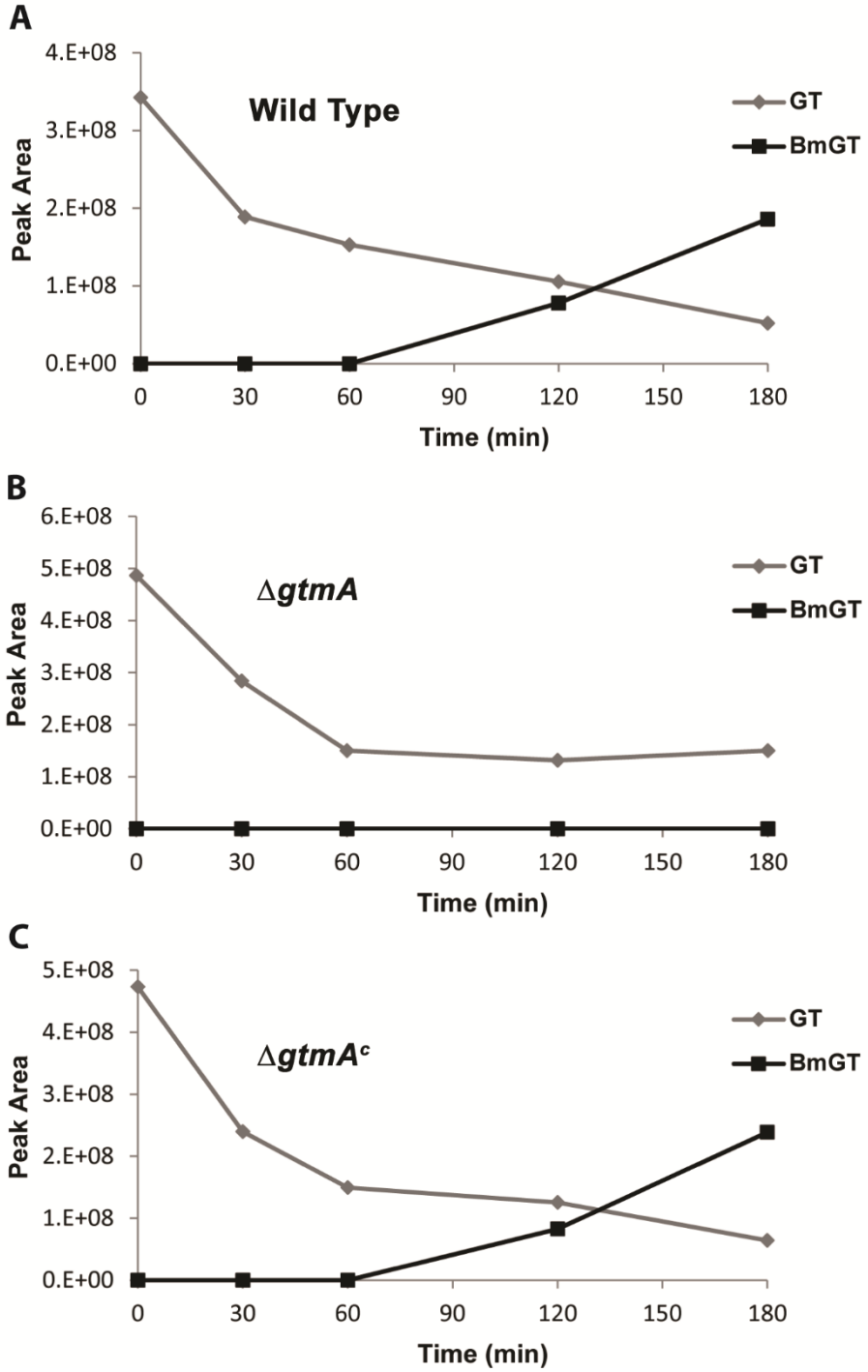

Figure 4.6. *A. fumigatus* converts exogenously-added gliotoxin to bis(methyl)gliotoxin in a time-dependent manner. Exogenously-added gliotoxin (5 μg/ml final) is taken up, but not converted to, bis(methyl)gliotoxin in *A. fumigatus* Δ*gtmA* whilst *gtmA* complementation restores the ability to biosynthesize bis(methyl)gliotoxin from exogenous gliotoxin. Graph depicts the levels of GT and BmGT in organically extracted culture supernatants. The depicted values are averaged from three independent samples.

4.2.6 *In Vitro* Enzyme-Mediated Gliotoxin Bismethylation

A. fumigatus wild-type, Δ*gliT* (Schrettl et al., 2010) and Δ*gtmA* mycelial lysates were obtained following 24 hr growth in Sabouraud-Dextrose media (21 h culture followed by 3 h supplementation with gliotoxin (5 mg/ml) or MeOH for 3 h. Mycelia were snap-frozen and ground in liquid N_2 and lysates were prepared as described in Section 2.2.16.5. Protein lysates were clarified by centrifugation prior to use in assays. Reaction mixtures comprised relevant lysate (20 µl), PBS (54 µl), SAM (25 mg/ml in PBS; 6 µl) and NADPH (60 mM; 10 µl). Negative controls used 20 µl lysis buffer in place of lysate. As demonstrated by Owens et al. (2015), lysates from *A. fumigatus* Δ*gliT* were shown to exhibit significantly elevated bisthiomethylation activity ($p<0.0013$) in comparison with those of wild-type *A. fumigatus* following prior gliotoxin exposure. Relevantly, Δ*gtmA* lysates did not exhibit any bisthiomethylation activity (Figure 4.7).

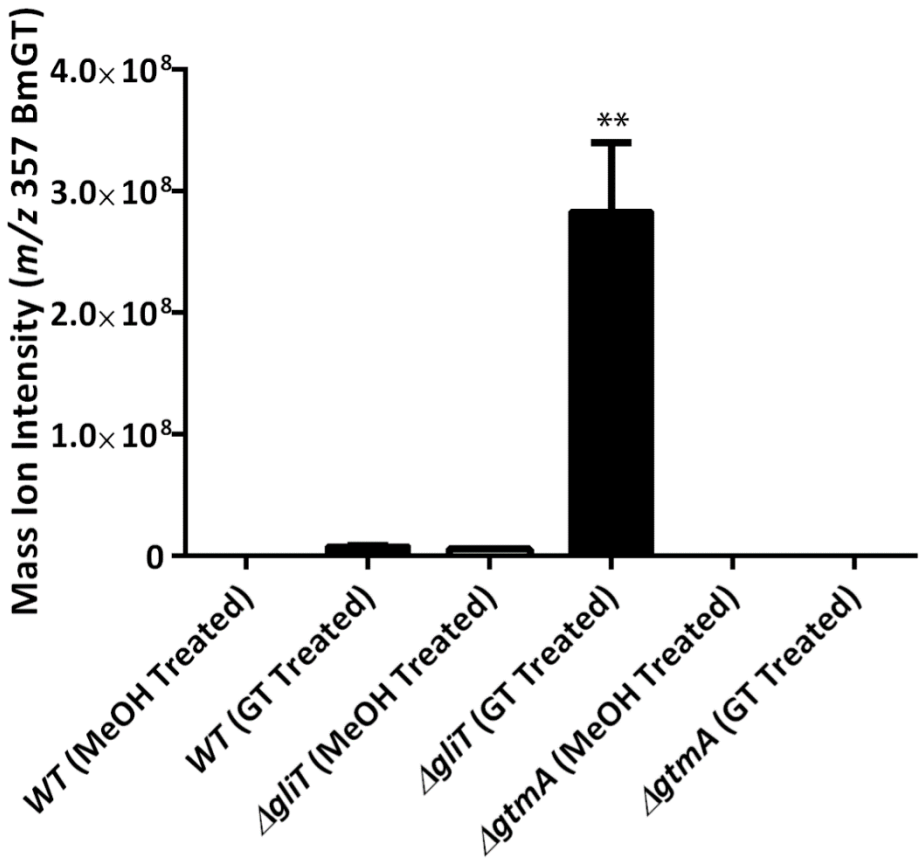

Figure 4.7. Detection of *bis*-thiomethylation activity by LC-MS exclusively in *A. fumigatus* Δ*gliT* protein lysates**.** Following gliotoxin induction (5 μg/ml for 3 h), protein lysates from *A. fumigatus* Δ*gliT* exhibit significantly elevated *bis*-thiomethylation activity (p<0.0013) when compared to wild-type *A. fumigatus* lysates. No bis(methyl)gliotoxin was detected in the Δ*gtmA* gliotoxin-exposed lysates. The depicted values are from three independent extracts. Error bars show calculated SD from the mean.

4.2.7 Confocal microscopy reveals that GtmA-eGFP is localised throughout the cytosol following gliotoxin exposure

As described in Section 2.2.8, the Δ*gtmA*::*gtmA-eGFP*::*H2A-mRFP* strain was prepared for confocal microscopy analysis. The results revealed that GtmA::eGFP accumulates in the cytosol of *A. fumigatus* following gliotoxin exposure (5 μg/ml, 3h) (Figure 4.8). Histone 2A monomeric red fluorescent protein fusion (H2A::mRFP), which was also transformed into this strain, clearly visualised the nuclei. No eGFP signal was detectable in either the methanol control or the Δ*gtmA* strain exposed to gliotoxin which contains no eGFP or mRFP.

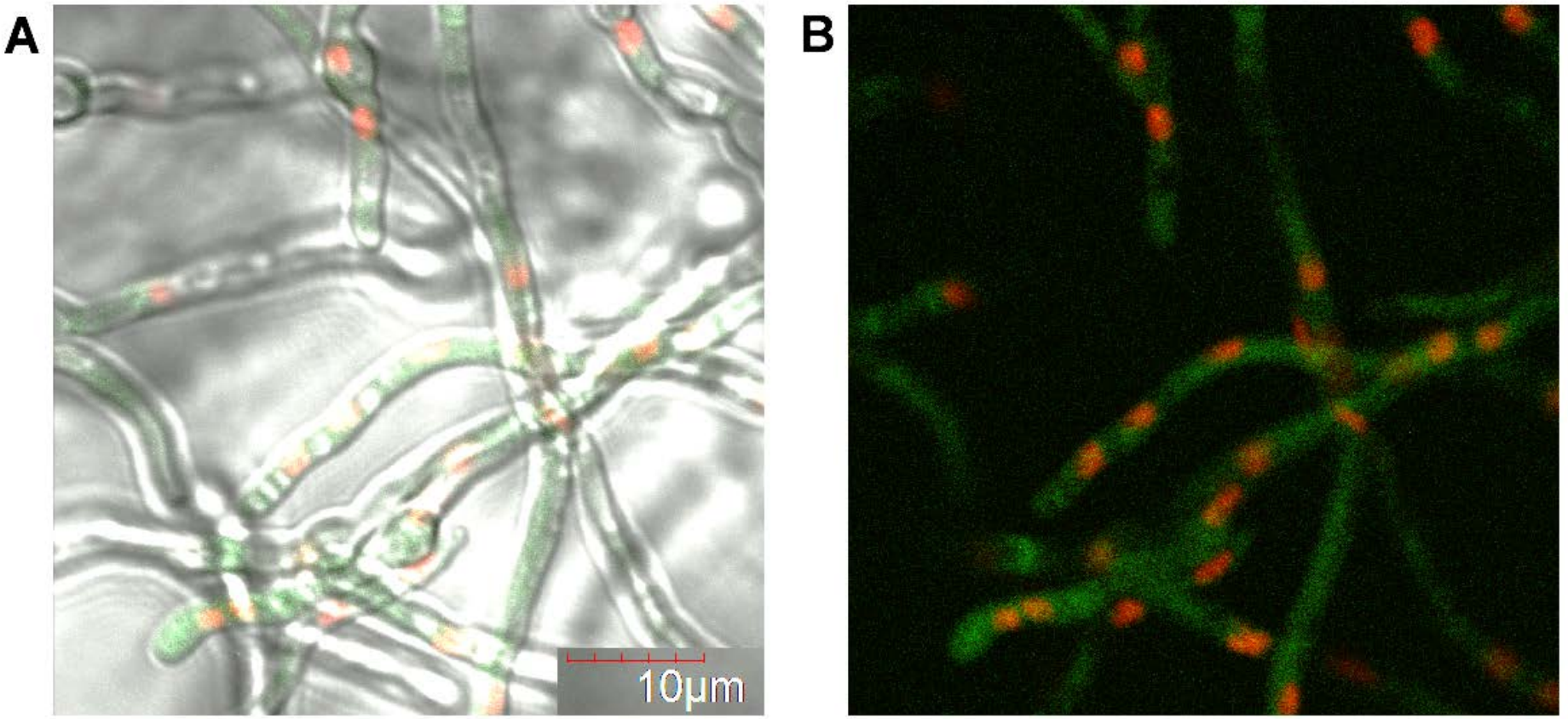

Figure 4.8. eGFP labelling of GtmA (GtmA::eGFP) revealed the rapid accumulation of this enzyme to the cytosol following 3h gliotoxin exposure (5 µg/ml). Histone 2A monomeric red fluorescent protein fusion (H2A::mRFP) visualizes the nuclei. The GtmA::eGFP signal was not detectable in the MeOH controls. A: Bright-field, eGFP and mRFP signal overlay. B: eGFP and mRFP signal overlay.

4.2.8 Comparative proteomic analysis of *A. fumigatus* wild-type and Δ*gtmA* exposed to gliotoxin

In order to elucidate the effect of exogenous gliotoxin exposure on the proteome of Δ*gtmA* following exposure to exogenous gliotoxin, quantitative label-free proteomics was carried out as described in Section 2.2.16.5. *A. fumigatus* wild-type and Δ*gtmA* were exposed to either gliotoxin (5 µg/ml) or a methanol control for 3 h following 21 h growth in Sabouraud-Dextrose broth. Mycelia was harvested and lysed and the samples were processed. A total of 8 proteins were uniquely detected in the wild-type samples exposed to gliotoxin when compared to the control. 12 proteins were detected with a significantly higher abundance upon gliotoxin treatment (Table 4.1). A total of 4 proteins were uniquely detected in the *A. fumigatus* Δ*gtmA* samples exposed to gliotoxin in comparison with the control. 7 proteins were detected with a significantly higher abundance upon gliotoxin treatment (Table 4.2).The quantitative proteomic results indicated *A. fumigatus* wild-type (Table 4.1) and Δ*gtmA* (Table 4.2) respond to gliotoxin exposure by increasing the abundance of Yap1 dependent catalases and *gli*-cluster encoded gliotoxin biosynthetic enzymes. Both strains exhibited a significantly increased abundance of mycelial catalase Cat1 (wild-type/Δ*gtmA*: $\log_2$ 3.552/ $\log_2$ 3.435), GliT ($\log_2$ 5.125/ $\log_2$ 4.869) and the bifunctional catalase-peroxidase Cat2 ($\log_2$ 1.947/ $\log_2$ 1.205). This indicated that both the wild-type and Δ*gtmA* strains have a very similar proteomic response to gliotoxin. Notably, GtmA is highly abundant in the wild-type samples following gliotoxin exposure whereas it is completely absent in *A. fumigatus* Δ*gtmA*.

Table 4.1. Proteins with **increased** abundance (or uniquely detected) in *A. fumigatus* wild-type with gliotoxin compared to wild-type with methanol. Data sorted by fold change, in descending order.

Protein Description	**Log_2(Fold Increase)**	**p-value**	**Peptides**	**Sequence coverage [%]**	**Protein IDs**
Putative zinc knuckle transcription factor; transcript induced by exposure to human airway epithelial cells	Unique	N/A	2	4.6	AFUA_3G10840
Has domain(s) with predicted hydrolase activity	Unique	N/A	5	28	AFUA_5G12770
Predicted *O*-methyltransferase, encoded in the putative gliotoxin biosynthetic gene cluster. **GliM.**	Unique	N/A	8	20.9	AFUA_6G09680
Glutathione S-transferase encoded in the gliotoxin biosynthetic gene cluster; not involved in self-protection against gliotoxin. **GliG.**	Unique	N/A	4	29.2	AFUA_6G09690
Ortholog(s) have role in circadian rhythm, hyphal growth and cytosol localization	Unique	N/A	3	3.4	AFUA_1G13060
Has domain(s) with predicted oxidoreductase activity and role in metabolic process	Unique	N/A	3	7.8	AFUA_5G10180

Protein Description	Log_2(Fold Increase)	p-value	Peptides	Sequence coverage [%]	Protein IDs
Ortholog(s) have cytoplasm localization	Unique	N/A	4	15	AFUA_5G11760
Has domain(s) with predicted oxidoreductase activity and role in metabolic process	Unique	N/A	11	22	AFUA_6G03490
Gliotoxin sulfhydryl oxidase required for gliotoxin biosynthesis; encoded in gliotoxin biosynthetic gene cluster; involved in self-protection against exogenous gliotoxin; **GliT.**	5.125	5.97E-05	13	62.9	AFUA_6G09740
Has domain(s) with predicted methyltransferase activity. **GtmA.**	4.991	5.34E-06	10	44.7	AFUA_2G11120
Uncharacterized ORF	4.379	7.92E-04	6	31.3	AFUA_6G09745
Predicted methyltransferase, encoded in the putative gliotoxin biosynthetic gene cluster. **GliN.**	3.990	1.48E-04	17	72	AFUA_6G09720
Mycelial catalase; induced in hyphae exposed to neutrophils; protein induced in amphotericin B and H2O2; stuA-dependent up-regulation	3.552	1.70E-07	13	26.4	AFUA_3G02270

Protein Description	Log_2(Fold Increase)	p-value	Peptides	Sequence coverage [%]	Protein IDs
in developmentally competent hyphae; hypoxia repressed; SrbA-regulated; repressed by gliotoxin exposure					
Glyoxalase family protein	2.574	3.19E-03	3	16.9	AFUA_7G05015
Putative bifunctional catalase-peroxidase; induction in response to hydrogen peroxide Yap1-dependent; transcript induced by exposure to human airway epithelial cells; SrbA-regulated during hypoxia	1.947	7.47E-05	34	63.6	AFUA_8G01670
Putative fructosyl amine; transcript induced by voriconazole	1.913	1.78E-02	11	32.2	AFUA_6G03440
Putative methoxylase	1.830	2.84E-02	9	42.1	AFUA_3G15010
ThiJ/PfpI family protein; abundant in conidia	1.649	5.91E-04	4	22.5	AFUA_5G01430
Ortholog(s) have intracellular localization	1.529	1.86E-03	11	52.8	AFUA_3G13140
Putative p-nitroreductase family protein; protein induced by heat shock; Yap1-dependent induction in response to hydrogen peroxide; induced by gliotoxin exposure	1.278	4.19E-02	6	35.5	AFUA_5G09910

Table 4.2. Proteins with **increased** abundance (or unique to) *A. fumigatus* Δ*gtmA* with gliotoxin (5 µg/ml; 3 h) compared to Δ*gtmA* with methanol. Data sorted by fold change, in descending order.

Protein Description	**Log_2(Fold Increase)**	**p-value**	**Peptides**	**Sequence coverage [%]**	**Protein IDs**
Ortholog(s) have cytosol, nucleus localization	Unique	N/A	4	18.3	AFUA_6G12780
Has domain(s) with predicted hydrolase activity	Unique	N/A	5	28	AFUA_5G12770
Predicted *O*-methyltransferase, encoded in the putative gliotoxin biosynthetic gene cluster. **GliM**.	Unique	N/A	8	20.9	AFUA_6G09680
Glutathione S-transferase encoded in the gliotoxin biosynthetic gene cluster; required for gliotoxin biosynthesis; **GliG**.	Unique	N/A	4	29.2	AFUA_6G09690
Gliotoxin sulfhydryl oxidase required for gliotoxin biosynthesis; involved in self-protection against exogenous gliotoxin; **GliT.**	4.879	6.26E-06	13	62.9	AFUA_6G09740
Uncharacterized ORF, **GliN**	4.023	3.99E-03	17	72	AFUA_6G09720
Mycelial catalase; induced in hyphae exposed to neutrophils; protein induced in amphotericin B and H_2O_2; stuA-dependent up-regulation	3.435	9.95E-06	13	26.4	AFUA_3G02270

Protein Description	Log_2(Fold Increase)	p-value	Peptides	Sequence coverage [%]	Protein IDs
in developmentally competent hyphae; hypoxia repressed; SrbA-regulated; repressed by gliotoxin exposure					
Ortholog of *Aspergillus brasiliensis*: Aspbr1_0199026, *Neosartorya fischeri NRRL 181*	3.178	5.30E-03	6	31.3	AFUA_6G09745
Glyoxalase family protein	2.367	2.28E-03	3	16.9	AFUA_7G05015
Putative bifunctional catalase-peroxidase; induction in response to hydrogen peroxide Yap1-dependent; SrbA-regulated during hypoxia.	2.028	1.44E-04	34	63.6	AFUA_8G01670
Ortholog(s) have intracellular localization	1.205	8.98E-03	11	52.8	AFUA_3G13140

4.2.9 Comparative proteomic analysis of *A. fumigatus* wild-type and Δ*gtmA* exposed to bis(methyl)gliotoxin compared to a methanol control

In order to elucidate the effect of exogenous bis(methyl)gliotoxin exposure on the proteome of Δ*gtmA* following exposure to exogenous bis(methyl)gliotoxin, quantitative label-free proteomics was carried out as outlined in Section 2.2.16.5. Briefly, *A. fumigatus* wild-type and Δ*gtmA* were exposed to either bis(methyl)gliotoxin (5 µg/ml) or a methanol control for 3 h following 21 h growth in Sabouraud-Dextrose broth. Mycelia were harvested and lysed and the samples were processed. LFQ proteomics analysis revealed that exogenous bis(methyl)gliotoxin exposure resulted in a significantly increased abundance of GliT, $\log_2$ 1.985 fold increase, and GtmA, $\log_2$ 1.933 fold increase, in *A. fumigatus* wild-type. It also highlighted that the abundance of only 4 other proteins were significantly altered (unique or increased) (Table 4.3). Of all the proteins to undergo differential abundance (bis(methyl)gliotoxin versus methanol exposure), GliT and GtmA abundance was observed to be the most significantly altered. Moreover, no other *gli* cluster-encoded proteins were found to exhibit an altered abundance following bis(methyl)gliotoxin exposure when compared to the methanol control. Δ*gtmA* also showed an increased abundance of GliT ($\log_2$ 1.985 fold increase) in response to bis(methyl)gliotoxin. (Table 4.4)

Table 4.3. Proteins with **increased** abundance, or unique to, *A. fumigatus* wild-type with BmGT (5 μg/ml; 3 h) compared to wild-type with methanol. Data sorted by fold change, in descending order.

Protein Description	**Log_2(Fold Increase)**	**p-value**	**Peptides**	**Sequence [%]**	**Protein IDs**
Has domain(s) with predicted oxidoreductase activity and role in metabolic process	Unique	N/A	3	7.8	AFUA_5G10180
Ortholog(s) have cytoplasm localization	Unique	N/A	4	15	AFUA_5G11760
Has domain(s) with predicted methyltransferase activity. **GtmA.**	1.933	5.01E-05	10	44.7	AFUA_2G11120
Gliotoxin sulfhydryl oxidase required for gliotoxin biosynthesis; encoded in gliotoxin biosynthetic gene cluster; involved in self-protection against exogenous gliotoxin; **GliT.**	1.985	8.69E-03	13	62.9	AFUA_6G09740
Conidial cell wall hydrophobin involved in conidial cell wall composition; not required for normal rodlet layer; protein repressed by amphotericin B; upregulated in biofilm vs planktonic culture; repressed by exposure to artemisinin	1.930	1.59E-02	4	52.1	AFUA_1G17250

Protein Description	Log_2(Fold Increase)	p-value	Peptides	Sequence [%]	Protein IDs
Non-heme Fe(II) and alpha-ketoglutarate-dependent dioxygenase; phytanoyl-CoA dioxygenase family protein; catalyses the conversion of fumitremorgin B to verruculogen	1.045	1.38E-02	13	56.7	AFUA_8G00230

Table 4.4. Proteins with **increased** abundance, or unique to, *A. fumigatus* with BmGT (5 µg/ml; 3 h) compared to wild-type with methanol. Data sorted by fold change, in descending order.

Protein Description	**Log_2(Fold Increase)**	**p-value**	**Peptides**	**Sequence [%]**	**Protein IDs**
Transcript up-regulated in conidia exposed to neutrophils	Unique	N/A	3	44.4	AFUA_2G13590
Ortholog(s) have Golgi apparatus, endoplasmic reticulum localization	Unique	N/A	3	23.4	AFUA_4G07390
Gliotoxin sulfhydryl oxidase required for gliotoxin biosynthesis; encoded in gliotoxin biosynthetic gene cluster; involved in self-protection against exogenous gliotoxin; **GliT**	1.678	2.16E-02	13	62.9	AFUA_6G09740
Ortholog of *A. nidulans FGSC A4*: AN5353, *A. niger CBS 513.88*: An02g05680,	1.032	1.78E-03	5	25.2	AFUA_6G14470

4.2.10 Label-free quantitative (LFQ) proteomics reveals elevated abundance of *gli*-encoded enzymes in *A. fumigatus* Δ*gtmA*

In order to elucidate the effect of the abrogation of *gtmA* expression on the proteome of *A. fumigatus* during incubation in secondary metabolite producing conditions (Section 4.2.2), quantitative label-free proteomics was carried out as described in Section 2.2.16.5. *A. fumigatus* wild-type, Δ*gtmA* and *gtmA*^{c} were cultured in Czapeks-Dox broth for 72 h, 200 rpm. The cultures were not exposed to gliotoxin for this experiment. Mycelia were harvested and lysed and the samples were processed.

The analysis revealed a significantly increased abundance ($p< 0.05$) of GliM ($\log_2$ 1.467 fold), GliP ($\log_2$ 1.399 fold) and GliF ($\log_2$ 1.297 fold) in Δ*gtmA* when compared to the wild-type (Table 2.5). This led to the conclusion that, in the absence of GtmA and abrogated bis(methyl)gliotoxin formation, expression of the *gli* cluster is significantly induced by *endogenous* gliotoxin in comparison with the wild-type strain. Notably, the unique presence of 7 proteins and significantly increased abundance of 18 additional proteins was observed in *A. fumigatus* Δ*gtmA* protein lysates (Table 4.5). As demonstrated in Table 4.7, GtmA presence is restored in *A. fumigatus gtmA*^{c} thus confirming the result observed following Southern analysis of the complementation of *gtmA* deletion (Section 3.2.7). Importantly, when the proteome of the wild-type versus *gtmA*^{c} was analysed, GliM, GliP and GliF were not differentially abundant which unambiguously confirms that *gtmA* complementation restored *gli* cluster regulation to that of the *A. fumigatus* wild-type (Table 4.7). Moreover, GliM, GliN and GliF abundance was significantly higher ($\log_2$ 1.324, 1.115 and 1.475, respectively) in *A. fumigatus* Δ*gtmA* than in *gtmA*^{c}, convincingly demonstrating that *gtmA* loss augments *gli* cluster-encoded enzyme levels.

Table 4.5. Proteins with **increased** abundance (or unique) in *A. fumigatus* Δ*gtmA* strains grown for 72 h in Czapeks Dox Media compared to wild-type. Data sorted by fold change, in descending order.

Protein Description	**Log_2(Fold Increase)**	**p-value**	**Peptides**	**Sequence [%]**	**Protein IDs**
Ortholog of A. oryzae RIB40 : AO090701000613, Neosartorya fischeri NRRL 181 : NFIA_094160	Unique	N/A	4	6.6	AFUA_8G00730
Ortholog(s) have role in austinol biosynthetic process, dehydroaustinol biosynthetic process, sporocarp development involved in sexual reproduction	Unique	N/A	4	13.5	AFUA_6G13970
Putative cyclophilin; peptidyl-prolyl cis-trans isomerase-like protein	Unique	N/A	3	23	AFUA_6G02140
Ortholog(s) have role in cellular response to drug, nuclear-transcribed mRNA catabolic process, rRNA processing,	Unique	N/A	2	16.6	AFUA_5G13470

Protein Description	Log_2(Fold Increase)	p-value	Peptides	Sequence [%]	Protein IDs
ribosomal large subunit assembly and nucleolus, nucleoplasm, preribosome, large subunit precursor localization					
Predicted aminopeptidase, metalloexopeptidase; encoded in the fma (fumagillin) secondary metabolite gene cluster	Unique	N/A	2	11.8	AFUA_8G00460
Ortholog(s) have role in ascospore formation, sporocarp development involved in sexual reproduction and nucleus localization	Unique	N/A	4	7.2	AFUA_1G15810
Predicted O-methyltransferase, encoded in the putative gliotoxin biosynthetic gene cluster, **GliM**	1.467	1.97E-03	4	11.6	AFUA_6G09680
Ortholog(s) have DNA binding, DNA-directed RNA polymerase activity, RNA binding activity and role in chromatin silencing by small RNA, transcription from RNA polymerase II promoter	1.457	3.21E-03	13	12.4	AFUA_7G01920

Protein Description	Log_2(Fold Increase)	p-value	Peptides	Sequence [%]	Protein IDs
Tubulin beta-2 subunit; predicted gene pair with AFUA_1G10910 (tubA)	1.409	4.00E-03	13	32.8	AFUA_7G00250
Non-ribosomal peptide synthetase encoded in the gliotoxin biosynthetic gene cluster; regulated by the transcription factor StuA; expression increases *in vivo*, **GliP**	1.399	4.42E-03	5	3.5	AFUA_6G09660
Ortholog(s) have cytosol, nucleus localization	1.366	3.07E-02	4	14.8	AFUA_1G06780
Ortholog(s) have cytoplasmic mRNA processing body localization	1.350	2.54E-02	3	5.7	AFUA_3G10220
Has domain(s) with predicted nucleotide binding, oxidoreductase activity and role in metabolic process	1.329	1.48E-02	10	67	AFUA_1G00990
Predicted cytochrome P450 monooxygenase, encoded in the putative gliotoxin biosynthetic gene cluster, **GliF**	1.297	1.67E-02	6	16.3	AFUA_6G09730

Protein Description	Log_2(Fold Increase)	p-value	Peptides	Sequence [%]	Protein IDs
Thiazole biosynthesis enzyme; hypoxia induced protein; induced by gliotoxin exposure	1.361	3.31E-03	12	38.3	AFUA_6G08360
Anthranilate phosphoribosyl transferase; no human homolog	1.185	3.89E-03	4	16.1	AFUA_4G11980
Ortholog of *A. nidulans FGSC A4*: AN3605, *A. niger CBS 513.88*: An03g02780	1.150	4.22E-03	6	26.5	AFUA_4G12710
Molecular chaperone; conidia-enriched protein	1.128	2.16E-02	36	63.2	AFUA_1G07440
Ortholog of *A. nidulans FGSC A4*: AN8072, *A. oryzae RIB40*: AO090003001347	1.111	2.39E-03	4	21.3	AFUA_5G01770
Eukaryotic translation initiation factor eIF4A; ATP-dependent RNA helicase; protein induced by heat shock; predicted gene pair with AFUA_5G02410	1.106	2.44E-02	16	53.2	AFUA_3G08160
Putative malate synthase; protein abundant in conidia	1.103	3.74E-02	5	11.5	AFUA_6G03540

Protein Description	Log_2(Fold Increase)	p-value	Peptides	Sequence [%]	Protein IDs
Putative mitogen-activated protein kinase (MAPK)	1.097	2.44E-02	9	31.7	AFUA_6G12820
Clathrin, heavy chain; transcript downregulated in response to amphotericin B	1.128	1.10E-03	53	48	AFUA_4G07700
Ortholog(s) have cytoplasm localization	1.065	2.59E-02	16	35	AFUA_1G03400
Septin; unique to filamentous fungi; localizes to long tubular structures within hyphae and to newly formed septa	1.059	4.67E-02	4	7.1	AFUA_3G07015
Ortholog(s) have preprotein binding activity, role in conidium formation, hyphal growth, protein targeting to mitochondrion and mitochondrial outer membrane translocase complex localization	1.034	1.73E-02	6	13.3	AFUA_2G01660

Table 4.6. Proteins with **decreased** abundance (or absent) in *A. fumigatus* Δ*gtmA* strains grown for 72 h in Czapeks Dox Media compared to wild-type. Data sorted by fold change, in descending order.

Protein Description	**Log_2(Fold Decrease)**	**p-value**	**Peptides**	**Sequence [%]**	**Protein IDs**
Ortholog(s) have cytosol, nucleus localization	Absent	N/A	2	14.9	AFUA_1G10960
Has domain(s) with predicted methyltransferase activity	Absent	N/A	10	41	AFUA_2G11120
Ortholog(s) have enzyme activator activity, heme binding activity, role in ergosterol biosynthetic process, regulation of ergosterol biosynthetic process and endoplasmic reticulum, endosome localization	Absent	N/A	2	19.4	AFUA_3G10490
Ortholog of *S. cerevisiae*: YER010C, *A. nidulans* FGSC A4: AN10700, *A. niger* CBS 513.88: An04g05730	Absent	N/A	2	8.2	AFUA_4G10940
Ortholog of *A. nidulans FGSC A4*: AN7836, *A. oryzae RIB40*: AO090003000833	Absent	N/A	4	14.6	AFUA_7G01060

Protein Description	**Log_2(Fold Decrease)**	**p-value**	**Peptides**	**Sequence [%]**	**Protein IDs**
Ortholog(s) have RNA polymerase II core binding, TFIIF-class binding transcription factor activity, chromatin binding activity	Absent	N/A	4	10.4	AFUA_2G11190
Protein of unknown function identified by mass spectrometry	Absent	N/A	2	9.8	AFUA_2G14370
Putative NIPSNAP family protein	Absent	N/A	3	9.9	AFUA_3G06660
Ortholog(s) have AMP deaminase activity, role in guanine salvage, purine nucleotide metabolic process and cytosol localization	Absent	N/A	3	2.3	AFUA_8G02860
Ortholog of *Neosartorya fischeri NRRL 181*: NFIA_105510, *Aspergillus wentii*: Aspwe1_0166738	-1.649	2.23E-02	2	19.8	AFUA_4G10560
Putative class III family 18 chitinase	-1.646	2.38E-02	2	7.6	AFUA_7G05140
Conserved protein, predicted adhesin; expression induced in biofilm	-1.083	4.42E-02	9	12.9	AFUA_7G05340

Table 4.7. Proteins with **increased** abundance (or uniquely detected) in *A. fumigatus* Δ*gtmA* compared to *gtmA*^{c} grown for 72 h in Czapeks Dox Media. Data sorted by fold change, in descending order.

Protein Description	Log_2(Fold Increase)	p-value	Peptides	Sequence coverage [%]	Protein IDs
Putative hydrolase; member of the pseurotin A gene cluster	Unique	N/A	2	5.5	AFUA_8G00570
Ortholog(s) have cell septum, fungal-type vacuole, late endosome, plasma membrane localization	Unique	N/A	2	17.8	AFUA_6G11270
Ortholog of *A. nidulans FGSC A4*: AN5204, *A. niger CBS 513.88*: An07g09060	Unique	N/A	2	7.7	AFUA_6G07370
Ortholog(s) have role in mRNA export from nucleus and nucleus localization	Unique	N/A	4	1.3	AFUA_4G10780
Putative secreted aminopeptidase; predicted signal sequence for secretion	Unique	N/A	3	13.6	AFUA_4G04210
Ortholog(s) have nitronate monooxygenase activity and role in denitrification pathway, detoxification of nitrogen compound	Unique	N/A	5	20.3	AFUA_2G17430
Ortholog(s) have nuclear pore localization	Unique	N/A	3	5.4	AFUA_2G08560
Ortholog of *Neosartorya fischeri NRRL 181*: NFIA_064340	1.650	4.06E-02	4	14.5	AFUA_3G12982

Protein Description	Log_2(Fold Increase)	p-value	Peptides	Sequence coverage [%]	Protein IDs
Predicted O-methyltransferase, encoded in the putative gliotoxin biosynthetic gene cluster, **GliM**	1.324	3.60E-03	4	11.6	AFUA_6G09680
Predicted cytochrome P450 monooxygenase, encoded in the putative gliotoxin biosynthetic gene cluster, **GliF**	1.475	1.48E-02	6	16.3	AFUA_6G09730
Protein of unknown function; transcript downregulated in response to voriconazole	1.283	2.65E-02	10	39.1	AFUA_4G14380
Ortholog of *A. fumigatus Af293*: Afu6g09720/gliN, Afu8g00550, *A. niger CBS 513.88*: An07g05460	1.151	2.10E-02	3	16.5	AFUA_5G13860
Predicted methyltransferase, encoded in the putative gliotoxin biosynthetic gene cluster, **GliN**	1.115	3.33E-02	18	74.8	AFUA_6G09720
Ortholog(s) have cytoplasm localization	1.084	4.69E-02	16	35	AFUA_1G03400
Baeyer-Villiger monooxygenase (BVMO); hypoxia induced protein; encoded in the fma (fumagillin) secondary metabolite gene cluster	1.079	2.69E-02	43	62.3	AFUA_8G00440

Table 4.8. Proteins with **decreased** abundance (or absent) in *A. fumigatus* Δ*gtmA* compared to *gtmA*^{c} grown for 72 h in Czapeks Dox Media. Data sorted by fold change, in descending order.

Protein Description	Log_2(Fold Increase)	p-value	Peptides	Sequence coverage [%]	Protein IDs
Ortholog(s) have role in positive regulation of RNA polymerase II transcriptional preinitiation complex assembly, proteasome regulatory particle assembly, ubiquitin-dependent protein catabolic process	Absent	N/A	2	6.7	AFUA_1G06170
Ortholog(s) have cytosol, nucleus localization	Absent	N/A	2	14.9	AFUA_1G10960
Has domain(s) with predicted methyltransferase activity	Absent	N/A	10	41	AFUA_2G11120
Ortholog(s) have RNA polymerase II core binding, TFIIF-class binding transcription factor activity, chromatin binding activity	Absent	N/A	4	10.4	AFUA_2G11190
Putative class V chitin synthase; required for normal hyphal growth, conidiation and normal conidiophore development; mutants have decreased chitin content	Absent	N/A	6	4.9	AFUA_2G13440

Protein Description	Log_2(Fold Increase)	p-value	Peptides	Sequence coverage [%]	Protein IDs
Ortholog(s) have enzyme activator activity, heme binding activity, role in ergosterol biosynthetic process, regulation of ergosterol biosynthetic process and endoplasmic reticulum, endosome localization	Absent	N/A	2	19.4	AFUA_3G10490
Ortholog of *A. nidulans FGSC A4*: AN5509, AN2837, AN2029, *A. oryzae RIB40* : AO090023000015	Absent	N/A	2	4.5	AFUA_4G00200
Ortholog(s) have Golgi apparatus localization	Absent	N/A	3	14	AFUA_1G05730
Protein of unknown function identified by mass spectrometry	Absent	N/A	2	9.8	AFUA_2G14370
Putative NIPSNAP family protein; transcript up-regulated in conidia exposed to neutrophils	Absent	N/A	3	9.9	AFUA_3G06660
Putative 30-kilodalton heat shock protein; conidia-enriched protein; protein levels increase in response to amphotericin B and hydrogen peroxide	Absent	N/A	2	17.8	AFUA_3G14540

Protein Description	Log_2(Fold Increase)	p-value	Peptides	Sequence coverage [%]	Protein IDs
Putative oxidosqualene:lanosterol cyclase (OSLC) with a role in protostadienol biosynthesis; SrbA-regulated during hypoxia	Absent	N/A	2	3.5	AFUA_5G04080
Galactofuranosyltransferase involved in biosynthesis of galactofuranose antigen of cell wall O-glycan	Absent	N/A	4	9.9	AFUA_6G02120
Ortholog of *A. nidulans FGSC A4*: AN3716, *A. niger CBS* 513.88 : An08g10710	Absent	N/A	3	7.4	AFUA_6G12770
Has domain(s) with predicted catalytic activity, pyridoxal phosphate binding activity	Absent	N/A	4	13.5	AFUA_7G01590
Ortholog(s) have AMP deaminase activity, role in guanine salvage, purine nucleotide metabolic process and cytosol localization	Absent	N/A	3	2.3	AFUA_8G02860
Putative coenzyme A transferase; transcript induced by exposure to human airway epithelial cells	Absent	N/A	2	5.7	AFUA_8G05580

Protein Description	Log_2(Fold Increase)	p-value	Peptides	Sequence coverage [%]	Protein IDs
Ortholog(s) have endoplasmic reticulum, extracellular region localization	-1.753	2.23E-02	4	12.3	AFUA_2G16720
Protein with Yap1-dependent induction in response to hydrogen peroxide; calcium downregulated; induced by gliotoxin exposure	-1.513	4.54E-03	9	41	AFUA_5G14680
Ortholog(s) have role in mitochondrial respiratory chain complex I assembly and mitochondrial membrane localization	-1.132	1.82E-02	6	38.6	AFUA_6G12280
Putative pyruvate decarboxylase with a predicted role in pyruvate metabolism; reacts with rabbit immunosera exposed to *A. fumigatus* conidia; higher expression in 48 h biofilm vs planktonic cells; protein increases during hypoxia	-1.123	1.33E-02	14	37.6	AFUA_3G11070
Putative amino acid permease; transcript up-regulated in conidia exposed to neutrophils and by growth on BSA as a sole nitrogen source	-1.106	1.81E-02	5	8.4	AFUA_7G04290

Protein Description	**Log_2(Fold Increase)**	**p-value**	**Peptides**	**Sequence coverage [%]**	**Protein IDs**
Ortholog of *A. nidulans FGSC A4* : AN2953, *A. niger CBS 513.88* : An02g11360,	-1.035	1.18E-02	10	40.6	AFUA_3G07890
Ras GTPase; hypoxia repressed protein	-1.000	5.31E-03	6	35.8	AFUA_1G02190

4.2.11 GtmA phylogeny

Phylogenetic analysis of GtmA was carried out in collaboration with Dr David Fitzpatrick of Maynooth University. As described in Section 4.2.11, using *A. fumigatus* GtmA as a query sequence, 124 homologs in 103 fungal genomes were located. GtmA orthology was inferred using three approaches. Firstly, proteins which shared a bidirectional best hit to *A. fumigatus* GtmA, AFUA_2G11120, were located (Figure 4.9). Secondly, a GtmA phylogenetic tree was reconstructed (Figure 4.10). Finally, the synteny around GtmA homologs was viewed to confirm orthology (Figure 4.11). All proteins that share a bidirectional BlastP hit with *A. fumigatus* GtmA are located in a single clade (Figure 4.9, clade-A). It is worth noting that all homologs were from the Ascomycota phylum. No homologs in the Basidiomycota, Chytridmycota or Zygomycota phyla were identified (Figure 4.9). Database searches showed that species belonging to the Taphrinomycotina subphylum and CTG clade, *Candida albicans* and close relatives (Fitzpatrick et al., 2006), contain GtmA homologs although no homologs were located in species that have undergone a whole genome duplication (WGD) or close relatives of WGD species such as *Kluyveromyces lactis* and *Ashbya gossypii* (Figure 4.9).

All species belonging to the filamentous ascomycetes (Pezizomycotina subphylum), with the exceptions of *Uniocarpus reesii*, *Verticillium dahliae* and *Verticillium alboatrum*, contain a homolog of GtmA (Figure 4.9). Furthermore, most Pezizomycotina species contain multiple GtmA homologs. For example, *A. fumigatus* has two homologs, AFUA_4G14510 and AFUA_6G08850. According to AspGD (http://www.aspgd.org/), AFUA_4G14510 is annotated as an uncharacterized protein with predicted methyltransferase activity whilst AFUA_6G08850 is a ubiquinone biosynthesis methyltransferase (Vödisch et al., 2011).

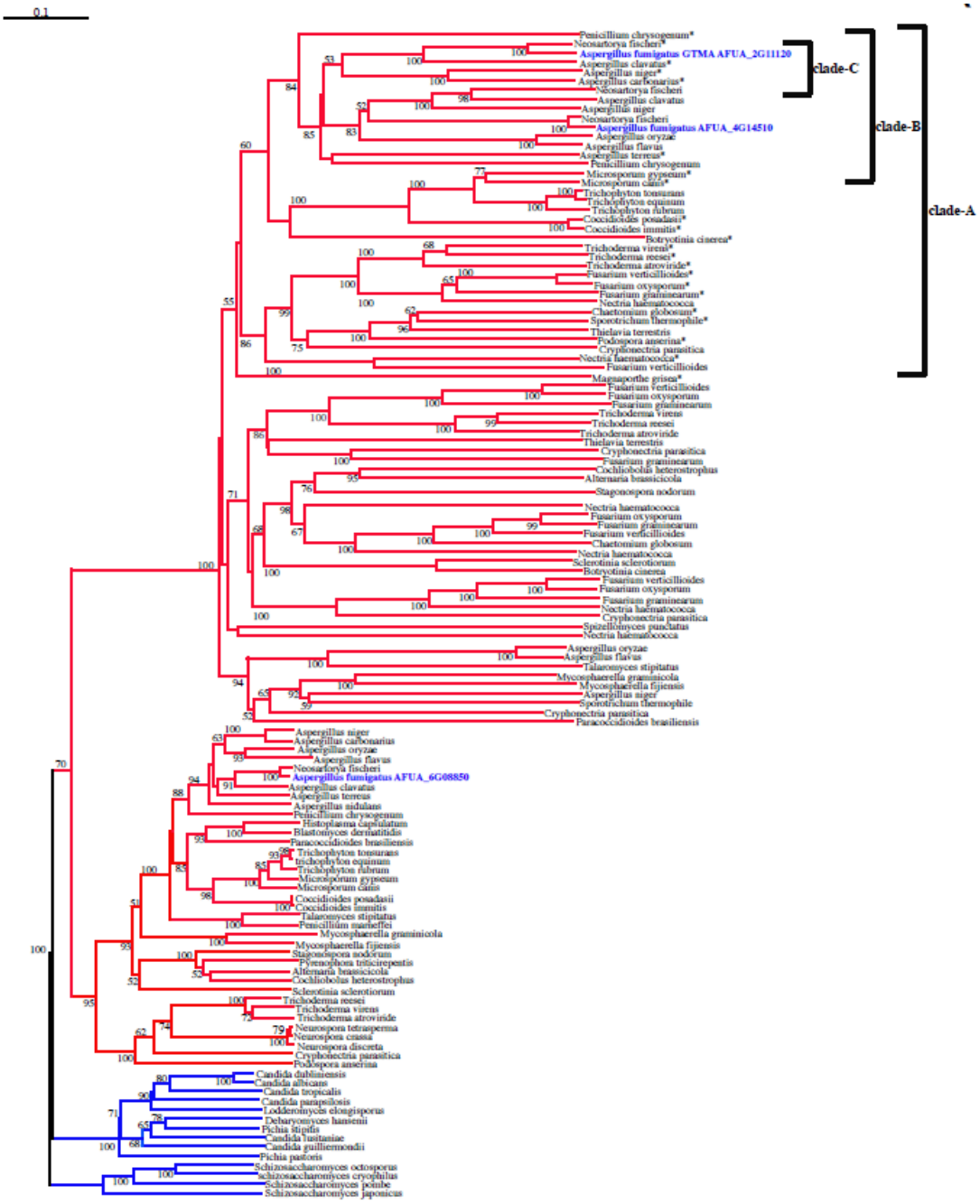

Figure 4.9. Maximum likelihood phylogenetic tree of GtmA homologs. Species with blue coloured branches belong to the Taphrinomycotina and Saccharomycotina subphyla. Red branches indicate species belonging to the Pezizomycotina subphylum. *A. fumigatus* homologs are coloured in blue for reference purposes. All proteins that share a bidirectional best hit with *A. fumigatus* GtmA (AFUA_2G11120) are located in clade-C and are indicated with an *. Clade-B contains species belonging to the Eurotiales order exclusively. GtmA orthologs are found in clade-C.

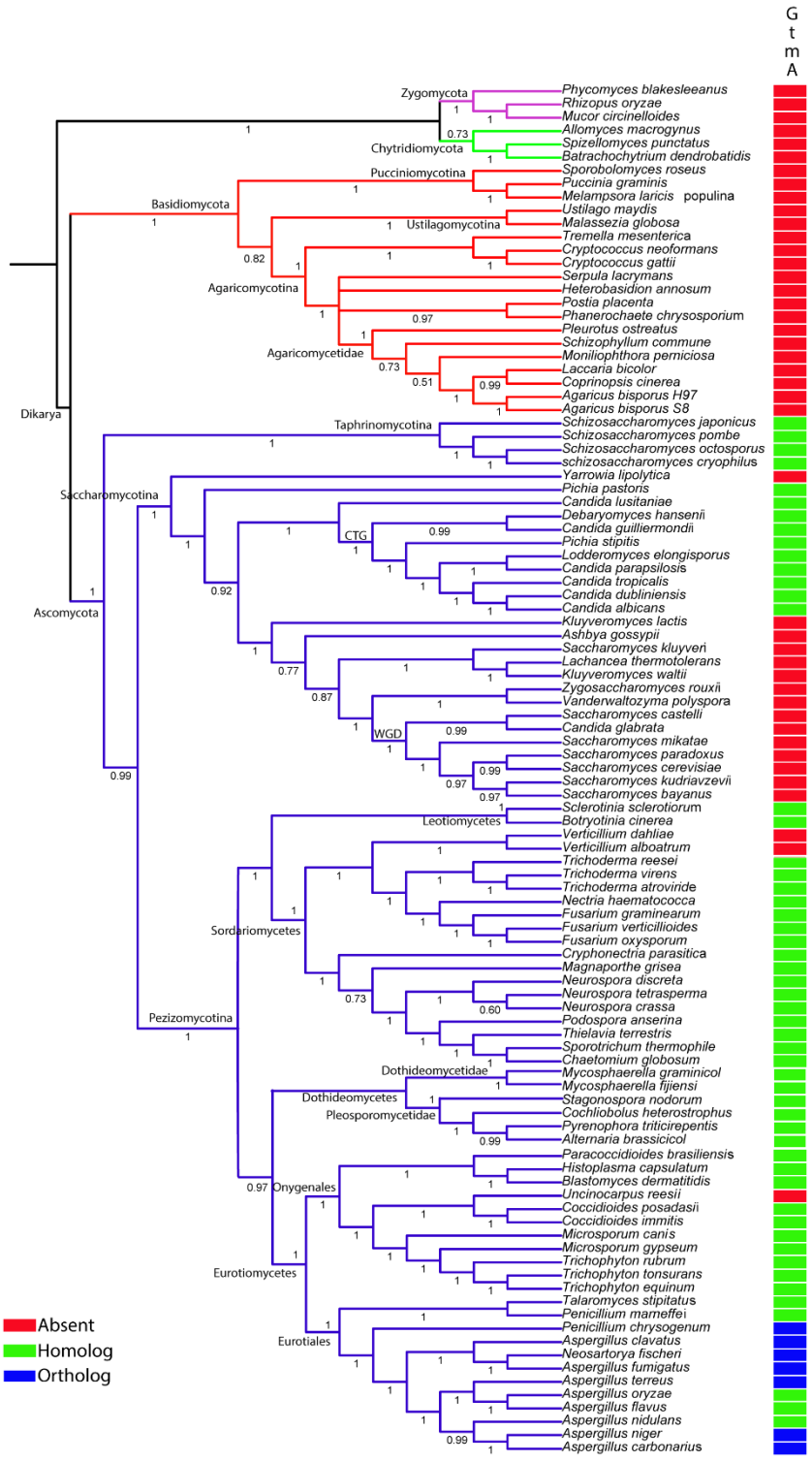

Figure 4.10. Fungal species phylogeny modified from (Medina et al., 2011). The presence and absence of GtmA is indicated. Species are deemed to contain an ortholog if they share a best bi-directional hit with *A. fumigatus* GtmA (AFUA_2G11120) and are located in the GtmA monophyletic clade (clade-c) in Figure 4.10.

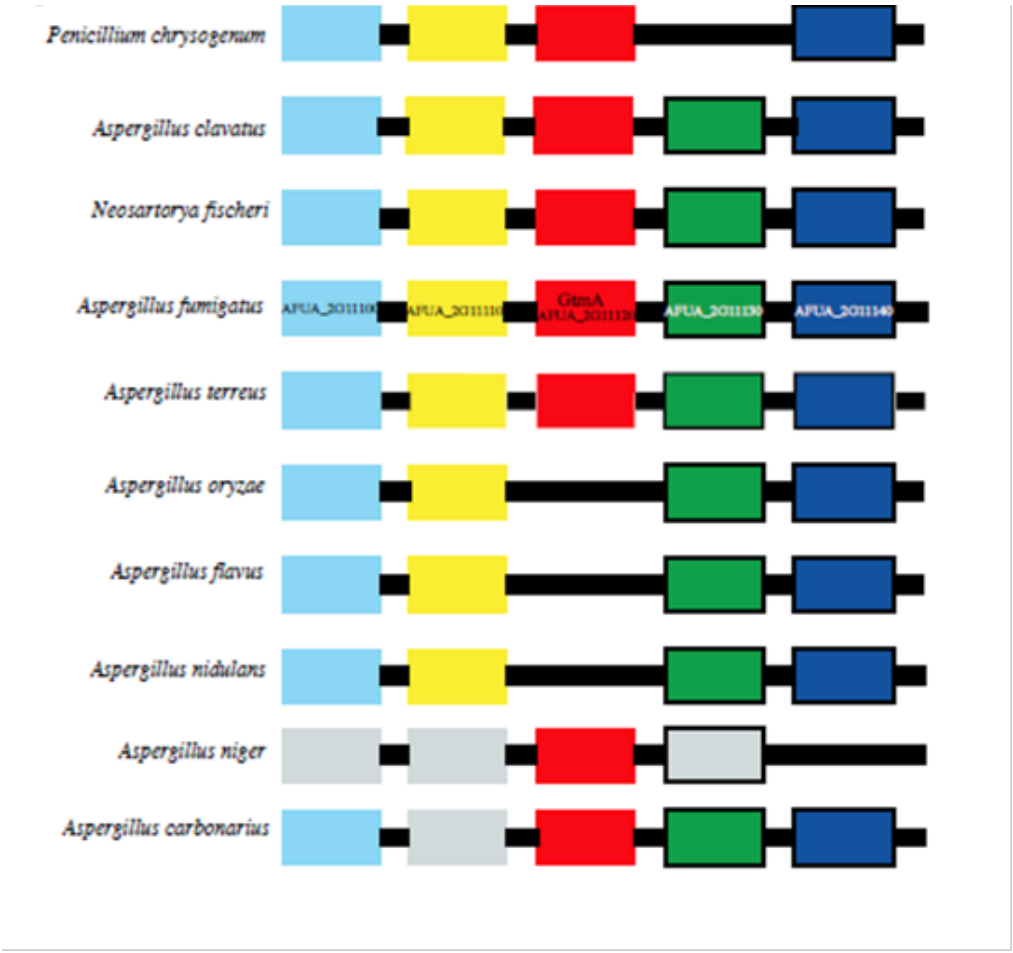

Figure 4.11. Synteny around GtmA in Eurotiales species relative to *A. fumigatus*. *A. fumigatus* accession numbers are shown for reference. Orthologs are arranged in pillars. Coloured boxes indicate that synteny is conserved. Grey boxes indicate that an ortholog is present but in a different part of the genome. Continuous black lines indicate that the ortholog is missing.

4.3 Discussion

The deletion of *gtmA* from the genome of *A. fumigatus* ATCC26933 provided an opportunity to functionally investigate a role for *gtmA*. It has been proposed (Li et al., 2012) that *bis*-thiomethylation represents a back-up detoxification strategy to the GliT-mediated gliotoxin self-protection system in *A. fumigatus* (Schrettl et al., 2010; Scharf et al., 2010). Furthermore, it has been speculated, not unreasonably, that the *gli* cluster-encoded GliN may be responsible for gliotoxin *bis*-thiomethylation (Li and Walsh, 2011). The work presented in this chapter shows that, unlike the gliotoxin oxidoreductase GliT, GtmA is not essential for gliotoxin biosynthesis or self-protection in *A. fumigatus*. The inability to detect bis(methyl)gliotoxin formation by *A. fumigatus* Δ*gtmA* also effectively excludes a role for either GliM or GliN in gliotoxin *bis*-thiomethylation and suggests that these enzymes are responsible for unrelated functionalities during gliotoxin biosynthesis.

Previously it has been demonstrated that *Gliocladium deliquescens* could convert exogenous gliotoxin to bis(methyl)gliotoxin (Kirby et al., 1980) – indeed, this metabolite has been identified to be endogenously produced by many fungal species (Amitani et al., 1995; Guimarães et al., 2010; Intaraudom et al., 2013; Li et al., 2006; Van der Pyl et al., 1992; Sun et al., 2011). In this thesis, it is shown that added gliotoxin (5 µg/ml) is taken up by *A. fumigatus* ATCC26933 over the course of 3 h and then converted to bis(methyl)gliotoxin which is then secreted into the culture medium over the 3 h period. Although *A. fumigatus* Δ*gtmA* does not have this bis(methyl)gliotoxin conversion ability, it responds in the same manner as the wild-type to exogenous gliotoxin presence. This is further supported on the proteomic level as both the wild-type and Δ*gtmA* strains respond almost identically to gliotoxin exposure. If bis(methyl)gliotoxin formation played a significant role in the detoxification of intracellular gliotoxin, the Δ*gtmA* strain would be expected to be more sensitive to gliotoxin than the wild-type. Since this is not observed,

it further underpins our hypothesis that GtmA activity is not directly involved in self-protection against gliotoxin.

However, despite endogenous or exogenous gliotoxin clearly undergoing conversion to bis(methyl)gliotoxin in *A. fumigatus*, initial attempts to detect *bis*-thiomethylation activity in wild-type lysates was unsuccessful. Interestingly, *in vitro* bis(methyl)gliotoxin formation was readily detectable by LC-MS in reaction mixtures containing TCEP-reduced gliotoxin, SAM and *A. fumigatus* Δ*gliT* mycelial lysates (Owens et al. 2015). As such, GliT absence facilitated GtmA-mediated gliotoxin bisthiomethylation, inferring that dithiogliotoxin is a co-substrate for both enzymes. *A. fumigatus* Δ*gtmA* mycelial lysates did not have any gliotoxin bisthiomethylation activity (Figure 4.12).

To the best of our knowledge, this is the first fungal thiomethyltransferase, and only *bis*-thiomethyltransferase, to be identified to date. The thiomethyltransferase (PpSABATH1) identified in a bryophyte *P. patens*, which can monomethylate a range of thiol-containing compounds including thiobenzoic acid in a SAM-dependent manner, has been proposed to play a role in the detoxification of xenobiotic thiols (Zhao et al., 2012). However, deletion of *gtmA* from *A. fumigatus,* which completely abrogated bis(methyl)gliotoxin production, did not result in the acquisition of a gliotoxin- or H_2O_2-sensitive phenotype. This leads us to conclude that GtmA is not primarily involved in the detoxification of gliotoxin or related biosynthetic intermediates (Forseth et al., 2011) as has previously been proposed (Li et al., 2012). While we cannot exclude the possibility that GliT activity compensates for the absence of GtmA, we consider that a counter-balance for the positive regulation of *gli* cluster expression by gliotoxin (Cramer et al., 2006; Davis et al., 2011; Schrettl et al., 2010) presented an alternative purpose for bis(methyl)gliotoxin formation. In fact, formerly, no consideration had been given to a mechanism by which gliotoxin-induced *gli* cluster activity could be attenuated. These

data suggest that bis(methyl)gliotoxin biosynthesis *via* GtmA, instead of GliT-catalyzed *de novo* gliotoxin formation, represents a post-biosynthetic "off-switch" for gliotoxin biosynthesis and leads to diminution of *gli* cluster expression and consequent diminished gliotoxin biosynthesis (Figure 4.12). This hypothesis is underpinned by the increased abundance of key gliotoxin biosynthetic enzymes (GliP, GliM and GliF) in *A. fumigatus* Δ*gtmA*, in comparison with wild-type or *gtmA*^{c}, under conditions permissive for gliotoxin biosynthesis. It is also established by the significant elevation (p<0.0056) in gliotoxin production in *A. fumigatus* Δ*gtmA* under identical conditions. Moreover, the positive regulation of *gtmA* expression and GtmA abundance by exposure to elevated gliotoxin levels further consolidates the biological role of this enzyme in attenuating *gli* cluster activity and gliotoxin biosynthesis. Notably, the significantly elevated abundance of gliotoxin-related biosynthetic enzymes excludes the possibility that increased gliotoxin biosynthesis is simply due to an absence of "competing" bis(methyl)gliotoxin biosynthesis (Table 4.5). In essence, ETP *bis*-thiomethylation in *A. fumigatus* may represent a strategy for suppressing ETP biosynthesis as opposed to, or in addition to, acting as an alternative self-protection strategy. Nonetheless, the removal of dithiogliotoxin by *bis*-thiomethylation likely confers some indirect element of self-protection against this reactive biosynthetic intermediate. Just as *A. fumigatus* Δ*gtmA* facilitates gliotoxin over-production, deletion mutants of *gtmA* orthologs in other ETP-producing fungi may result in similar outcomes in addition to attenuating the *bis*-thiomethylation of reactive biosynthetic intermediates (Forseth et al., 2011). Compellingly, the overexpression of RsmA, a Yap-like bZIP transcriptional enhancer, in *A. fumigatus* (*OErsmA*) resulted in increased *gliT* expression and enhanced production of gliotoxin, resulting in the effective abolition of bis(methyl)gliotoxin formation (Sekonyela et al., 2013). Our observation that GtmA is the SAM-dependent methyltransferase which *bis*-thiomethylates GT-$(SH)_2$ is in complete accordance with

these investigations and provides a definitive explanation for the loss of bis(methyl)gliotoxin formation by *A. fumigatus OErsmA*.

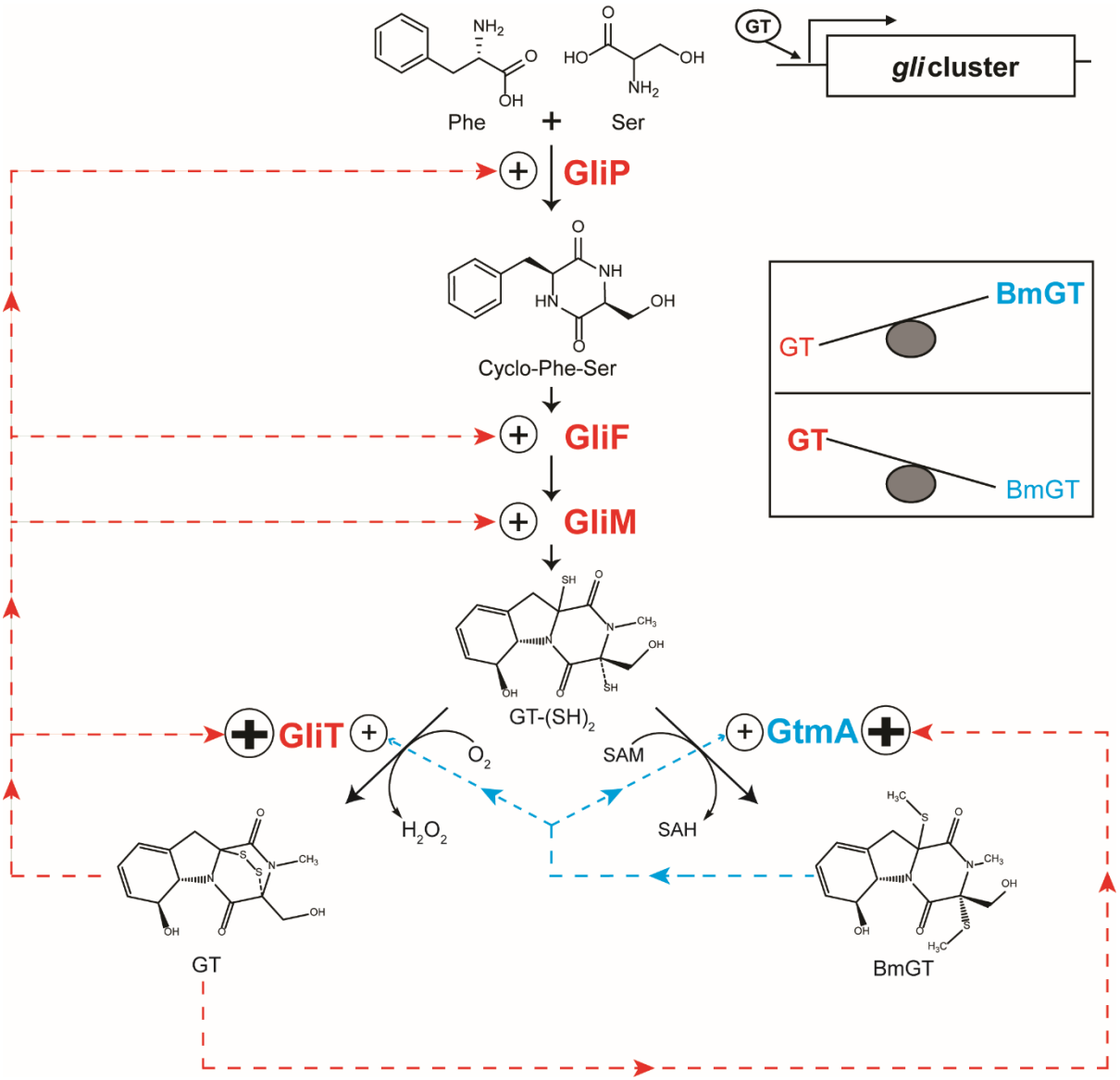

Figure 4.12. Model of GtmA-mediated regulation gliotoxin biosynthesis. Gliotoxin induces *gli* cluster expression and acts to potentiate its own biosynthesis. The toxic biosynthetic intermediate, GT-$(SH)_2$ (dithiol gliotoxin), is a shared substrate between GliT and GtmA and is either converted to gliotoxin or bis(methyl)gliotoxin. Gliotoxin production is suppressed by increased conversion to bis(methyl)gliotoxin which occurs due to an increased GtmA abundance once gliotoxin levels increase (gliotoxin significantly induces *gtmA* expression and GtmA abundance). The consequent depletion of gliotoxin may lead to a reduction in *gli* cluster expression and *gli* enzyme abundance. Bis(methyl)gliotoxin may also promote self- and gliotoxin-formation to dissipate reactive GT-$(SH)_2$.

Localisation of *gtmA* on chromosome 2, distal to the *gli* cluster on chromosome 6 (Cramer et al., 2006) is highly relevant to assigning a role for *gtmA* in either self-protection against a toxic biosynthetic intermediate or, as a regulator of gliotoxin production. It has been proposed that the co-localization of genes within metabolite-encoding clusters has evolved to protect against toxic biosynthetic intermediates (McGary et al., 2013). Our demonstration that *gtmA* deletion completely abrogates bis(methyl)gliotoxin formation without enhancing sensitivity to exogenous gliotoxin is in accordance with this proposal, strongly implicating an alternative function for GtmA in gliotoxin biosynthesis. Moreover, our data endorse the key role of GliT, located within the *gli* cluster, in mediating self-protection against reactive dithiogliotoxin.

The Δ*gtmA*::*gtmA-eGFP*::*H2A-mRFP* strain was analysed by confocal microscopy analysis (Section 4.2.7). The results revealed that GtmA::eGFP accumulates in the cytosol of *A. fumigatus* following exposure to 5 µg/ml gliotoxin for 3 h (Figure 4.8). Cytosolic localisation is a feature of methyltransferases involved in the detoxification of thiol compounds in other organisms. The thiol methyltransferase from *Euglena gracilis* (Drotar et al., 1987) and the methyl chloride transferase form *E. muricata* (Wuosmaa and Hager, 1990) are also localized in the cytosol. These are involved in the general detoxification of thiols and halides. The cytosolic location of these enzymes gives them rapid access to their substrates. In contrast, the fungal methyl chloride transferase, which is not involved in detoxification (Harper, 1993) and which differs from our TMT in substrate preference (Saxena et al., 1998), is membrane-bound.

This work represents the first characterisation of an enzyme responsible for non-ribosomal peptide *bis*-thiomethylation in microbial secondary metabolism whereby GtmA catalyzes bis(methyl)gliotoxin biosynthesis in *A. fumigatus*. The data suggests that bis(methyl)gliotoxin production may act as a negative regulatory mechanism for *gli* cluster expression by disrupting the gliotoxin-mediated *gli* cluster positive feedback

system – a model which may be applicable to all ETPs synthesised by various filamentous fungi. Unusually, *gtmA* is located outside the *gli* cluster despite the fact that bis(methyl)gliotoxin production is conserved across all gliotoxin-producing species.

GtmA orthology was inferred using three approaches: Firstly, proteins were located that shared a bidirectional best hit to *A. fumigatus* GtmA (AFUA_2G11120). Secondly, a GtmA phylogenetic tree was reconstructed (Figure 4.10). Finally the synteny around GtmA homologs was viewed to confirm orthology (Figure 4.11). All proteins that share a bidirectional BlastP hit with *A. fumigatus* GtmA are located in a single clade (Figure 4.9, clade-A). Based on the GtmA phylogeny, paralogs seem to have arisen in a species/lineage dependent manner as some species, such as *A. niger* and *Nectria haematococca*, contain multiple homologs (4 and 6, respectively) while others, such as *A. nidulans*, contain a single GtmA homolog. The most robust manner to ascertain orthology is through phylogenetic reconstruction and confirmation by synteny. Phylogenetic analysis inferred a GtmA ortholog clade containing *A. clavatus*, *N. fischeri*, *A. fumigatus*, *A. niger* and *A. carbonarius* (Figure 4.9). These species, along with *Penicillium chrysogenum*, *A. terreus*, *A. oryzae*, *A. flavus* and *A. nidulans*, all belong to the Eurotiales order (Figure 4.9, clade-B). *A. terreus* and *P. chrysogenum* both contain proteins that have reciprocal best blast hits to *A. fumigatus* GtmA, yet, neither is found within the GtmA ortholog clade (Figure 4.9). However, based on our synteny analysis, it is confirmed that both species possess orthologs of GtmA (Figure 4.11). In accordance with the phylogeny and reciprocal best-hit strategy, there are two scenarios which explain the evolutionary history of GtmA. Firstly, GtmA is the result of a duplication of the ortholog of AFUA_4G14510 in the last common ancestor of all these species. Species-specific losses of GtmA have since occurred in *A. terreus*, *A. oryzae*, *A. flavus* and *A. nidulans*. Alternatively, AFUA_4G14510 may be the result of GtmA duplication with subsequent retention of the GtmA paralog and loss of the GtmA ortholog in these species.

The presence of GtmA orthologs in fungi non-permissive for gliotoxin biosynthesis (e.g., *A. niger*) is interesting and perhaps represents a self-protection mechanism in these species.

In summary, we have identified the first *bis*-thiomethyltransferase and demonstrated its role in the *bis*-thiomethylation of dithiol gliotoxin (Figure 4.12) therefore proposing that it primarily acts as a molecular switch to attenuate *gli* cluster expression and, consequently, gliotoxin biosynthesis in *A. fumigatus*.

Chapter 5

Recombinant Expression and Structural Elucidation of Gliotoxin Thiomethyltransferase A

5.1 Introduction

The mechanism responsible for *bis*-thiomethyl ETP biosynthesis is of substantial interest due to the clear value of these natural products. Furthermore, SAM-dependent methyltransferases have been established as highly versatile enzymes for applications in biocatalysis, metabolic engineering, chemical biology and other areas of biotechnology (Struck et al., 2012). The chemospecific and regiospecific methylation of natural products using classical chemical alkylating agents requires multistep reactions which can be costly and time consuming (Wessjohann et al., 2013). However, despite the fact that a vast number of natural product methyltransferases have been characterised, thiol directed NPMTs remain a largely unclassified group of biosynthetic enzymes (Liscombe et al., 2012).

The ability to express and purify desired recombinant proteins in large quantities has facilitated the rapid biochemical characterization of a variety of enzymes. *Escherichia coli* is one of the organisms of choice for the production of recombinant proteins. Its use as a cell factory is well-established and it has become the most popular expression platform (Gräslund et al., 2008). For this reason, there are many molecular tools and protocols at hand for the high-level production of heterologous proteins; these include a vast catalog of expression plasmids, a great number of engineered strains and many cultivation strategies (Rosano and Ceccarelli, 2014).

Affinity-tagged protein purification is a widely used method for the purification of proteins of interest. The two most commonly used tags are the polyhistidine tag, which generally consists of six histidine residues, and GST (Kimple et al., 2013). Proteins tagged with histidine bind strongly with metal ions such as Ni^{2+}, Co^{2+}, Cu^{2+}, and Zn^{2+}. They are purified by binding to a metal ion immobilized on a support resin through the IMAC method (immobilized metal ion affinity chromatography). For GST tags, the purification principle is based on the binding of GST to glutathione immobilized on the support resin.

After sample impurities are washed from the resin, the bound GST-tagged protein is eluted by reduced glutathione. The GST protein has a molecular mass of 26 kDa and is most often fused to the target protein at the N-terminus. The GST protein is a dimer in solution and, thus, the fusion protein dimerizes as well. The use of GST as a fusion tag is desirable because it can act as a chaperone to facilitate protein folding and, consequently, the fusion protein can often be expressed as a soluble protein rather than in inclusion bodies (Lichty et al., 2005; Harper et al., 2011).

Several methods are currently used to determine the structure of a protein. These include X-ray crystallography, NMR spectroscopy and electron microscopy. Each method has both advantages and disadvantages. In each of these methods many pieces of information are used to create the final atomic model based on experimental data about the structure of the molecule (Egli, 2010). In the case of X-ray crystallography, this is the X-ray diffraction pattern. Most of the structures included in the Protein Data Bank (PDB) archive were determined using X-ray crystallography (Callaway, 2014). For this method, the protein is purified and crystallized and then subjected to an intense beam of X-rays. The proteins in the crystal diffract the X-ray beam into a characteristic pattern of spots which are then analyzed to determine the distribution of electrons in the protein. The resulting map of the electron density is then interpreted to determine the location of each atom (Wlodawer et al., 2008).

X-ray crystallography can provide very detailed atomic information: it shows every atom in a protein or nucleic acid along with atomic details of ligands, inhibitors, ions, and other molecules which are incorporated into the crystal (Egli, 2010). However, the process of crystallization is difficult and can impose limitations on the types of proteins that may be studied by this method. For example, X-ray crystallography is an excellent method for determining the structures of rigid proteins that form nice, ordered

crystals. Conversely, flexible proteins are far more difficult to study with this method as crystallography relies on having a large quantity of molecules aligned in exactly the same orientation. Flexible portions of protein will often be invisible in crystallographic electron density maps since their electron density will be smeared over a large space (Pflugrath, 1999; Wlodawer et al., 2008).

Despite tremendous progress in experimental determination of protein three-dimensional structures, it has not kept pace with the explosive growth of sequence information that results from massively parallel sequencing technology (Marks et al., 2012). As a result of this there are many more protein sequences than protein three-dimensional structures - the gap is widening rather than diminishing. Many proteins contain enough information in their amino acid sequence to determine their three-dimensional structure, thus opening the possibility of predicting three-dimensional structure from sequence (Stolte et al., 2015).

Critical Assessment of protein Structure Prediction (CASP) is a community-wide, worldwide experiment for protein structure prediction which takes place every two years. CASP provides research groups with the opportunity to objectively test their structure prediction methods (Boutros et al., 2014). I-TASSER (Iterative Threading ASSEmbly Refinement) is a hierarchical method for protein structure and function prediction (Yang et al., 2015). First, structural templates are identified from the PDB by multiple threading approach LOMETS. Following this, full-length atomic models are then constructed using iterative template fragment assembly simulations. Finally, function inslights of the target are derived by threading the 3D models through the protein function database BioLiP. I-TASSER was ranked as the No. 1 server for protein structure prediction in recent CASP7, CASP8, CASP9, CASP10, and CASP11 experiments (Zhang, 2008; Roy et al., 2010; Yang et al., 2015).

The overall objectives of the work presented in this chapter were to:

(vii) Recombinantly express GtmA as a GST tagged fusion protein, cleave off the GST tag and purify the active protein at high yields and purity.

(viii) Carry out activity analysis on GtmA using a variety of substrate and cofactor concentrations in order to determine both the kinetics and the oligomeric state of GtmA.

(ix) Predict the structure of GtmA using the latest computational methods and carry out any subsequent database predictions on this enzyme.

(x) Prepare sufficient quantities of this enzyme for crystallography studies, carry out crystallisation trials on this enzyme and determine the structure of GtmA.

(xi) Use the GtmA structural and computational data to carry out targeted site directed mutagenesis on this enzyme.

5.2 Results

5.2.1 Recombinant expression of GtmA in *E. coli*

Primers GtmA_F and GtmA_R (Table 2.4) were designed to amplify the *gtmA* coding sequence and, also, to incorporate two restriction sites, *Xho*I and *Hind*III, into the forward and reverse primers in order to allow for directional cloning into the pEX_N_GST vector. GT treated *A. fumigatus* ATCC26933 cDNA (Section 2.2.5) was used as a template for the PCR amplification of the *gtmA* gene.

The *gtmA* gene was predicted to have three introns (186 bp). The difference in the *gtmA* cDNA and gDNA was discernible by gel electrophoresis (Figure 5.1). The amplified *gtmA* cDNA (880 bp) was visible as a slightly lower band than the *gtmA* gDNA 1066 bp. The *gtmA* cDNA product was digested with *Xho*I and *Hind*III and then gel extracted.

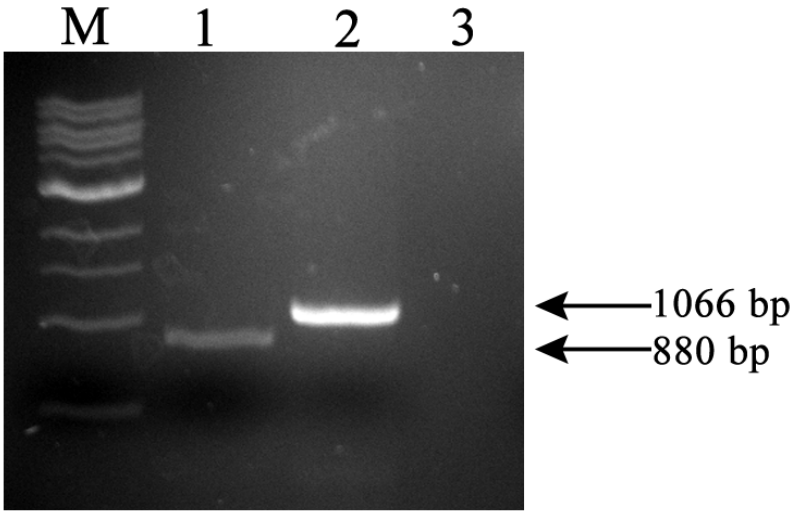

Figure 5.1. Amplification of *gtmA* coding sequence from *A. fumigatus* GT induced cDNA. Lane 1: cDNA, Lane 2: gDNA positive control, Lane 3: Negative control.

The *gtmA* product was cloned into the pEX_N_GST vector and transformed into *E. coli* BL21 (DE3) competent cells for expression. The resulting colonies were tested for integration of the DNA by restriction digest using XhoI and *Hind*III. The resulting colonies were first screened by PCR (Figure 5.2) for successful integration of the *gtmA* gene (Figure 5.3). A positive colony with the expected 880 bp amplification product was then screened by restriction digestion using *Xho*I and *Hind*III. The correct digestion pattern for the insertion of *gtmA* cDNA into the pEX_N_GST vector was observed (5159 bp, 870 bp).

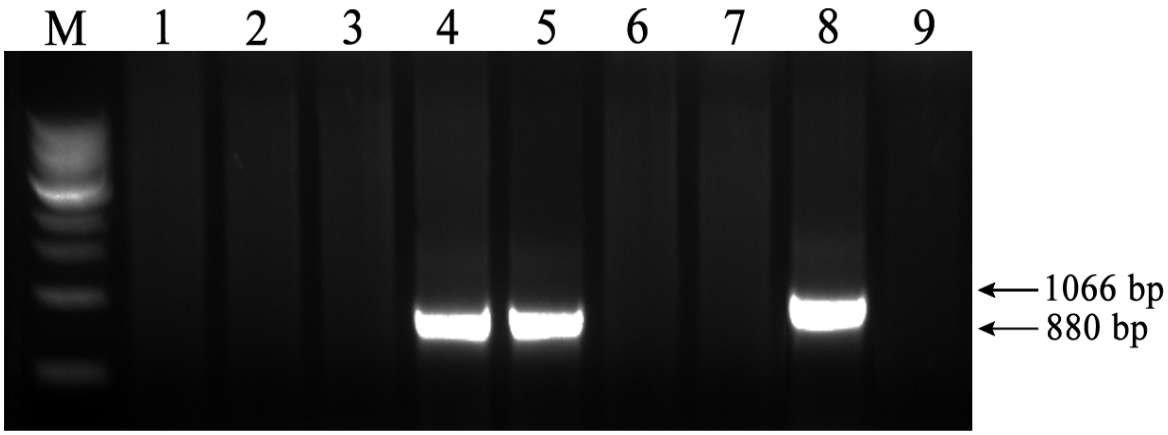

Figure 5.2. Colony PCR on *gtmA*-pEX_N_GST transformants. Colonies 4 and 5 contain the predicted 880 bp band indicating successful *gtmA* integration. Lane 8: gDNA positive control. Lane 9: negative control.

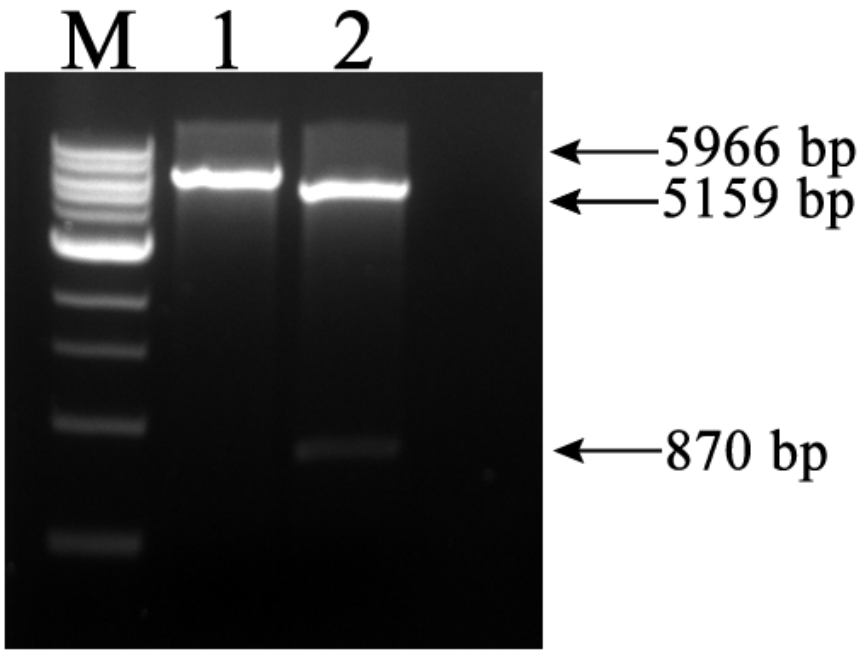

Figure 5.3. *gtmA*-pEX_N_GST digestion to confirm *gtmA* integration. Lane 1: Single digestion with *Xho*I, Lane 2: Double digestion using *Xho*I and *Hind*III.

The plasmid was sequenced to confirm that *gtmA* remained in frame in order to enable protein expression. Sequence analysis was performed on a commercial basis (Source Bioscience) and was compared to the predicted sequence according to CADRE (http://www.cadre-genomes.org.uk) with ID AFUA_2G11120. The sequencing of the *gtmA* cDNA confirmed the correct sequence of *gtmA*. Interestingly, the three CADRE predicted introns were incorrectly annotated - the actual *gtmA* sequence encodes 287 amino acids rather than the 266 predicted by the CADRE annotation. The correct GtmA amino acid sequence is shown in Figure 5.4.

Identities	Positives	Gaps
256/287(89%)	**259/287(90%)**	**21/287(7%)**

```
Query  1    MSKSDYIQNMFQTKSFVDRYKYTEKLTGLYAQTLVDYSGVANTSQKPLVVLDNACGIGAV  60
            MSKSDYIQNMFQTKSFVDRYKYTEKLTGLYAQTLVDYSGVANTSQKPLVVLDNACGIGAV
Sbjct  1    MSKSDYIQNMFQTKSFVDRYKYTEKLTGLYAQTLVDYSGVANTSQKPLVVLDNACGIGAV  60

Query  61   SSVLNHTLQDEAKKTWKLTCGDLSEGMLETTKRRLQDEGWVNAETKIVNALDTGLPDGHY  120
            SSVLNHTLQDEAKKTWKLTCGDLSEGMLETTKRRLQDEGWVNAETKIVNAL
Sbjct  61   SSVLNHTLQDEAKKTWKLTCGDLSEGMLETTKRRLQDEGWVNAETKIVNAL---------  111

Query  121  THVFVAFGFQSFPDANAALKECFRILASGGILASSTWQNFNWIPIMKAAIETIPGNLPFP  180
                                    RILASGGILASSTWQNFNWIPIMKAAIETIPGNLPFP
Sbjct  112  ------------PELSRRQRRLERILASGGILASSTWQNFNWIPIMKAAIETIPGNLPFP  159

Query  181  TQKEFIALHNAGWDSESYIQSELEKLGFRDVKVIPVPKETSIPIDEFFEVCMMIIPYLLP  240
            TQKEFIALHNAGWDSESYIQSELEKLGFRDVKVIPVPKETSIPIDEFFEVCMMIIPYLLP
Sbjct  160  TQKEFIALHNAGWDSESYIQSELEKLGFRDVKVIPVPKETSIPIDEFFEVCMMIIPYLLP  219

Query  241  KFWTEEQRESHEKDVPMVLRQYLQDTYGANGQVPLEAVALITTGLKP  287
            KFWTEEQRESHEKDVPMVLRQYLQDTYGANGQVPLEAVALITTGLKP
Sbjct  220  KFWTEEQRESHEKDVPMVLRQYLQDTYGANGQVPLEAVALITTGLKP  266
```

Figure 5.4. Alignment of the confirmed GtmA amino acid sequence (Query) against the CADRE annotated amino acid sequence (Sbjct). Incorrect annotation of the three intron regions resulted in a predicted sequence of 266 amino acids whilst the confirmed sequence contains 287 amino acids.

5.2.2 SDS-PAGE, Western Blot and Mass Spectrometry Analysis of GST-GtmA

Detection of GST-GtmA protein expression was carried out by induction using IPTG followed by SDS-PAGE and Western Blot analysis. Small scale cultures were induced and grown for 3 h – samples were taken pre-induction and also at hourly time points. As shown in Figure 5.5, both the SDS-PAGE and Western Blot analysis resulted in a band with an approximate molecular mass of 58 kDa, agreeing with the prediction for the recombinant GST-GtmA fusion protein. The pellet and supernatant extracts from the *E. coli* cell lysate were separated. This confirmed that the GST-GtmA protein was present in both the soluble and insoluble fractions. The SDS-PAGE band corresponding to the GST-GtmA protein was excised, digested and analysed by LC-MS as described in Section 2.2.16.1. This analysis confirmed the identity of the band as GtmA (15% protein sequence coverage) (Figure 5.6).

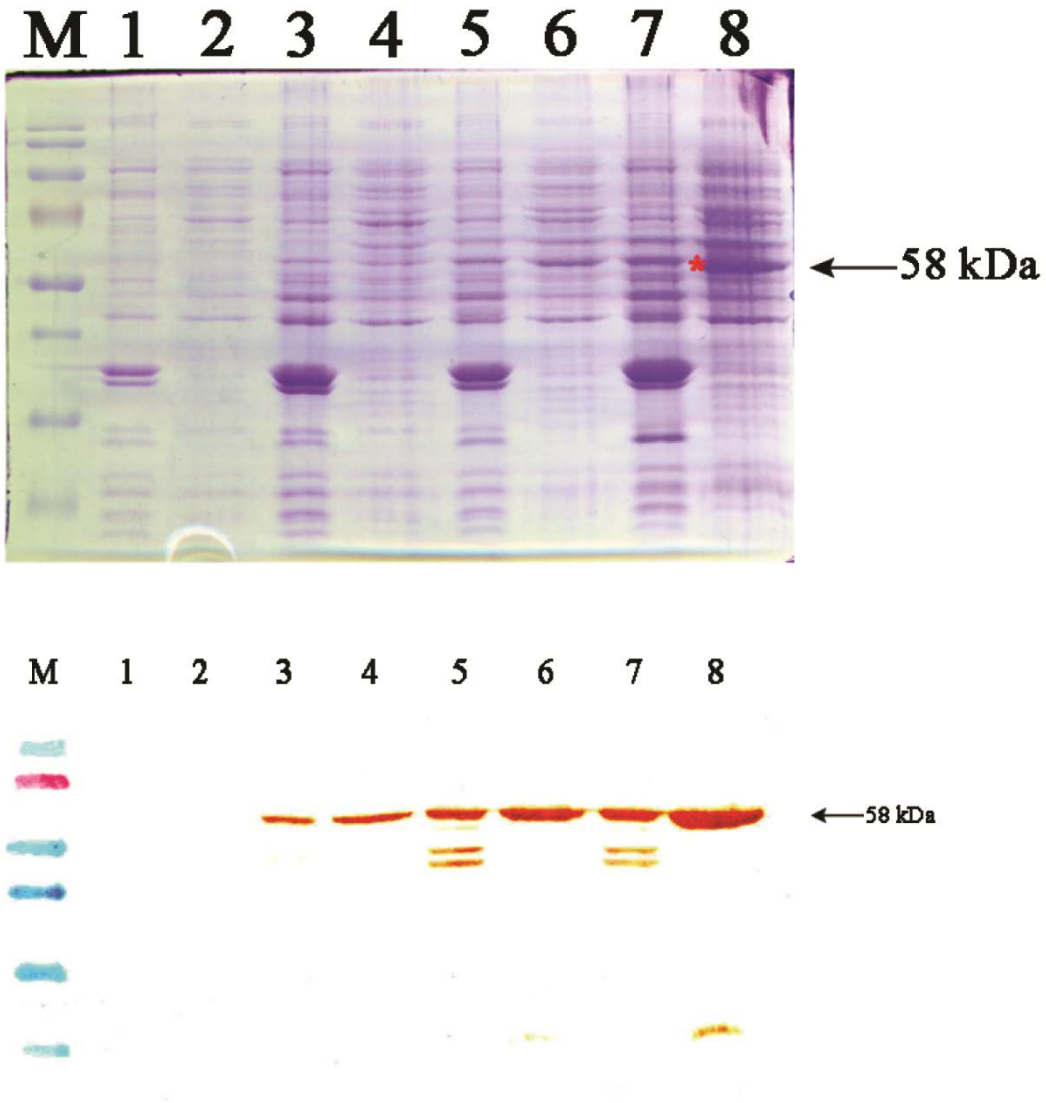

Figure 5.5. Time course small scale induction of GST-GtmA expression over 3 h in LB broth using 1 mM IPTG. Lane 1: 0 h IPTG soluble fraction. Lane 2: 0 h IPTG insoluble fraction. 1 h IPTG soluble fraction. 1 h IPTG insoluble fraction. 2 h IPTG soluble fraction. 2 h IPTG insoluble fraction. 3 h IPTG soluble fraction. 3 h IPTG insoluble fraction. B: Below: Western Blot of cell lysates displaying band with an approximate molecular mass of 58 kDa in the IPTG induced samples, agreeing with the predicted mass for the recombinant GST-GtmA fusion protein.

```
  1 MSKSDYIQNM FQTKSFVDRY KYTEKLTGLY AQTLVDYSGV ANTSQKPLVV
 51 LDNACGIGAV SSVLNHTLQD EAKKTWKLTC GDLSEGMLET TKRRLQDEGW
101 VNAETKIVNA LPELSRRQRR LERILASGGI LASSTWQNFN WIPIMKAAIE
151 TIPGNLPFPT QKEFIALHNA GWDSESYIQS ELEKLGFRDV KVIPVPKETS
201 IPIDEFFEVC MMIIPYLLPK FWTEEQRESH EKDVPMVLRQ YLQDTYGANG
251 QVPLEAVALI TTGLKP
```

Figure 5.6. LC-MS confirmation of GtmA expression by LC-MS. 15% sequence coverage of GtmA was detected.

5.2.3 Large Scale Expression and Purification of GST-GtmA from *E. coli*

As outlined in Section 2.2.7.1, 10 L of GST-GtmA was induced overnight at 30 °C. The resulting cells were pelleted and lysed as described in Section 2.2.7.3. Glutathione-Sepharose affinity chromatography was first carried out to purify the GST-GtmA from the cell lysate (Figure 5.7). This was carried out as highlighted in Section 2.2.11.1. 10 L of *E. coli* lysate yielded 140 mg of GST-GtmA. The GST tag was then removed from GST-GtmA using TEV protease. The cleavage of GST-GtmA was monitored by SDS-PAGE (Figure 5.8). Following dialysis against 20 mM Tris HCL, 20 mM NaCl, pH 8.0, the cleaved sample was subjected to Q-Sepharose anion exchange chromatography to remove the free GST tag from the sample. As shown in Figure 5.9, the anion exchange 1 ml fractions containing GST (as indicated by anti-GST signal by immunoblot) were excluded from the final pooled sample. The final pooled fraction containing cleaved GtmA was concentrated to 2 mg/ml and simultaneously buffer exchanged into 50 mM Tris HCl, 50 mM NaCl, pH 7.4. The final sample was subjected to SDS-PAGE. This indicated a single band at approximately 32 kDa which corresponded to the molecular mass of GtmA (Figure 5.10).

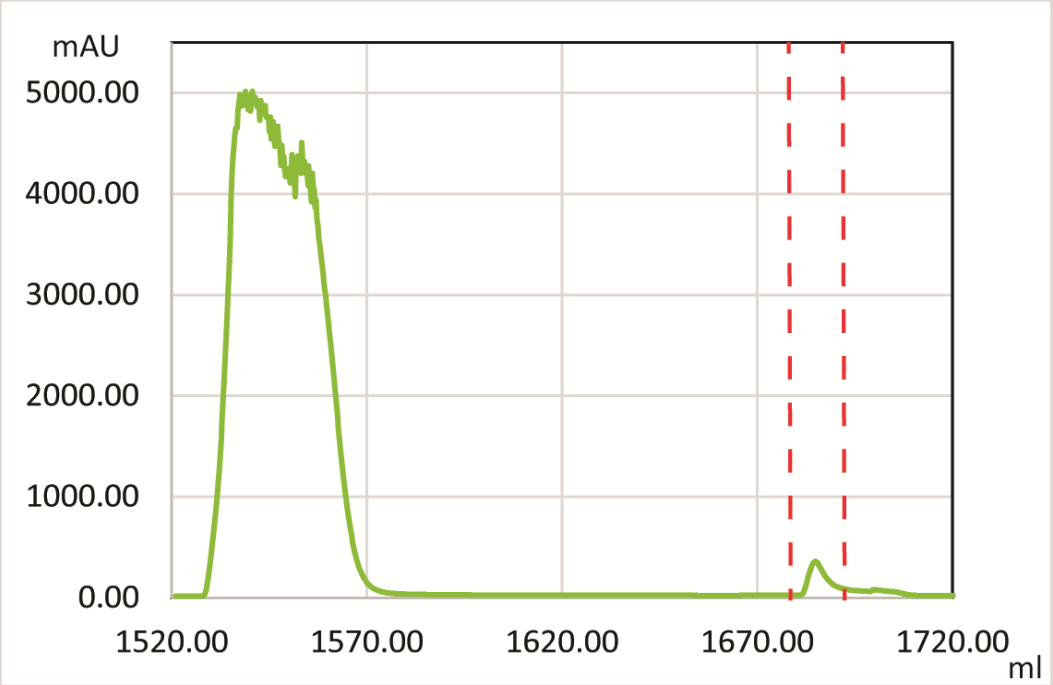

Figure 5.7. Large scale purification of GST-GtmA from E. coli lysates using GSH-Sepharose affinity chromatography. The red lines indicate the eluted GST-GtmA from the crude *E. coli* cell lysate.

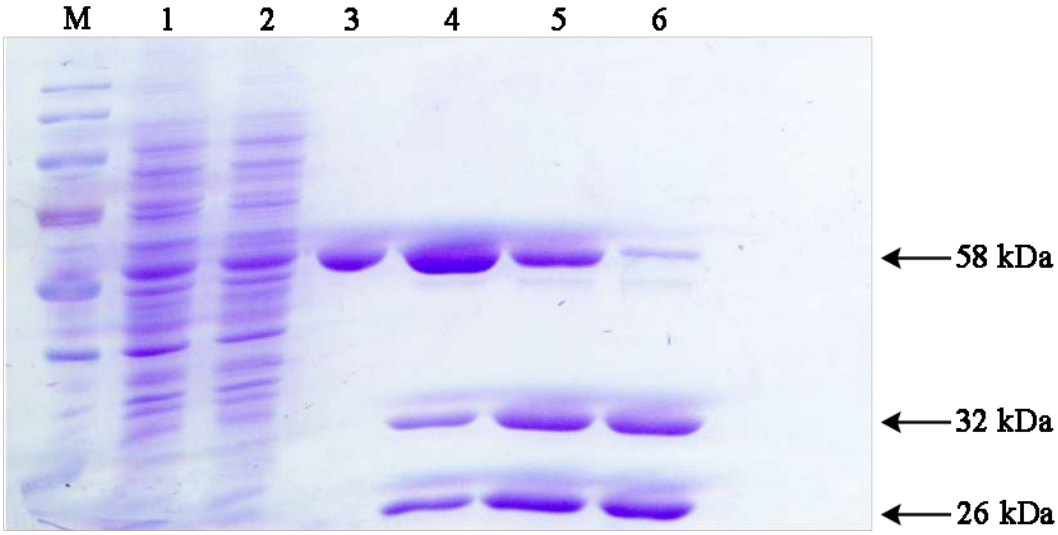

Figure 5.8. Large scale expression, purification and TEV cleavage of GST-GtmA. Lane 1: GST-GtmA lysate, Lane 2: GST-GtmA flow through, Lane 3: GST-GtmA affinity purified using GSH agarose, Lane 4: GST-GtmA cleavage 1 h (37 °C), Lane 5: GST-GtmA cleavage 2 h (37 °C). Lane 6: GST-GtmA cleavage overnight at 4°C.

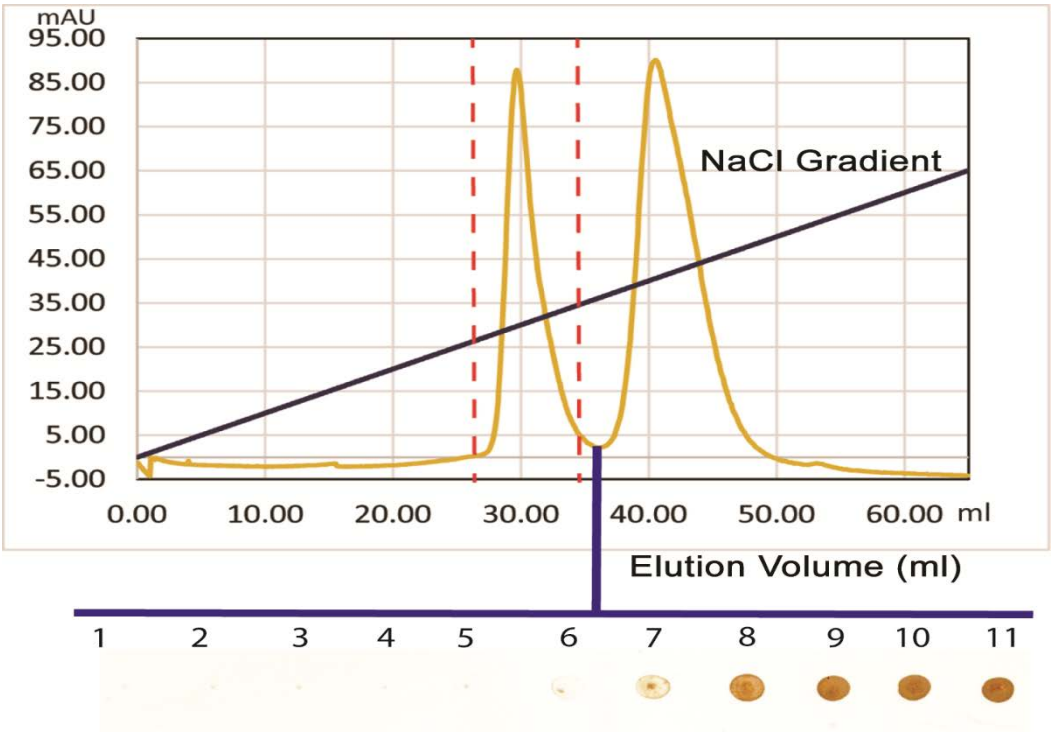

Figure 5.9. Large scale purification of GtmA from free GST using Q-Sepharose anion exchange chromatography. Blue line: Anti-GST immunoblot illustrating the absence of GST signal in the first peak of the chromatogram.

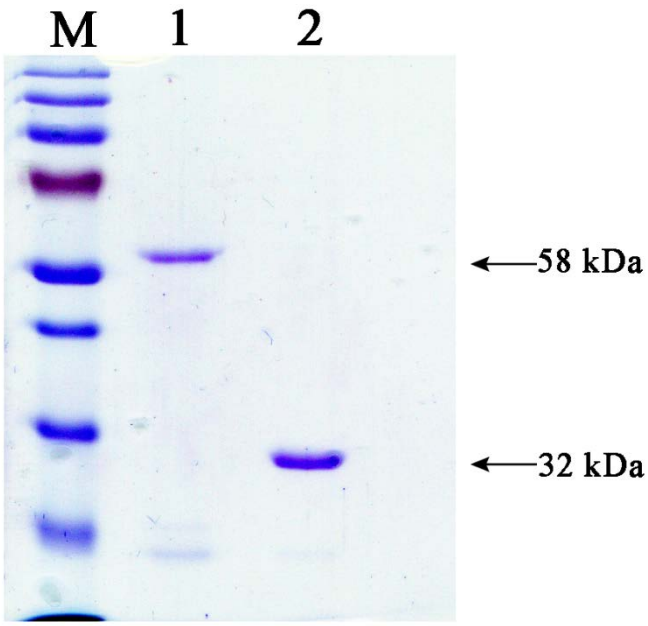

Figure 5.10. SDS-PAGE analysis of large scale anion exchange purification of GtmA from free GST. Lane 1: GST-GtmA. Lane 2: GtmA purified by anion exchange chromatography

5.2.4 Size Exclusion Chromatography Analysis of recombinant GtmA

As illustrated in Figure 5.10, purified and concentrated GtmA (1 mg) was loaded onto a Superdex 200 10/300 GL column (GE Healthcare, Germany). Figure 5.10 shows GtmA analysed by size exclusion chromatography (SEC) as a single, monodisperse peak. This indicated that, following GSH-Sepharose affinity chromatography and anion exchange chromatography, the resulting protein was at high purity. A selection of molecular mass calibrants (BSA, Ovalbumin and Lysozyme) were applied to the column in order to uncover the oligomeric state of the methyltransferase. The GtmA peak eluted after the BSA (66.5 kDa) and Ovalbumin (42.7 kDa) proteins, indicating that GtmA is present as the monomeric form in solution (Figure 5.11).

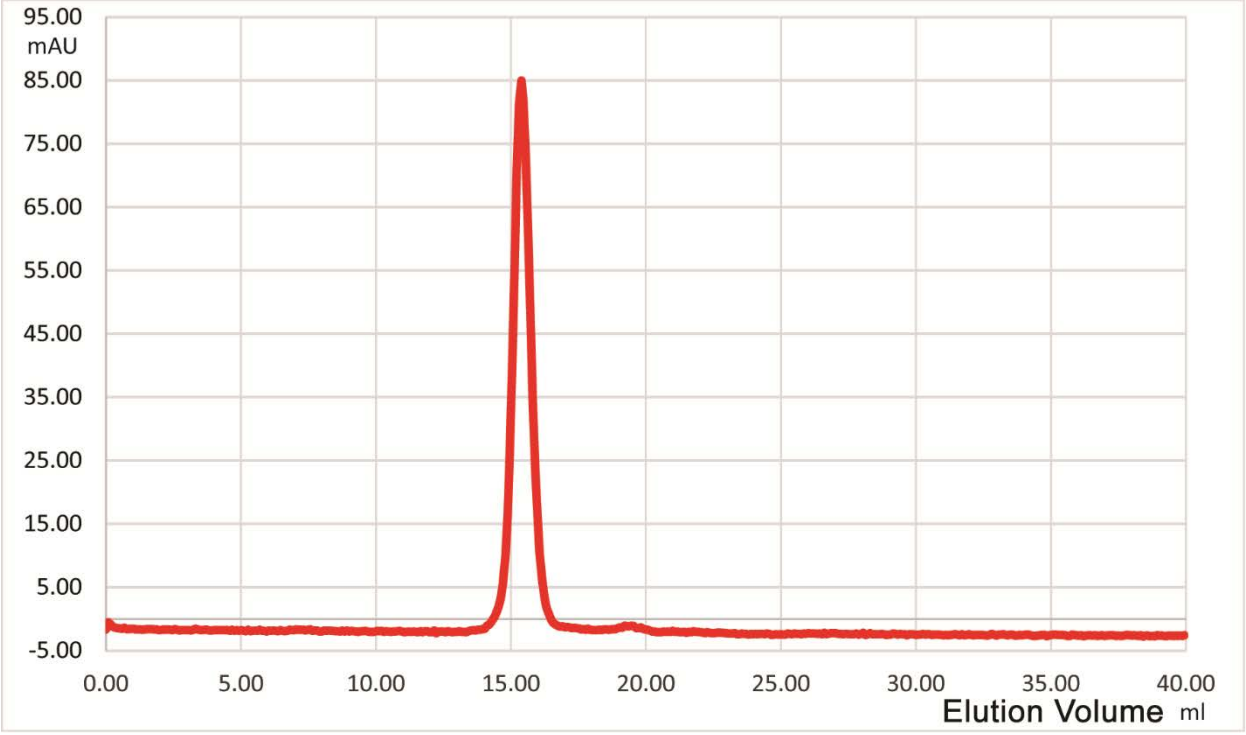

Figure 5.10. GtmA analysis by size exclusion chromatography showing a single peak at 15.2 min.

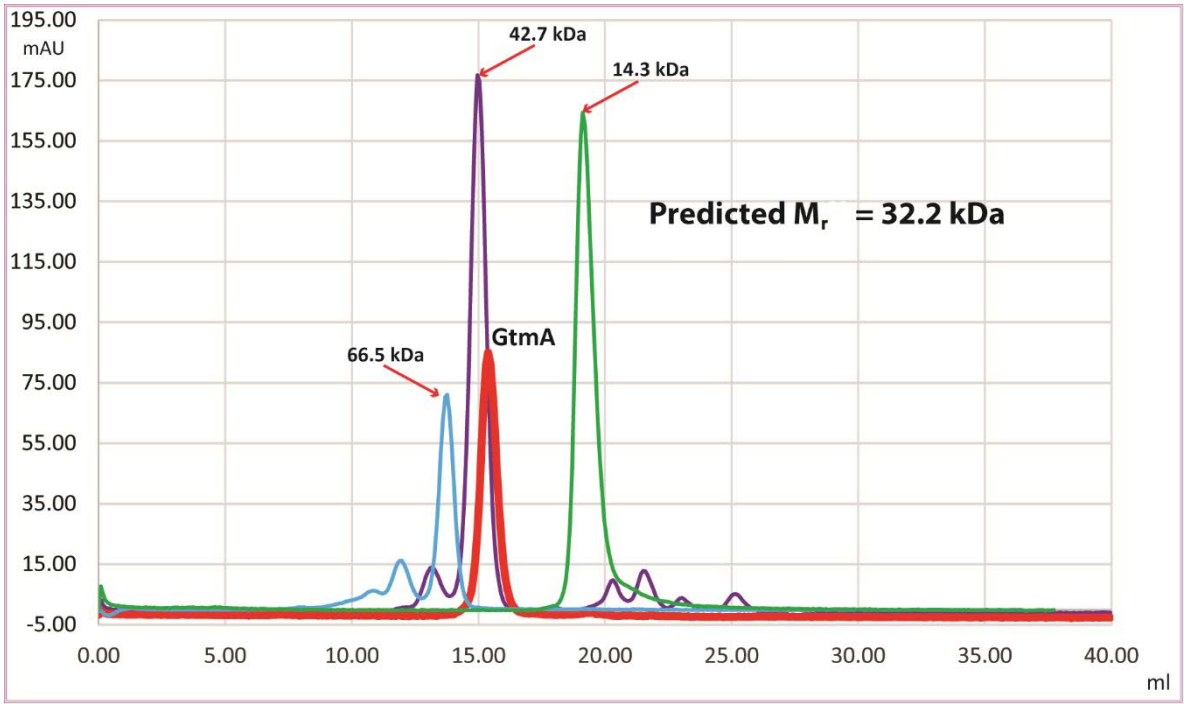

Figure 5.11. Size exclusion of GtmA alongside commercial protein standards (GE Healthcare Life Sciences). This indicated that the GtmA protein is present as a monomer.

5.2.5 Activity analysis of GtmA

Purified GtmA was tested for bisthiomethyltransferase activity. The reaction consisted of 60 µl PBS, 6 µl SAM (25 mg/ml in PBS) and 10 µl TCEP reduced GT (1 mg/ml). 5 µl GtmA (2 mg/ml) was added to the reaction. For the control sample, the 6 µl SAM was substituted with 6 µl PBS. The samples were incubated at 37 °C for 1 h and processed for LC-MS analysis as described in Section 2.2.16.4. As shown in Figure 5.12, the addition of recombinant GtmA and SAM to the reaction resulted in the conversion of dithiol gliotoxin (*m/z* 329) to bis(methyl)gliotoxin (*m/z* 357). This conversion did not occur when SAM was excluded from the reaction.

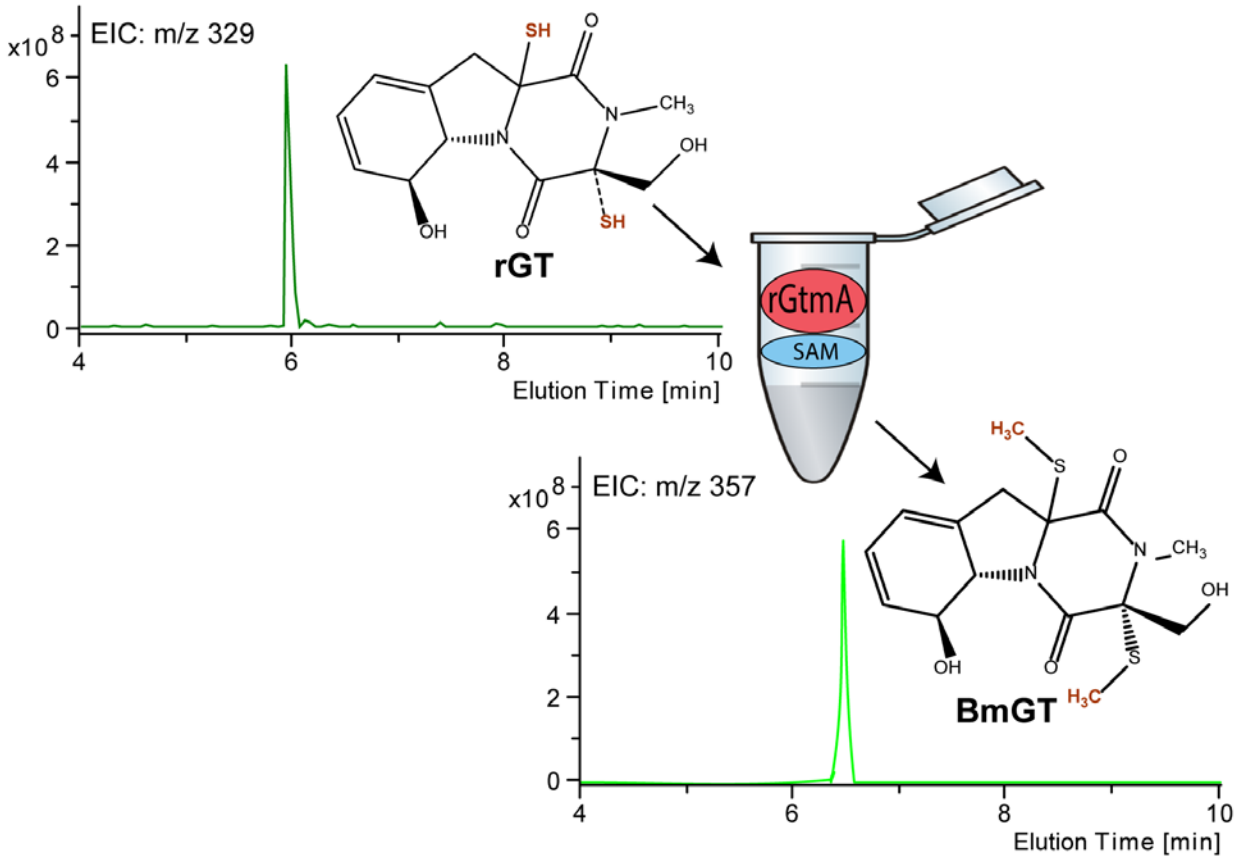

Figure 5.12. Recombinant GtmA converts dithiol gliotoxin to bis(methyl)gliotoxin in a SAM dependent manner. Dithiol gliotoxin (rGT) (*m/z* 329) is present in the control sample which does not contain SAM. The addition of SAM and GtmA to the reaction results in the formation of bis(methyl)gliotoxin (*m/z* 357).

5.2.6 GtmA bisthiomethyltransferase activity occurs sequentially

GtmA methyltransferase activity was monitored by RP-HPLC in 50 mM Tris HCl, 50 mM NaCl, pH 7.4 using a range of SAM concentrations (100 μM to 400 μM) and 500 μM dithiol GT. The samples were incubated at 37 °C for 1 h. As shown in Figure 5.13, increasing the SAM concentration results in the conversion of dithiol gliotoxin (green peak) to monomethylgliotoxin (orange peak) followed by the generation of bis(methyl)gliotoxin (red peak). This indicated that MmGT generation occurs first and is followed by bis(methyl)gliotoxin generation. This was also confirmed by LC-MS (Figure 5.14). The putative MmGT peak was fraction-collected and analysed by LC-MS to confirm the identity of this compound (Figure 5.15).

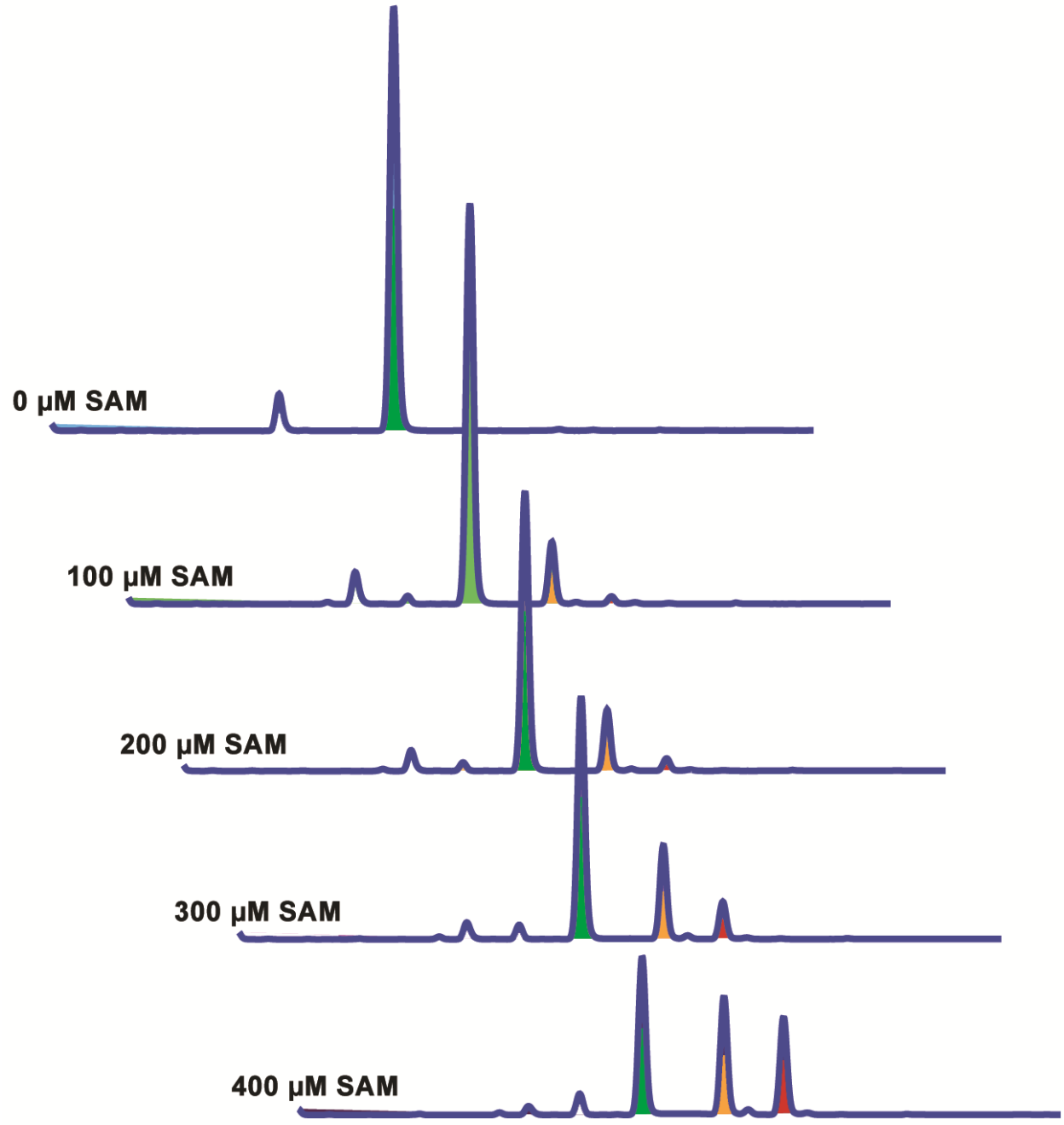

Figure 5.13. GtmA mediated bisthiomethylation occurs sequentially. The addition of increasing amounts of SAM (100 µM to 400 µM) results in the increased formation of bis(methyl)gliotoxin (red) compared to monomethylgliotoxin (orange). Dithiol gliotoxin is shown in green.

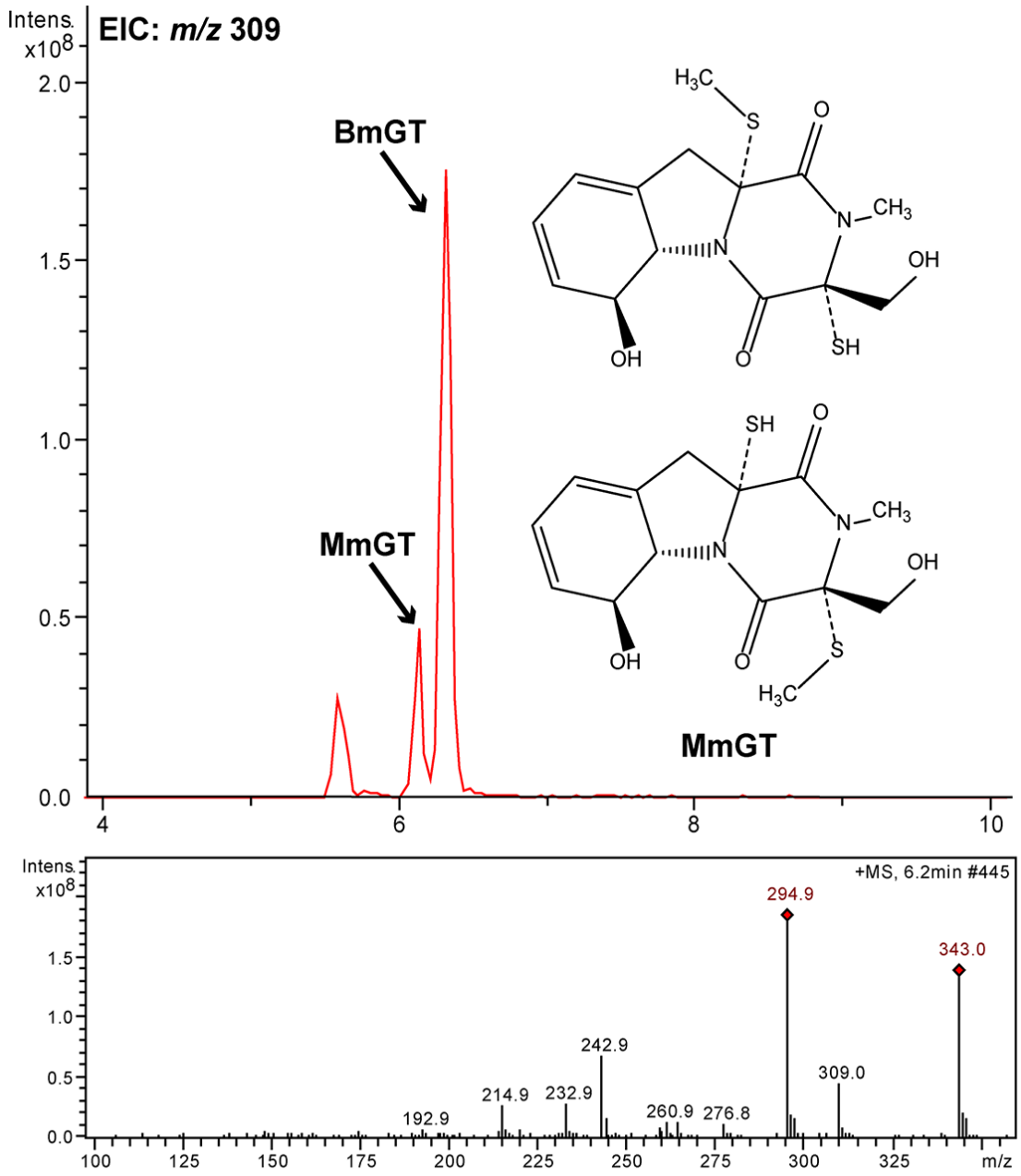

Figure 5.14. Activity analysis in the presence of limiting amounts of SAM, whereby a putative monodethiomono(methylthio)gliotoxin (MmGT) form is detectable, reveals that this reaction may proceed in a sequential manner with MmGT formation preceding that of bis(methyl)gliotoxin.

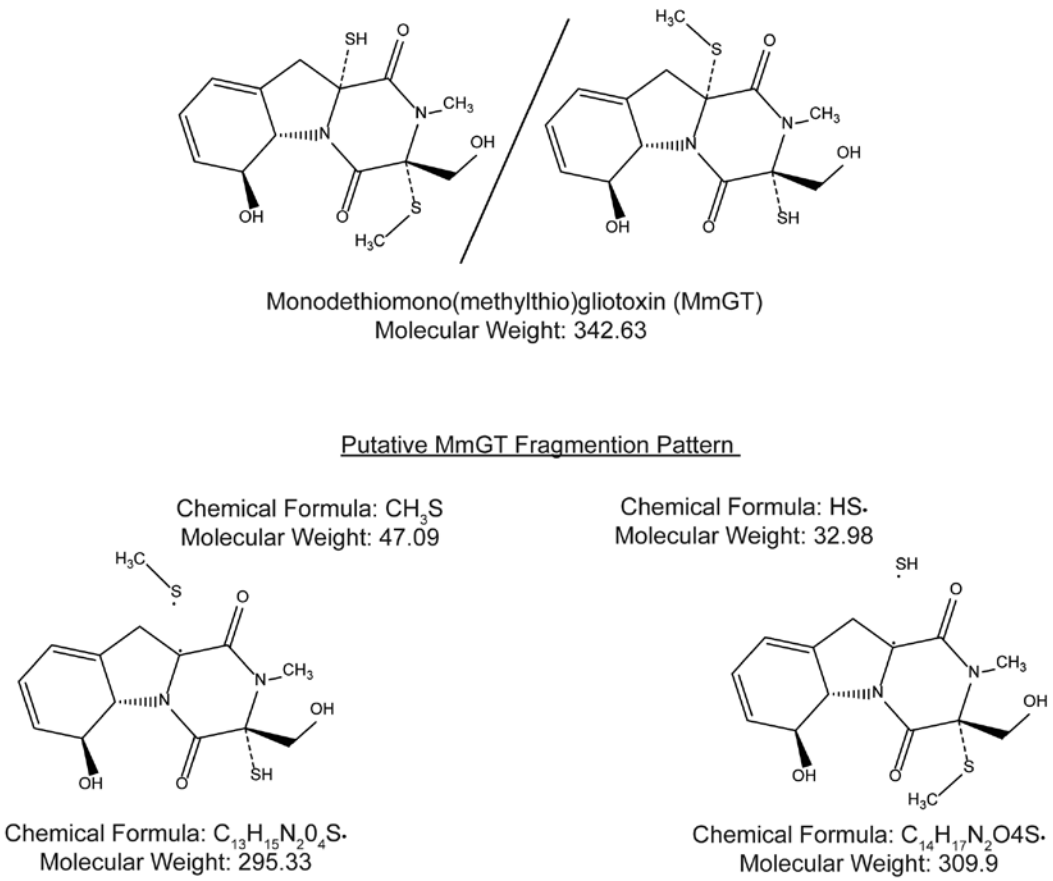

Figure 5.15. Potential LC-MS fragmentation pattern of MmGT. *m/z* 295 and *m/z* 309 fragments. The existence of *m/z* 295 fragment confirms that the CH_3 is located on the sulfhydral of MmGT.

5.2.7 Sporidesmin A is not converted to the *bis*-thiomethyl form by GtmA

Sporidesmin A is an ETP produced by *Pithomyces chartarum*. Sporidesmin D, a bisthiomethyl form of this metabolite, is also produced by this ascomycete. To test the specificity of GtmA for dithiol GT, *A. fumigatus* was exposed to sporidesmin A under conditions which promote bis(methyl)gliotoxin formation. As shown in Figure 5.16, after 3 h sporidesmin exposure, no sporidesmin D is detectable in the *A. fumigatus* culture supernatant. This indicated that GtmA shows specificity towards dithiol GT and not all thiol containing ETPs. This experiment was also carried out with purified GtmA and TCEP reduced sporidesmin A. No sporidesmin D was detected in the samples.

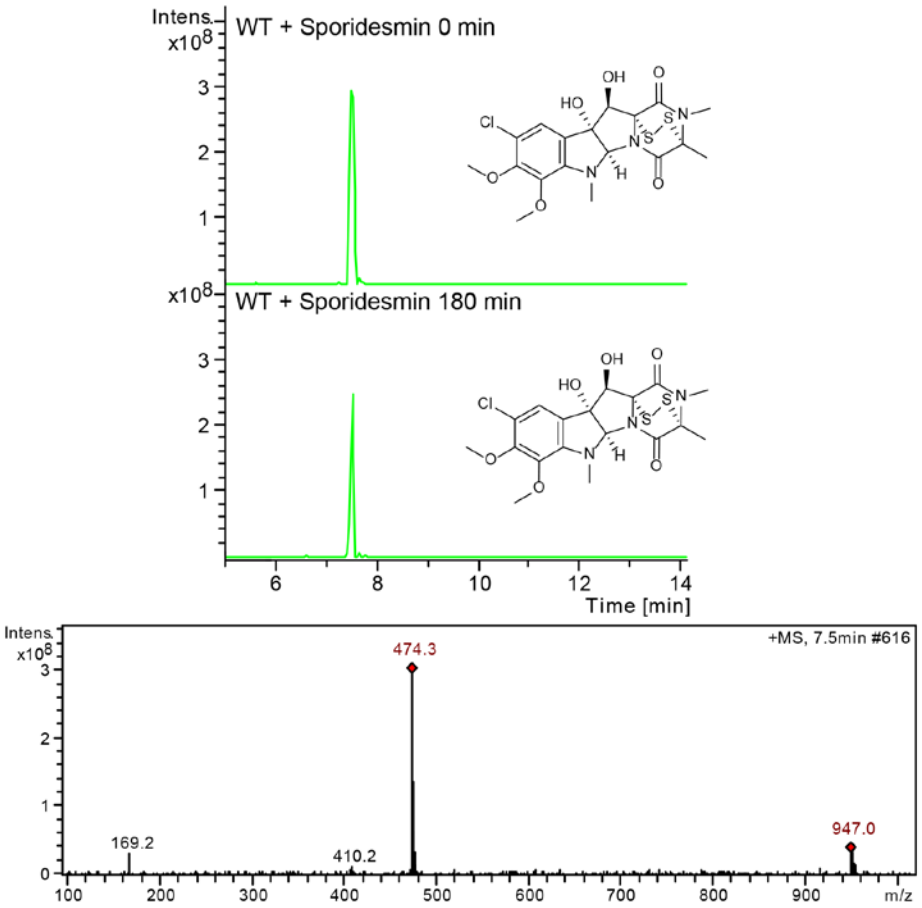

Figure 5.16. Sporidesmin (*m/z* 474) is not converted to *bis*-thiomethylsporidesmin by *A. fumigatus* wild-type under conditions (3 h exposure) which promote bis(methyl)gliotoxin formation.

5.2.8 SAH does not act as a GtmA inhibitor

The majority of SAM-dependent methyltransferases are known to be inhibited by SAH, the methyl-depleted version of SAM (Hendricks et al., 2004). GtmA was pre-incubated with SAH for 30 min (400 µM) to determine if this metabolite had an inhibitory effect on the dithiol gliotoxin bisthiomethylation activity. Dithiol gliotoxin was added and the reactions were incubated at 37 °C for 1 h. No significant difference was noted for the bis(methyl)gliotoxin peak area in the assay samples containing SAH or control samples as detected by RP-HPLC (Figure 5.17). This result suggested that GtmA was resistant to SAH mediated feedback inhibition.

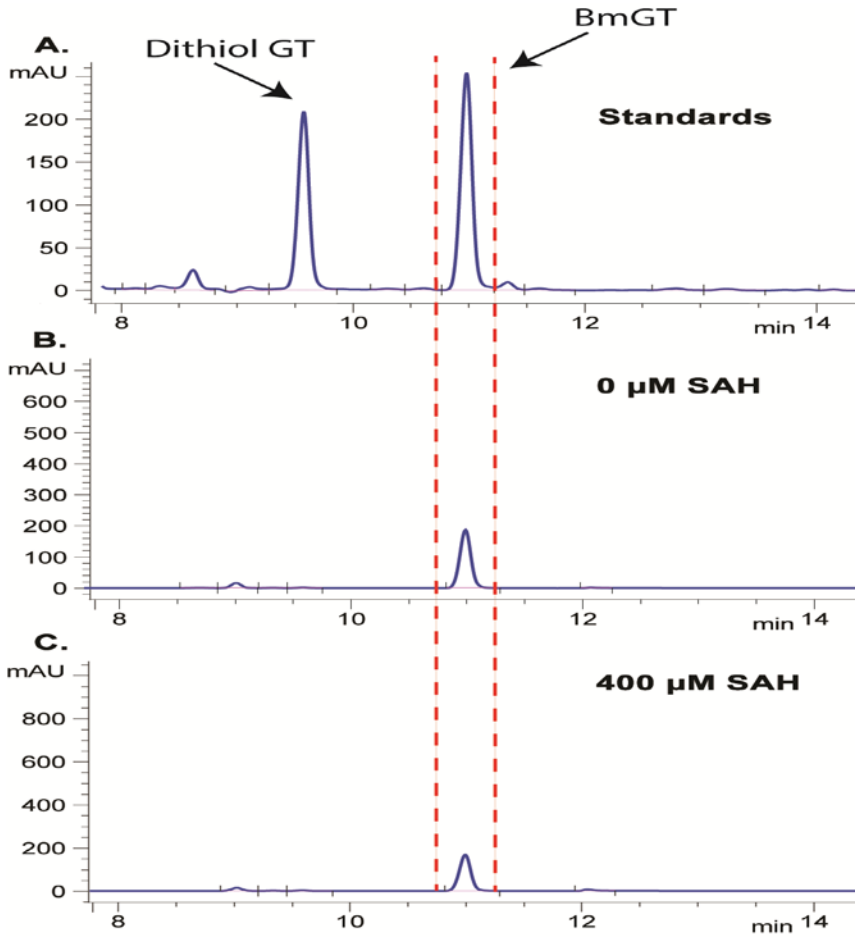

Figure 5.17. SAH does not significantly inhibit the activity of GtmA. A: RP-HPLC standards of dithiol gliotoxin and bis(methyl)gliotoxin showing the respective retention times. B: GtmA without added SAH. C: GtmA with SAH (400 µM) added to the reaction.

5.2.9 GtmA 3D Structure Prediction using I-TASSER

I-TASSER (Iterative Threading ASSEmbly Refinement) is a hierarchical method for protein structure and function prediction. The confidence of each model is quantitatively measured using a 'C-score' that is calculated based on the significance of threading template alignments and the convergence parameters of the structure assembly simulations (Roy et al., 2010)

The GtmA amino acid sequence (Section 5.2.2) was sent to the I-TASSER server. This program uses the templates of the highest significance in the threading alignments, the significance of which are measured by the Z-score (the difference between the raw and average scores in the unit of standard deviation). The top matching PDB structures used for comparison were 4OBW (yeast Coq5 in the SAM bound form), 1VL5 (A putative methyltransferase, BH2331, from *Bacillus halodurans* C-125), 4OBX (yeast Coq5 in the apo form), 2YQZ (Hypothetical methyltransferase TTHA0223 from *Thermus thermophilus* HB8 complexed with SAM) and 3CCF (putative methyltransferase (YP_321342.1) from *Anabaena variabilis* ATCC 29413). The structure shown in Figure 5.18 was the best predicted GtmA structural model with a C-score of -0.89; C-score is typically in the range of [-5, 2], where a C-score of a higher value signifies a model with a higher confidence and vice-versa. The structure had an estimated root-mean-square deviation (RMSD) of 8.1 ± 4.4 Å.

Figure 5.19 details the local accuracy and predicted normalized B-factor of the GtmA model. The local accuracy is defined as the distance deviation (in Angstroms) between residue positions in the model and the native structure. Since the native structure is unknown, the distance errors in the plot are estimated by ResQ using support vector regression which makes use of the coverage of threading alignment, divergence of I-TASSER simulation decoys and sequence-based secondary structure and solvent

accessibility predictions. Large-scale benchmark tests show that the estimated local quality has an average error of 1.4 Angstrom units and AUC score of 0.89 for well-predicted I-TASSER models (Roy et al., 2010).

B-factor is a value to indicate the extent of the inherent thermal mobility of residues/atoms in proteins. The normalized B-factor for a target protein is defined as z-score-based normalization of the raw B-factor values. The normalized B-factor (called B-factor profile, BFP) is predicted using a combination of both template-based assignment and profile-based prediction. Based on the distributions and predictions of the BFP, residues with BFP values higher than 0 are less stable in experimental structures (Zhang, 2008; Roy et al., 2010).

TM-align was used to identify proteins which were structurally close to the GtmA model. This program uses TM-score as a metric for measuring the structural similarity of two protein models. This analysis is favoured over traditional metrics such as RMSD. This is due to the fact that TM-score measures the global fold similarity and is less sensitive to the local structural variations. Also, the magnitude of TM-score for random structure pairs is length-independent. TM-score has the value in [0, 1], where 1 indicates a perfect match between two structures. Following strict statistics of structures in the PDB, scores below 0.17 correspond to randomly chosen unrelated proteins whereas a score higher than 0.5 generally assumes the same fold in SCOP/CATH (Zhang, 2008). Figure 5.20 shows this GtmA model overlaid with the salicylic acid carboxyl methyltransferase (SAMT) from *Clarkia breweri*. This protein had the highest TM-score of 0.741. In addition, the GtmA model was overlaid with the yeast C-methyltransferase Coq5, which had a TM-score of 0.723.

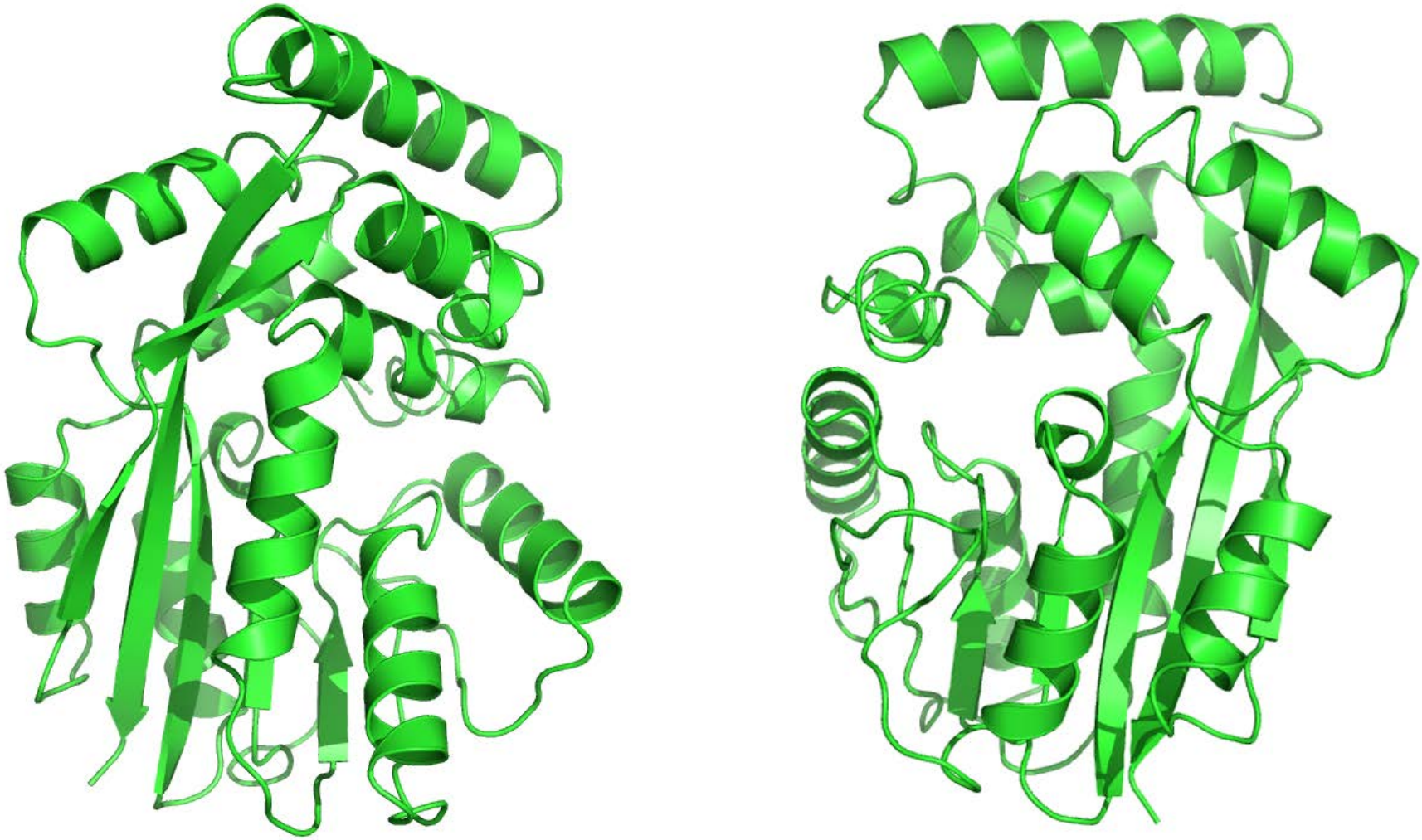

Figure 5.18. A, I-TASSER generated model of GtmA. Threading templates used were 4OBWA, IVL5A, 4OBXA, 2YQZA, 3CCFA.

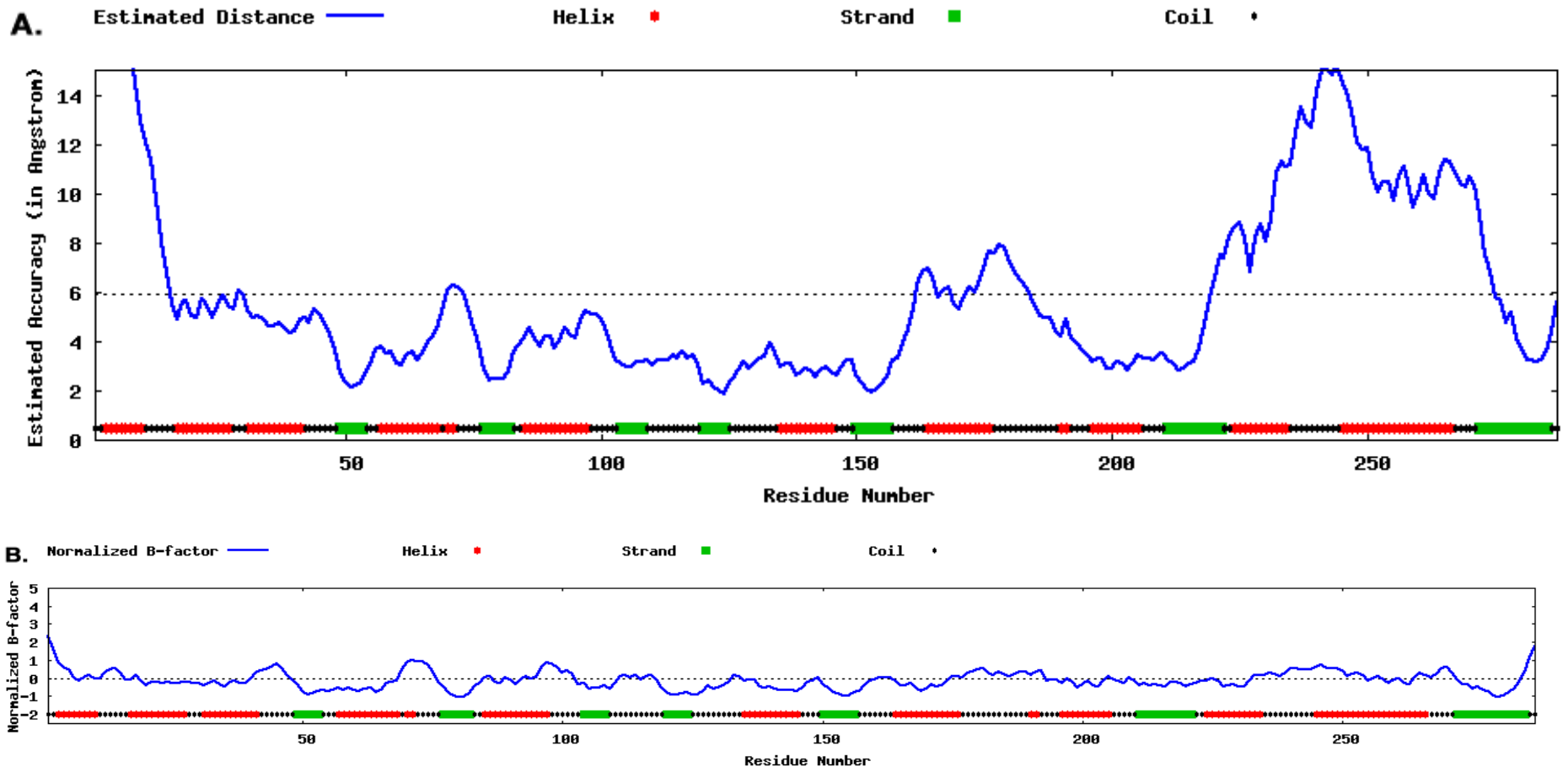

Figure 5.19. A: The local accuracy of the GtmA model based on the distance deviation (in Angstrom units) between residue positions in the model and the ResQ generated test 'native' structure. **B**: Predicted normalized B-factor for GtmA. Residues with BFP values higher than 0 are less stable in experimental structures.

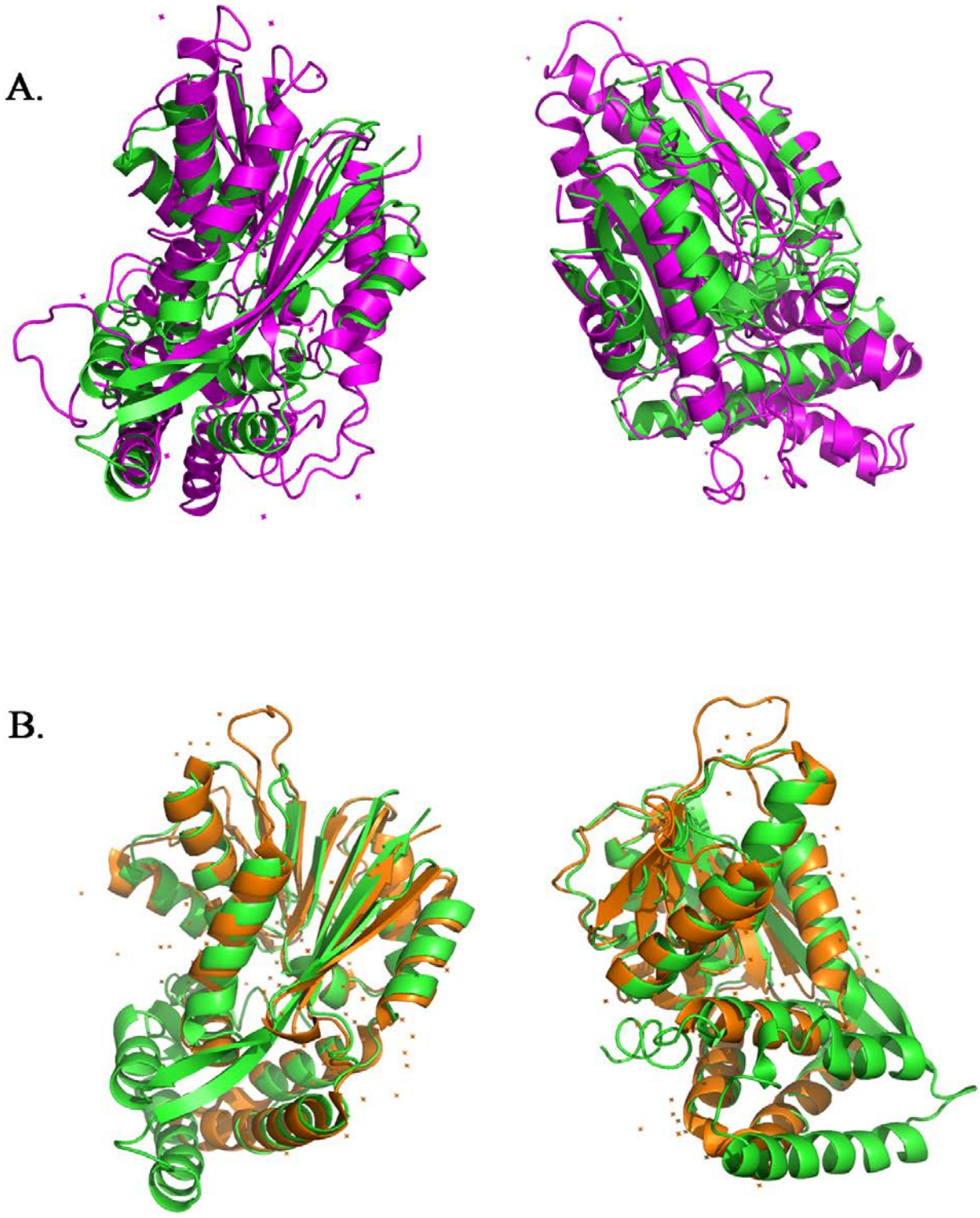

Figure 5.20. GtmA overlaid with **A:** the salicylic acid carboxyl methyltransferase (SAMT) from *Clarkia breweri* (TM-score 0.741) and **B:** the yeast C-methyltransferase Coq5 (TM-score 0.723). These proteins were calculated to be structurally close to GtmA.

The GtmA SAH binding site was predicted using COACH, a meta-server approach that combines multiple function annotation results from the COFACTOR, TM-SITE and S-SITE programs. Beginning with the given structure of target proteins, COACH generated complementary ligand binding site predictions using the comparative methods - TM-SITE and S-SITE - which recognize ligand-binding templates from the BioLiP protein function database by binding-specific substructure and sequence profile comparisons. These predictions were combined with results from other methods (including COFACTOR, FINDSITE and ConCavity) to generate final ligand binding site predictions. The I-TASSER generated 3D model of GtmA was fed into the COACH pipeline for ligand-binding site prediction. The PDB structure 4NEC (Echinomycin methyltransferase Ecm18) was selected as a model for the GtmA structure (Hotta et al., 2014). Based on this analysis, the GtmA residues which may interact with SAH were shown to be 7,11,24,54,55,56,82,83,84,108,109,110,126,127,128 and 132. These SAH interacting residues were illustrated using LIGPLOT^{+} as shown in Figure 5.21. The dithiol gliotoxin binding residues could not be predicted using this method (Roy et al., 2010; Zhang, 2008; Laskowski and Swindells, 2011).

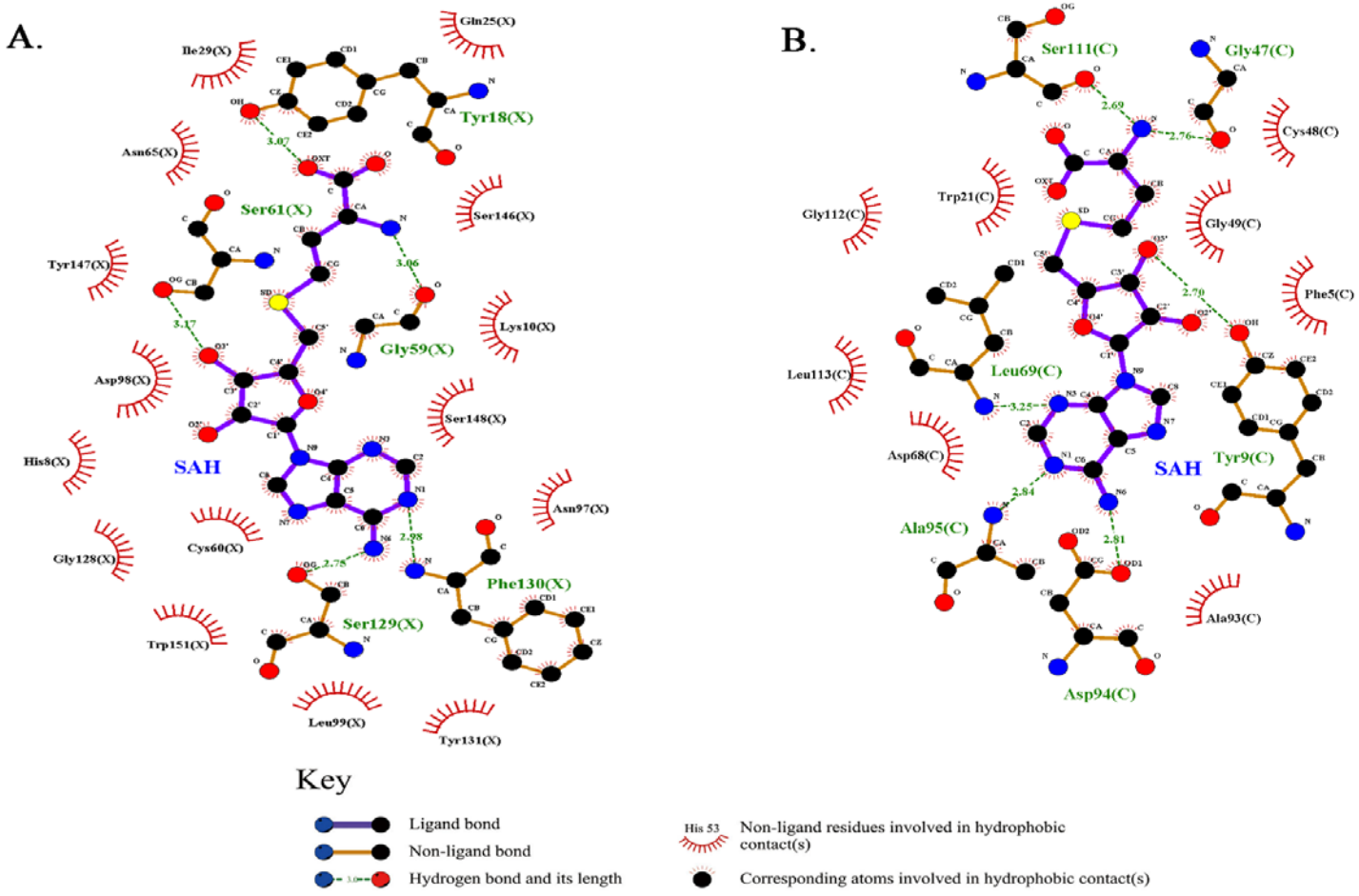

Figure 5.21. **A:** GtmA-SAH potential interactions based on the COACH analysis. **B:** Ecm18-SAH interacting residues based on the published complex. Figures were prepared using LIGPLOT^{+}.

5.2.10 Crystallisation of GtmA

Purified GtmA was concentrated to 15 mg/ml in 50 mM Tris HCl, 50 mM NaCl, pH 7.4. The protein (40 mg total) was snap frozen in liquid nitrogen and was then sent to the Helmholtz Centre for Infection Research for crystallisation trials. The initial crystallization conditions of GtmA were determined with the vapor diffusion method in a sitting drop 96-well format with the JCSG Core Suites I–IV. Drops were set up using a dispensing robot (Honeybee, Zinsser Analytic) mixing 0.1 µL of GtmA solution (15 mg mL^{-1}) with 0.1 µL of reservoir solution equilibrated against 70 µL reservoir solution. The screens were stored at 20 °C in an automated imaging system (Formulatrix). Crystals of different morphology appeared with various precipitants which were optimized with respect to pH and component concentrations. The final condition of GtmA crystals contained 0.2 M Ammonium acetate, 0.1 M tri-Sodium Citrate pH 5.84, 26% (w/v) PEG 4000. Apo crystals of GtmA were cryoprotected in reservoir solution supplemented with 20 %(v/v) glycerol, flash cooled in liquid nitrogen and tested on an X-ray home source including a Saturn 944+ CCD detector (Rigaku). Well-diffracting crystals of GtmA were sent to a synchrotron (Bessy II, HZB, Berlin, Germany) for data collection. Crystals of the seleno-L-methionine-labelled protein were obtained by keeping the composition of the crystallization solution the same as for native protein. High-quality crystals appeared after 7 days (Figure 5.22).

A.

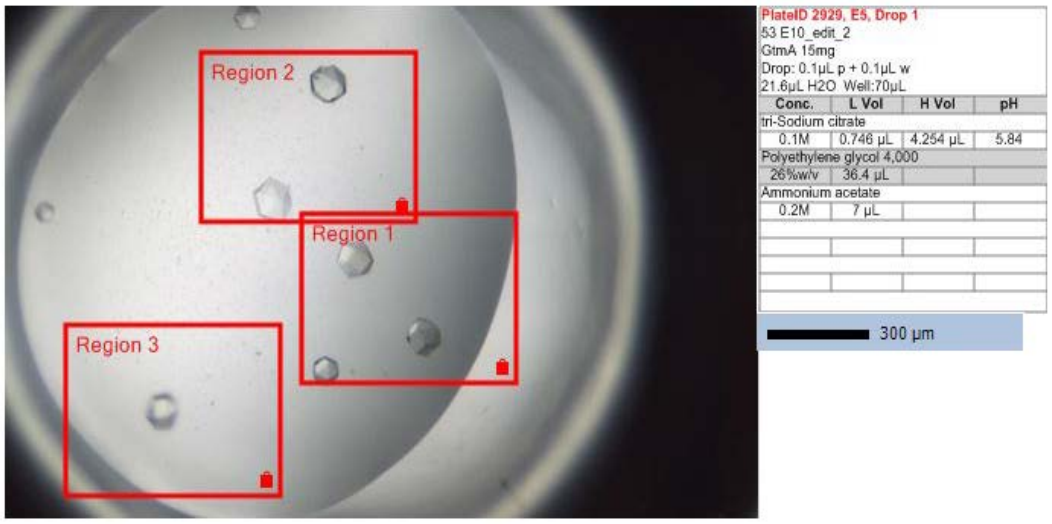

B.

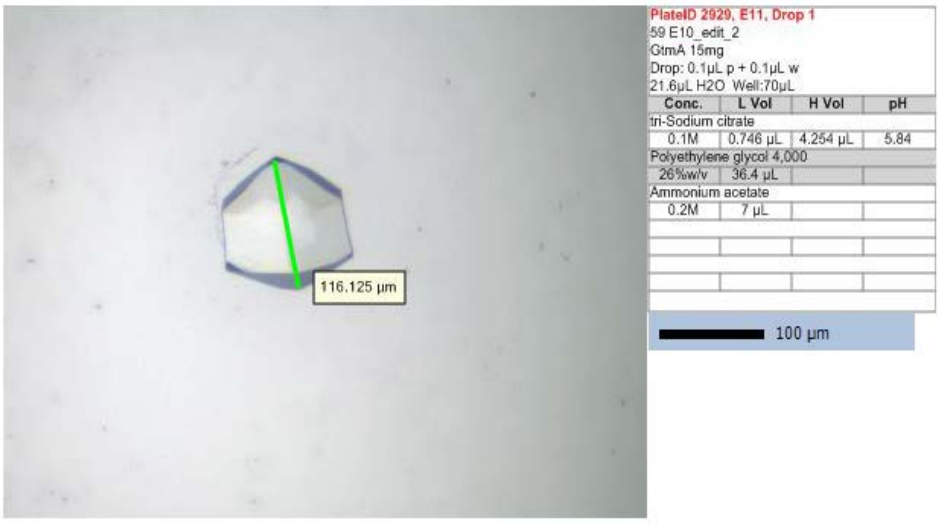

Figure 5.22. A: GtmA apo crystals imaged after 7 days by the automatic imaging system.

B: Magnified image of a single GtmA crystal with dimensions.

5.2.11 Preparation of seleno-L-methionine-labeled GtmA

SeMet incorporation and multiwavelength anomalous diffraction (MAD) phasing are routinely used and have become the norm in protein crystallography. Production of seleno-L-methionine-labelled GtmA was achieved by cultivation of *E. coli* BL21 (DE3) cells in artificial medium suppressing L-methionine biosynthesis as described in Section 2.1.2.4. Purification steps were performed as for the native protein (Section 5.2.3). Figure 5.23 shows the SDS-PAGE analysis of the purification steps. The identity of the proteins and the incorporation of seleno- L -methionine were confirmed by ESI mass-spectrometric analysis. 5 mg of SeMet GtmA was concentrated to 15 mg/ml for crystallisation trials.

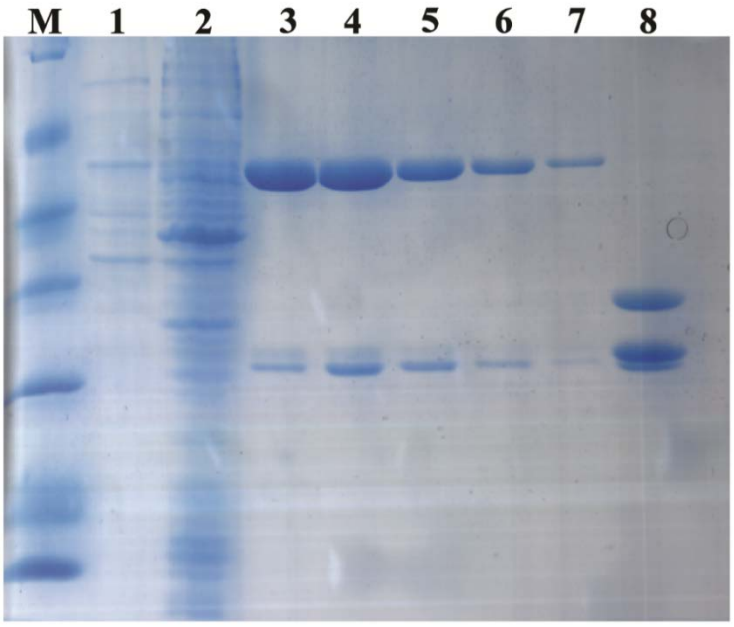

Figure 5.23. Expression and purification of SeMet-GtmA. GST-SeMet-GtmA was first purified by GSH-Sepharose affinity chromatography. The protein was then cleaved using TEV protease and purified by size exclusion chromatography. Fractions containing Se-Met-GtmA (5 mg) were pooled and concentrated. Lane 1: Uninduced sample, Lane 2: Induced sample, Lane 3-7: fractions eluted from GSH affinity chromatography. Lane 8: TEV cleaved GtmA and GST. The double bands indicate the Se-Met-GST cleaved from GtmA and endogenous GST.

5.2.12 Data collection, data processing, structure solution and refinement

Diffraction data for seleno-L-methionine-labeled and native GtmA apo form crystals were collected at the BESSY II Synchrotron (HZB, Berlin, Germany) using a Pilatus 2M detector (Dectris). A native dataset was collected from a different GtmA apo-crystal at a wavelength of 2.1 Å. All data were indexed and integrated with XDS (Kabsch, 2010) and scaled with AIMLESS (Evans, 2011) from the CCP4 program suite (Winn et al., 2011). For the MAD data, hkl2map (Pape and Schneider, 2004) was used to employ SHELXC (Sheldrick, 2010) in extraction of the anomalous signal and SHELXD (Schneider and Sheldrick, 2002) in locating the anomalous scatterers, before SHELXE was used for density modification and automated model building. Since native data extended to a resolution of 2.05 Å, MAD data and native data were combined. An initial model was generated using arp/Warp 7.0 (Langer et al., 2008). Data were processed with XDS and Aimless. Manual adjustment of all models was done in COOT (Emsley and Cowtan, 2004) which included the placement of ions. Figures were prepared with PyMOL. Data collection and refinement statistics are presented in Table 5.1. Indexing and integration with XDS (Kabsch, 2010) revealed that the investigated GtmA crystals belonged to space group P62.

Table 5.1. GtmA Crystallography Model Statistics and General Data

R Values	R_{work} 23.37 R_{free} 26.27
Space Group	P62
Cell	94.74 94.74 53.76 90 90 120
Resolution Low	82.06
Resolution High	2.05
Number of Reflections	17398
Number of Datasets	4

5.2.13 GtmA Structure as determined by X-Ray Crystallography

Based on the X-ray crystallography data gathered in Section 5.2.12, a structural model of GtmA was constructed. This structure is shown in Figure 5.24. The overall apo structure of the GtmA monomer consists of a globular domain which contains the extended sheet characteristic of all other SAM-dependent methyltransferases (Cheng and Blumenthal, 1999) and a unique -helical cap that forms the top one-third of the active site cavity. These structures confirmed that GtmA possesses the expected class I AdoMet-dependent MTase core fold which consists of a seven-stranded β sheet flanked on each side by three α helices. Class I MTases bind AdoMet (or the demethylated product AdoHcy) at the same methyl donor site in their structures reflecting their shared AdoMet dependence. However, they must have diverse active sites to accommodate their wide variety of acceptor substrates (Schubert et al., 2003).

Several loops and the N-terminus (residues 0-24) of GtmA are absent from the structure. This happens when regions of protein molecules in the protein crystal are disordered, mobile or "floppy" and, as such, do not generate an interpretable X-ray diffraction pattern. The N-terminal part of methyltransferases are generally flexible, facilitating the entry of the substrates and cofactor into the active site and the exit of the reaction products. As shown in Figure 5.25, the I-TASSER generate GtmA model was overlaid with the crystallographic model. This allowed for a comparison of the effectiveness of the computer generated models. Also, the loops which are absent from the crystal structure can be modelled in based on the I-TASSER model (Figure 5.26).

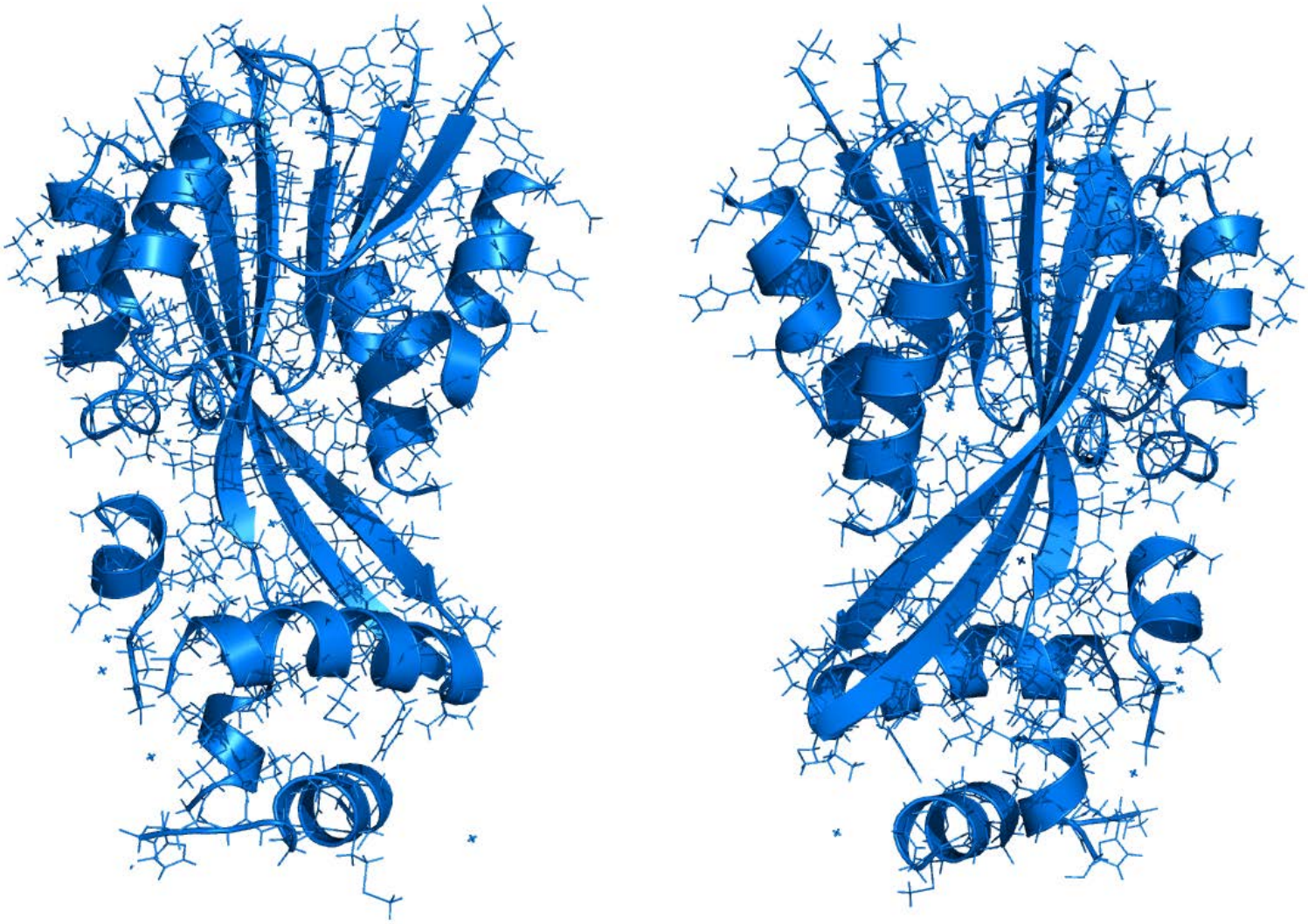

Figure 5.24. Structural model of GtmA based on the crystallographic data.

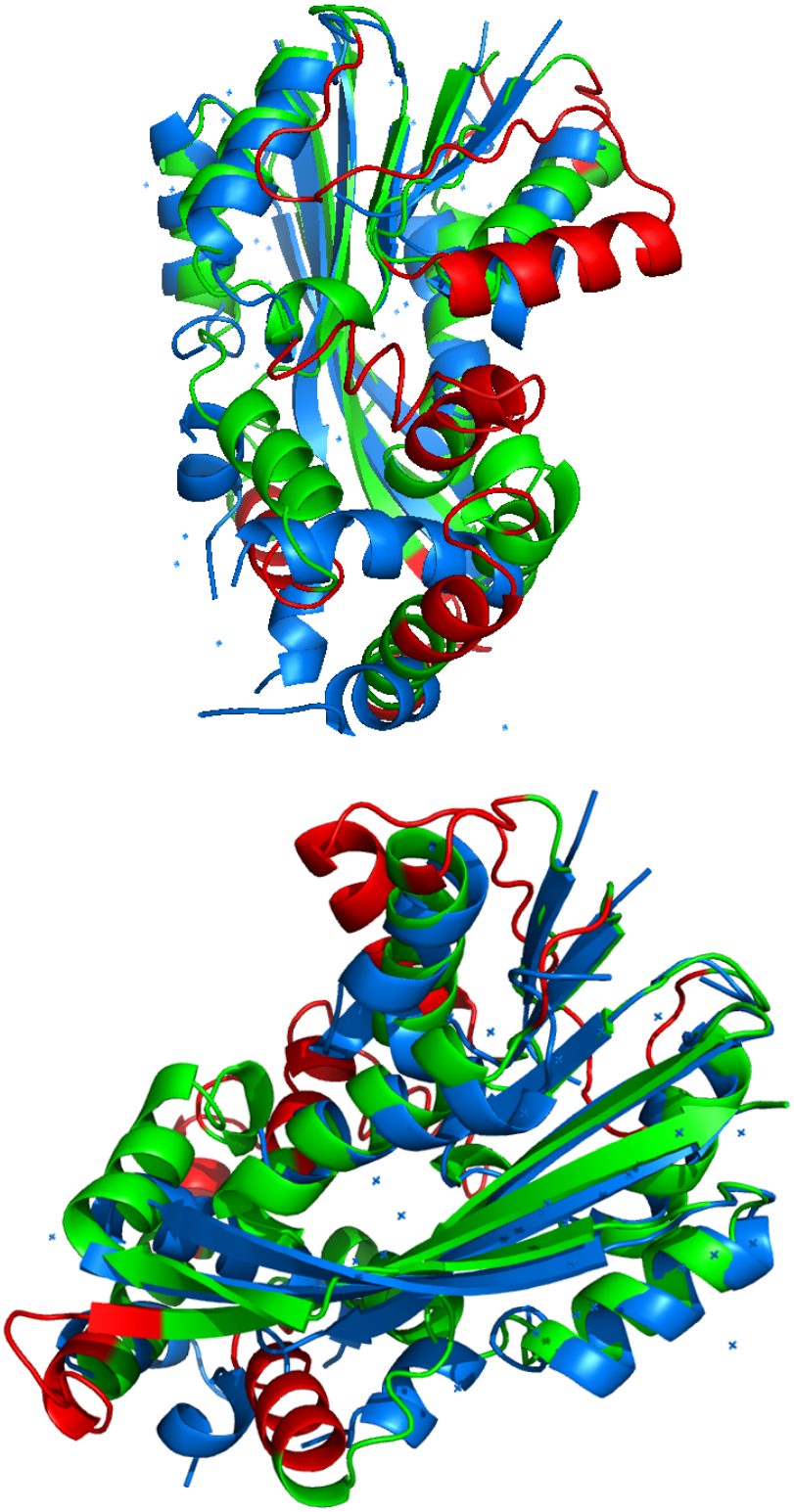

Figure 5.25. Overlay of GtmA model based on the crystallographic structural data (blue) with the I-TASSER generated GtmA model (green). Flexible regions of the GtmA structure which were not resolved by X-ray crystallography are shown in red within the I-TASSER model.

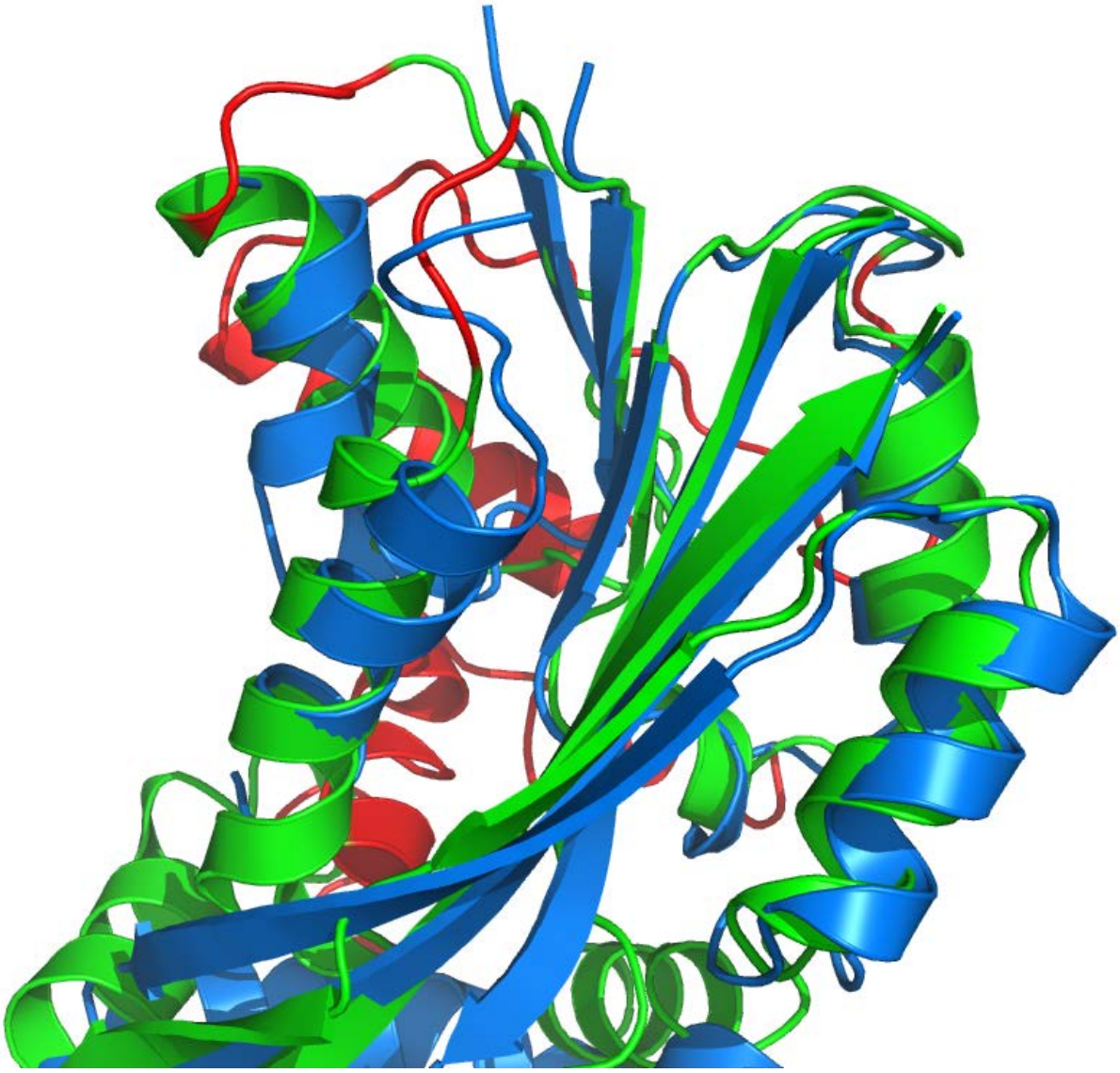

Figure 5.26. Detailed overlay of the GtmA model based on the crystallographic structural data (blue) with the I-TASSER generated GtmA model (green). Flexible regions of the GtmA structure which were not resolved by X-ray crystallography are shown in red within the I-TASSER model. Several conserved regions of the methyltransferase structure were predicted accurately by I-TASSER.

5.2.14 PDBeFold pairwise comparison and 3D alignment of GtmA against similar protein structures

PDBeFold structure alignment is based on identification of residues occupying "equivalent" geometrical positions (Mcwilliam et al., 2009). The PDBefold service is a very powerful structure alignment tool which can perform both pairwise and multiple three dimensional alignment. The results of the Secondary Structure Matching are sorted based on the Q Score (Cα-alignment), P score (taking into account RMSD, number of aligned residues, number of gaps, number of matched Secondary Structure Elements and the SSE match score), Z score (based on Gaussian Statistics), RMSD and % Sequence Identity. The structural relatedness of the proteins involves consideration of average root-mean-square deviation (RMSD) of Cα atoms and Z-score between structures. The GtmA coordinates from the structure shown in Section 5.2.10 were uploaded to the server. PDBeFold structural similarity searches were conducted using WWW interface at http://www.ebi.ac.uk/msd-srv/ssm/.

The structural alignment results indicated that the best structural matches to GtmA were an N-methyltransferase NodS from *Bradyrhizobium japonicum* (PDB: 3OFK) [Q-Score 0.27] and, also, the N-terminal methyltransferase-like domain of anamorsin from *Homo sapiens* (PDB: 4M7R) [Q-Score 0.18]. GtmA overlaid with these other structures is illustrated in Figure 5.27.

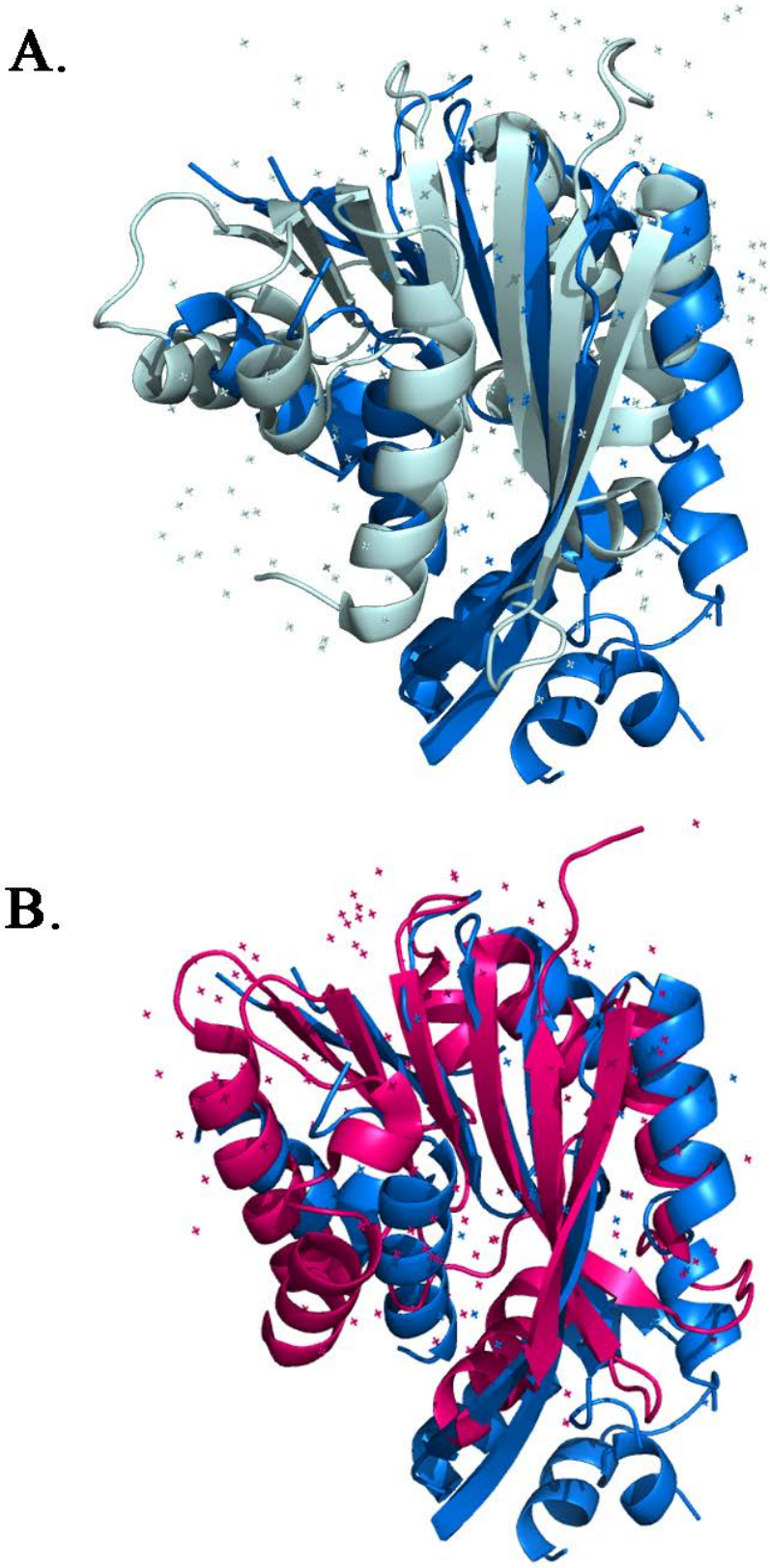

Figure 5.27. Overlay of GtmA model based on the structural data (blue) with **A:** N-methyltransferase NodS from *Bradyrhizobium japonicum* (PDB: 3OFK) and **B:** the N-terminal methyltransferase-like domain of anamorsin from *Homo sapiens* (PDB: 4M7R).

5.2.15 Alignment of GtmA with other methyltransferases

Multiple sequence alignment of GtmA with other methyltransferases was carried out using Jalview. A ClustalWS alignment was selected in the parameters and the resulting illustrations were exported. Figure 5.28 shows the alignment of GtmA with an *A. niger* GtmA homolog (MT) which has been shown to also bisthiomethylate dithiol gliotoxin, a methyltransferase from *Methanosarcina mazei* (3MGG), a C-methyltransferase from *Saccharomyces cerevisiae* (Coq5) and the rebeccamycin 4′-O-methyltransferase (RebM) from *Lechevalieria aerocolonigenes*. This alignment was used to identify conserved motifs which are found across the entire family of methyltransferases. GtmA was also aligned solely with *A. niger* MTII (MacKenzie et al., 2005, Manzanares et al., 2015) in order to highlight the similarity between these two methyltransferases (Figure 5.29). In addition to the high sequence similarity (51%), 71% of GtmA residues have substitutions with amino acids with similar characteristics. Zappo colours were used in the alignment illustrations as described in Table 5.3.

Table 5.3. Legend for the Zappo colour scheme. Residues are coloured according to their physico-chemical properties as follows:

Residues	Description	Colour
ILVAM	Aliphatic/hydrophobic residues	Pink
FWY	Aromatic	Orange
KRH	Positive	Red
DE	Negative	Green
STNQ	Hydrophilic	Blue
PG	Proline/Glycine (conformationally special)	Magenta
C	Cysteine	Yellow

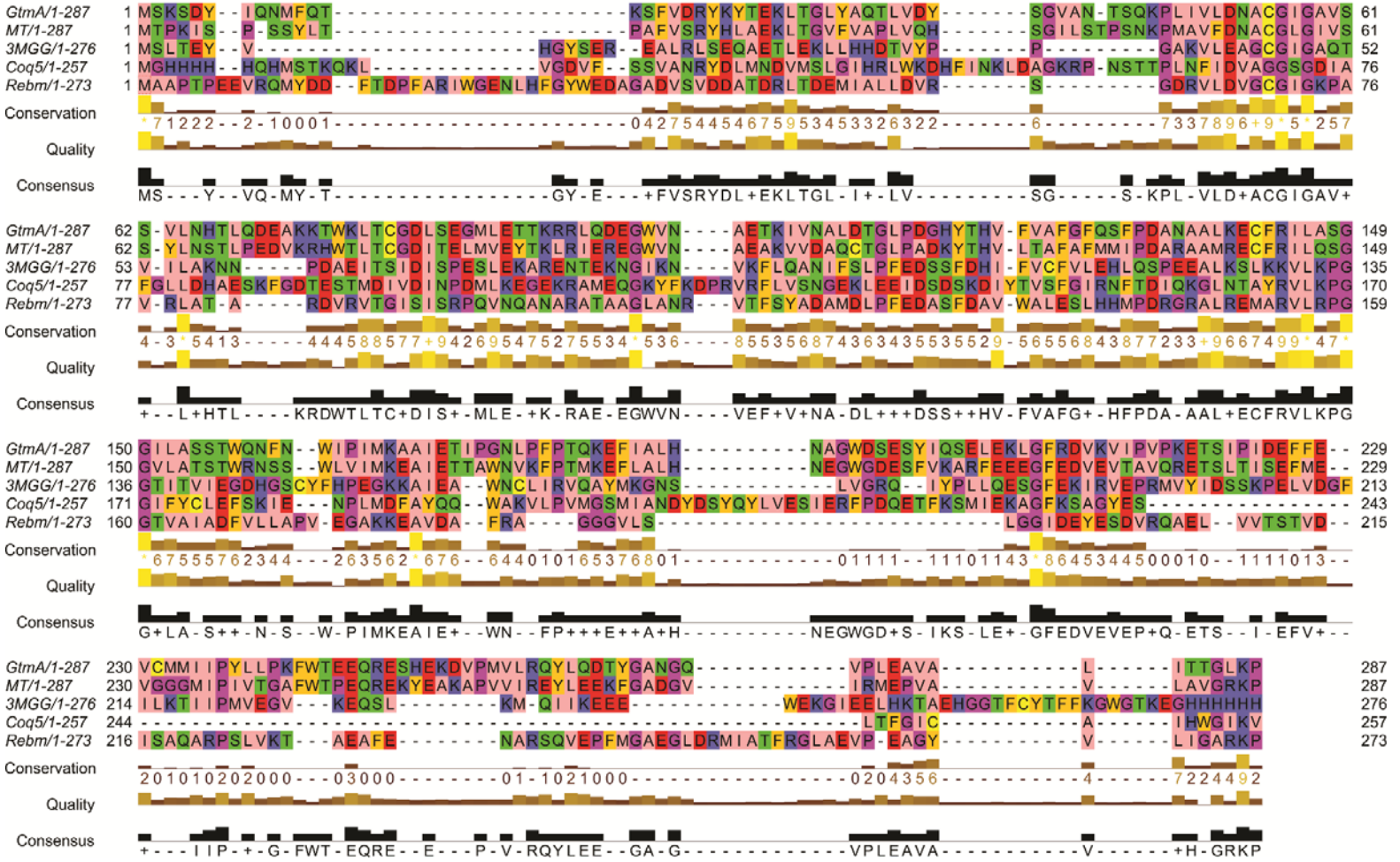

Figure 5.28. Alignment of GtmA with other methyltransferases showing conserved residues which are likely to be essential for the catalytic activity of these enzymes.

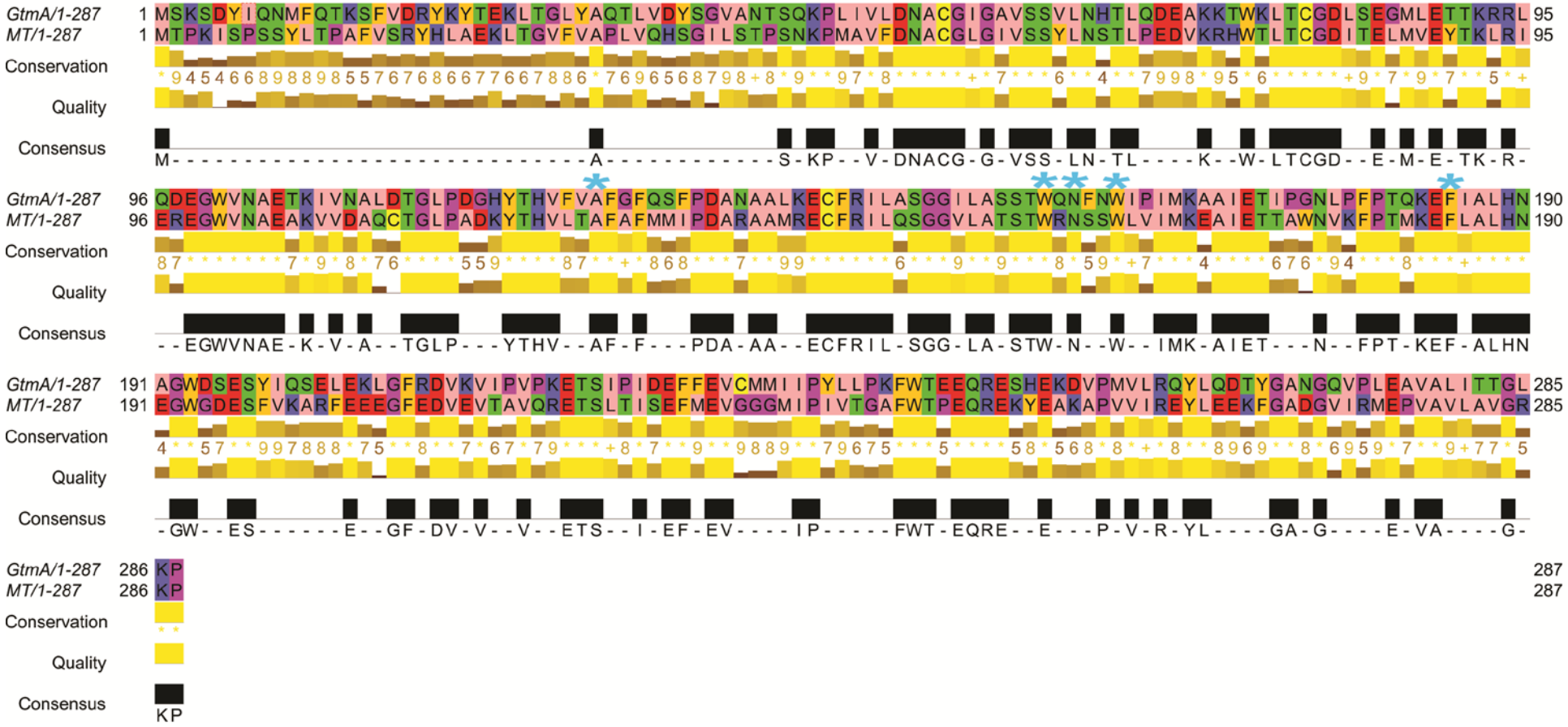

Figure 5.29. Alignment of *A. fumigatus* GtmA with an *A. niger* GtmA homolog (MTII) which has been shown to also bisthiomethylate dithiol gliotoxin. This data was used in combination with the structural data to select residues for mutation (blue asterisks) which may be essential for the substrate binding of this enzyme.

5.2.16 Cloning of *gtmA* into Pet19m

In order to express GtmA as a His-tagged protein the *gtmA* gene was cloned into Pet19m from pEX-N-GST using the primers stated in Table 2.4. Pet19m contained a His_6 affinity tag which facilitated rapid purification of GtmA from cell lysates. Amplified *gtmA* and Pet19m were digested using the restriction enzymes *Nde*I and *Xho*I and ligated using Promega rapid DNA ligase. Colonies were screened by PCR as described in Section 2.2.2.2. Correct cloning was verified by sequencing. GtmA was expressed and purified as described in Section 5.2.3, however, NiNTA affinity resin was used instead of GSH-Sepharose. The samples containing protein were tested by SDS-PAGE (Figure 5.30). The fractions containing His-GtmA were pooled and this His-tag was cleaved using TEV protease while simultaneously carrying out dialysis of the sample into 50 mM Tris-HCl, 50 mM NaCl, pH 7.4. 110 mg of purified, cleaved GtmA was prepared for further crystallisation trials. This was snap frozen in liquid nitrogen and sent to the Helmholtz Infection Centre.

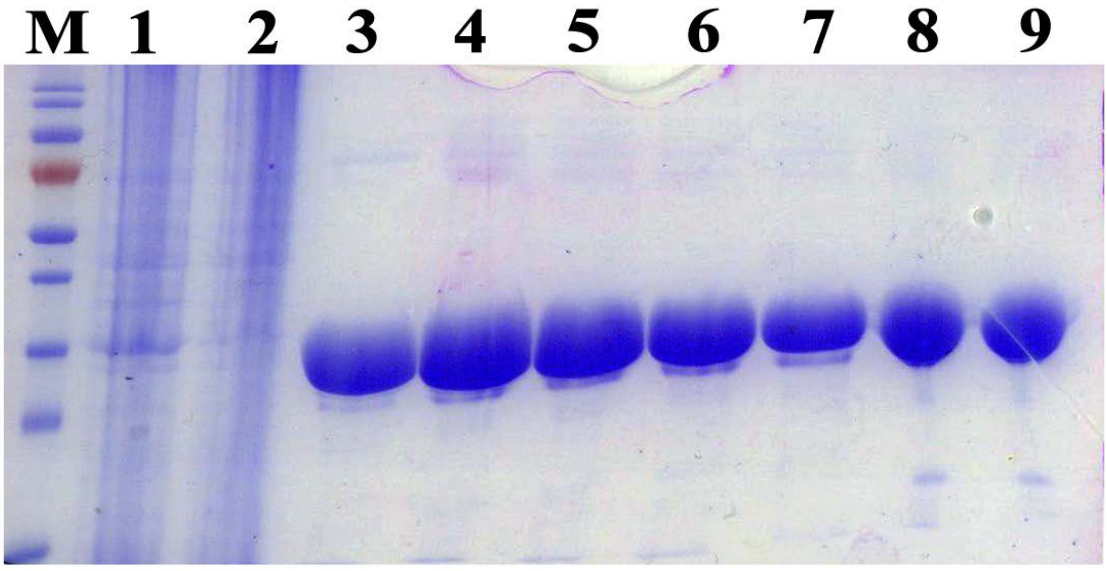

Figure 5.30. SDS-PAGE analysis of fractions containing His-GtmA. 5 µl was loaded per well. M; protein molecular mass marker, Lane 1: Induced His_6-GtmA lysate, Lane 2: NiNTA column flow through, Lane 3-9: His_6-GtmA fractions eluted from NiNTA resin (approximately 32 kDa)

5.2.17 Site Directed Mutagenesis of Selected GtmA Residues

Single GtmA residues which may be important for the activity of this enzyme were selected by using a combination of the structural data and modelling from Section 5.2.13 and also by analysing the alignment of *A. fumigatus* GtmA and *A. niger* MT-II (Section 5.2.15). Conserved residues within the putative SAM binding domain and putative SAH interacting residues identified by the COACH analysis (Figure 5.21) were avoided as they have been extensively characterised previously in other methyltransferases. The following residues were selected for mutagenesis using a QuickChange XL Site-Directed Mutagenesis Kit (Section 2.2.7.2): Trp157 to Val, Trp162 to Val, Asp159 to Val, and Phe185 to Gly and Phe127 to Val. Successful single amino acid mutagenesis was confirmed by sequencing the mutated plasmids. The recombinant GtmA mutants were then expressed and purified as shown in Figure 5.31. The locations of these selected residues within the GtmA structure are shown in Figure 5.32.

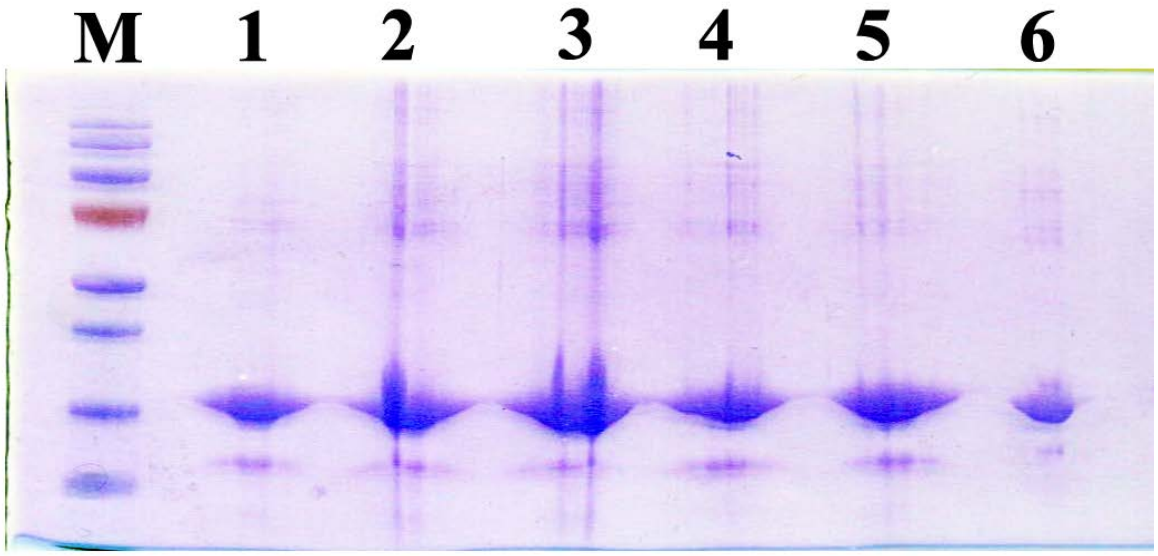

Figure 5.31. Recombinant expression and purification of GtmA with single amino acid mutations (1 µg loaded per well). 1: GtmA wild-type, 2: GtmA W157V, 3: GtmA W162V, 4: GtmA N159V, 5: GtmA F185G, 6: GtmA F127V.

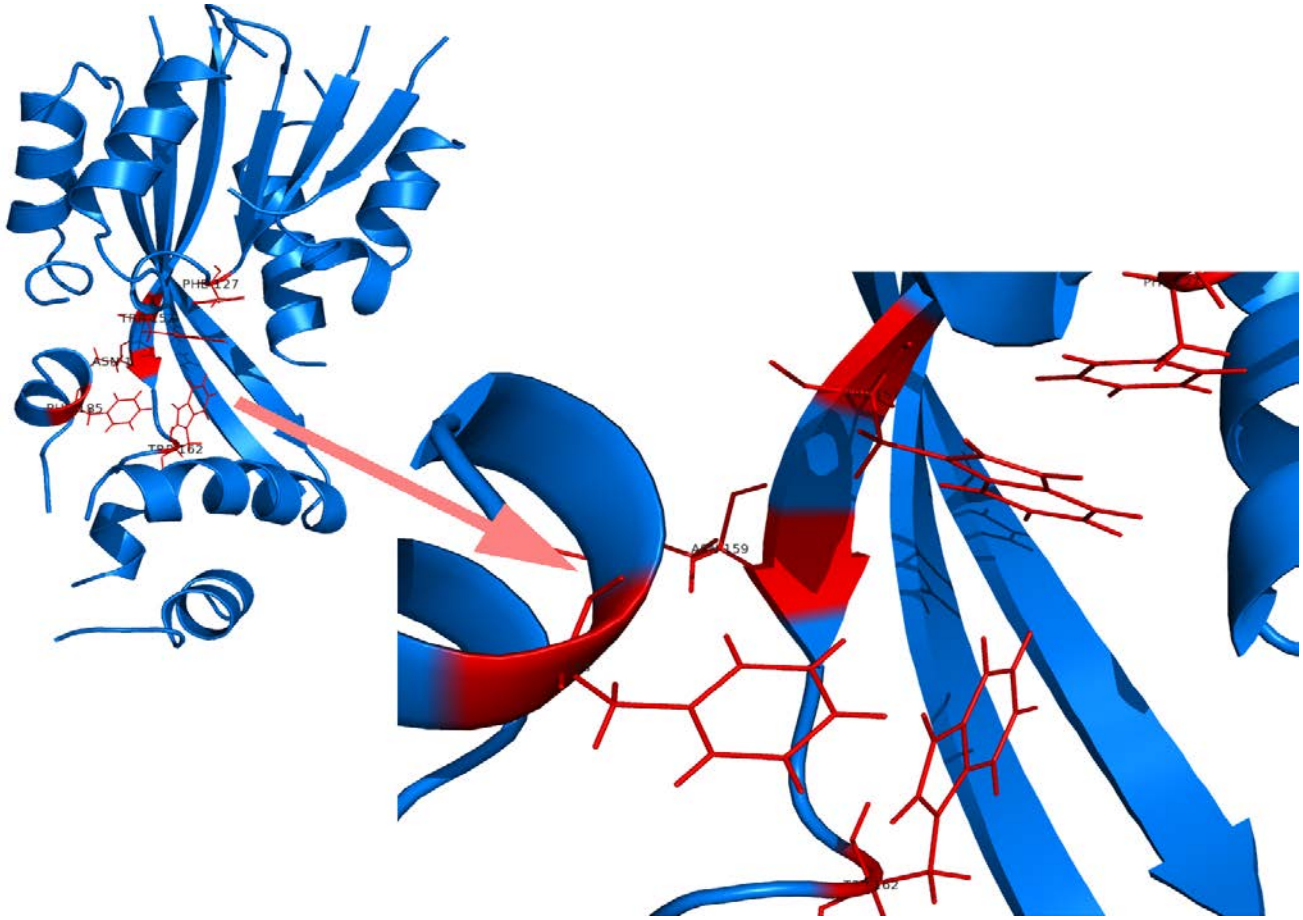

Figure 5.32. The location of GtmA residues selected for site directed mutagenesis highlighted in red. Trp157 to Val, Trp162 to Val, Asp159 to Val, and Phe185 to Gly and Phe127 to Val. These residues were selected for mutagenesis as they are conserved between GtmA and MTII (Figure 5.29) and contain prominent side chains which may form part of the GtmA ligand binding site.

5.2.18 RP-HPLC Analysis of GtmA Mutants

GtmA methyltransferase activity of the GtmA mutants was monitored by RP-HPLC in 50 mM Tris HCl, 50 mM NaCl, pH 7.4 using 750 μM SAM and 300 μM dithiol GT. 1 μM of purified enzyme was added to each reaction. The samples were incubated at 37 °C for 1 h prior to RP-HPLC analysis. The resulting chromatograms are shown in Figure 5.33. Wild-type GtmA converted all of the dithiol gliotoxin in the reaction (green) to bis(methyl)gliotoxin (red). The F185G GtmA mutation had no apparent effect on the activity of the enzyme. W157V had a significant effect on the activity of the enzyme. As shown in Figure 5.33, the conversion of dithiol gliotoxin to bis(methyl)gliotoxin is significantly diminished when this enzyme is used to effect catalysis. Almost no bis(methyl)gliotoxin (red) is generated by this enzyme and, also, low quantities of mono(methylthio)gliotoxin (orange). W162V and F127V also resulted in a significant decrease in GtmA activity. Notably, an extra peak (pink) was apparent in the GtmA F127V supernatants which eluted just after the mono(methylthio)gliotoxin peak. This peak may represent mono(methylthio)gliotoxin which has been methylated on the opposite sulfhydral. GtmA N159V had an unusual effect on enzyme activity. Although activity was diminished in this mutant when compared to the wild-type, almost no mono(methylthio)gliotoxin was detected in the supernatants whereas significant amounts of bis(methyl)gliotoxin were present.

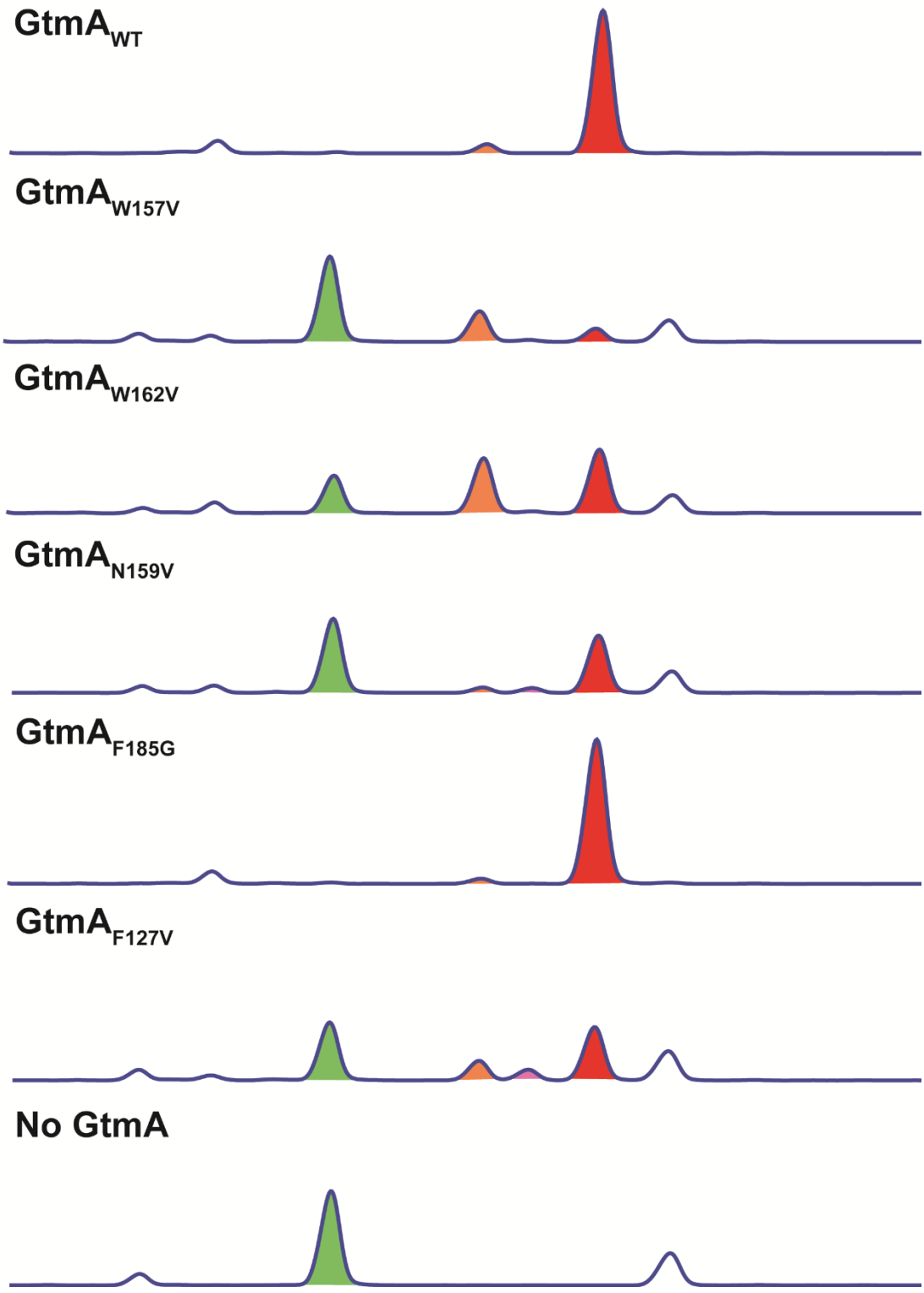

Figure 5.33. RP-HPLC chromatograms of GtmA wild-type, GtmA W157V, GtmA W162V, GtmA N159V, GtmA F185G, GtmA F127V and a No GtmA control incubated with dithiol gliotoxin and SAM. Dithiol gliotoxin (green), mono(methylthio)gliotoxin (orange), mono(methylthio)gliotoxin * (pink), bis(methyl)gliotoxin (red).

5.3 Discussion

In this chapter the first identified ETP bisthiomethyltransferase, GtmA, was recombinantly expressed in *E. coli*, purified and characterised. The structure was also solved using X-ray crystallography and residues which are important for the catalytic activity of this enzyme were identified.

As described in Section 5.2.1, GtmA was expressed as a fusion protein with a glutathione S-transferase (GST) moiety located at the N-terminus. The GST fusion protein was affinity purified by immobilised glutathione and impurities were removed. The fusion protein was then eluted using reduced glutathione. The GST affinity tag was then removed by using the site-specific TEV protease which recognised the sequence located between the GST moiety and GtmA. Size exclusion chromatography of GtmA alongside a selection of molecular mass calibrants showed that this enzyme is present in solution as a monomer. This analysis also indicated that the enzyme was purified to homogeneity, which is essential for protein structural analysis. The majority of NPMTs characterised to date have been shown to be dimeric although several monomers have been identified also (Liscombe et al., 2012). The dimerization interface of methyltransferase homodimers can be quite extensive. For example, the dimerization interface of the methyltransferase RdmB involved in anthracycline biosynthesis in *Streptomyces purpurascens* comprises of 3600 $Å^2$ or 23% of the total monomer surface while Catechol-O-methyltransferase (COMT) buries about 30% of the total surface area of the dimer (Jansson et al., 2003; Zubieta, 2002).

Activity analysis of GtmA showed that the cleaved protein was capable of rapidly S-methylating dithiol gliotoxin to bis(methyl)gliotoxin in the presence of the methyl donor SAM. It was also shown that, under SAM limiting conditions, a monomethyl version of gliotoxin (mono(methylthio)gliotoxin) is produced. This suggested that the

production of bis(methyl)gliotoxin is preceded by a singly methylated mono(methylthio)gliotoxin intermediate. Increasing the SAM concentration in the reaction resulted in the conversion of mono(methylthio)gliotoxin to bis(methyl)gliotoxin. Similarly, the plantazolicin N-methyltransferase BamL which dimethylates the N-terminus of this antibiotic is also capable of producing a monoalkylated intermediate under limiting conditions of SAM (Hao et al., 2015). Following mutagenesis of Tyr182Phe in BamL the enzyme primarily yields a monomethylated product instead of the dimethylated product. Importantly, the authors also obtained co-crystal structures with the monomethylated product which showed that this substrate sits in the active site with a nearly identical conformation as the corresponding desmethyl substrate. The active site pocket is predominantly hydrophobic (formed by Phe20, Leu130, and Leu134) and accommodates both forms of the substrate for the two distinct methyl-transfer reactions (Hao et al., 2015). A similar structural arrangement may occur in GtmA to accommodate both the dithiol and monomethylated gliotoxin.

In order to check the specificity of GtmA for other metabolites the ETP sporidesmin was reduced with TCEP to its dithiol form and incubated with GtmA in the presence of SAM. No sporidesmin D (a bisthiomethyl form of this metabolite) was detected in the reaction following LC-MS analysis. This modification was also carried attempted by exposing *A. fumigatus* sporidesmin A under conditions which promote bis(methyl)gliotoxin formation. Similarly, no sporidesmin D was detected. This indicated the specificity of GtmA for dithiol gliotoxin and suggests that GtmA is not a general defence against thiol-containing metabolites.

SAH has been shown to be a potent feedback inhibitor of SAM-dependent methyltransferases (Lee et al., 2005). Interestingly, this inhibition does not occur for GtmA, which appears to be resistant to SAH-mediated inhibition. This may be due to the

fact that GtmA catalyses the transfer of two methyl groups, which means that if SAH was capable of inhibiting the enzyme, this would affect its ability to rapidly bind a second SAM molecule for the second methyl transfer. Similarly, the plantazolicin N-methyltransferase BamL which dimethylates the N-terminus of this antibiotic is also resistant to SAH by-product inhibition (Lee et al., 2013b).

The structure of GtmA was predicted computationally using I-TASSER. Based on this analysis the overall structure of GtmA was predicted to consist of a globular domain containing the extended β-sheet characteristic of all other SAM-dependent methyltransferases (Cheng and Blumenthal, 1999) and a helical cap that forms the top one-third of the active site cavity. Based on the generated 3D model, GtmA was proposed be a structural analog of the salicylic acid carboxyl methyltransferase (SAMT) from *C. breweri* (Zubieta et al., 2001) and the yeast C-methyltransferase Coq5 (Dai et al., 2014). Interestingly, these proteins exist as homodimers in solution whereas the SEC data in Section 5.2.4 shows that GtmA likely functions as a monomer (Zubieta et al., 2003; Dai et al., 2014).

GtmA (40 mg) was expressed, purified to high purity and concentrated to 15 mg/ml for crystallisation trials which were carried out at the Helmholtz Centre for Infection Research. As the structure could not be solved by molecular replacement, a SeMet-substituted protein was produced by inhibiting methionine biosynthesis in amino acid supplemented minimal medium. Crystals of SeMet-substituted GtmA were obtained using the same conditions as for wildtype enzyme. The apo-GtmA structure was solved to 2.1 Å using multiwavelength anomalous dispersion (MAD) phasing.

In order to test the conformity between the computationally derived I-TASSER GtmA model and the GtmA structure as determined by X-ray crystallography the two structures were overlaid as shown in Figures 5.25 and 5.26. This illustrated the accuracy

of computational methods in predicting conserved domains of structures as several folds within the GtmA crystallographic model were accurately depicted in the GtmA computational model. Some folds were not accurately predicted in the I-TASSER model. These included the α-helices between residues 224-239 and 253-261 and the β sheets between residues 211-222 and 76-80.

As shown in Figure 5.26, several loops (e.g. residues 83-115) and the N-terminus (residues 0-24) of GtmA are absent from the structure. Since X-ray crystallography relies on obtaining crystals with many proteins in exactly identical positions, flexible proteins can be problematic. Regions in a protein that move are generally not observed in X-ray structures, so coordinates for these regions are not included in the structural model. Figure 5.19 indicated that several regions of the GtmA structure are predicted to have high normalized B-factors. The B-factor can be thought of as a measure of how much an atom oscillates or vibrates around the position specified in the model which indicates flexibility in these regions. Consequently residues 69-75, 93-102, 239-251 and 265-271 which are predicted to have high normalised B-factors by I-TASSER are regions of the GtmA crystallographic structure which have missing density. This suggests that these regions are missing from the GtmA model due to the flexibility of the structure. An advantage of the I-TASSER model is that regions which are missing in the GtmA crystallographic model can be overlaid with the I-TASSER model to show the putative folds in these regions. As shown in Figure 5.26, residues 83-115 are likely to form an α-helix followed by an extended loop which possibly acts as a substrate "gatekeeping" loop which changes conformation and becomes ordered upon SAM or dithiol gliotoxin binding. This region may play a role in substrate access and recognition as shown previously for other methyltransferases (Lim et al., 2001).

The putative N-terminus (residues 0-24) of GtmA is also shown in the I-TASSER model as a loop which may partially shield the active site. Most NPMTs also have an active site 'cover' contributed by several inserts in the fold and many have insertions between β5 and α2- α3, and between β6 and β7 (Vidgren et al., 1994; Fu et al., 1996). The N-terminal part of methyltransferases are generally flexible, facilitating the entry of the substrates and cofactor into the active site and the exit of the reaction products. This region may also be stabilised in the substrate bound form, however, in the crystal structure of Hma, a methyltransferase involved in keto- and methoxymycolates in *Mycobacterium tuberculosis*, helical stabilisation of the flexible N-terminal extremities did not seem to depend on the presence of a cofactor (Boissier et al., 2006).

NPMTs usually methylate their substrates through an SN2-like nucleophilic substitution reaction that is categorized by three distinct mechanisms: 1) proximity and desolvation (PD) effects, 2) general acid-base catalysis and 3) metal-dependent mechanism (Liscombe et al., 2012). To elucidate the catalytic mechanism, structural and biochemical approaches have a strong contribution to identify whether pivotal residues or metal ions exist or not.

DnrK is considered to use a PD mechanism because the mutagenesis of Tyr142, a key residue nearby the catalytic centre, did not dramatically reduce the enzyme activity (Jansson et al., 2004). As for general acid-base catalysis, many methyltransferases have been structurally and biochemically characterized to use a general base in active site for catalysis (Liscombe et al., 2012). Several plant O-methyltransferases such as the caffeic acid/5-hydroxyferulic acid 3/5-O-methyltransferase (COMT) from alfalfa and PRMT3, a protein Arg N-methyltransferase from rat use a catalytic His as a general base (Zubieta, 2002; Zhang et al., 2000).

NovP and MycE utilize a divalent ion to coordinate substrate and a nearby residue abstracts a proton from the methyl acceptor. Therefore, understanding the roles of crucial residues near the active centre from a structural perspective seems to be indispensable in NPMTs (Gómez García et al., 2010). For the echinomycin methyltransferase Ecm18, which converts a disulfide bond into a thioacetal group, the structure of this enzyme shows that the methionyl sulfur atom of SAH, the transferred methyl group, and the nucleophilic sulfur atom of the substrate are present in a linear arrangement. Unlike the situation in most other SAM-MTases, where the nucleophile is a carbon, nitrogen, or oxygen atom that may require activation through deprotonation, the nucleophile in the Ecm 18-catalyzed methyl transfer reaction is an electron-rich sulfur atom of a disulfide bond. Thus, activation of the sulfur atom as a nucleophile is perhaps not required for the methyl transfer reaction to proceed. Instead, the Ecm 18-catalyzed methyl transfer reaction is likely to be driven by the proximity effect (Hotta et al., 2014).

The crystal structure of the methyltransferase YecO from *Haemophilus influenzae* (HI0319) is proposed to undergo a conformational transition following substrate binding as access to the active site cavity is blocked. The aromatic residues Phe17 and Phe19 after the disordered N-terminus region block access to the cavity. These residues may provide a flexible gate that enables a substrate molecule to enter the cavity. Closure of this gate may then desolvate the substrate and ensure catalysis. The exquisite arrangement of the residues that delineate the cavity supports the notion that it is designed to be small, so that only a highly specific, small substrate may be accommodated (Lim et al., 2001). GtmA methyl-transfer may proceed by either proximity and desolvation effects or general acid-base catalysis. More detailed structural analysis with bound SAM/SAH or substrate will elucidate this catalytic mechanism.

As detailed in Section 5.2.14 the PDBefold structural alignments indicated that the best structural matches to GtmA were an N- methyltransferase NodS from B*radyrhizobium japonicum* (PDB: 3OFK) [Q-Score 0.27] and also the N-terminal methyltransferase-like domain of anamorsin from *Homo sapiens* (PDB: 4M7R) [Q-Score 0.18] (Cakici et al., 2010; Song et al., 2014). Despite the low sequence identity (10-15%) of these proteins several regions of these methyltransferases overlap as shown in Figure 5.27. Indeed, this method of structure comparison highlights how the chemical properties of residues should be given preference over residue identity in structure and function analysis. Residue identity may play a much less significant role in protein structure than often believed and the role of residue identity in protein function may often be overestimated.

Multiple sequence alignment of GtmA with other SAM-dependent methyltransferases was carried out using Jalview. This was carried out to identify conserved residues which may be essential for the catalytic activity of SAM-dependent methyltransferases. Based on this analysis several highly conserved residues (G56, G58, L64, G99, L146, G149, G150) were identified. Glycine is a conformationally special residue, which explains the conservation of this residue across functionally diverse members of this family. The Zappo colour scheme used in the alignment also highlighted which residues have conserved physicochemical properties. For example, V17 is substituted by leucine in the methyltransferase from *Methanosarcina mazei* (3MGG) and by alanine in the C-methyltransferase from *Saccharomyces cerevisiae* (Coq5), however, these are all aliphatic/hydrophobic residues. This may suggest that a residue with such characteristics is crucial in this position. The universal glycine-rich motif (often referred to as motif I) E/DXGXGXG in SAM-MTases is found as DNAGGIG in GtmA, with a minor variation of Ala54 instead of a glycine (Kozbial and Mushegian, 2005).

The sequence alignment of *A. fumigatus* GtmA with an *A. niger* GtmA homolog (MTII) indicated the residues within this sequence which have a high degree of conservation (Figure 5.29) (MacKenzie et al., 2005). Considering both of these methyltransferases catalyse the same reaction residues which are essential for controlling substrate specificity or catalysis are likely to be conserved. In combination with the crystallographic data shown in Figure 5.32 the five residues W157V, W162V, N159V, F185G, and F127V were selected for mutagenesis. These residues are conserved in *A. fumigatus* GtmA and *A. niger* MTII.

Attempts to cocrystallise GtmA in the presence of SAM, SAH, dithiol gliotoxin or bis(methyl)gliotoxin were unsuccessful. It was noted that following GST tag cleavage from GtmA using TEV protease, 11 residues (GAIAGAPDLKL) remain on the N-terminus before methionine. This may impede cocrystal formation by limiting certain crystal packing arrangements. For this reason GtmA was expressed as a His-tagged protein the vector Pet19m. Following His_6 affinity tag cleavage using TEV, only two residues (GH) remain before the N-terminal methionine. This vector was successfully used previously to express the ergothioneine-biosynthetic methyltransferase EgtD and crystallise it in the presence of its substrate and SAH (Vit et al., 2014, 2015). This, 110 mg of purified, cleaved GtmA was prepared for further crystallisation trials.

Following the successful expression of the wild-type GtmA using the His vector, this sequence was used as a template for site-directed mutagenesis as described in Section 5.2.17. RP-HPLC analysis on the respective GtmA mutants indicated that four of the mutants had significantly reduced dithiol gliotoxin bisthiomethylation activity compared to the wild-type protein. F185G had no effect on the activity of GtmA. Although this result did not identify a catalytic residue it confirmed that mutant enzymes were purified to the same degree as wild-type GtmA. As shown in Figure 5.33 the conversion of dithiol

gliotoxin to bis(methyl)gliotoxin is depleted in the W157V mutant. Almost no bis(methyl)gliotoxin (red) is generated by this mutant and low quantities of mono(methylthio)gliotoxin (orange) were evident.

W162V and F127V also resulted in a decrease in GtmA activity. Notably, an extra peak (pink) was apparent in the GtmA F127V supernatants which eluted just after the mono(methylthio)gliotoxin peak. This peak may represent mono(methylthio)gliotoxin which has been methylated on the opposite sulfhydral. This mutation may have resulted in a widening of the substrate binding pocket such that it facilitates dithiol GT in the opposite orientation. GtmA N159V had a particularly unusual effect on enzyme activity. Although activity was diminished in this mutant compared to the wild-type, almost no mono(methylthio)gliotoxin was detected in the supernatants whereas significant amounts of bis(methyl)gliotoxin were present. In the mutants where catalytic activity is decreased (F157V, W162V, F127V) significant amounts of monomethylated gliotoxin is generated. The N159V mutation may increase the GtmA affinity for monomethylgliotoxin such that the enzyme preferentially binds this intermediate instead of dithiol gliotoxin. It is also possible that this mutant is unable to efficiently release the monomethylated intermediate, resulting in the two methylation steps occurring consecutively. As mentioned previously, GtmA catalysis may proceed through proximity and desolvation effects or by general acid-base catalysis. Based on this mutagenesis result, the residue N159 could act as a general base in GtmA, however the activity of the enzyme is still quite substantial in the N159V mutant. A co-crystal structure of GtmA with dithiol gliotoxin bound or docked into the GtmA structure will be essential to elucidate the exact roles of the above residues and carry out more targeted mutagenesis on this enzyme.

Overall the data presented in this chapter have characterised GtmA-mediated thiomethylation on both the enzymatic and structural level. The enzyme was

recombinantly expressed to high yields and purity to facilitate enzymatic and structural studies. The power of in-silico structural modelling was also demonstrated in this chapter. The GtmA model generated by the I-TASSER suite of programs was reasonably accurate, considering the low sequence similarity of GtmA to any other structurally elucidated methyltransferase. The structural data facilitated guided site-directed mutagenesis to modify specific residues which may be located in the substrate binding site of this enzyme. Four of the single residue changes had drastic effects on GtmA activity. As described in Chapter 4, GtmA has 124 homologs in 103 fungal genomes. As GtmA is the first member of this family to be structurally elucidated this work will facilitate a future in-depth analysis of this family of methyltransferases and their applications in biocatalysis, metabolic engineering, chemical biology and other areas of biotechnology.

Chapter 6

Systems effects of gliotoxin bisthiomethylation in *Aspergillus fumigatus*

6.1 Introduction

As described in Chapter 4, GtmA has become specialised and is associated with the regulation of gliotoxin production in *A. fumigatus*. The deletion of *gtmA* results in no additional sensitivity to exogenous gliotoxin (Dolan et al., 2014). Chapter 5 detailed the recombinant expression and structural elucidation of this methyltransferase. Residues which are important to the catalytic activity of this enzyme were also uncovered. Interestingly, GtmA was shown to be resistant to SAH mediated competitive inhibition (Figure 5.2.8), a negative feedback mechanism which affects the majority of SAM dependent methyltransferases (Lee et al., 2005).

Based on the results from Chapter 4, the deletion of *gtmA* from *A. fumigatus* completely abrogated bis(methyl)gliotoxin production. However, it did not result in the acquisition of a gliotoxin- or H_2O_2-sensitive phenotype. This led us to conclude that GtmA is not primarily involved in the detoxification of gliotoxin or related biosynthetic intermediates (Forseth et al., 2011) as has been previously proposed (Li et al., 2012). There remained the possibility that GliT activity actively compensates for the absence of GtmA in *A. fumigatus* Δ*gtmA*, masking the protective role of GtmA during gliotoxin exposure. As illustrated in Chapter 3, the deletion of *gtmA* was carried out in the gliotoxin sensitive mutants, Δ*gliA* and Δ*gliT*. This facilitated an investigation into the redundancy of GtmA as a defensive strategy against gliotoxin in *A. fumigatus*.

The data from Chapter 4 also showed that *A. fumigatus* Δ*gtmA* produces more gliotoxin than the wild-type and that several *gli*-cluster encoded gliotoxin biosynthetic enzymes are more abundant in this mutant under secondary metabolite producing conditions. This led to an investigation into the effect of this gliotoxin production alteration on the levels of primary and unrelated secondary metabolites produced by *A. fumigatus*.

Many cellular components which are more commonly associated with primary metabolism are required for NRPS and PKS (Sheridan et al., 2015). These include, amongst others, *S*-adenosylmethionine (SAM), isoprenyl and mevalonyl moieties, NADPH, glutathione (GSH), malonyl CoA and acetyl CoA (Yasmin *et al*., 2012; Davis *et al*., 2011: Scharf *et al*., 2011; Haas, 2012). This suggests significant interplay between what is currently considered to be primary and secondary metabolism. The bisthiomethylation of gliotoxin by *A. fumigatus* demands two molecules of SAM per gliotoxin molecule. It has previously been shown that the methyl cycle is significantly altered in Δ*gliT* when exposed to gliotoxin (O'Keeffe et al., 2014).

In addition to the clear interactions between primary and secondary metabolism described above, there are also several examples of cross-talk amongst gene clusters which direct the synthesis of fungal natural products. Overexpression of the *A. fumigatus* putative $Zn(II)_2Cys_6$ transcription factor *hasA* (which is part of the hexadehydro-astechrome (HAS) biosynthetic gene cluster) also resulted in the production of large amounts of fumitremorgins compared to the wild-type strain (Yin et al., 2013). Deletion of the HAS NRPS in a background overexpressing *hasA* (OE*::hasA*Δ*hasD*) resulted in significantly increased fumitremorgin production. The authors hypothesised that the diversion of tryptophan and prenylation activity from HAS production towards fumitremorgin biosynthesis may occur in OE*::hasA*Δ*hasD* due to the inability of this mutant to utilise the pathway intermediates from HAS production. As fumitremorgins are potent tremorgenic mycotoxins this may account for the increased virulence of the OE*::hasA*Δ*hasD* strain compared to wild-type (Yin et al., 2013).

The overall objectives of the work presented in this chapter were to:

(i) Determine if Afu2g11120*, gtmA*, has a secondary role in self-protection against gliotoxin using the Δ*gliT::*Δ*gtmA and* Δ*gliA::*Δ*gtmA* double mutant strains.

(ii) Observe any phenotype associated with *A. fumigatus* Δ*gliT::*Δ*gtmA* and Δ*gliA::*Δ*gtmA* in comparison to the corresponding single deletion mutants under various conditions of oxidative stress or gliotoxin resistance through a series of phenotypic assays.

(iii) Evaluate any connection between SAM utilisation and gliotoxin bisthiomethylation utilising a series of *A. fumigatus* deletion mutants.

(iv) Perform quantitative proteomic analysis of the Δ*gliT* and Δ*gliT::*Δ*gtmA* strain in response to gliotoxin exposure.

(v) Carry out late stage culture (28 d) metabolomics and proteomics on *A. fumigatus* wild-type, Δ*gtmA* and *gtmA*^{c} in order for further functionally characterise this methyltransferase as bisthiomethylation of gliotoxin is a process which occurs late in terms of fungal growth.

6.2 Results

6.2.1 Phenotypic Analysis of *A. fumigatus* Δ*gliT::*Δ*gtmA and* Δ*gliA::*Δ*gtmA* in Response to Gliotoxin

Plate assays were performed to determine the response of both Δ*gliT::*Δ*gtmA* and Δ*gliA*::Δ*gtmA* to exogenous GT exposure. All strains were grown on Czapeks Dox agar plates with a range of GT concentrations (0 – 20 μg/ml) (Section 2.2.6). Radial growth was observed at 24 h time points and the plates were imaged at 72 h (Figure 6.1). Upon exposure to gliotoxin, both *A. fumigatus* Δ*gliT*::Δ*gtmA* ($p < 0.0001$) and Δ*gliA*::Δ*gtmA* ($p < 0.0021$) exhibited a decrease in growth in comparison with their single deletion counterparts. In particular, Δ*gliT*::Δ*gtmA* was shown to be extremely sensitive to exogenous gliotoxin exposure. The reduction in radial growth of these mutants is represented in Figure 6.2.

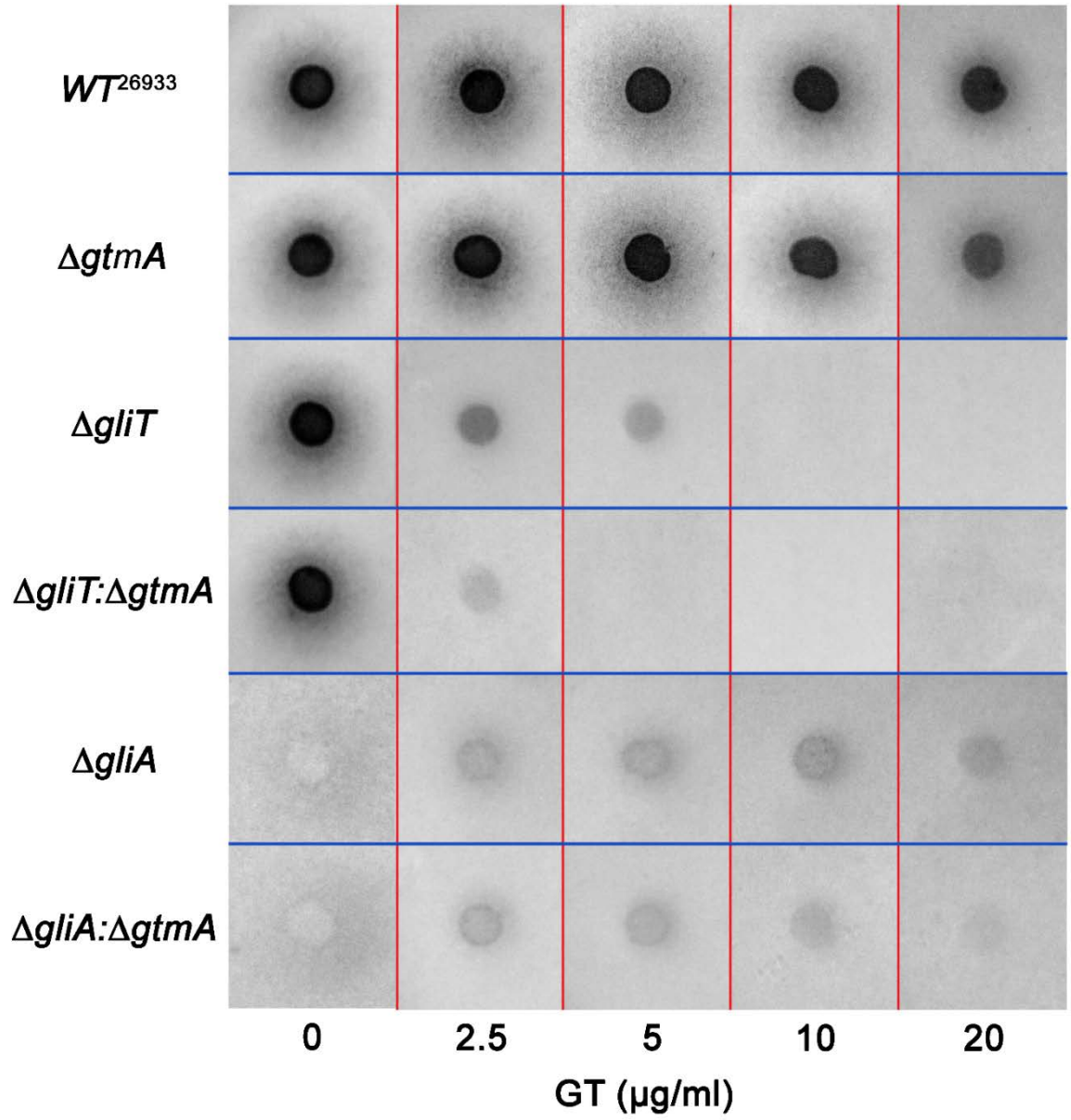

Figure 6.1. Deletion of *gtmA* does not result in gliotoxin sensitivity when compared to *A. fumigatus* wild-type. Deletion of *gtmA* in the gliotoxin sensitive strains Δ*gliT* and Δ*gliA* resulted in double mutants with an increased sensitivity to gliotoxin exposure. *A. fumigatus* Δ*gliT*::Δ*gtmA* was shown to be particularly sensitive to exogenous gliotoxin whereby the radial growth of this mutant was inhibited at 2.5 µg/ml gliotoxin.

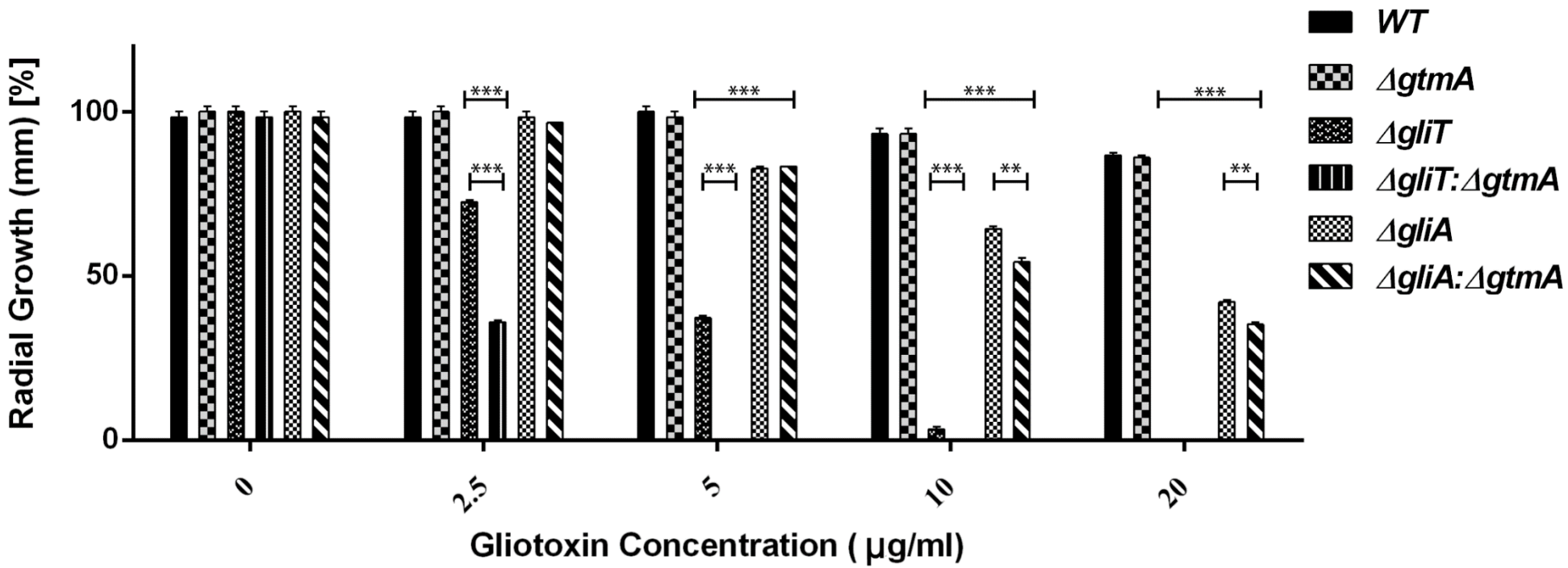

Figure 6.2. Graphical representation of Figure 6.1. Exposure of selected *A. fumigatus* strains to 0 – 20 µg/ml exogenous gliotoxin. The depicted values are from three independent samples. Error bars are SDs from the mean.

6.2.2 Bis(methyl)gliotoxin production is severely affected by the absence of *gliT* or *gliA*

Czapeks Dox media (100 ml) was inoculated with 10^6/ml conidia from *A. fumigatus* wild-type, gene deletion and complementation strains (triplicate) and the cultures were incubated at 37 °C, shaking 200 rpm for 21 h. Following this, 500 µl methanol was added and the cultures were incubated for a further 3 h before the supernatants were harvested. As highlighted in Section 2.2.16.4, the supernatants were organically extracted and then analysed by LC-MS. The results revealed that the levels of bis(methyl)gliotoxin detected in the Δ*gliT* or Δ*gliA* mutant supernatants were significantly lower than in the wild-type strain (Figure 6.3). This demonstrated that endogenously produced bis(methyl)gliotoxin was not produced or effluxed by either Δ*gliT* or Δ*gliA* to the same degree as in the wild-type strain. No bis(methyl)gliotoxin was detectable in *A. fumigatus* Δ*gtmA,* Δ*gliT*::Δ*gtmA* and Δ*gliA*::Δ*gtmA*. In line with previous data, the Δ*gtmA* mutant produced significantly more gliotoxin than the wild-type strain at 24 h (Figure 6.4).

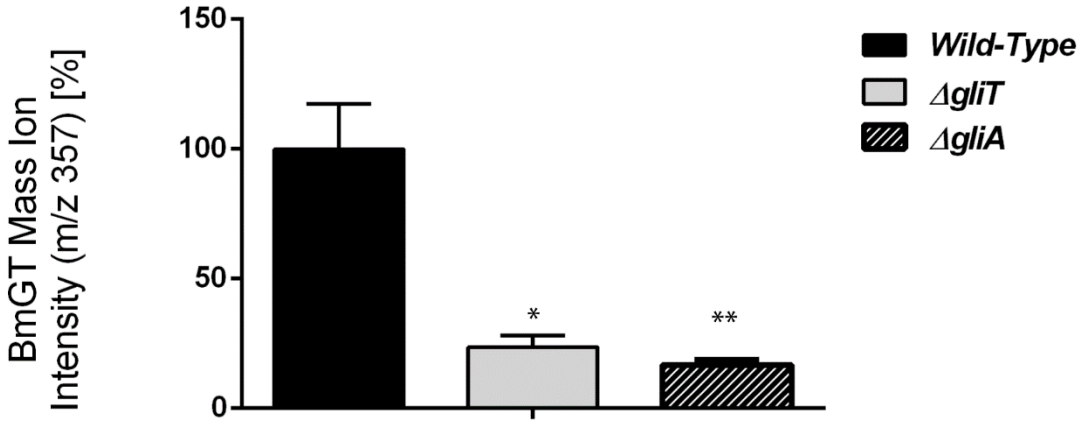

Figure 6.3. LC-MS detection of bis(methyl)gliotoxin (*m/z* 357) signal intensity in the culture supernatants of *A. fumigatus wild-type*, Δ*gliT* and Δ*gliA* following 24 h growth in Czapeks Dox liquid media (triplicate). Both the Δ*gliT* ($p = 0.0129$) and Δ*gliA* ($p = 0.0088$) mutants were shown to secrete significantly reduced bis(methyl)gliotoxin in comparison with the wild-type at this time point. Error bars show calculated SD from the mean.

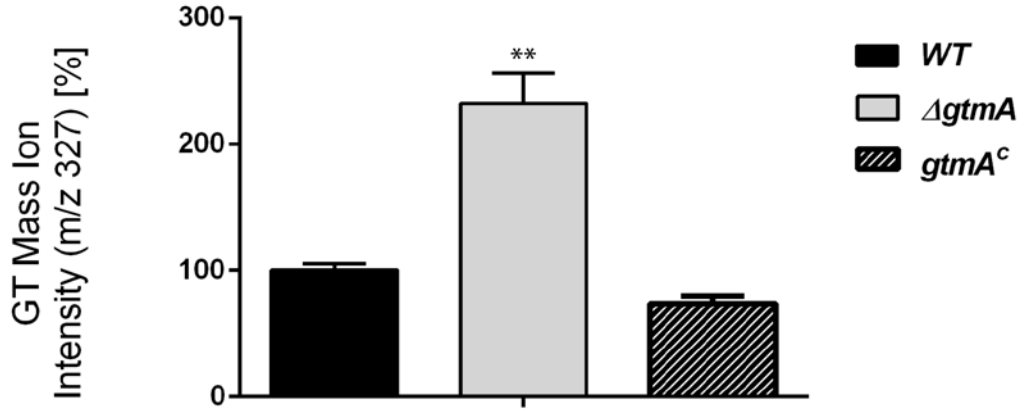

Figure 6.4. LC-MS detection of gliotoxin (*m/z* 327) signal intensity in the culture supernatants of *A. fumigatus wild-type*, Δ*gtmA* and *gtmA*^{c} following 24 h growth in Czapeks Dox liquid media (triplicate). Δ*gtmA* was shown to secrete a significantly increased ($p = 0.0058$) amount of gliotoxin when compared to the wild-type at the same time point. The levels were restored in the complement (*gtmA*^{c}) strain. Error bars show calculated SD from the mean.

6.2.3 Δ*gliT* produces significantly more bis(methyl)gliotoxin than wild-type or Δ*gliA* following exogenous gliotoxin exposure

Czapeks-Dox media (100 ml) was inoculated with 10^6/ml conidia from *A. fumigatus* wild-type, gene deletion and complemented strains (triplicate) and the cultures were incubated at 37 °C, shaking 200 rpm for 21 h. Gliotoxin (5 µg/ml final conc.) was then added and the cultures were incubated for a further 3 h before the supernatants were harvested and organically extracted as described in Section 2.2.16.4. They were then analysed by LC-MS. The results demonstrated that the levels of bis(methyl)gliotoxin detected in the Δ*gliT* mutant supernatants were significantly higher ($p = 0.0039$) than in that of the wild-type or Δ*gliA* strain (Figure 6.5).

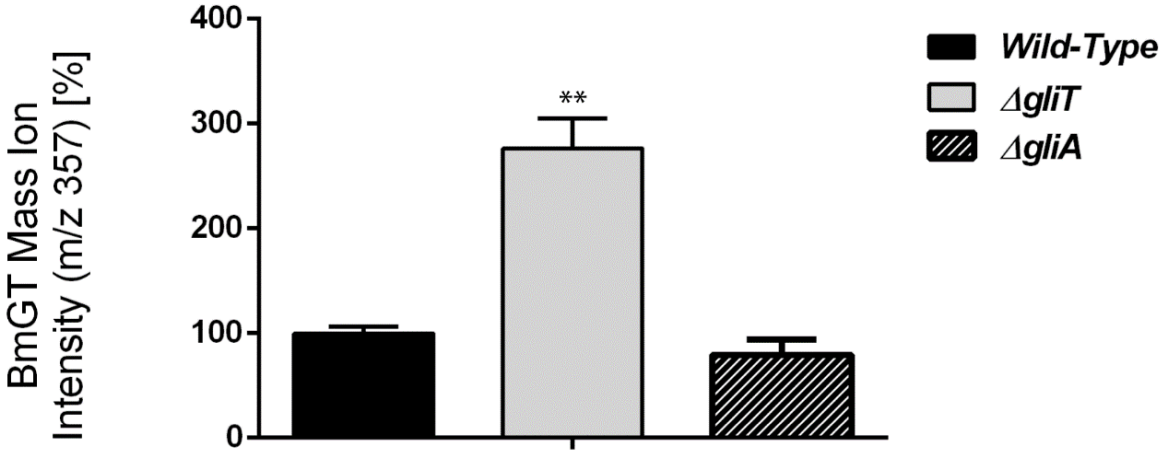

Figure 6.5. LC-MS detection of bis(methyl)gliotoxin (*m/z* 357) signal intensity in the culture supernatants of *A. fumigatus wild-type*, Δ*gliT* and Δ*gliA* following 21 h growth in Czapeks Dox liquid media and, subsequently, gliotoxin exposure (5 µg/ml) for 3 h (triplicate). *A. fumigatus* Δ*gliT* was shown to secrete significantly increased ($p = 0.0039$) bis(methyl)gliotoxin compared to the wild-type at this time point. The levels of bis(methyl)gliotoxin were not significantly altered between Δ*gliA* and the wild-type strain. Error bars show calculated SD from the mean.

6.2.4 Detection and quantification of *S*-adenosylmethionine from *A. fumigatus* mycelial lysates

Mycelia were harvested from the cultures as described in Section 6.2.2. In accordance with Section 2.2.14, mycelia were then snap frozen in liquid N_2 and, following this, SAM was extracted. A SAM commercial standard was used to obtain the retention time and fragmentation pattern of this metabolite. As revealed in Figure 6.6, the comparison of SAM levels across the *gli*-cluster deletion strains revealed a close link between *gtmA* activity and cellular SAM availability following gliotoxin exposure. Due to the absence of bis-thiomethylation, the Δ*gtmA* mutant was shown to have significantly ($p = 0.0021$) higher cellular SAM levels than the wild-type strain after gliotoxin exposure. The SAM levels were restored to wild-type levels in the $gtmA^C$ complement strain. Notably, the severe SAM depletion which was identified in Δ*gliT* following gliotoxin exposure ($p = 0.0001$) was alleviated in the double deletion mutant Δ*gliT*::Δ*gtmA*. *A. fumigatus* Δ*gliA::*Δ*gtmA* was also shown to retain higher levels of cellular SAM than Δ*gliA* following gliotoxin exposure: however, this was not as drastic as the changes seen in Δ*gliT* vs. Δ*gliT*::Δ*gtmA*. The corresponding LC-MS chromatograms for these samples are shown in Figure 6.7.

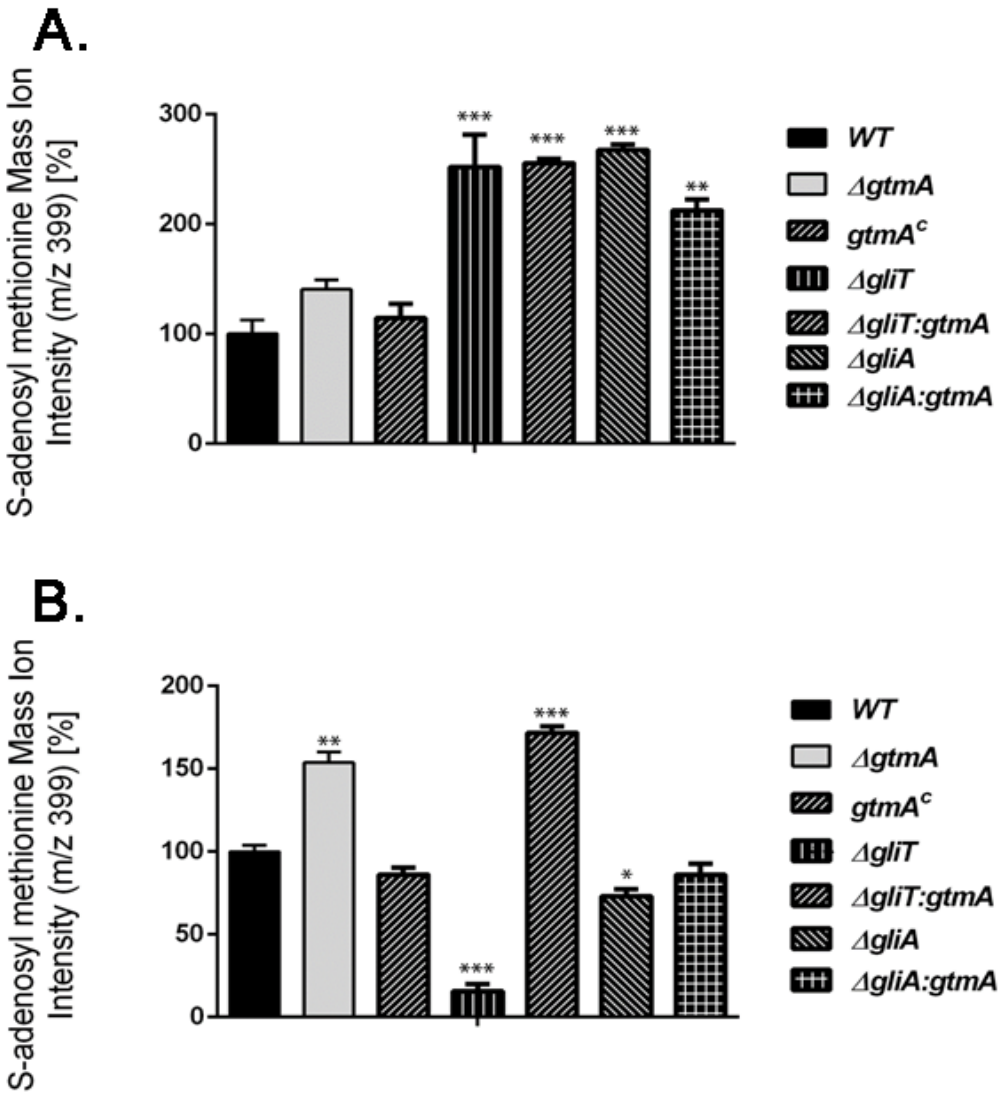

Figure 6.6. SAM detection in *A. fumigatus* wild-type and selected mutants (triplicate) after 21 h growth in Czapeks Dox liquid media followed by 3 h exposure to **A:** Control (MeOH) or **B:** Gliotoxin exposure (5 µg/ml final). Compared with the wild-type, significantly higher cellular SAM was detectable in Δ*gliT* (p = 0.0093), Δ*gliA* (p = 0.0003), Δ*gliT*::Δ*gtmA* (p = 0.0003) and Δ*gliA*::Δ*gtmA* (p = 0.0021). GT exposure results in highly significant SAM depletion in Δ*gliT* (p = 0.0001). This SAM depletion does not occur in the Δ*gliT*::Δ*gtmA* mutant. SAM levels were also significantly reduced in Δ*gliA* upon gliotoxin exposure (p = 0.0100). In comparison, this reduction was not significant in the Δ*gliA*::Δ*gtmA* double mutant. Finally, SAM depletion did not occur in Δ*gtmA* to the same degree as in the wild-type or complemented strain (p = 0.0021). Error bars show calculated SD from the mean.

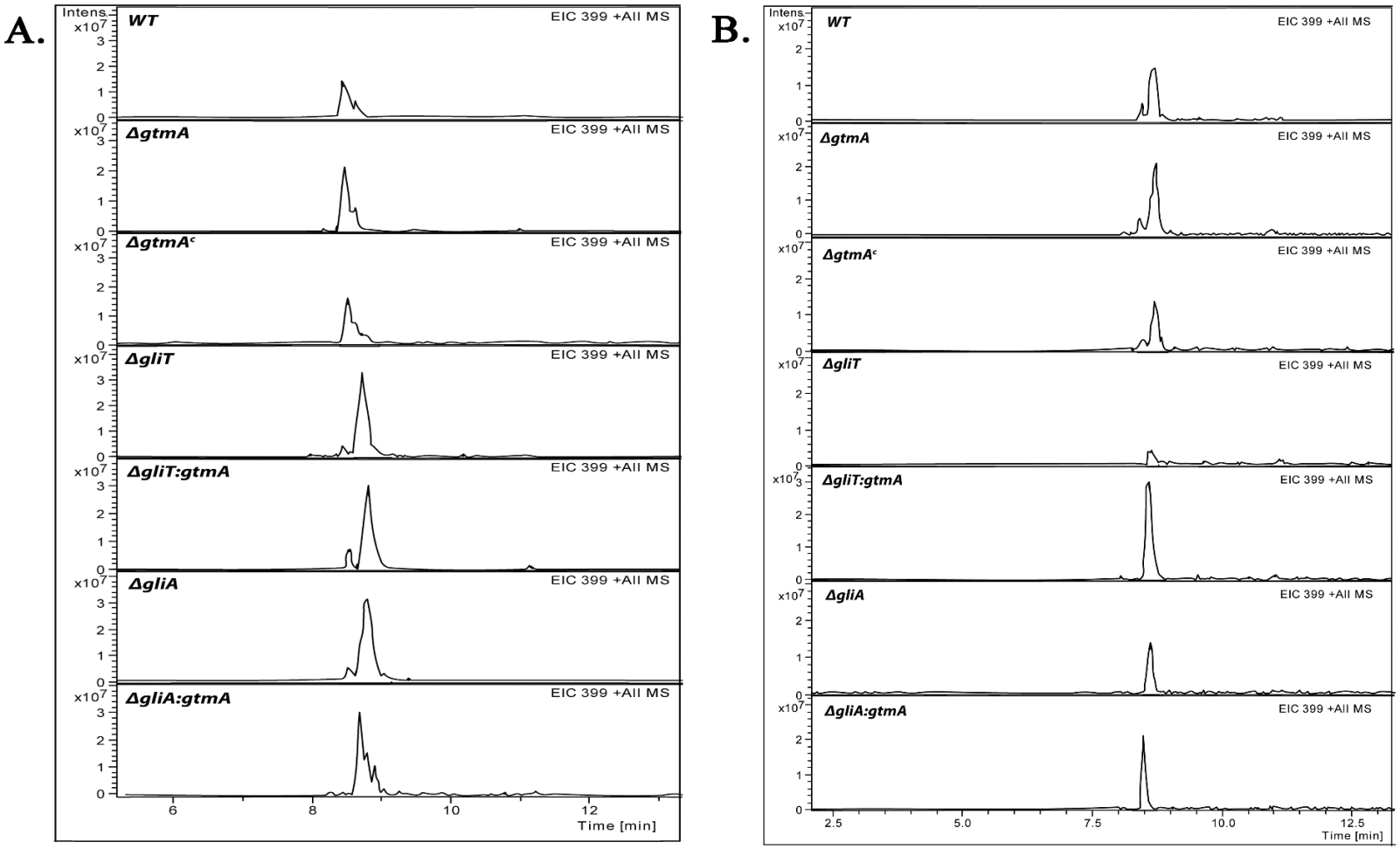

Figure 6.7. Corresponding chromatograms for SAM detection in *A. fumigatus* wild-type and selected mutants after 21h growth in Czapeks Dox liquid media followed by 3 h of **A:** methanol exposure and **B:** Gliotoxin exposure.

6.2.5 Following gliotoxin exposure *ΔgliT:ΔgtmA* may accumulate high levels of intracellular dithiol gliotoxin

Sabouraud dextrose media (50 ml) was inoculated with 10^6/ml conidia from *A. fumigatus* wild-type and gene deletion mutants in triplicate and incubated at 37 °C, shaking 200 rpm for 21 h. The cultures were exposed to either 2.5 µg/ml gliotoxin or a 250 µl methanol control and then incubated for a further 3 h. Mycelia were harvested and snap frozen in liquid nitrogen. The supernatants were harvested and organically extracted as illustrated in Section 2.2.15. Finally, they were analysed by RP-HPLC. It was established that the levels of extracellular gliotoxin and bis(methyl)gliotoxin (GT/BmGT) in the mutants correlated with the level of gliotoxin sensitivity which was observed in the mutants (Figure 6.8 and Figure 6.9). Δ*gliT*::Δ*gtmA* has significantly lower extracellular GT/BmGT than Δ*gliT* after 3 h (p = 0.0118). This suggests that the gliotoxin is accumulating intracellularly in the dithiol form, which cannot pass out of the cell. It has been shown previously that gliotoxin is reduced and actively concentrated in P388D1 cells in a glutathione-dependent manner, facilitating gliotoxin toxicity (Bernardo et al., 2003).

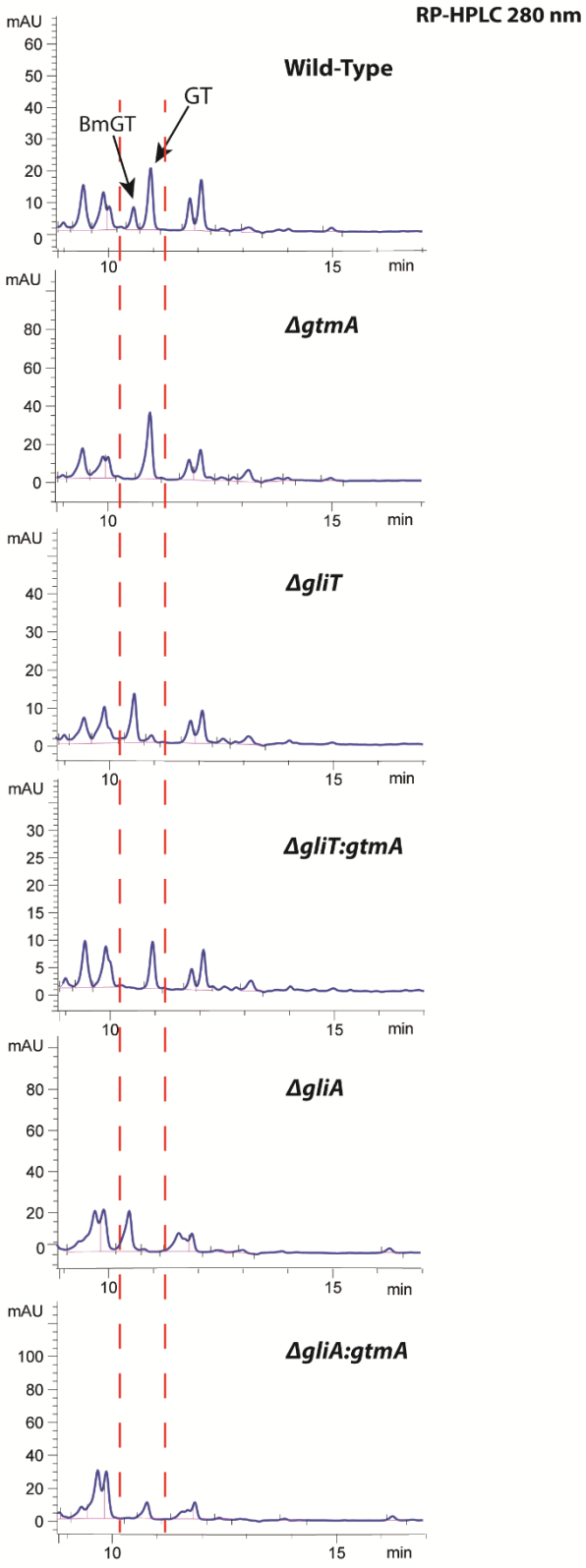

Figure 6.8. Exposure of wild-type and mutant strains to 2.5 µg/ml gliotoxin for 3 h and quantification of the remaining GT/BmGT in the organically extracted supernatant. Bis(methyl)gliotoxin (10.5 min) is the first peak followed by GT (10.8 min)

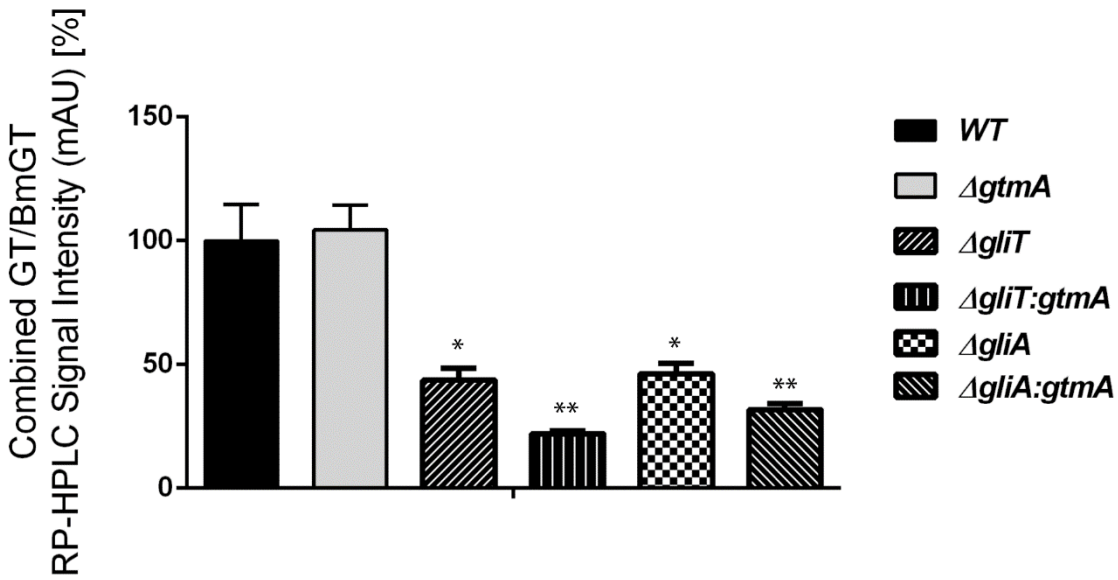

Figure 6.9. Exposure of wild-type and mutant strains (triplicate) to 2.5 µg/ml gliotoxin for 3 h and quantification of the remaining GT/BmGT in the organically extracted supernatants. The bars represent the combined intensity of GT/BmGT signal on the RP-HPLC 280 nm chromatogram. Δ*gliT*::Δ*gtmA* has significantly lower extracellular GT/BmGT than Δ*gliT* after 3 h ($p = 0.0118$). This would suggest that, due to its inability to methylate or oxidise dithiol gliotoxin, Δ*gliT*::Δ*gtmA* is accumulating more intracellular dithiol gliotoxin than any of the other mutants. This correlates with the highest gliotoxin sensitivity seen in this strain. Intracellular GT or BmGT could not be detected. Error bars show calculated SD from the mean.

6.2.6 Quantitative Proteomic Analysis of *ΔgliT* vs. *ΔgliT:gtmA* exposed gliotoxin

Gliotoxin sensitivity assays (Figure 6.1) demonstrated that Δ*gliT::*Δ*gtmA* is extremely sensitive to exogenous gliotoxin but, unlike *A. fumigatus* Δ*gliT*, this mutant did not undergo SAM depletion following gliotoxin exposure (Figure 6.6). In addition, the amount of gliotoxin remaining in the supernatant of Δ*gliT::*Δ*gtmA* when exposed to gliotoxin is significantly lower than that of the other mutants. This suggested that the likely mechanism of increased gliotoxin sensitivity in this mutant is the intracellular accumulation of dithiol gliotoxin. As Δ*gliT*::Δ*gtmA* is significantly more sensitive to gliotoxin than Δ*gliT*, the proteomic response of these mutants in response to either gliotoxin or a methanol control was examined. The snap-frozen mycelial samples from Section 6.2.5 were processed as demonstrated in Section 2.2.16.5 and were then analysed by quantitative proteomics in triplicate. This may help elucidate whether the increased gliotoxin sensitivity of Δ*gliT*::Δ*gtmA* was manifested on the proteomic level.

A total of 2136 proteins were detected in the Δ*gliT::*Δ*gtmA* vs Δ*gliT* gliotoxin treatment. 24 proteins were uniquely detected in the Δ*gliT::*Δ*gtmA* mutant under gliotoxin exposure and 37 proteins were significantly more abundant in this mutant. Under the same conditions, 12 proteins were uniquely detected in the Δ*gliT* mutant and 22 proteins were shown to be significantly more abundant in this mutant. As shown in Table 6.1, it appears that proteins most significantly increased in abundance in Δ*gliT*::Δ*gtmA* upon gliotoxin exposure are encoded by the gliotoxin biosynthetic cluster. Four gliotoxin biosynthetic enzymes, GliG (AFUA_6G09690; 4.52528), GliN (AFUA_6G09720; 3.2664), GliH (AFUA_6G09745; 2.7334) and GliM (AFUA_6G09680; 2.52137), were highly abundant in this mutant when compared to Δ*gliT*. GliP (AFUA_6G09660) was also uniquely detected in the Δ*gliT*::Δ*gtmA* mutant. Notably, a putative cysteine synthase (CysB) (AFUA_4G03930; 1.89937) was also significantly more abundant.

Several proteins which are associated with driving protein translation and folding were shown to be significantly more abundant in the Δ*gliT*::Δ*gtmA* mutant. These include Prefoldin subunit 3, putative (AFUA_2G02230; 1.36956) and a putative mitochondrial DnaJ chaperone (Mdj1) (AFUA_2G11750; 1.57627). Additionally, Seryl-tRNA synthetase (AFUA_3G12640), D-3-phosphoglycerate dehydrogenase (AFUA_2G04490) were uniquely detected in this condition.

An increased abundance of proteins which are commonly associated with mRNA synthesis was evident in the Δ*gliT*::Δ*gtmA* mutant. These included the polymerase (RNA) II (DNA directed) polypeptide D (AFUA_3G08040; Unique), Pre-mRNA splicing factor Dim1 (AFUA_3G12290; Unique), an uncharacterized protein (AFUA_2G03210; Unique) with orthologs involved in the positive regulation of transcription from RNA polymerase II promoter, SWI-SNF complex subunit (Snf5), putative (AFUA_2G16840; Unique), THO complex subunit Tho1, putative (AFUA_4G04330; Unique).

` Additionally, proteins which are associated with mitochondrial activity and vacuolar transport were found to be more abundant. These included the mitochondrial F1F0-ATP synthase g subunit (AFUA_1G16280; 1.27137), Mitochondrial 2-oxodicarboxylate carrier protein, putative (AFUA_1G09660; 1.48277), mitochondrial import receptor subunit (Tom20), putative (AFUA_6G11380; Unique), a putative vacuolar transporter chaperone Vtc4 (AFUA_2G09040; 1.42043) and a vacuolar armadillo repeat protein Vac8, putative (AFUA_5G13540; 1.38502). The acid phosphatases AphA (AFUA_5G01330; 2.0362) and PhoA (AFUA_1G03570; 1.05516) were significantly more abundant in the double mutant.

Proteins which have previously been shown to be upregulated by gliotoxin exposure were more abundant in Δ*gliT*::Δ*gtmA* (Dolan et al., 2014). These included a ThiJ/PfpI family protein which is abundant in conidia (AFUA_5G01430; 1.50109) and a protein of unknown function induced by hypoxia (AFUA_6G11850; 1.57101).

As shown in Table 6.2, the majority of proteins detected as significantly less abundant in the Δ*gliT*::Δ*gtmA* mutant were shown to be associated with the ribosome. These included the 40S ribosomal protein S19 (AFUA_1G05340; 1.64506), the ribosome assembly and transport protein Srp40, putative (AFUA_1G04370; 1.50622), the nascent polypeptide-associated complex (NAC) subunit beta (AFUA_6G02750; 1.35069), 40S ribosomal protein S6 (AFUA_4G10800; 1.32211), 40S ribosomal protein S17 (AFUA_2G10300; 1.26034), 40S ribosomal protein S26 (AFUA_1G06770; 1.1822), 40S ribosomal protein S5 (AFUA_1G15020; 1.12063), 60S ribosomal protein L37a (AFUA_2G16880; 1.12053), the ribosome associated DnaJ chaperone Zuotin (AFUA_4G03650; 1.09331), the ribosomal protein S13p/S18e (AFUA_6G13550; 1.05296), Nucleoporin NUP49/NSP49, putative (AFUA_6G10730; 1.0383), and the ribosomal S30/ubiquitin fusion protein (AFUA_6G02450; 1.00763).

The thiol methyltransferase GtmA (AFUA_2G11120) was not detectable in the Δ*gliT*::Δ*gtmA* mutant whereas it was highly abundant in Δ*gliT* upon gliotoxin exposure. As described above, proteins induced by hypoxia were more abundant in Δ*gliT*::Δ*gtmA*. In support of these data, a hypoxia repressed protein (AFUA_2G15290; 1.89792) with a glutathione-dependent formaldehyde-activating enzyme domain was significantly less abundant in this mutant.

Table 6.1. Proteins with **increased** abundance in *A. fumigatus ΔgliT:gtmA* compared to *ΔgliT* grown for 21 h in Sabouraud Dextrose Media followed by 2.5 μg/ml gliotoxin exposure for 3h. Data sorted by fold change, in descending order.

Protein Description	**Log_2(Fold Increase)**	**p-value**	**Peptides**	**Sequence coverage [%]**	**Protein IDs**
Pre-mRNA splicing factor Dim1	Unique	N/A	3	30.2	AFUA_3G12290
Seryl-tRNA synthetase	Unique	N/A	5	13.9	AFUA_3G12640
dUTPase, putative	Unique	N/A	4	38.1	AFUA_3G14580
Hypothetical protein	Unique	N/A	4	8.6	AFUA_4G14190
Protein of unknown function; transcript induced by voriconazole	Unique	N/A	2	29.7	AFUA_5G00740
GliP, Non-ribosomal peptide synthetase encoded in the gliotoxin biosynthetic gene cluster; catalyzes the first step in gliotoxin biosynthesis; regulated by the transcription factor StuA; expression increases *in vivo*	Unique	N/A	8	5.8	AFUA_6G09660
Has domain(s) with predicted nucleotide binding activity, isoflavone reductase family protein	Unique	N/A	5	23.6	AFUA_1G12510
Ortholog(s) have nucleus localization, WD repeat protein	Unique	N/A	3	8.4	AFUA_1G14650
Has P-loop containing nucleoside triphosphate hydrolase domain	Unique	N/A	3	10.3	AFUA_1G15260

Protein Description	Log_2(Fold Increase)	p-value	Peptides	Sequence coverage [%]	Protein IDs
Ortholog(s) have role in positive regulation of transcription from RNA polymerase II promoter, telomere maintenance and EKC/KEOPS complex localization	Unique	N/A	4	24.9	AFUA_2G03210
D-3-phosphoglycerate dehydrogenase, Role in L-serine biosynthetic process	Unique	N/A	5	10.6	AFUA_2G04490
DUF185 domain protein	Unique	N/A	3	6.6	AFUA_2G09740
SWI-SNF complex subunit (Snf5), putative, Has domain(s) with predicted role in chromatin remodeling and nuclear chromosome localization	Unique	N/A	4	8.3	AFUA_2G16840
Polymerase (RNA) II (DNA directed) polypeptide D	Unique	N/A	2	18.9	AFUA_3G08040
Has domain(s) with predicted heme binding activity, Indoleamine 2,3-dioxygenase subfamily	Unique	N/A	2	4.6	AFUA_3G14250
Has P-loop containing nucleoside triphosphate hydrolase domain	Unique	N/A	3	17.3	AFUA_4G03890
THO complex subunit Tho1, putative	Unique	N/A	3	6.7	AFUA_4G04330
50S ribosomal protein L24	Unique	N/A	3	12.3	AFUA_4G10740
L-PSP endoribonuclease family protein (Brt1), putative	Unique	N/A	2	34.4	AFUA_5G03780

Protein Description	Log_2(Fold Increase)	p-value	Peptides	Sequence coverage [%]	Protein IDs
Has domain(s) with predicted guanylate cyclase activity, heme binding activity and role in cGMP biosynthetic process, BET3 family protein	Unique	N/A	3	23.6	AFUA_5G12880
Mitochondrial import receptor subunit (Tom20), putative	Unique	N/A	3	20.7	AFUA_6G11380
Translin-associated factor TraX, putative, Has domain(s) with predicted sequence-specific DNA binding activity	Unique	N/A	2	17.3	AFUA_7G01330
Has domain(s) with predicted carbon-nitrogen ligase activity, with glutamine as amido-N-donor activity	Unique	N/A	2	6.1	AFUA_8G01360
AAA family ATPase, putative	Unique	N/A	4	9	AFUA_7G06680
Glutathione S-transferase encoded in the gliotoxin biosynthetic gene cluster; required for gliotoxin biosynthesis; increased expression in biofilm, GliG	4.52528	2.9462E-03	10	61.2	AFUA_6G09690
N methyltransferase, encoded in the putative gliotoxin biosynthetic gene cluster, GliN	3.2664	8.6092E-04	19	89	AFUA_6G09720
Conserved hypothetical protein, encoded in the putative gliotoxin biosynthetic gene cluster, GliH	2.7334	9.0091E-04	5	30.7	AFUA_6G09745
Predicted O-methyltransferase, encoded in the putative gliotoxin biosynthetic gene cluster, GliM	2.52137	4.1063E-04	22	74.5	AFUA_6G09680

Protein Description	Log_2(Fold Increase)	p-value	Peptides	Sequence coverage [%]	Protein IDs
Allergen Asp f 2;expressed in alkaline zinc-limiting conditions; shares a divergent promoter with zrfC; higher expression in biofilm vs planktonic cells; fibrinogen binding protein	2.08334	1.3464E-03	8	39.5	AFUA_4G09580
Acid phosphatase AphA, Has domain(s) with predicted acid phosphatase activity, metal ion binding activity	2.0362	2.0674E-02	4	10.7	AFUA_5G01330
Putative cysteine synthase B; transcript induced by exposure to human airway epithelial cells	1.89937	2.1559E-05	33	81.2	AFUA_4G03930
Amidase, putative	1.74772	1.9580E-02	6	15.9	AFUA_2G00410
Has domain(s) with predicted cytoplasm, nucleus localization	1.70609	1.7907E-02	2	10.5	AFUA_1G11120
Mitochondrial DnaJ chaperone (Mdj1), putative	1.57627	4.4759E-02	3	11	AFUA_2G11750
Protein of unknown function; hypoxia induced protein	1.57101	3.1364E-02	2	4	AFUA_6G11850
ThiJ/PfpI family protein; abundant in conidia	1.50109	4.7688E-03	7	36.4	AFUA_5G01430
Mitochondrial 2-oxodicarboxylate carrier protein, putative	1.48277	3.5118E-02	2	11.8	AFUA_1G09660
Putative glucosamine-6-phosphate deaminase; transcript up-regulated in conidia exposed to neutrophils)	1.46	2.2835E-03	5	25.3	AFUA_8G04070
Uncharacterized protein. Transcript up-regulated in conidia exposed to neutrophils	1.44322	1.5158E-03	4	56.8	AFUA_2G13590

Protein Description	Log_2(Fold Increase)	p-value	Peptides	Sequence coverage [%]	Protein IDs
Has domain(s) with predicted oxidoreductase activity and role in oxidation-reduction process	1.43412	9.1269E-03	11	51.2	AFUA_2G02950
Putative vacuolar transporter chaperone Vtc4, phoB-regulated	1.42043	5.9550E-03	8	11.7	AFUA_2G09040
Vacuolar armadillo repeat protein Vac8, putative, Ortholog(s) have fungal-type vacuole localization	1.38502	1.8178E-04	11	31.1	AFUA_5G13540
Prefoldin subunit 3, putative, Ortholog(s) have tubulin binding activity, role in tubulin complex assembly and polysome, prefoldin complex localization	1.36956	1.7077E-03	3	20.7	AFUA_2G02230
Chitin synthase F	1.36251	1.9773E-02	4	6.7	AFUA_8G05630
beta-N-acetylhexosaminidase NagA, putative, highly expressed in biofilm	1.3414	3.0090E-02	12	34.7	AFUA_8G05020
NAD-dependent 15-hydroxyprostaglandin dehydrogenase	1.28311	1.0685E-02	6	27.3	AFUA_5G09290
Mitochondrial F1F0-ATP synthase g subunit, putative	1.27137	2.8867E-02	6	40.8	AFUA_1G16280
Conserved hypothetical protein, DinB/YfiT-like putative metal-dependent hydrolase domain	1.26802	8.1446E-03	8	52.4	AFUA_3G00960
Cellular morphogenesis protein (Rax2), putative, predicted adhesin; expression induced in biofilm	1.25678	2.6139E-02	4	5.5	AFUA_7G05340

Protein Description	Log_2(Fold Increase)	p-value	Peptides	Sequence coverage [%]	Protein IDs
Isocitrate lyase AcuD, conidia-enriched protein; transcript up-regulated in conidia exposed to neutrophils	1.2476	1.1466E-02	21	55.8	AFUA_4G13510
Has domain(s) with predicted oxidoreductase activity and role in oxidation-reduction process	1.24757	2.3722E-04	20	47.6	AFUA_7G06810
Has domain(s) with predicted methyltransferase activity and role in metabolic process	1.21381	8.2554E-03	2	9.4	AFUA_6G06380
Putative carboxypeptidase S1;predicted signal sequence for secretion; predicted gene pair with AFUA_A_1G00420	1.14751	5.5440E-03	10	32.3	AFUA_8G04120
Has domain(s) with predicted acyl-CoA dehydrogenase activity, flavin adenine dinucleotide binding activity and role in oxidation-reduction process	1.13788	1.8716E-02	10	33.6	AFUA_3G01920
1,3-beta-glucanosyltransferase Bgt1, induced by exposure to artemisinin	1.11353	1.1206E-02	8	28.9	AFUA_1G11460
Has domain(s) with predicted acetyltransferase activity	1.09426	1.3740E-02	3	21.8	AFUA_1G08765
Putative acyl-CoA dehydrogenase; transcript up-regulated in conidia exposed to neutrophils	1.05527	4.0845E-02	13	43.3	AFUB_065590
Acid phosphatase PhoA	1.05516	1.4299E-03	6	15	AFUA_1G03570
Phosphatidylglycerol specific phospholipase C, putative	1.05015	3.9238E-02	11	34.3	AFUA_7G04910

Protein Description	Log_2(Fold Increase)	p-value	Peptides	Sequence coverage [%]	Protein IDs
Secreted protein of unknown function	1.04991	5.4175E-03	4	19.2	AFUA_6G02010
Cell wall glucanase, putative	1.00409	1.6853E-02	4	15.1	AFUA_6G08510
Aldehyde reductase (AKR1), putative	1.00253	1.2992E-03	20	81.7	AFUA_6G10260

Table 6.2. Proteins with **decreased** abundance in *A. fumigatus ΔgliT:gtmA* compared to *ΔgliT* grown for 21 h in Sabouraud Dextrose Media followed by 2.5 μg/ml gliotoxin exposure for 3 h. Data sorted by fold change, in descending order.

Protein Description	Log_2(Fold Decrease)	p-value	Peptides	Sequence coverage [%]	Protein IDs
Has domain(s) with predicted catalytic activity and role in trehalose biosynthetic process	Absent	N/A	6	13.5	AFUA_7G03940
Putative frequenin with homology to *S. cerevisiae* Frq1p;has four EF-hand calcium binding domains	Absent	N/A	3	19.5	AFUA_6G14240
Ortholog(s) have mitochondrion localization. Translation elongation factor G2, putative	Absent	N/A	5	12.3	AFUA_5G07140
Has domain(s) with predicted 2-dehydropantoate 2-reductase activity, NADP binding activity, role in oxidation-reduction process, pantothenate biosynthetic process and cytoplasm localization	Absent	N/A	2	9.4	AFUA_4G13960
Ortholog(s) have role in ascospore-type prospore membrane assembly, late endosome to vacuole transport, protein retention in Golgi apparatus, protein targeting to vacuole	Absent	N/A	9	3.7	AFUA_4G11560
Has domain(s) with predicted 4-hydroxyphenylpyruvate dioxygenase activity and role in aromatic amino acid family metabolic process, oxidation-reduction process	Absent	N/A	5	18	AFUA_4G10620
CASC3/Barentsz eIF4AIII binding Btz domain	Absent	N/A	4	6.8	AFUA_3G05830

Protein Description	Log_2(Fold Decrease)	p-value	Peptides	Sequence coverage [%]	Protein IDs
Putative phosphoketolase;calcium downregulated	Absent	N/A	4	5.3	AFUA_3G00370
Putative nonsense-mediated mRNA decay protein	Absent	N/A	5	12.2	AFUA_2G16750
Gliotoxin Thiomethyltransferase A (GtmA)	Absent	N/A	10	45.1	AFUA_2G11120
Has domain(s) with predicted ATP binding, protein serine/threonine kinase activity and role in protein phosphorylation	Absent	N/A	3	4.1	AFUA_1G09620
Serine/threonine protein kinase related to the PKA catalytic subunit;involved in cAMP signaling	Absent	N/A	5	8.7	AFUA_1G06400
C-8 sterol isomerase, involved in sterol biosynthesis;upregulated in 48h biofilm vs planktonic culture;SrbA-regulated during hypoxia	Absent	N/A	2	20.1	AFUA_1G04720
Conidia-enriched protein of unknown function; transcript downregulated in response to voriconazole; hypoxia repressed protein	-1.89792	7.7642E-04	5	69.1	AFUA_2G15290
Has domain(s) with predicted role in nuclear mRNA splicing, via spliceosome and nucleus localization, mRNA splicing factor (Prp1/Zer1), putative	-1.81827	3.3116E-02	6	8.3	AFUA_2G06070
40S ribosomal protein S19	-1.64506	2.3371E-04	5	25.8	AFUA_1G05340
Ribosome assembly and transport protein Srp40, putative	-1.50622	5.9257E-03	2	5.7	AFUA_1G04370

Protein Description	Log_2(Fold Decrease)	p-value	Peptides	Sequence coverage [%]	Protein IDs
Nascent polypeptide-associated complex (NAC) subunit beta; protein level decreases upon heat shock	-1.35069	1.0968E-03	13	55.4	AFUA_6G02750
40S ribosomal protein S6	-1.32211	2.0131E-03	10	34.2	AFUA_4G10800
40S ribosomal protein S17	-1.26034	3.7943E-02	7	35.4	AFUA_2G10300
Putative zinc-dependent alcohol dehydrogenase; predicted gene pair with AFUA_A_7G01010 (adh1);protein induced by hydrogen peroxide; reacts with rabbit immunosera exposed to *A. fumigatus* conidia; calcium downregulated	-1.21622	1.7292E-02	20	72	AFUA_5G06240
40S ribosomal protein S26	-1.1822	1.1508E-02	4	37.8	AFUA_1G06770
Hypothetical protein	-1.17746	2.7839E-02	5	16.1	AFUA_8G03950
40S ribosomal protein S5; reacts with rabbit immunosera exposed to *A. fumigatus* conidia	-1.12063	4.6129E-03	14	60.2	AFUA_1G15020
60S ribosomal protein L37a	-1.12053	8.2945E-03	5	48.9	AFUA_2G16880
Putative fatty acid elongase with a predicted role in fatty acid biosynthesis; induced by exposure to artemisinin	-1.10096	1.3282E-02	2	7.8	AFUA_5G02760
Ribosome associated DnaJ chaperone Zuotin	-1.09331	3.0942E-03	14	42.8	AFUA_4G03650

Protein Description	Log_2(Fold Decrease)	p-value	Peptides	Sequence coverage [%]	Protein IDs
Ribosomal protein S13p/S18e	-1.05296	6.9708E-03	8	52.8	AFUA_6G13550
ATP dependent RNA helicase (Dbp1), putative	-1.05164	7.0398E-03	24	49.9	AFUA_4G07660
Nucleoporin NUP49/NSP49, putative	-1.0383	3.4327E-02	6	16.6	AFUA_6G10730
Has domain(s) with predicted exonuclease activity, nucleic acid binding, nucleotide binding, zinc ion binding activity and intracellular localization	-1.02234	3.5262E-02	7	24.1	AFUA_5G02160
Copper resistance protein Crd2, putative	-1.02119	4.3498E-03	4	42.3	AFUA_4G04318
Ribosomal S30/ubiquitin fusion	-1.00763	5.4432E-03	2	17.7	AFUA_6G02450
Ortholog(s) have glutamate-5-semialdehyde dehydrogenase activity, role in proline biosynthetic process and cytoplasm, nucleus localization	-1.00457	2.4349E-02	15	49.1	AFUA_2G07350

6.2.7 Late stage culture metabolomics reveals that *gtmA* may also influence the biosynthesis of other secondary metabolites

A. fumigatus wild-type, Δ*gtmA* and *gtmA*^{c} strains were grown in quadruplicate in Czapeks dox broth, 200 rpm, 72 h; 37 °C. The conical flasks were then transferred to a 37°C static incubator whereby the cultures were incubated for a further 25 days (a total of 28 days incubation) in darkness. The culture supernatants were then organically extracted using chloroform and analysed by RP-HPLC (Section 2.2.15). The results showed the significant decrease in four compounds detected at the 254 nm and 351 nm (Figure 6.10 and 6.12). These compounds were fraction collected based on their respective retention times (RT) and analysed by LC-MS. Their identities were then elucidated based on their *m/z* values and fragmentation patterns. Based on this analysis, the compounds pseurotin A ($p = 0.0035$) (Figure 6.11) and fumagillin ($p = 0.00154$) (Figure 6.13) were produced at significantly decreased levels in the Δ*gtmA* strain. The levels of these metabolites were restored in the *gtmA*^{c} strain. This suggested that GtmA activity may influence the production of other secondary metabolites through the production of bis(methyl)gliotoxin or, alternatively, by influencing the induction of the *gli*-gene cluster through the mechanism described in Section 4.3.

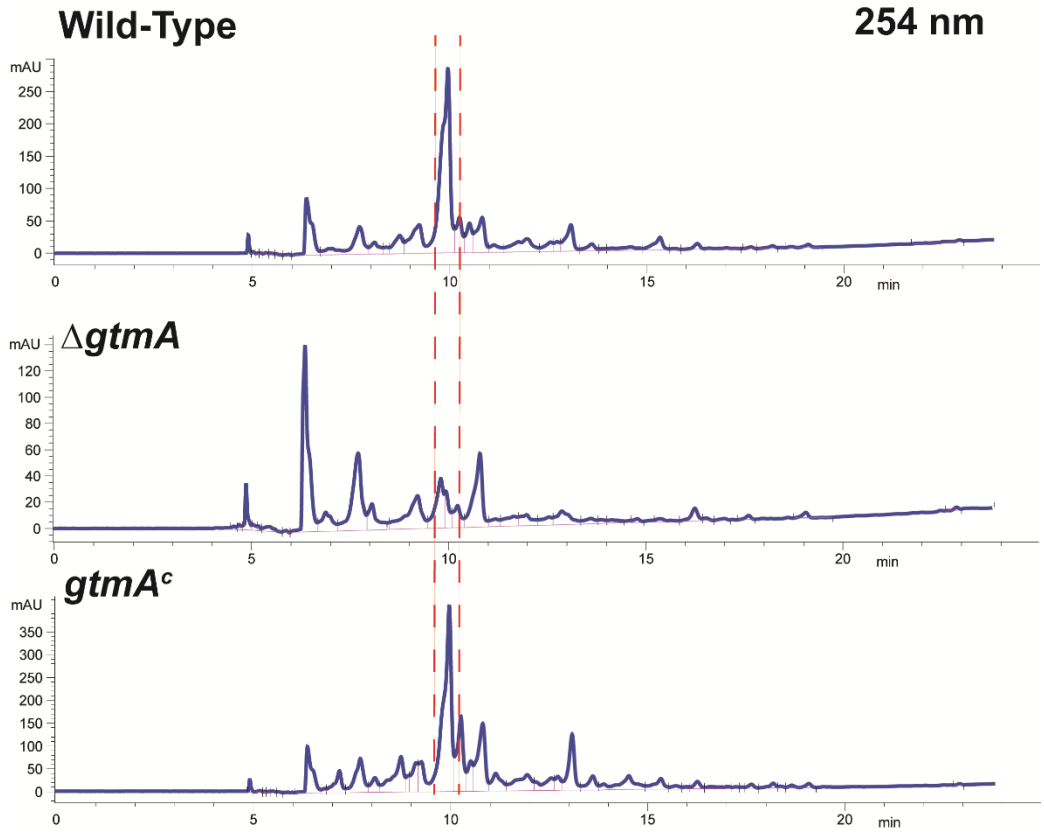

Figure 6.10. RP-HPLC chromatogram (254 nm) where a single compound (RT: 9.9 min) was shown to be detected at a significantly reduced intensity (p = 0.0035) in the *A. fumigatus* Δ*gtmA*. The levels of this metabolite were restored in the *gtmA*^{c} strain.

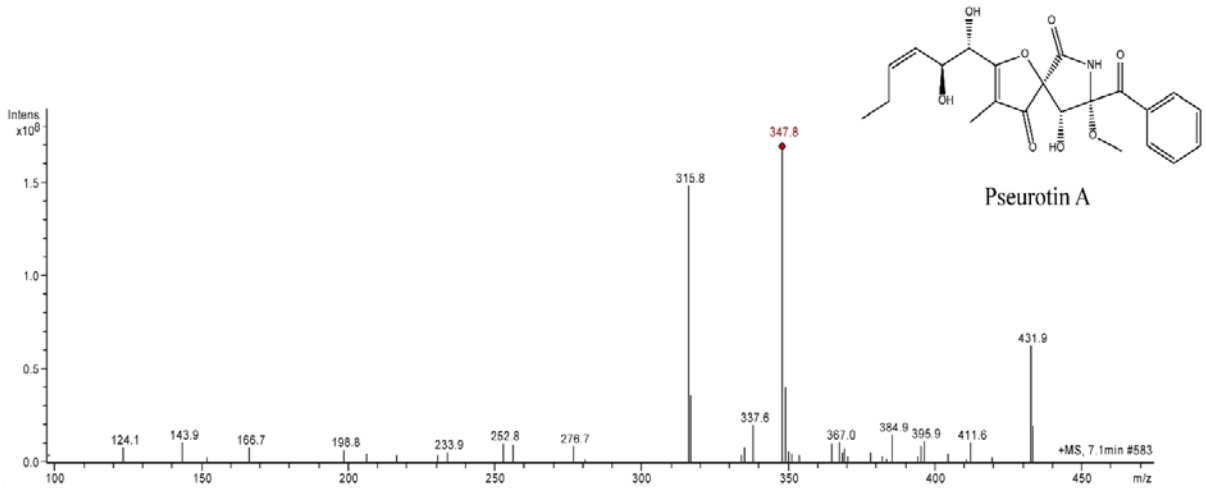

Figure 6.11. The LC-MS fragmentation pattern of the compound in Figure 6.10 confirms its identity as pseurotin A.

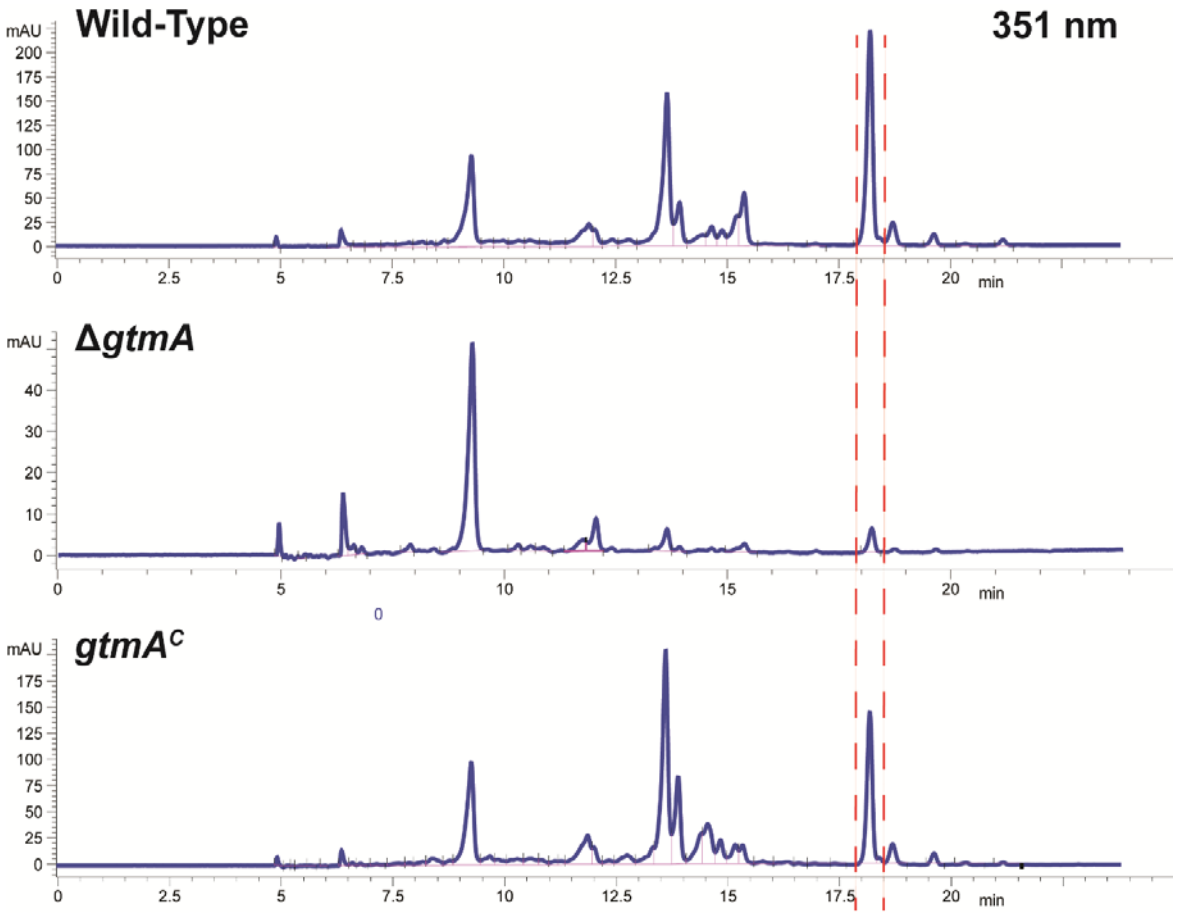

Figure 6.12. RP-HPLC chromatogram (351 nm) where an 18.2 min compound was shown to be detected at a significantly reduced intensity in the *A. fumigatus* Δ*gtmA* (p = 0.00194). The levels of this metabolite were restored in the *gtmA*^{c} strain. The compounds at RT 9.2 min and 13.6 min could not be identified by mass spectrometry analysis.

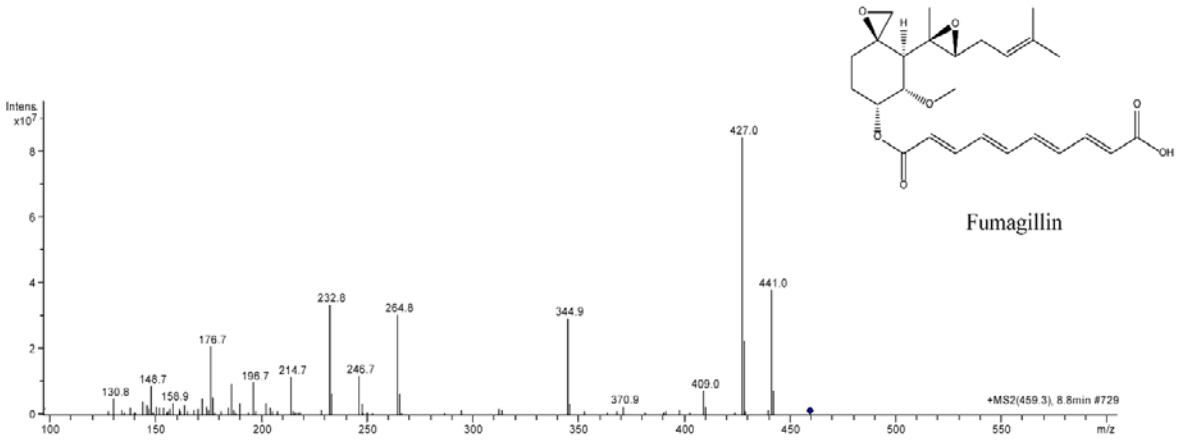

Figure 6.13. The LC-MS fragmentation pattern of the compound in Figure 6.12 confirms its identity as fumagillin.

6.2.8 Addition of bis(methyl)gliotoxin to Δ*gtmA* does not restore wild-type levels of pseurotin A production

In order to uncover whether the absence of bis(methyl)gliotoxin was directly responsible for the metabolite alterations uncovered in Section 6.2.7, bis(methyl)gliotoxin (10 µg/ml final) was added to Δ*gtmA* prior to static incubation for 25 days (quadruplicate). Methanol was added as a control. As outlined in Figure 6.14, this did not result in the restoration of wild-type pseurotin A production, indicating that bis(methyl)gliotoxin does not directly alter the production of these metabolites.

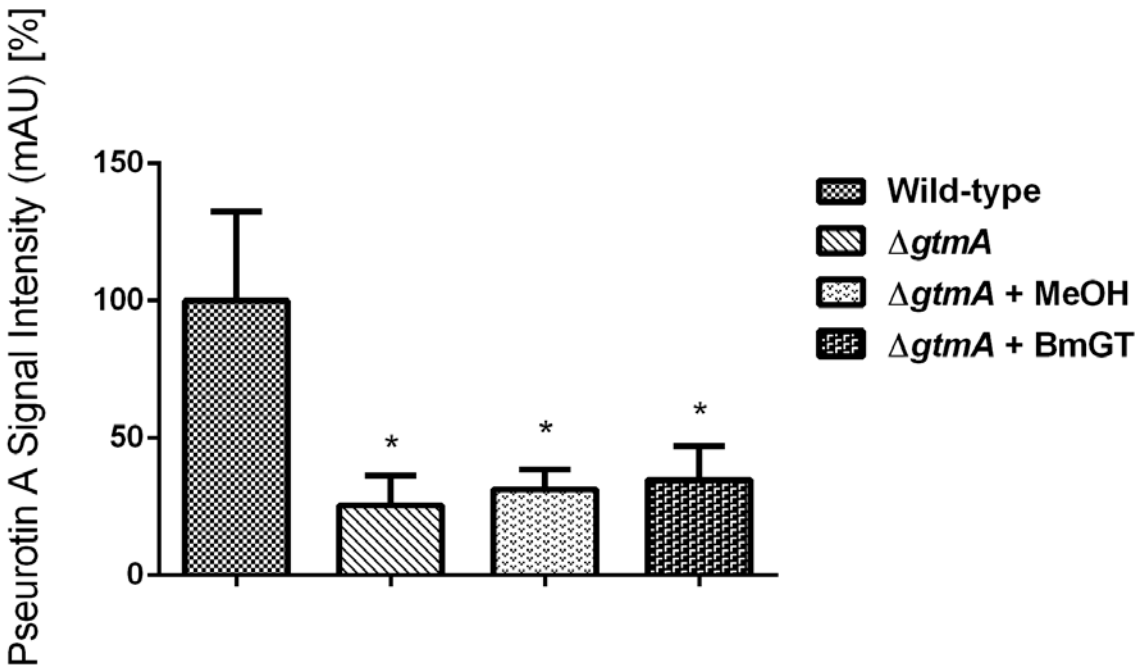

Figure 6.14. Exogenous addition of methanol or bis(methyl)gliotoxin (10 µg/ml) to *A. fumigatus* Δ*gtmA* (quadruplicate) prior to static incubation for 25 days does not result in the restoration of pseurotin A production levels to that of the wild-type strain. Bars represent pseurotin A RP-HPLC intensity (mAU) at 254 nm.

6.2.9 Quantitative proteomics of late-stage cultures reveals that the absence of *gtmA* expression leads to widespread proteomic alterations

The RP-HPLC chromatograms shown in Figures 6.10 and 6.11 demonstrated that *A. fumigatus* Δ*gtmA* has an altered secondary metabolite profile in comparison with that of the wild-type or *gtmA*^{C} cultured in the same conditions. In order to elucidate the involvement of GtmA activity in this metabolite profile alteration, quantitative comparative proteomic analysis was carried out. The snap frozen mycelial samples from Section 6.2.7 were processed as detailed in Section 2.2.16.5. These samples were then analysed by quantitative proteomics in quadruplicate. A total of 1648 proteins were detected in the wild type vs. Δ*gtmA* analysis. 59 proteins were uniquely detected in the wild-type and 135 proteins were significantly more abundant in this strain. Two proteins were uniquely detected in *A. fumigatus* Δ*gtmA* under this condition and 88 proteins were significantly more abundant in this mutant. Due to the large number of proteins altered in abundance, this dataset was cross referenced with the *gtmA*^{C} vs. Δ*gtmA* dataset in order to confirm which of these changes were directly due to the absence of Δ*gtmA*. Based on this enrichment, 44 proteins were uniquely detected in the wild-type and 92 proteins were significantly more abundant in this strain. Two proteins were uniquely detected in *A. fumigatus* Δ*gtmA* under this condition and 70 proteins were significantly more abundant in this mutant.

Four proteins encoded by the gliotoxin cluster were shown to be significantly more abundant in Δ*gtmA* compared to the wild type. The MFS gliotoxin efflux transporter GliA (AFUA_6G09710; 1.82652), the membrane dipeptidase GliJ (AFUA_6G09650; 1.66652), a predicted *O*-methyltransferase GliM (AFUA_6G09680; 1.62724) and the glutathione S-transferase GliG (AFUA_6G09690; 1.40425) were increased in abundance in Δ*gtmA*. Additionally, a putative short chain dehydrogenase (AFUA_4G08710; 1.37478) and a ThiJ/PfpI family protein (AFUA_5G01430; 1.93416), which were

previously shown to be induced by gliotoxin exposure were more abundant in this condition.

Proteins which had previously been shown to be induced by hypoxia exposure were significantly more abundant in the Δ*gtmA* mutant compared to the wild type (Vödisch et al., 2011). These include a putative transaldolase (AFUA_5G09230; 1.58072), a putative glyceraldehyde 3-phosphate dehydrogenase (AFUA_5G01030; 1.34405), an argininosuccinate lyase (AFUA_3G07790; 1.34137), a 6-phosphogluconate dehydrogenase (AFUA_6G08050; 1.31184), a putative mevalonate kinase (AFUA_4G07780; 1.07826) and an essential 1,3-beta-glucanosyltransferase (AFUA_2G05340; 1.0025). Additionally, glutathione synthase (AFUA_5G06610; 1.67077) was more abundant which is an ortholog of the *S. cerevisiae* GSH2 glutathione biosynthetic protein, which is induced by oxidative stress in this organism (Sugiyama et al., 2000).

Proteins formerly shown to be induced by neutrophil exposure were also more abundant in Δ*gtmA* (Sugui et al., 2008). These included a putative carbon-nitrogen family hydrolase (AFUA_5G02350; 1.567), a putative short chain dehydrogenase (AFUA_4G08710; 1.37478), ZrfB, a low affinity plasma membrane zinc transporter (AFUA_2G0386; 1.30673), a putative myo-inositol-phosphate synthase (AFUA_2G01010 - 1.21826), an aldehyde reductase (AKR1) (AFUA_6G10260; 1.09358) and a putative amino acid permease (Gap1) (AFUA_7G04290; 1.03424). Mannitol 2-dehydrogenase which has a predicted role in mannitol metabolism (AFUA_4G14450; 1.52766) was also more abundant. Mannitol is an important virulence determinant of pathogenic fungi. Its high antioxidant capacity aids in suppressing the reactive oxygen species mediated attacks from neutrophils (Wyatt et al., 2014).

Four transporter proteins were found to be significantly more abundant in Δ*gtmA***.** These were an ABC transporter AbcC (AFUA_1G14330; 2.4345), a putative MFS monocarboxylate transporter (AFUA_3G03320; 2.29482) and the ABC multidrug transporter Mdr1 (AFUA_5G06070; 2.19999).

Aminoacyl-tRNA synthetases are central enzymes in protein translation which provide the charged tRNAs needed for protein synthesis (Guo et al., 2010). Tyrosyl-tRNA synthetase (AFUA_5G10640; 2.85558), Glutamyl-tRNA (Gln) amidotransferase, subunit A (AFUA_2G00410; 1.93045), Seryl-tRNA synthetase (AFUA_5G05490; 1.22428), Putative valyl-tRNA synthetase (AFUA_8G04800; 1.22314), Isoleucyl-tRNA synthetase (AFUA_1G13710; 1.10632) and a putative Lysyl-tRNA synthetase (AFUA_6G07640; 1.05645) were significantly more abundant in in the Δ*gtmA* mutant compared to the wild type.

Several cell wall- related proteins were increased in abundance in *A. fumigatus* Δ*gtmA*. These included the GPI-anchored cell wall beta-1,3-endoglucanase Bgt2 (AFUA_3G00270; 1.35218) and three beta(1-3)glucanosyltransferases which belong to the 7-member GEL family (Gastebois et al., 2010; Fontaine et al., 2003); Gel 5 (AFUA_8G02130; 1.23988), Gel3 (AFUA_2G12850; 1.00391), and Gel4 (AFUA_2G05340; 1.0025).

An intertwined secondary metabolite supercluster on chromosome 8 of *A. fumigatus* (AFUA_8G00100-00720) has been found to encode for at least three bioactive metabolites, fumitremorgin, pseurotin, and fumagillin (Wiemann et al., 2013). Several proteins encoded by this supercluster were significantly decreased in abundance in *A. fumigatus* Δ*gtmA*.

Four proteins involved in the synthesis of fumitremorgins were significantly decreased in abundance in Δ*gtmA***.** FtmPT1 (AFUA_8G00210; Unique) and FtmPT2

(AFUA_8G00250; Unique), two prenyltransferases involved in fumitremorgin B biosynthesis, FtmD, an O-methyltransferase involved in fumitremorgin B synthesis (AFUA_8G00200; Unique), and FtmF, an alpha-ketoglutarate-dependent dioxygenase which catalyses the conversion of fumitremorgin B to verruculogen (AFUA_8G00230; 4.32466),

Seven proteins associated with fumagillin biosynthesis were significantly less abundant. These were the fumagillin polyketide synthase (Fma-PKS) (AFUA_8G00370; Unique), the fumagillin oxidoreductase FmaG (AFUA_8G00510; Unique), the fumagillin phytanoyl-CoA-oxidase FmaF (AFUA_8G00480; 4.17772), FmaD, the fumagillin O-methyltransferase (AFUA_8G00390; 3.85167), a hypoxia induced protein; encoded in the fma gene cluster (AFUA_8G00430; 3.24847), FmaC, a putative fumagillin alpha/beta hydrolase (AFUA_8G00380; 3.16375) and a putative *O*-methyltransferase; encoded in the *fma* gene cluster (AFUA_8G00400; 2.85247).

Six proteins identified with pseurotin A biosynthesis were significantly less abundant. PsoB, a putative pseurotin A alpha/beta hydrolase (AFUA_8G00530; Unique), PsoD, a putative pseurotin A P450 monooxygenase (AFUA_8G00560; Unique), PsoC, a putative pseurotin A methyltransferase (AFUA_8G00550; 3.28917), PsoA, the pseurotin A non-ribosomal peptide synthetase (AFUA_8G00540; 1.60039), a pseurotin A dual-functional mono- oxygenase/methyltransferase PsoE (AFUA_8G00580; Unique) and PsoF, a putative pseurotin A dual methyltransferase/monooxygenase (AFUA_8G00440; 2.74114).

Two proteins shown previously to be repressed by gliotoxin exposure were shown to be significantly decreased in abundance in the Δ*gtmA* mutant when compared to the wild type (Carberry et al., 2012). These were a mitochondrial peroxiredoxin (AFUA_4G08580; 1.96889) with predicted role in cell redox homeostasis regulation and a putative alcohol dehydrogenase (AFUA_7G01000; 1.17862) involved in ethanol

metabolism. A putative thioredoxin (AFUA_8G01090; Unique) and an M repeat protein (AFUA_6G08660; 1.99673), which were shown to be hypoxia repressed were also decreased in expression (Vödisch et al., 2011). The thiol methyltransferase GtmA was uniquely detected in the wild-type condition and abundance was restored in the complemented strain.

Several cell wall associated proteins were also decreased in abundance in the Δ*gtmA* mutant in comparison with the wild type. These included the conidial hydrophobin RodA (AFUA_5G09580; Unique), a putative antigenic cell wall galactomannoprotein (AFUA_4G00870; Unique), a putative glycophosphatidylinositol (GPI)-anchored cell wall protein MP-2 (AFUA_2G05150; Unique) and a putative phiA family cell wall protein (AFUA_3G03060; 1.5461).

Several mitochondrial-associated proteins were less abundant in Δ*gtmA*. These included the mitochondrial F1F0-ATP synthase g subunit (AFUA_1G16280; Unique), an uncharacterized protein (AFUA_1G13195; Unique) with orthologs involved in cristae formation and integral to mitochondrial inner membrane, a putative iron-sulfur cluster biosynthesis protein extrinsic to mitochondrial inner membrane (AFUA_3G06492, Unique), a putative mitochondrial intermembrane space translocase subunit (AFUA_1G04470; 1.97737), a putative mitochondrial peroxiredoxin (AFUA_4G08580; 1.96889) with a predicted role in cell redox homeostasis regulation, a putative prohibitin (AFUA_2G09090; 1.5947) with orthologs involved in mitochondrion inheritance, a putative mitochondrial 2-oxodicarboxylate carrier protein (AFUA_1G09660; 1.56908), a putative adenylate kinase with mitochondrial intermembrane space localization (AFUA_1G07530; 1.4474), a putative outer mitochondrial membrane protein porin (AFUA_4G06910; 1.31711), a putative mitochondrial genome maintenance protein Mgm101 (AFUA_2G09560; 1.26767), a mitochondrial glycerol-3-phosphate

dehydrogenase (AFUA_1G08810; 1.19813) and a putative mitochondrial processing peptidase alpha subunit with a role in protein processing involved in protein targeting to mitochondrion (AFUA_1G11870; 1.1768) .

Interestingly, several hypoxia induced proteins were decreased in abundance in the Δ*gtmA* mutant (Blatzer et al., 2011). These included a gamma-glutamyltranspeptidase (AFUA_4G13580, Unique); SrbA-regulated during hypoxia, Putative flavohemoprotein (AFUA_4G03410; 1.42304), Putative outer mitochondrial membrane protein porin (AFUA_4G06910; 1.31711), Ubiquinol-cytochrome c reductase iron-sulphur subunit precursor (AFUA_5G10610; 1.19224) with a predicted role in oxidative phosphorylation, an aspartic acid endopeptidase (AFUA_3G11400; 1.18445) and a thiamine biosynthesis protein (AFUA_5G02470; 1.11766),

Table 6.3. Proteins with **increased** abundance in *A. fumigatus ΔgtmA* compared to wild-type and *gtmA*^{c} grown for 28 days in Czapeks Dox media. Data sorted by fold change, in descending order.

Protein Description	Log_2(Fold Increase)	p-value	Peptides	Sequence coverage [%]	Protein IDs
Hypothetical protein	Unique	N/A	2	8.5	AFUA_5G10240
DnaJ domain protein Psi, putative	Unique	N/A	7	22.6	AFUA_5G07340
Has domain(s) with predicted oxidoreductase activity and role in oxidation-reduction process	2.85624	8.19E-04	9	36.2	AFUA_2G01410
Tyrosyl-tRNA synthetase	2.85558	1.49E-02	10	34.5	AFUA_5G10640
Putative ABC transporter; mutation causes increased azole sensitivity	2.4345	1.20E-02	18	16.2	AFUA_1G14330
MFS monocarboxylate transporter, putative	2.29482	6.99E-04	2	4.5	AFUA_3G03320
ABC multidrug transporter Mdr1	2.19999	5.97E-04	25	25	AFUA_5G06070
Has domain(s) with predicted catalytic activity, pyridoxal phosphate binding activity and role in metabolic process	2.09468	4.09E-04	12	38	AFUA_2G13295
Glycerate dehydrogenase	2.01153	1.59E-04	7	28	AFUA_1G13630
ThiJ/PfpI family protein; abundant in conidia	1.93416	5.71E-05	9	55.1	AFUA_5G01430

Protein Description	Log_2(Fold Increase)	p-value	Peptides	Sequence coverage [%]	Protein IDs
Glutamyl-tRNA(Gln) amidotransferase, subunit A	1.93045	2.75E-03	12	34.5	AFUB_092380
MFS gliotoxin efflux transporter GliA, encoded in the putative gliotoxin biosynthetic gene cluster	1.82652	1.09E-04	4	9.2	AFUA_6G09710
Zinc-binding oxidoreductase ToxD, putative	1.76982	5.73E-06	16	69.7	AFUA_6G10120
Transesterase (LovD), putative	1.73026	4.44E-04	11	43.1	AFUA_5G00920
Putative extracellular aspartic endopeptidase; acid protease; predicted signal sequence for secretion; allergen Asp f 10;transcript induced by growth on hydrogen peroxide and by growth on BSA as a sole nitrogen source	1.70013	1.75E-02	10	41	AFUA_5G13300
Glutathione synthetase, putative	1.67077	1.39E-05	17	49.2	AFUA_5G06610
Membrane dipeptidase GliJ, encoded in the putative gliotoxin biosynthetic gene cluster; higher expression in biofilm	1.66652	2.19E-02	7	30.2	AFUA_6G09650
RAS small monomeric GTPase RasA	1.65165	1.29E-03	14	72.8	AFUA_5G11230
Predicted O-methyltransferase GliM, encoded in the putative gliotoxin biosynthetic gene cluster	1.62724	1.26E-02	16	52	AFUA_6G09680
60S ribosome biogenesis protein Sqt1, putative	1.62446	5.79E-03	7	23.3	AFUA_5G07390

Protein Description	Log_2(Fold Increase)	p-value	Peptides	Sequence coverage [%]	Protein IDs
Has domain(s) with predicted UDP-N-acetylmuramate dehydrogenase activity, flavin adenine dinucleotide binding activity and role in oxidation-reduction process	1.61997	1.26E-03	10	18.3	AFUA_1G00980
Putative transaldolase; abundant protein in conidia and mycelia; protein induced by hydrogen peroxide and hypoxia	1.58072	1.59E-04	29	86.4	AFUA_5G09230
Putative carbon-nitrogen family hydrolase; transcript up-regulated in conidia exposed to neutrophils	1.567	9.08E-03	4	19	AFUA_5G02350
Putative polyketide synthase	1.55075	1.15E-02	55	36.8	AFUA_1G01010
Has domain(s) with predicted oxidoreductase activity and role in oxidation-reduction process	1.54785	3.55E-03	32	57.7	AFUA_7G06810
Mannitol 2-dehydrogenase with a predicted role in mannitol metabolism	1.52766	1.07E-03	28	85.7	AFUA_4G14450
NADH-dependent flavin oxidoreductase, putative	1.48197	5.84E-04	29	83.7	AFUB_049990
Nonribosomal peptide synthase SidE	1.46547	3.85E-03	34	21.9	AFUA_3G03350
Has domain(s) with predicted hydrolase activity	1.42593	5.66E-03	5	36.5	AFUA_5G13840
Glutathione S-transferase encoded in the gliotoxin biosynthetic gene cluster; required for gliotoxin biosynthesis	1.40425	1.31E-02	18	87.9	AFUA_6G09690

Protein Description	Log_2(Fold Increase)	p-value	Peptides	Sequence coverage [%]	Protein IDs
Plasma membrane H+-ATPase Pma1	1.3888	1.02E-05	40	47.8	AFUA_3G07640
Putative short chain dehydrogenase; transcriptionally up-regulated in conidia exposed to neutrophils; induced by gliotoxin exposure	1.37478	9.33E-03	10	47.7	AFUA_4G08710
Hypothetical protein	1.36026	1.87E-02	5	43.9	AFUA_5G01420
GPI-anchored cell wall beta-1,3-endoglucanase EglC	1.35218	7.27E-03	10	27.1	AFUA_3G00270
Putative glyceraldehyde 3-phosphate dehydrogenase, hypoxia induced protein	1.34405	2.56E-04	35	87.3	AFUA_5G01030
Argininosuccinate lyase; hypoxia induced protein	1.34137	3.29E-04	17	50.5	AFUA_3G07790
Putative UDP-galactopyranose mutase, enzyme in the first step of galactofuranose biosynthesis; mutant unmasks mannan residues on the cell surface, which is thought to contribute to increased cell adhesion	1.3312	3.72E-04	26	64.1	AFUA_3G12690
6-phosphogluconate dehydrogenase; conidia-enriched protein; protein induced by heat shock; reacts with rabbit immunosera exposed to conidia; hypoxia-induced protein; transcript induced by exposure to human airway epithelial cells	1.31184	5.88E-05	33	74.4	AFUA_6G08050
ZrfB, low affinity plasma membrane zinc transporter; induced by zinc depletion, ZafA-dependent; overexpression decreases zinc uptake, heme biosynthesis and triacetylfusarinine C (TAFC) siderophore production; induced in neutrophil-exposed conidia	1.30673	1.01E-02	8	33.7	AFUA_2G0386

Protein Description	Log_2(Fold Increase)	p-value	Peptides	Sequence coverage [%]	Protein IDs
Aldehyde reductase, has domain(s) with predicted oxidoreductase activity and role in oxidation-reduction process	1.29593	2.29E-03	9	34.2	AFUA_2G02950
Has domain(s) with predicted N-acetyltransferase activity and role in metabolic process	1.28379	1.55E-04	8	56.2	AFUA_7g00850
YjgH family protein	1.25488	1.80E-03	8	59.6	AFUA_3G02253
NADPH cytochrome P450 reductase (CprA), putative	1.24203	4.90E-05	32	65.6	AFUA_6G10990
Putative beta(1-3)glucanosyltransferase, belongs to the 7-member GEL family	1.23988	1.34E-04	4	8.8	AFUA_8G02130
Has domain(s) with predicted ATP binding, serine-tRNA ligase activity, role in seryl-tRNA aminoacylation and cytoplasm localization	1.22428	1.04E-04	23	56.1	AFUA_5G05490
Putative valyl-tRNA synthetase; transcript induced by exposure to human airway epithelial cells	1.22314	1.16E-04	28	36.3	AFUA_8G04800
Has domain(s) with predicted nucleotide binding activity	1.21908	2.18E-04	6	38.2	AFUA_2G02490
Putative myo-inositol-phosphate synthase; transcript up-regulated in conidia exposed to neutrophils	1.21826	3.95E-03	22	68.5	AFUA_2G01010
Phosphoribosylformylglycinamidine synthase, Ortholog(s) have role in purine nucleotide biosynthetic process and cytoplasm localization	1.21743	1.12E-03	39	51.1	AFUA_5G02720

Protein Description	Log_2(Fold Increase)	p-value	Peptides	Sequence coverage [%]	Protein IDs
Amidase; secreted protein; fibrinogen-binding	1.21641	3.92E-02	13	36.3	AFUA_5G10490
D-xylulokinase similar to xkiA	1.19871	3.27E-04	19	45.7	AFUA_5G09840
Has domain(s) with predicted pyridoxal phosphate binding, threonine synthase activity and role in threonine biosynthetic process	1.19834	2.15E-02	10	28.7	AFUA_3G08980
Putative pyridoxine biosynthesis protein	1.17091	4.45E-03	24	82.8	AFUA_5G08090
Putative adenosine kinase	1.15756	4.96E-03	23	80.8	AFUA_5G06390
Thiamin pyrophosphokinase-related protein	1.15446	3.88E-03	9	43.5	AFUA_5G11110
Ran GTPase activating protein 1 (RNA1 protein)	1.1377	2.60E-03	18	58.3	AFUA_3G07680
Septin; unique to filamentous fungi; localizes to long tubular structures within hyphae and to newly formed septa	1.13412	1.26E-02	6	10.5	AFUA_3G07015
Isoleucyl-tRNA synthetase, cytoplasmic	1.10632	2.72E-02	33	38.1	AFUA_1G13710
Aldehyde reductase (AKR1), putative, transcript up-regulated in conidia exposed to neutrophils and to human airway epithelial cells	1.09358	4.82E-05	27	85	AFUA_6G10260
Cytosine deaminase-uracil phosphoribosyltransferase fusion protein; transcript induced by exposure to human airway epithelial cells	1.09242	1.52E-03	12	60.3	AFUA_5G05460

Protein Description	Log_2(Fold Increase)	p-value	Peptides	Sequence coverage [%]	Protein IDs
Mevalonate kinase Erg12; SrbA-regulated during hypoxia	1.07826	3.01E-03	13	33.8	AFUA_4G07780
Histone H4 arginine methyltransferase RmtA	1.06182	4.71E-04	9	28.1	AFUA_1G06190
Has domain(s) with predicted ATP binding, lysine-tRNA ligase activity, nucleic acid binding activity, role in lysyl-tRNA aminoacylation and cytoplasm localization	1.05645	1.30E-04	19	35.5	AFUA_6G07640
Putative adenosylhomocysteinase;protein induced by heat shock	1.05614	2.10E-03	31	72.2	AFUA_1G10130
Hypothetical protein	1.03521	1.61E-03	20	16.9	AFUA_1G07090
Putative amino acid permease (Gap1); transcript up-regulated in conidia exposed to neutrophils and by growth on BSA as a sole nitrogen source	1.03424	7.12E-05	9	20.4	AFUA_7G04290
Putative extracellular lipase; repressed by exposure to artemisinin	1.03203	4.13E-03	7	30.1	AFUA_5G02040
Hypothetical protein	1.02294	7.75E-03	14	47.6	AFUA_1G15260
Ortholog(s) have Ran GTPase binding activity, role in G1/S transition of mitotic cell cycle, RNA export from nucleus, protein import into nucleus, ubiquitin-dependent protein catabolic process and cytoplasm, nucleus localization	1.01922	6.25E-03	9	45.3	AFUA_5G12180
1,3-beta-glucanosyltransferase Gel3, belongs to the 7-member GEL family	1.00391	4.13E-05	15	43	AFUA_2G12850
Essential 1,3-beta-glucanosyltransferase, GPI-anchored to the plasma membrane; constitutively expressed during hyphal growth; hypoxia induced protein	1.0025	5.43E-03	16	33.6	AFUA_2G05340

Table 6.4. Proteins with **decreased** abundance in *A. fumigatus ΔgtmA* compared to wild-type and *gtmA*^{c} grown for 28 days in Czapeks Dox media. Data sorted by fold change, in descending order.

Protein Description	Log_2(Fold Decrease)	p-value	Peptides	Sequence coverage [%]	Protein IDs
Has domain(s) with predicted iron ion binding, iron-sulfur cluster binding activity and role in iron-sulfur cluster assembly	Absent	N/A	5	33.1	AFUA_1G04680
Ortholog(s) have role in cristae formation and integral to mitochondrial inner membrane, mitochondrial crista junction localization	Absent	N/A	3	34.1	AFUA_1G13195
Protein of unknown function; abundant in conidia	Absent	N/A	11	45	AFUA_1G13670
Allergen Asp f 4;higher expression in biofilm vs planktonic cells; transcript induced by growth on hydrogen peroxide	Absent	N/A	5	23	AFUA_4G13960
Putative glycophosphatidylinositol (GPI)-anchored cell wall protein; putative adhesin; antigenic galactomannoprotein; induced by exposure to artemisinin	Absent	N/A	3	5.9	AFUA_2G05150
Has domain(s) with predicted methyltransferase activity; GtmA	Absent	N/A	8	42.1	AFUA_2G11120
Has domain(s) with predicted electron carrier activity, protein disulfide oxidoreductase activity and role in cell redox homeostasis	Absent	N/A	4	18.8	AFUA_2G15180
Ortholog(s) have enzyme activator activity, role in iron-sulfur cluster assembly and extrinsic to mitochondrial inner membrane, mitochondrial matrix localization	Absent	N/A	4	28.5	AFUA_3G06492

Protein Description	Log_2(Fold Decrease)	p-value	Peptides	Sequence coverage [%]	Protein IDs
Has domain(s) with predicted oxidoreductase activity, acting on a sulfur group of donors, oxygen as acceptor activity and role in oxidation-reduction process, prenylcysteine catabolic process	Absent	N/A	10	18.1	AFUA_3G09330
Has domain(s) with predicted metal ion binding activity; class II aldolase/adducin domain protein	Absent	N/A	11	52.5	AFUA_3G09800
Putative succinate-semialdehyde dehydrogenase	Absent	N/A	10	21.1	AFUA_4G08170
Conserved hypothetical protein	Absent	N/A	2	19.8	AFUA_4G10560
Gamma-glutamyltranspeptidase; SrbA-regulated during hypoxia	Absent	N/A	2	5.3	AFUA_4G13580
Conidial hydrophobin; conidial surface associated; required for formation of the rodlet layer of conidia	Absent	N/A	5	52.2	AFUA_5G09580
Protein of unknown function	Absent	N/A	12	35.4	AFUA_5G14930
Protein of unknown function	Absent	N/A	2	18.5	AFUA_6G10450
Has domain(s) with predicted nucleic acid binding, nucleotide binding activity	Absent	N/A	4	22	AFUA_7G05260
Putative prenyltransferase involved in fumitremorgin B biosynthesis	Absent	N/A	16	39.8	AFUA_8G00250
Polyketide synthase (PKS), encoded in the fma (fumagillin) secondary metabolite gene cluster; required for fumagillin biosynthesis	Absent	N/A	27	15.4	AFUA_8G00370

Protein Description	Log_2(Fold Decrease)	p-value	Peptides	Sequence coverage [%]	Protein IDs
Protein of unknown function	Absent	N/A	8	18.2	AFUA_8G00630
MFS multidrug transporter, putative	Absent	N/A	4	5.8	AFUA_8G00940
Putative thioredoxin; hypoxia repressed protein	Absent	N/A	7	71.6	AFUA_8G01090
Has domain(s) with predicted oxidoreductase activity, acting on the aldehyde or oxo group of donors, NAD or NADP as acceptor activity and role in oxidation-reduction process	Absent	N/A	9	19.9	AFUA_8G02310
Putative coenzyme A transferase; transcript induced by exposure to human airway epithelial cells	Absent	N/A	8	21.1	AFUA_8G05580
translation elongation factor eEF-1, gamma subunit, putative	Absent	N/A	9	36.7	AFUA_8G00580
Putative brevianamide F prenyltransferase, predicted to convert brevianamide F to tryprostatin B; involved in the biosynthesis of fumitremorgins	Absent	N/A	13	32.3	AFUA_8G00210
Putative O-methyltransferase with a predicted role in fumitremorgin B synthesis	Absent	N/A	22	68.9	AFUA_8G00200
Has domain(s) with predicted structural molecule activity, role in intracellular protein transport, vesicle-mediated transport and COPI vesicle coat localization	Absent	N/A	9	11.1	AFUA_1G10970
Ortholog(s) have proton-transporting ATPase activity, rotational mechanism, structural molecule activity and role in ATP synthesis coupled proton transport, cristae formation, protein oligomerization	Absent	N/A	3	26	AFUA_1G16280

Protein Description	Log_2(Fold Decrease)	p-value	Peptides	Sequence coverage [%]	Protein IDs
Has domain(s) with predicted catalytic activity and role in metabolic process	Absent	N/A	23	79.1	AFUA_2G00540
NADH-ubiquinone oxidoreductase 49 kDa subunit	Absent	N/A	7	22.1	AFUA_2G13710
Putative FAD binding monooxygenase; calcium downregulated	Absent	N/A	6	16.3	AFUA_3G03280
BAR adaptor protein RVS167, putative, calcium induced	Absent	N/A	7	20.7	AFUA_3G14230
Antigenic cell wall galactomannoprotein, putative	Absent	N/A	2	15.8	AFUA_4G00870
Has domain(s) with predicted 4 iron, 4 sulfur cluster binding, NADH dehydrogenase (ubiquinone) activity, quinone binding activity and role in oxidation-reduction process	Absent	N/A	2	11.7	AFUA_4G05860
Protein of unknown function identified by mass spectrometry	Absent	N/A	2	4	AFUA_4G08030
Has domain(s) with predicted actin binding activity and intracellular localization	Absent	N/A	4	50.8	AFUA_5G11200
Has domain(s) with predicted sulfuric ester hydrolase activity and role in metabolic process	Absent	N/A	12	25.4	AFUA_5G12940
Has domain(s) with predicted nucleotide binding, oxidoreductase activity and role in oxidation-reduction process	Absent	N/A	4	20.7	AFUA_6G09140

Protein Description	Log_2(Fold Decrease)	p-value	Peptides	Sequence coverage [%]	Protein IDs
Has domain(s) with predicted electron carrier activity, heme binding, oxidoreductase activity, acting on paired donors, with incorporation or reduction of molecular oxygen activity and role in oxidation-reduction process	Absent	N/A	7	19	AFUA_8G00510
Putative alpha/beta hydrolase; member of the pseurotin A gene cluster; hypoxia induced protein	Absent	N/A	16	42.9	AFUA_8G00530
Putative P450 monooxygenase; member of the pseurotin A gene cluster; transcript induced by voriconazole	Absent	N/A	4	10.6	AFUA_8G00560
Putative chitinase with a predicted role in the degradation and recycling of fungal chitin during autolysis; N-terminal signal peptide that targets to the secretory pathway	Absent	N/A	6	23.6	AFUA_8G01410
Conserved hypothetical protein	Absent	N/A	3	7.7	AFUA_8G01980
Non-heme Fe(II) and alpha-ketoglutarate-dependent dioxygenase; phytanoyl-CoA dioxygenase family protein; catalyses the conversion of fumitremorgin B to verruculogen	-4.32466	1.20E-05	21	87.3	AFUA_8G00230
Putative iron-dependent oxygenase; encoded in the *fma* (fumagillin) secondary metabolite gene cluster	-4.17772	3.18E-03	12	46.8	AFUA_8G00480
Predicted O-methyltransferase; encoded in the *fma* (fumagillin) secondary metabolite gene cluster	-3.85167	1.01E-04	11	70.6	AFUA_8G00390
IgE-binding protein	-3.76683	2.05E-04	3	34.5	AFUA_6G00430

Protein Description	Log_2(Fold Decrease)	p-value	Peptides	Sequence coverage [%]	Protein IDs
Putative methyl transferase; member of the pseurotin A gene cluster; conidia-enriched protein; hypoxia induced protein	-3.28917	9.98E-05	28	79.7	AFUA_8G00550
Cysteine-rich secreted protein	-3.27599	4.28E-05	15	63.3	AFUA_7G01060
Hypoxia induced protein; encoded in the fma (fumagillin) secondary metabolite gene cluster	-3.24847	6.95E-06	12	84.7	AFUA_8G00430
Putative alpha/beta hydrolase; encoded in the fma (fumagillin) secondary metabolite gene cluster	-3.16375	1.38E-05	15	78.4	AFUA_8G00380
Protein of unknown function; transcript downregulated in response to voriconazole	-2.96915	1.79E-02	11	41	AFUA_4G14380
Putative secreted 1,4-beta-D-glucan glucanhydrolase	-2.90284	1.49E-04	27	53.3	AFUA_7G06140
Protein of unknown function; encoded in the fma (fumagillin) secondary metabolite gene cluster	-2.85247	6.11E-04	10	45.1	AFUA_8G00400
Hypothetical protein	-2.82667	4.14E-03	7	62.3	AFUA_2G11860
Baeyer-Villiger monooxygenase (BVMO); hypoxia induced protein; encoded in the fma (fumagillin) secondary metabolite gene cluster	-2.74114	6.34E-05	41	63.4	AFUA_8G00440
Putative theta class glutathione S-transferase	-2.25371	4.53E-03	10	64.4	AFUA_4G14530
Allergen Asp f 13;putative alkaline serine protease; higher expression in biofilm vs planktonic cells; transcript induced by growth on hydrogen peroxide	-2.06535	6.01E-04	8	81.6	AFUA_2G12630

Protein Description	Log_2(Fold Decrease)	p-value	Peptides	Sequence coverage [%]	Protein IDs
Putative GTP cyclohydrolase II;transcript up-regulated in conidia exposed to neutrophils	-2.05509	3.52E-03	13	43.8	AFUA_2G01220
Has domain(s) with predicted peroxidase activity	-2.02461	1.66E-03	10	32.6	AFUA_4G02780
Ortholog of *A. nidulans* AN3906; hypoxia repressed protein	-1.99673	2.21E-03	49	48.1	AFUA_6G08660
Allergen Asp f 8;putative ribosomal protein P2;transcript induced by growth on hydrogen peroxide and menadione	-1.97795	5.13E-03	7	82	AFUA_2G10100
(Ortholog(s) have protein transporter activity, unfolded protein binding activity and role in protein import into mitochondrial inner membrane	-1.97737	9.85E-03	4	50.5	AFUA_1G04470
Mitochondrial peroxiredoxin; predicted role in cell redox homeostasis regulation; protein levels increase with amphotericin B and H2O2 exposure; transcript up-regulated in conidia exposed to neutrophils; repressed by gliotoxin exposure	-1.96889	1.96E-02	16	84.5	AFUA_4G08580
Putative FK506-binding protein (FKBP)-type peptidyl-prolyl cis-trans isomerase; transcript induced by exposure to human airway epithelial cells	-1.85773	1.55E-05	11	93.8	AFUA_6G12170
Has domain(s) with predicted zinc ion binding activity, role in ER to Golgi vesicle-mediated transport, intracellular protein transport and COPII vesicle coat localization	-1.84388	2.71E-02	10	15.2	AFUA_6G12830
Asp-hemolysin;hemolytic toxin; highly secreted; enriched in conidia; expression increases *in vivo*; binds lysophosphatidylcholine	-1.82658	1.50E-03	10	71.9	AFUA_3G00590

Protein Description	Log_2(Fold Decrease)	p-value	Peptides	Sequence coverage [%]	Protein IDs
Transcript up-regulated in conidia exposed to neutrophils	-1.81415	1.73E-03	3	13.9	AFUA_4G07030
Pathogenesis associated protein Cap20	-1.78879	3.73E-02	12	70.1	AFUA_1G06350
Putative tripeptidyl-peptidase of the sedolisin family; predicted signal sequence for secretion	-1.73219	2.95E-02	7	12.3	AFUA_4G14000
Guanyl-specific ribonuclease, putative	-1.72977	1.63E-02	10	34.1	AFUB_079800
Hypothetical protein	-1.70645	2.22E-03	8	66.5	AFUA_6G00600
Putative NADH-ubiquinone oxidoreductase 39 kDa subunit	-1.63808	5.32E-03	12	51.3	AFUA_6G12790
Putative enoyl-CoA hydratase/isomerase family protein with a predicted role in beta oxidation of fatty acids; transcript up-regulated in conidia exposed to neutrophils	-1.63382	2.82E-03	9	34.7	AFUA_2G10920
Non-ribosomal peptide synthetase (NRPS); PKS/NRPS hybrid; multidomain protein; required for pseurotin A production; pseurotin A gene cluster member; transcript induced by voriconazole; induced by hypoxia and in infected mouse lungs	-1.60039	7.06E-03	105	36.9	AFUB_086030
Ortholog(s) have role in mitochondrion inheritance, negative regulation of proteolysis, protein folding, replicative cell aging and mitochondrial inner membrane localization	-1.5947	2.18E-03	9	31.8	AFUA_2G09090

Protein Description	Log_2(Fold Decrease)	p-value	Peptides	Sequence coverage [%]	Protein IDs
Ortholog(s) have dicarboxylic acid transmembrane transporter activity, role in mitochondrial transport and mitochondrial inner membrane localization	-1.56908	2.64E-02	5	23.6	AFUA_1G09660
Putative alpha-glucosidase B	-1.55841	1.95E-03	30	44.4	AFUA_1G16250
Allergen Asp f 34;putative phiA family cell wall protein; induced calcium; repressed by exposure to artemisinin	-1.5461	3.85E-02	7	79.5	AFUA_3G03060
Allergen Asp f 29;putative thioredoxin	-1.50915	9.52E-03	9	82.7	AFUA_5G11320
Has domain(s) with predicted oxidoreductase activity and role in oxidation-reduction process	-1.50563	2.59E-02	6	27.8	AFUA_4G12710
Putative tropomyosin 1;protein induced by hydrogen peroxide; reacts with rabbit immunosera exposed to *A. fumigatus* conidia	-1.50549	2.05E-02	17	81.8	AFUA_7G04210
Allergen Asp f 1; ribonuclease mitogillin family of cytotoxins; similar to restrictocin; inhibits protein synthesis in mammalian cells	-1.48966	1.08E-03	10	61.4	AFUA_5G02330
Putative NADH dehydrogenase; mutation causes increased azole resistance	-1.48604	2.71E-02	6	42.1	AFUA_2G10600
Putative NADPH isocitrate dehydrogenase; transcript induced during conidial germination	-1.46226	2.70E-02	20	58.2	AFUA_1G12800
Ortholog(s) have adenylate kinase activity, role in ADP biosynthetic process, DNA-dependent DNA replication initiation and mitochondrial intermembrane space localization	-1.4474	-1.4474	9	47.5	AFUA_1G07530

Protein Description	Log_2(Fold Decrease)	p-value	Peptides	Sequence coverage [%]	Protein IDs
Putative flavohemoprotein; protein induced by heat shock and hypoxia	-1.42304	3.39E-02	12	41.9	AFUA_4G03410
Putative glutathione transferase	-1.4093	2.46E-02	7	40.6	AFUA_3G10830
Glycosyl hydrolase family 75 chitosanase; hydrolyzes beta-1,4-glycosidic linkage of chitosan; repressed by exposure to artemisinin	-1.3902	4.01E-02	10	40.8	AFUA_4G01290
Ortholog(s) have thiosulfate sulfurtransferase activity, role in tRNA wobble position uridine thiolation and cytoplasm localization	-1.38091	5.01E-03	11	47.9	AFUA_7G01370
Has domain(s) with predicted transporter activity, role in transport and intracellular localization	-1.36724	9.32E-03	10	42.3	AFUA_3G09910
Ran-interacting protein Mog1, putative	-1.32425	9.02E-03	9	66.7	AFUA_6G12430
Putative outer mitochondrial membrane protein porin; hypoxia induced protein	-1.31711	3.51E-02	12	52.8	AFUA_4G06910
Protein with Yap1-dependent induction in response to hydrogen peroxide; calcium downregulated	-1.30285	2.42E-02	7	85.2	AFUA_1G09890
ThiJ/PfpI family protein	-1.29656	3.71E-03	4	13.1	AFUA_5G02670
RhoGAP and Fes/CIP4 domain protein; calcium induced	-1.28477	2.91E-02	11	17.5	AFUA_7G04300

Protein Description	Log_2(Fold Decrease)	p-value	Peptides	Sequence coverage [%]	Protein IDs
Has domain(s) with predicted UDP-N-acetylmuramate dehydrogenase activity, flavin adenine dinucleotide binding activity and role in oxidation-reduction process	-1.27887	5.18E-03	15	46.4	AFUA_6G14340
Mitochondrial genome maintenance protein Mgm101, putative	-1.26767	4.83E-02	6	30.9	AFUA_2G09560
Putative FK506-binding protein (FKBP)-type peptidyl-prolyl cis-trans isomerase	-1.26433	2.11E-03	6	60.4	AFUA_2G03870
Putative acylCoA binding family protein	-1.25198	1.63E-04	11	70.3	AFUA_2G11060
Has domain(s) with predicted structural molecule activity, role in intracellular protein transport, vesicle-mediated transport and COPI vesicle coat localization	-1.25084	2.61E-02	14	19	AFUA_2G02560
Putative translation elongation factor EF-2 subunit; protein abundant in conidia; protein induced by heat shock	-1.24914	6.58E-03	64	75.9	AFUA_2G13530
Hypothetical protein	-1.24131	1.03E-02	10	25.9	AFUA_5G09640
Ortholog(s) have hydrolase activity, role in nucleotide metabolic process and cytoplasm, nucleus localization	-1.22323	2.14E-02	5	38.5	AFUA_6G12680
Has domain(s) with predicted catalytic activity and role in metabolic process	-1.20739	4.69E-02	6	18.3	AFUA_1G06780
Mitochondrial glycerol-3-phosphate dehydrogenase; hypoxia repressed protein	-1.19813	2.06E-02	25	53.9	AFUA_1G08810

Protein Description	Log_2(Fold Decrease)	p-value	Peptides	Sequence coverage [%]	Protein IDs
Ubiquinol-cytochrome c reductase iron-sulphur subunit precursor with a predicted role in oxidative phosphorylation; hypoxia induced protein; induced by exposure to artemisinin; SrbA-regulated during hypoxia	-1.19224	4.54E-04	8	40.6	AFUA_5G10610
Has domain(s) with predicted protein serine/threonine phosphatase activity, role in protein dephosphorylation and protein serine/threonine phosphatase complex localization	-1.18685	6.53E-03	11	34.7	AFUA_1G09280
Hypothetical protein	-1.18577	4.05E-02	22	43.4	AFUA_6G09920
Aspartic acid endopeptidase; conidia-enriched protein; conidial surface associated; predicted signal secretion sequence; hypoxia induced protein; transcript up-regulated in conidia exposed to neutrophils and by growth on BSA	-1.18445	2.82E-02	21	52.3	AFUA_3G11400
Putative 60S ribosomal protein P0;reacts with rabbit immunosera exposed to *A. fumigatus* conidia	-1.18381	3.58E-02	10	43.1	AFUA_1G05080
Ortholog(s) have role in response to DNA damage stimulus	-1.17873	3.59E-02	8	25.2	AFUA_1G13020
Putative alcohol dehydrogenase involved in ethanol metabolism; predicted gene pair with AFUA_A_6G11430 (AldA);increased expression in biofilm; induced by L-tyrosine; induced in neutrophil-exposed conidia; repressed by gliotoxin exposure	-1.17862	3.06E-02	11	26.4	AFUA_7G01000
Ortholog(s) have metalloendopeptidase activity, role in protein processing involved in protein targeting to mitochondrion and mitochondrial processing peptidase complex localization	-1.1768	1.68E-02	11	29.8	AFUA_1G11870

Protein Description	Log_2(Fold Decrease)	p-value	Peptides	Sequence coverage [%]	Protein IDs
Ortholog(s) have ubiquitin-protein ligase activity, role in free ubiquitin chain polymerization, postreplication repair, protein polyubiquitination and cytoplasm, nucleus, ubiquitin conjugating enzyme complex localization	-1.17177	4.46E-02	6	38.8	AFUA_4G12080
Ortholog of *S. cerevisiae* NFS1;putative novel ncRNA AFUA_-203 encoded within the intron	-1.15836	1.41E-02	16	46.6	AFUA_3G14240
Has domain(s) with predicted oxidoreductase activity and role in cell redox homeostasis	-1.14876	2.37E-02	11	59.5	AFUA_6G12500
Thiamine biosynthesis protein, phoB-regulated; protein induced by H2O2;reacts with rabbit immunosera exposed to conidia; hypoxia induced protein; transcript induced by exposure to human airway epithelial cells	-1.11766	4.54E-03	20	68.1	AFUA_5G02470
Putative extracellular serine carboxypeptidase; predicted signal sequence for secretion; induced by growth on BSA as a sole nitrogen source	-1.11575	1.53E-02	13	32.3	AFUA_2G17330
Ortholog(s) have carbonyl reductase (NADPH) activity and cytoplasm, nucleus localization	-1.10991	9.48E-03	8	21.9	AFUA_2G10280
Putative fumarate hydratase; reacts with rabbit immunosera exposed to *A. fumigatus* conidia	-1.0972	2.37E-02	17	46	AFUA_6G02470
Putative 40S ribosomal protein S0	-1.08214	1.98E-02	9	40.7	AFUA_3G13320
Endonuclease/exonuclease/phosphatase family protein	-1.07779	1.13E-02	15	56.3	AFUA_2G16830

Protein Description	Log_2(Fold Decrease)	p-value	Peptides	Sequence coverage [%]	Protein IDs
Putative 2,3-bisphosphoglycerate-independent phosphoglycerate mutase; protein abundant in conidia; transcript induced by exposure to human airway epithelial cells	-1.07141	1.74E-02	12	32.7	AFUA_3G09290
GTP-binding protein YchF	-1.06875	1.51E-02	19	59.9	AFUA_1G09800
Ortholog(s) have ubiquitin binding activity, role in late endosome to vacuole transport, protein targeting to vacuole and ESCRT-0 complex localization	-1.06689	4.68E-02	6	12.3	AFUA_2G04670
mRNA binding post-transcriptional regulator (Csx1), putative	-1.05534	4.16E-02	9	30.1	AFUA_7G02230
Putative polyADP-ribose polymerase (PARP)	-1.05271	7.65E-03	13	24.7	AFUA_5G07320
Calmodulin	-1.05167	5.05E-03	16	98.7	AFUA_4G10050
Alpha/beta hydrolase	-1.03265	3.93E-02	8	25.4	AFUA_1G05590
Putative family 18 (class V) chitinase; secreted protein	-1.01758	2.53E-03	6	21.6	AFUA_3G11280
Phosducin family protein	-1.01644	4.60E-03	4	75.9	AFUA_2G02550
Ortholog(s) have G-protein beta/gamma-subunit complex binding, actin binding activity, role in positive regulation of transcription from RNA polymerase II promoter by pheromones, protein folding and cytoplasm localization	-1.01409	7.29E-03	5	17.9	AFUA_2G02550
Putative microtubule associated protein	-1.01289	6.56E-03	10	42.8	AFUA_3G11860
Karyopherin alpha subunit	-1.01042	2.30E-03	13	34.1	AFUA_2G16090

Protein Description	Log_2(Fold Decrease)	p-value	Peptides	Sequence coverage [%]	Protein IDs
Ortholog(s) have urease activity and role in urea catabolic process	-1.00997	1.92E-02	13	24.8	AFUA_1G04560

6.3 Discussion

The deletion of *gtmA* in the *A. fumigatus*^{ATCC26933} mutant backgrounds Δ*gliT* and Δ*gliA* (Section 3.2.9) facilitated an exploration of the underlying contribution of this methyltransferase to the self-protection against gliotoxin. Also, as SAM is a cofactor required for the thiomethylation of dithiol gliotoxin, the levels of this metabolite were quantified in various *A. fumigatus* deletion mutants upon gliotoxin exposure. Finally, late stage culture incubation was utilised to explore the interplay between GtmA activity and the production of other bioactive secondary metabolites produced by *A. fumigatus*.

The data shown in Figure 6.1 indicated that Δ*gliT::*Δ*gtmA* is more sensitive to exogenous gliotoxin in comparison with *A. fumigatus* Δ*gliT*. In addition, Δ*gliA*:Δ*gtmA* was shown to be significantly more sensitive to gliotoxin than Δ*gliA*. This suggests that, when the primary method of self-protection is disabled, *gtmA* provided some level of resistance against gliotoxin. Data in Section 6.2.2 demonstrated that endogenous bis(methyl)gliotoxin production is severely affected by the absence of *gliT* or *gliA* (Figure 6.3). The decreased production of bis(methyl)gliotoxin by Δ*gliT* is surprising considering that the absence of *gliT* should result in an increased substrate availability for GtmA. Deletion of the dithiol oxidase gene, *hlmI*, results in an increase in dimethyldihydroholomycin production in a holomycin overexpression background (Li et al., 2012). However, it was demonstrated that dimethyldihydroholomycin is produced at higher levels by Δ*hlml* compared to the wild-type under secondary metabolite producing conditions (Li et al., 2012). The decreased production of bis(methyl)gliotoxin by Δ*gliT* may be due to the possibility that the bis(methyl)gliotoxin which is detected in the wild-type culture supernatants may be largely a product of the conversion of exogenously effluxed gliotoxin which is re-taken up by *A. fumigatus* and converted to bis(methyl)gliotoxin by GtmA. This result might also be explained by pathway cellular compartmentalisation during gliotoxin biosynthesis which may limit the endogenously

produced dithiol gliotoxin reaching GtmA. Compartmentalisation in secondary metabolism has been demonstrated for several other natural product biosynthetic pathways (Lim and Keller, 2014).

Furthermore, it was demonstrated in Section 6.2.3 that Δ*gliT* produces significantly more bis(methyl)gliotoxin than wild-type or Δ*gliA* following exogenous gliotoxin exposure. This suggested that the inability to oxidise dithiol gliotoxin to gliotoxin by GliT results in a higher substrate availability for GtmA. This in turn results in higher levels of bis(methyl)gliotoxin production upon gliotoxin exposure (Figure 6.15). The lower conversion by Δ*gliA* may be explained by this strain's ability to oxidise gliotoxin; this may result in the reduction of the GtmA substrate availability. These data were in agreement with the SAM levels quantified in Section 6.2.4. The severe SAM depletion noted in Δ*gliT* following gliotoxin exposure (O'Keeffe et al., 2014) was alleviated in the double deletion mutant Δ*gliT*::Δ*gtmA*. *A. fumigatus* Δ*gliA::*Δ*gtmA* was also found to have higher remaining levels of cellular SAM than Δ*gliA* following gliotoxin exposure. These data support the RNAseq analysis of Δ*gliT* exposed to gliotoxin which revealed the significant up-regulated expression ($p < 0.005$) of genes involved in sulfur assimilation, methionine and SAM biosynthesis (O'Keeffe et al., 2014). The expression of methylenetetrahydrofolate reductase (*mtrA*), cobalamin-independent methionine synthase (*metH*) and S-adenosylmethionine synthetase (*sasA*) were significantly increased ($p < 5 \times 10^{-5}$ - 0.003) (Amich et al., 2010). Expression of the bZIP transcription factor, *metR* and S-adenosylhomocysteinase (*sahA*) was also up regulated ($p < 0.00015$-0.001), as was that of glycine dehydrogenase (GDH; $p < 0.0056$) and serine hydroxymethyltransferase (SHMT; $p < 0.0001$). GDH and SHMT act in concert with the folate cycle to transfer methyl groups to homocysteine (Hcy) for methionine biosynthesis (Suliman et al., 2007).

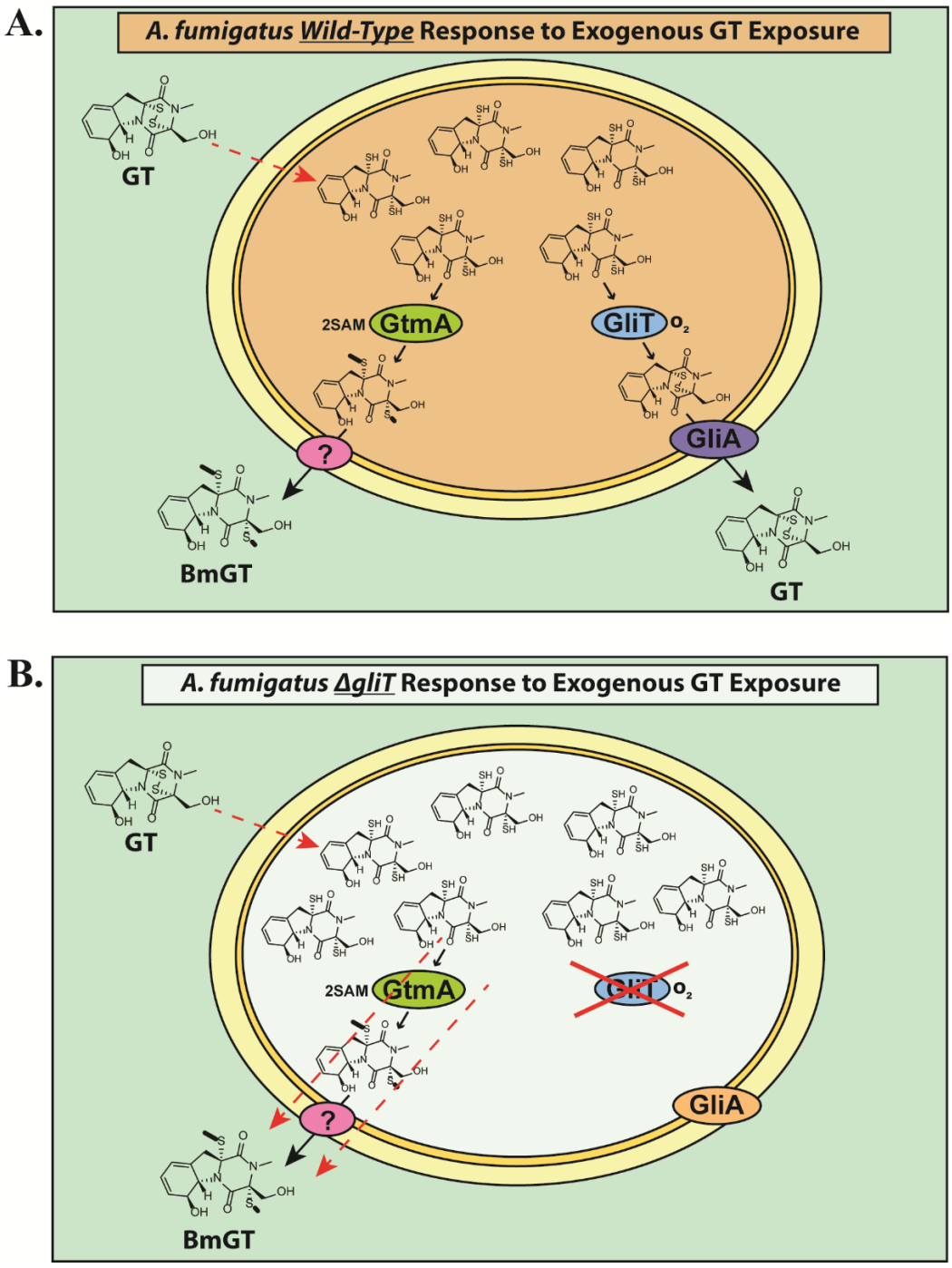

Figure 6.15. A: *A. fumigatus* wild-type responds to exogenous gliotoxin by a combination of GliT mediated dithiol gliotoxin oxidation and GliA-mediated export. GtmA-mediated bisthiomethylation and export also occur. **B:** In the Δ*gliT* strain the absence of GliT results in an increased GtmA substrate availability, which in turn results in maximal bisthiomethylation activity in the presence of exogenous GT. As each dithiol gliotoxin requires two SAM molecules, this process results in a rapid depletion of cellular SAM.

Overall, these observations reveal the impact of gliotoxin thiomethylation on the cellular levels of SAM and the importance of GliT for the control of sulfur metabolism during gliotoxin exposure. Moreover, these data directly implicate GtmA activity in the dysregulation of SAM:SAH levels and strongly implicate gliotoxin exposure as impacting on the methyl/methionine cycle within *A. fumigatus* in the absence of *gliT* (Owens et al., 2015).

Based on the above data, it is hypothesised that, following gliotoxin exposure, Δ*gliT*:Δ*gtmA* accumulates high levels of intracellular dithiol gliotoxin which cannot exit the cell by either oxidation (GliT) and subsequent efflux by GliA, or by GtmA-mediated bisthiomethylation. As shown in Section 6.2.5, this hypothesis is supported by the RP-HPLC based gliotoxin uptake/efflux investigation. The gliotoxin sensitivity of *A. fumigatus* mutants is most significant where the removal of intracellular dithiol gliotoxin (Dolan et al., 2014) is hampered by a combined deficit of the inability to oxidise, efflux or bisthiomethylate this toxin. Δ*gliT*::Δ*gtmA* was shown to have the lowest levels of extracellular gliotoxin present following 3 h gliotoxin exposure; this is in complete agreement with the inability of this mutant to directly dissipate any dithiol gliotoxin which enters the cell. The fact that Δ*gliA*::Δ*gliT* is more sensitive to gliotoxin than Δ*gliA* (Wang et al., 2014) suggests that GliT is able to maintain a discrete level of intracellular gliotoxin in the oxidised state. This explains why Δ*gliT* converts more added gliotoxin to bis(methyl)gliotoxin than Δ*gliA* (Figure 6.8) and why Δ*gliT*::Δ*gtmA* is more sensitive to gliotoxin than Δ*gliA*::Δ*gtmA*.

Figure 6.1 demonstrated that Δ*gliT*::Δ*gtmA* is very sensitive to exogenous gliotoxin compared to *A. fumigatus* Δ*gliT*. These results, in combination with the gliotoxin uptake and conversion data in Section 6.2.5, suggested that the increased accumulation of intracellular gliotoxin (as dithiol gliotoxin) may lead to toxicity in this

mutant. Considering that gliotoxin exposure results in the induction of *gli*-cluster expression (O'Keeffe et al., 2014) (possibly by intracellular accumulation), the heightened sensitivity of Δ*gliT::*Δ*gtmA* may also be the result of the over-activation of the *gli*-cluster leading to a sustained expression of these proteins. As described in Section 6.2.6, upon exposure to gliotoxin for 3 h five gliotoxin biosynthesis enzymes (GliG, GliN, GliH, GliM and GliP) were found to be highly abundant in the Δ*gliT::*Δ*gtmA* mutant compared to Δ*gliT*. As these gliotoxin biosynthetic enzymes have been synthesised, it is plausible that the gliotoxin pathway could proceed to the penultimate step (dithiol gliotoxin) before being trapped in the cell due to the absence of both GliT and GtmA. This trapped dithiol gliotoxin may then further activate the *gli*-cluster. It is likely that this *in-vivo*-produced dithiol gliotoxin would contribute to cellular oxidative stress in conjunction with the exogenously-added gliotoxin, which undergoes intracellular GSH-mediated reduction, hampering its export from the cell (Figure 6.16).

A putative cysteine synthase (CysB) was significantly more abundant in the Δ*gliT::*Δ*gtmA* mutant compared to Δ*gliT* (Amich et al., 2013). *A. fumigatus* detoxifies oxidative threats via glutathione synthesis (Tekaia and Latgé, 2005). However, it has been shown that gliotoxin is actively concentrated in P388D1 cells in a glutathione-dependent manner and that this normally protective mechanism actually facilitates gliotoxin toxicity (Bernardo et al., 2003). An increased intracellular dithiol gliotoxin load in Δ*gliT::*Δ*gtmA* may result in a more substantial depletion of GSH compared to Δ*gliT*. In addition, the glutathione S-transferase GliG, responsible for transferring two GSH molecules onto the gliotoxin scaffold resulting in sulfurization of the metabolite was the protein with the most significant abundance increase in Δ*gliT*::Δ*gtmA* exposed to gliotoxin compared to Δ*gliT*. (Davis et al., 2011; Scharf et al., 2011). This may also contribute to the increase in CysB abundance in *A. fumigatus* Δ*gliT::*Δ*gtmA* due to GSH utilisation by this secondary metabolite biosynthetic pathway.

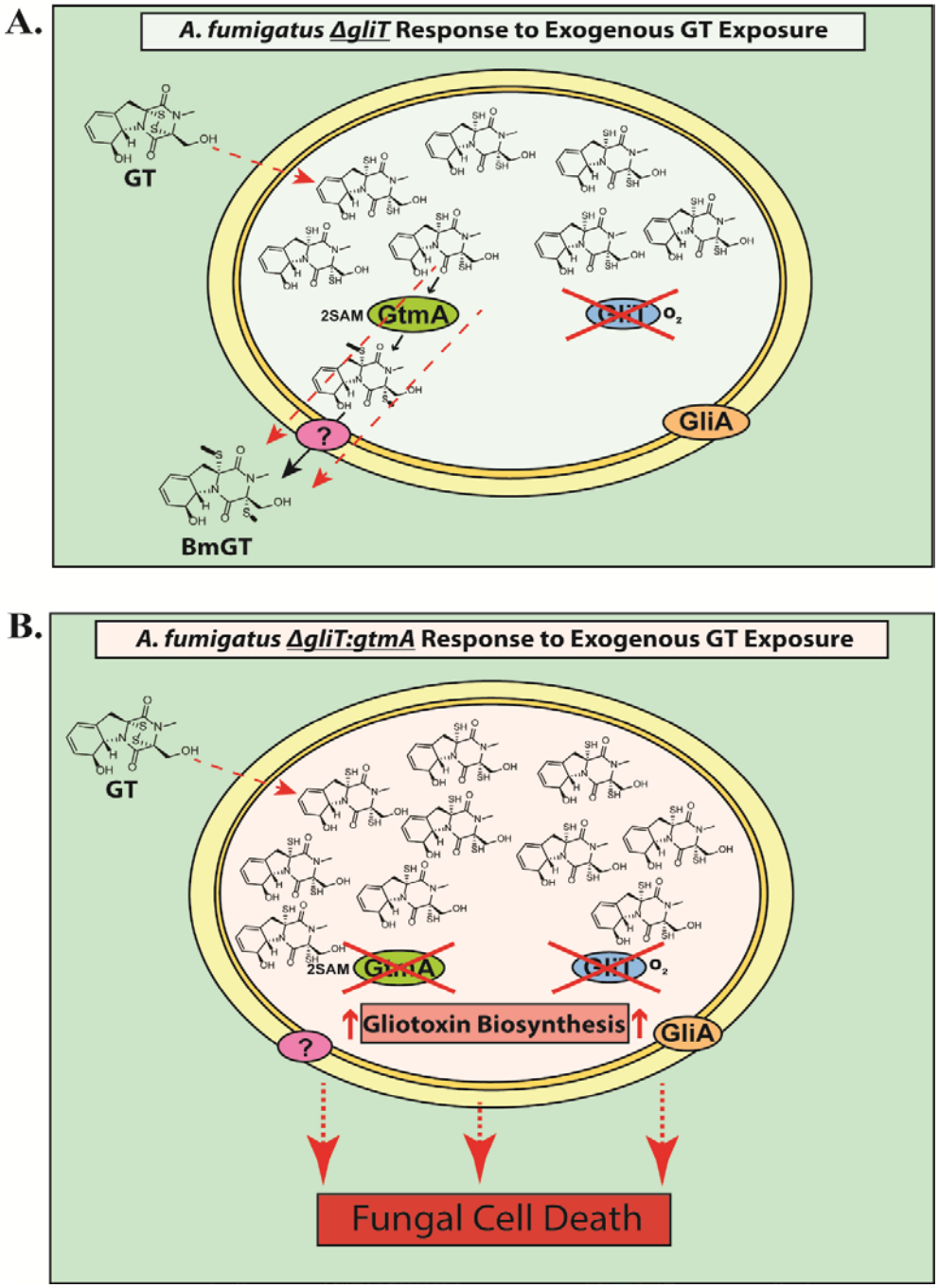

Figure 6.16. A: *A. fumigatus* Δ*gliT* responds to exogenous gliotoxin by effecting excessive bisthiomethylation on this metabolite, resulting in cellular SAM depletion. **B:** The highly sensitive *A. fumigatus* Δ*gliT*::Δ*gtmA* cannot remove intracellular accumulated dithiol gliotoxin by S-methylation or oxidation. This likely results in cell death as a result of the combined effect of gliotoxin toxicity and *gli*-cluster over-activation due to the sustained presence of dithiol gliotoxin.

The non-ribosomal peptide synthetase GliP was uniquely detected in the Δ*gliT*::Δ*gtmA*. Exposure of *A. fumigatus* to gliotoxin has been shown to induce the expression of genes in the gliotoxin biosynthetic cluster (Cramer et al., 2006). This was also shown on the proteomic level (Dolan et al., 2014), demonstrating that the pathway can be completely activated by this external signal (O'Keeffe et al., 2014). Also, the addition of gliotoxin to the culture medium of a *gliP* deficient mutant restored the expression of several *gli*-cluster genes in a dose-dependent manner from 500 ng/ml to 20 µg/ml (Cramer et al., 2006). This further supports the idea that the intracellular accumulation of gliotoxin in Δ*gliT*::Δ*gtmA* results in higher *gli*-cluster induction. GliP activates and tethers L-Phe on thiolation domain 1 and L-Ser on thiolation domain 2 before generating the L-Phe-L-Ser-*S*-T_2 dipeptidyl enzyme intermediate (Balibar and Walsh, 2006). A D-3-phosphoglycerate dehydrogenase (AFUA_2G04490) which synthesizes L-serine from 3-phospho-D-glycerate was uniquely detected in Δ*gliT*::Δ*gtmA* exposed to gliotoxin vs. Δ*gliT*. In addition, Seryl-tRNA synthetase was uniquely detected in Δ*gliT*::Δ*gtmA*; this may be linked to increased serine utilisation in Δ*gliT*::Δ*gtmA* by GliP and concomitant depletion or competition for endogenous serine.

It has been shown that, in response to a diverse range of stresses, fungi undergo a common response termed the "environmental stress response" (Moye-Rowley, 2003). This involves the expression of (i) heat shock proteins or chaperones that protect against protein unfolding, (ii) proteins with anti-oxidant functions (glutathione metabolism) that repair against oxidative stress induced damage, (iii) carbohydrate metabolism which generates metabolic energy required for stress adaptation. Protein synthesis and cellular growth is repressed indicating the requirement to preserve energy (Gasch et al., 2000). This response is evident in the *A. fumigatus* Δ*gliT*::Δ*gtmA* vs. *A. fumigatus* Δ*gliT* quantitative proteomic data.

A putative mitochondrial DnaJ chaperone (MDJ1) (AFUA_2G11750; 1.57627) was significantly more abundant in Δ*gliT*::Δ*gtmA*. In *S. cerevisiae*, MDJ1 has been localised to the mitochondrial matrix where it participates in the folding of certain imported proteins and may also help prevent heat induced protein aggregation. The lack of MDJ1 resulted in the reduced competence of mitochondria to properly fold imported monomeric proteins (Rowley et al., 1994). A putative prefoldin subunit 3 (AFUA_2G02230; 1.36956) was also significantly more abundant. Prefoldin is a molecular chaperone that acts in conjunction with chaperonin to assist in the correct folding of other proteins in the crowded molecular environment that exists in living cells. Chaperonins are multisubunit toroidal assemblies which undergo major ATP-dependent conformational changes as part of the mechanism of facilitated folding (Vainberg et al., 1998).

A notable characteristic of neutrophil activation is the production of copious amounts of oxidants in a process known as the respiratory burst (Dahlgren and Karlsson, 1999). Several genes are induced *in-vivo* to protect against this oxidative stress. Five proteins with increased abundance in Δ*gliT*::Δ*gtmA* exposed to gliotoxin were previously shown to have their transcripts up-regulated in conidia exposed to neutrophils (Sugui et al., 2008). These included AFUA_2G13590, a protein with a protease inhibitor propeptide domain, which are generally responsible for the modulation of zymogen folding and activity, the isocitrate lyase AcuD (AFUA_4G13510) and a putative acyl-CoA dehydrogenase (AFUB_065590), a putative aldehyde reductase (AFUA_6G10260) and a putative glucosamine-6-phosphate deaminase (AFUA_8G04070). A hypoxia-induced protein, AFUA_6G11850, was also increased in abundance. An uncharacterized protein with oxidoreductase activity (AFUA_2G02950) was also shown to be more abundant in this condition.

Proteins associated with energy providing pathways were also deregulated in Δ*gliT*::Δ*gtmA*, possibly as a result of stress adaptation. These included a mitochondrial 2-oxodicarboxylate carrier protein (AFUA_1G09660; 1.48277), a mitochondrial F1F0-ATP synthase g subunit (AFUA_1G16280; 1.27137), a putative mitochondrial import receptor subunit (Tom20) (AFUA_6G11380; Unique), the *are*A-dependent nitrogen-scavenging enzyme L-amino acid oxidase LaoA (AFUA_7G06810; 1.24757) which enables *Aspergilli* to catabolise a broad spectrum of amino acids in nitrogen starvation condition, and the isocitrate lyase AcuD (AFUA_4G13510; 1.2476) which facilitates the growth of *A. fumigatus* on C2-generating carbon sources (Schöbel et al., 2007). The abundance of the allergen Aspf2 (AFUA_4G09580; 2.08334) was significantly more abundant in the Δ*gliT*::Δ*gtmA* mutant. This protein is known to be expressed under zinc limiting conditions and is required for fungal growth in extreme zinc-limiting media (Amich et al., 2010).

As described above, oxidative stress leads to a general repressed expression of protein synthesis and cellular growth indicating the requirement to preserve energy (Gasch et al., 2000). This is represented in the proteomic data described in Section 6.2.6, which shows an enrichment of ribosome and ribosome associated proteins. 13 of the 24 proteins detected as significantly decreased in abundance in *A. fumigatu*s Δ*gliT*::Δ*gtmA* mutant compared to *A. fumigatu*s Δ*gliT* are associated with the ribosome.

Interestingly, the putative zinc-dependent alcohol dehydrogenase AlcC (AFUA_5G06240; 1.21622) was shown to be less abundant in this mutant compared to Δ*gliT*. The mRNA abundance of *alcC* was shown to be significantly increased in response to hypoxia, suggesting that *alcC* is the primary gene encoding an alcohol dehydrogenase that responds to hypoxia in *A. fumigatus* (Grahl et al., 2011).

Overall the gliotoxin sensitivity data, SAM quantification and quantitative proteomic data suggest that, in the absence of GliT, GtmA plays a key role in protecting

against exogenous gliotoxin. The results also highlight the complexity of the interactions between primary and secondary metabolism in this organism. The intricate mechanism of *gli*-cluster positive feedback by intracellular dithiol gliotoxin was also explored by this analysis.

The filamentous fungus *A. terreus* produces the ETP acetylaranotin (Guo et al., 2013). Similar to gliotoxin, this metabolite and its derivatives have been shown to display an array of interesting bioactivities including the induction of apoptosis in cancer cell lines and antifungal activity (Guo et al., 2013; Choi et al., 2011; Suzuki et al., 2000). Extending the incubation duration of *A. terreus* cultures from 6 d to 42 d resulted in the production of four thiomethylated forms of acetlyaranotin. One of these forms (bisdethiobis(methylsulfanyl)apoaranotin) had not been characterised previously (Haritakun et al., 2012). As the generation of these thiomethylated forms of acetylaranotin was likely carried out by the *A. terreus* GtmA homolog, this experiment prompted us to explore the effect of extended culture incubation on *A. fumigatus* wild-type and Δ*gtmA*.

As described in Section 6.2.7, *A. fumigatus* Δ*gtmA* 28 d cultures showed a significant decrease in the production of pseurotin A and fumagillin compared to the wild-type strain. The levels of these metabolites were restored in the complemented strain. It was first explored if the absence of bisthiomethylgliotoxin was affecting the expression of the *A. fumigatus* chromosome 8 intertwined secondary metabolite supercluster (Wiemann et al., 2013). Bisthiomethylgliotoxin may act as a signal for the activation of other secondary metabolite clusters by an unknown mechanism which is not unlike the mechanism of gliotoxin induction of *gli*-cluster expression. As described in Section 6.2.8, the addition of exogenous bisthiomethylgliotoxin did not restore the production of the affected metabolites to wild-type levels, thus ruling out bisthiomethylgliotoxin-mediated induction of the supercluster.

This then prompted the analysis of the cultures by quantitative proteomics in order to study the modified metabolome of *A. fumigatus* Δ*gtmA*. As described in Section 6.2.9, the results showed that, after 28 d cultured in Czapeks Dox, Δ*gtmA* still has *gli*-cluster encoded proteins (GliA, GliM , GliJ and GliG) significantly increased in abundance compared to the wild-type. As described in Section 4.2.10, GliP, GliM and GliF were significantly increased in abundance in Δ*gtmA* compared to the wild-type after 72 h growth in Czapeks Dox broth. This indicated that the absence of *gtmA* results in a sustained induction of *gli*-cluster expression.

Several proteins which have transcripts shown previously to be induced by hypoxia or by exposure to neutrophils were shown to be upregulated in Δ*gtmA*. Two proteins which are repressed by gliotoxin exposure and two which are repressed by hypoxia were significantly decreased in abundance in Δ*gtmA* (Vödisch et al., 2011). This may be a response to the sustained gliotoxin production in this mutant as the abundance of these proteins are returned to wild-type levels in the complemented strain.

A clear result of the analysis was the large decrease in abundance of several proteins encoded by the chromosome 8 supercluster (Afu_8g00100-00720) (Wiemann et al., 2013). This was in agreement with the metabolomic analysis of culture supernatants from these samples (Section 6.2.7) which revealed the decreased production of pseurotin A and fumagillin. A total of 17 proteins from this cluster were detected as less abundant in Δ*gtmA*. Interestingly, 23 of the 136 proteins detected as significantly decreased in abundance in Δ*gtmA* are encoded on Chromosome 8. This is in comparison to 2 of the 72 proteins detected as increased in abundance in Δ*gtmA* being encoded on Chromosome 8.

In addition to the interactions between primary and secondary metabolism described above, there are also several examples of cross-talk amongst gene clusters which are responsible for the synthesis of fungal natural products. Over-expression of the

silent *inp* putative secondary metabolism cross-pathway regulator gene (*scpR*) in *A. nidulans* resulted in the overproduction of both the *inp* gene cluster and, also, production of the polyketide, asperfuranone. As no link had previously been described between these unrelated metabolites, this work highlighted some additional complexity of regulatory cross-talk in fungal secondary metabolism (Bergmann *et al*., 2010). Further recent findings are changing previously held views of distinct SM clusters encoding for a single class of, or closely related, secondary metabolites. A FAD-dependent monooxygenase (FqzB) which is encoded by the fumiquinazoline biosynthetic pathway in *A. fumigatus* was also shown to catalyse spiro-carbon formation in the indole alkaloid spirotryprostatin A via an epoxidation route. The authors speculated that these interactions between unrelated fungal natural product encoding cluster genes may be a strategy of natural product producers to generate structural diversity (Tsunematsu *et al*., 2013).

Fumigaclavine C, an ergot alkaloid, was demonstrated to aid in oxidative stress defense in *A. fumigatus* whereby deletion of either of the NRP synthetase genes, *pesL* or *pes1*, resulted in abrogation of the metabolite (O'Hanlon *et al*., 2012). Loss of fumigaclavine C in *A. fumigatus* resulted in H_2O_2 sensitivity, suggestive of its role in oxidative stress defense. It should be noted that, in contrast to *Claviceps purpurea* (Haarmann *et al.,* 2005), the role of an NRPS in alkaloid synthesis has yet to be proven in *A. fumigatus*. Loss of fumigaclavine C was accompanied by elevated levels of another class of SM, the fumitremorgins. The increased production of fumitremorgins such as TR-2, fumitremorgin C and verruculogen in response to fumigaclavine C diminution is indicative of cross-talk within the secondary metabolome. These authors have speculated that increased fumitremorgin levels are possibly caused by increased isoprene availability due to decreased prenylation of fumigaclavine A as a result of PesL/Pes1 absence (O'Hanlon et al., 2012).

Further to the observations regarding fumitremorgin and fumigaclavine biosynthesis (O'Hanlon *et al*., 2012), overexpression of the *A. fumigatus* putative $Zn(II)_2Cys_6$ transcription factor *hasA* (which is part of the hexadehydro-astechrome (HAS) biosynthetic gene cluster) also resulted in the production of large amounts of fumitremorgins compared to the wild-type strain. Deletion of the HAS NRPS in a background overexpressing *hasA* (OE*::hasA*Δ*hasD*) resulted in significantly increased fumitremorgin production. The authors hypothesised that the diversion of tryptophan and prenylation activity from HAS production towards fumitremorgin biosynthesis may occur in OE*::hasA*Δ*hasD* due to the inability of this mutant to utilise the pathway intermediates from HAS production. As fumitremorgins are potent tremorgenic mycotoxins this may account for the increased virulence of the OE*::hasA*Δ*hasD* strain compared to wild-type (Yin et al., 2013).

O'Keeffe *et al*. (2014) have demonstrated that an intact gliotoxin self-protection mechanism (Schrettl *et al*., 2010; Scharf *et al*., 2010), mediated by GliT, is essential to regulate the biosynthesis of apparently unrelated metabolites such as pseurotin A, fumagillin and fumitremorgins. Specifically, using RNA-seq these authors have demonstrated that gene cluster expression encoding the biosynthesis of helvolic acid, pseurotin A, fumagillin and fumitremorgins is significantly attenuated in *A. fumigatus* Δ*gliT* upon gliotoxin exposure.

Overall these data suggest that GtmA directs the production of bis(methyl)gliotoxin and that the deletion of this methyltransferase results in a deregulation of the gliotoxin biosynthetic pathway. When these *A. fumigatus* cultures are incubated for extended durations, the absence of GtmA has downstream effects on seemingly unrelated natural products produced by this organism. LaeA, a global regulator of secondary metabolism, controls the expression of gliotoxin, pseurotin A, fumagillin and the fumitremorgins (Bok and Keller, 2004). It is possible that the absence of GtmA

alters the activity of LaeA or other global regulators of secondary metabolism, which in turn impacts on the production of co-regulated secondary metabolites.

Overall the data presented in this chapter suggests GtmA-mediated thiomethylation as an ancestral protection strategy against dithiol compounds. This ability is also shared by multiple Ascomycota such as *A. nidulans* and *A. niger* which do not synthesise ETPs. Data in this chapter also highlighted the metabolic cost of gliotoxin bisthiomethylation by *A. fumigatus* as this process demands two molecules of SAM per dithiol gliotoxin molecule. As SAM is an essential cellular cofactor that is required for cellular function, this is quite an expensive metabolic commitment. Quantitative proteomic data from *ΔgliT: gtmA* uncovered further details behind the elaborate mechanism of *gli*-cluster control in *A. fumigatus* – a process which remains to be elucidated. Also, late-stage culture proteomics and metabolomics reveals that GtmA activity affects the production of other secondary metabolites produced by *A. fumigatus*. Gliotoxin is a potent toxin with a very elaborate mechanism regulating its production. Targeting this pathway may serve as a mechanism to turn this toxin against its producer.

Chapter 7

Bis(methyl)gliotoxin as a biomarker for *A. fumigatus* Infection

7.1 Introduction

As described in Section 1.9, IA is the most commonly found invasive mould disease and is a major source of mortality in immunocompromised individuals. Incidences of IA have increased markedly over recent years (Perfect, 2013). It is well established that sensitive, nonculture-based diagnostic mechanisms which rapidly detect the onset of infection are of critical importance to permit the rational administration of antifungal drugs (Johnson et al., 2014).

The detection of nonribosomal cyclic peptides and depsipeptides by MS may serve as highly specific fungal markers (Jegorov and Hajduch, 2006). Gliotoxin, which is produced by most *A. fumigatus* strains is present in plasma and serum (Fox and Howlett, 2008). Also, its inactive derivative bis(methylthio)gliotoxin is recoverable from blood (Domingo et al., 2012). A recent report described the MS detection of a gliotoxin precursor, cyclo (L-Phe-L-Ser), in the lungs of mice which were colonised by *A. fumigatus*. This metabolite may serve as an alternative marker for the diagnosis of invasive aspergillosis (Sekonyela et al., 2013). Immunodetection of human IgG directed against the *Aspergillus* gliotoxin oxidoreductase may have potential as a diagnostic biomarker of IA in nonimmunocompromised individuals (Shi et al., 2012).

The ELISA has been established as a robust method for clinical diagnostics. This technique relies on the interaction of the analyte with specific antibodies. A major advantage of competition ELISA is its high sensitivity to minimally expressed antigens in complex mixtures even when the detecting antibody is present in relatively small amounts (Gan and Patel, 2013). An inherent problem with producing antibodies against small molecules is that these molecules are too small to initiate an immune response on their own (Tuomola et al., 2000). In order to raise high affinity antibodies, the small molecule, or a modified version of the molecule (a hapten), is covalently bound to a

carrier protein to form an immunogenic toxin (hapten)–protein conjugate. Vaccination of an animal with the conjugate, when formulated with a suitable adjuvant, results in the *in vivo* production of a polyclonal suite of antibodies, some of which will be cross-reactive to the toxin (hapten) portion (epitope) of the immunogenic conjugate. The toxin-specific antibodies which are thereby generated are incorporated into various ELISA formats. These formats rely on the capture of the analyte by the antibodies and a resultant induction of change (e.g. color) which correlates with the level of analyte present in the sample (Singh et al., 2004).

Several chemistries have successfully been utilised to create hapten-protein conjugates (Lu et al., 2006; Fox et al., 2004). A common method for coupling these haptens to carrier proteins involves the use of a heterobifunctional crosslinker containing an N-Hydroxysuccinimide (NHS) ester and a maleimide group. This type of crosslinker allows better control over the coupling process than homobifunctional or zero-length conjugation methods as it incorporates a 2- or 3-step reaction strategy which is directed against two different functional targets. In this approach, the carrier protein is initially activated with the crosslinker through its amine groups. It is subsequently purified to remove excess reactants and, finally, it is crosslinked to a hapten molecule containing a sulfhydryl group. One of the most useful reagents for this conjugation approach is sulfosuccinimidyl 4-(N-maleimidomethyl)cyclohexane-1-carboxylate (sulfo-SMCC) (Kafi et al., 2009).

The reactions associated with a sulfo-SMCC conjugation are shown in Figure 7.1. This crosslinking reagent mediates the conjugation of a carrier protein through primary amino groups to a peptide or other hapten through sulfhydryl groups. It contains both a reasonably long spacer and an extremely stable maleimide group which is due to the adjacent cyclohexane ring in its cross-bridge. The active N-hydroxysulfosuccinimide

ester (sulfo-NHS) end of sulfo- SMCC is first reacted with available primary amino groups on the carrier protein. This reaction results in the formation of an amide bond between the protein and the crosslinker with the release of sulfo-NHS as a by-product. The carrier protein is then isolated by gel filtration in order to remove excess reagents. At this point, the purified carrier possesses modifications which were generated by the crosslinker. This results in a number of reactive maleimide groups projecting from its surface. The maleimide portion of sulfo-SMCC is a thiol-reactive group that can be used in a secondary step to conjugate with a free sulfhydryl (i.e., a cysteine residue) on a peptide or other hapten, resulting in a stable thioether bond. A disadvantage to using SMCC, or other NHS–maleimide type crosslinkers with hindered ring structures, is the relatively high immunogenicity of the cross-bridge. A PEG group used as a cross-bridge in a heterobifunctional reagent to prepare immunogen conjugates will result in non-immunogenic modifications on the carrier protein and, thus, no antibody production against the polyether linker (Hermanson, 2008).

Due to its intrinsic immunogenicity, KLH is a popular carrier protein and a frequent choice for the development of immunogen conjugates (Presicce et al., 2008). KLH contains an abundance of functional groups which are available for conjugation with hapten molecules. On a per-mole basis (using an average multi-subunit MW of 5 x 10^6 Da), KLH has over 2,000 amines from lysine residues, over 700 sulfhydryls from cysteine groups and over 1,900 tyrosines. Activation of the protein with sulfo-SMCC typically results in 300–600 maleimide groups per molecule for coupling to sulfhydryl-containing hapten (Hermanson, 2008).

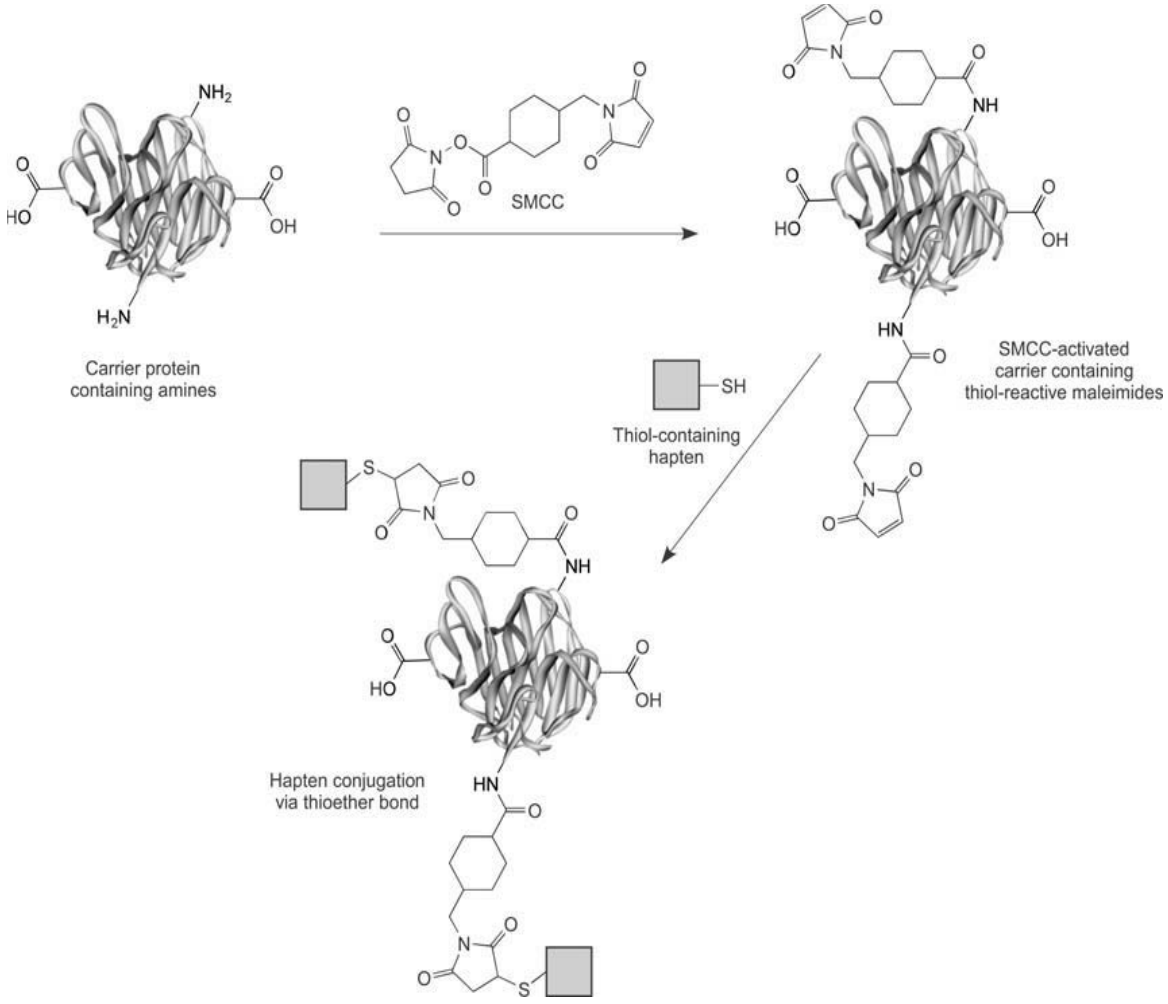

Figure 7.1. NHS Ester-Maleimide Heterobifunctional Crosslinker-Mediated Hapten–Carrier Conjugation. A common way of conjugating sulfhydryl-containing haptens to carrier proteins is to activate the carrier with sulfo-SMCC in order to create an intermediate maleimide derivative. The maleimide groups can then be coupled to thiols to form thioether bonds.

The aim of the work presented in this chapter was to explore the potential of the inactive derivative of gliotoxin, bis(methylthio)gliotoxin (BmGT), as a marker for *A. fumigatus* presence. NHS ester-maleimide mediated hapten–carrier conjugation requires that the hapten has a free sulfhydral group. However, bis(methylthio)gliotoxin does not possess any free sulfhydrals to avail of this conjugation chemistry. Furthermore, bis(methylthio)gliotoxin has no carboxyl groups which could be activated for carbodiimide conjugation using the popular crosslinker EDC. Due to the lack of functional groups which are available to conjugate bis(methylthio)gliotoxin to a carrier protein, traditional conjugation methodologies could not be used.

Mono(methylthio)gliotoxin was shown in Chapter 5 to be an intermediate in the conversion of dithiol gliotoxin to bis(methylthio)gliotoxin (Section 5.2.6). Based on the similar structures of these metabolites, we hypothesise that it was likely that MmGT and bis(methylthio)gliotoxin have similar epitopes. These may result in antisera generation which is cross reactive to both of these metabolites. Mono(methylthio)gliotoxin has a free sulfhydryl available for NHS ester-maleimide mediated hapten–carrier conjugation. This infers that standard conjugation methodologies could be used to conjugate this hapten to a carrier protein such as bovine serum albumin (BSA) or keyhole limpet hemocyanin (KLH). An additional might lie in the fact that these antibodies may also be cross-reactive to gliotoxin.

The overall objectives of the work presented in this chapter were to:

(i) Explore the detection capabilities of gliotoxin and bis(methylthio)gliotoxin by RP-HPLC and LC-MS

(ii) Develop and optimise a conjugation strategy to generate an immunogen to raise antisera against bis(methylthio)gliotoxin.

(iii) Develop a competitive ELISA for bis(methylthio)gliotoxin detection.

7.2 Results

7.2.1 Bis(methylthio)gliotoxin is detected at a higher intensity than gliotoxin by LC-MS, but not by RP-HPLC

Commercial standards of gliotoxin and bis(methylthio)gliotoxin (5 µg) were analysed by RP-HPLC. As shown in Figure 7.2 A, 5 µg bis(methylthio)gliotoxin and gliotoxin were detected at similar intensities by RP-HPLC at 254 nm. In addition, the RP-HPLC analysis of organically extracted *A. fumigatus* Czapeks Dox broth 72 h culture supernatants indicated that the level of bis(methylthio)gliotoxin detected in the supernatants was significantly lower than that of gliotoxin (Figure 7.2, B). Although bis(methylthio)gliotoxin was detected at extremely low levels in culture supernatants by RP-HPLC, the same samples, when analysed by electrospray LC-MS, showed a significantly higher intensity of detectable bis(methylthio)gliotoxin in comparison with gliotoxin (Figure 7.3). Serial dilutions of commercial bis(methylthio)gliotoxin and gliotoxin standards were analysed by LC-MS (Figure 7.4). Identical concentrations of each were analysed by LC-MS with bis(methylthio)gliotoxin proving to be consistently detectable at higher intensities than gliotoxin. This unusual property explains the differential detection of bis(methylthio)gliotoxin and gliotoxin by RP-HPLC and LC-MS, respectively.

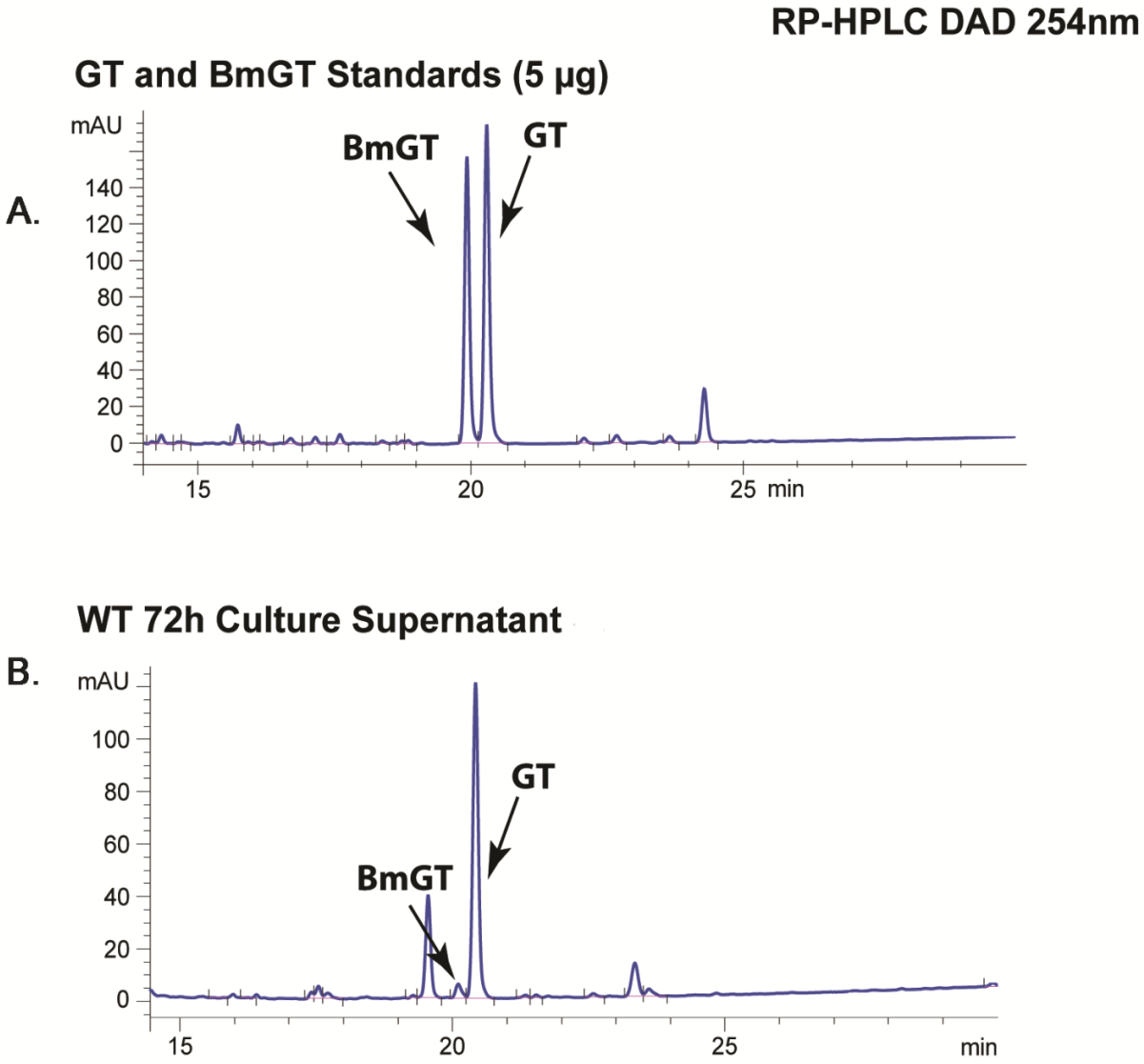

Figure 7.2. A: RP-HPLC detection of gliotoxin and bis(methylthio)gliotoxin commercial standards. 5 µg of each standard was injected. Bis(methylthio)gliotoxin elutes at a slightly earlier retention time than gliotoxin. The compounds have similar mAU intensities at 254 nm. **B:** *A. fumigatus* wild-type organically extracted Czapeks dox both 72 h culture supernatants showing the relative gliotoxin and bis(methylthio)gliotoxin intensities. Bis(methylthio)gliotoxin is present in culture supernatants at low levels when compared to gliotoxin.

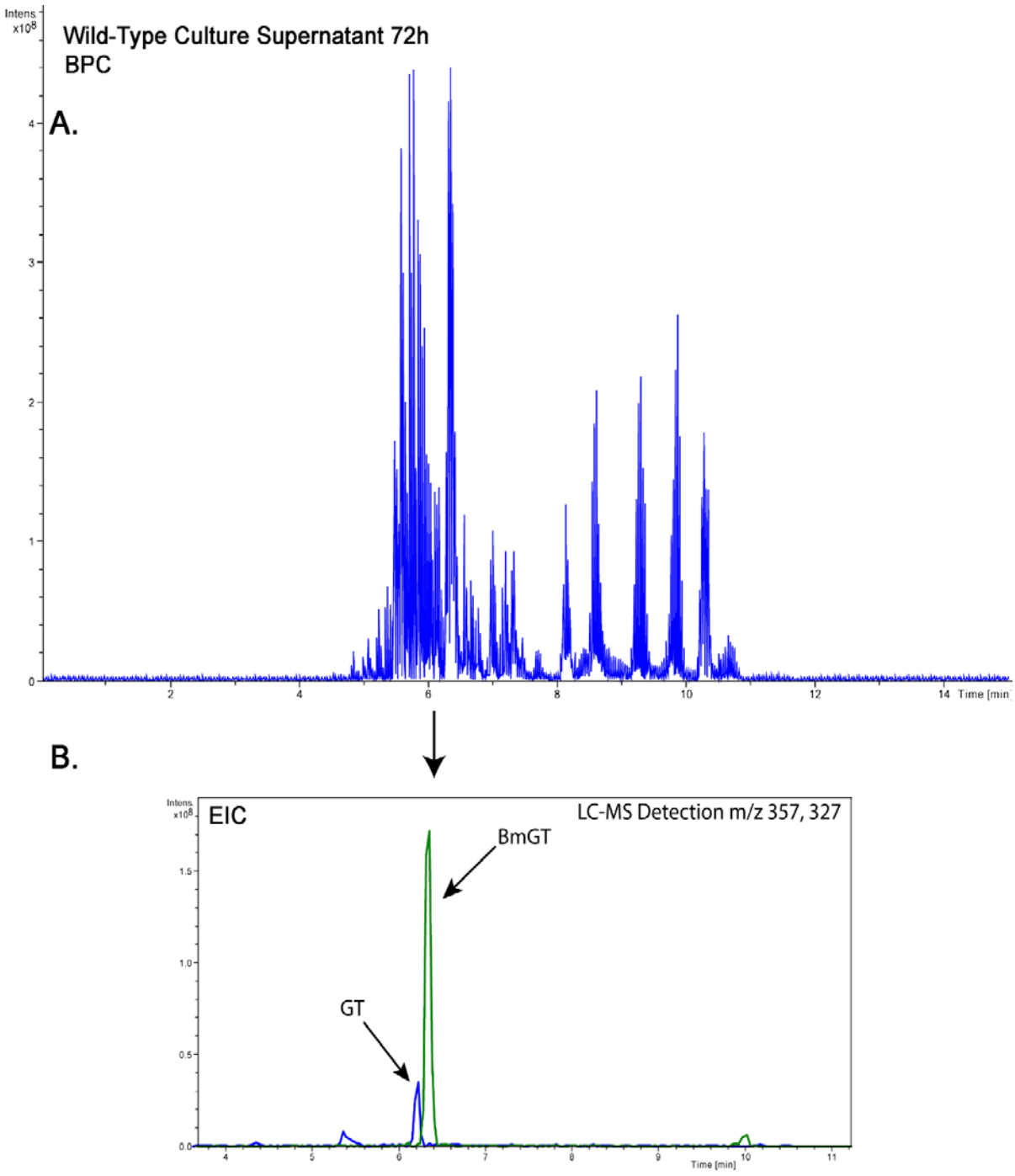

Figure 7.3. LC-MS detection of gliotoxin and bis(methylthio)gliotoxin in *A. fumigatus* wild-type organically extracted culture supernatants. **A:** Base peak chromatogram of sample showing all compounds detected. **B:** Extracted ion chromatogram showing the overlaid extracted *m/z* 357 (BmGT) and 327 (GT) compound intensities. Note the significantly higher bis(methylthio)gliotoxin intensity which contrasts with that of gliotoxin.

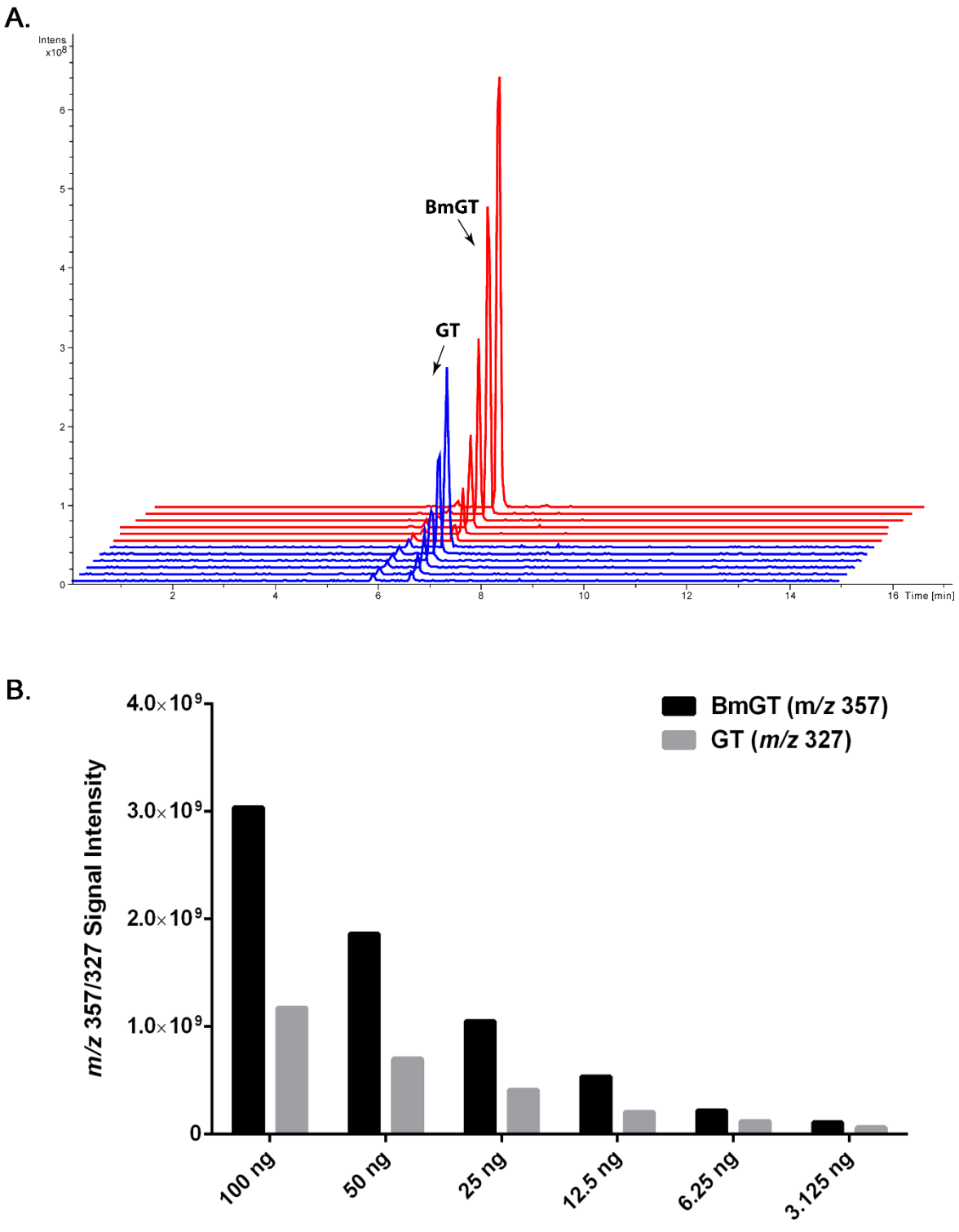

Figure 7.4. A: Differential detection of serially diluted gliotoxin and bis(methylthio)gliotoxin commercial standards by LC-MS. Bis(methylthio)gliotoxin (red) is detected at a substantially greater intensity by electrospray LC-MS than gliotoxin (blue) by LC-MS. **B:** Bis(methylthio)gliotoxin and gliotoxin detection intensities plotted across the dilution series.

7.2.2 Strategy for the generation of antibodies against bis(methylthio)gliotoxin

A. fumigatus GtmA generates mono(methylthio)gliotoxin as an intermediate in the generation of bis(methylthio)gliotoxin. The use of a high GtmA enzyme concentration and a low concentration of SAM cofactor resulted in the preferential generation of mono(methylthio)gliotoxin rather than bis(methylthio)gliotoxin (Section 5.2.6). Initially, mono(methylthio)gliotoxin generation for immunogen generation was carried out using the rGtmA protein with SAM as the methyl donor in the reaction. This method efficiently generated MmGT. However, as dithiol gliotoxin requires an organic solvent for solubility at high concentrations, a large reaction volume was necessary in order to maintain GtmA solubility and activity in the reaction. As additional steps were required to concentrate the sample after the methylation reaction, it resulted in a lower overall yield of MmGT. This highlighted the need to carry out the generation of MmGT using the alternative strategy which is illustrated in Figure 7.5. Methyl iodide is a methylation reagent which can be used to add methyl groups to substrates such as phenols, amines, thiols or carboxylic acids. This reagent is frequently used in a variety of studies to chemically synthesise ETPs and other biologically active secondary metabolites (Boyer et al., 2013). As such, it was used as a chemical alternative to GtmA in order to generate MmGT.

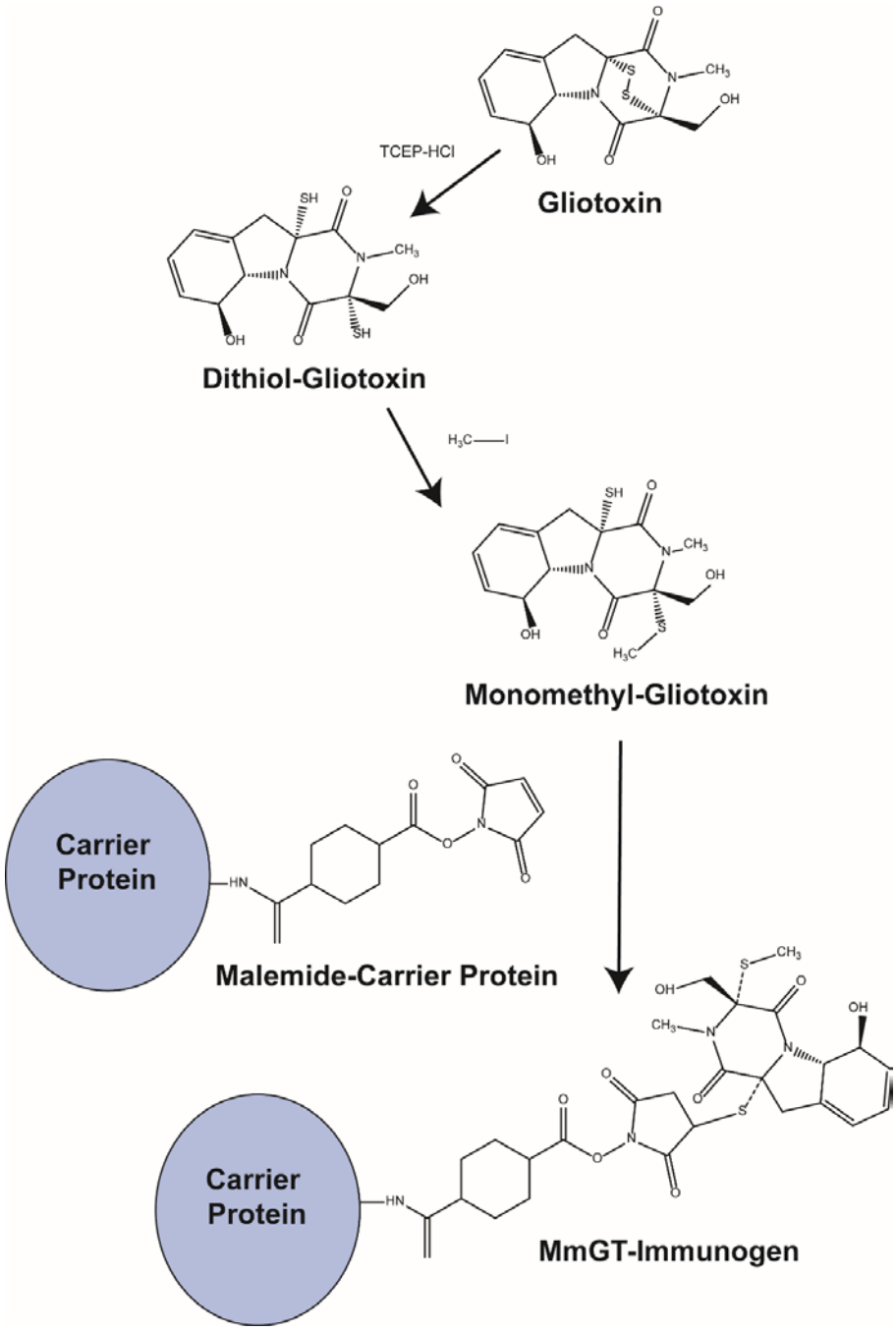

Figure 7.5. Strategy for the generation of the mono(methylthio)gliotoxin immunogen. MmGT has a free sulfhydral group available for NHS ester-maleimide mediated conjugation. This allows for the hapten to be conjugated to a large carrier protein for immunisation trials.

7.2.3 Generation of mono(methylthio)gliotoxin (MmGT) using Methyl Iodide

Methyl iodide (Figure 7.6) is a widely employed methylation agent which is used in organic synthesis for the covalent modification of thiol groups. It is an excellent substrate for S_N2 substitution reactions as it is sterically open for attack by nucleophiles (Bolt and Gansewendt, 1993). Figure 7.7 shows the optimisation of mono(methylthio)gliotoxin generation using methyl iodide as a methyl donor. The final optimised reaction conditions for mono(methylthio)gliotoxin generation are outlined in Section 2.2.18. Confirmation of mono(methylthio)gliotoxin generation was carried out by RP-HPLC fractionation of the metabolite followed by LC-MS analysis. The fragmentation patterns of ICH_3 and GtmA generated mono(methylthio)gliotoxin were identical (Figure 7.8). Confirmation of available free thiol on mono(methylthio)gliotoxin was carried out by the addition of sulfo-SMCC to the reaction. This reagent contains a sulfhydryl-reactive maleimide group (Figure 7.1). As outlined in Figure 7.9, the addition of sulfo-SMCC to the reaction resulted in a reduction in the mono(methylthio)gliotoxin peak but not the bis(methyl)gliotoxin peak; this was shown by RP-HPLC following reaction with sulfo-SMCC.

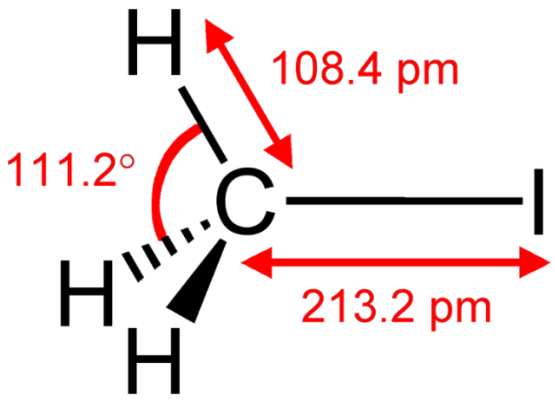

Figure 7.6. Structural formula of the methyl iodide (iodomethane) molecule, MeI, CH_3I. Structural information (determined by microwave and infrared spectroscopy) (Lide, 2007).

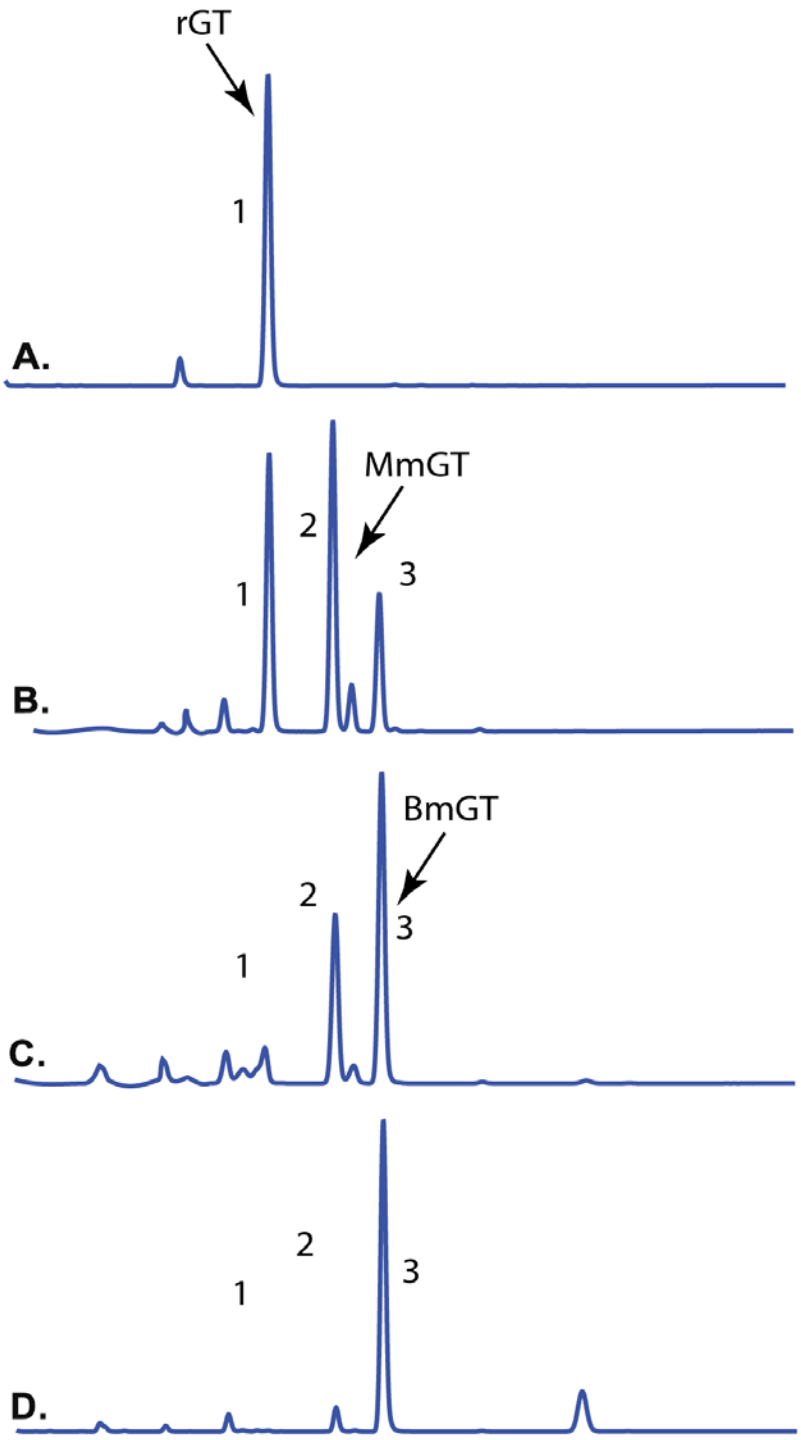

Figure 7.7. S-methylation of 3 mM dithiol gliotoxin using 5 mM Iodomethane (ICH_3) at 37°C as monitored by RP-HPLC. Increasing the reaction incubation time results in a sequential increase in the amount of mono(methylthio)gliotoxin and bis(methyl)gliotoxin. **A:** No ICH_3, **B:** 15 min ICH_3,**C:** 30 min ICH_3, **D:** 60 min ICH_3. 1: dithiol gliotoxin (rGT), 2: MmGT, 3: BmGT.

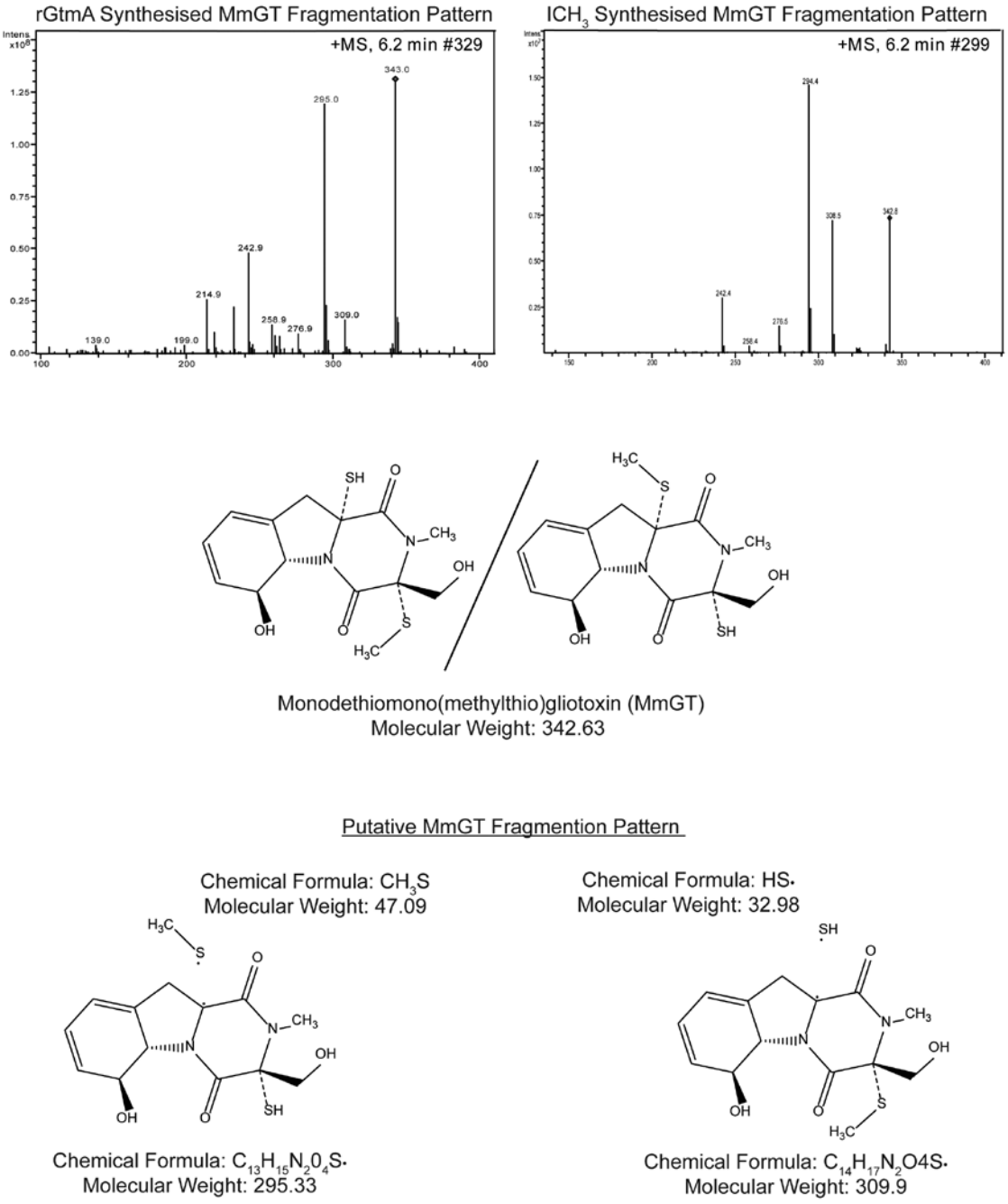

Figure 7.8. LC-MS fragmentation pattern of rGtmA and ICH_3 generated mono(methylthio)gliotoxin. The identical LC-MS retention times and fragmentation patterns of mono(methylthio)gliotoxin are also shown with the potential source of the *m/z* 295 and *m/z* 309 fragments. The existence of *m/z* 295 fragment confirms that the CH_3 is located on the sulfhydral of mono(methylthio)gliotoxin.

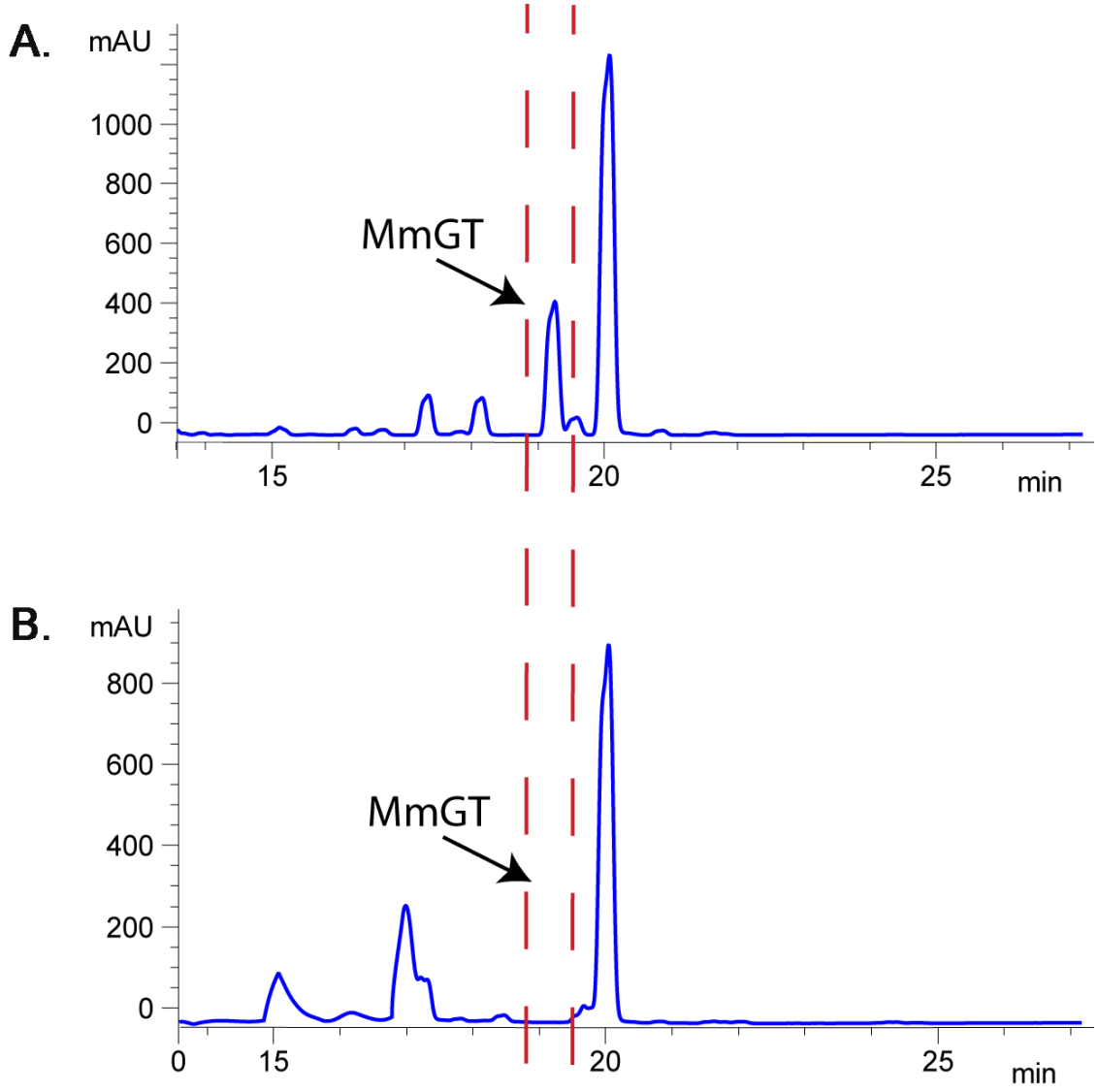

Figure 7.9. A: Following the methylation reaction, bis(methylthio)gliotoxin elutes at RT 20.1 min on the chromatogram: mono(methylthio)gliotoxin (19.2 min) and dithiol gliotoxin (18.3 min) are also present. **B:** Following the addition of SMCC to the reaction, the peaks for dithiol gliotoxin and mono(methylthio)gliotoxin are no longer detectable. This indicates that the mono(methylthio)gliotoxin compound has a free thiol which is capable of reacting with sulfo-SMCC.

7.2.4 Mono(methylthio)gliotoxin conjugation to BSA-sulfo-SMCC

BSA-sulfo-SMCC was generated as described in Section 2.2.19. The mono(methylthio)gliotoxin generated in Section 7.2.3 was immediately added to the BSA-sulfo-SMCC and the reaction was left to incubate overnight at room temperature. Figure 7.10 shows that the addition of mono(methylthio)gliotoxin to BSA-sulfo-SMCC results in a decrease in free mono(methylthio)gliotoxin from the reaction. This was detected by RP-HPLC. No reduction in the mono(methylthio)gliotoxin peak was observed when sulfo-SMCC was omitted from the reaction therefore confirming that the hapten was covalently linked to the carrier protein.

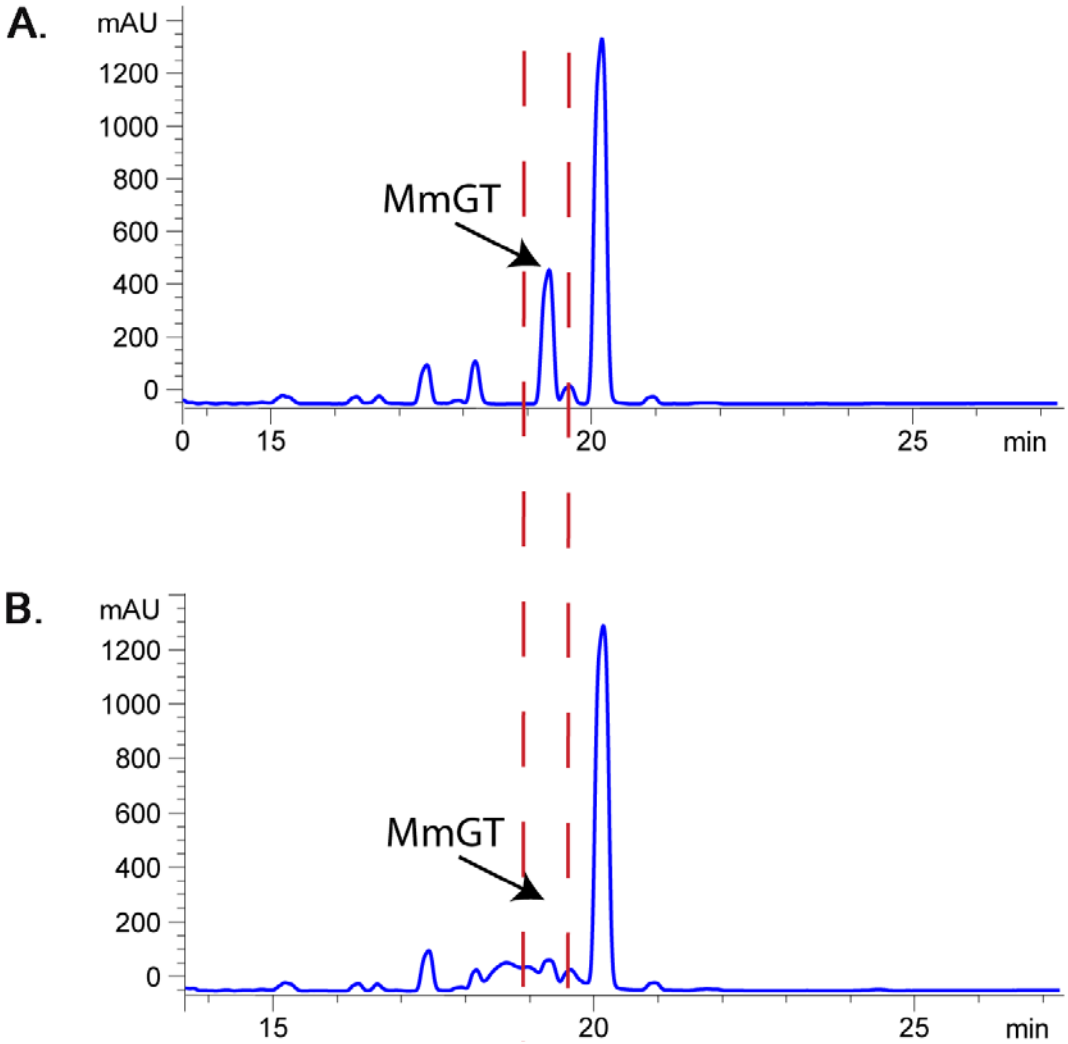

Figure 7.10. A: In the control sample (MmGT + BSA Control (No SMCC), bis(methylthio)gliotoxin is detectable at 20.1 min on the chromatogram - MmGT (RT 19.2 min) and dithiol gliotoxin (18.3 min) are also visible. **B:** Following the addition of sulfo-SMCC-BSA to the reaction, the peaks for MmGT are reduced in the chromatogram. This indicates that the MmGT has covalently attached to the sulfo-SMCC-BSA.

7.2.5 SDS-PAGE Confirmation of MmGT-sulfo-SMCC-BSA Generation

The covalent attachment of mono(methylthio)gliotoxin to the carrier protein (MmGT-sulfo-SMCC-BSA) was predicted to have an increased molecular mass when compared to that of BSA-sulfo-SMCC alone. As confirmed by SDS-PAGE analysis, an increased molecular mass for the BSA-SMCC-MmGT immunogen in comparison with that of the BSA-SMCC control was evident (Figure 7.11). In contrast with the unconjugated BSA-SMCC or BSA controls, the BSA-mono(methylthio)gliotoxin immunogen was visible as a higher band on the SDS-PAGE gel. As BSA contains one free cysteine sulfhydryl, the appearance of two separate protein bands in the BSA-SMCC-MmGT and BSA-SMCC lanes is likely due to the dimerization of BSA-SMCC through this free thiol group. This data further substantiates the success of the conjugation.

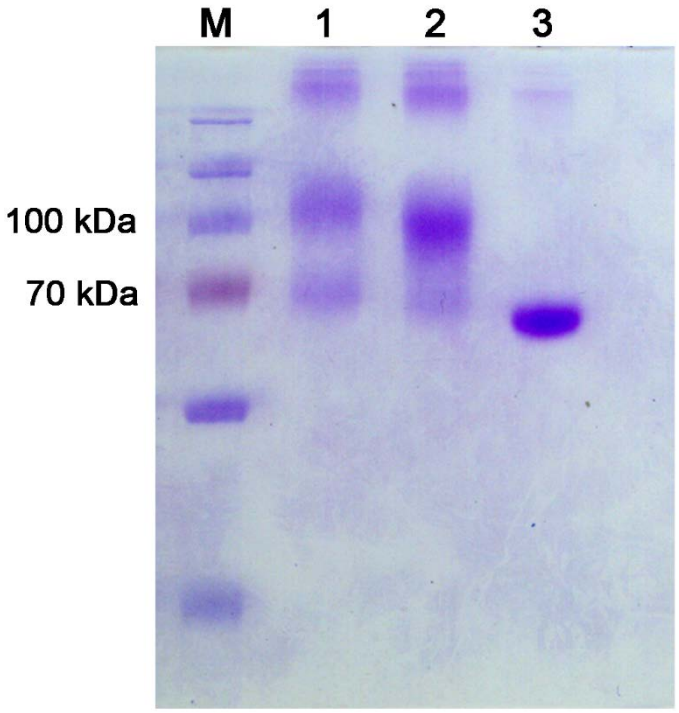

Figure 7.11. SDS-PAGE analysis demonstrating an increased M_r for the BSA-sSMCC-MmGT conjugate (Lane 1) when compared to that of the BSA-SMCC control (Lane 2). The appearance of two bands in the BSA-sSMCC-MmGT / BSA-sSMCC lanes in comparison to the single unmodified BSA band (Lane 3) is likely due to the dimerization of BSA-sSMCC through its free thiol groups. 2 μg protein was loaded per well.

7.2.6 Generation of MmGT-KLH

As described in Section 7.1, keyhole limpet hemocyanin, KLH, is a popular carrier protein and a common choice for developing immunogen conjugates. Furthermore, the employment of the KLH carrier protein for immunisation processes allows the MmGT-sulfo-SMCC-BSA immunogen generated in Section 7.2.4 to be utilised in the screening of the resulting antisera for mono(methylthio)gliotoxin reactivity. Section 2.2.19 describes the procedure which was adopted for KLH immunogen generation. RP-HPLC confirmed the successful generation of MmGT-sulfo-SMCC-KLH. Figure 7.12 shows that, following incubation with maleimide-KLH, the level of mono(methylthio)gliotoxin in the conjugation reaction drops over time. The SDS-PAGE electrophoresis bands of KLH and MmGT-KLH yielded non-conclusive results as the KLH protein is too large to move in the polyacrylamide gel (data not shown). As such, the sole purpose of RP-HPLC was to corroborate the success of this conjugation.

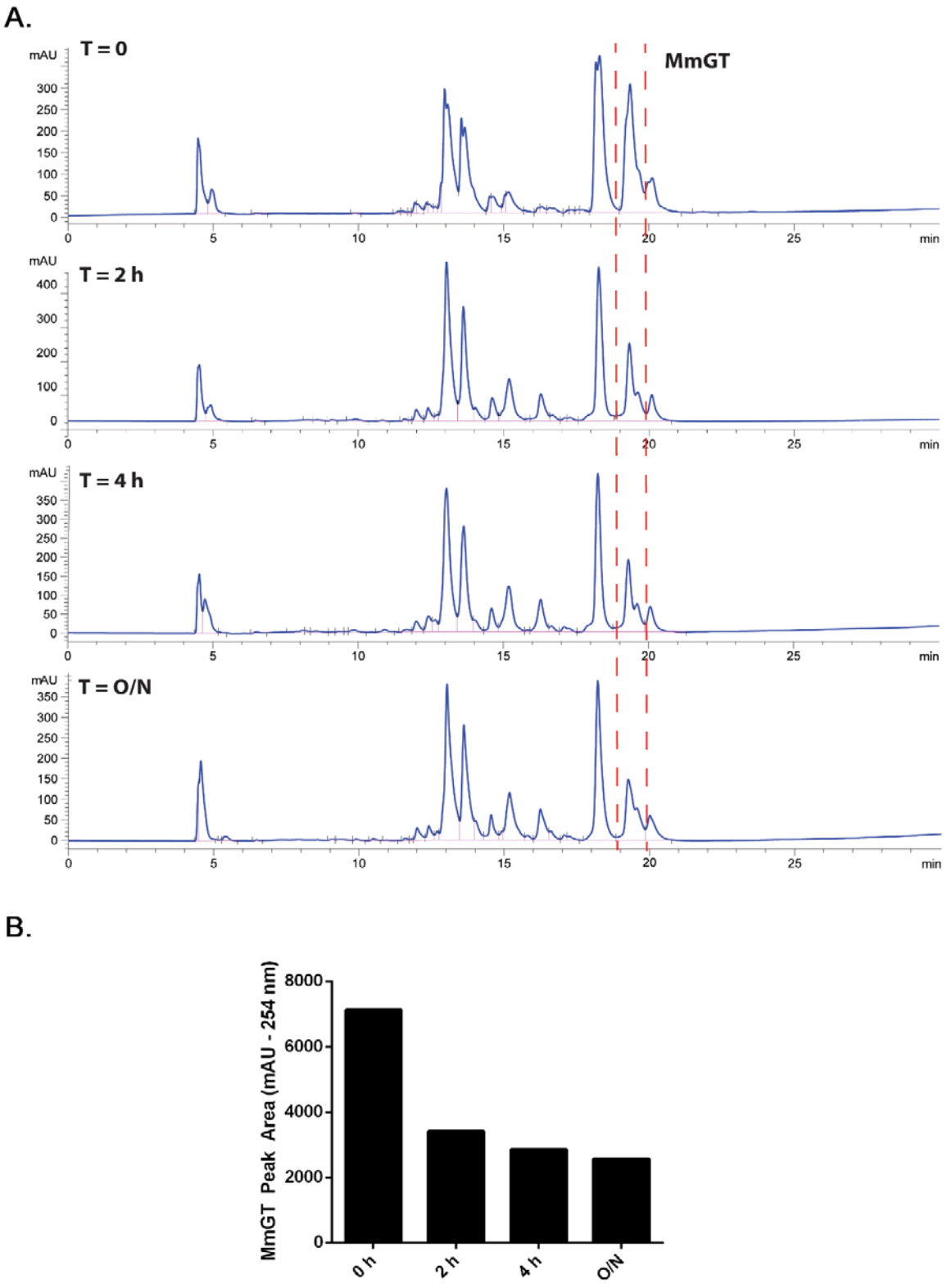

Figure 7.12. A: RP-HPLC chromatograms illustrating the reduction in the mono(methylthio)gliotoxin peak over the course of the conjugation reaction with maleimide KLH (0 h to O/N). **B:** A graphical representation of the MmGT peak area reduction (mAU, 254 nm) over the course of the conjugation reaction.

7.2.7 Immunisation of Mice with MmGT-KLH Immunogen

MmGT-KLH at 1 mg/ml in PBS was provided to Dublin City University for murine immunisation. For primary immunisations and booster injections, 50 µl of Pam-Cys Adjuvant was added to 50 µl of immunogen. The mice received a single intraperitoneal injection of 100 µl each (50 µg immunogen/injection). This was repeated in three boosters each of which were administered over 3 week intervals. Following the third booster, tail bleeds were taken and the sera was fractionated. 20 µl sera per mouse was harvested for screening.

7.2.8 Development of a Competitive ELISA for the screening of antibodies specific for bis(methylthio)gliotoxin from immunised mice

A competitive ELISA was developed to screen the antisera generated in Section 7.2.7 for antibodies reactive to bis(methylthio)gliotoxin. The schematic for this assay is illustrated in Figure 7.13. This screening process would identify the immunised mouse (Section 7.2.7) which would be most suitable to proceed to monoclonal BmGT antibody development. MmGT-BSA was coated onto the ELISA plate and wells were blocked to prevent non-specific binding. Bis(methylthio)gliotoxin was then added to selected wells as a free competitor in order to determine whether this metabolite was capable of competing for the antibodies which bind to the MmGT-BSA coated ELISA plate. Sera, which potentially contained antibodies that are reactive against bis(methylthio)gliotoxin, was then added to the ELISA wells. After washing away the unbound antibody, any antibodies which were bound to the plate were detected by anti-mouse IgG-HRP. This detection was then visualised by the addition of HRP substrate, TMB and the signal measured photometrically at 450/ 620 nm. Following completion of the assay, a reduction in the binding signal in the wells containing added bis(methylthio)gliotoxin confirmed that the antisera contains antibodies which are specific for this metabolite.

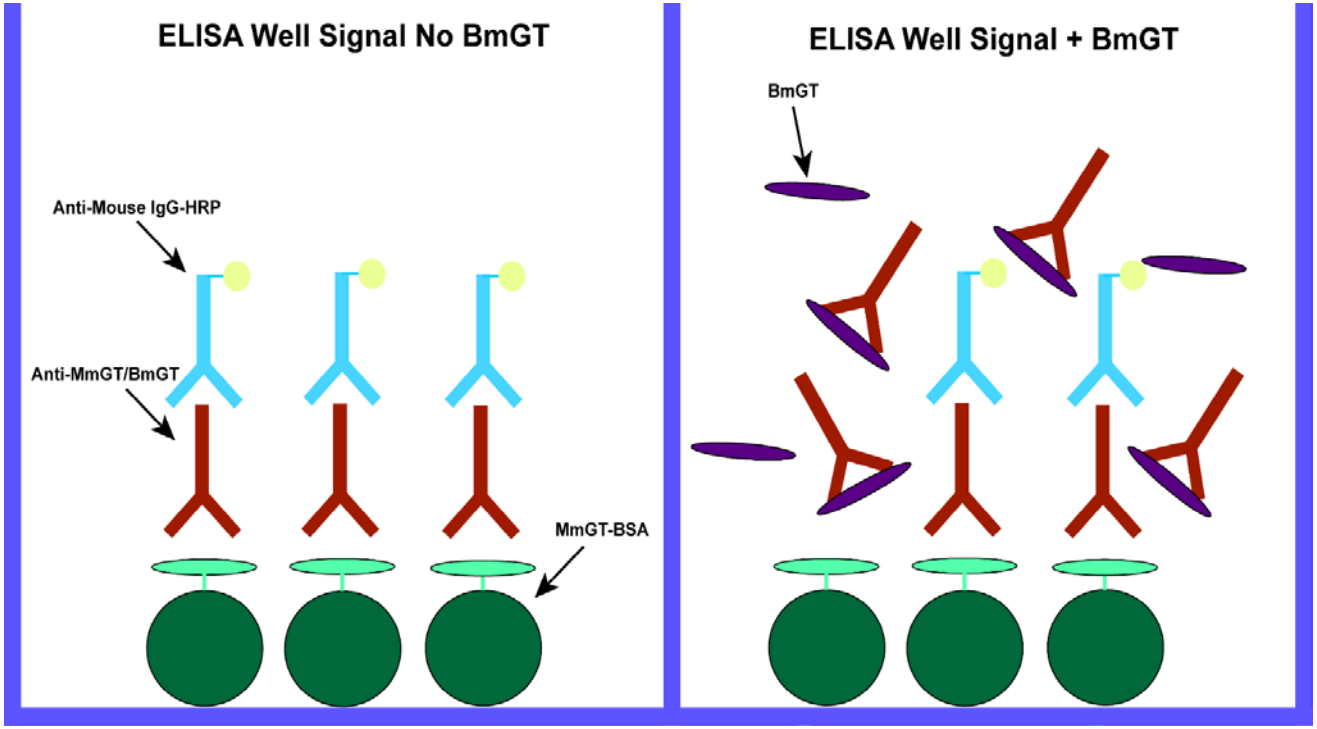

Figure 7.13. Illustration of the competitive ELISA format for screening MmGT-KLH immunised mice sera for antibodies specific for bis(methylthio)gliotoxin. MmGT-BSA was coated on the ELISA plate. Varying concentrations of competing free BmGT were then added to select wells in order to establish whether the BmGT metabolite was capable of competing for the antibodies which were binding to the ELISA plate. Sera were then added to the ELISA wells. Following a plate wash step, detection was visualised via the addition of HRP substrate, A significant signal reduction in the wells containing BmGT (right panel) when compared to the background signal (left panel) was indicative of the presence of anti-BmGT antibodies in the test antiserum.

7.2.9 Determination of working dilution of serum for competitive ELISA screening

An indirect ELISA with a range of antiserum titres and MmGT-BSA coating was carried out to identify the optimal ELISA conditions. ELISA plates were coated with MmGT-BSA at 1 µg/ml. After blocking, antisera dilutions of 1/40,000, 1/80,000, 1/120,000, 1/160,000 and 1/200,000 were added to ELISA wells for mice A, B and C. As shown in Figure 7.14, the antisera dilution of 1/160,000 was deemed to be within the parameters of the assay (Delta OD < 2). This antisera dilution was used during further sera analysis by indirect competitive ELISA (Section 7.2.10).

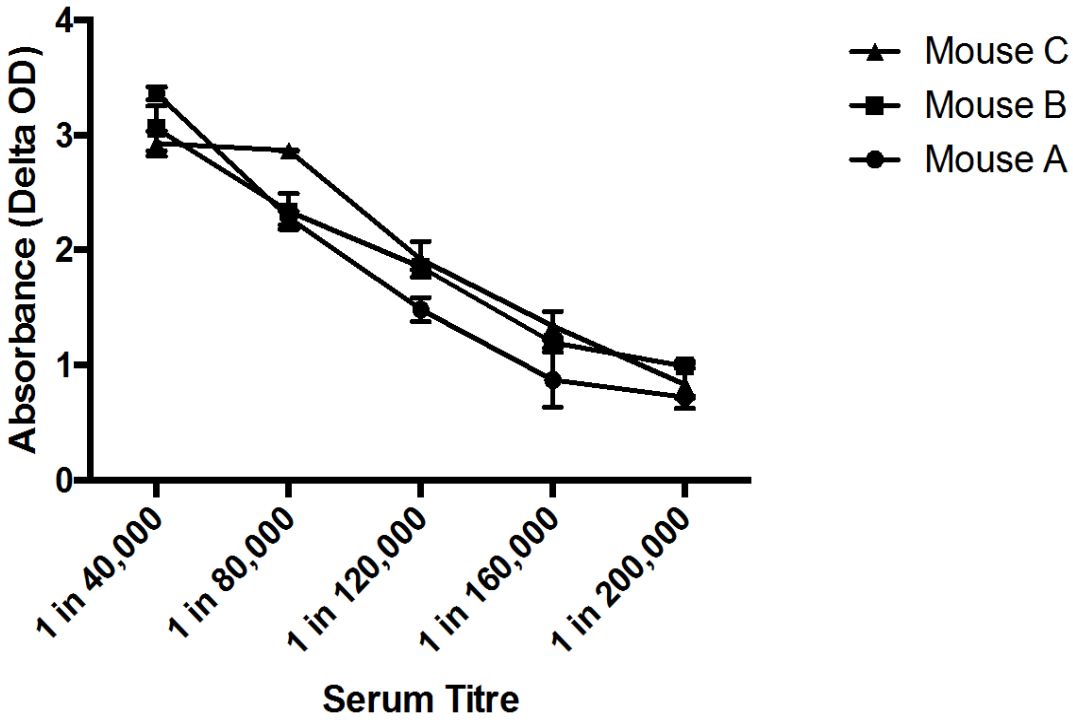

Figure 7.14. Optimisation of antiserum dilutions for polyclonal antibody analysis. The absorbance readings for the 1/40,000 to 1/120,000 were deemed to be outside of the assay parameters.

7.2.10 ELISA Testing of Tail-Bleeds from Mice (3) Immunised with MmGT-KLH Immunogen

The optimised ELISA conditions are detailed in Section 2.2.20. Plates were coated with MmGT-BSA at 1 μg/ml. After blocking, a titre of free competing BmGT 0-150 μM was added to ELISA wells. Sera from mice A, B and C was then added to each well at a 1/ 160,000 dilution. As shown in Figure 7.15, free BmGT significantly ($p < 0.05$) inhibited antibodies from sera A and C binding to the coated MmGT-BSA. Mouse C sera was shown to have the most significant ($p = 0.001$) reduction in signal following the addition of competing BmGT when compared with the DMSO control. The control plate coated with SMCC-BSA confirmed that the reaction was specific to the MmGT antigen. This result indicated that the Mouse C sera contained antibodies with an affinity for bis(methylthio)gliotoxin. Subsequently, based on the results of the various antisera dilutions and conditions tested, the ELISA was replicated using the Mouse C antisera which was diluted to 1/120,000 (Table 7.1). The addition of 100 μM bis(methylthio)gliotoxin to the reaction resulted in a significant depletion ($p = 0.001$) of the assay signal which contrasted with that of the DMSO control.

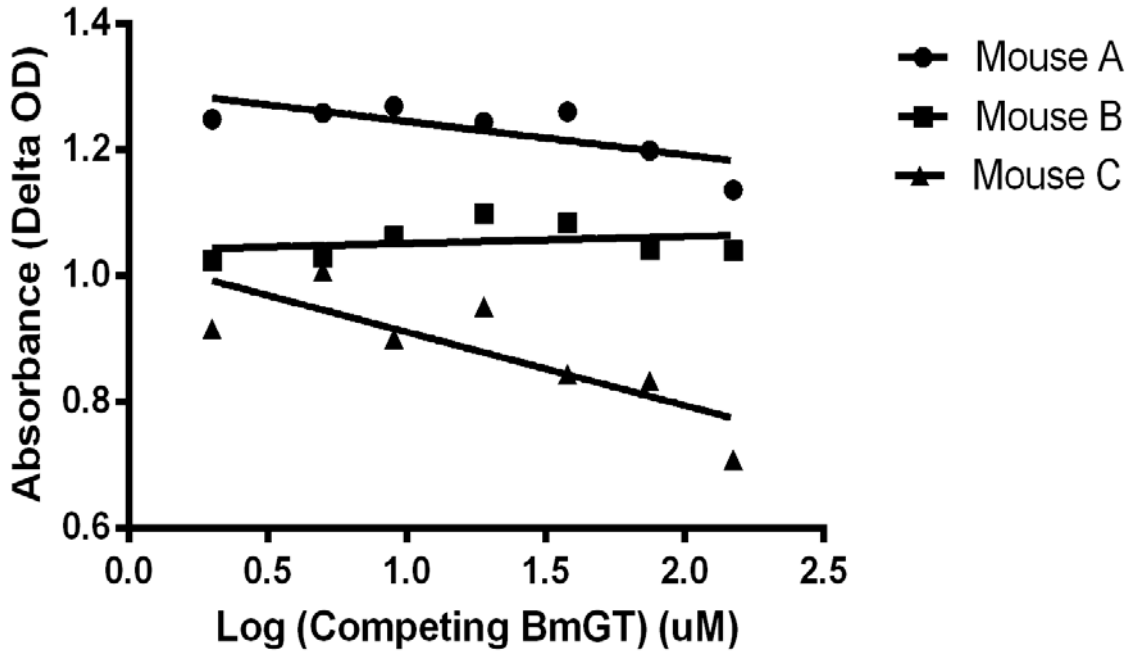

Figure 7.15. Linear regression analysis of competitive ELISA data from sera A, B and C. Mouse C sera was shown to have the most significant (*p*= 0.001) reduction in signal following the addition of competing BmGT.

Table 7.1. Mouse C Sera competes with bis(methylthio)gliotoxin for MmGT-BSA

Mouse C Sera (1 in 120,000)				
MmGT-BSA (µg/ml)	**100 uM BmGT**	**100 uM BmGT**	**0 uM BmGT**	**0 uM BmGT**
1	1.535	1.566	1.89	1.875
0.5	2.004	1.914	2.193	2.218
0.25	2.085	2.173	2.251	2.206
0.125	2.12	2.208	2.383	2.424
0.06125	2.318	2.067	2.421	2.564
0.03	2.201	2.056	2.306	2.321
0.015	2.038	1.852	1.926	1.9
0	0.034	0.018	0.021	0.034

7.2.11 Mouse C Antisera Competes with bis(methylthio)gliotoxin but not TAFC for MmGT-Sulfo-SMCC-BSA

Based on the results from the sera dilution optimisation carried out in Section 7.2.9, the selected antisera dilution was 1/120,000 and the MmGT-sSMCC-BSA coating concentration was 1 μg/ml. As shown in Figure 7.16, the concentration of competing free bis(methylthio)gliotoxin was titred down the plate. This demonstrated that the antisera contains antibodies which compete for bis(methylthio)gliotoxin in a dose dependent manner. No competition for bis(methylthio)gliotoxin was observed when the pre-bleed sera from mouse C was used or when sSMCC-BSA was coated on the plates. Critically, the addition of triacetylfusarinine C (TAFC), another small natural product of *A. fumigatus*, did not result in a reduction in the assay signal. Overall, these results confirm that mouse C, which was immunised with MmGT-sSMCC-KLH immunogen, generated antibodies which are reactive against bis(methylthio)gliotoxin. The spleen of mouse C was selected for harvesting for the generation monoclonal antibodies against bis(methylthio)gliotoxin.

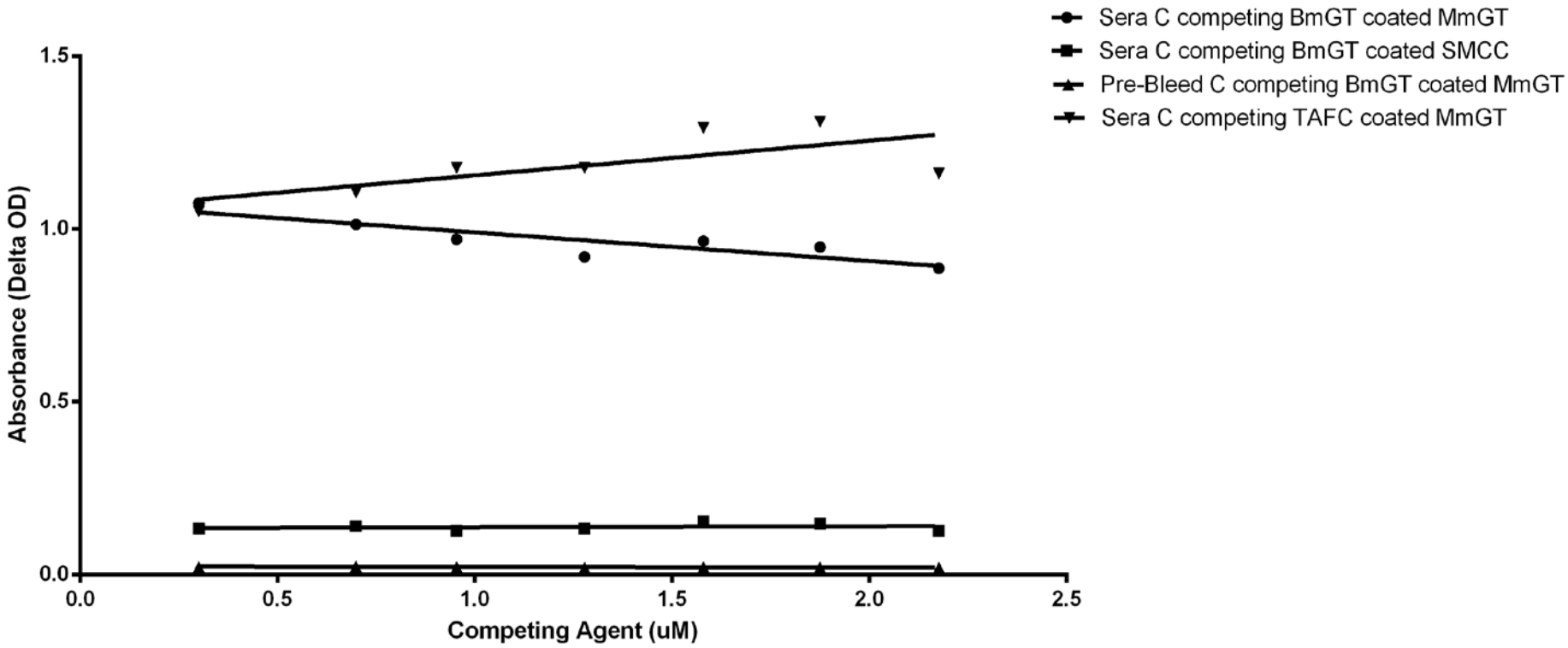

Figure 7.16. Sera C competes with bis(methylthio)gliotoxin for coated MmGT. This is confirmation that the sera contains antibodies against the bis(methylthio)gliotoxin antigen.

7.3 Discussion

Recent literature has explored the potential of fungal secondary metabolites as specific methods to rapidly diagnose AI in patient samples (Johnson et al., 2014; Petrik et al., 2012). This chapter explored the potential of the ETP derivative bis(methylthio)gliotoxin to act as a marker for *A. fumigatus* and described a new method for generating antibodies which are specific for this metabolite.

Bis(methylthio)gliotoxin was shown to have a superior sensitivity of detection to gliotoxin by LC-MS. However, this was not the case with RP-HPLC. The bisthiomethylation of dithiol gliotoxin is, essentially, a chemical derivatization of this metabolite. Analyte chemical derivatization for liquid chromatography/electrospray ionization tandem mass spectrometry is routinely carried out to enhance the detection sensitivity for a variety of compounds (Santa et al., 2007). For example, ketones are neutral functional groups which have low ionization efficiencies in ESI. Hydroxylamine has been successfully utilised to derivatize ketones such as testosterone in order to enhance the ionization efficiency of these compounds (Borrey et al., 2007). The chemoselective derivatization of cellular thiols is an established technique in proteomics and metabolomics. This method is known to increase the dynamic range for low abundance metabolites and to reduce ionization suppression (Gori et al., 2014). It is likely that the bisthiomethylation of gliotoxin has the same effect on this metabolite resulting in enhanced detection by LC-MS.

A recently developed HPLC-MS/MS method to detect gliotoxin in the serum of patients with suspected aspergillosis was shown to have a lower limit of quantification (LLOQ) of 10 ng mL^{-1}. Of the 10 samples which tested positive by ELISA for the presence of galactomannan, five were shown to test positive for gliotoxin using this HPLC-MS/MS method (Cerqueira et al., 2014). Bis(methylthio)gliotoxin quantification

was not carried out on these samples. Considering the enhanced detectability of bis(methylthio)gliotoxin when compared to that of gliotoxin by electrospray MS, a rapid TCEP/ICH_3 method which reduces and S-alkylates the gliotoxin in these samples may enhance the sensitivity of this assay.

Gliotoxin is known to be extremely reactive and is capable of undergoing rapid cellular association. Using a variety of human cell lines, approximately 80% of the spiked toxin was shown to undergo cellular uptake in less than 1 min (Waring et al., 1994). It is possible that this rapid uptake hampers detection of the metabolite by reducing the detectable level of gliotoxin in biological fluids. Gliotoxin was shown to rapidly associate with whole blood resulting in less than 10 % recovery of the toxin when up to 20 μg was added. Interestingly, over 90% of bis(methylthio)gliotoxin spiked into blood was recoverable (Domingo et al., 2012). Although we have shown that bis(methylthio)gliotoxin is produced at substantially lower levels than gliotoxin, the non-reactive nature of bis(methylthio)gliotoxin may result in this compound being readily detectable.

Typically, small molecule detection has relied upon techniques such as liquid/gas chromatography in conjunction with UV absorbency/mass spectrometry detectors. Despite the high sensitivity of these methods, they require expensive instrumentation and highly trained users to interpret the data (Zhao et al., 2007). The ELISA has been established as a robust method of clinical diagnostics. One major advantage of competition ELISA is its high sensitivity to minimally expressed antigens in complex mixtures even when the detecting antibody is present in relatively small amounts (Gan and Patel, 2013). Antibody generation against small molecules can be a challenging task; bis(methylthio)gliotoxin contains no suitable functional groups for conjugation to a protein or carrier molecule. As a result, a synthetic strategy for the generation of a MmGT

hapten containing a single free thiol group was developed. It involved the selective S-methylation of a single thiol group of dithiol gliotoxin through careful control of the reaction conditions. Mass spectral analysis was performed to confirm the correct molecular mass of the compound. This hapten was then conjugated to a KLH carrier protein and used for mouse immunisation. The conjugation of the hapten to the carrier protein was confirmed by RP-HPLC. The resulting tail bleeds were used to develop an immunoassay to detect bis(methylthio)gliotoxin. Specific anti-mycotoxin based antibodies have been used in competitive ELISA systems to detect the presence of these compounds in both feed and biological samples (Zhang et al., 2011).

Gallagher et al. (1992) prepared hemisuccinate derivatives of sporidesmin A using succinic anhydride in which the disulfide moiety of this metabolite was preserved. These hemisuccinate derivatives were then conjugated to carrier proteins using the active ester method. The resulting sera was cross-reactive against both sporidesmin A and its bisthiomethylated derivative sporidesmin D (Briggs et al., 1994). We considered using this succinylation method to prepare bis(methylthio)gliotoxin haptens for conjugation to carrier proteins. However, considering that bis(methylthio)gliotoxin contains two free hydroxyl groups, treatment with succinic anhydride would generate reaction side-products which would then have to be purified from the final sample by preparative RP-HPLC. As such, a large amount of expensive starting material would be required. For this reason, we looked at an alternative hapten generation method using a mono-methylated derivative of gliotoxin. This method minimised the reaction starting material as few purification steps were necessary. Also, maleimide reaction chemistry is a highly established one-step mechanism for immunogen generation.

The success of this strategy proves that using monomethylated ETPs maleimide coupled to carrier proteins is a viable method for the generation of antisera against

bisthiomethylated ETPs. This technique may be applicable for the whole family of ETPs in order to generate antibodies against stable methyl-derivatives.

Chapter 8

Discussion

Prior to the work presented in this thesis it was known that *A. fumigatus* produces a bisthiomethylated derivative of gliotoxin, bis(methyl)gliotoxin, by an uncharacterised enzymatic process. No methyltransferases which carry out such a transformation had previously been described in fungal secondary metabolism. The exact role of this mechanism and its contribution in protecting *A. fumigatus* against gliotoxin were also unknown. Additionally, it was shown that bis(methyl)gliotoxin can be recovered from blood, suggesting that this gliotoxin derivative is a potential biomarker for invasive fungal infection (Domingo et al., 2012).

Afu2g11120 was identified as an uncharacterised methyltransferase, located outside of the gliotoxin biosynthetic gene cluster, which was highly upregulated in expression following gliotoxin exposure. Chapter 3 detailed the molecular techniques which facilitated an investigation into the role of this methyltransferase in bis(methyl)gliotoxin and/or gliotoxin biosynthesis. In Chapter 4, Afu2g11120 was shown to encode gliotoxin thiomethyltransferase A (*gtmA*), the methyltransferase responsible for bis(methyl)gliotoxin biosynthesis in *A. fumigatus*. Gliotoxin sensitivity assays and comparative quantitative proteomic analysis of *A. fumigatus* wild type and Δ*gtmA* showed that this mutant strain is not more sensitive to gliotoxin. This suggested that, despite the high induction of this gene following gliotoxin exposure (O'Keeffe et al., 2014), *gtmA* did not play a role in the self-protection of *A. fumigatus* against gliotoxin toxicity. The localisation of GtmA-eGFP throughout the cytosol was significant in that it suggested that this is a feature of previously characterised methyltransferases involved in the detoxification of thiol compounds.

A combination of comparative quantitative proteomic analysis and metabolomics carried out on *A. fumigatus* wild-type, Δ*gtmA* and *gtmA*^{c} indicated that several enzymes involved in gliotoxin biosynthesis are significantly more abundant in *A. fumigatus* Δ*gtmA*.

This in turn resulted in higher levels of gliotoxin production in this mutant. This suggested that *gtmA* was not involved in self-protection against this toxin but, instead, that GtmA was primarily involved in regulating the expression of the gliotoxin gene cluster.

Phylogenetic analysis of GtmA identified 124 homologs in 103 fungal genomes, all of which were found in the Ascomycota phylum. This was significant in that ETP production has been shown to be limited to this fungal phylum (Patron et al., 2007). The identification of these GtmA homologs in other ascomycetes means that the substrates of these enzymes may be predicted based on the known ETPs produced by these species. For example *A. terreus* produces the ETP acetylaranotin. It also produces bisdethiobis(methylthio)-acetylaranotin; a bisthiomethylated derivative of acetylaranotin. Genome based deletion analysis was unable to identify the thiomethyltransferase responsible for this transformation. However, based on the GtmA phylogenetic analysis, the *A. terreus* gene ATEG_01465 is likely to encode the dithiol acetylaranotin thiomethyltransferase, which is located outside of the acetylaranotin biosynthetic gene cluster. This highlights both the power of in-silico analysis of secondary metabolite associated genes while and the importance of reverse genetics in functionally annotating uncharacterised proteins within secondary metabolism.

As described in Chapter 5, the novelty of this enzyme justified its recombinant expression, enzyme activity analysis, structural studies and site directed mutagenesis for detailed biochemical characterisation. The data showed that the monomeric GtmA bisthiomethylates gliotoxin in two sequential steps producing mono(methylthio)gliotoxin as an intermediate during this transformation. Also, unlike the majority of characterised methyltransferases, GtmA was shown to be resistant to SAH mediated inhibition.

The methyltransferases involved in rebeccamycin, aminocoumarin and CypM biosynthesis methylate a wide range of substrates (Zhang et al., 2006a; Anderle et al.,

2007; Zhang and van der Donk, 2012). As GtmA did not S-methylate dithiol sporidesmin A, an ETP produced by *P. chartarum*, this indicated that GtmA shows some level of specificity against dithiol gliotoxin. It would be interesting to explore the extent of this substrate specificity by testing a variety of other ETPs such as sirodesmin A, acetylaranotin and hyalodendrin. Gliotoxin related metabolites such as acetylgliotoxin, gliotoxin E and gliotoxin G could also be tested to investigate if GtmA can S-methylate these slightly larger compounds (Van der Pyl et al., 1992; Forseth et al., 2011).

RebM was the first NPMT shown to accept synthetic cofactors to generate a number of new rebeccamycin analogues (Zhang et al., 2006). Subsequently, BamL, the N-methyltransferase involved in plantazolicin biosynthesis, was shown to accept ethyl SAM and transfer a single ethyl group to desmethylPZN. Interestingly, although this enzyme is normally capable of transferring two methyl groups to desmethylPZN, diethylPZN or even monomethyl-monoethylPZN could not be generated (Lee et al., 2013b). The discovery that NPMTs can also accept SAM analogues with alternative alkylating groups has expanded their biocatalytic repertoire, enabling broader bioalkylation reactions to be developed for biomolecular labelling and the development of natural product analogs (Klimašauskas and Weinhold, 2007). GtmA may also be capable of accepting synthetic cofactors which in turn could be used to generate synthetic ETPs with novel activities.

The structural elucidation of NPMTs has advanced our understanding of both the molecular determinants for substrate specificity and the varied catalytic mechanisms of NPMTs, whilst also providing a foundation for structure based engineering to generate new enzymes with altered specificities (Liscombe et al., 2012). Prediction of the 3D structure of GtmA was carried out using I-TASSER. This program predicted that GtmA was structurally similar to the salicylic acid carboxyl methyltransferase (SAMT) from *Clarkia breweri* and the yeast C-methyltransferase Coq5.

X-ray crystallographic analysis of apo GtmA revealed that the true structure of the GtmA monomer consists of a globular domain which contains the extended sheet characteristic of all other SAM-dependent methyltransferases (Cheng and Blumenthal, 1999) and a unique -helical cap that forms the top one-third of the active site cavity. The structure confirmed that GtmA possesses the expected class I AdoMet-dependent MTase core fold which consists of a seven-stranded β sheet flanked on each side by three a helices. Based on this structural data, targeted mutagenesis of GtmA revealed four residues (W157V, W162V, N159V and F127V) which when mutated significantly affected the activity of this enzyme. The exact role of these residues will be revealed in a cocrystal structure of GtmA bound to SAM and/or dithiol gliotoxin.

Through protein engineering and directed evolution, it is also envisaged that new mutant MTases with altered regioselectivities and/or substrate specificities capable of effectively methylating a wider range of natural and unnatural substrates, for example, high- value pharmaceutical intermediates can be generated. To date most activity in this area has focused on the more common O- and N-methyltranserases (Liscombe et al., 2012). The work described in this thesis highlights the potential of S-directed methyltransferases as future tools for both metabolic engineering and synthetic biology.

As natural product synthesis needs to produce larger quantities of target compounds, a constant supply of SAM in the form of a regeneration system is therefore crucial for the preparative use of NPMTs. It is a considerable drawback of SAM dependent reactions that this cofactor is unstable and degrades quickly under assay conditions. A practical and rapid method for the preparation of active SAM for chemoenzymatic synthesis has recently been described. This method uses the SAM-dependent chlorinase SalL to generate SAM in situ from L-Methionine and 5'-chloro-5'-deoxyadenosine (ClDA) (Lipson et al., 2013). In addition, enzymatically active and stable

SAM analogs have been generated using metabolically engineered SalL and another halogenase, FDAS (Thomsen et al., 2013). As these recent developments address the sustainable production and stability of SAM, this may lead to rapid methyltransferase based biocatalysis in the coming years.

Chapter 6 revealed that *A. fumigatus* Δ*gliT::*Δ*gtmA* is very sensitive to exogenous gliotoxin in comparison with *A. fumigatus* Δ*gliT*. This suggested that GliT activity effectively compensates for the absence of GtmA in *A. fumigatus* Δ*gtmA* and that GtmA may have been an ancestral protective strategy against gliotoxin and/or other ETPs prior to the acquisition of the gliotoxin cluster by this organism. The presence of a gtmA homolog (MTII) in *A. niger* supports this hypothesis as MTII has been shown to be involved in protection against gliotoxin and possibly other ETPs (Manzanares et al., 2015). *A. niger* does not produce any ETPs which suggests that the role of MTII is purely as a self-protection strategy against dithiol compounds. Subsequent redundancy of this superseded protection mechanism in *A. fumigatus* may have resulted in the neofunctionalization of GtmA and its interlinked association with the gliotoxin biosynthetic gene cluster.

Is GtmA wired in the network of *A. fumigatus* secondary metabolism? Gliotoxin *bis*-thiomethylation appears to be controlled by transcription factors involved in regulating *A. fumigatus* secondary metabolism. *veA* is a global regulator of secondary metabolism in *A. fumigatus* and *gtmA* was noted as significantly downregulated in a *veA* overexpression mutant (and also down-regulated in Δ*veA*) (Dhingra et al., 2013). Indeed, differentially regulated genes in these mutants were dramatically enriched for secondary metabolism-associated processes. In addition, *stuA* encodes a developmental transcription factor and regulates the expression of six secondary metabolite gene clusters in *A. fumigatus* (including gliotoxin) and *gtmA* was also differentially regulated in Δ*stuA* (Twumasi-Boateng et al., 2009). Interestingly, *gtmA* was downregulated at all time points

(up to 12 h) during co-incubation of *A. fumigatus* with human immature dendritic cells (Morton et al., 2011). Several *gli*-cluster genes were also downregulated during this interaction. This further suggests that, that although *gtmA* is located outside of the *gli* cluster, this gene is under the control of secondary metabolism-associated transcription factors.

Quantitative proteomic analysis on *A. fumigatus* Δ*gliT* vs. *ΔgliT:ΔgtmA* following 3 h gliotoxin exposure revealed that the highly sensitive *ΔgliT:ΔgtmA* mutant has several gliotoxin biosynthetic enzymes highly abundant at this time point when compared to Δ*gliT*. The exact mechanism as to how gliotoxin exposure induces the expression of the gliotoxin cluster is not understood. This work has shown that the abundance of several gliotoxin cluster encoded enzymes can be enhanced through the deletion of *A. fumigatus* GliT/GliA in combination with GtmA. This may occur due to the intracellular accumulation of gliotoxin in either the oxidised form or as dithiol gliotoxin which may then be directly potentiating the cluster induction signal.

Gliotoxin may act as a specific elicitor of secondary metabolism as shown in other systems but the chemical and molecular complexity of these elicitation processes means that the precise mechanism of activation is poorly understood. The hypothetical mechanisms of elicitation of secondary metabolism in bacterial cells are shown in Figure 8.1 (Abdelmohsen et al., 2015). Induction of the orsellinic acid gene cluster in *A. nidulans* by the bacterium *Streptomyces rapamycinicus* was shown to be dependent on the Saga/Ada complex containing the histone acetyltransferase proteins GcnE and the AdaB. A Saga/Ada-dependent increase of histone 3 acetylation at lysine 9 and 14 was shown to occur during this interaction between the fungus and bacterium. However, the exact nature of the bacterial signal remains to be elucidated (Nützmann et al., 2011). It is conceivable that gliotoxin mediated induction of the *A. fumigatus* gliotoxin biosynthetic

cluster may occur through a related mechanism. The plant specific messenger molecules jasmonic acid and its methyl ester, methyl jasmonate (MJ) have been shown to activate many classes of secondary metabolites in different plant species. This elicitation has been shown to be triggered by a variety of different signalling pathways and cascades. The activation of the Ca^{2+} cascade is an essential requirement for MJ-induced diterpene production in *S. dulcis* (Kurosaki and Taura, 2015). It has also been shown that Sdrac-1 and Sdrac-2, Rac/Rop GTPase proteins of *S. dulcis*, rapidly translocate to microsomal fractions in response to MJ stimulation, thus implicating monomeric GTP-binding proteins in this process (Mitamura et al., 2011). Future work may examine the role of these characterised triggers in relation to gliotoxin cluster induction in *A. fumigatus*.

SAM is severely depleted in *A. fumigatus ΔgliT*. However, this does not occur when *gtmA* is deleted in this genetic background (Δ*gliT*::Δ*gtmA*). This result established a direct link between the depletion of cellular SAM and gliotoxin bisthiomethylation. This result also highlighted the complexity of the *A. fumigatus* response to this toxin. It preferentially oxidises the toxin, and methylation appears to be a secondary process. Considering the metabolic expense of bisthiomethylation on SAM depletion in *A. fumigatus* Δ*gliT* and the fast, reversible nature of GliT mediated dithiol gliotoxin oxidation it is understandable that the process of dithiol bisthiomethylation may have been relegated to a backup strategy in *A. fumigatus*.

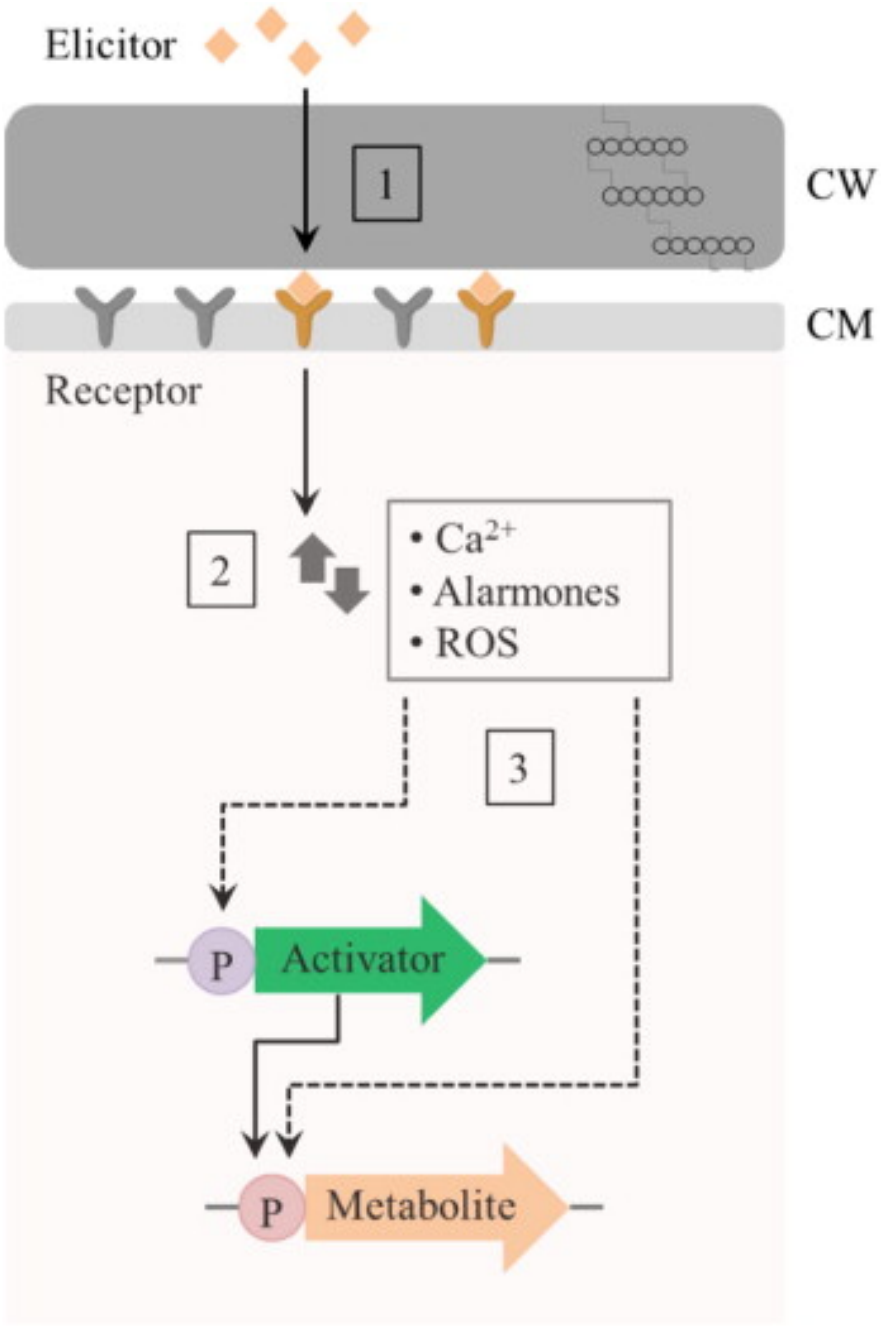

Figure 8.1. Hypothetical mechanisms of elicitation of secondary metabolism in bacterial cells, Elicitation may occur though the binding of elicitor to a specific receptor or its internalization, changes in the levels of intracellular molecules as a response to the elicitors or activation of either the metabolite activator or the metabolite gene cluster itself (via unknown mechanisms). CW= cell wall, CM=cytoplasmic membrane and P=promoter (Abdelmohsen et al., 2015).

Recent literature has highlighted the clear crosstalk and blurred lines between what has been characterised as primary and secondary metabolism (Sheridan et al., 2015). However, it is clear from this work that the flux of primary metabolites such as SAM into these specialised metabolic pathways is tightly regulated by the organism. Secondary metabolism has recently been described as biochemistry's 'Panda's Thumb', due to the loose enzyme specificity and rapid evolutionary innovations within these pathways (Bar-Even and Salah Tawfik, 2013). As illustrated in Figure 8.2, enzymes operating within these secondary metabolite pathways are far from kinetic perfection. The selection pressure on these enzymes may not be to increase the catalytic rate but rather to optimise the regulation, control and localisation of these systems (Bar-Even et al., 2011). The interaction between GtmA and its substrate dithiol gliotoxin is likely to be a non-optimised reaction akin to most within secondary metabolism. It is conceivable that if GtmA activity was as optimised as those found in primary metabolism, it would commit the majority of the pathway intermediate dithiol gliotoxin to the production of bis(methyl)gliotoxin instead of gliotoxin. Poor GtmA kinetics may be advantageous in this case as bis(methyl)gliotoxin appears to be a metabolically expensive inactive mycotoxin. It is also possible that substrate compartmentalisation within *A. fumigatus* limits GtmA access to dithiol gliotoxin.

It was also revealed that in late stage cultures the absence of *gtmA* expression has profound effects on the levels of other secondary metabolites which are produced by *A. fumigatus*. The wild type phenotype was not restored following the addition of bis(methyl)gliotoxin into these cultures. This suggested that the deregulation of gli-cluster expression in *A. fumigatus* Δ*gtmA* may result in crosstalk amongst secondary metabolite clusters within this organism. This phenomenon has been identified previously in *A. fumigatus*. Gliotoxin exposure has recently been shown to enhance conidiation by approximately 2.5-fold in *A. nidulans*; which suggests that this metabolite can operate as

a conserved signal affecting fungal development. This study also highlighted that the conidiation induction response to these metabolites occurs through fine-tuned oxidative stress regulation in the fungus (Zheng et al., 2014). As GtmA plays a role in regulating the induction of gliotoxin biosynthesis, the absence of this gene could, in theory, have an effect on the oxidative stress response of *A. fumigatus*. In turn, this could have an effect on the conidiation induction response in this organism. As fungal development and secondary metabolism are closely linked processes (Calvo et al., 2002), this altered gliotoxin cluster expression could result in the significant alterations evident in the Δ*gtmA* secondary metabolite biosynthesis during late stage culture incubation.

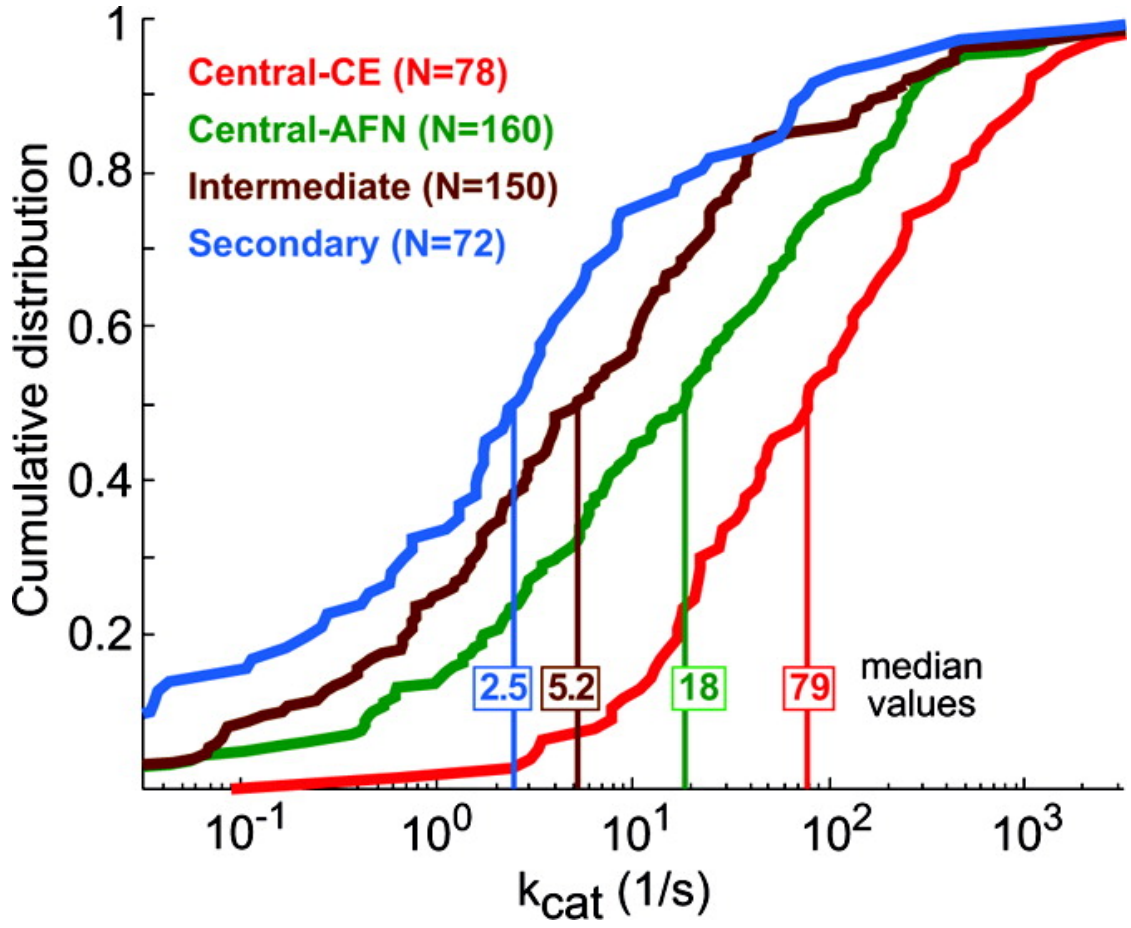

Figure 8.2. Enzymes operating within different metabolic groups have different k_{cat} and k_{cat}/K_M values. All modules were classified into four central groups: *Central-CE* (carbohydrate-energy) metabolism, involving the main carbon and energy flow; *Central-AFN* (amino-acids, fatty-acids and nucleotide) metabolism; *Intermediate* metabolism, including the biosynthesis and degradation of various common cellular components, such as co-factors and co-enzymes and *Secondary* metabolism related to metabolites which are produced in specific cells or tissues, under specific conditions and/or in relatively limited quantities. The cumulative distribution of k_{cat} values for enzyme-substrate pairs belonging to different metabolic contexts. The distributions are significantly different with p-value <0.0005, rank-sum test, except those of intermediate and specialized metabolisms (p-value <0.05) (Bar-Even et al., 2011).

In Chapter 7 a novel mono(methylthio)gliotoxin conjugate was generated. This was subsequently used to develop polyclonal antisera which were cross-reactive to bis(methyl)gliotoxin. A competitive ELISA was established to rapidly test the different mice where were immunised with the immunogen. This rapid method of antibody generation may be applicable all bisthiomethylated ETP derivatives.

The definitive demonstration that GtmA is the only enzyme which *bis*-thiomethylates GT-$(SH)_2$ raises questions as to the function of both methyltransferases encoded within the *gli* cluster (Figure 8.3). The methyltransferase *gliN* was recently shown to encode the *N*-methyltransferase which inserts the N-CH_3 in gliotoxin, conferring stability to the ETP, damping the spontaneous formation of tri- and tetrasulfides (Scharf et al., 2014a). GliM has been putatively annotated as an O-methyltransferase but this may not be its actual function. GliM contains a winged helix-turn-helix (HTH) DNA-binding domain. This domain consists of two wings, three α(alpha) helices, and three β(beta) strands and is frequently found in protein families such as the forkhead and E26 transformation-specific (ETS) transcription factors (Teichmann et al., 2012; Sharrocks, 2001). The winged-helix transcription factor CPCR1 and its interacting protein AcFKH1 positively regulate cephalosporin C biosynthesis in *Acremonium chrysogenum* (Schmitt et al., 2004a, 2004b). In addition, GipA, a C_2H_2 transcription factor which regulates *gliA* expression interdependently with *gliZ*, was shown to have a putative binding site within all the gliotoxin cluster encoded genes except *gliM*. This may suggest that *gliM* may have some level of independence from the gli-cluster (Schoberle et al., 2014).

Interestingly, the acetylaranotin cluster in *A. terreus* encodes a trimodular gene (*ataIMG*) with modules homologous to *gliI*, *gliM* and *gliG*, despite acetylaranotin not having any N or O-methyl groups. The authors state that this *gliM* homolog may be responsible for S-methylation but this is likely to be carried out by ATEG_01465 (Guo et

al., 2013). Also, the sirodesmin encoding cluster of *L. maculans* has both *gliM* and *gliN* homologs but like gliotoxin, this metabolite has only a single N-methyl group (Gardiner et al, 2004). It's also possible that *gliM* encodes a putative *O*-methyltransferase which transiently modifies a gliotoxin biosynthetic intermediate/shunt metabolite. Indeed, such an intermediate, 6-benzyl-6-hydroxy-1-methoxy-3-methylenepiperazine-2,5-dione, has been identified by two groups following deletion of *A. fumigatus gliG* (Davis et al., 2011; Scharf et al., 2011).

Figure 8.3 summarises the main contribution of this thesis to understanding the complexity of *A. fumigatus* secondary metabolism and ETP biosynthesis in general. GtmA is a thiol directed methyltransferase which synthesises bis(methyl)gliotoxin from dithiol gliotoxin. A combination of reverse genetics, metabolomics and quantitative proteomics were used to uncover the intricate feedback induction mechanism of gliotoxin biosynthesis and the role of GtmA in dissipating this signal. In addition, the apo crystal structure of GtmA was solved and this data will be used to direct future mechanistic studies of this unusual transformation. Furthermore, the role of gliotoxin bisthiomethylation as a self-protection mechanism against this toxin and the metabolic consequences of this transformation were also explored through the generation a series of *A. fumigatus* mutants. Finally, the potential of bis(methylthio)gliotoxin to act as a marker for *A. fumigatus* was explored and a new method of generating antibodies which are specific for this metabolite was developed.

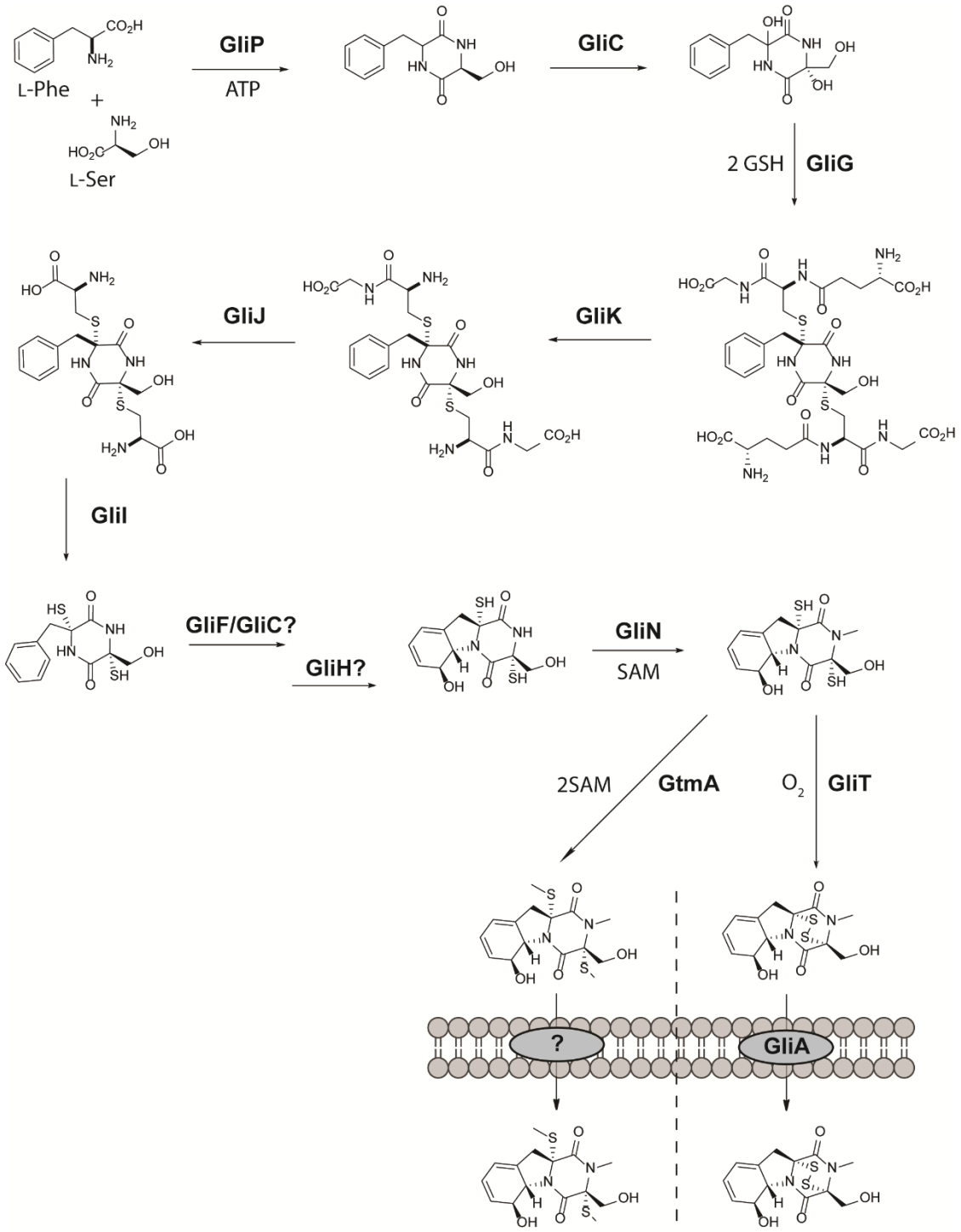

Figure 8.3. Gliotoxin biosynthesis, secretion, and regulation. A series of enzyme-catalyzed steps convert phenylalanine and serine to gliotoxin or BmGT via the formation of reactive intermediates, *bis*-glutathionylation, degradation steps, methylation and oxidation. Please note that the precise order of some reaction steps, and *gliM*/*H* involvement, remains to be fully elucidated.

Bibliography

Abad, A., Fernández-Molina, J. V., Bikandi, J., Ramírez, A., Margareto, J., Sendino, J., Hernando, F. L., Pontón, J., Garaizar, J., and Rementeria, A. (2010). What makes Aspergillus fumigatus a successful pathogen? Genes and molecules involved in invasive aspergillosis. *Rev. Iberoam. Micol.* 27, 155–82.

Abdelmohsen, U. R., Grkovic, T., Balasubramanian, S., Kamel, M. S., Quinn, R. J., and Hentschel, U. (2015). Elicitation of secondary metabolism in actinomycetes. *Biotechnol. Adv.* 33, 798–811.

Aimanianda, V., Bayry, J., Bozza, S., Kniemeyer, O., Perruccio, K., Elluru, S. R., Clavaud, C., Paris, S., Brakhage, A. a, Kaveri, S. V, et al. (2009). Surface hydrophobin prevents immune recognition of airborne fungal spores. *Nature* 460, 1117–21.

Ajees, A. A., Marapakala, K., Packianathan, C., Sankaran, B., and Rosen, B. P. (2012). Structure of an As(III) S-adenosylmethionine methyltransferase: insights into the mechanism of arsenic biotransformation. *Biochemistry* 51, 5476–85.

Al-Bader, N., Vanier, G., Liu, H., Gravelat, F. N., Urb, M., Hoareau, C. M.-Q., Campoli, P., Chabot, J., Filler, S. G., and Sheppard, D. C. (2010). Role of trehalose biosynthesis in Aspergillus fumigatus development, stress response, and virulence. *Infect. Immun.* 78, 3007–18.

Altschul, S. F., Madden, T. L., Schäffer, a a, Zhang, J., Zhang, Z., Miller, W., and Lipman, D. J. (1997). Gapped BLAST and PSI-BLAST: a new generation of protein database search programs. *Nucleic Acids Res.* 25, 3389–402.

Amich, J., and Krappmann, S. (2012). Deciphering metabolic traits of the fungal pathogen Aspergillus fumigatus: redundancy vs. essentiality. *Front. Microbiol.* 3, 414.

Amich, J., Schafferer, L., Haas, H., and Krappmann, S. (2013). Regulation of Sulphur Assimilation Is Essential for Virulence and Affects Iron Homeostasis of the Human-Pathogenic Mould Aspergillus fumigatus. *PLoS Pathog.* 9, e1003573.

Amich, J., Vicentefranqueira, R., Leal, F., and Calera, J. A. (2010). Aspergillus fumigatus survival in alkaline and extreme zinc-limiting environments relies on the induction of a zinc homeostasis system encoded by the zrfC and aspf2 genes. *Eukaryot. Cell* 9, 424–37.

Amitani, R., Taylor, G., Elezis, E. N., Llewellyn-Jones, C., Mitchell, J., Kuze, F., Cole, P. J., and Wilson, R. (1995). Purification and characterization of factors produced by Aspergillus fumigatus which affect human ciliated respiratory epithelium. *Infect. Immun.* 63, 3266–71.

Anderle, C., Hennig, S., Kammerer, B., Li, S.-M., Wessjohann, L., Gust, B., and Heide, L. (2007). Improved mutasynthetic approaches for the production of modified aminocoumarin antibiotics. *Chem. Biol.* 14, 955–67.

Anitha, R., and Murugesan, K. (2005). Production of gliotoxin on natural substrates by

Trichoderma virens. *J. Basic Microbiol.* 45, 12–9.

Attieh, J., Sparace, S. A., and Saini, H. S. (2000). Purification and properties of multiple isoforms of a novel thiol methyltransferase involved in the production of volatile sulfur compounds from Brassica oleracea. *Arch. Biochem. Biophys.* 380, 257–66.

Axelsson, V., Pikkarainen, K., and Forsby, a (2006). Glutathione intensifies gliotoxin-induced cytotoxicity in human neuroblastoma SH-SY5Y cells. *Cell Biol. Toxicol.* 22, 127–36.

Balibar, C. J., and Walsh, C. T. (2006). GliP, a multimodular nonribosomal peptide synthetase in Aspergillus fumigatus, makes the diketopiperazine scaffold of gliotoxin. *Biochemistry* 45, 15029–38.

Bar-Even, A., Noor, E., Savir, Y., Liebermeister, W., Davidi, D., Tawfik, D. S., and Milo, R. (2011). The Moderately Efficient Enzyme: Evolutionary and Physicochemical Trends Shaping Enzyme Parameters. *Biochemistry* 50, 4402–4410.

Bar-Even, A., and Salah Tawfik, D. (2013). Engineering specialized metabolic pathways--is there a room for enzyme improvements? *Curr. Opin. Biotechnol.* 24, 310–9.

Bayram, O., Krappmann, S., Ni, M., Bok, J. W., Helmstaedt, K., Valerius, O., Braus-Stromeyer, S., Kwon, N.-J., Keller, N. P., Yu, J.-H., et al. (2008). VelB/VeA/LaeA complex coordinates light signal with fungal development and secondary metabolism. *Science* 320, 1504–6.

Beauvais, A., Maubon, D., Park, S., Morelle, W., Tanguy, M., Huerre, M., Perlin, D. S., and Latgé, J. P. (2005). Two alpha(1-3) glucan synthases with different functions in Aspergillus fumigatus. *Appl. Environ. Microbiol.* 71, 1531–8.

Ben-Ami, R., Lewis, R. E., Leventakos, K., and Kontoyiannis, D. P. (2009). Aspergillus fumigatus inhibits angiogenesis through the production of gliotoxin and other secondary metabolites. *Blood* 114, 5393–9.

Bergmann, S., Funk, A. N., Scherlach, K., Schroeckh, V., Shelest, E., Horn, U., Hertweck, C., and Brakhage, A. A. (2010). Activation of a silent fungal polyketide biosynthesis pathway through regulatory cross talk with a cryptic nonribosomal peptide synthetase gene cluster. *Appl. Environ. Microbiol.* 76, 8143–9.

Bernardo, P. H., Brasch, N., Chai, C. L. L., and Waring, P. (2003). A novel redox mechanism for the glutathione-dependent reversible uptake of a fungal toxin in cells. *J. Biol. Chem.* 278, 46549–55.

Bhabhra, R., and Askew, D. S. (2005). Thermotolerance and virulence of Aspergillus fumigatus: role of the fungal nucleolus. *Med. Mycol.* 43 Suppl 1, S87–93.

Bhabhra, R., Miley, M. D., Mylonakis, E., Boettner, D., Fortwendel, J., Panepinto, J. C., Postow, M., Rhodes, J. C., and Askew, D. S. (2004). Disruption of the Aspergillus fumigatus gene encoding nucleolar protein CgrA impairs thermotolerant growth and reduces virulence. *Infect. Immun.* 72, 4731–40.

Blatzer, M., Barker, B. M., Willger, S. D., Beckmann, N., Blosser, S. J., Cornish, E. J., Mazurie, A., Grahl, N., Haas, H., and Cramer, R. A. (2011). SREBP coordinates iron and ergosterol homeostasis to mediate triazole drug and hypoxia responses in the human fungal pathogen Aspergillus fumigatus. *PLoS Genet.* 7, e1002374.

Bodey, G., Bueltmann, B., Duguid, W., Gibbs, D., Hanak, H., Hotchi, M., Mall, G., Martino, P., Meunier, F., Milliken, S., et al. (1992). Fungal infections in cancer patients: An international autopsy survey. *Eur. J. Clin. Microbiol. Infect. Dis.* 11, 99–109.

Boente, M., and Kirby, G. (1991). Biosynthesis of hyalodendrin and didethiobis (methylthio) hyalodendrin, sulphur-containing 2, 5-dioxopiperazines of the 3S, 6S series. *J. Chem. Soc. Perkin Trans.* 8, 1283–1290.

Boissier, F., Bardou, F., Guillet, V., Uttenweiler-Joseph, S., Daffé, M., Quémard, A., and Mourey, L. (2006). Further insight into S-adenosylmethionine-dependent methyltransferases: structural characterization of Hma, an enzyme essential for the biosynthesis of oxygenated mycolic acids in Mycobacterium tuberculosis. *J. Biol. Chem.* 281, 4434–45.

Bok, J., Balajee, S., and Marr, K. (2005). LaeA, a regulator of morphogenetic fungal virulence factors. *Eukaryot. Cell* 4, 1574–1582.

Bok, J. W., Chung, D., Balajee, S. A., Marr, K. a, Andes, D., Nielsen, K. F., Frisvad, J. C., Kirby, K. a, and Keller, N. P. (2006). GliZ, a transcriptional regulator of gliotoxin biosynthesis, contributes to Aspergillus fumigatus virulence. *Infect. Immun.* 74, 6761–8.

Bok, J. W., and Keller, N. P. (2004). LaeA , a Regulator of Secondary Metabolism in Aspergillus spp . *Eukaryot. Cell* 8, 527–535.

Bolt, H. M., and Gansewendt, B. (1993). Mechanisms of carcinogenicity of methyl halides. *Crit. Rev. Toxicol.* 23, 237–53.

Boonsarngsuk, V., Niyompattama, A., Teosirimongkol, C., and Sriwanichrak, K. (2010). False-positive serum and bronchoalveolar lavage Aspergillus galactomannan assays caused by different antibiotics. *Scand. J. Infect. Dis.* 42, 461–8.

Borrey, D., Moerman, E., Cockx, A., Engelrelst, V., and Langlois, M. R. (2007). Column-switching LC-MS/MS analysis for quantitative determination of testosterone in human serum. *Clin. Chim. Acta.* 382, 134–7.

Boutros, P. C., Margolin, A. A., Stuart, J. M., Califano, A., and Stolovitzky, G. (2014). Toward better benchmarking: challenge-based methods assessment in cancer genomics. *Genome Biol.* 15, 462.

Boyer, N., Morrison, K. C., Kim, J., and Hergenrother, J. (2013). Synthesis and anticancer activity of epipolythiodiketopiperazine alkaloids 1646–1657.

Bradshaw, R. E., Feng, Z., Schwelm, A., Yang, Y., and Zhang, S. (2009). Functional

analysis of a putative Dothistromin toxin MFS transporter gene. *Toxins (Basel).* 1, 173–87.

Briggs, L. R., Towers, N. R., and Molan, P. C. (1994). Development of an Enzyme-Linked Immunosorbent Assay for Analysis of Sporidesmin A and Its Metabolites in Ovine Urine and Bile. *J. Agric. Food Chem.* 42, 2769–2777.

Brochado, A. R., and Patil, K. R. (2013). Overexpression of O-methyltransferase leads to improved vanillin production in baker's yeast only when complemented with model-guided network engineering. *Biotechnol. Bioeng.* 110, 656–9.

Burns, C., Geraghty, R., Neville, C., Murphy, A., Kavanagh, K., and Doyle, S. (2005). Identification, cloning, and functional expression of three glutathione transferase genes from Aspergillus fumigatus. *Fungal Genet. Biol.* 42, 319–27.

Cakici, O., Sikorski, M., Stepkowski, T., Bujacz, G., and Jaskolski, M. (2010). Crystal Structures of NodS N-Methyltransferase from Bradyrhizobium japonicum in Ligand-Free Form and as SAH Complex. *J. Mol. Biol.* 404, 874–889.

Callaway, E. (2014). Data bank struggles as protein imaging ups its game. *Nature* 514, 416.

Calvo, A. M., Wilson, R. A., Bok, J. W., and Keller, N. P. (2002). Relationship between secondary metabolism and fungal development. *Microbiol. Mol. Biol. Rev.* 66, 447–59.

Carberry, S., Molloy, E., Hammel, S., O'Keeffe, G., Jones, G. W., Kavanagh, K., and Doyle, S. (2012). Gliotoxin effects on fungal growth: mechanisms and exploitation. *Fungal Genet. Biol.* 49, 302–12.

Cerqueira, L. B., de Francisco, T. M. G., Gasparetto, J. C., Campos, F. R., and Pontarolo, R. (2014). Development and validation of an HPLC-MS/MS method for the early diagnosis of aspergillosis. *PLoS One* 9, e92851.

Chang, S.-L., Chiang, Y.-M., Yeh, H.-H., Wu, T.-K., and Wang, C. C. C. (2013). Reconstitution of the early steps of gliotoxin biosynthesis in Aspergillus nidulans reveals the role of the monooxygenase GliC. *Bioorg. Med. Chem. Lett.* 23, 2155–7.

Cheng, X., and Blumenthal, R. (1999). S-adenosylmethionine-dependent methyltransferases: structures and functions, World Scientific, 1st Ed.

Chocklett, S. W., and Sobrado, P. (2010). Aspergillus fumigatus SidA is a highly specific ornithine hydroxylase with bound flavin cofactor. *Biochemistry* 49, 6777–83.

Choi, E. J., Park, J.-S., Kim, Y.-J., Jung, J.-H., Lee, J. K., Kwon, H. C., and Yang, H. O. (2011). Apoptosis-inducing effect of diketopiperazine disulfides produced by Aspergillus sp. KMD 901 isolated from marine sediment on HCT116 colon cancer cell lines. *J. Appl. Microbiol.* 110, 304–13.

Choi, H., Shim, J., and Kim, J. (2007). Discovery of gliotoxin as a new small molecule

targeting thioredoxin redox system. *Biochem. Biophys. Res. Commun.* 359, 523–528.

Chujo, T., and Scott, B. (2014). Histone H3K9 and H3K27 methylation regulates fungal alkaloid biosynthesis in a fungal endophyte-plant symbiosis. *Mol. Microbiol.* 92, 413–34.

Coiner, H., Schröder, G., Wehinger, E., Liu, C.-J., Noel, J. P., Schwab, W., and Schröder, J. (2006). Methylation of sulfhydryl groups: a new function for a family of small molecule plant O-methyltransferases. *Plant J.* 46, 193–205.

Coleman, J. J., and Mylonakis, E. (2009). Efflux in fungi: la pièce de résistance. *PLoS Pathog.* 5, e1000486.

Cook, K. M., Hilton, S. T., Mecinovic, J., Motherwell, W. B., Figg, W. D., and Schofield, C. J. (2009). Epidithiodiketopiperazines block the interaction between hypoxia-inducible factor-1alpha (HIF-1alpha) and p300 by a zinc ejection mechanism. *J. Biol. Chem.* 284, 26831–8.

Cramer, R. A., Gamcsik, M. P., Brooking, R. M., Najvar, L. K., Kirkpatrick, W. R., Patterson, T. F., Balibar, C. J., Graybill, J. R., Perfect, J. R., Abraham, S. N., et al. (2006). Disruption of a nonribosomal peptide synthetase in Aspergillus fumigatus eliminates gliotoxin production. *Eukaryot. Cell* 5, 972–80.

Cullen, D., Leong, S., Wilson, L., and Henner, D. (1987). Transformation of Aspergillus nidulans with the hygromycin-resistance gene, hph. *Gene* 57, 21–26.

Dagenais, T. R. T., and Keller, N. P. (2009). Pathogenesis of Aspergillus fumigatus in Invasive Aspergillosis. *Clin. Microbiol. Rev.* 22, 447–65. d

Dahlgren, C., and Karlsson, A. (1999). Respiratory burst in human neutrophils. *J. Immunol. Methods* 232, 3–14.

Dai, Y.-N., Zhou, K., Cao, D.-D., Jiang, Y.-L., Meng, F., Chi, C.-B., Ren, Y.-M., Chen, Y., and Zhou, C.-Z. (2014). Crystal structures and catalytic mechanism of the C-methyltransferase Coq5 provide insights into a key step of the yeast coenzyme Q synthesis pathway. *Acta Crystallogr. D. Biol. Crystallogr.* 70, 2085–92.

Darriba, D., Taboada, G. L., Doallo, R., and Posada, D. (2011). ProtTest 3: fast selection of best-fit models of protein evolution. *Bioinformatics* 27, 1164–5.

Davis, C., Carberry, S., Schrettl, M., Singh, I., Stephens, J. C., Barry, S. M., Kavanagh, K., Challis, G. L., Brougham, D., and Doyle, S. (2011). The role of glutathione S-transferase GliG in gliotoxin biosynthesis in Aspergillus fumigatus. *Chem. Biol.* 18, 542–52.

Dhingra, S., Andes, D., and Calvo, A. A. M. (2012). VeA regulates conidiation, gliotoxin production, and protease activity in the opportunistic human pathogen Aspergillus fumigatus. *Eukaryot. Cell* 11, 1531–43.

Dhingra, S., Lind, A. L., Lin, H.-C., Tang, Y., Rokas, A., and Calvo, A. M. (2013). The

Fumagillin Gene Cluster, an Example of Hundreds of Genes under veA Control in Aspergillus fumigatus. *PLoS One* 8, e77147.

Díez, B., Alvarez, E., Cantoral, J. M., Barredo, J. L., and Martín, J. F. (1987). Selection and characterization of pyrG mutants of Penicillium chrysogenum lacking orotidine-5'-phosphate decarboxylase and complementation by the pyr4 gene of Neurospora crassaa. *Curr. Genet.* 12, 277–282.

Dolan, S. K., O'Keeffe, G., Jones, G. W., and Doyle, S. (2015). Resistance is not futile: gliotoxin biosynthesis, functionality and utility. *Trends Microbiol.*, 1–10.

Dolan, S. K., Owens, R. a, O'Keeffe, G., Hammel, S., Fitzpatrick, D. a, Jones, G. W., and Doyle, S. (2014). Regulation of Nonribosomal Peptide Synthesis: bis-Thiomethylation Attenuates Gliotoxin Biosynthesis in Aspergillus fumigatus. *Chem. Biol.* 21, 999–1012.

Domingo, M. P., Colmenarejo, C., Martínez-Lostao, L., Müllbacher, A., Jarne, C., Revillo, M. J., Delgado, P., Roc, L., Meis, J. F., Rezusta, A., et al. (2012). Bis(methyl)gliotoxin proves to be a more stable and reliable marker for invasive aspergillosis than gliotoxin and suitable for use in diagnosis. *Diagn. Microbiol. Infect. Dis.* 73, 57–64.

Drotar, a, Fall, L. R., Mishalanie, E. a, Tavernier, J. E., and Fall, R. (1987). Enzymatic methylation of sulfide, selenide, and organic thiols by Tetrahymena thermophila. *Appl. Environ. Microbiol.* 53, 2111–8.

Duncan, E. J., Thompson, M. P., and Phua, S. H. (2005). Zinc protection of HepG2 cells from sporidesmin toxicity does not require de novo gene transcription. *Toxicol. Lett.* 159, 164–172.

Duthie, R., and Denning, D. W. (1995). Aspergillus fungemia: report of two cases and review. *Clin. Infect. Dis.* 20, 598–605.

Edgar, R. C. (2004). MUSCLE: multiple sequence alignment with high accuracy and high throughput. *Nucleic Acids Res.* 32, 1792–7.

Edmond, M. B., Wallace, S. E., McClish, D. K., Pfaller, M. A., Jones, R. N., and Wenzel, R. P. (1999). Nosocomial bloodstream infections in United States hospitals: a three-year analysis. *Clin. Infect. Dis.* 29, 239–44.

Egli, M. (2010). Diffraction techniques in structural biology. *Curr. Protoc. Nucleic Acid Chem.* Chapter 7, Unit 7.13.

Emsley, P., and Cowtan, K. (2004). Coot: model-building tools for molecular graphics. *Acta Crystallogr. D. Biol. Crystallogr.* 60, 2126–32.

Evans, P. R. (2011). An introduction to data reduction: space-group determination, scaling and intensity statistics. *Acta Crystallogr. D. Biol. Crystallogr.* 67, 282–92.

Fitzpatrick, D. A., Logue, M. E., Stajich, J. E., and Butler, G. (2006). A fungal phylogeny

based on 42 complete genomes derived from supertree and combined gene analysis. *BMC Evol. Biol.* 6, 99.

Fitzpatrick, L. R., Wang, J., and Le, T. (2002). Gliotoxin, an inhibitor of nuclear factor-kappa B, attenuates peptidoglycan-polysaccharide-induced colitis in rats. *Inflamm. Bowel Dis.* 8, 159–67.

Fontaine, T., Magnin, T., Melhert, A., Lamont, D., Latge, J.-P., and Ferguson, M. a J. (2003). Structures of the glycosylphosphatidylinositol membrane anchors from Aspergillus fumigatus membrane proteins. *Glycobiology* 13, 169–77.

Forseth, R. R., Fox, E. M., Chung, D., Howlett, B. J., Keller, N. P., and Schroeder, F. C. (2011). Identification of cryptic products of the gliotoxin gene cluster using NMR-based comparative metabolomics and a model for gliotoxin biosynthesis. *J. Am. Chem. Soc.* 133, 9678–81.

Fox, E. M., and Howlett, B. J. (2008). Biosynthetic gene clusters for epipolythiodioxopiperazines in filamentous fungi. *Mycol. Res.* 112, 162–9.

Fox, M., Gray, G., Kavanagh, K., Lewis, C., and Doyle, S. (2004). Detection of Aspergillus fumigatus mycotoxins: immunogen synthesis and immunoassay development. *J. Microbiol. Methods* 56, 221–230.

Frisvad, J. C., and Larsen, T. O. (2015). Chemodiversity in the genus Aspergillus. *Appl. Microbiol. Biotechnol.* 99, 7859–77.

Fu, Z., Hu, Y., Konishi, K., Takata, Y., Ogawa, H., Gomi, T., Fujioka, M., and Takusagawa, F. (1996). Crystal Structure of Glycine N -Methyltransferase from Rat Liver *Biochemistry* 35, 11985–11993.

Gallagher, L., Owens, R. A., Dolan, S. K., O'Keeffe, G., Schrettl, M., Kavanagh, K., Jones, G. W., and Doyle, S. (2012). The Aspergillus fumigatus protein GliK protects against oxidative stress and is essential for gliotoxin biosynthesis. *Eukaryot. Cell* 11, 1226–38.

Gan, S. D., and Patel, K. R. (2013). Enzyme immunoassay and enzyme-linked immunosorbent assay. *J. Invest. Dermatol.* 133, e12.

Garcia-Vidal, C., Peghin, M., Cervera, C., Gudiol, C., Ruiz-Camps, I., Moreno, A., Royo-Cebrecos, C., Roselló, E., de la Bellacasa, J. P., Ayats, J., et al. (2015). Causes of death in a contemporary cohort of patients with invasive aspergillosis. *PLoS One* 10, e0120370.

Gardiner, D. M., Cozijnsen, A. J., Wilson, L. M., Pedras, M. S. C., and Howlett, B. J. (2004). The sirodesmin biosynthetic gene cluster of the plant pathogenic fungus Leptosphaeria maculans. *Mol. Microbiol.* 53, 1307–18.

Gardiner, D. M., and Howlett, B. J. (2005). Bioinformatic and expression analysis of the putative gliotoxin biosynthetic gene cluster of Aspergillus fumigatus. *FEMS Microbiol. Lett.* 248, 241–8.

Gardiner, D. M., Jarvis, R. S., and Howlett, B. J. (2005). The ABC transporter gene in the sirodesmin biosynthetic gene cluster of Leptosphaeria maculans is not essential for sirodesmin production but facilitates self-protection. *Fungal Genet. Biol.* 42, 257–63.

Gasch, A. P., Spellman, P. T., Kao, C. M., Carmel-Harel, O., Eisen, M. B., Storz, G., Botstein, D., and Brown, P. O. (2000). Genomic expression programs in the response of yeast cells to environmental changes. *Mol. Biol. Cell* 11, 4241–57.

Gastebois, A., Clavaud, C., Aimanianda, V., and Latgé, J.-P. (2009). Aspergillus fumigatus: cell wall polysaccharides, their biosynthesis and organization. *Future Microbiol.* 4, 583–95.

Gastebois, A., Fontaine, T., Latgé, J.-P., and Mouyna, I. (2010). beta(1-3)Glucanosyltransferase Gel4p is essential for Aspergillus fumigatus. *Eukaryot. Cell* 9, 1294–8.

Geissler, A., Haun, F., Frank, D. O., Wieland, K., Simon, M. M., Idzko, M., Davis, R. J., Maurer, U., and Borner, C. (2013). Apoptosis induced by the fungal pathogen gliotoxin requires a triple phosphorylation of Bim by JNK. *Cell Death Differ.* 20, 1317–29.

Giacchino, M., Chiapello, N., Bezzio, S., Fagioli, F., Saracco, P., Alfarano, A., Martini, V., Cimino, G., Martino, P., and Girmenia, C. (2006). Aspergillus galactomannan enzyme-linked immunosorbent assay cross-reactivity caused by invasive Geotrichum capitatum. *J. Clin. Microbiol.* 44, 3432–4.

Gómez García, I., Stevenson, C. E. M., Usón, I., Freel Meyers, C. L., Walsh, C. T., and Lawson, D. M. (2010). The crystal structure of the novobiocin biosynthetic enzyme NovP: the first representative structure for the TylF O-methyltransferase superfamily. *J. Mol. Biol.* 395, 390–407.

Gori, S. S., Lorkiewicz, P., Ehringer, D. S., Belshoff, A. C., Higashi, R. M., Fan, T. W.-M., and Nantz, M. H. (2014). Profiling thiol metabolites and quantification of cellular glutathione using FT-ICR-MS spectrometry. *Anal. Bioanal. Chem.* 406, 4371–9.

Grahl, N., Puttikamonkul, S., Macdonald, J. M., Gamcsik, M. P., Ngo, L. Y., Hohl, T. M., and Cramer, R. A. (2011). In vivo hypoxia and a fungal alcohol dehydrogenase influence the pathogenesis of invasive pulmonary aspergillosis. *PLoS Pathog.* 7, e1002145.

Gräslund, S., Nordlund, P., Weigelt, J., Hallberg, B. M., Bray, J., Gileadi, O., Knapp, S., Oppermann, U., Arrowsmith, C., Hui, R., et al. (2008). Protein production and purification. *Nat. Methods* 5, 135–46.

Gravelat, F. N., Doedt, T., Chiang, L. Y., Liu, H., Filler, S. G., Patterson, T. F., and Sheppard, D. C. (2008). In vivo analysis of Aspergillus fumigatus developmental gene expression determined by real-time reverse transcription-PCR. *Infect. Immun.*

76, 3632–9.

Guimarães, D. O., Borges, W. S., Vieira, N. J., de Oliveira, L. F., da Silva, C. H. T. P., Lopes, N. P., Dias, L. G., Durán-Patrón, R., Collado, I. G., and Pupo, M. T. (2010). Diketopiperazines produced by endophytic fungi found in association with two Asteraceae species. *Phytochemistry* 71, 1423–9.

Guindon, S., and Gascuel, O. (2003). A Simple, Fast, and Accurate Algorithm to Estimate Large Phylogenies by Maximum Likelihood. *Syst. Biol.* 52, 696–704.

Guo, C.-J., Yeh, H.-H., Chiang, Y.-M., Sanchez, J. F., Chang, S.-L., Bruno, K. S., and Wang, C. C. C. (2013). Biosynthetic pathway for the epipolythiodioxopiperazine acetylaranotin in Aspergillus terreus revealed by genome-based deletion analysis. *J. Am. Chem. Soc.* 135, 7205–13.

Guo, H., Sun, B., Gao, H., and Chen, X. (2009). Diketopiperazines from the Cordyceps-colonizing fungus Epicoccum nigrum. *J. Nat. Prod.* 72, 2115–2119.

Guo, M., Yang, X.-L., and Schimmel, P. (2010). New functions of aminoacyl-tRNA synthetases beyond translation. *Nat. Rev. Mol. Cell Biol.* 11, 668–74.

Haas, H. (2012). Iron - A Key Nexus in the Virulence of Aspergillus fumigatus. *Front. Microbiol.* 3, 28.

Haas, H., Eisendle, M., and Turgeon, B. G. (2008). Siderophores in fungal physiology and virulence. *Annu. Rev. Phytopathol.* 46, 149–87.

Hachem, R. Y., Kontoyiannis, D. P., Chemaly, R. F., Jiang, Y., Reitzel, R., and Raad, I. (2009). Utility of galactomannan enzyme immunoassay and (1,3) beta-D-glucan in diagnosis of invasive fungal infections: low sensitivity for Aspergillus fumigatus infection in hematologic malignancy patients. *J. Clin. Microbiol.* 47, 129–33.

Häcker, G. (2013). A Bim-activating mould. *Cell Death Differ.* 20, 1289–90.

Hao, Y., Blair, P. M., Sharma, A., Mitchell, D. A., and Nair, S. K. (2015). Insights into methyltransferase specificity and bioactivity of derivatives of the antibiotic plantazolicin. *ACS Chem. Biol.* 10, 1209–16.

Haritakun, R., Rachtawee, P., Komwijit, S., Nithithanasilp, S., and Isaka, M. (2012). Highly Conjugated Ergostane-Type Steroids and Aranotin-Type Diketopiperazines from the Fungus Aspergillus terreus BCC 4651. *Helv. Chim. Acta* 95, 308–313.

Harper, D. . (1993). *Metal Ions in Biological Systems: Volume 29: Biological Properties of Metal Alkyl Derivatives - CRC Press Book.* , ed. H. S. & A. Sigel.

Harper, S., Speicher, D. W., and Ph, D. (2011). Purification of proteins fused to glutathione S-tranferase. 681, 1–15.

Heinekamp, T., Schmidt, H., Lapp, K., Pähtz, V., Shopova, I., Köster-Eiserfunke, N., Krüger, T., Kniemeyer, O., and Brakhage, A. A. (2015). Interference of Aspergillus fumigatus with the immune response. *Semin. Immunopathol.* 37, 141–52.

Hendricks, C. L., Ross, J. R., Pichersky, E., Noel, J. P., and Zhou, Z. S. (2004). An enzyme-coupled colorimetric assay for S-adenosylmethionine-dependent methyltransferases. *Anal. Biochem.* 326, 100–5.

Herbrecht, R., Letscher-Bru, V., Oprea, C., Lioure, B., Waller, J., Campos, F., Villard, O., Liu, K.-L., Natarajan-Amé, S., Lutz, P., et al. (2002). Aspergillus galactomannan detection in the diagnosis of invasive aspergillosis in cancer patients. *J. Clin. Oncol.* 20, 1898–906.

Herfarth, H., Brand, K., Rath, H. C., Rogler, G., Schölmerich, J., and Falk, W. (2000). Nuclear factor-kappa B activity and intestinal inflammation in dextran sulphate sodium (DSS)-induced colitis in mice is suppressed by gliotoxin. *Clin. Exp. Immunol.* 120, 59–65.

Hermanson, G. (2008). *Bioconjugate Techniques*. Second Ed. Elsevier Inc.

Hohl, T. M., and Feldmesser, M. (2007). Aspergillus fumigatus: principles of pathogenesis and host defense. *Eukaryot. Cell* 6, 1953–63.

Hope, W. W., Kruhlak, M. J., Lyman, C. A., Petraitiene, R., Petraitis, V., Francesconi, A., Kasai, M., Mickiene, D., Sein, T., Peter, J., et al. (2007). Pathogenesis of Aspergillus fumigatus and the kinetics of galactomannan in an in vitro model of early invasive pulmonary aspergillosis: implications for antifungal therapy. *J. Infect. Dis.* 195, 455–66.

Hope, W. W., Walsh, T. J., and Denning, D. W. (2005). The invasive and saprophytic syndromes due to Aspergillus spp. *Med. Mycol.* 43 Suppl 1, S207–38.

Hotta, K., Keegan, R. M., Ranganathan, S., Fang, M., Bibby, J., Winn, M. D., Sato, M., Lian, M., Watanabe, K., Rigden, D. J., et al. (2014). Conversion of a disulfide bond into a thioacetal group during echinomycin biosynthesis. *Angew. Chem. Int. Ed. Engl.* 53, 824–8.

Ingham, C. J., Kalisman, O., Finkelshtein, A., and Ben-Jacob, E. (2011). Mutually facilitated dispersal between the nonmotile fungus Aspergillus fumigatus and the swarming bacterium Paenibacillus vortex. *Proc. Natl. Acad. Sci. U. S. A.* 108, 19731–6.

Intaraudom, C., Boonyuen, N., Suvannakad, R., Rachtawee, P., and Pittayakhajonwut, P. (2013). Penicolinates A–E from endophytic Penicillium sp. BCC16054. *Tetrahedron Lett.* 54, 744–748.

Irmer, H., Tarazona, S., Sasse, C., Olbermann, P., Loeffler, J., Krappmann, S., Conesa, A., and Braus, G. H. (2015). RNAseq analysis of Aspergillus fumigatus in blood reveals a just wait and see resting stage behavior. *BMC Genomics* 16, 640.

Jain, R., Valiante, V., Remme, N., Docimo, T., Heinekamp, T., Hertweck, C., Gershenzon, J., Haas, H., and Brakhage, A. a (2011). The MAP kinase MpkA controls cell wall integrity, oxidative stress response, gliotoxin production and iron

adaptation in Aspergillus fumigatus. *Mol. Microbiol.* 82, 39–53.

Jansson, A., Koskiniemi, H., Mäntsälä, P., Niemi, J., and Schneider, G. (2004). Crystal structure of a ternary complex of DnrK, a methyltransferase in daunorubicin biosynthesis, with bound products. *J. Biol. Chem.* 279, 41149–56.

Jansson, A., Niemi, J., Lindqvist, Y., Mäntsälä, P., and Schneider, G. (2003). Crystal structure of aclacinomycin-10-hydroxylase, a S-adenosyl-L-methionine-dependent methyltransferase homolog involved in anthracycline biosynthesis in Streptomyces purpurascens. *J. Mol. Biol.* 334, 269–80.

Jegorov, A., and Hajduch, M. (2006). Nonribosomal cyclic peptides: specific markers of fungal infections. *J. Mass Spectrom*, 41, 563–576.

de Jesus Carrion, S., Leal Jr., S. M. . J., Paul-Latge, J., and Pearlman, E. (2012). Hydrophobin RodA protein is essential for masking the host immune response and enhancing fungal survival of Aspergillus fumigatus during corneal infection. *J. Immunol.* 188, 55.9.

Johnson, G., Ferrini, A., Dolan, S. K., Nolan, T., Agrawal, S., Doyle, S., and Bustin, S. A. (2014). Biomarkers for invasive aspergillosis: the challenges continue. *Biomark. Med.* 8, 429–51.

Kabsch, W. (2010). Integration, scaling, space-group assignment and post-refinement. *Acta Crystallogr. D. Biol. Crystallogr.* 66, 133–44.

Kafi, K., Betting, D. J., Yamada, R. E., Bacica, M., Steward, K. K., and Timmerman, J. M. (2009). Maleimide conjugation markedly enhances the immunogenicity of both human and murine idiotype-KLH vaccines. *Mol. Immunol.* 46, 448–56.

Kanamori, H., Kanemitsu, K., Miyasaka, T., Ameku, K., Endo, S., Aoyagi, T., Inden, K., Hatta, M., Yamamoto, N., Kunishima, H., et al. (2009). Measurement of (1-3)-beta-D-glucan derived from different gauze types. *Tohoku J. Exp. Med.* 217, 117–21.

Kankaanranta, H., Ilmarinen, P., Zhang, X., Adcock, I. M., Lahti, A., Barnes, P. J., Giembycz, M. A., Lindsay, M. A., and Moilanen, E. (2014). Tumour necrosis factor-α regulates human eosinophil apoptosis via ligation of TNF-receptor 1 and balance between NF-κB and AP-1. *PLoS One* 9, e90298.

Kim, S., and Shin, K. (2013). The developmental regulators, FlbB and FlbE, are involved in the virulence of Aspergillus fumigatus. *J. Microbiol. Biotechnol.* 23, 766–70.

Kim, S.-S., Kim, Y. H., and Shin, K.-S. (2013). The Developmental Regulators, FlbB and FlbE, are Involved in the Virulence of Aspergillus fumigatus. *J. Microbiol. Biotechnol.* 23, 766–70.

Kimple, M. E., Brill, A. L., and Pasker, R. L. (2013). Overview of affinity tags for protein purification. *Curr. Protoc. Protein Sci.* 73, Unit 9.9.

Kirby, G. W., Robins, D. J., Sefton, M. A., and Talekar, R. R. (1980). Biosynthesis of

bisdethiobis(methylthio)gliotoxin, a new metabolite of Gliocladium deliquescens. *J. Chem. Soc. Perkin Trans. 1*, 119.

Klimašauskas, S., and Weinhold, E. (2007). A new tool for biotechnology: AdoMet-dependent methyltransferases. *Trends Biotechnol.* 25, 99–104.

Koo, S., Thomas, H. R., Daniels, S. D., Lynch, R. C., Fortier, S. M., Shea, M. M., Rearden, P., Comolli, J. C., Baden, L. R., and Marty, F. M. (2014). A breath fungal secondary metabolite signature to diagnose invasive aspergillosis. *Clin. Infect. Dis.* 59, 1733–40.

Kozbial, P. Z., and Mushegian, A. R. (2005). Natural history of S-adenosylmethionine-binding proteins. *BMC Struct. Biol.* 5, 19.

Kubodera, T., Yamashita, N., and Nishimura, A. (2000). Pyrithiamine resistance gene (ptrA) of Aspergillus oryzae: cloning, characterization and application as a dominant selectable marker for transformation. *Biosci. Biotechnol.Biochem.* 64, 1416-21

Kubodera, T., Yamashita, N., and Nishimura, A. (2002). Transformation of Aspergillus sp. and Trichoderma reesei using the pyrithiamine resistance gene (ptrA) of Aspergillus oryzae. *Biosci. Biotechnol. Biochem.* 66, 404–6.

Kupfahl, C., Heinekamp, T., Geginat, G., Ruppert, T., Härtl, A., Hof, H., and Brakhage, A. a (2006). Deletion of the gliP gene of Aspergillus fumigatus results in loss of gliotoxin production but has no effect on virulence of the fungus in a low-dose mouse infection model. *Mol. Microbiol.* 62, 292–302.

Kurosaki, F., and Taura, F. (2015). Transcriptional activation of sesquiterpene biosynthetic enzyme δ-guaiene synthase gene in cell cultures of Aquilaria microcarpa overexpressing cam1 and rac2 encoding calmodulin and Rac GTPase. *Plant Gene* 2, 25–28.

Kwon, N.-J., Shin, K.-S., and Yu, J.-H. (2010). Characterization of the developmental regulator FlbE in Aspergillus fumigatus and Aspergillus nidulans. *Fungal Genet. Biol.* 47, 981–93.

Kwon-Chung, K., and Sugui, J. (2013). Aspergillus fumigatus—What Makes the Species a Ubiquitous Human Fungal Pathogen? *PLoS Pathog.* 9, e1003743.

Kwon-Chung, K., and Sugui, J. (2008). What do we know about the role of gliotoxin in the pathobiology of Aspergillus fumigatus? *Med. Mycol.* 47, 1–12.

Langer, G., Cohen, S. X., Lamzin, V. S., and Perrakis, A. (2008). Automated macromolecular model building for X-ray crystallography using ARP/wARP version 7. *Nat. Protoc.* 3, 1171–9.

Langfelder, K., Jahn, B., Gehringer, H., Schmidt, A., Wanner, G., and Brakhage, A. A. (1998). Identification of a polyketide synthase gene (pksP) of Aspergillus fumigatus involved in conidial pigment biosynthesis and virulence. *Med. Microbiol. Immunol.* 187, 79–89.

Langfelder, K., Philippe, B., and Jahn, B. (2001). Differential expression of the Aspergillus fumigatus pksP gene detected in vitro and in vivo with green fluorescent protein. *Infect.immun.* 69, 6411-8

Laskowski, R. A., and Swindells, M. B. (2011). LigPlot+: Multiple Ligand–Protein Interaction Diagrams for Drug Discovery. *J. Chem. Inf. Model.* 51, 2778–2786.

Latgé, J. P. (1999). Aspergillus fumigatus and aspergillosis. *Clin. Microbiol. Rev.* 12, 310–50.

Lee, D. J., Kang, D. H., Choi, M., Choi, Y. J., Lee, J. Y., Park, J. H., Park, Y. J., Lee, K. W., and Kang, S. W. (2013a). Peroxiredoxin-2 represses melanoma metastasis by increasing E-Cadherin/β-Catenin complexes in adherens junctions. *Cancer Res.* 73, 4744–57.

Lee, H. J., Lee, J. H., Hwang, B. Y., Kim, H. S., and Lee, J. J. (2001). Anti-angiogenic activities of gliotoxin and its methylthio-derivative, fungal metabolites. *Arch. Pharm. Res.* 24, 397–401.

Lee, I., Oh, J.-H., Shwab, E. K., Dagenais, T. R. T., Andes, D., and Keller, N. P. (2009). HdaA, a class 2 histone deacetylase of Aspergillus fumigatus, affects germination and secondary metabolite production. *Fungal Genet. Biol.* 46, 782–90.

Lee, J., Hao, Y., Blair, P. M., Melby, J. O., Agarwal, V., Burkhart, B. J., Nair, S. K., and Mitchell, D. a (2013b). Structural and functional insight into an unexpectedly selective N-methyltransferase involved in plantazolicin biosynthesis. *Proc. Natl. Acad. Sci. U. S. A.*, 12954-9

Lee, W. J., Shim, J.-Y., and Zhu, B. T. (2005). Mechanisms for the inhibition of DNA methyltransferases by tea catechins and bioflavonoids. *Mol. Pharmacol.* 68, 1018–30.

Li, B., Forseth, R. R., Bowers, A. a, Schroeder, F. C., and Walsh, C. T. (2012). A backup plan for self-protection: S-methylation of holomycin biosynthetic intermediates in Streptomyces clavuligerus. *Chembiochem* 13, 2521–6.

Li, B., and Walsh, C. T. (2011). Streptomyces clavuligerus HlmI is an intramolecular disulfide-forming dithiol oxidase in holomycin biosynthesis. *Biochemistry* 50, 4615–22.

Li, M., Kim, T.-J., Kwon, H.-J., and Suh, J.-W. (2008). Effects of extracellular ATP on the physiology of Streptomyces coelicolor A3(2). *FEMS Microbiol. Lett.* 286, 24–31.

Li, X., Kim, S., Nam, K. W., Kang, J. S., and Choi, H. D. (2006). A New Antibacterial Dioxopiperazine Alkaloid Related to Gliotoxin from a Marine Isolate of the Fungus Pseudallescheria. *J. Antibiot. (Tokyo).* 59, 248–250.

Lichty, J. J., Malecki, J. L., Agnew, H. D., Michelson-Horowitz, D. J., and Tan, S. (2005). Comparison of affinity tags for protein purification. *Protein Expr. Purif.* 41, 98–105.

Lim, F. Y., and Keller, N. P. (2014). Spatial and temporal control of fungal natural product synthesis. *Nat. Prod. Rep.* 31, 1277–1286.

Lim, K., Zhang, H., Tempczyk, A., Bonander, N., Toedt, J., Howard, A., Eisenstein, E., and Herzberg, O. (2001). Crystal structure of YecO from Haemophilus influenzae (HI0319) reveals a methyltransferase fold and a bound S-adenosylhomocysteine. *Proteins* 45, 397–407.

Lin, H.-C., Chooi, Y.-H., Dhingra, S., Xu, W., Calvo, A. M., and Tang, Y. (2013). The fumagillin biosynthetic gene cluster in Aspergillus fumigatus encodes a cryptic terpene cyclase involved in the formation of β-trans-bergamotene. *J. Am. Chem. Soc.* 135, 4616–9.

Lin, S. J., Schranz, J., and Teutsch, S. M. (2001). Aspergillosis case-fatality rate: systematic review of the literature. *Clin. Infect. Dis.* 32, 358–66.

Lipson, J. M., Thomsen, M., Moore, B. S., Clausen, R. P., La Clair, J. J., and Burkart, M. D. (2013). A Tandem Chemoenzymatic Methylation by S-Adenosyl-L-methionine. *Chembiochem* 14, 950–3.

Liscombe, D. K., Louie, G. V, and Noel, J. P. (2012). Architectures, mechanisms and molecular evolution of natural product methyltransferases. *Nat. Prod. Rep.* 29, 1238–50.

Loenen, W. a M. (2006). S-adenosylmethionine: jack of all trades and master of everything? *Biochem. Soc. Trans.* 34, 330–3.

Lu, S., Zhang, Y., Liu, J., Zhao, C., Liu, W., and Xi, R. (2006). Preparation of anti-pefloxacin antibody and development of an indirect competitive enzyme-linked immunosorbent assay for detection of pefloxacin residue in chicken liver. *J. Agric. Food Chem.* 54, 6995–7000.

Ma, D., and Li, R. (2012). Current Understanding of HOG-MAPK Pathway in Aspergillus fumigatus. *Mycopathologia* 175, 13–23.

MacKenzie, D. a, Guillemette, T., Al-Sheikh, H., Watson, a J., Jeenes, D. J., Wongwathanarat, P., Dunn-Coleman, N. S., van Peij, N., and Archer, D. B. (2005). UPR-independent dithiothreitol stress-induced genes in Aspergillus niger. *Mol. Genet. Genomics* 274, 410–8.

Maertens, J. A., Klont, R., Masson, C., Theunissen, K., Meersseman, W., Lagrou, K., Heinen, C., Crépin, B., Van Eldere, J., Tabouret, M., et al. (2007). Optimization of the cutoff value for the Aspergillus double-sandwich enzyme immunoassay. *Clin. Infect. Dis.* 44, 1329–36.

Mah, J.-H., and Yu, J.-H. (2006). Upstream and downstream regulation of asexual development in Aspergillus fumigatus. *Eukaryot. Cell* 5, 1585–95.

Marks, D. S., Hopf, T. A., and Sander, C. (2012). Protein structure prediction from sequence variation. *Nat. Biotechnol.* 30, 1072–80.

Marty, F. M., and Koo, S. (2009). Role of (1-->3)-beta-D-glucan in the diagnosis of invasive aspergillosis. *Med. Mycol.* 47 Suppl 1, S233–40.

McCarthy, A. a, and McCarthy, J. G. (2007). The structure of two N-methyltransferases from the caffeine biosynthetic pathway. *Plant Physiol.* 144, 879–889.

McDonagh, A., Fedorova, N. D., Crabtree, J., Yu, Y., Kim, S., Chen, D., Loss, O., Cairns, T., Goldman, G., Armstrong-James, D., et al. (2008). Sub-telomere directed gene expression during initiation of invasive aspergillosis. *PLoS Pathog.* 4, e1000154.

McGary, K. L., Slot, J. C., and Rokas, A. (2013). Physical linkage of metabolic genes in fungi is an adaptation against the accumulation of toxic intermediate compounds. *Proc. Natl. Acad. Sci.* 110, 11481–6.

Mcwilliam, H., Valentin, F., Goujon, M., Li, W., Narayanasamy, M., Martin, J., Miyar, T., and Lopez, R. (2009). Web services at the European Bioinformatics Institute-2009. *Nucleic Acids Res.* 37, W6–W10.

Medina, E. M., Jones, G. W., and Fitzpatrick, D. A. (2011). Reconstructing the fungal tree of life using phylogenomics and a preliminary investigation of the distribution of yeast prion-like proteins in the fungal kingdom. *J. Mol. Evol.* 73, 116–33.

Min, Z., Baddley, J. W., Rodriguez, J. M., Moser, S. A., and Patel, M. (2012). Cross-reactivity of Aspergillus galactomannan in an HIV-infected patient with histoplasmosis. *Med. Mycol. Case Rep.* 1, 119–22.

Mitamura, T., Yamamura, Y., and Kurosaki, F. (2011). Modification and translocation of Rac/Rop guanosine 5'-triphosphate-binding proteins of Scoparia dulcis in response to stimulation with methyl jasmonate. *Biol. Pharm. Bull.* 34, 845–9.

Mitchell, C. G., Slight, J., and Donaldson, K. (1997). Diffusible component from the spore surface of the fungus Aspergillus fumigatus which inhibits the macrophage oxidative burst is distinct from gliotoxin and other hyphal toxins. *Thorax* 52, 796–801.

Mitsuguchi, H., Seshime, Y., Fujii, I., Shibuya, M., Ebizuka, Y., and Kushiro, T. (2009). Biosynthesis of steroidal antibiotic fusidanes: functional analysis of oxidosqualene cyclase and subsequent tailoring enzymes from Aspergillus fumigatus. *J. Am. Chem. Soc.* 131, 6402–11.

Miyazaki, T., Kohno, S., Mitsutake, K., Maesaki, S., Tanaka, K., Ishikawa, N., and Hara, K. (1995). Plasma (1-->3)-beta-D-glucan and fungal antigenemia in patients with candidemia, aspergillosis, and cryptococcosis. *J. Clin. Microbiol.* 33, 3115–8.

Moreno, M. A., Ibrahim-Granet, O., Vicentefranqueira, R., Amich, J., Ave, P., Leal, F., Latgé, J.-P., and Calera, J. A. (2007). The regulation of zinc homeostasis by the ZafA transcriptional activator is essential for Aspergillus fumigatus virulence. *Mol. Microbiol.* 64, 1182–97.

Morton, C. O., Varga, J. J., Hornbach, A., Mezger, M., Sennefelder, H., Kneitz, S.,

Kurzai, O., Krappmann, S., Einsele, H., Nierman, W. C., et al. (2011). The temporal dynamics of differential gene expression in Aspergillus fumigatus interacting with human immature dendritic cells in vitro. *PLoS One* 6, e16016.

Mouyna, I., Morelle, W., Vai, M., Monod, M., Léchenne, B., Fontaine, T., Beauvais, A., Sarfati, J., Prévost, M.-C., Henry, C., et al. (2005). Deletion of GEL2 encoding for a beta(1-3)glucanosyltransferase affects morphogenesis and virulence in Aspergillus fumigatus. *Mol. Microbiol.* 56, 1675–88.

Moye-Rowley, W. S. (2003). Regulation of the transcriptional response to oxidative stress in fungi: similarities and differences. *Eukaryot. Cell* 2, 381–9.

Mulinti, P., Allen, N. A., Coyle, C. M., Gravelat, F. N., Sheppard, D. C., and Panaccione, D. G. (2014). Accumulation of ergot alkaloids during conidiophore development in Aspergillus fumigatus. *Curr. Microbiol.* 68, 1–5.

Munday, R., Thompson, A., Smith, B., Towers, N., O'Donnell, K., McDonald, R., and M, S. (2001). A zinc-containing intraruminal device for prevention of the sporidesmin-induced cholangiopathy of facial eczema in calves. *N. Z. Vet. J.* 40, 29–33.

Nielsen, M. L., Albertsen, L., Lettier, G., Nielsen, J. B., and Mortensen, U. H. (2006). Efficient PCR-based gene targeting with a recyclable marker for Aspergillus nidulans. *Fungal Genet. Biol.* 43, 54–64.

Nützmann, H.-W., Reyes-Dominguez, Y., Scherlach, K., Schroeckh, V., Horn, F., Gacek, A., Schümann, J., Hertweck, C., Strauss, J., and Brakhage, A. A. (2011). Bacteria-induced natural product formation in the fungus Aspergillus nidulans requires Saga/Ada-mediated histone acetylation. *Proc. Natl. Acad. Sci. U. S. A.* 108, 14282–7.

O'Gorman, C. M. (2011). Airborne Aspergillus fumigatus conidia: a risk factor for aspergillosis. *Fungal Biol. Rev.* 25, 151–157.

O'Gorman, C. M., Fuller, H. T., and Dyer, P. S. (2009). Discovery of a sexual cycle in the opportunistic fungal pathogen Aspergillus fumigatus. *Nature* 457, 471–4.

O'Hanlon, K. a, Gallagher, L., Schrettl, M., Jöchl, C., Kavanagh, K., Larsen, T. O., and Doyle, S. (2012). Nonribosomal peptide synthetase genes pesL and pes1 are essential for Fumigaclavine C production in Aspergillus fumigatus. *Appl. Environ. Microbiol.* 78, 3166–76.

O'Keeffe, G., Hammel, S., Owens, R. A., Keane, T. M., Fitzpatrick, D. A., Jones, G. W., and Doyle, S. (2014). RNA-seq reveals the pan-transcriptomic impact of attenuating the gliotoxin self-protection mechanism in Aspergillus fumigatus. *BMC Genomics* 15, 894.

Odabasi, Z., Paetznick, V. L., Rodriguez, J. R., Chen, E., McGinnis, M. R., and Ostrosky-Zeichner, L. (2006). Differences in beta-glucan levels in culture supernatants of a

variety of fungi. *Med. Mycol.* 44, 267–72.

Okamoto, M., Yoshida, K., Uchida, I., Nishikawa, M., Kohsaka, M., and Aoki, H. (1986). Studies of platelet activating factor (PAF) antagonists from microbial products. I. Bisdethiobis(methylthio)gliotoxin and its derivatives. *Chem. Pharm. Bull. (Tokyo).* 34, 340–4.

Onishi, A., Sugiyama, D., Kogata, Y., Saegusa, J., Sugimoto, T., Kawano, S., Morinobu, A., Nishimura, K., and Kumagai, S. (2012). Diagnostic accuracy of serum 1,3-β-D-glucan for pneumocystis jiroveci pneumonia, invasive candidiasis, and invasive aspergillosis: systematic review and meta-analysis. *J. Clin. Microbiol.* 50, 7–15.

Outten, C. E., and O'Halloran, T. V (2001). Femtomolar sensitivity of metalloregulatory proteins controlling zinc homeostasis. *Science* 292, 2488–92.

Owens, R. A., O'Keeffe, G., Smith, E. B., Dolan, S. K., Hammel, S., Sheridan, K. J., Fitzpatrick, D. A., Keane, T. M., Jones, G. W., and Doyle, S. (2015). Interplay between Gliotoxin Resistance, Secretion, and the Methyl/Methionine Cycle in Aspergillus fumigatus. *Eukaryot. Cell* 14, 941–57.

Pahl, H. L., Krauss, B., Schulze-Osthoff, K., Decker, T., Traenckner, E. B., Vogt, M., Myers, C., Parks, T., Warring, P., Mühlbacher, A., et al. (1996). The immunosuppressive fungal metabolite gliotoxin specifically inhibits transcription factor NF-kappaB. *J. Exp. Med.* 183, 1829–40.

Palazon, A., Goldrath, A. W., Nizet, V., and Johnson, R. S. (2014). HIF Transcription Factors, Inflammation, and Immunity. *Immunity* 41, 518–528.

Palmer, J. M., Bok, J. W., Lee, S., Dagenais, T. R. T., Andes, D. R., Kontoyiannis, D. P., and Keller, N. P. (2013). Loss of CclA, required for histone 3 lysine 4 methylation, decreases growth but increases secondary metabolite production in Aspergillus fumigatus. *PeerJ* 1, e4.

Pandey, S., Hoselton, S. A., and Schuh, J. M. (2013). The impact of Aspergillus fumigatus viability and sensitization to its allergens on the murine allergic asthma phenotype. *Biomed Res. Int.* 2013, 619614.

Pape, T., and Schneider, T. R. (2004). HKL2MAP : a graphical user interface for macromolecular phasing with SHELX programs. *J. Appl. Crystallogr.* 37, 843–844.

Pardo, J., Urban, C., Galvez, E. M., Ekert, P. G., Müller, U., Kwon-Chung, J., Lobigs, M., Müllbacher, A., Wallich, R., Borner, C., et al. (2006). The mitochondrial protein Bak is pivotal for gliotoxin-induced apoptosis and a critical host factor of Aspergillus fumigatus virulence in mice. *J. Cell Biol.* 174, 509–19.

Park, H. B., Kim, Y.-J., Park, J.-S., Yang, H. O., Lee, K. R., and Kwon, H. C. (2011). Glionitrin B, a cancer invasion inhibitory diketopiperazine produced by microbial coculture. *J. Nat. Prod.* 74, 2309–12.

Park, H.-S., Bayram, O., Braus, G. H., Kim, S. C., and Yu, J.-H. (2012). Characterization

of the velvet regulators in Aspergillus fumigatus. *Mol. Microbiol.* 86, 937–53.

Pathak, V., Hurtado Rendon, I. S., and Ciubotaru, R. L. (2011). Invasive pulmonary aspergillosis in an immunocompetent patient. *Respir. Med. CME* 4, 105–106.

Patron, N. J., Waller, R. F., Cozijnsen, A. J., Straney, D. C., Gardiner, D. M., Nierman, W. C., and Howlett, B. J. (2007). Origin and distribution of epipolythiodioxopiperazine (ETP) gene clusters in filamentous ascomycetes. *BMC Evol. Biol.* 7, 174.

Patterson, T. F. (2011). Clinical utility and development of biomarkers in invasive aspergillosis. *Trans. Am. Clin. Climatol. Assoc.* 122, 174–83.

De Pauw, B., Walsh, T. J., Donnelly, J. P., Stevens, D. A., Edwards, J. E., Calandra, T., Pappas, P. G., Maertens, J., Lortholary, O., Kauffman, C. A., et al. (2008). Revised definitions of invasive fungal disease from the European Organization for Research and Treatment of Cancer/Invasive Fungal Infections Cooperative Group and the National Institute of Allergy and Infectious Diseases Mycoses Study Group (EORTC/MSG) C. *Clin. Infect. Dis.* 46, 1813–21.

Peng, G., Ren, Y., Sun, X., Zhou, J., and Li, D. (2012). Inhibition of farnesyltransferase reduces angiogenesis by interrupting endothelial cell migration. *Biochem. Pharmacol.* 83, 1374–82.

Perfect, J. R. (2013). Fungal diagnosis: how do we do it and can we do better? *Curr. Med. Res. Opin.* 29 Suppl 4, 3–11.

Perrin, R. M., Fedorova, N. D., Bok, J. W., Cramer, R. a, Wortman, J. R., Kim, H. S., Nierman, W. C., and Keller, N. P. (2007). Transcriptional regulation of chemical diversity in Aspergillus fumigatus by LaeA. *PLoS Pathog.* 3, e50.

Petrik, M., Franssen, G. M., Haas, H., Laverman, P., Hörtnagl, C., Schrettl, M., Helbok, A., Lass-Flörl, C., and Decristoforo, C. (2012). Preclinical evaluation of two 68Ga-siderophores as potential radiopharmaceuticals for Aspergillus fumigatus infection imaging. *Eur. J. Nucl. Med. Mol. Imaging* 39, 1175–83.

Petrik, M., Haas, H., Dobrozemsky, G., Lass-Flörl, C., Helbok, A., Blatzer, M., Dietrich, H., and Decristoforo, C. (2010). 68Ga-siderophores for PET imaging of invasive pulmonary aspergillosis: proof of principle. *J. Nucl. Med.* 51, 639–45.

Pfaffenbach, B., Donhuijsen, K., Pahnke, J., Bug, R., Adamek, R. J., Wegener, M., and Ricken, D. (1994). [Systemic fungal infections in hematologic neoplasms. An autopsy study of 1,053 patients]. *Med. Klin. (Munich).* 89, 299–304.

Pflugrath, J. W. (1999). The finer things in X-ray diffraction data collection. *Acta Crystallogr. Sect. D Biol. Crystallogr.* 55, 1718–1725.

Pickering, J. W., Sant, H. W., Bowles, C. A. P., Roberts, W. L., and Woods, G. L. (2005). Evaluation of a (1->3)-beta-D-glucan assay for diagnosis of invasive fungal infections. *J. Clin. Microbiol.* 43, 5957–62.

Presicce, P., Taddeo, A., Conti, A., Villa, M. L., and Della Bella, S. (2008). Keyhole limpet hemocyanin induces the activation and maturation of human dendritic cells through the involvement of mannose receptor. *Mol. Immunol.* 45, 1136–45.

Van der Pyl, D., Inokoshi, J., Shiomi, K., Yang, H., Takeshima, H., and Omura, S. (1992). Inhibition of farnesyl-protein transferase by gliotoxin and acetylgliotoxin. *J. Antibiot. (Tokyo).* 45, 1802–5.

Rateb, M., Hallyburton, I., and Houssen, W. (2013). Induction of diverse secondary metabolites in Aspergillus fumigatus by microbial co-culture. *RSC Adv.*, 14444–14450.

Reategui, R., Rhea, J., Adolphson, J., Waikins, K., Newell, R., Rabenstein, J., Mocek, U., Luche, M., and Carr, G. (2013). Leporizines A-C: epithiodiketopiperazines isolated from an Aspergillus species. *J. Nat. Prod.* 76, 1523–7.

Reece, K. M., Richardson, E. D., Cook, K. M., Campbell, T. J., Pisle, S. T., Holly, A. J., Venzon, D. J., Liewehr, D. J., Chau, C. H., Price, D. K., et al. (2014). Epidithiodiketopiperazines (ETPs) exhibit in vitro antiangiogenic and in vivo antitumor activity by disrupting the HIF-1α/p300 complex in a preclinical model of prostate cancer. *Mol. Cancer* 13, 91.

Reyes-Dominguez, Y., Bok, J. W., Berger, H., Shwab, E. K., Basheer, A., Gallmetzer, A., Scazzocchio, C., Keller, N., and Strauss, J. (2010). Heterochromatic marks are associated with the repression of secondary metabolism clusters in Aspergillus nidulans. *Mol. Microbiol.* 76, 1376–86.

Rhodes, J. C. (1988). Virulence factors in fungal pathogens. *Microbiol. Sci.* 5, 252–4.

Richard, J. L. (2007). Some major mycotoxins and their mycotoxicoses--an overview. *Int. J. Food Microbiol.* 119, 3–10.

Rokas, A. (2013). Aspergillus. *Curr. Biol.* 23, R187–8.

Rosano, G. L., and Ceccarelli, E. A. (2014). Recombinant protein expression in Escherichia coli: advances and challenges. *Front. Microbiol.* 5, 172.

Rowley, N., Prip-Buus, C., Westermann, B., Brown, C., Schwarz, E., Barrell, B., and Neupert, W. (1994). Mdj1p, a novel chaperone of the DnaJ family, is involved in mitochondrial biogenesis and protein folding. *Cell* 77, 249–259.

Roy, A., Kucukural, A., and Zhang, Y. (2010). I-TASSER: a unified platform for automated protein structure and function prediction. *Nat. Protoc.* 5, 725–38.

Sakamoto, H., Egashira, S., Saito, N., Kirisako, T., Miller, S., Sasaki, Y., Matsumoto, T., Shimonishi, M., Komatsu, T., Terai, T., et al. (2014). Gliotoxin suppresses NF-κB activation by selectively inhibiting linear ubiquitin chain assembly complex (LUBAC). *ACS Chem. Biol.* 3, 675-681

Sales-Campos, H., Tonani, L., Cardoso, C. R. B., and Kress, M. R. V. Z. (2013). The

immune interplay between the host and the pathogen in Aspergillus fumigatus lung infection. *Biomed Res. Int.* 2013, 693023.

Santa, T., Al-Dirbashi, O. Y., and Fukushima, T. (2007). Derivatization reagents in liquid chromatography/electrospray ionization tandem mass spectrometry for biomedical analysis. *Drug Discov. Ther.* 1, 108–18.

Sarikaya Bayram, O., Bayram, O., Valerius, O., Park, H. S., Irniger, S., Gerke, J., Ni, M., Han, K.-H., Yu, J.-H., and Braus, G. H. (2010). LaeA control of velvet family regulatory proteins for light-dependent development and fungal cell-type specificity. *PLoS Genet.* 6, e1001226.

Saxena, D., Aouad, S., Attieh, J., and Saini, H. S. (1998). Biochemical Characterization of Chloromethane Emission from the Wood-Rotting Fungus Phellinus pomaceus. *Appl. Envir. Microbiol.* 64, 2831–2835.

Scharf, D. H., Chankhamjon, P., Scherlach, K., Heinekamp, T., Roth, M., Brakhage, A. a., and Hertweck, C. (2012). Epidithiol Formation by an Unprecedented Twin Carbon-Sulfur Lyase in the Gliotoxin Pathway. *Angew. Chem. Int. Ed. Engl.* 124, 10211–10215.

Scharf, D. H., Chankhamjon, P., Scherlach, K., Heinekamp, T., Willing, K., Brakhage, A. A., and Hertweck, C. (2013). Epidithiodiketopiperazine biosynthesis: a four-enzyme cascade converts glutathione conjugates into transannular disulfide bridges. *Angew. Chem. Int. Ed. Engl.* 52, 11092–5.

Scharf, D. H., Habel, A., Heinekamp, T., Brakhage, A. a, and Hertweck, C. (2014a). Opposed effects of enzymatic gliotoxin N- and s-methylations. *J. Am. Chem. Soc.* 136, 11674–9.

Scharf, D. H., Heinekamp, T., and Brakhage, A. A. (2014b). Human and plant fungal pathogens: the role of secondary metabolites. *PLoS Pathog.* 10, e1003859.

Scharf, D. H., Remme, N., Habel, A., Chankhamjon, P., Scherlach, K., Heinekamp, T., Hortschansky, P., Brakhage, A. a, and Hertweck, C. (2011). A dedicated glutathione S-transferase mediates carbon-sulfur bond formation in gliotoxin biosynthesis. *J. Am. Chem. Soc.* 133, 12322–5.

Scharf, D. H., Remme, N., Heinekamp, T., Hortschansky, P., Brakhage, A. A., and Hertweck, C. (2010). Transannular disulfide formation in gliotoxin biosynthesis and its role in self-resistance of the human pathogen Aspergillus fumigatus. *J. Am. Chem. Soc.* 132, 10136–10141.

Schmidberger, J. W., James, A. B., Edwards, R., Naismith, J. H., and O'Hagan, D. (2010). Halomethane biosynthesis: structure of a SAM-dependent halide methyltransferase from Arabidopsis thaliana. *Angew. Chem. Int. Ed. Engl.* 49, 3646–8.

Schmitt, E. K., Bunse, A., Janus, D., Hoff, B., Friedlin, E., Kürnsteiner, H., and Kück, U. (2004a). Winged helix transcription factor CPCR1 is involved in regulation of beta-

lactam biosynthesis in the fungus Acremonium chrysogenum. *Eukaryot. Cell* 3, 121–34.

Schmitt, E. K., Hoff, B., and Kück, U. (2004b). AcFKH1, a novel member of the forkhead family, associates with the RFX transcription factor CPCR1 in the cephalosporin C-producing fungus Acremonium chrysogenum. *Gene* 342, 269–81.

Schneider, T. R., and Sheldrick, G. M. (2002). Substructure solution with SHELXD. *Acta Crystallogr. D. Biol. Crystallogr.* 58, 1772–9.

Schöbel, F., Ibrahim-Granet, O., Avé, P., Latgé, J.-P., Brakhage, A. A., and Brock, M. (2007). Aspergillus fumigatus does not require fatty acid metabolism via isocitrate lyase for development of invasive aspergillosis. *Infect. Immun.* 75, 1237–44.

Schoberle, T. J., Nguyen-Coleman, C. K., Herold, J., Yang, A., Weirauch, M., Hughes, T. R., McMurray, J. S., and May, G. S. (2014). A novel C2H2 transcription factor that regulates gliA expression interdependently with GliZ in Aspergillus fumigatus. *PLoS Genet.* 10, e1004336.

Schrettl, M., Bignell, E., Kragl, C., Sabiha, Y., Loss, O., Eisendle, M., Wallner, A., Arst, H. N., Haynes, K., and Haas, H. (2007). Distinct roles for intra- and extracellular siderophores during Aspergillus fumigatus infection. *PLoS Pathog.* 3, 1195–207.

Schrettl, M., Carberry, S., and Kavanagh, K. (2010). Self-protection against gliotoxin—a component of the gliotoxin biosynthetic cluster, GliT, completely protects Aspergillus fumigatus against exogenous. *PLoS Pathog.* 6, e1000952.

Schrettl, M., and Haas, H. (2011). Iron homeostasis-Achilles' heel of Aspergillus fumigatus? *Curr. Opin. Microbiol.* 14, 400–5.

Schubert, H. L., Blumenthal, R. M., and Cheng, X. (2003). Many paths to methyltransfer: A chronicle of convergence. *Trends Biochem. Sci.* 28, 329–335.

Sekonyela, R., Palmer, J. M., Bok, J.-W., Jain, S., Berthier, E., Forseth, R., Schroeder, F., and Keller, N. P. (2013). RsmA Regulates Aspergillus fumigatus Gliotoxin Cluster Metabolites Including Cyclo(L-Phe-L-Ser), a Potential New Diagnostic Marker for Invasive Aspergillosis. *PLoS One* 8, e62591.

Sharrocks, A. D. (2001). The ETS-domain transcription factor family. *Nat. Rev. Mol. Cell Biol.* 2, 827–37.

Sheldrick, G. M. (2010). Experimental phasing with SHELXC/D/E: combining chain tracing with density modification. *Acta Crystallogr. D. Biol. Crystallogr.* 66, 479–85.

Sheridan, K. J., Dolan, S. K., and Doyle, S. (2015). Endogenous cross-talk of fungal metabolites. *Front. Microbiol.* 5, 10.3389.

Shevchenko, A., Tomas, H., Havlis, J., Olsen, J. V, and Mann, M. (2006). In-gel digestion for mass spectrometric characterization of proteins and proteomes. *Nat. Protoc.* 1,

2856–60.

Shi, L., Li, F., Lu, J., Kong, X., Wang, S., Huang, M., Shao, H., and Shao, S. (2012). Antibody specific to thioredoxin reductase as a new biomarker for serodiagnosis of invasive aspergillosis in non-neutropenic patients. *Clin. Chim. Acta.* 413, 938–43.

Shin, K. K., Park, H. H., Kim, Y. Y., and Yu, J.-H. J. (2013). Comparative proteomic analyses reveal that FlbA down-regulates gliT expression and SOD activity in Aspergillus fumigatus. *J. Proteomics*.

Shwab, E. K., Bok, J. W., Tribus, M., Galehr, J., Graessle, S., and Keller, N. P. (2007). Histone deacetylase activity regulates chemical diversity in Aspergillus. *Eukaryot. Cell* 6, 1656–64.

Singh, K. V, Kaur, J., Varshney, G. C., Raje, M., and Suri, C. R. (2004). Synthesis and characterization of hapten-protein conjugates for antibody production against small molecules. *Bioconjug. Chem.* 15, 168–73.

Smith, T. D., and Calvo, A. M. (2014). The mtfA transcription factor gene controls morphogenesis, gliotoxin production, and virulence in the opportunistic human pathogen Aspergillus fumigatus. *Eukaryot. Cell* 13, 766–75.

Song, G., Cheng, C., Li, Y., Shaw, N., Xiao, Z.-C., and Liu, Z.-J. (2014). Crystal structure of the N-terminal methyltransferase-like domain of anamorsin. *Proteins* 82, 1066–71.

Spikes, S., and Xu, R. (2008). Gliotoxin production in Aspergillus fumigatus contributes to host-specific differences in virulence. *J. Infect. Dis.* 197, 479–486.

Srinivasan, U., Bala, A., Jao, S., Starke, D. W., Jordan, T. W., and Mieyal, J. J. (2006). Selective inactivation of glutaredoxin by sporidesmin and other epidithiopiperazinediones. *Biochemistry* 45, 8978–87.

Stack, D., Neville, C., and Doyle, S. (2007). Nonribosomal peptide synthesis in Aspergillus fumigatus and other fungi. *Microbiology* 153, 1297–306.

Stolte, C., Sabir, K. S., Heinrich, J., Hammang, C. J., Schafferhans, A., and O'Donoghue, S. I. (2015). Integrated visual analysis of protein structures, sequences, and feature data. *BMC Bioinformatics* 16, S7.

Struck, A., Thompson, M. L., Wong, L. S., and Micklefield, J. (2012). S-adenosyl-methionine-dependent methyltransferases: highly versatile enzymes in biocatalysis, biosynthesis and other biotechnological applications. *Chembiochem* 13, 2642–55.

Stynen, D., Sarfati, J., Goris, A., Prévost, M. C., Lesourd, M., Kamphuis, H., Darras, V., and Latgé, J. P. (1992). Rat monoclonal antibodies against Aspergillus galactomannan. *Infect. Immun.* 60, 2237–45.

Sugiyama, K., Izawa, S., and Inoue, Y. (2000). The Yap1p-dependent induction of glutathione synthesis in heat shock response of Saccharomyces cerevisiae. *J. Biol.*

Chem. 275, 15535–40.

Sugui, J. a, Pardo, J., Chang, Y. C., Zarember, K. a, Nardone, G., Galvez, E. M., Müllbacher, A., Gallin, J. I., Simon, M. M., and Kwon-Chung, K. J. (2007). Gliotoxin is a virulence factor of Aspergillus fumigatus: gliP deletion attenuates virulence in mice immunosuppressed with hydrocortisone. *Eukaryot. Cell* 6, 1562–9.

Sugui, J. A., Kim, H. S., Zarember, K. A., Chang, Y. C., Gallin, J. I., Nierman, W. C., and Kwon-Chung, K. J. (2008). Genes differentially expressed in conidia and hyphae of Aspergillus fumigatus upon exposure to human neutrophils. *PLoS One* 3, e2655.

Sulahian, A., Porcher, R., Bergeron, A., Touratier, S., Raffoux, E., Menotti, J., Derouin, F., and Ribaud, P. (2014). Use and limits of (1-3)-β-d-glucan assay (Fungitell), compared to galactomannan determination (Platelia Aspergillus), for diagnosis of invasive aspergillosis. *J. Clin. Microbiol.* 52, 2328–33.

Suliman, H. S., Appling, D. R., and Robertus, J. D. (2007). The gene for cobalamin-independent methionine synthase is essential in Candida albicans: A potential antifungal target. *Arch. Biochem. Biophys.* 467, 218–226.

Sun, Y., Takada, K., and Takemoto, Y. (2011). Gliotoxin analogues from a marine-derived fungus, Penicillium sp., and their cytotoxic and histone methyltransferase inhibitory activities. *J. Nat. Prod.* 75, 111–4.

Suzuki, Y., Takahashi, H., Esumi, Y., Arie, T., Morita, T., Koshino, H., Uzawa, J., Uramoto, M., and Yamaguchi, I. (2000). Haematocin, a new antifungal diketopiperazine produced by Nectria haematococca Berk. et Br. (880701a-1) causing nectria blight disease on ornamental plants. *J. Antibiot. (Tokyo).* 53, 45–9.

Tan, R. X., Jensen, P. R., Williams, P. G., and Fenical, W. (2004). Isolation and structure assignments of rostratins A-D, cytotoxic disulfides produced by the marine-derived fungus Exserohilum rostratum. *J. Nat. Prod.* 67, 1374–82.

Taylor, A. (1963). Sporidesmins. Isolation and Structure of Sporidesmin-D and Sporidesmin-F. *J. Chem. Soc. C Org.* 95, 1564–1567.

Teichmann, M., Dumay-Odelot, H., and Fribourg, S. (2012). Structural and functional aspects of winged-helix domains at the core of transcription initiation complexes. *Transcription* 3, 2–7.

Tekaia, F., and Latgé, J.-P. (2005). Aspergillus fumigatus: saprophyte or pathogen? *Curr. Opin. Microbiol.* 8, 385–392.

Thomsen, M., Vogensen, S. B., Buchardt, J., Burkart, M. D., and Clausen, R. P. (2013). Chemoenzymatic synthesis and in situ application of S-adenosyl-L-methionine analogs. *Org. Biomol. Chem.* 11, 7606–10.

Thykaer, J., and Nielsen, J. (2003). Metabolic engineering of beta-lactam production.

Metab. Eng. 5, 56–69.

Tsunawaki, S., Yoshida, L. S., Nishida, S., Kobayashi, T., and Shimoyama, T. (2004). Fungal metabolite gliotoxin inhibits assembly of the human respiratory burst NADPH oxidase. *Infect. Immun.* 72, 3373–82.

Tsunematsu, Y., Ishikawa, N., Wakana, D., Goda, Y., Noguchi, H., Moriya, H., Hotta, K., and Watanabe, K. (2013). Distinct mechanisms for spiro-carbon formation reveal biosynthetic pathway crosstalk. *Nat. Chem. Biol.*, 1–78.

Tuomola, M., Harpio, R., Mikola, H., Knuuttila, P., Lindström, M., Mukkala, V.-M., Matikainen, M.-T., and Lövgren, T. (2000). Production and characterisation of monoclonal antibodies against a very small hapten, 3-methylindole. *J. Immunol. Methods* 240, 111–124.

Twumasi-Boateng, K., Yu, Y., Chen, D., Gravelat, F. N., Nierman, W. C., and Sheppard, D. C. (2009). Transcriptional profiling identifies a role for BrlA in the response to nitrogen depletion and for StuA in the regulation of secondary metabolite clusters in Aspergillus fumigatus. *Eukaryot. Cell* 8, 104–15.

Vainberg, I. E., Lewis, S. A., Rommelaere, H., Ampe, C., Vandekerckhove, J., Klein, H. L., and Cowan, N. J. (1998). Prefoldin, a Chaperone that Delivers Unfolded Proteins to Cytosolic Chaperonin. *Cell* 93, 863–873.

Valerio, M., Rodriguez-Gonzalez, C. G., Muñoz, P., Caliz, B., Sanjurjo, M., and Bouza, E. (2014). Evaluation of antifungal use in a tertiary care institution: antifungal stewardship urgently needed. *J. Antimicrob. Chemother.* 69, 1993–9.

Valiante, V., Heinekamp, T., and Jain, R. (2008). The mitogen-activated protein kinase MpkA of Aspergillus fumigatus regulates cell wall signaling and oxidative stress response. *Fungal Genet. Biol.* 45, 618–27.

Valiante, V., Macheleidt, J., Föge, M., and Brakhage, A. a. (2015). The Aspergillus fumigatus cell wall integrity signaling pathway: drug target, compensatory pathways, and virulence. *Front. Microbiol.* 06.

Vicentefranqueira, R., Amich, J., Laskaris, P., Ibrahim-Granet, O., Latgé, J. P., Toledo, H., Leal, F., and Calera, J. A. (2015). Targeting zinc homeostasis to combat Aspergillus fumigatus infections. *Front. Microbiol.* 6, 160.

Vidgren, J., Svensson, L. A., and Liljas, A. (1994). Crystal structure of catechol O-methyltransferase. *Nature* 368, 354–8.

Vit, A., Misson, L., Blankenfeldt, W., and Seebeck, F. P. (2014). Crystallization and preliminary X-ray analysis of the ergothioneine-biosynthetic methyltransferase EgtD. *Acta Crystallogr. Sect. F, Struct. Biol. Commun.* 70, 676–80.

Vit, A., Misson, L., Blankenfeldt, W., and Seebeck, F. P. (2015). Ergothioneine Biosynthetic Methyltransferase EgtD Reveals the Structural Basis of Aromatic Amino Acid Betaine Biosynthesis. *Chembiochem* 16, 119–25.

Vödisch, M., Scherlach, K., Winkler, R., Hertweck, C., Braun, H.-P., Roth, M., Haas, H., Werner, E. R., Brakhage, A. a, and Kniemeyer, O. (2011). Analysis of the Aspergillus fumigatus proteome reveals metabolic changes and the activation of the pseurotin A biosynthesis gene cluster in response to hypoxia. *J. Proteome Res.* 10, 2508–24.

Wagener, J., Echtenacher, B., Rohde, M., Kotz, A., Krappmann, S., Heesemann, J., and Ebel, F. (2008). The putative alpha-1,2-mannosyltransferase AfMnt1 of the opportunistic fungal pathogen Aspergillus fumigatus is required for cell wall stability and full virulence. *Eukaryot. Cell* 7, 1661–73.

Wallwey, C., Matuschek, M., Xie, X.-L., and Li, S.-M. (2010). Ergot alkaloid biosynthesis in Aspergillus fumigatus: Conversion of chanoclavine-I aldehyde to festuclavine by the festuclavine synthase FgaFS in the presence of the old yellow enzyme FgaOx3. *Org. Biomol. Chem.* 8, 3500–8.

Wang, D.-N., Toyotome, T., Muraosa, Y., Watanabe, A., Wuren, T., Bunsupa, S., Aoyagi, K., Yamazaki, M., Takino, M., and Kamei, K. (2014). GliA in Aspergillus fumigatus is required for its tolerance to gliotoxin and affects the amount of extracellular and intracellular gliotoxin. *Med. Mycol.* 52, 506–18.

Ward, C., Chilvers, E., Lawson, M., and Pryde, J. (1999). NF-kappa B Activation Is a Critical Regulator of Human Granulocyte Apoptosis in Vitro. *J. Biol. Chem.* 274, 4309–4318.

Ward, O. P., Qin, W. M., Dhanjoon, J., Ye, J., and Singh, A. (2005). Physiology and Biotechnology of Aspergillus. *Adv. Appl. Microbiol.* 58C, 1–75.

Waring, P., Newcombe, N., Edel, M., Lin, Q. H., Jiang, H., Sjaarda, A., Piva, T., and Mullbacher, A. (1994). Cellular uptake and release of the immunomodulating fungal toxin gliotoxin. *Toxicon* 32, 491–504.

Watts, K., Ratnam, J., and Ang, K. (2010). Assessing the trypanocidal potential of natural and semi-synthetic diketopiperazines from two deep water marine-derived fungi. *Bioorg. Med. Chem.* 18, 2566–2574.

Weissman, K. J. (2015). Uncovering the structures of modular polyketide synthases. *Nat. Prod. Rep.* 32, 436–453.

Welch, T. R., and Williams, R. M. (2014). Epidithiodioxopiperazines. occurrence, synthesis and biogenesis. *Nat. Prod. Rep.* 31, 1376–404.

Wessjohann, L., Keim, J., Weigel, B., and Dippe, M. (2013). Alkylating enzymes. *Curr. Opin. Chem. Biol.* 17, 229–35.

Wheat, L. J. (2003). Rapid diagnosis of invasive aspergillosis by antigen detection. *Transpl. Infect. Dis.* 5, 158–166.

Wiemann, P., Guo, C.-J., Palmer, J. M., Sekonyela, R., Wang, C. C. C., and Keller, N. P. (2013). Prototype of an intertwined secondary-metabolite supercluster. *Proc. Natl.*

Acad. Sci. U. S. A., 1–6.

Wiemann, P., and Keller, N. P. (2013). Strategies for mining fungal natural products. *J Ind Microbiol Biotechnol*.

Wiemann, P., Lechner, B. E., Baccile, J. A., Velk, T. A., Yin, W.-B., Bok, J. W., Pakala, S., Losada, L., Nierman, W. C., Schroeder, F. C., et al. (2014). Perturbations in small molecule synthesis uncovers an iron-responsive secondary metabolite network in Aspergillus fumigatus. *Front. Microbiol.* 5, 530.

Winn, M. D., Ballard, C. C., Cowtan, K. D., Dodson, E. J., Emsley, P., Evans, P. R., Keegan, R. M., Krissinel, E. B., Leslie, A. G. W., McCoy, A., et al. (2011). Overview of the CCP4 suite and current developments. *Acta Crystallogr. D. Biol. Crystallogr.* 67, 235–42.

Wlodawer, A., Minor, W., Dauter, Z., and Jaskolski, M. (2008). Protein crystallography for non-crystallographers, or how to get the best (but not more) from published macromolecular structures. *FEBS J.* 275, 1–21.

Wuosmaa, A. M., and Hager, L. P. (1990). Methyl chloride transferase: a carbocation route for biosynthesis of halometabolites. *Science* 249, 160–2.

Wyatt, T. T., van Leeuwen, M. R., Wösten, H. A. B., and Dijksterhuis, J. (2014). Mannitol is essential for the development of stress-resistant ascospores in Neosartorya fischeri (Aspergillus fischeri). *Fungal Genet. Biol.* 64, 11–24.

Xiao, P., Shin, K.-S., Wang, T., and Yu, J.-H. (2010). Aspergillus fumigatus flbB encodes two basic leucine zipper domain (bZIP) proteins required for proper asexual development and gliotoxin production. *Eukaryot. Cell* 9, 1711–23.

Yang, J., Yan, R., Roy, A., Xu, D., Poisson, J., and Zhang, Y. (2015). The I-TASSER Suite: protein structure and function prediction. *Nat. Methods* 12, 7–8.

Yasmin, S., Alcazar-fuoli, L., Gründlinger, M., Puempel, T., Cairns, T., Blatzer, M., Lopez, J. F., Grimalt, J. O., Bignell, E., and Haas, H. (2012). Mevalonate governs interdependency of ergosterol and siderophore biosyntheses in the fungal pathogen Aspergillus fumigatus. *Proc. Natl. Acad. Sci. U. S. A.*109, E497–504.

Yin, W.-B., Baccile, J. a, Bok, J. W., Chen, Y., Keller, N. P., and Schroeder, F. C. (2013). A Nonribosomal Peptide Synthetase-Derived Iron(III) Complex from the Pathogenic Fungus Aspergillus fumigatus. *J. Am. Chem. Soc.* 135, 2064–7.

Zhang, A., Ma, Y., Feng, L., Wang, Y., He, C., Wang, X., and Zhang, H. (2011). Development of a sensitive competitive indirect ELISA method for determination of ochratoxin A levels in cereals originating from Nanjing, China. *Food Control* 22, 1723–1728.

Zhang, C., Albermann, C., Fu, X., Peters, N. R., Chisholm, J. D., Zhang, G., Gilbert, E. J., Wang, P. G., Van Vranken, D. L., and Thorson, J. S. (2006a). RebG- and RebM-Catalyzed Indolocarbazole Diversification. *ChemBioChem* 7, 795–804.

Zhang, C., Weller, R. L., Thorson, J. S., and Rajski, S. R. (2006b). Natural product diversification using a non-natural cofactor analogue of S-adenosyl-L-methionine. *J. Am. Chem. Soc.* 128, 2760–1.

Zhang, Q., and van der Donk, W. A. (2012). Catalytic promiscuity of a bacterial α-N-methyltransferase. *FEBS Lett.* 586, 3391–7.

Zhang, X., Zhou, L., and Cheng, X. (2000). Crystal structure of the conserved core of protein arginine methyltransferase PRMT3. *EMBO J.* 19, 3509–3519.

Zhang, Y. (2008). I-TASSER server for protein 3D structure prediction. *BMC Bioinformatics* 9, 40.

Zhao, C., Liu, W., Ling, H., Lu, S., Zhang, Y., Liu, J., and Xi, R. (2007). Preparation of anti-gatifloxacin antibody and development of an indirect competitive enzyme-linked immunosorbent assay for the detection of gatifloxacin residue in milk. *J. Agric. Food Chem.* 55, 6879–84.

Zhao, N., Ferrer, J.-L., Moon, H. S., Kapteyn, J., Zhuang, X., Hasebe, M., Stewart, C. N., Gang, D. R., and Chen, F. (2012). A SABATH Methyltransferase from the moss Physcomitrella patens catalyzes S-methylation of thiols and has a role in detoxification. *Phytochemistry* 81, 31–41.

Zheng, H., Kim, J., Liew, M., Yan, J. K., Herrera, O., Bok, J. W., Kelleher, N. L., Keller, N. P., and Wang, Y. (2014). Redox Metabolites Signal Polymicrobial Biofilm Development via the NapA Oxidative Stress Cascade in Aspergillus. *Curr. Biol.* 25, 29–37.

Zubieta, C. (2002). Structural Basis for the Modulation of Lignin Monomer Methylation by Caffeic Acid/5-Hydroxyferulic Acid 3/5-O-Methyltransferase. *Plant Cell* 14, 1265–1277.

Zubieta, C., He, X. Z., Dixon, R. a, and Noel, J. P. (2001). Structures of two natural product methyltransferases reveal the basis for substrate specificity in plant O-methyltransferases. *Nat. Struct. Biol.* 8, 271–9.

Zubieta, C., Ross, J. R., Koscheski, P., Yang, Y., Pichersky, E., and Noel, J. P. (2003). Structural basis for substrate recognition in the salicylic acid carboxyl methyltransferase family. *Plant Cell* 15, 1704–16.